

# Rehabilitation Robotics and Systems

Special Issue Editor in Chief: Rafael Morales

Guest Editors: Antonio Fernández-Caballero, José A. Somolinos,  
and Carlo Ferraresi



# **Rehabilitation Robotics and Systems**

Journal of Healthcare Engineering

---

## **Rehabilitation Robotics and Systems**

Special Issue Editor in Chief: Rafael Morales

Guest Editors: Antonio Fernández-Caballero, José A. Somolinos,  
and Carlo Ferraresi



Copyright © 2018 Hindawi. All rights reserved.

This is a special issue published in "Journal of Healthcare Engineering." All articles are open access articles distributed under the Creative Commons Attribution License, which permits unrestricted use, distribution, and reproduction in any medium, provided the original work is properly cited.

## **Editorial Board**

Saverio Affatato, Italy	Valentina Hartwig, Italy	David Moratal, Spain
Francesca Apollonio, Italy	David Hewson, UK	Angkoon Phinyomark, Canada
Hasan Ayaz, USA	Andreas H. Hielscher, USA	Vincenzo Positano, Italy
William Bertucci, France	Ernesto Iadanza, Italy	Alessandro Ramalli, Italy
Patrick Boissy, Canada	Norio Iriguchi, Japan	Alessandro Reali, Italy
Hongwei Chen, USA	Jingfeng Jiang, USA	Lei Ren, UK
Daniel H.K. Chow, Hong Kong	Zhongwei Jiang, Japan	Jose Joaquin Rieta, Spain
Gianluca Ciardelli, Italy	Rashed Karim, UK	Emanuele Rizzuto, Italy
Elena De Momi, Italy	Pasi A. Karjalainen, Finland	Sébastien Roth, France
Costantino Del Gaudio, Italy	Chandan Karmakar, Australia	Simo Saarakkala, Finland
Tiago H. Falk, Canada	John S. Katsanis, Greece	Hélder A. Santos, Finland
Mostafa Fatemi, USA	Terry K.K. Koo, USA	Emiliano Schena, Italy
Jesus Favela, Mexico	Panagiotis Kosmas, UK	Maurizio Schmid, Italy
David Dagan Feng, Australia	Michel Labrosse, Canada	Jiann-Shing Shieh, Taiwan
Joseph Finkelstein, USA	Jui-Yang Lai, Taiwan	Tiago H. Silva, Portugal
Jesus Fontecha, Spain	Xiang Li, USA	Redha Taiar, France
Jean-Luc Gennisson, France	Feng-Huei Lin, Taiwan	Jinshan Tang, USA
Shahram M. Ghanaati, Germany	Yuan-Pin Lin, Taiwan	Vinoy Thomas, USA
Luca Giancardo, USA	Maria Lindén, Sweden	Ioannis G. Tollis, Greece
Antonio Gloria, Italy	Dongfei Liu, Finland	Kazunori Uemura, Japan
Kheng-Lim Goh, Singapore	Francisco Lopez-Valdes, Spain	Uche Wejinya, USA
Pedro Gomes, Portugal	Zufu Lu, Australia	Ying Yang, UK
Carlos Gómez, Spain	Ilias Maglogiannis, Greece	Haihong Zhang, Singapore
Philippe Gorce, France	Andreas Maier, Germany	Hongbo Zhang, Finland
Sophia Z. Gu, Australia	Mehran Moazen, UK	Ping Zhou, USA
Vincenzo Guarino, Italy	Rafael Morales, Spain	Loredana Zollo, Italy

# Contents

## **Rehabilitation Robotics and Systems**

Rafael Morales , José A. Somolinos, Antonio Fernández-Caballero , and Carlo Ferraresi  
Editorial (3 pages), Article ID 5370127, Volume 2018 (2018)

## **Manipulability Inclusive Principle for Assistive Result Evaluation of Assistive Mechanism**

Wenyuan Liang  and Yong Yu  
Research Article (16 pages), Article ID 2767129, Volume 2018 (2018)

## **An Orthopaedic Robotic-Assisted Rehabilitation Method of the Forearm in Virtual Reality Physiotherapy**

Miguel A. Padilla-Castañeda , Edoardo Sotgiu, Michele Barsotti, Antonio Frisoli , Piero Orsini, Alessandro Martiradonna, Cristina Laddaga, and Massimo Bergamasco  
Research Article (20 pages), Article ID 7438609, Volume 2018 (2018)

## **Experimental Characterization of NURSE, a Device for Arm Motion Guidance**

Betsy Dayana Marcela Chaparro-Rico , Daniele Cafolla , Marco Ceccarelli , and Eduardo Castillo-Castaneda   
Research Article (15 pages), Article ID 9303282, Volume 2018 (2018)

## **Human-Inspired Reflex to Autonomously Prevent Slip of Grasped Objects Rotated with a Prosthetic Hand**

Zachary Ray and Erik D. Engeberg   
Research Article (11 pages), Article ID 2784939, Volume 2018 (2018)

## **Evaluating the Effects of Kinesthetic Biofeedback Delivered Using Reaction Wheels on Standing Balance**

Muhammad Raheel Afzal , Amre Eizad , Carlos Ernesto Palo Peña , and Jungwon Yoon   
Research Article (10 pages), Article ID 7892020, Volume 2018 (2018)

## **Assessing Effectiveness and Costs in Robot-Mediated Lower Limbs Rehabilitation: A Meta-Analysis and State of the Art**

Giorgio Carpino , Alessandra Pezzola, Michele Urbano, and Eugenio Guglielmelli  
Review Article (9 pages), Article ID 7492024, Volume 2018 (2018)

## **Dynamic Modeling and Interactive Performance of PARM: A Parallel Upper-Limb Rehabilitation Robot Using Impedance Control for Patients after Stroke**

Hui Guang , Linhong Ji , Yingying Shi, and Berno J. E. Misgeld  
Research Article (11 pages), Article ID 8647591, Volume 2018 (2018)

## **Motor Imagery-Based Brain-Computer Interface Coupled to a Robotic Hand Orthosis Aimed for Neurorehabilitation of Stroke Patients**

Jessica Cantillo-Negrete , Ruben I. Carino-Escobar, Paul Carrillo-Mora , David Elias-Vinas, and Josefina Gutierrez-Martinez  
Research Article (10 pages), Article ID 1624637, Volume 2018 (2018)

## **A Lower Limb Rehabilitation Robot in Sitting Position with a Review of Training Activities**

Trinnachoke Eiammanussakul  and Viboon Sangveraphunsiri   
Research Article (18 pages), Article ID 1927807, Volume 2018 (2018)

---

### **A Review of Robotics in Neurorehabilitation: Towards an Automated Process for Upper Limb**

E. D. Oña , R. Cano-de la Cuerda , P. Sánchez-Herrera, C. Balaguer, and A. Jardón

Review Article (19 pages), Article ID 9758939, Volume 2018 (2018)

### **Rehabilitation of Upper Limb in Children with Acquired Brain Injury: A Preliminary Comparative Study**

Elena Beretta, Ambra Cesareo, Emilia Biffi , Carolyn Schafer, Sara Galbiati, and Sandra Strazzer

Research Article (12 pages), Article ID 4208492, Volume 2018 (2018)

### **Social Robotics in Therapy of Apraxia of Speech**

José Carlos Castillo , Diego Álvarez-Fernández , Fernando Alonso-Martín, Sara Marques-Villarroya , and Miguel A. Salichs 

Research Article (11 pages), Article ID 7075290, Volume 2018 (2018)

### **Obtaining Natural Sit-to-Stand Motion with a Biomimetic Controller for Powered Knee Prostheses**

Molei Wu, Md Rejwanul Haque, and Xiangrong Shen

Research Article (6 pages), Article ID 3850351, Volume 2017 (2018)

## Editorial

# Rehabilitation Robotics and Systems

Rafael Morales ,<sup>1</sup> José A. Somolinos,<sup>2</sup> Antonio Fernández-Caballero ,<sup>1</sup> and Carlo Ferraresi<sup>3</sup>

<sup>1</sup>*Escuela de Ingenieros Industriales de Albacete, Universidad de Castilla-La Mancha, 02071 Albacete, Spain*

<sup>2</sup>*Escuela de Ingenieros Navales, Universidad Politécnica de Madrid, Madrid, Spain*

<sup>3</sup>*Politecnico di Torino, Torino, Italy*

Correspondence should be addressed to Rafael Morales; rafael.morales@uclm.es

Received 9 September 2018; Accepted 10 September 2018; Published 17 December 2018

Copyright © 2018 Rafael Morales et al. This is an open access article distributed under the Creative Commons Attribution License, which permits unrestricted use, distribution, and reproduction in any medium, provided the original work is properly cited.

## 1. Introduction

Development of novel engineering solutions that incorporate robotic systems offers huge potential, as both assistive devices and therapeutic aids, for patients with reduced motor and/or cognitive abilities. Indeed, such technologies are capable of outperforming existing therapeutic systems for improving patients' achievable functional recovery. As a result, advanced engineering solutions for rehabilitation robotics have received a considerable amount of interest in recent years, from both the academic community and the industrial sector. Emphasis is typically focused on the improvement of sensor systems, control engineering, computer vision, robotic mechanics, human-machine interfaces, modelling and simulation, in-built intelligence, and informatics, to meet the broad range of challenges posed during patient rehabilitation.

This special issue is aimed at exhibiting the latest research achievements, findings, and ideas in the field of rehabilitation robotics and systems. Researchers were invited to contribute with their original research articles, as well as review articles, that summarize the most recent developments in the field of rehabilitation robotics and systems.

Potential topics included but were not limited to the following:

- (i) Plasticity and motor-learning robotic devices
- (ii) Assistive and therapeutic robotic aids
- (iii) Upper and lower limb rehabilitation robotics
- (iv) Human-machine and brain-machine interfaces
- (v) Mobile, wearable, and prosthetic robotic devices
- (vi) Sensors, intelligent sensors, and sensor networks

- (vii) Artificial intelligence-based rehabilitation systems
- (viii) Complex, nonlinear, and intelligent systems
- (ix) Vision, awareness, perception, and signal processing
- (x) Sensor networks for precise motion control and visual servoing
- (xi) Adaptive control, robust control, and active disturbance rejection control
- (xii) Modelling and simulation for robotic rehabilitation systems
- (xiii) Networked rehabilitation robotics
- (xiv) Intelligent automation of rehabilitation robotics
- (xv) Informational monitoring, control, and data fusion for rehabilitation systems

## 2. The Papers

A total of 22 papers were submitted to this special issue. After peer review, finally 13 of them were accepted and published, covering a wide range of the topics proposed in the call for papers.

Three interesting papers are based on reviews of literature papers on rehabilitation robotics and systems. Firstly, a work by G. Carpino et al. includes a meta-analysis of robot-mediated lower limbs rehabilitation for stroke-affected patients; it is aimed at evaluating the effectiveness of the robotic approach using wearable robots or operational machines with respect to the conventional approach. The primary assessed outcome is the patient's ability to regain walking independence, whereas the secondary

outcome is the average walking speed. Also, E. D. Oña et al. conduct a systematic literature review to identify the contribution of robotics to upper limb neurorehabilitation, highlighting its relationship with the rehabilitation cycle, and to clarify the prospective research directions in the development of more autonomous rehabilitation processes. In addition, a series of technical requirements that should be considered when designing and implementing autonomous robotic systems for rehabilitation are presented and discussed. Lastly, T. Eiammanussakul and V. Sangveraphunsiri review the training activities that were realized by rehabilitation robots in the literature to offer insights into developing a novel robot suitable for stroke rehabilitation. The control system of the lower limb rehabilitation robot in sitting position of the authors' previous work is discussed in detail to demonstrate the behavior of the robot while training a subject. A preliminary experiment is conducted on a healthy subject to show that the robot can perform active assistive exercises with various training activities and assist the subject to complete the training with a desired level of assistance.

Next, other six papers are more directed towards the experimental evaluation of rehabilitation mechanics. Thus, W. Liang and Y. Yu propose the so-called manipulability inclusive principle (MIP) to evaluate the assistive mechanism's assistive feasibility and assistive effect through the manipulability comparison between the assisted limb and slave-active-assistive mechanism. The optimization based on MIP can make the assistive mechanism realize better kinematical performance and assistance. Another paper by B. D. M. Chaparro-Rico et al. presents an experimental characterization of NURSE, a device for arm motion guidance. The laboratory setup and testing modes are presented. Two exercises for the upper limb are used to test the NURSE behavior. Trajectories and linear accelerations are tested when the device performs the exercises with and without load. Z. Ray and E. D. Engeberg face the problem of autonomously preventing grasped objects from slipping out of prosthetic hands for limb-absent people. Their paper explores a human-inspired grasp reflex controller for prosthetic hands to prevent slip of objects when they are rotated. This human-inspired grasped object slip prevention controller is evaluated with six different objects in benchtop tests and by 12 able-bodied subjects during realistic tasks of daily life. Moreover, in another article, M. Wu, M. R. Haque, and X. Shen present a new sit-to-stand (STS) control approach for powered lower limb prostheses, which can regulate the power delivery of the prosthetic knee joint to obtain natural STS motion like that displayed by healthy subjects. Mimicking the dynamic behavior of the knee in both phases of the STS, a unified control structure provides the desired control actions by combining an impedance function with a time-based ramp-up function. In addition, H. Guang et al. present an interactive upper limb rehabilitation robot with a parallel mechanism and an isometric screen embedded in the platform to display trajectories. In the dynamic modeling for impedance control, the effects of friction and inertia are reduced by introducing the principle of virtual work and derivative of

the Jacobian matrix. To achieve the assist-as-needed impedance control for arbitrary trajectories, the strategy based on orthogonal deviations is proposed. Simulations and experiments were performed to validate the dynamic modeling and impedance control. Lastly, in a study by M. R. Afzal et al., a wearable system based on the reaction wheel is used to deliver light-touch-based balance biofeedback on the subject's back. The system can sense torso tilt and, using reaction wheels, generates light-touch. A group of 7 healthy young individuals performed balance tasks under 12 trial combinations based on two conditions each of standing stance and surface types and three of biofeedback device status.

A last group of four papers is directly focused demonstrating implementations for rehabilitation. A paper by J. Cantillo-Negrete et al. presents the implementation of a brain-computer interface system, coupled to a robotic hand orthosis, driven by hand motor imagery of healthy subjects and the paralyzed hand of stroke patients. A novel processing stage is designed using a bank of temporal filters, the common spatial patterns algorithm for feature extraction, and particle swarm optimization for feature selection. The system's performance shows that it has potential to be used for hand rehabilitation of stroke patients. The aim of an article by J. C. Castillo et al. is in the line of robotic therapies in which a robot can perform partially or autonomously a therapy session, endowing a social robot with the ability of assisting therapists in apraxia of speech rehabilitation exercises. The authors integrate computer vision and machine-learning techniques to detect the mouth pose of the user, and on top of that, our social robot performs autonomously the different steps of the therapy using multimodal interaction. Then, M. A. Padilla-Castañeda et al. introduce the development and evaluation of a robotic-assisted rehabilitation system as a new methodology of assisted physiotherapy in orthopedics. The proposal consists of an enhanced end-effector haptic interface mounted in a passive mechanism for allowing patients to perform upper limb exercising and integrates virtual reality games conceived explicitly for assisting the treatment of the forearm after injuries at the wrist or elbow joints. The authors design specific game scenarios enriched by proprioceptive and haptic force feedback in three training modes: passive, active, and assisted exercising. Finally, in a study by E. Beretta et al., a group of 18 children and adolescents with hemiplegia, an impairment due to acquired brain injuries, was enrolled and underwent intensive rehabilitation treatment including flank physical therapy and constrained-induced movement therapy or Armeo®Spring therapy. The effects of the treatments are assessed using clinical functional scales and upper limb kinematic analysis during horizontal and vertical motor tasks. The results of this study may be of help to define the best rehabilitation treatment for each patient, depending on the goal, and may thus support clinical decision.

## Conflicts of Interest

The editors declare that they have no conflicts of interest.

## Acknowledgments

This special issue would not be possible without the contributions of the authors who submitted their valuable papers. We would like to thank all reviewers and editorial team of *Journal of Healthcare Engineering* for their great work. Lastly, we acknowledge the financial support from Spanish Ministerio de Ciencia, Innovación y Universidades and Agencia Estatal de Investigación (AEI)/European Regional Development Fund (FEDER, EU) under DPI2016-80894-R grant.

*Rafael Morales  
José A. Somolinos  
Antonio Fernández-Caballero  
Carlo Ferraresi*

## Research Article

# Manipulability Inclusive Principle for Assistive Result Evaluation of Assistive Mechanism

Wenyuan Liang  <sup>1,2</sup> and Yong Yu<sup>3</sup>

<sup>1</sup>College of Engineering, Peking University, Beijing, China

<sup>2</sup>National Research Center for Rehabilitation Technical Aids, Beijing, China

<sup>3</sup>Graduate School of Science and Engineering, Kagoshima University, Kagoshima, Japan

Correspondence should be addressed to Wenyuan Liang; lwy123@hotmail.com

Received 3 March 2018; Accepted 26 August 2018; Published 24 September 2018

Academic Editor: Rafael Morales

Copyright © 2018 Wenyuan Liang and Yong Yu. This is an open access article distributed under the Creative Commons Attribution License, which permits unrestricted use, distribution, and reproduction in any medium, provided the original work is properly cited.

In this paper, from the aspect of kinematics, we reveal the physical significance of assistance for the assistive mechanism. Then, Manipulability Inclusive Principle (MIP) is proposed to evaluate assistive mechanism's assistive feasibility and assistive effect through the manipulability comparison between the assisted limb and slave-active-assistive mechanism. The optimization based on MIP can make the assistive mechanism realize better kinematical performance and assistance. The design and optimization of the assistive mechanism should keep the assistive mechanism from interfering with human's movements in the expected workspace. More importantly, it should also keep the assistive mechanism not only have better kinematical performance on symmetry, isotropy, etc. but also be able to provide better assistance for human. The application on the human lower-limb straight-walking power-assisting mechanism shows that the design and optimization based on MIP can find out the assistive mechanism which satisfies assistive feasibility and realizes better assistive effect in the whole expected workspace.

## 1. Introduction

For the purpose of helping the elders and disabled, a power-assisting robot [1, 2] has been devised and defined as an active mechanical device that fits closely for the operator's body and works in concert with the operator's movements. In the last century, late 60s and early 70s, the Hardiman project [3], a large two-armed, bipedal exoskeletal system, operated at GE was controlled by using a master-slave system. The Belgrade exoskeleton [4] was a human-sized lower-extremity robot designed to help the paraplegics realize rehabilitation. The Lokomat system [5] is a walker system for standing assistance [6].

In recent years, there are more assistive devices appeared. The wearable power-assisting system also becomes an attractive method of power assisting since it can be adapted to a wide range of applications. For example, Sarcos Exoskeleton [7], Wearable Power Suit [8], and Hybrid Assistive Limb (HAL) [9] are full-body assistive robots;

MGA Exoskeleton [10], SUEFUL-6 [11], and CADEN-7 [12] focus on upper-limb assistance; Berkeley Lower Extremity Exoskeleton (BLEEX) [13], MIT Exoskeleton [14], Robo-Knee [15], Human Universal Load Carrier (HULC) [16], Wearable Walking Helper-KH [17], and Bodyweight Support System [18] are the assistive robots which are used for lower-limb assistance. On the power-assisting robot, we also have made some research studies, such as PAWL [19, 20] which is designed for human lower-limb assistance, upper-limb assistive mechanism [21], and a parallel assisting mechanism for hip joint 3-DOF power assisting [22].

In this paper, we focus on the wearable assistive mechanism which belongs to the following type: the human is acting actively, and simultaneously, the assistive robot works actively to provide assistance with matching human's moving intention, where [7–22] all belong to this type. When this kind of assistive mechanism is mounted to the human body, the assistive mechanism and human are considered as a parallel mechanism, where the active joints

of this parallel mechanism are divided into two types: master-active joints and slave-active joints. For this parallel mechanism, it has several kinds of problems, such as selecting slave-active joints, confirming types of joints, configurations and sizes, motion interference, sensors, and control. All these problems will have the influence on the final assistance, including assistive feasibility and assistive effect.

In order to realize better assistance, these problems should be partly considered during the assistive mechanism design and optimization, where the rest is determined by the sensors and control. Generally, for the mechanism design and optimization [23, 24], researchers have considered it from these aspects: workspace, symmetry, isotropy, and so on. For this parallel mechanism which consists of the assistive mechanism and human, by considering that the assistive mechanism's own special characteristic is that the assistive mechanism and human cooperate together to realize assistance; the design and optimization should keep the assistive mechanism from interfering with human's movements in the expected workspace. And especially, the design and optimization should also keep the assistive mechanism not only have better kinematical performance on symmetry, isotropy etc., but also be able to provide better assistance for human. In recent research studies, the research in [30] uses the Jacobian matrices to analyze the assistive isotropy and assistive efficiency; researchers in [31] use the global performance index to represent the dexterity, and the manipulability ellipsoids for the 4-DOF assistive robot is obtained in [32]. However, the research studies shown in [30–32] have not considered the influence of the motions of the human limb. For example, the problem of assistive feasibility should compare the manipulability between the assistive mechanism and the human limb. Additionally, compared to [30–32], this paper will show more systemic research on optimization problem including assistive feasibility and assistive efficiency.

In this paper, from the aspect of kinematics, we propose Manipulability Inclusive Principle (MIP), which is derived from the physical significance of assistance and based on robotics manipulability theory [25–27], to consider the problems during assistive mechanism's design and optimization. The prototype of MIP first appeared in our pre-study [22], used on hip joint 3-DOF assistive mechanism's design and optimization. The MIP is related to actuators' maximum velocities, assistive mechanism's fixed and connected locations, mechanical structure, configuration, types of joints, sizes, and so on. The optimization algorithm based on MIP is helpful for designing and optimizing the assistive mechanism in terms of kinematics, finding out the structure which can realize better kinematical performance and assistance. In theory, the MIP is also applicable for many kinds of power-assisting robots which belong to the type where human is acting actively, and the assistive mechanism is matching human's moving intention.

The MIP has been partially discussed in the pre-work [22, 28, 29], where the content in this paper is the supplement for the pre-work. For the sake of discussing, an example of lower-limb assistive robot is used in this paper.

This paper is organized as follows: some definitions and the problems are shown in Section 2. Section 3 presents the definition of MIP. In Section 4, with some examples and analysis, the MIP is proved to be able to evaluate lower-limb assistive mechanism's design and optimization. Conclusions are presented in Section 5.

## 2. Slave-Active-Assistive Mechanism

As well known, for the human lower limb, hip joint has 3 DOFs, and the knee joint is a 1-DOF joint. Similar to the lower-limb straight-walking assistive robots in [16, 17], in this paper, the lower-limb straight-walking assistive mechanism also only assists hip joint's and knee joint's flexion/extension motions, where the assistive mechanism includes a revolute joint and a prismatic joint as shown in Figure 1. This assistive mechanism is fixed to the human waist and connected to the calf with a revolute joint. For example, research studies in [16, 17] place the assistive robots just as shown in Figure 1(a), where the assistive mechanism is in the behind of the human body; Figure 1(b) shows the model where the assistive mechanism is in front of the human body.

For the sake of discussing and understanding, before discussing the problems for this lower-limb assistive mechanism, first of all, we propose some important and useful definitions for power assisting as follows.

**2.1. Master-Active Joint and Slave-Active Joint.** When the assistive mechanism is mounted to the human body, the assistive mechanism and human can be considered as a parallel mechanism. In general, the joints of parallel mechanism are divided into two types: active joints and passive joints, where the joint with driven source is defined as the active joint and the joint without driven source is defined as the passive joint. If too many joints are considered as active joints, it will lead to an interference between these active joints, and if too few joints are considered as active joints, this parallel mechanism cannot be driven well. Hence for a parallel mechanism, the number of active joints should be equal to the number of the DOFs of the parallel mechanism.

However, during assisting, both human's joints and the actuators installed on the assistive mechanism are with the driven source, providing power on human motions, where the assistance cannot be realized without these actuators. Hence, in this parallel mechanism which consists of the assistive mechanism and human, there is a problem that the number of active joints is not equal to the number of the DOFs of the parallel mechanism, where it seems that this problem will lead to interference between the human and assistive mechanism. This problem can be considered as follows:

For a power-assisting robot, the human is at the master level and generating the moving intention, and the assistive mechanism is at the slave level to match human's moving intention, where the assistive mechanism itself cannot generate moving intention. Therefore, for the active joints in

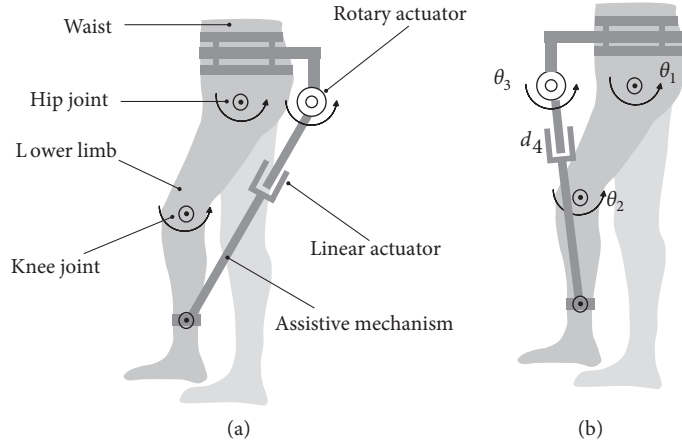


FIGURE 1: Lower-limb assistive mechanism for straight-walking assistance.

this parallel mechanism, human's joints are acting actively and generating moving intention; therefore, human's joints are defined as master-active joints; the assistive mechanism is matching human's moving intention and then working actively to provide necessary assistance; therefore, assistive mechanism's joints with driven sources are defined as slave-active joints.

The slave-active joints drive the parallel mechanism to match human's movements; therefore, the number of slave-active joints should be equal to the number of the DOFs of this parallel mechanism. In addition, when selecting different assistive mechanisms' joints as slave-active joints, the assistive results will be different.

In this paper, the parallel mechanism, which consists of the lower limb and assistive mechanism, has 2 DOFs just the same as the lower limb; therefore, it is necessary to use 2 slave-active joints to assist the lower limb. By considering the actuators' installed locations and weight, the revolute joint (with rotary actuator) and prismatic joint (with linear actuator) are selected as slave-active joints just as shown in Figure 1. The left revolute joint connecting the assistive mechanism and lower limb is passive joint.

**2.2. Assisted Limb and Slave-Active-Assistive Mechanism.** For power assisting, the active joints are divided into master-active joints and slave-active joints. In other words, human and master-active joints are at the master level, and assistive mechanism and slave-active joints are at the slave level. For these two levels, we can have another two definitions.

The assisted limb represents the part of the human body which is to be assisted and only driven by the master-active joints. In this paper, the assisted limb is the human lower limb, and the master-active joints are composed of the hip joint and the knee joint.

Slave-Active-Assistive Mechanism (SAAM), a parallel mechanism consisting of the assistive mechanism and assisted limb, is only driven by the slave-active joints, where in this parallel mechanism, master-active joints are also considered as passive joints. The reason for proposing the definition of SAAM is that since the assistive mechanism is

finally mounted to the assisted limb, discussing assistive mechanism's assistive performance should combine with the assisted limb.

The discussions and comparisons in this paper are based on these two definitions: the assisted limb representing lower limb's performance and SAAM representing assistive mechanism's performance. Actually, the assisted limb and SAAM are acting simultaneously as a whole during assisting. By comparing their kinematical performances, assistive mechanism's assistive results can be judged in terms of kinematics.

**2.3. Problems: Assistive Feasibility and Assistive Effect.** Combined with the definitions above, the problems for lower-limb assistive mechanism's design and optimization are discussed as follows. As shown in Figure 1, the assistive mechanism is mounted to the assisted limb with different locations, and the assistive results may be different. Besides, the parameters such as actuators' maximum velocities, mechanical structure, types of joints and actuators, and sizes would also have the influence on the assistive results. In general, with different parameters, assistive mechanism's assistive results are different.

Therefore, the purpose in this paper is optimizing lower-limb assistive mechanism's parameters to realize better assistive results, where in this paper, the discussions focus on the parameters of actuators' maximum velocities and assistive mechanism's fixed location.

Realizing better assistive results includes a double meaning: first, the assistive mechanism must satisfy assistive feasibility; then further, it should realize better assistive effect. Assistive feasibility means that the assistive mechanism is able to provide necessary assistance on the expected motions, where in this paper, the expected motions are lower limb's straight-walking motions. Assistive effect is used to evaluate the final assistance, where the assistive effect includes three aspects such as assistive efficiency, assistive ability, and assistive isotropy.

In order to realize better assistive results, during lower-limb assistive mechanism's design and optimization, we

should consider these two problems: assistive feasibility and assistive effect, where these two problems also exist in many other assistive mechanisms.

### 2.3.1. Problem of Assistive Feasibility.

On the problem of assistive feasibility, it does have three concerns.

First, the corresponding type of SAAM end-effector's DOF should be the same as the lower limb. Second, SAAM end-effector's DOF space and lower-limb end-effector's DOF space should be in the same space. Avoiding interfering lower limb's movements, these two concerns ensure that when the slave-active joints are without actuators, the assistive mechanism can move with lower limb's movements.

Third, the assistive mechanism, where the slave-active joints are driven by the actuators, should be able to catch the lower limb's movements. As said before, during the assisting process, the assistive mechanism is acting actively to match lower limb's moving intention. If the assistive mechanism cannot catch lower limb's movements, the assistive mechanism still cannot assist even if their end-effectors' DOF spaces are in the same space.

Thus, satisfying these three concerns ensures that the assistive mechanism is able to shadow lower limb's movements and provide necessary assistance for the lower limb.

### 2.3.2. Problem of Assistive Effect.

Another problem is the assistive effect. When the assistive mechanism satisfies assistive feasibility, SAAM end-effector's and lower-limb end-effector's DOF spaces are in the same space. However, since the DOF direction and magnitude may be different, the assistive effect may be different.

In order to realize better assistive effect, it is necessary to discuss its included three aspects further. Assistive ability means the assisting power which the assistive mechanism owns. Assistive efficiency shows that how much assistive mechanism's assisting power can apply on assisted limb's motions. And the similarity of assistive ability on each DOF is considered as assistive isotropy.

Assistive mechanism's assistive feasibility and assistive effect are related to the parameters, such as actuators' maximum velocities, assistive mechanism's fixed location, and so on. Therefore, proposing an evaluation criterion which can consider the assistive feasibility and assistive effect is of great significance. Then the evaluation criterion can be used for assistive mechanism's design and optimization.

In this paper, Manipulability Inclusive Principle (MIP) is proposed to consider the problems of assistive feasibility and assistive effect. When SAAM's manipulability ellipsoid and lower limb's manipulability ellipsoid are in the same space, their end-effector's DOF spaces are also in the same space. Then, while SAAM's manipulability ellipsoid can cover lower limb's manipulability ellipsoid, the assistive mechanism satisfies assistive feasibility to provide assistance on all the DOFs. The assistive effect is considered from the differences of principle axes' directions and volume and axes' magnitude between SAAM's and lower limb's manipulability ellipsoids.

Better assistance means the assistive mechanism can use less power to realize more assistance. In order to realize better assistance in the whole expected workspace, optimization based on MIP is helpful for optimizing assistive mechanism in terms of kinematics.

## 3. Manipulability Inclusive Principle

In order to consider the problems of assistive feasibility and assistive effect, from the aspect of kinematics, Manipulability Inclusive Principle (MIP) is proposed to evaluate lower-limb assistive mechanism's design and optimization to realize better assistance. In the following, we will show the definition of the MIP evaluation criterion which is derived from the physical significance of assistance.

**3.1. Physical Significance of Assistance for Assistive Mechanism.** Let us see an example, where the lower limb and assistive mechanism in Figure 1(b) is simply represented as an RR-R-PR parallel mechanism ABCD shown in Figure 2. In this parallel mechanism, lower limb ABC and assistive mechanism DC are connected at C; assistive mechanism's fixed location is D, and connected location is C. As the discussion for the definitions of master-active joints and slave-active joints before, here master-active joints A and B separately represent hip joint and knee joint; rotary actuator and linear actuator are adopted as the two slave-active joints' driven sources; the left revolute joint C is a passive joint.

Figure 2 shows that the lower limb and assistive mechanism are at three different postures, where on the distance, there are  $\overline{DC} = \overline{DC}'$  and  $\overline{AC} = \overline{AC}''$ . In this example, we focus on the assistance on the directions which are vertical to the direction from assistive mechanism's fixed location D to end-effector C, such as  $\overrightarrow{EF}$ ,  $\overrightarrow{E'F'}$ ,  $\overrightarrow{E''F''}$ , and so on. Assume that each joint for the lower limb and assistive mechanism separately has its own maximum velocity; at posture (1), when lower limb's end-effector C moves on direction  $\overrightarrow{EF}$  at maximum velocity, the slave-active joint D also just reaches its maximum velocity to make the assistive mechanism shadow lower limb's movement to provide certain assistance on this direction.

Compared to the results on the direction  $\overrightarrow{EF}$  of posture (1), intuitively at posture (2), lower-limb end-effector's maximum velocity decreases on direction  $\overrightarrow{E'F'}$ , so that slave-active joint D is able to use lower velocity to shadow lower limb's movement in this direction, where in this case assistive mechanism also can assist the lower limb much better on this direction; at posture (3), the distance between D and  $C''$  becomes much shorter, leading that even slave-active joint D uses its maximum velocity, assistive mechanism still cannot shadow and assist the lower limb on direction  $\overrightarrow{E''F''}$ .

The above is an intuitive description; however, it reveals the physical significance of assistance described as following. After the assistive mechanism is mounted to the assisted limb, when lower limb's end-effector reaches maximum velocity on a certain direction, in this case, that slave-active joints' velocities do not exceed their own maximum

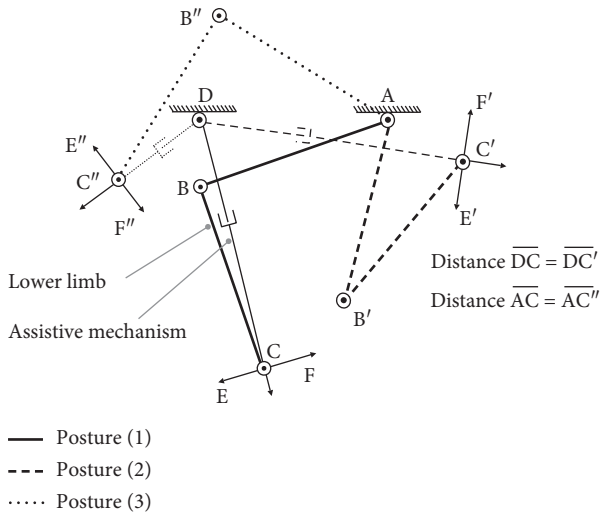


FIGURE 2: Lower limb with assistive mechanism at different postures.

velocities ensures the assistive mechanism is able to shadow the lower limb's movement to assist lower limb in this direction. And further, that slave-active joints can use lower velocities to shadow lower limb's movement means assistive mechanism can provide better assistance in this direction.

In other words, combined with the definitions of the assisted limb and SAAM, the physical significance of assistance also can be described as following. While SAAM end-effector's maximum velocity is not lower than assisted-limb end-effector's velocity on a certain direction, it means during the assisted limb's movements even assisted limb's end-effector reaches its maximum velocity, and slave-active joints' velocities are still lower than or equal to their own maximum velocities. Then, in this case, it ensures the assistive mechanism is able to shadow assisted limb's movement to assist on this direction. Therefore, we can compare assisted limb end-effector's and SAAM end-effector's maximum velocities to evaluate the assistive result in a certain direction.

In order to evaluate the assistive results on all the directions, comparing their end-effectors' maximum velocities one direction by one direction is a feasible method. For example, in this example, through comparing, at posture (2), the assistive mechanism can shadow lower limb's movements on all the directions; at posture (3), the assistive mechanism can shadow lower limb's movements on part of the whole directions.

However, the aforementioned method will incur a huge cost and will be ineffective to be applicable in practices, whereas another method based on the manipulability concept is adopted to consider evaluating assistive results on all the directions. Manipulability is a useful means of quantifying end-effector's velocity on each DOF, where it includes two ideas: manipulability direction and manipulability magnitude of each DOF. As a mathematical tool, velocity manipulability ellipsoid is used to describe end-effector's velocities on all the directions: along the manipulability direction of the major axis of the manipulability ellipsoid, the end-effector can move at large velocity, while

along the manipulability direction of the minor axis, small end-effector velocities are obtained. In this paper, the velocity manipulability ellipsoid is simply called as manipulability ellipsoid.

Therefore, this adopted method, MIP, is based on comparing assisted limb's manipulability and SAAM's manipulability to consider the two problems of assistive feasibility and assistive effect, whereas in this paper, the manipulability only represents end-effector's manipulability. Then, the definition of MIP can be derived from the physical significance of assistance as follows.

**3.2. Definition of Manipulability Inclusive Principle.** Based on the manipulability concept, during the design and optimization for the assistive mechanism which belongs to the type where human is acting actively and simultaneously the assistive mechanism is matching human's moving intention just as shown in Section 1, the Manipulability Inclusive Principle (MIP) evaluation criterion is proposed to evaluate the assistive mechanism's assistive feasibility and assistive effect in terms of kinematics. Assuming that SAAM and the assisted limb are both at the same posture, for the same end-effector, the definition of MIP can be set out as follows:

- (i) On the assistive feasibility, if assisted limb's manipulability ellipsoid is whole inclusive by SAAM's manipulability ellipsoid, the assistive mechanism can shadow the assisted limb's movements well to satisfy assistive feasibility and be used to provide power assisting on all the DOFs.
- (ii) On the assistive effect, if the corresponding manipulability directions of SAAM align with assisted limb's better, the assistive efficiency is higher; if the manipulability magnitude of SAAM is larger, the assistive mechanism owns more assistive ability; if the manipulability magnitude of SAAM on each DOF is closer, the assistive isotropy is better.

Assisting all the DOFs also means assisting all the directions, and manipulability directions represent the directions of the manipulability ellipsoid's principle axes.

As for the definition of MIP, from the macroscopic perspective, three inclusive cases can be derived from the assistive feasibility: whole inclusive case, part inclusive case, and no inclusive case. The whole inclusive case ensures that the assistive mechanism satisfies assistive feasibility to shadow assisted limb's movements well to assist all the DOFs, while the part inclusive case or no inclusive case means the assistive mechanism cannot assist assisted limb's movements in some directions or at all.

From the microscopic perspective, the inclusive results will have the influence on the assistive effect. The assisted limb's manipulability directions represent assisted limb's most needed assisted directions. The SAAM's manipulability directions are the directions where SAAM can provide its largest assistance. Therefore, the SAAM's manipulability directions align with assisted limb's better, the assistive efficiency is higher. In practice, as their directions cannot align completely, the other two factors, assistive ability and

assistive isotropy, are needed to be considered. Too small assistive ability will lead to that SAAM's manipulability ellipsoid cannot cover assisted limb's, while too large assistive ability means a waste. Hence, during design and optimization for the assistive mechanism, we should select suitable actuators for the assistive mechanism to make the assistive mechanism satisfy assistive feasibility. With the limited assistive ability, we should keep the assistive mechanism have close assistive ability in each direction or DOF. Then, this assistive mechanism can realize better assistive effect.

From assisted limb's manipulability and SAAM's manipulability, the following can be obtained: Manipulability Ellipsoid of Assisted Limb (ME-al) and Manipulability Directions of Assisted Limb (MD-al) where in this case, the assisted limb is without assistive mechanism, the Manipulability Ellipsoid of SAAM (ME-saam) and Manipulability Directions of SAAM (MD-saam) where the SAAM is only driven by the slave-active joints. Then, EV-al and EV-saam separately represent end-effector's velocity of assisted limb and end-effector's velocity of SAAM, respectively.

#### 4. MIP Studies with the Example of Lower-Limb Assistance

With Manipulability Inclusive Principle (MIP), it is necessary to validate that MIP is applicable on the lower-limb assistive mechanism, and then, the design and optimization for the lower-limb assistive mechanism can be operated with MIP. Therefore, it is needed to validate that MIP is applicable to evaluate assistive feasibility for lower-limb assistive mechanism and then, analyze and discuss the factors which will have the influence on assistive feasibility and assistive effect.

In this section, the validation, analysis, and discussion all are based on the manipulability. Manipulability can be obtained through singular value decomposition of the kinematical Jacobian. Associated with the normalized kinematical Jacobian  $J$ , there is a mathematical form:

$$J = U \cdot S \cdot V. \quad (1)$$

Consequently, the above equation can generate a velocity manipulability ellipsoid which represents end-effector's moving velocities on all the directions. The principal axes of the ellipsoid, representing the manipulability directions of all the DOFs, are aligned with the matrix  $U$ , and the length of each principal axis which is equal to manipulability magnitude of each DOF is diagonal with matrix  $S$ . With the computing results, we can draw manipulability ellipsoids locating their centers at the locations of the end-effector in the workspace so that the globe characteristics of the end-effector's velocities can be represented in the whole.

In this section, the Jacobian and manipulability for assisted limb and SAAM are built at first. With the results generated from the Jacobian and manipulability, the validation on evaluating assistive feasibility for MIP is operated with some examples. Then, through the analysis between ME-al and ME-saam, an inclusive judgement algorithm is

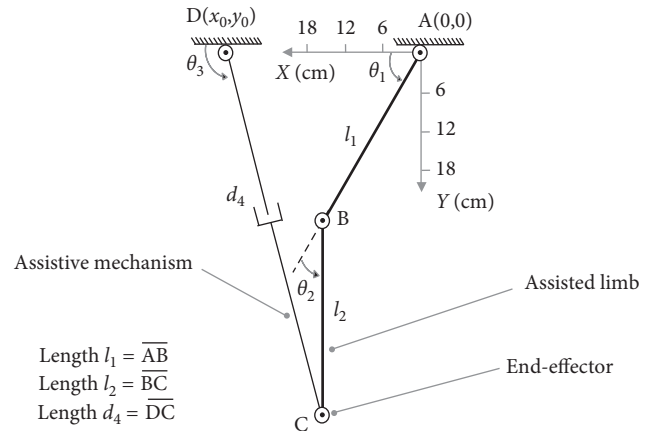


FIGURE 3: RR-R-PR mechanical configuration.

proposed to evaluate the inclusive cases. By learning about all kinds of inclusive cases, we can find out which inclusive case is our need. At last with the analysis and discussion on the influence factors of MIP, we will find the ways to improve assistance.

**4.1. Jacobian and Manipulability for Lower Limb and SAAM.** As shown in Figure 3, the reference coordinate A – XY is located at the hip joint. In this parallel mechanism ABCD,  $l_1$  represents the length between hip joint A and knee joint B, and  $l_2$  is the length from knee joint B to assistive mechanism's connected location C;  $\theta_1$  and  $\theta_2$  are the angular variables for the hip joint and knee joint on the motions of flexion/extension; in this assistive mechanism,  $\theta_3$  represents the angular variable for revolute joint C, and  $d_4$  represents the variable of the length of the prismatic joint. In this paper, the unit of the length is (cm), and the unit for the angular variable is (rad); hence, the unit of linear velocity is (cm/s), and the unit of angular velocity is (rad/s). Therefore, the Jacobian for the lower limb and SAAM can be built as follows.

For lower limb, master-active joints A and B can determine the position of end-effector C, where  $f_1$  represents its X-position component, and  $f_2$  is the X-position component. The expressions for  $f_1$  and  $f_2$  are as follows:

$$f_1 = l_1 \cos \theta_1 + l_2 \cos(\theta_1 + \theta_2), \quad (2)$$

$$f_2 = l_1 \sin \theta_1 + l_2 \sin(\theta_1 + \theta_2). \quad (3)$$

For the assistive mechanism end-effector's position C,  $f_3$  and  $f_4$  separately represents its X-position component and Y-position component,

$$f_3 = x_0 + d_4 \cos \theta_3, \quad (4)$$

$$f_4 = y_0 + d_4 \sin \theta_3, \quad (5)$$

where  $(x_0, y_0)$  represents assistive mechanism's fixed location D. While the assistive mechanism is mounted to the lower limb, there are  $x_C = f_1 = f_3$  and  $y_C = f_2 = f_4$ , where  $(x_C, y_C)$  represents the position of C.

For the lower limb which is driven by the master-active joints A and B, combined with Equations (2) and (3), the Jacobian is

$$[\dot{x}_C \ \dot{y}_C]^T = J_{01} \cdot [\dot{\theta}_1 \ \dot{\theta}_2]^T, \quad (6)$$

where  $[*]^T$  is the transpose of matrix  $[*]$ . In Equation (6),  $J_{01}$  is

$$J_{01} = \begin{bmatrix} g_{11} & g_{12} \\ g_{21} & g_{22} \end{bmatrix}, \quad (7)$$

where  $g_{11} = \partial f_1 / \partial \theta_1$ ,  $g_{12} = \partial f_1 / \partial \theta_2$ ,  $g_{21} = \partial f_2 / \partial \theta_1$ , and  $g_{22} = \partial f_2 / \partial \theta_2$ .

The Jacobian of SAAM is about the velocity relation between end-effector C and slave-active joints in the parallel mechanism ABCD; therefore, the Jacobian of SAAM has the following mathematical form:

$$[\dot{x}_C \ \dot{y}_C]^T = J_{02} \cdot [\dot{\theta}_3 \ \dot{d}_4]^T. \quad (8)$$

Then, it is needed to find out the expression of  $J_{02}$ . As C connects the lower limb and assistive mechanism, the velocity of SAAM's end-effector C is related to the lower limb and assistive mechanism. Lower limb's Jacobian is expressed as Equation (6), and combined with Equations (4) and (5), the Jacobian of the assistive mechanism is

$$\begin{aligned} [\dot{x}_C \ \dot{y}_C]^T &= J_{03} \cdot [\dot{\theta}_3 \ \dot{d}_4]^T, \\ J_{03} &= \begin{bmatrix} g_{31} & g_{32} \\ g_{41} & g_{42} \end{bmatrix}, \end{aligned} \quad (9)$$

where  $g_{31} = \partial f_3 / \partial \theta_3$ ,  $g_{32} = \partial f_3 / \partial \theta_4$ ,  $g_{41} = \partial f_4 / \partial \theta_3$ , and  $g_{42} = \partial f_4 / \partial \theta_4$ . When the assistive mechanism is mounted to the lower limb, there is

$$J_{01} \cdot [\dot{\theta}_1 \ \dot{\theta}_2]^T = J_{03} \cdot [\dot{\theta}_3 \ \dot{d}_4]^T. \quad (10)$$

Therefore, the SAAM which is only driven by the slave-active joints, its Jacobian is

$$\begin{aligned} [\dot{x}_C \ \dot{y}_C]^T &= \frac{\left( J_{01} \cdot [\dot{\theta}_1 \ \dot{\theta}_2]^T + J_{03} \cdot [\dot{\theta}_3 \ \dot{d}_4]^T \right)}{2} \\ &= \frac{\left( J_{01} \cdot J_{01}^+ \cdot J_{03} + J_{03} \right)}{2 \cdot [\dot{\theta}_3 \ \dot{d}_4]^T}, \end{aligned} \quad (11)$$

where  $[*]^+$  represents the pseudo-inverse of  $[*]$ ,  $J_{02} = (J_{01} \cdot J_{01}^+ \cdot J_{03} + J_{03})/2$ . When assisted limb is not at the singular postures, the Jacobian for SAAM becomes

$$\begin{aligned} [\dot{x}_C \ \dot{y}_C]^T &= \frac{\left( J_{01} \cdot J_{01}^{-1} \cdot J_{03} [\dot{\theta}_3 \ \dot{d}_4]^T + J_{03} \cdot [\dot{\theta}_3 \ \dot{d}_4]^T \right)}{2} \\ &= J_{03} \cdot [\dot{\theta}_3 \ \dot{d}_4]^T, \end{aligned} \quad (12)$$

where  $[*]^{-1}$  represents the inverse matrix of  $[*]$ ,  $J_{02} = J_{03}$ . In this case, the Jacobian for SAAM and assistive mechanism are the same.

Then for assisted limb's and SAAM's separate Jacobian shown in Equations (6) and (8), the inputs are needed to be normalized [25] with their maximum input velocities, and the outputs are also needed to be normalized by limiting them with the maximum expected output velocities, where usually the maximum expected output velocities are assisted limb end-effector's maximum moving velocities. After normalization, there are

$$\left[ \frac{\dot{x}_C}{(\dot{x}_C)_{\max}} \ \frac{\dot{y}_C}{(\dot{y}_C)_{\max}} \right]^T = A_{03}^{-1} \cdot J_{01} \cdot A_{01} \cdot \left[ \frac{\dot{\theta}_1}{(\dot{\theta}_1)_{\max}} \ \frac{\dot{\theta}_2}{(\dot{\theta}_2)_{\max}} \right]^T, \quad (13)$$

$$\left[ \frac{\dot{x}_C}{(\dot{x}_C)_{\max}} \ \frac{\dot{y}_C}{(\dot{y}_C)_{\max}} \right]^T = A_{03}^{-1} \cdot J_{02} \cdot A_{02} \cdot \left[ \frac{\dot{\theta}_3}{(\dot{\theta}_3)_{\max}} \ \frac{\dot{d}_4}{(\dot{d}_4)_{\max}} \right]^T, \quad (14)$$

where  $(\dot{\theta}_1)_{\max}$ ,  $(\dot{\theta}_2)_{\max}$ ,  $(\dot{\theta}_3)_{\max}$ , and  $(\dot{d}_4)_{\max}$  are the maximum velocities of master-active joints and slave-active joints, and  $(\dot{x}_C)_{\max}$ ,  $(\dot{y}_C)_{\max}$  are end-effector's maximum expected output velocities. Matrices  $A_{01}$ ,  $A_{02}$ , and  $A_{03}$  are defined as

$$\begin{aligned} A_{01} &= \text{diag}((\dot{\theta}_1)_{\max}, (\dot{\theta}_2)_{\max}), \\ A_{02} &= \text{diag}((\dot{\theta}_3)_{\max}, (\dot{d}_4)_{\max}), \\ A_{03} &= \text{diag}((\dot{x}_C)_{\max}, (\dot{y}_C)_{\max}), \end{aligned} \quad (15)$$

where  $\text{diag}(\cdot)$  represents a diagonal matrix. In Equations (13) and (14), the value of the inputs for lower limb and SAAM is between 0 and 1, and the outputs are also the same.

According to Equation (1), through the singular value decomposition [25] of the normalized matrices  $J'_{01}$  and  $J'_{02}$ , which separately describe the kinematical performance without and with the assistive mechanism, there are

$$\begin{aligned} J'_{0i_0} &= U_{0i_0} \cdot S_{0i_0} \cdot V_{0i_0}, \\ J'_{0i_0} &= A_{03}^{-1} \cdot J_{0i_0} \cdot A_{0i_0}, \\ i_0 &= 1, 2. \end{aligned} \quad (16)$$

Some results, such as ME-al, MD-al, ME-saam, and MD-saam can be obtained from Equation (16). With the inputs, EV-al and EV-saam also can be obtained through Equations (6) and (8).

With the results above, in the following parts, it will validate and show MIP can be applicable on lower-limb assistive mechanism's design and optimization to evaluate the assistive feasibility and assistive ability.

**4.2. MIP Study on Assistive Feasibility Validation.** In this part, with some examples, MIP will be validated to be applicable to evaluate assistive feasibility for the lower-limb assistive mechanism. For a certain posture, satisfying assistive feasibility means the assistive mechanism can assist on all the directions. Hence, the first step is to validate assistive feasibility by considering one direction, and then, the validation extends to all the directions logically. Since MIP describes the relation between end-effectors' manipulability and velocities, the validation is based on

end-effectors' maximum output velocities comparison and manipulability magnitude comparison.

At first, end-effectors' maximum output velocities on a certain direction for the lower limb and SAAM should be performed. As their end-effectors have the same two translational DOFs in the  $X - Y$  planar,  $v_{1x}$  and  $v_{1y}$  separately represents  $X$ -velocity component and  $Y$ -velocity component for end-effectors' velocity of the lower limb (EV-al);  $v_{2x}$  and  $v_{2y}$  also separately represent  $X$ -velocity component and  $Y$ -velocity component for end-effectors' velocity of SAAM (EV-saam). For lower limb and SAAM, while their end-effectors separately reaches the maximum velocity on direction  $(j_i)_w$ , the constraint equations are

$$\begin{cases} |\dot{\theta}_1| = (\dot{\theta}_1)_{\max} \text{ or } |\dot{\theta}_2| = (\dot{\theta}_2)_{\max}, \\ [(v_{1x})_w \ (v_{1y})_w]^T // \overrightarrow{(j_i)_w} \end{cases} \quad (17)$$

$$\begin{cases} |\dot{\theta}_3| = (\dot{\theta}_3)_{\max} \text{ or } |\dot{d}_4| = (\dot{d}_4)_{\max}, \\ [(v_{2x})_w \ (v_{2y})_w]^T // \overrightarrow{(j_i)_w} \end{cases} \quad (18)$$

where in this paper,  $(*)_w$  represents the results of case  $(w)$ . In Equation (17), the constraint equations mean almost on all the directions, while lower limb's end-effector reaches its maximum velocity, only one master-active joint can reach its maximum velocity, where only on four directions both lower limb's master-active joints can reach maximum velocities simultaneously. Equation (18) also shows similar meaning for the SAAM.

Then for the manipulability, on direction  $\overrightarrow{(j_i)_w}$ , the lower limb's manipulability magnitude is

$$(m_1)_w = \sqrt{(S_{01}^2(1))_w \cos^2(\alpha_1)_w + (S_{01}^2(4))_w \sin^2(\alpha_1)_w}, \\ (\alpha_1)_w = \langle \overrightarrow{(j_i)_w}, [U_{01}(1) \ U_{01}(2)]_w^T \rangle. \quad (19)$$

Here,  $\langle *, * \rangle$  represents two vectors' intersection angle. And on this direction, the manipulability magnitude of SAAM is

$$(m_2)_w = \sqrt{(S_{02}^2(1))_w \cos^2(\alpha_2)_w + (S_{02}^2(4))_w \sin^2(\alpha_2)_w}, \\ (\alpha_2)_w = \langle \overrightarrow{(j_i)_w}, [U_{02}(1) \ U_{02}(2)]_w^T \rangle. \quad (20)$$

In this paper, the items in a certain matrix  $H$  are defined as

$$H = \begin{bmatrix} H(1) & H(n+1) & \cdots & : \\ \vdots & \vdots & \cdots & \vdots \\ H(n) & H(2n) & \cdots & H(n \times m) \end{bmatrix}_{n \times m}. \quad (21)$$

Combined with Equations (17)–(20), on a certain direction, lower limb end-effector's and SAAM end-effector's maximum output velocities comparison is shown between Equations (17) and (18), and manipulability magnitude comparison is shown between Equations (19) and (20). Based on these two comparisons, the following examples will

show MIP is applicable to evaluate assistive feasibility for the lower-limb assistive mechanism.

In these examples, assume the parameters are set as  $l_1 = 30(\text{cm})$ ,  $l_2 = 30(\text{cm})$ ,  $(\dot{\theta}_1)_{\max} = \pi/5(\text{rad/s})$ ,  $(\dot{\theta}_2)_{\max} = \pi/4(\text{cm/s})$ ,  $x_0 = 30(\text{cm})$ ,  $y_0 = 0(\text{cm})$ ,  $(\dot{\theta}_3)_{\max} = \pi/4(\text{rad/s})$ ,  $(\dot{d}_4)_{\max} = 24(\text{cm/s})$ , and  $(\dot{x}_C)_{\max} = (\dot{y}_C)_{\max} = l_1 \cdot (\dot{\theta}_3)_{\max} + l_2 \cdot (\dot{\theta}_2)_{\max} = 42.951(\text{cm/s})$ . As shown in Figure 4, for posture (a):  $\{\theta_1 = \pi/6, \theta_2 = \pi/3\}$ , through the singular value decomposition of  $(J'_{01})_a$  and  $(J'_{02})_a$ , there are

$$(U_{01})_a = \begin{bmatrix} -0.938 & 0.344 \\ 0.344 & 0.938 \end{bmatrix}, \quad (22)$$

$$(S_{01})_a = \text{diag}(0.92, 0.23),$$

$$(U_{02})_a = \begin{bmatrix} 0.996 & -0.09 \\ 0.09 & 0.996 \end{bmatrix}, \quad (23)$$

$$(S_{02})_a = \text{diag}(0.84, 0.57),$$

where  $(U_{01})_a$  represents the MD-al, and  $(S_{01})_a$  represents the manipulability magnitude of assisted limb on each DOF. Similarly,  $(U_{02})_a$  represents the MD-saam, and  $(S_{02})_a$  is the manipulability magnitude of SAAM for each DOF.

Both the end-effectors of the assisted limb and SAAM move along direction  $a_1 : [0.938, -0.344]$ . According to the constraint Equations (17) and (18), while the velocities of lower limb's joints are  $\{\dot{\theta}_1 = -(\dot{\theta}_1)_{\max} = -\pi/5, \dot{\theta}_2 = -0.541\}$ , where master-active joint A reaches its maximum velocity, and in the SAAM, the velocities slave-active's joints are  $\{\dot{\theta}_3 = -(\dot{\theta}_3)_{\max} = -\pi/4, \dot{d}_4 = -9.531\}$ , where  $\dot{\theta}_3$  reaches its maximum velocity, the assisted limb's end-effector and SAAM's end-effector separately reaches their maximum velocities on direction  $a_1$

$$\begin{bmatrix} (v_{1x})_{a_1} \\ (v_{1y})_{a_1} \end{bmatrix} = (J_{01})_a \cdot \begin{bmatrix} -(\dot{\theta}_1)_{\max} \\ -0.541 \end{bmatrix} = \begin{bmatrix} 44.511 \\ -16.323 \end{bmatrix}, \quad (24)$$

$$\begin{bmatrix} (v_{2x})_{a_1} \\ (v_{2y})_{a_1} \end{bmatrix} = (J_{02})_a \cdot \begin{bmatrix} -(\dot{\theta}_3)_{\max} \\ -9.531 \end{bmatrix} = \begin{bmatrix} 34.494 \\ -12.651 \end{bmatrix}, \quad (25)$$

where the result of  $44.511/(-16.323) = 34.494/(-12.651) = 0.938/(-0.344)$  shows end-effectors' velocities are along direction  $a_1$ . In Figure 4, on direction  $a_1$ , it also shows both the EV-al and EV-saam parallel with  $a_1$ , where EV-al is the resultant velocity of  $v_{1x}$  and  $v_{1y}$ , and EV-saam is the resultant velocity of  $v_{2x}$  and  $v_{2y}$ . In Figure 4, end-effectors' maximum velocities comparison between Equations (24) and (25) shows that lower limb's end-effector can reach larger velocity than SAAM's end-effector in this case. From the aspect of manipulability, on direction  $a_1$ , lower limb's manipulability magnitude is

$$(m_1)_{a_1} = \sqrt{(S_{01}^2(1))_a \cos^2(\alpha_1)_{a_1} + (S_{01}^2(4))_a \sin^2(\alpha_1)_{a_1}} \\ = 0.92, \quad (26)$$

where  $(\alpha_1)_{a_1} = \langle (0.938, -0.344), (-0.938, 0.344) \rangle = 0$ . The manipulability magnitude of SAAM is

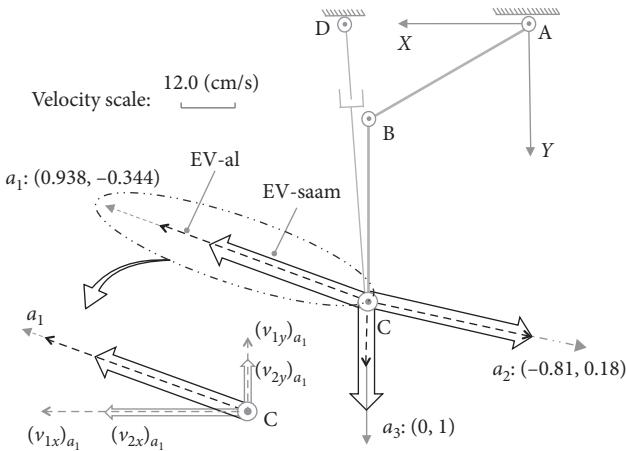


FIGURE 4: Maximum velocities comparison on different directions at posture (a):  $\{\theta_1 = \pi/6, \theta_2 = \pi/3\}$ .

$$\begin{aligned} (m_2)_{a_1} &= \sqrt{(S_{02}(1))_a \cos^2(\alpha_2)_{a_1} + (S_{02}(4))_a \sin^2(\alpha_2)_{a_1}} \\ &= 0.8, \end{aligned} \quad (27)$$

where  $(\alpha_2)_{a_1} = \langle(0.938, -0.344), (0.996, 0.09)\rangle = 0.044$ . Thereby, there is  $(m_1)_{a_1} > (m_2)_{a_1}$ . In this example, the comparison results mean that while SAAM's manipulability magnitude is smaller than lower limb's, SAAM end-effector's velocity is also smaller than lower limb end-effector's.

In the second example, on direction  $a_2 : [-0.807, 0.184]$ , while the velocities of lower limb's joints are:  $\{\dot{\theta}_1 = 3.429, \dot{\theta}_2 = (\dot{\theta}_2)_{\max} = \pi/4\}$ , and the velocities of assistive mechanism's joints are:  $\{\dot{\theta}_3 = (\dot{\theta}_3)_{\max} = \pi/4, \dot{d}_4 = 4.839\}$ , their end-effectors' maximum velocities on direction  $a_2$  are

$$\begin{bmatrix} (v_{1x})_{a_2} \\ (v_{1y})_{a_2} \end{bmatrix} = (J_{01})_a \cdot \begin{bmatrix} 3.429 \\ (\dot{\theta}_2)_{\max} \end{bmatrix} = \begin{bmatrix} -36.96 \\ 8.442 \end{bmatrix}, \quad (28)$$

$$\begin{bmatrix} (v_{2x})_{a_2} \\ (v_{2y})_{a_2} \end{bmatrix} = (J_{02})_a \cdot \begin{bmatrix} (\dot{\theta}_3)_{\max} \\ 4.839 \end{bmatrix} = \begin{bmatrix} -36.96 \\ 8.442 \end{bmatrix}. \quad (29)$$

The results in Equations (28) and (29) mean, just as shown in Figure 4, on direction  $a_2$ , the end-effectors for the lower limb and SAAM can achieve the same maximum velocity. Their separate manipulability magnitude is  $(m_1)_{a_2} = (m_2)_{a_2} = 0.816$ . In this example, it means while the manipulability magnitude for lower limb and SAAM is equal, the maximum output velocities on the certain direction are also equal.

The last example is on direction  $a_3 : [0, 1]$ , where there are  $\{\dot{\theta}_1 = 0.524, \dot{\theta}_2 = -(\dot{\theta}_2)_{\max} = -\pi/4\}$ , and  $\{\dot{\theta}_3 = -0.047, \dot{d}_4 = (\dot{d}_4)_{\max} = 24\}$ . Therefore, we can have

$$\begin{bmatrix} (v_{1x})_{a_3} \\ (v_{1y})_{a_3} \end{bmatrix} = (J_{01})_a \cdot \begin{bmatrix} 0.524 \\ -(\dot{\theta}_2)_{\max} \end{bmatrix} = \begin{bmatrix} 0 \\ 13.59 \end{bmatrix}, \quad (30)$$

$$\begin{bmatrix} (v_{2x})_{a_3} \\ (v_{2y})_{a_3} \end{bmatrix} = (J_{02})_a \cdot \begin{bmatrix} -0.047 \\ (\dot{d}_4)_{\max} \end{bmatrix} = \begin{bmatrix} 0 \\ 24.09 \end{bmatrix}.$$

Surely, SAAM can act quicker than the lower limb just as shown in Figure 4 on direction  $a_3$ . Their manipulability magnitude on this direction is  $(m_1)_{a_3} = 0.383$  and  $(m_2)_{a_3} = 0.573$ . There is  $(m_1)_{a_3} < (m_2)_{a_3}$ . Thereby, in this example, while SAAM end-effector's manipulability magnitude is larger than lower limb end-effector's, SAAM end-effector's velocity is also larger than lower limb end-effector's. Therefore, it can ensure the assistive mechanism shadows and assist lower limb's movement on this direction.

Through these three examples, the comparison results verify that on a certain direction, if SAAM end-effector's manipulability magnitude is equal to, larger than, or smaller than lower limb end-effector's, SAAM end-effector's maximum velocities are equal to, larger than, or smaller than lower limb end-effector's. It shows the end-effectors' manipulability magnitude comparison is directly related to end-effectors' maximum velocities comparison.

Further, as well known, the manipulability magnitude and velocity for mechanism's end-effector have the same change tendency, where the manipulability magnitude becomes smaller or larger on certain directions, and the maximum velocity also decreases or increases on certain directions. Thereby, we can extend the comparison results from one direction to all directions logically: if SAAM's manipulability magnitude is larger than lower limb's on all the directions, assistive mechanism satisfies the assistive feasibility since it can shadow lower-limb end-effector's velocity on all the directions; if SAAM's manipulability magnitude is smaller than lower limb's on all the directions, assistive mechanism cannot satisfy the assistive feasibility since it cannot shadow lower-limb end-effector's velocity at all; if SAAM's manipulability magnitude is larger than, equal to, or smaller than lower limb's on part of all the directions, the assistive mechanism may or may not shadow lower limb's velocity on part of all the directions, where in this case, the assistive mechanism also cannot satisfy assistive feasibility.

The above can be concluded as follows: when assisted limb's manipulability magnitude is smaller than or equal to SAAM's on all directions, in other words, when ME-al is whole inclusive by ME-saam, the assistive mechanism can shadow the assisted limb's movements well to satisfy assistive feasibility and be used to provide assistance on all the directions. This conclusion accords to the assistive feasibility evaluation criterion shown in the definition of MIP; therefore, MIP is proved to be applicable to evaluate lower-limb assistive mechanism's assistive feasibility.

In order to evaluate assistive feasibility for assistive mechanism, manipulability magnitude comparison with one direction by one direction is almost inefficient. Therefore, it is necessary to find an inclusive judgement algorithm which can judge the inclusive case on the whole directions quickly.

**4.3. Inclusive Judgement Algorithm.** Since the manipulability ellipsoid is used to represent the manipulability magnitude on the whole directions, we can compare the ME-al and ME-saam in terms of geometry to obtain the manipulability magnitude comparison results on all the

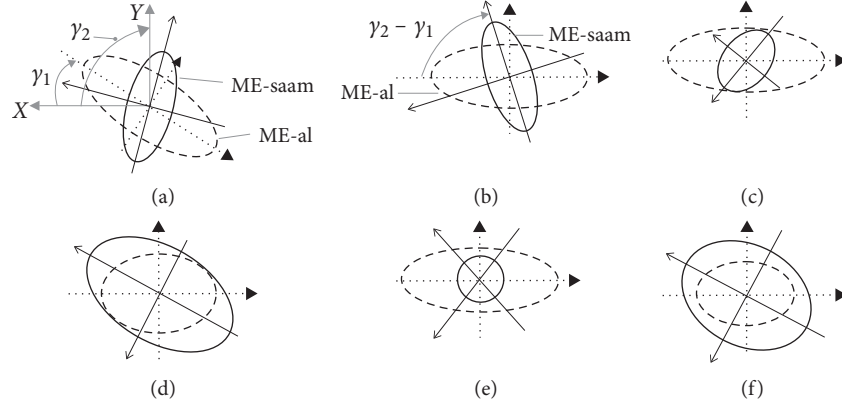


FIGURE 5: Inclusive cases between ME-al and ME-saam. (a) Initial, (b) after rotation, (c) internally tangent, (d) externally tangent, (e) internally inclusive, (f) externally inclusive.

directions. Through the inclusive judgement algorithm, we can judge whether the assistive mechanism can satisfy assistive feasibility or not.

At first, according to the first two concerns shown in the problem of assistive feasibility, lower limb end-effector's and SAAM end-effector's DOF spaces should be in the same space. It means their manipulability ellipsoids should be also in the same space. For the lower limb assistance, the manipulability ellipsoids of lower limb and SAAM both degenerate to ellipses. That whether these two ellipses are in the same space or not can be judged by their major and minor axes' normal lines: if these two normal lines are parallel to each other, these two ellipses are in the same space; otherwise they are not in the same space.

Then, the third concern can be judged by the intersection of these two ellipses. Assuming the intersection angles between these two ellipses and axis  $X$  are  $\gamma_1$  and  $\gamma_2$ , just as shown in Figure 5(a), the expressions for the manipulability ellipses of lower limb and SAAM are

$$\begin{aligned} \frac{(\cos \gamma_1 \cdot x + \sin \gamma_1 \cdot y)^2}{S_1^2(1)} + \frac{(-\sin \gamma_1 \cdot x + \cos \gamma_1 \cdot y)^2}{S_1^2(4)} &= 1, \\ \frac{(\cos \gamma_2 \cdot x + \sin \gamma_2 \cdot y)^2}{S_2^2(1)} + \frac{(-\sin \gamma_2 \cdot x + \cos \gamma_2 \cdot y)^2}{S_2^2(4)} &= 1. \end{aligned} \quad (31)$$

For the sake of computation, make the same rotations for these two ellipses. Then, Figure 5(b) is the rotation results of Figure 5(a), where the major and minor axes of MD-al align with axes  $X$  and  $Y$ . There are

$$\frac{x^2}{S_1^2(1)} + \frac{y^2}{S_1^2(4)} = 1, \quad (32)$$

$$\frac{(\cos \gamma \cdot x + \sin \gamma \cdot y)^2}{S_2^2(1)} + \frac{(-\sin \gamma \cdot x + \cos \gamma \cdot y)^2}{S_2^2(4)} = 1, \quad (33)$$

where  $\gamma = \gamma_2 - \gamma_1$ .

Since the ME-al and ME-saam are both odd symmetry about axis  $X$  as shown in Figure 5(b), we can only discuss

the case of  $\gamma \geq 0$  to judge their intersection or inclusive cases,

$$\gamma \geq 0. \quad (34)$$

By solving the set of Equations (32)–(34) which are quadratic equations about  $\{x, y\}$  to obtain real roots, there exist three cases: two roots, sole root, and no root. The cases of roots are directly related to the intersection or inclusive cases.

For example, just as shown in Figure 5(b), ME-al is part inclusive by ME-saam with two different points of intersection, where in this case, the set of equations has two roots. When the set of equations has sole root, the inclusive cases are internally tangent (Figure 5(c)) or externally tangent (Figure 5(d)), where we can separate them by considering their major and minor axes extremities distribution. If the set of equations has no root, it means ME-al and ME-saam have no point of intersection. In this case, it also has two types which can also be separated by considering their major and minor axes extremities distribution: internally inclusive (Figure 5(e)) and externally inclusive (Figure 5(f)).

The inclusive cases between ME-al and ME-saam are considered to be divided into three types: part inclusive case (Figures 5(a) and 5(b)), no inclusive case (Figures 5(c) and 5(e)), and whole inclusive case (Figures 5(d) and 5(f)). With this inclusive judgement algorithm, the inclusive case between ME-al and ME-saam can be obtained quickly.

In the following part, through the study on kinds of inclusive cases, we can understand which case is as our expected. Moreover, by the study on all kinds of inclusive cases, we can further understand MIP is applicable to evaluate assistive feasibility for lower-limb assistive mechanism, where it is also needed to check whether this inclusive judgement algorithm is applicable to judge inclusive cases or not.

#### 4.4. Cases of Part Inclusive, No Inclusive, and Whole Inclusive.

Through comparing the ME-al and ME-saam with inclusive judgement algorithm, for a certain assistive mechanism, at

different postures there may exist three cases: part inclusive case, no inclusive case, and whole inclusive case.

**4.4.1. Part Inclusive Case.** For posture (a):  $\{\theta_1 = \pi/6, \theta_2 = \pi/3\}$ , combined with Equation (22), we can draw the ME-al (denoted with dashed ellipse) with  $(U_{01})_a$  and  $(S_{01})_a$  to represent the manipulability of lower limb just as shown in Figure 6. Similarly, the ME-saam (denoted with solid ellipse) is generated with  $(U_{02})_a$  and  $(S_{02})_a$  to represent the manipulability of SAAM. In Figure 6, ME-al is part inclusive by the ME-saam, where by the inclusive judgement algorithm, the set of Equations (32)–(34) also shows that it has two different roots in this case.

With MIP, for the part inclusive case, there must be the conclusion: in different directions, SAAM end-effector's manipulability magnitude may be smaller than, equal to, or larger than lower-limb end-effector's; correspondingly, on these different directions, SAAM end-effector's maximum velocity is smaller than, equal to, or larger than lower limb's. In Figure 4, the maximum velocities comparison results on different directions certify this conclusion.

As the discussion before (Figure 4), in direction  $a_1$ , SAAM cannot catch lower limb's movement; on direction  $a_2$ , their end-effectors' maximum velocities are equal; on direction  $a_3$ , SAAM end-effector's maximum velocity is larger than lower-limb end-effector's.

The above means, for the case of part inclusive, in some directions, the assistive mechanism cannot shadow lower limb's movements to assist, but on the rest of the directions it can.

**4.4.2. No Inclusive Case.** At posture (b):  $\{\theta_1 = -1.1, \theta_2 = 2.02\}$ , there are

$$\begin{aligned} (U_{01})_b &= \begin{bmatrix} 0.52 & 0.854 \\ 0.854 & -0.52 \end{bmatrix}, \\ (S_{01})_b &= \text{diag}(0.64, 0.35), \\ (U_{02})_b &= \begin{bmatrix} 0.517 & 0.856 \\ 0.856 & -0.517 \end{bmatrix}, \\ (S_{02})_b &= \text{diag}(0.57, 0.06). \end{aligned} \quad (35)$$

In this case, with the inclusive judgement algorithm, the set of Equations (32)–(34) shows it has no real roots, and the major and minor axes extremities of ME-al are at the outer of ME-saam. Hence, this posture belongs to no inclusive case just as shown in Figure 7. According to MIP, in this case, on all the directions, SAAM's manipulability magnitude is smaller than lower limb's (Figure 7); correspondingly, SAAM end-effector's maximum velocities are also smaller than lower limb end-effector's. This conclusion can be certified by the maximum velocities comparison results shown in Figure 8.

As shown in Figure 8, while lower limb and SAAM move along direction  $b_1 : [0.854, -0.52]$ , there are

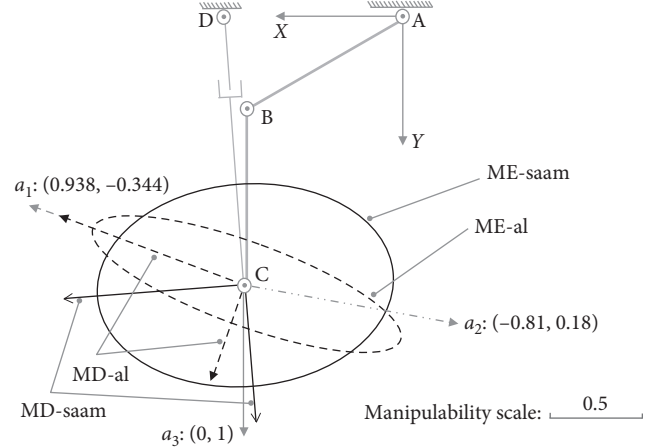


FIGURE 6: Part inclusive case at posture (a):  $\{\theta_1 = \pi/6, \theta_2 = \pi/3\}$ .

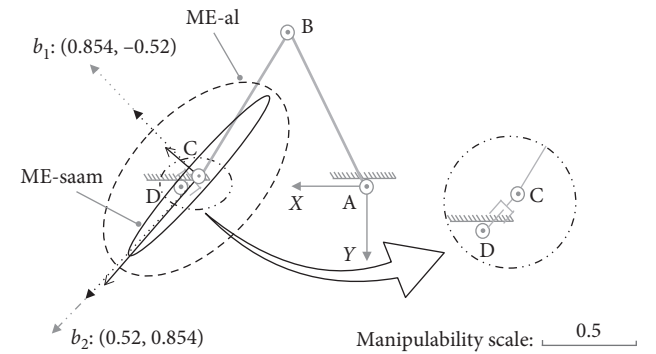


FIGURE 7: No inclusive case at posture (b):  $\{\theta_1 = -1.1, \theta_2 = 2.02\}$ .

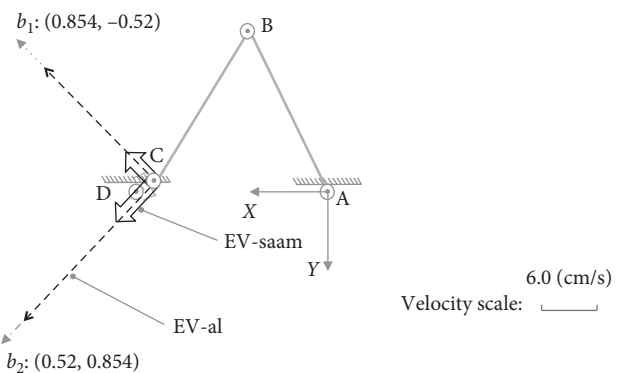


FIGURE 8: Maximum velocity comparison on different directions for part inclusive case at posture (b).

$$\begin{bmatrix} (v_{1x})_{b_1} \\ (v_{1y})_{b_1} \end{bmatrix} = (J_{01})_b \cdot \begin{bmatrix} 0.085 \\ -(\dot{\theta}_2)_{\max} \end{bmatrix} = \begin{bmatrix} 18.99 \\ -5.25 \end{bmatrix}, \quad (36)$$

$$\begin{bmatrix} (v_{2x})_{b_1} \\ (v_{2y})_{b_1} \end{bmatrix} = (J_{02})_b \cdot \begin{bmatrix} (\dot{\theta}_3)_{\max} \\ 5.25 \end{bmatrix} = \begin{bmatrix} 5.01 \\ -3.06 \end{bmatrix}. \quad (37)$$

In Equations (36) and (37), lower limb end-effector's velocity is larger. On direction  $b_2 : [0.52, 0.854]$ , there are

$$\begin{bmatrix} (v_{1x})_{b_2} \\ (v_{1y})_{b_2} \end{bmatrix} = (J_{01})_b \cdot \begin{bmatrix} (\dot{\theta}_1)_{\max} \\ -0.3 \end{bmatrix} = \begin{bmatrix} 8.88 \\ 14.58 \end{bmatrix}, \quad (38)$$

$$\begin{bmatrix} (v_{2x})_{b_2} \\ (v_{2y})_{b_2} \end{bmatrix} = (J_{02})_b \cdot \begin{bmatrix} (\dot{\theta}_3)_{\max} \\ -1.35 \end{bmatrix} = \begin{bmatrix} 1.56 \\ 2.55 \end{bmatrix}. \quad (39)$$

The results in Equations (38) and (39) also show SAAM cannot catch lower limb end-effector's velocities.

Therefore, in the case of no inclusive, SAAM cannot catch lower-limb end-effector's movements on all the directions. Moreover, since SAAM end-effector's velocities are lower than lower limb end-effector's, it will drag lower limb's movements. Hence, in the case of no inclusive, the assistive mechanism cannot assist the lower limb at all.

**4.4.3. Whole Inclusive Case.** In order to assist the lower limb on all the directions, part inclusive case and no inclusive case must be avoided. For posture (c):  $\{\theta_1 = \pi/5, \theta_2 = 3.02\}$ , there are

$$\begin{aligned} (U_{01})_c &= \begin{bmatrix} -0.615 & 0.788 \\ 0.788 & 0.615 \end{bmatrix}, \\ (S_{01})_c &= \text{diag}(0.556, 0.005), \\ (U_{02})_c &= \begin{bmatrix} -0.084 & 0.996 \\ 0.996 & 0.084 \end{bmatrix}, \\ (S_{02})_c &= \text{diag}(0.603, 0.566). \end{aligned} \quad (40)$$

For this posture, by the inclusive judgement algorithm, the set of Equations (32)–(34) shows it has no real roots, and the major and minor axes extremities of ME-al are at the inner of ME-saam. Therefore, ME-al is whole inclusive by ME-saam just as shown in Figure 9. According to MIP, in the case of whole inclusive, SAAM end-effector's velocities are larger than lower-limb end-effector's on all the directions.

In this case, as shown in Figure 10, on direction  $c_1 : [-0.615, 0.788]$ , there are

$$\begin{bmatrix} (v_{1x})_{c_1} \\ (v_{1y})_{c_1} \end{bmatrix} = (J_{01})_c \cdot \begin{bmatrix} (\dot{\theta}_1)_{\max} \\ -0.49 \end{bmatrix} = \begin{bmatrix} -9.06 \\ 11.61 \end{bmatrix}, \quad (41)$$

$$\begin{bmatrix} (v_{2x})_{c_1} \\ (v_{2y})_{c_1} \end{bmatrix} = (J_{02})_c \cdot \begin{bmatrix} (\dot{\theta}_3)_{\max} \\ -1.62 \end{bmatrix} = \begin{bmatrix} -18.39 \\ 23.55 \end{bmatrix}. \quad (42)$$

And on direction  $c_2 : [-0.788, -0.615]$ , we have

$$\begin{bmatrix} (v_{1x})_{c_2} \\ (v_{1y})_{c_2} \end{bmatrix} = (J_{01})_c \cdot \begin{bmatrix} (\dot{\theta}_1)_{\max} \\ 0.007 \end{bmatrix} = \begin{bmatrix} -1.83 \\ -1.41 \end{bmatrix}, \quad (43)$$

$$\begin{bmatrix} (v_{2x})_{c_2} \\ (v_{2y})_{c_2} \end{bmatrix} = (J_{02})_c \cdot \begin{bmatrix} 0.48 \\ -(\dot{d}_4)_{\max} \end{bmatrix} = \begin{bmatrix} -22.44 \\ -17.49 \end{bmatrix}. \quad (44)$$

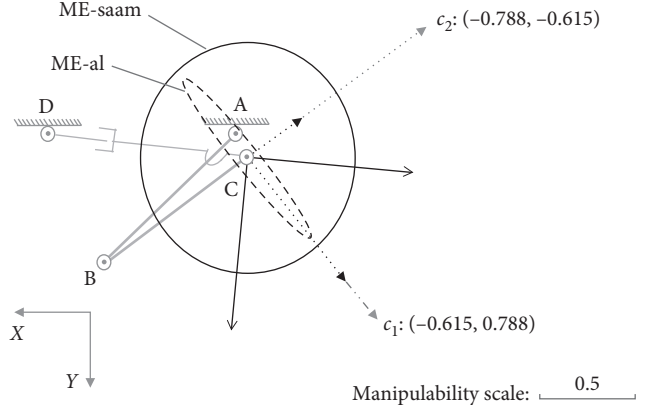


FIGURE 9: Whole inclusive case at posture (c):  $\{\theta_1 = \pi/5, \theta_2 = 3.02\}$ .

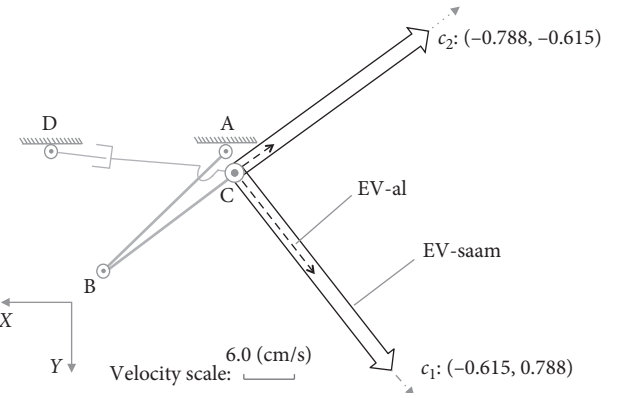


FIGURE 10: Maximum velocity comparison on different directions for whole inclusive case at posture (c).

From the results above shown in Equations (41)–(44), on these directions, SAAM's end-effector can act quicker than lower limb's end-effector. Thereby, in the case of whole inclusive, the assistive mechanism can shadow lower limb's movements well to provide power assisting for lower limb on all the directions.

Through the study on these three kinds of inclusive cases, it shows the inclusive case can be confirmed with the inclusive judgement algorithm effectively. It also shows the MIP is quite useful on evaluating assistive feasibility for lower limb assistive mechanism. In order to provide assistance on all the directions, the ME-al must be whole inclusive by ME-saam. Otherwise, when the ME-saam cannot cover ME-al on some directions, it means the assistive mechanism cannot provide power assisting on these directions, and even worse, human will feel difficulty increased on these directions. Hence, only the case of whole inclusive ensures the assistive mechanism can be used to assist lower limb's movements on all the directions.

Therefore, the problem of evaluating assistive feasibility in fact is converted to the following: with the inclusive judgement algorithm, comparing the ME-saam and ME-al to ascertain assistive mechanism's assistive feasibility. Through the study on these parts, MIP is validated to be able to evaluate assistive feasibility for lower-limb assistive mechanism.

Different from the problem of evaluating assistive feasibility whose answer is about being able to assist or being not able to assist these two aspects, the problem of evaluating effect is about that how the assistive mechanism assist lower limb, where the evaluation for assistive effect is shown in Section 4. In the next part, we will analyze and discuss the influence factors for assistive feasibility and assistive effect.

**4.5. Study on the Influence Factors of MIP.** As the discussions above, for a certain assistive mechanism, at different postures, the inclusive cases may be different. Our purpose is the assistive mechanism can satisfy assistive feasibility and realize better assistive effect in the whole expected workspace. Thereby, it is necessary to analyze and discuss which factors will have the influence on MIP, and then, we can develop the assistance for the assistive mechanism, where the influence on MIP also means the influence on inclusive results or assistive results.

The definition of MIP is based on manipulability which can be obtained through kinematical Jacobian. Hence, the MIP is related to mechanical structure, sizes, types of joints, actuators' maximum velocities, assistive mechanism's connected and fixed locations, and so on. In this paper, we focus on the influence factors of actuators' maximum velocities and assistive mechanism's fixed location.

**4.5.1. Influence Factor of Actuators' Maximum Velocities.** In this part, we will discuss the factor of actuators' maximum velocities, where in this case, only actuators' maximum velocities change. At posture (d), which is the same as posture (a), for the slave-active joints, the maximum velocity of  $(\dot{d}_4)_{\max}$  decreases from 24 (cm/s) to 8.28 (cm/s), and  $(\dot{\theta}_3)_{\max}$  decreases from  $\pi/4$  (rad/s) to 0.18 (rad/s). Then, SAAM's manipulability becomes

$$(U_{02})_d = \begin{bmatrix} 0.996 & -0.09 \\ 0.09 & 0.996 \end{bmatrix}, \quad (45)$$

$$(S_{02})_d = \text{diag}(0.2, 0.2),$$

while the manipulability of lower limb remains the same as posture (a) shown in Equation (22).

Compared to Figure 6, the inclusive case becomes from part inclusive case to no inclusive case just as shown in Figure 11. It shows the change of actuators' maximum velocities will have the influence on the MIP.

The change will also have the influence on end-effector's velocity. Compared to Figure 4, in Figure 12, besides directions  $d_1 (= a_1)$ ,  $d_2 (= a_2)$ , and  $d_3 (= a_3)$ , SAAM end-effector's velocities also decrease on the other directions.

In this case, if the maximum velocities of actuators change, inclusive results will also change. In addition, in this case, driven by the assistive mechanism, the ME-saam in Figure 11 becomes a circle which possesses good features on symmetry and isotropy, where Figure 12 also shows SAAM end-effector's velocities on each direction are equal. However, in this case the assistive mechanism cannot assist at all. Therefore, during the design and optimization for assistive mechanism, only considering the symmetry and isotropy is

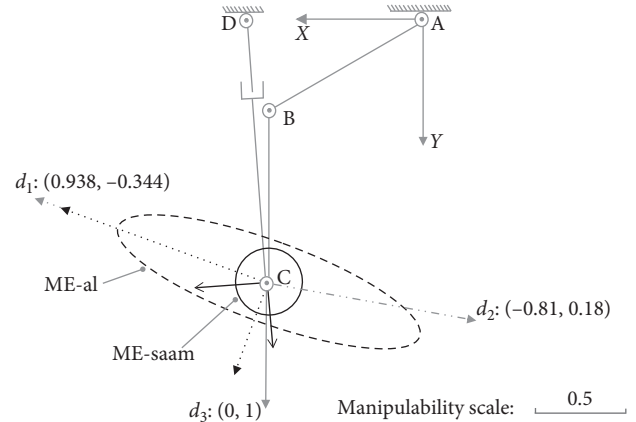


FIGURE 11: Influence with the change of actuators' maximum velocities at posture (d)=(a):  $\{\theta_1 = \pi/6, \theta_2 = \pi/3\}$ .

not enough. For assistive mechanism, we must also consider the basic feature for assistive mechanism at first: assistive feasibility.

**4.5.2. Influence Factor of Fixed Location.** For assistive mechanism's fixed location  $D(x_0, y_0)$ , in Figure 13, it shows only  $D$  changes from  $(30, 0)$  to  $(15, -30)$  with the same actuators, where lower limb is at posture (e) which is also the same as posture (a). In this case, the manipulability magnitude of SAAM becomes  $(S_{02})_e = \text{diag}(1.40, 0.57)$ . Compared to  $(S_{02})_a = \text{diag}(0.84, 0.57)$ , the manipulability magnitude of revolute DOF is enhanced. Then compared to Figure 6, the inclusive case becomes from part inclusive case to whole inclusive case.

In this case, just as shown in Figure 14, SAAM end-effector's velocities are also enhanced. Compared to Figure 4, in Figure 14, SAAM end-effector's velocities becomes larger than lower limb end-effector's on all the directions. It shows that changing fixed location will also have influence on the MIP.

From the discussions on the MIP influence factors, for the same posture, actuators' maximum velocities change and fixed location change will have influence on the inclusive case or assistive feasibility. Moreover, the changes of these factors will also have influence on the assistive effect. For example, at posture (a), the intersection angle between the major axes of MD-al and MD-saam in Figure 6 is 0.436 (rad). While the fixed location changes, at the same posture (e) just as shown in Figure 13, the intersection angle decreases to 0.192 (rad), where this development means after changing parameters, the MD-saam can align with MD-al much better to realize higher assistive efficiency. Meanwhile, compared to Figure 6, the volume of ME-saam in Figure 13 becomes much larger showing its assistive ability is enhanced. The change of assistive isotropy can be easily seen by comparing the ME-saam in Figures 6 and 11.

Hence, based on MIP, the optimization by considering the influence factors is helpful to make the assistive mechanism fit MIP. In other words, optimizing these parameters can relieve the problem of assistive feasibility,

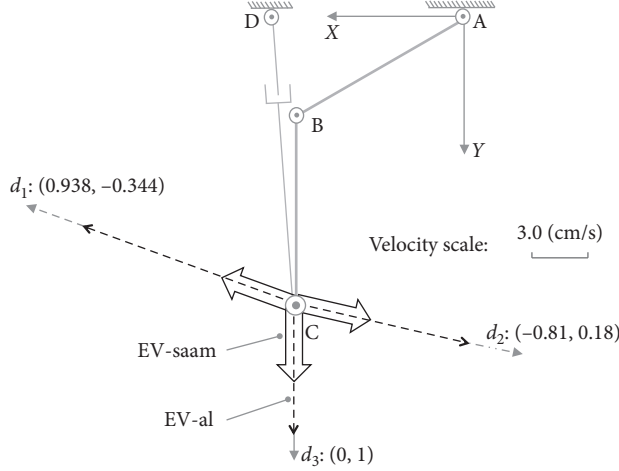


FIGURE 12: Maximum velocity comparison on different directions at posture (d)=(a) while actuators' maximum velocities change.

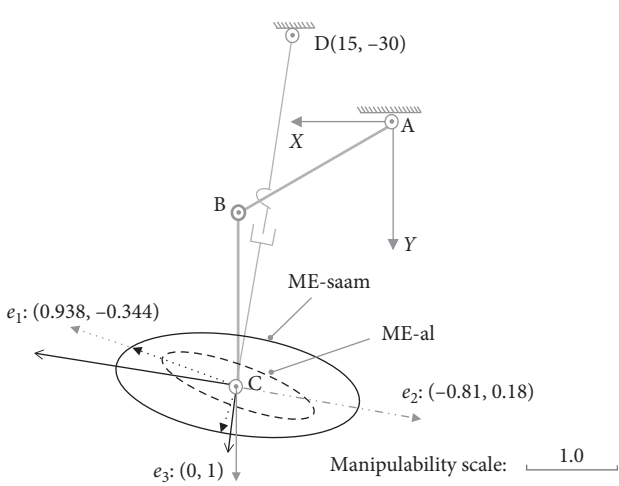


FIGURE 13: Influence with the change of fixed location at posture (e)=(a):  $\{\theta_1 = \pi/6, \theta_2 = \pi/3\}$ .

where changing the parameters can make no inclusive case or part inclusive case become whole inclusive case. And optimizing the parameters also makes sense for developing the assistive effect.

Through the studies on MIP in this section, it is certified that MIP can be used as the evaluation criterion for evaluating assistive feasibility and assistive effect for lower-limb assistive mechanism design and optimization. In order to realize better assistance in the whole expected workspace, the optimization algorithm based on MIP is needed.

## 5. Conclusions

In this paper, by considering satisfying assistive feasibility and realizing better assistive effect, the Manipulability Inclusive Principle (MIP) evaluation criterion for assistive mechanism design and optimization is proposed. This principle can be applicable on the assistive mechanisms which belong to the type where the human is acting actively,

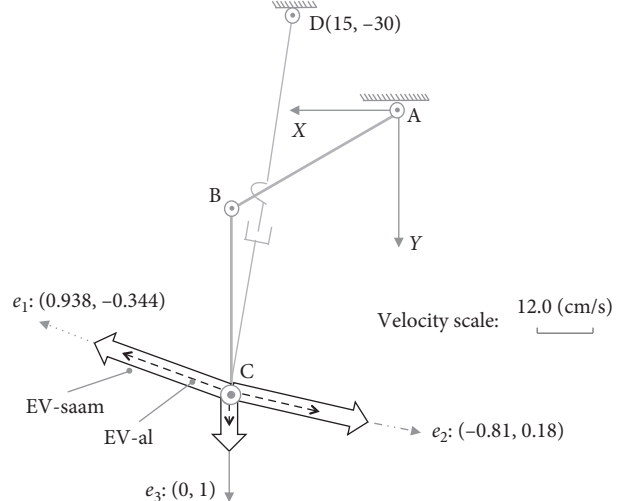


FIGURE 14: Maximum velocity comparison on different directions at posture (e)=(a) while fixed location changes.

and simultaneously the assistive mechanism is matching human's moving intention.

In order to ensure that the expected assistive mechanism satisfies assistive feasibility, the manipulability ellipsoid of the assisted limb must be whole inclusive by the slave-active-assistive mechanism's manipulability ellipsoid. The inclusive cases can be confirmed with the inclusive judgement algorithm. The MIP also shows that different parameters, such as actuators' maximum velocities, fixed and connected locations, types of joints, mechanical structure, and sizes, will have the influence on the assistive results.

The manipulability inclusive principle can also be applied on other various assistive mechanisms. Through building the model for the assisted limb and slave-active-assistive mechanism and then comparing their manipulability, manipulability inclusive principle is useful for evaluating assistive mechanism's assistive feasibility and assistive effect during design and optimization.

## Data Availability

The data used to support the findings of this study are included within the article.

## Conflicts of Interest

The authors declare that there are no conflicts of interest regarding the publication of this paper.

## Acknowledgments

This work was supported by the Fundamental Research Funds for Central Public Welfare Research Institutes (118009001000160001).

## References

- [1] M. Vukobratovic, V. Circ, and D. Hristic, "Contribution to the study of active exoskeletons," in *Proceedings of the 5th IFAC Congress*, Paris, France, June 1972.
- [2] H. Kazerooni and J. Guo, "Human extenders," *Journal of Dynamic Systems, Measurement, and Control*, vol. 115, pp. 281–290, 1993.
- [3] B. J. Makinson, "Research and development prototype for machine augmentation of human strength and endurance, Hardiman I Project," General Electric Report, S-71-1056, General Electric Co., New York, NY, USA, 1971.
- [4] M. Vukobratovic, D. Hristic, and Z. Stojiljkovic, "Development of active anthropomorphic exoskeletons," *Medical & Biological Engineering*, vol. 12, no. 1, pp. 66–80, 1974.
- [5] J. Hidler, W. Wismanc, and N. Neckel, "Kinematic trajectories while walking within the Lokomat robotic gait-orthosis," *Clinical Biomechanics*, vol. 23, no. 10, pp. 1251–1259, 2008.
- [6] D. Chugo and K. Takase, "A rehabilitation walker with a standing assistance device," in *Rehabilitation Engineering*, Y. K. Tan, Ed., pp. 109–128, InTech Publisher, Rijeka, Croatia, 2009.
- [7] G. T. Huang, *Wearable Robots*, MIT Technology Review, Cambridge, MA, USA, 2004.
- [8] K. Yamamoto, K. Hyodo, M. Ishi, and T. Matsuo, "Development of power assisting suit for assistive nurse labor," *JSME International Journal Series C*, vol. 45, no. 3, pp. 703–711, 2002.
- [9] K. Kasaoka and Y. Sankai, "Predictive control estimating operator's intention for stepping-up motion by exoskeleton type power assist system HAL," in *Proceedings of the IEEE/RSJ International Conference on Intelligent Robots and Systems*, pp. 1578–1583, Sendai, Japan, 2004.
- [10] C. R. Carignan, M. P. Naylor, and S. N. Roderick, "Controlling shoulder impedance in a rehabilitation arm exoskeleton," in *Proceedings of the 2008 IEEE International Conference on Robotics and Automation*, pp. 2453–2458, Pasadena, CA, USA, 2008.
- [11] R. A. R. C. Gopura and K. Kiguchi, "Development of a 6DOF exoskeleton robot for human upper-limb motion assist," in *Proceedings of International Conference on Information and Automation for Sustainability*, pp. 13–18, Colombo, Sri Lanka, 2008.
- [12] J. C. Perry, J. Rosen, and S. Burns, "Upper-limb powered exoskeleton design," *IEEE/ASME Transactions on Mechatronics*, vol. 12, no. 4, pp. 408–417, 2007.
- [13] H. Kazerooni and R. Steger, "The Berkeley lower extremity exoskeleton," *Journal of Dynamic Systems, Measurement, and Control*, vol. 128, no. 1, pp. 14–25, 2006.
- [14] C. J. Walsh, K. Pasch, and H. Herr, "An autonomous, underactuated exoskeleton for load-carrying augmentation," in *Proceedings of IEEE/RSJ International Conference on Intelligent Robots and Systems*, pp. 1410–1415, Beijing, China, October 2006.
- [15] J. E. Pratt, B. T. Krupp, and C. J. Morse, "The RoboKnee: an exoskeleton for enhancing strength and endurance during walking," in *Proceedings of the 2004 IEEE International Conference on Robotics and Automation*, pp. 2430–2435, New Orleans, LA, USA, April 2004.
- [16] <http://www.lockheedmartin.com/us/products/hulc.html>.
- [17] T. Nakamura, K. Saito, Z. Wang, and K. Kosuge, "Realizing a posture-based wearable antigravity muscles support system for lower extremities," in *Proceedings of the 2005 IEEE 9th International Conference on Rehabilitation Robotics*, pp. 273–276, Chicago, IL, USA, June-July 2005.
- [18] <http://www.honda.co.jp/ASIMO/new-tech>.
- [19] F. Chen, Y. Yu, Y. Ge, J. Sun, and X. Deng, "A PAWL for enhancing strength and endurance during walking using interaction force and dynamical information," in *Climbing & Walking Robots, towards New Applications*, H. Zhang, Ed., pp. 417–428, I-Tech Publishers, Vienna, Austria, 2007.
- [20] F. Chen, Y. Yu, Y. Ge, and Y. Fang, "WAPL for human power assist during walking using dynamic equation," in *Proceedings of the 2009 IEEE International Conference on Mechatronics and Automation*, pp. 1039–1043, Changchun, China, August 2009.
- [21] Y. Yu, D. Yoshimitsu, S. Tsujio, and R. Hayashi, "Power assist system with power-damped operation information feedbacking," in *Proceedings of the 2007 IEEE International Conference on Robotics and Biomimetics*, pp. 1709–1714, Rome, Italy, 2007.
- [22] Y. Yu and W. Liang, "Design optimization for parallel mechanism using on human hip joint power assisting based on manipulability inclusive principle," in *Proceedings of the 2012 IEEE International Conference on Robotics and Automation*, St. Paul, MN, USA, May 2012.
- [23] C. Gosselin and J. Angeles, "A global performance index for the kinematic optimization of robotic manipulators," *Journal of Mechanical Design*, vol. 113, no. 3, pp. 220–226, 1991.
- [24] L. W. Tsai and S. Joshi, "Kinematics and optimization of a spatial 3-UPU parallel manipulator," *Journal of Mechanical Design*, vol. 122, no. 4, pp. 439–446, 2000.
- [25] T. Yoshikawa, *Foundations of Robotics: Analysis and Control*, MIT Press, Cambridge, MA, USA, 1990.
- [26] H. Asada, "Dynamic analysis and design of robot manipulators using inertia ellipsoids," in *Proceedings of the 1984 IEEE International Conference on Robotics and Automation*, pp. 94–102, Atlanta, GA, USA, 1984.
- [27] J. P. Merlet, "Jacobian, manipulability, condition number, and accuracy of parallel robots," *Journal of Mechanical Design*, vol. 128, no. 1, pp. 199–206, 2006.
- [28] Y. Yu and W. Liang, "Design optimization for lower limb assistive mechanism based on Manipulability Inclusive Principle," in *Proceedings of IEEE International Conference on Robotics and Biomimetics*, pp. 174–180, IEEE, Guangzhou, China, December 2012.
- [29] Y. Yu and W. Liang, "Manipulability inclusive principle for hip joint assistive mechanism design optimization," *International Journal of Advanced Manufacturing Technology*, vol. 70, no. 5–8, pp. 929–945, 2014.

- [30] J. Li, B. Shen, L. Zhang, C. Tao, and R. Ji, "Kinematics and performance analysis of a serial hip assistive mechanism," *Advances in Mechanical Engineering*, vol. 10, no. 4, 2018.
- [31] Y. Miao, F. Gao, and D. Pan, "Prototype design and size optimization of a hybrid lower extremity exoskeleton with a scissor mechanism for load-carrying augmentation," *Proceedings of the Institution of Mechanical Engineers, Part C: Journal of Mechanical Engineering Science*, vol. 229, no. 1, pp. 155–167, 2015.
- [32] M. Gunasekara, R. Gopura, and S. Jayawardena, "6-REXOS: upper limb exoskeleton robot with improved pHRI," *International Journal of Advanced Robotic Systems*, vol. 12, no. 4, p. 47, 2015.

## Research Article

# An Orthopaedic Robotic-Assisted Rehabilitation Method of the Forearm in Virtual Reality Physiotherapy

Miguel A. Padilla-Castañeda<sup>1,2</sup>, Edoardo Sotgiu,<sup>1,3</sup> Michele Barsotti,<sup>1</sup> Antonio Frisoli<sup>1,4</sup>, Piero Orsini,<sup>4</sup> Alessandro Martiradonna,<sup>5</sup> Cristina Laddaga,<sup>5</sup> and Massimo Bergamasco<sup>1</sup>

<sup>1</sup>Laboratory of Perceptual Robotics, Pisa, Scuola Superiore Sant' Anna, Italy

<sup>2</sup>Instituto de Ciencias Aplicadas y Tecnología, Universidad Nacional Autónoma de México, México City, Mexico

<sup>3</sup>Microfabrication and Exploratory Nanotechnology, International Iberian Nanotechnology Laboratory, Braga, Portugal

<sup>4</sup>Research Center "E.Piaggio", University of Pisa, Pisa, Italy

<sup>5</sup>Adult Rehabilitation Centre "Luciana Segnini" USL5, Fornacette, Italy

Correspondence should be addressed to Miguel A. Padilla-Castañeda; [miguel.padilla@icat.unam.mx](mailto:miguel.padilla@icat.unam.mx)

Received 18 November 2017; Revised 28 February 2018; Accepted 28 March 2018; Published 1 August 2018

Academic Editor: Rafael Morales

Copyright © 2018 Miguel A. Padilla-Castañeda et al. This is an open access article distributed under the Creative Commons Attribution License, which permits unrestricted use, distribution, and reproduction in any medium, provided the original work is properly cited.

The use of robotic rehabilitation in orthopaedics has been briefly explored. Despite its possible advantages, the use of computer-assisted physiotherapy of patients with musculoskeletal injuries has received little attention. In this paper, we detailed the development and evaluation of a robotic-assisted rehabilitation system as a new methodology of assisted physiotherapy in orthopaedics. The proposal consists of an enhanced end-effector haptic interface mounted in a passive mechanism for allowing patients to perform upper-limb exercising and integrates virtual reality games conceived explicitly for assisting the treatment of the forearm after injuries at the wrist or elbow joints. The present methodology represents a new approach to assisted physiotherapy for strength and motion recovery of wrist pronation/supination and elbow flexion-extension movements. We design specific game scenarios enriched by proprioceptive and haptic force feedback in three training modes: passive, active, and assisted exercising. The system allows the therapist to tailor the difficulty level on the observed motion capacity of the patients and the kinesiology measurements provided by the system itself. We evaluated the system through the analysis of the muscular activity of two healthy subjects, showing that the system can assign significant working loads during typical physiotherapy treatment profiles. Subsequently, a group of ten patients undergoing manual orthopaedic rehabilitation of the forearm tested the system, under similar conditions at variable intensities. Patients tolerated changes in difficulty through the tests, and they expressed a favourable opinion of the system through the administered questionnaires, which indicates that the system was well accepted and that the proposed methodology was feasible for the case study for subsequently controlled trials. Finally, a predictive model of the performance score in the form of a linear combination of kinesiology observations was implemented in function of difficult training parameters, as a way of systematically individualising the training during the therapy, for subsequent studies.

## 1. Introduction

Musculoskeletal disorders or lesions in conjunction are one of the leading causes of chronic disability around the world. For example, in the United States, orthopaedic surgery is one of the first causes of medical visits and physical therapy is one of the nonmedicated treatments [1].

Among orthopaedic injuries, wrist fractures had a high incidence in the elderly population in 2001 [2]; forearm fractures of the distal radius are the most common in humans

[3]. Patients with a distal radial fracture must require staying out of work around 67 days up to 20 weeks for recovery, what poses relevant economic and social implications. Indeed, at the moment of suffering the radius injury, more than half of the patients are currently employed [4]. A study for evaluating the relationship of pain, occupational performance, and quality of life in a women population after upper limb fractures indicates that half of the reported problems were related with productivity, almost 40% with self-care, and 10% with leisure [5].

Although less frequent, elbow fractures might lead to severe limitations of the forearm, affecting its fundamental role in placing and supporting the hand in the space and as a stabiliser [6]. Elbow fractures can occur at the distal humerus, the proximal radius, or the proximal ulna. Such injuries result in considerable variability of postfracture symptoms (swelling, pain, and loss of motion) and might lead to functional disability [4, 6] because these joints should hold mobility, stability, strength, and absence of pain [7, 8]. Loss of motion of the elbow may affect essential independent functions in daily life activities, including personal care, mobility, eating, or even walking safely with aids especially for the elderly [8].

The treatment depends on the lesion severity; if the fracture is stable and without dislocation of fragments, a cast or a splint made of thermoplastic material is used for external immobilisation of the lesion area. An unstable and dislocated fracture requires a surgical intervention of reduction and stabilisation and the following immobilisation with a cast or a splint [8, 9]. In any case, after the immobilisation period, an early rehabilitation treatment consisting of exercise physiotherapy must start as early as possible to have a positive recovery of the forearm motion. Four aspects have been suggested as crucial factors for recovery functional movement in patients with fractures affecting the forearm joints: the number of therapy visits [10], the intensity and individualising level of the therapy, the adherence to the postoperative treatment [10], and the objective and continuous monitoring of the patient evolution during the intervention. Thus, on the one hand, the need for reducing the duration of the post-operative treatment for functional restoration is a crucial factor for many patients. On the other hand, the need for therapists for incrementing the number of attending patients with a better understanding of the progress of the patients motivates the research of treatment strategies that would optimise the type, intensity, and duration of the treatment according to the patient's condition.

An approach based on rehabilitation robotics with physiotherapy games would be a valuable tool for rendering the physiotherapy process more efficient. However, most of the current research in rehabilitation robotics focuses on neurorehabilitation for patients with lesions at the central nervous system (CNS), with more emphasis on stroke patients and with lesser extent in patients with other neural injuries, such as in the spinal cord. Exoskeletons [11–14] or end-effector robots [15] in combination with virtual reality (VR) serious games [16–19] have shown advantages for the neuromotor rehabilitation of upper limbs [20–23]: to mention, higher intensity of the training, higher level of motor control of the joints, longer duration, and more number of the sessions [13, 24], which can give variable assistance [25] or resistance [26] force feedback and may provide kinesiology information of the patient performance that facilitates the evaluation during the treatment [23], among others.

Unfortunately, despite the possible benefits, the high incidence of musculoskeletal injuries, and the current demand for faster and better physical therapies, the use of robotics for orthopaedic rehabilitation remains practically uncovered, and the research in this field is quite scarce, in comparison with neurorehabilitation systems [27].

The main difference between neuromotor and orthopaedic rehabilitation relies on the clinical goal of the recovery. For neurologic patients (with injuries at the level of the CNS), the primary goal is to achieve a cortical reorganisation which could lead to the restoration of motor functionalities [28, 29]. Instead, for orthopaedic patients (with musculoskeletal lesions but without cognitive impairments), the primary goal of any system should be the restoration of functional ranges of motion, muscular strength recovery, and pain reduction [5, 6, 8, 9, 30]. Robotic neurorehabilitation focuses on the mobilisation of the limbs through complex multijoint movements (reaching, grasp, and bimanual coordination, among others) and neuroplasticity stimulation with cognitive task assignment [17]. After a period of immobilisation, robotic rehabilitation in orthopaedics should focus on mobilisation of single joints within moderate increments [8, 9, 30].

Due to its severity, the treatment of a musculoskeletal lesion, such as elbow fracture, must be carried out with precaution and special care must be taken during all the phases of the intervention [8]. First, if the fracture is stable and without dislocation of fragments, a cast or a splint made of thermoplastic material is used for external immobilisation of the lesion area. An unstable and dislocated fracture requires a surgical intervention of reduction and stabilisation and the following immobilisation with a cast or a splint [31]. Aside from ensuring stabilisation of fragments, immobilisation aids to decrease pain and swelling and importantly prevents radiological deformity [32]. However, a common complication of postsurgery immobilisation is the development of joint stiffness and consequently long-term loss of range of motion [33]; in the case of the elbow, up to 25% of distal humerus fractures result in elbow stiffness [34]. For this reason, the rehabilitation must start as early as possible, immediately after the absence of severe pain, oedema, or instability of fragments [31]. Besides preventing contracture formation and post-traumatic rigidity, this facilitates the recovery of functional range of motion (RoM) and muscular strength [6].

The rehabilitation relies on the intensive practice of isolated movements [6, 8], actively performed by the patient or passively assisted by the therapist. Usually, the orthopaedic rehabilitation consists of three subsequent set of exercises: passive, active-assistive, and active. Passive exercises consist of the manual mobilisation of the patients' articulations performed by the therapist. Then, active-assistive exercises are performed when patients' muscles are still feeble and they have difficulties to perform the exercises independently. Finally, active exercises are performed in the latest phase (usually the longer) of the rehabilitation when the patient can move without external assistance [8, 9]. Mobilisation must be done gradually from passive to active movements of the single joints, starting from moderate movements within reduced RoM and mild working loads, especially at the early days after immobilisation, up to functional RoM and higher loads for strength recovery. This process is challenging for the therapist: it must focus on functional motion recovery and avoiding at the same time any aggressive movement that may provoke postinjury complications, for example, trauma to the arm's brachialis muscle and the elbow joint capsule due to forced passive manipulation of the elbow [33].

With these motivations, some devices have been designed specifically for wrist [15, 35–38] and elbow joints [36, 39], but to date, they have not been integrated with physiotherapy applications specifically designed for such patients. In particular, Vanderniepen et al. [39] presented an elbow orthosis intended explicitly for orthopaedic rehabilitation of the elbow, with an adaptable compliance mechanism designed for slow and constrained motions in a single DoF for protection of the patient and then for extending its device to an exoskeleton considering the shoulder [14]. Both apparatus seem suitable for orthopaedic rehabilitation of the upper limb. However, they did not include any integration with specific software for this purpose, and they did not report any experience with patients.

On the contrary, even if some of the rehabilitation robots reported for neurorehabilitation could have the potential use in orthopaedic rehabilitation, the adopted human-robot interaction schemes and assisted physiotherapy approaches of such systems cannot be directly applied for the needs of orthopaedic patients [40, 41]. At most, they should be used with precaution, but in any case, it is not clear if neurorehabilitation approaches would be valid for orthopaedic lesions, given the noticeable different clinical goals [41].

Up to the best of our knowledge, nowadays, the work reported by Schwickert et al. [42] is the only study detailing the use of robotic-assisted rehabilitation in orthopaedics with patients for proximal humerus fractures in virtual environments using the ArmeoSpring system (Hocoma AG, Zurich, Switzerland). The study consisted of an uncontrolled intervention of eight case series, with robotic sessions 2–3 times per week during 2–4 weeks in robotic sessions in combination with manual therapy; some single- to multijoint movements were tested with patients playing in goal-oriented game scenarios and with difficulty increments manually adjusted. Their results indicated that the system was safe and the treatment was feasible. However, the study gives no details regarding the specificity of the games for the characteristics of orthopaedic physiotherapy and nor the adopted criteria of how to adapt the difficulty levels during the sessions, which is not a straightforward aspect but still an open-research aspect. Thus, more research should be done both for the development of new devices and software-based physiotherapy methodologies for orthopaedic patients and for studying the feasibility, validation, and effectiveness of such developments through clinical experimentation with patients.

On these bases, we developed a robotic system for the orthopaedic rehabilitation of the upper limb, which integrates a novel methodology for assisted physiotherapy in VR serious games. The system consists of four modules: (1) a robotic rehabilitation device (PERCRO-BRANDO); (2) VR serious games for motion task execution of the forearm; (3) the therapist graphic interface; and (4) and a task difficulty adaptation module based on the monitored patient kinesiological performance through time.

The BRANDO robot consists of the integration of a 6-DoF end-effector-based robotic arm and a passive arm, mounted together in a common platform. Three of the 6 DoFs are actuated allowing the mobilisation of the elbow and shoulder joints. The three passive DoFs correspond to a 3-DoF gimbal for passive motions of the wrist joint. The passive arm

provides full gravity compensation of the upper limb, to aid the patient to perform movements without carrying its weight, which is often considered a useful configuration in manual physiotherapy [6]. The VR serious game applications were conceived for assigning isolated motion tasks of pronation/supination (PS) or flexion/extension (FE) movements within constrained RoM and moderate but incremental strength loads, within motivating game scenarios at different levels of difficulty. With the user-friendly graphical interface, the therapist can evaluate the current mobility of the FE and PS, modify the difficulty parameters of the exergames, and monitor the kinetic progress during the sessions. Finally, the task difficulty adaptation module allows to help the therapists to tailor the physical demanding of exercises based on the monitored kinesiological information and through the estimation of the performance score through a regression model, previously calibrated experimentally.

To the best of our knowledge, the system described in this paper is the first one designed that combines these four components in a single framework on the basis of the specific needs of orthopaedic rehabilitation of the upper limb, in particular for the recovery of strength and range of motion of elbow movements affecting the forearm. With the aim of studying the suitability of the proposed methodology with the system, we carried out two experiments: first in healthy subjects and second in a group of patients under orthopaedic rehabilitation of the forearm. Firstly, through the analysis of electromyographic surface signals (sEMG) placed at the arm muscles of the two healthy subjects practising with the system under the same conditions conceived for patients, we verified the capability of the method of assigning different working loads without physically overloading the patients until their muscular fatigue. Secondly, we tested the system on ten patients (9 performing PS movements and 7 performing PS and FE movements) confirming not only the acceptance by the patients but also its functional ability in delivering customised demanding levels of exercises systematically and safely. In conclusion, the proposed system is a suitable platform for carrying out more clinical studies towards the validation and effectiveness of robotic-assisted orthopaedic rehabilitation of the forearm and paves the way to the design of new therapeutic interventions for the rehabilitation of other upper limb fractures.

The rest of the paper is organised as follows: Section 2 presents the development of the full rehabilitation system. Section 3 presents the assessment of the system performance with the healthy volunteers and the feasibility and acceptance assessment by patients. Section 4 presents the discussion, and Section 5 the conclusions.

## 2. The BRANDO Rehabilitation System

Our system called BRANDO consists of the robotic device integrated with a control scheme for active/pассив rehabilitation of the upper limb, through VR exercising gaming scenarios. With this system, we propose a new methodology of assisted physiotherapy for the orthopaedic rehabilitation of the forearm, as detailed in this section.

**2.1. Robotic Rehabilitation Device.** The BRANDO system (Figure 1(a)) consists of a haptic interface in the form of a 6-DoF robotic arm with 3 actuated DoFs [43], enhanced with a 3-DoF passive gimbal for the patient's hand and mounted in a passive mechanism for giving support to the upper limb [44].

The haptic interface consists of a 3 actuated DoF end-effector (EE) mechanism (Figure 1(b)), kinematically equivalent to 2 orthogonal, one incident rotational joints ( $q_1 \pm 25^\circ$  and  $q_2 \pm 45^\circ$ ) and one prismatic joint ( $q_3 = 0.630$  mm) that drives a barrel along a third incident axis. The following direct kinematic equations define the tracking of the EE position in space:

$$\begin{aligned}x &= L \cos(q_1) \cos(q_2), \\y &= L \sin(q_1) \cos(q_2), \\z &= -L \sin(q_2),\end{aligned}\quad (1)$$

where  $L = q_3 + L_o$  is the length of the barrel's displacement, with  $L_o = 441$  mm being the minimum displacement.

Two DoFs are actuated by means of a differential transmission, composed of 2 capstans acting on a commonly driven pulley. The differential transmission was designed to allowing high kinematic isotropy along  $x$ - and  $z$ -directions and high regularity of the diagonal elements of the corresponding mass matrix of the mechanism. Three brushed DC motors are used for actuation: two grounded motors for reducing the amount of moving mass and the third motor for providing the translational motion of the barrel. No reduction gear was employed to minimise the backlash. The mechanism allows backdrivability of the DoFs with low friction perceived at the EE. Two weights are fixed to the rear of the barrel to counterbalance its weight in the central position of the workspace.

A passive gimbal with three spherical DoFs was mounted at the EE to allow the patient to handle the interface (wrist position W). The gimbal allows the tracking of the flexion/extension (FE) and abduction/adduction (AA) of the wrist and the pronation/supination (PS) of the elbow of the patient. It includes two buttons to let the patient trigger simple commands during the exercises.

The passive mechanism consists of one prismatic joint to adjust the height of the interface to the vertical position of the hand of the patient and a balancing column to mount a 2-DoF passive arm. The mechanism allows compensating the weight of the forearm through an ergonomic base supported by an industrial tool (with a maximum payload of 4 kg). A mobile platform mounts the full mechanism and allows placing the full device stable in the clinical room.

The full BRANDO system resulted in the optimal configuration shown in Figure 1(c). The configuration allows the patient to place comfortably in a seated posture and perform upper limb movements by placing the wrist within a minimal workspace of  $400 \times 800 \times 800$  mm up to an approximately  $900 \times 800 \times 1500$  mm conic workspace, under maximum continuous force feedback of 10 N up to a peak force of 20 N.

**2.2. Patient's Upper Limb Tracking and Modelling.** The system integrates a virtual reality model of the human upper limb [45], consisting of a multibody rigid dynamic system with 7 DoFs for the arm (Figure 2(a)) and 17 DoFs with 18

links for the hand (Figure 2(b)), in the form of revolute joints [46]. We implemented the model in the XVR software for VR (VRMedia s.r.l., Pisa, Italy) and C++ using the PhysX SDK (Nvidia, USA) for the physics engine simulation.

The tracking of the patient's movements is done by the estimation of the joint angles of the patient limb ( $q_1$  to  $q_7$ ), given the estimated positions W, E, and S using the analytical inverse kinematic solution reported in [47]. The shoulder position S is estimated from the starting posture of the patient sitting and with the elbow half flexed. The estimation of the elbow position E is according to the physical interpretation illustrated in Figure 2(b), where due to the redundant mechanism of the upper limb, even fixing W, the elbow E is still free to swivel on an arc with origin c lying in a plane that is orthogonal to the composed axis from the wrist to the shoulder S [47]. Given the local coordinates frame by the vectors n, u, and v, it is possible to geometrically estimate E in function of the swivel angle  $\phi$ , as detailed in [47], where n is the normal vector of the wrist-shoulder axis, u is the projection of the arbitrary unit vector a on the plane which corresponds to  $\phi = 0$ ,  $L_1$  is the length of the upper arm, and  $L_2$  is the length of the forearm.

For the game scenarios presented in this paper, we set up the swivel angle to two possible training postures, for the games in Section 2.4: (1) with the arm adducted at  $10^\circ$  approximately and (2) with the arm abducted at about  $80^\circ$ . Both configurations were estimated empirically with an extendable goniometer (Lafayette Instrument Co, Inc.; model 01135) during preliminary tests. For the first posture, variations of the swivel angle were minimised by instructing the patient to avoid shoulder movements or by fixing the upper arm to the trunk with an elastic bandage; for the second posture, the swivel angle was maintained by placing the patient's upper arm in the arm support of the device. Possible singularities occurring at the elbow fully extended were procedurally detected and corrected at runtime using the gradient information of the position in joint space.

**2.3. Control Scheme for Patient-Robot Interaction.** The control scheme was implemented at two levels (Figure 3). An industrial PC with a real-time operating system (xPC Target by MathWorks<sup>®</sup>) runs the low-level controller. This controller estimates the EE position in space given the  $\mathbf{q}$  angular positions of the robot joints, executes the gravity compensation ( $G(\mathbf{q})$ ) to avoid carrying the load of the robot arm, and performs the proportional-derivative (PD) position control for placing the EE in space. The high-level controller runs on a graphics workstation. This controller runs (1) the inverse kinematics for tracking the patient's movements; (2) the virtual reality games; (3) the target pose selection and the minimum-jerk reference path generator to the target position; and (4) the haptic feedback rendering. The communication between low-level and high-level controllers is executed via UDP.

The motion tasks consist of placing the current EE position ( $\mathbf{p}$ ) until touching a virtual object T at different target positions in the game. The interaction loop consists of three phases: (1) selecting T and computing the corresponding target position ( $\mathbf{p}_T$ ); (2) exerting haptic forces ( $\mathbf{F}_{path}$ ) tending

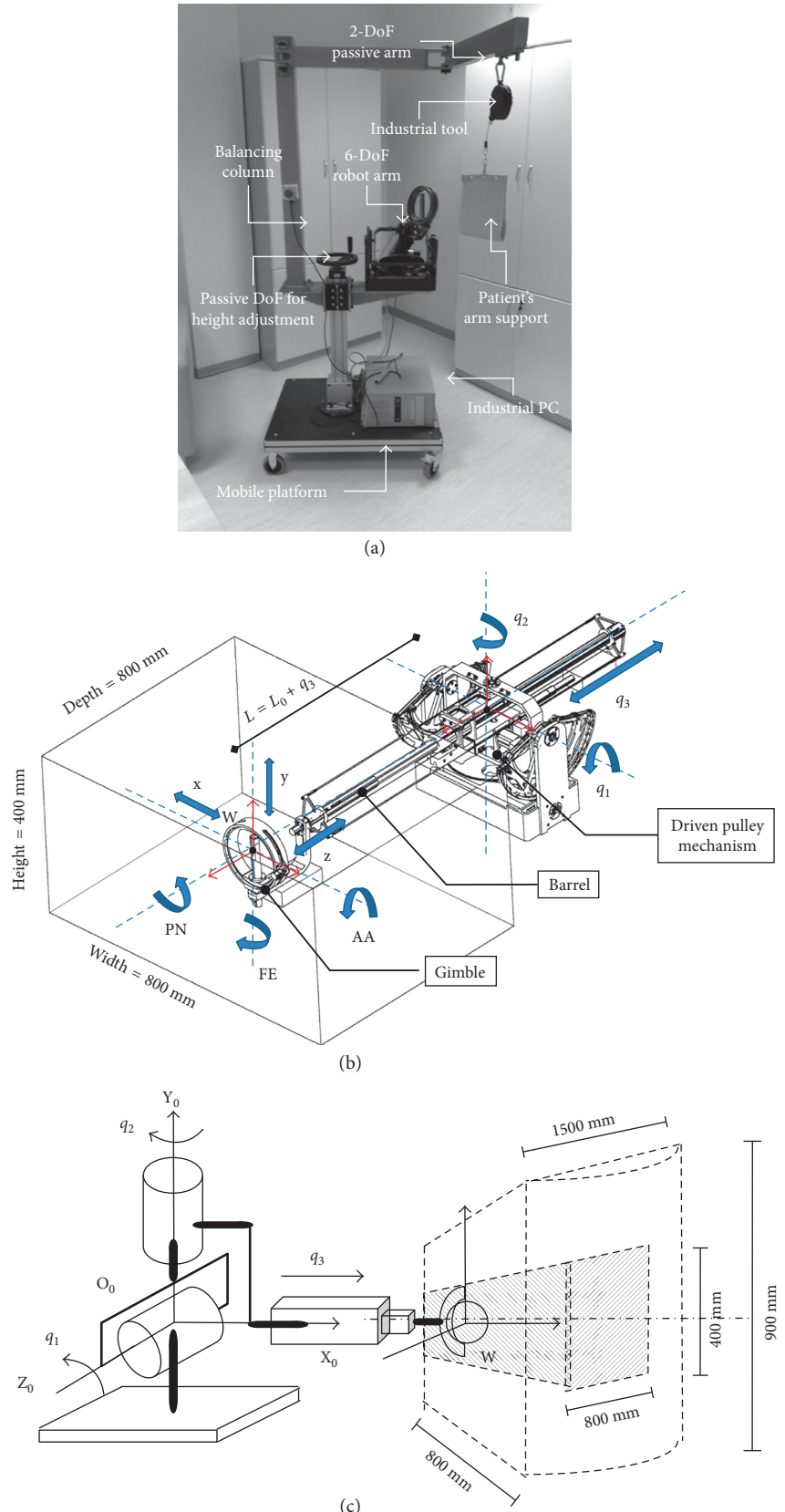


FIGURE 1: BRANDO rehabilitation robotic system consisting of a 6-DoF robot device mounted on the passive mobile platform, with a passive handle attached at the end-effector. (a) The full final system. (b) The mechanism of the 6-DoF robotic arm. (c) Conical workspace of the robot, with a minimum reachable square workspace of  $400 \times 800 \times 800$  mm.

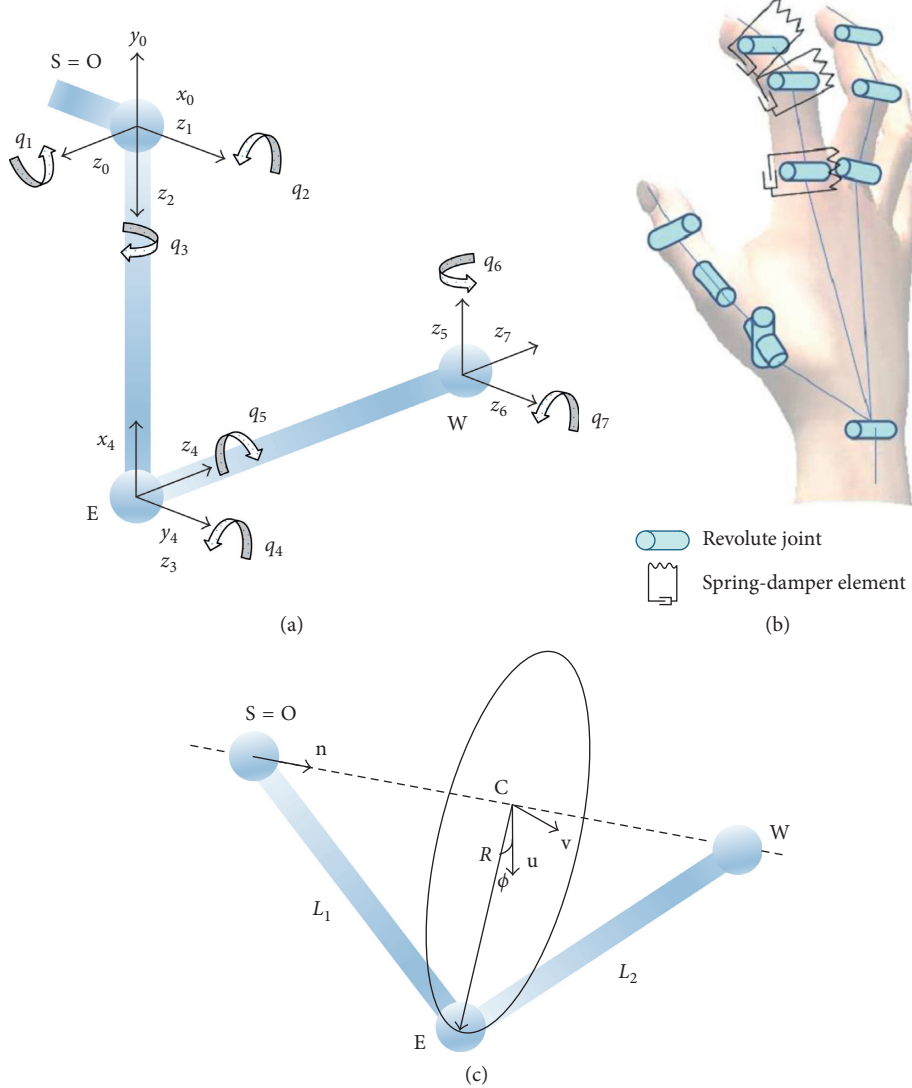


FIGURE 2: A simulation model of the upper limb. (a) 7-DoF kinematic model of the arm. (b) 17-DoF kinematic model of the hand, with the physical interpretation as a multirigid body system with spring-damper joints. (c) Elbow position as a function of the swivel angle  $\phi$ .

to place  $\mathbf{p}$  at a reference position ( $\mathbf{p}_{\text{ref}}$ ), by following a reference minimum-jerk trajectory  $R$ ; and (3) exerting collision forces ( $\mathbf{F}_{\text{collision}}$ ) when the virtual hand ( $\mathbf{p}_{\text{hand}}$ ) touches  $T$ .

The trajectory  $R$  from the starting position  $\mathbf{p}_S$  to  $\mathbf{p}_T$  is generated in real time given the polynomial time law reported in [25] (Figure 4(a)):

$$\begin{aligned} \mathbf{p}_{\text{ref}}(t) = & \mathbf{p}_S + \left( 10\left(\frac{t}{t_{\text{task}}}\right)^3 - 15\left(\frac{t}{t_{\text{task}}}\right)^4 + 6\left(\frac{t}{t_{\text{task}}}\right)^5 \right) \\ & \times (\mathbf{p}_T - \mathbf{p}_S), \end{aligned} \quad (2)$$

where  $t$  is the current time and  $t_{\text{task}}$  is the assigned time for completing the task. The equation assumes that the velocity and acceleration are zero at the beginning and the end of  $R$ .  $R$  could be linear or circular, depending on the motion task: linear for reaching or circular for single-joint motion tasks.

Positioning the EE is done by a PD controller given the proportional ( $K_p$ ) and derivative control coefficients ( $K_d$ ), as follows:

$$\begin{aligned} \mathbf{F}_{\text{path}}(t) &= K_p \Delta \mathbf{p} + K_d \Delta \dot{\mathbf{p}}, \\ \Delta \mathbf{p} &= \mathbf{p}_{\text{ref}}(t) - \mathbf{p}(t). \end{aligned} \quad (3)$$

The therapist can manually adjust the values of  $K_p$ ,  $K_d$ , and  $t_{\text{task}}$ . The value of  $K_p$  is within the range  $[0, 1]\text{Nm}$ , while for stability,  $K_d$  is proportionally computed to keep the ratio  $K_p/K_d$  always constant; such a ratio has been determined empirically during the preliminary tests. As illustrated in Figure 4(a), during the passive or active-assisted training, the resulting haptic positioning forces are exerted as an aid to the patient to follow the reference trajectory towards the target position. For the active exercise, the generated force field is applied to the patient movement by pushing the EE towards the opposite side of the current target object  $T$  [26] (Figure 4(b)). The resulting resistance force is generated by

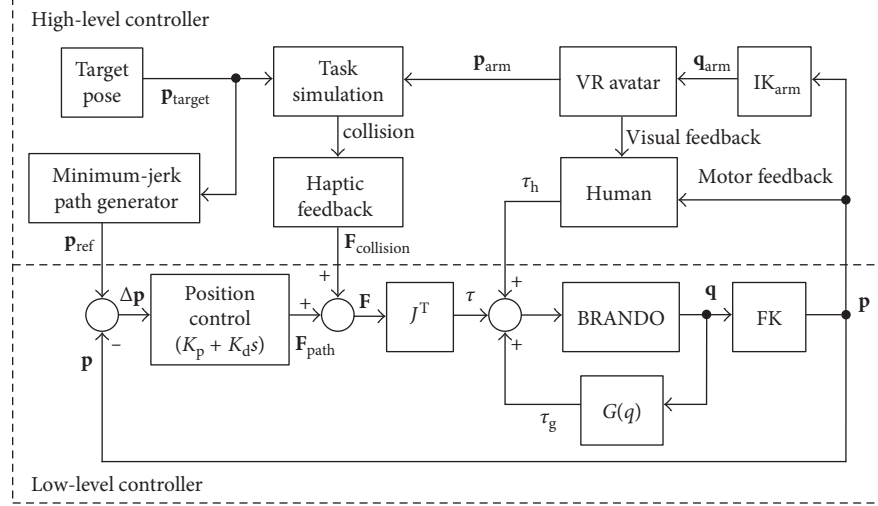


FIGURE 3: Control architecture for the task simulation through the patient’s movements.  $G(q)$  is the gravity model to compute the gravity compensation torque; FK is the direct kinematics block; IK<sub>arm</sub> is the inverse kinematics algorithm of the patient arm.  $\tau$  and  $\tau_g$  are the torque supplied by the motors given the control position and gravity compensation, respectively.

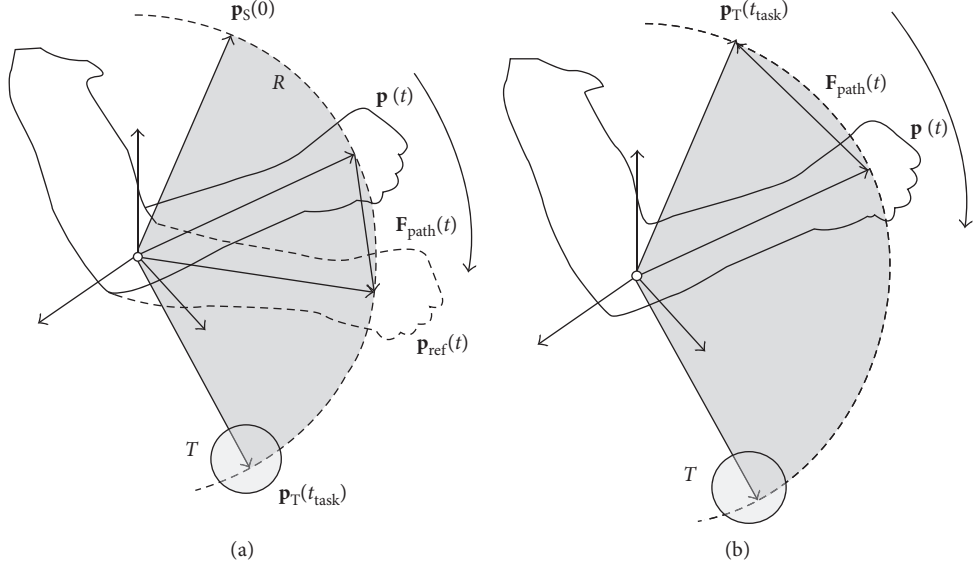


FIGURE 4: Force feedback scheme to the patient during the execution of elbow joint movements. (a) The assisted mode is activated during passive or active-assisted exercising by aiding the patient to follow a trajectory from the starting to the target positions, where the target position corresponded to the current target object in the VR scenario. (b) The resistive mode is activated during assisted exercising, pushing the end-effector towards the opposite side of the patient movement.

placing  $\mathbf{p}_T$  at the opposite limit position of the training workspace with respect to T. This solution provided opposite resistive forces to the patient during active training, proportional to the amount of elbow joint excursion.

Finally, for safety reasons, manually locking the end-effector position by the therapist is also possible at any moment, which is useful for recording the motion limits of the patient at the beginning of the session.

**2.4. Virtual Reality Gaming Scenarios.** A software application with VR game scenarios designed explicitly for elbow’s FE and wrist’s PS motion tasks was developed [36]. Two haptic

feedback modes were considered: free PS movements with weight support, while variable force assistance/resistance for FE movements. The software provides the therapist with a user-friendly graphical user interface (GUI) (developed in Python) which allows the therapist to intuitively set the parameters of the current session (speed, the range of movements, and workloads), to select the training modality (passive/active), manually calibrate, and personalise the exercise parameters (Figure 5). After the physiotherapist has chosen the training modality (passive/active) and the game parameters, the system allows him/her to monitor the kinesthesiology patients’ performance (RoM, joint angular velocities, and tolerated haptic force intensities), as well as the

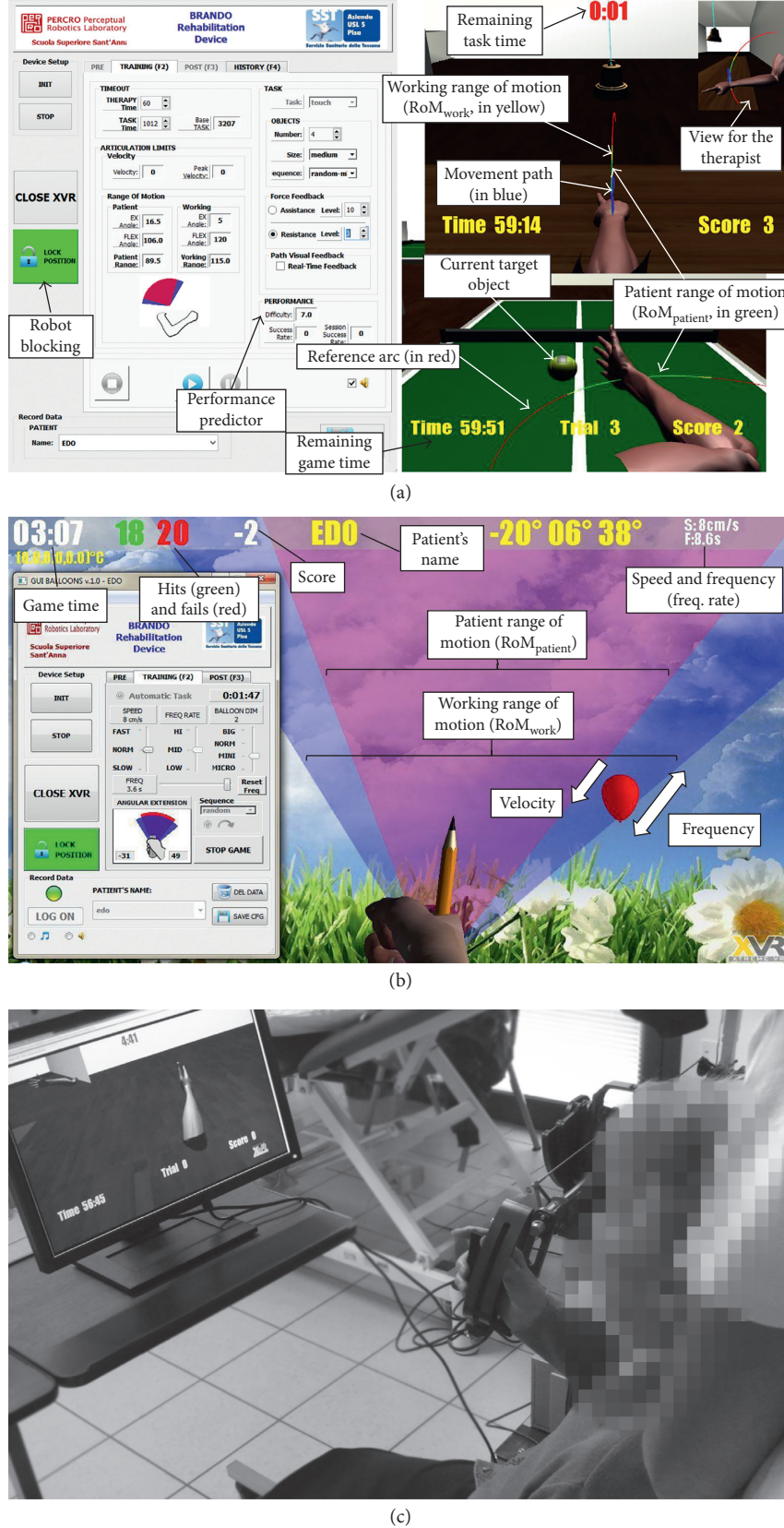


FIGURE 5: Three views of the full system with the Therapist GUI console and the gaming scenarios with different implemented tasks for the training. (a) FE movements; (b) PS movements; (c) a patient performing with the system.

TABLE 1: Design specification of the simulated tasks to perform during training exercises.

Exercise	Scenario	Upper arm posture	Movement	Joint motion	Virtual task
1	Bells	Adducted	Upward/downward	FE	Ring
2	Balls	Abducted	Lateral/medial	FE	Hit
3	Balloons	Adducted	Internal/external	PS	Burst

patients' achievements regarding game exercises (score, time for completing the task, and the achieved difficulty level). At the end of each session, it could be possible also to generate a report with graphs and statistics corresponding to the patients' evolution (knowledge of performance).

**2.4.1. Session Calibration.** The session starts with the evaluation of the current motion capacity of the patient. First, the patient is sitting in the correct posture in front of the screen, as explained in Section 2.2. Second, the therapist sets up the lengths of the patient's upper limb and calibrates the training movements. For FE, the calibration is defined by  $\mathbf{M}(q_4^{\text{EX}}, q_4^{\text{FLEX}}, \bar{q}_4, \dot{q}_4^{\text{peak}}, t_{\text{base}}, K_p^{\text{EX}}, K_p^{\text{FLEX}}, F^{\text{EX}}, F^{\text{FLEX}})_{\text{patient}}$ , where  $q_4^{\text{EX}}$  and  $q_4^{\text{FLEX}}$  are the maximum extension and flexion angles of the elbow,  $\bar{q}_4$  and  $\dot{q}_4^{\text{peak}}$  are the mean and peak angular velocities,  $t_{\text{base}}$  is the amount of time for performing movements within  $\text{RoM}_{\text{patient}} = [q_4^{\text{EX}}, q_4^{\text{FLEX}}]$ , and  $F^{\text{EX}}$  and  $F^{\text{FLEX}}$  are the tolerated interacting force amplitudes that the robot will exert during the training. The therapist manually adjusts the gains  $K_p^{\text{EX}}$  and  $K_p^{\text{FLEX}}$  of the PD controller, in a way that the observed  $\dot{q}_4$  relies on the range  $[\bar{q}_4, \dot{q}_4^{\text{peak}}]$ . For security,  $K_p^{\text{EX}}$  and  $K_p^{\text{FLEX}}$  are constrained to be incrementally tuned up by iteratively testing the force step by step within a range of  $[0, 0.2n]\text{Nm/rad}$ , where  $n = 1 \dots 10$  is the applied  $n$ -test by the therapist on the GUI.

For PS, the calibration is defined by  $\mathbf{M}(q_5^{\text{PRON}}, q_5^{\text{SUP}}, \bar{q}_5, \dot{q}_5^{\text{peak}})_{\text{patient}}$ , where  $q_5^{\text{PRON}}$  and  $q_5^{\text{SUP}}$  are the angular limits of the pronation and supination movements, and  $\bar{q}_5$  and  $\dot{q}_5^{\text{peak}}$  are the mean and peak angular velocities of the wrist during PS.

**2.4.2. VR Games for Motion Recovery.** Three kinds of movements commonly used in manual therapies were selected: (1) FE with the upper arm adducted (*exercise 1*); (2) FE with the upper arm abducted (*exercise 2*); and (3) PS with the arm adducted (*exercise 3*). Correspondingly, three different VR exergaming scenarios were created (Figure 5). The scenarios simulate different virtual tasks to complete through repetitive movements (Table 1). A scene for touching and ringing a bell with the index finger is for *exercise 1* (scenario *Bells*; Figure 5(a)). A scenario for hitting a tennis ball on a table is for *exercise 2* (scenario *Balls*; Figure 5(a)). A scenario for *exercise 3* is avoiding collisions with balloons gradually getting closer to the virtual hand by bursting them by orienting the pointer through wrist PS movements (scenario *Balloons*; Figure 5(b)).

With the aim to motivate the patient to perform challenging movements and to sustain his/her attention and interest, the difficulty level of the training may increment over the sessions. At the end of the session, the therapist may assess the observed patient's performance; then, the current

calibration and game parameters may be used as a baseline for the calibration of the next session and for historical comparison of the patient evolution.

For this purpose, the GUI allows the therapist to manually modify the game (Figures 5(a) and 5(b)) and consequently the demanding working load level, at any time during the training. To aid the therapist to systematically individualise the training as a function of the game input parameters, a predictive model of patient performance indicates in the GUI the expected performance score (normalised difficulty level from 0 to 10, as detailed in Section 3.4.2).

For FE movements, the following game parameters define the difficulty of both *Bells* and *Balls* exergames, as illustrated in Figure 5(a):

- (1) The training workspace  $\text{RoM}_{\text{work}}$  within the range of  $[1.0, 1.5]$  times the current patient  $\text{RoM}_{\text{patient}}$
- (2) The virtual object's size
- (3) The timeout ( $t_{\text{task}}$ ) for completing the task by scaling  $[0.5, 1.5]$  the registered  $t_{\text{base}}$  value
- (4) The number of positions of objects within  $\text{RoM}_{\text{work}}$
- (5) The sequence of appearance of objects at a random position (*random sequence*) or at an arbitrary location in alternate sequences of the extension and flexion (*random mirror sequence*)
- (6) The exerted haptic forces  $\text{Force}_{\text{work}}$  by scaling the impedance gain  $K_p$  proportionally to the calibrated gains ( $K_p^{\text{EX}}$  or  $K_p^{\text{FLEX}}$  for extension and flexion, resp.), within a range of  $[0, 1]$  for the assistance feedback and  $[0, 0.5]$  for the resistive one

For PS movements, the difficulty parameters of *Balloons* game are the following, as illustrated in Figure 5(b):

- (1) The game workspace  $\text{RoM}_{\text{work}}$  beyond  $\text{RoM}_{\text{patient}}$ .
- (2) The speed and size of the balloons.
- (3) The sequence of appearance of balloons in an *ordered sequence*, at *random* within  $\text{RoM}_{\text{patient}}$  or farther within the lateral cones defined by the intersection  $\text{RoM}_{\text{work}} \cap \text{RoM}_{\text{patient}}$ .
- (4) The frequency rate of the balloons progressively rises as the number score of the patient increases.

Figure 5(c) shows a patient performing a rehabilitation session with the BRANDO system while receiving supervision of a physiotherapist.

### 3. Experimental Assessment of System Feasibility and Performance

**3.1. Objectives of the Study.** The objective of the study was to bear out the suitability of the system to be used as an aided

TABLE 2: Clinical characteristics of the patients' population of the pilot study.

Patient	Gender	Age	Fracture injury	Injury treatment	Flex (deg)	Ext (deg)	FE RoM (deg)	Pron (deg)	Sup (deg)	PS RoM (deg)	JAMAR test	VAS test	DASH test
P1	M	24	Humerus, radius and ulna	Operative with internal fixation	138	36	102	78	48	109	14	2	71.33
P2	W	87	Humerus, radius and ulna	Operative with internal fixation	135	40	95	22	87	126	0	1	54.33
P3	M	66	Radius, capitate	Nonoperative with a fixed splint	115	10	105	26	95	121	16	4	63.33
P4	W	35	Humerus, radius and ulna	Operative with internal fixation	100	-5	105	70	40	110	0	5	53.33
P5	W	22	Distal epifisi, radius, ulnar styloid, scaphoid	Operative with internal fixation	128	31	97	80	30	110	15	6	47.41
P6	M	42	Humerus	Operative for removal of internal fixation	90	-5	95	78	55	133	48	6	49.17
P7	M	45	Humerus, radius and ulna	Operative with internal fixation	124	12	112	52	55	107	36	7	50
P8	W	60	Epifisi, radius, ulnar styloid, scaphoid	Nonoperative with a fixed splint	—	—	—	68	56	124	5	5	67.50
P9	M	58	Capitate	Nonoperative with a fixed splint	—	—	—	52	57	109	0	5	77.67
P10	M	33	Radius, capitate	Operative with internal fixation	—	—	—	62	75	137	20	2	48.5

method for orthopaedic physiotherapy of the forearm involving both PS and FE joint movements. To this aim, we investigated the following three aspects:

- (1) The capability of the system to assign different levels of physiotherapy exercises of the forearm, involving both PS and FE joint movements; thus, to elucidate whether, despite the variable working loads, the training remained under controlled and moderate motion conditions according to the current clinical condition of the patient, to avoid any harmful movement, as a fundamental requirement in orthopaedic rehabilitation.
- (2) The effects of the variable difficulty training conditions on the kinesiologic patient's performance (demanding incremental movements regarding higher ranges of motion, opposite force resistance, and speed) and its possible relationship with their current clinical condition; then, to design a new predictive model of the patient's progress, as a tool for the therapist for individualising the training intensity.
- (3) The evaluation and acceptance of the system by patients.

For these purposes, the experimental procedure was separated into two parts: (i) a preliminary evaluation of the functionality of the system in healthy subjects and (ii) a pilot study with patients undergoing manual physiotherapy due to forearm lesions.

**3.2. Recruitment and Patient Population.** Two healthy volunteers and ten patients (six males and four females;  $47.20 \pm 20.47$  years old) were recruited at the USL 5 Rehabilitation

Centre at Fornacette (Pisa), Italy. Nine performed PS training, while seven performed both PS and FE movements. All patients received a medical indication of the following traditional rehabilitation physiotherapy of the forearm due to fracture(s) at the elbow or wrist joints and after at least a period of 7 to 10 days after the splint withdrawal. None presented fragments instability, severe pain sensation, kinaesthetic or tactile sensorial disorders in the upper limb, or cognitive impairment. The subjects were informed regarding the aspects of the study and signed their informed consent before the experimental sessions. The study was reviewed by the local ethics committee.

All patients underwent a battery of clinical assessments: (i) the ranges of motion with extendable goniometers and following standard procedures [7], (ii) the strength of the affected hand by the Jamar strength test [48], and (iii) the pain sensation using the VAS pain test (Visual Analogue Scale for the pain test) [49]. The musculoskeletal ability to perform activities of daily life applying the Italian version of the DASH Questionnaire (Disabilities of the Arm Shoulder and Hand Questionnaire) normalised to a scale from 0 to 100 where the zero score means no impairment and proper functionality, while 100 means severe impairment and limited functionality [50]. The patients presented reduction of mobility at the limits of functional FE RoM ( $90.17 \pm 23.08^\circ$ , with  $104.25 \pm 28.89^\circ$  of flexion below a functional range of  $130^\circ$  [51] and  $13.83 \pm 18.48^\circ$  of extension) and also at the limits of functional PS RoM ( $118.60 \pm 11.07^\circ$ , with  $58.80 \pm 20.89^\circ$  of pronation and  $59.80 \pm 20.27^\circ$  of supination), presented a small registered hand strength of  $15.40 \pm 16.09$  kg, reported mild pain sensation of  $4.3 \pm 2.0$ , and self-perceived disability of  $59.46 \pm 10.79\%$  according to the DASH score. Table 2 shows the clinical characteristics of the patient population.

**3.3. Preliminary Evaluation in Healthy Subjects.** With the first aim of evaluating the functionality of the system, we recruited two healthy volunteers for testing the system before the evaluation in patients. We were particularly interested in studying the capability of the system for assigning incremental working profiles at moderate loads, under safe conditions at any moment and without overloading the patients.

We analysed their muscular activity to verify the effectiveness of the system in assigning different working loads in a training session under similar conditions, as for patients.

The subjects were invited to perform 45 minutes of training with the *Bells* game. Three motion velocities (low, medium, and high), under three haptic feedback modalities, were applied: zero force (ZF), assistance force (AF), and resistance force (RF) feedback. Two different force intensities were used for AF and RF, for a total of 15 working load combinations: 3 velocities  $x$  (2 AF + 2 RF + 1 ZF). The velocity levels for FE were 80°/s (low), 110°/s (medium), and 190°/s (high) (corresponding to movements within an RoM of 125° in time periods of 1.5 s, 0.9 s, and 0.65 s, resp.). The force feedback consisted of estimated mean values of 2.73 N (medium) and 5 N (high) for AF, while 1.8 N (medium) and 2.5 N (high) for RF. The ZF + medium velocity condition corresponded to natural movements during the calibration at the beginning of the session.

The muscular activation was monitored through surface electromyography (sEMG) by seven pairs of surface electrodes placed on two muscles of the subjects' upper limb: the biceps brachii (BB) and triceps brachii long head (TBL). SENIAM recommendations were followed for sensor positioning and the skin preparation (<http://www.seniam.org>) [52]. Ag/AgCl foam pregelled electrodes with a diameter of 24 mm were used with an interelectrode distance set to 20 mm for each bipolar derivation. The ground and the reference electrodes for all bipolar derivations were positioned at the elbow. All electrodes were connected to an amplifier (g.USBamp amplifier; <http://www.gtec.at/>) and digitally converted (1200 Hz sample frequency, 12-bit resolution). We preprocessed the envelopes of the activation signals for analysing isolated movements, as follows.

A band-pass filter was applied (5–500 Hz bandwidth), followed by high-pass filtering (cutoff frequency of 20 Hz), full-wave rectification, and low-pass filtering (1 Hz cutoff frequency). Then, the signals were divided into epochs using the maximum peak of the recorded FE elbow angle as a reference trigger and resampled using a cubic spline interpolation. Figure 6 shows the average muscle profiles of a healthy volunteer under the different tested conditions.

**3.4. Pilot Tests in Patients.** To verify the suitability of the system to be used as an aided method for orthopaedic physiotherapy of the forearm, we carried out a second experiment with patients. The tests were done to confirm the capability of the system for providing controlled and moderate motion tasks with patients, after the preliminary evaluation with two healthy volunteers. To this purpose, first, we analysed the kinesiologic patient's performance and the relationship of the variable difficulty training levels with the current patient clinical conditions according to the standard

clinical outcomes (JAMAR, VAS, and DASH tests). We were also interested in two other issues: (i) the possibility of introducing a new predictive metric of performance as a critical tool for guiding the recovery by the therapist and (ii) assessing the system and verifying its acceptance by patients.

**3.4.1. Experimental Session.** The tests lasted 30 minutes of exercising divided into three parts, with two pauses of 2 minutes for resting, for a total of 45 minutes per session, including the initial calibration phase. For practicality, for FE movements, all tested the *Bells* game because it did not require the external support of the arm.

Before starting the session, the patient was assisted to sit down in the correct posture. Next, we evaluated the current motion capability (RoM, velocity, and force) of the patient and then calibrated the starting difficulty level of the game. The difficulty was progressively adjusted by the hand during the session, always within safe tolerances. In other words, with the aim of preventing any manual error by the therapist, the system constrained the game parameters to ranges that matched from half to the full current capacity of the patient according to the calibration. In particular, for FE, completion task time  $t_{\text{task}}$  was constrained up to  $2t_{\text{base}}$ , maximum force intensity up to half of the tolerated force intensity (through the impedance gain  $K_p$  up to  $1/2K_p^{\text{EX}}$  or  $1/2K_p^{\text{FLEX}}$ ), and  $\text{RoM}_{\text{work}}$  up to 1.2  $\text{RoM}_{\text{patient}}$ . For PS,  $\text{RoM}_{\text{work}}$  was constrained up to 1.2  $\text{RoM}_{\text{patient}}$ . Then, patients were invited to perform and were kindly instructed to concentrate and to express if they felt pain or discomfort during the exercising.

**3.4.2. Predictive Model of Patient Performance.** With the aim of aiding the therapist to manually individualise the physiotherapy by systematically incrementing the training demand levels, we implemented a model of the *performance* of the patients. For this purpose, a principal component analysis (PCA) was applied to the observed kinesiology information of patients. The model resulted in the linear combination of a performed range of motion, velocity, and tolerated exerted resistive force by the system ( $\text{RoM}_{\text{performed}}$ ,  $\text{Velocity}_{\text{performed}}$ , and  $\text{Force}_{\text{performed}}$ ) for FE, while  $\text{RoM}_{\text{performed}}$  and  $\text{Velocity}_{\text{performed}}$  for PS. Then, for providing a prior estimation of *performance*, predictive regression models of normalised outcomes of  $\text{RoM}^*$  and  $\text{Velocity}^*$  for FE and PS and  $\text{Force}^*$  for FE were developed, all regarding game input parameters, as follows:

$$\text{Outcome} = b_o + \sum_{i=1}^p b_i x_i + \sum_{j,k} b_{jk} x_j x_k, \quad (4)$$

where  $x_i$  is the  $i$ th input parameter among the  $p$  significant input variables (significant main factors) for the corresponding outcome,  $x_j$  and  $x_k$  correspond to significant interacting factors, and  $b_n$  are constant values. Significant main factors and interactions over outcomes ( $\text{RoM}_{\text{performed}}$ ,  $\text{Velocity}_{\text{performed}}$ , and  $\text{Force}_{\text{performed}}$ ) were identified through a series of multifactorial ANOVAs (MANOVAs). The MANOVA series followed a design of 3 target sequences  $\times$  3 levels of  $t_{\text{task}}$   $\times$  3 levels of  $\text{RoM}_{\text{work}}$   $\times$  3 levels of  $\text{Force}_{\text{work}}$  for

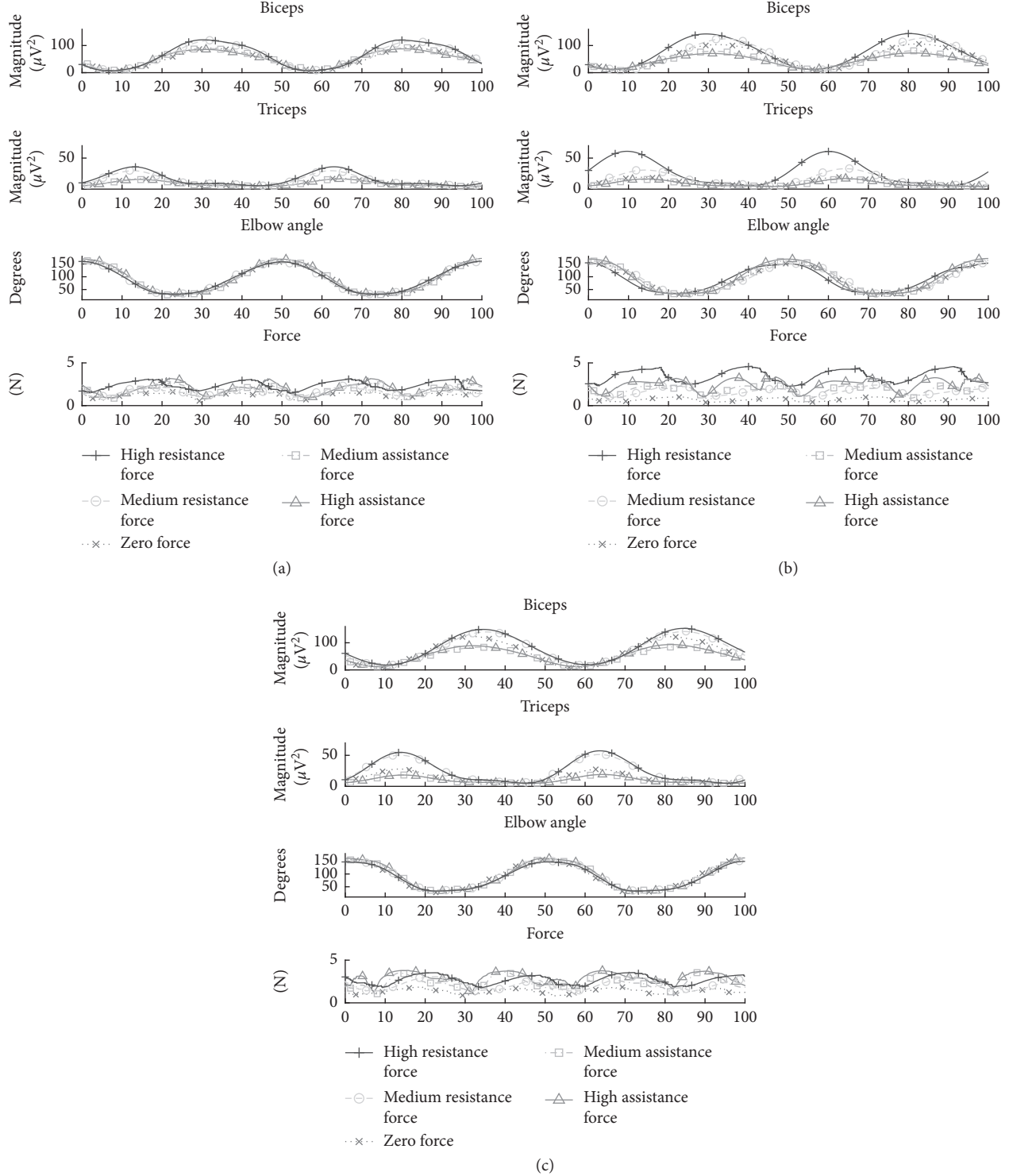


FIGURE 6: Postprocessed sEMG signals of the monitored muscular activity from the BB and TBL muscles of a healthy subject. The curves represent the median activations of different working load profiles of 3 force levels (resistance, zero or no force, assistance)  $\times$  3 movement's speed levels: (a) low, (b) medium, and (c) high.

FE movements, while  $2 \text{ sequences} \times 3 \text{ RoM}_{\text{work}} \times 3 \text{ balls' number} \times 3 \text{ balls' speed} \times 3 \text{ balls' frequency}$  for PS movements.

Finally, optimisation of the regression models was carried out over the training data set of 7 patients for PS and six patients for FE, while we used the data of 2 patients for PS and one patient for FE for model comparison and validation.

**3.4.3. System Acceptance Evaluation.** We applied an ad hoc designed questionnaire with eight items, all rated on a 7-point Likert scale (where 1 was the minimum, 7 the maximum, and 4 the neutral scores), for qualifying diverse perceived aspects regarding the confidence and acceptability of the system (Table 3). Six items assessed the usability and

TABLE 3: Self-rated questionnaire for assessing the acceptance of the system and the experience of the patient during the robotic session.

Item	Assessment	Statement	Tag
Q1	Acceptance	How much you consider that the session was enjoyable and engaging?	Enjoy
Q2	Acceptance	How much difficult seemed to you the game?	Difficult
Q3	Acceptance	How much you consider your level of fatigue after the session?	Fatigue
Q4	Acceptance	How much attention did you pay during the execution of the game?	Attention
Q5	Acceptance	How much you consider your level of pain after the session?	Pain
Q6	Acceptance	How much you consider your level of annoyance during the session?	Annoyance
Q7	Embodiment sensation	Sometimes I felt that the virtual arm was my own arm.	Ownership
Q8	Embodiment sensation	The movements of the virtual hand and arm were caused by my movements.	Agency

acceptance of the system: (1) How much the patients perceived it enjoyable (*enjoy*)? (2) How much difficult it was (*difficult*)? (3) How much exhausting they felt (*fatigue*)? (4) How much attention they paid (*attention*)? (5) How much physical pain patients felt in the affected limb during the exercises (*pain*)? (6) How much annoyed they felt during the exercises (*annoyance*)? Two extra items evaluated the embodiment sensation during the sessions [45, 53], regarding two sensations: (1) the sense of *ownership*, which means how much they perceived that the virtual avatar was their own limb, and (2) the sense of *agency* that indicates how much they recognised that the movements and actions of the virtual avatar were caused by their own actions.

## 4. Results

**4.1. Preliminary Evaluation in Healthy Subjects.** Different activation levels were observed for both BB and TBL (Figure 6), being the biggest motor activation of arm muscles associated with the movements performed under resistance forces, following by free movements (zero force) and those with the lowest level of assistance forces. We also observed decreasing motor activations from high to medium and from medium to low velocity movements. The increments in motor activation were due to dynamic isometric contractions during voluntary active movements under assistance or resistance forces and revealed by the increase of the amplitude of the sEMG [54]. A repeated measures ANOVA (SPSS 15 statistical package) according to 3 forces  $\times$  3 velocity conditions over mean amplitudes of the signal envelopes (Figure 7) revealed main factor effects for both force ( $F(2, 10) = 97.069, p < 0.05$ ) and velocity ( $F(2, 10) = 26.872, p < 0.05$ ) and a significant interaction ( $F(4, 20) = 12.222, p < 0.05$ ) for BB, and similarly for force ( $F(2, 10) = 606.725, p < 0.05$ ) and velocity ( $F(2, 10) = 24.106, p < 0.05$ ) and a significant interaction ( $F(4, 20) = 16.037, p < 0.05$ ) for TBL, which confirmed the recruitment of higher motor units as the system increments the required resistance force and velocity of movements, as expected. No significant changes in the mean frequency of the signals were observed, which indicates variable muscular working load at the arm while flexing and extending the elbow

with the system but without overloading it until excessive muscle fatigue [55].

**4.2. Pilot Tests in Patients.** For assessing the capability of the system for estimating the range of motion of the patients' movements, a comparative analysis was carried out between the standard clinical RoM outcome manually estimated by the therapist with the manual goniometer (Table 2) and the online estimation performed by the system (RoM<sub>patient</sub>) during the calibration step at the beginning of the session (Table 4).

For FE RoM, an underestimation was observed, from a mean clinical RoM of  $101.57 \pm 6.32^\circ$  for the seven patients performing FE training, in comparison to the mean calibrated RoM<sub>patient</sub> =  $92 \pm 10.63^\circ$ . An error of  $11.66 \pm 10.69\%$  was observed between both measures, with a medium value of the Pearson correlation of  $r = -0.278$ , but not still significant given the small sample size. For PS, a mean clinical RoM of  $118.60 \pm 11.067^\circ$  was observed among patients, while a mean calibrated RoM<sub>patient</sub> =  $117.90 \pm 10.59^\circ$  was observed with an error of  $5.66 \pm 6.64\%$  and a high value of the Pearson correlation of  $r = 0.520$  but again not still significant.

An interpretation of the observed errors is that the estimation of RoM<sub>patient</sub> during the calibration phase of the training session is consistent with the clinical observation and valuable for personalising the level of the working load difficulty of the training and the scoring of the estimated performance as a function of real-time kinaesthetic information. However, on the contrary, the RoM<sub>patient</sub> estimation must not be considered as a valid clinical measure that may replace the current standard manual method.

During the experiments, we incremented the difficulty levels from the observed motion capacity of the patients after the calibration phase. The increments included force resistance levels and working range of motion, decrements in the task's time, increasing number of targets, and different sequences of targets' position. Patients were invited to test the system just one session, so we expected that, at first sight, patients would probably perceive the system with suspiciousness. For this reason, the game parameters were manually adjusted to maintain the achieved game score as

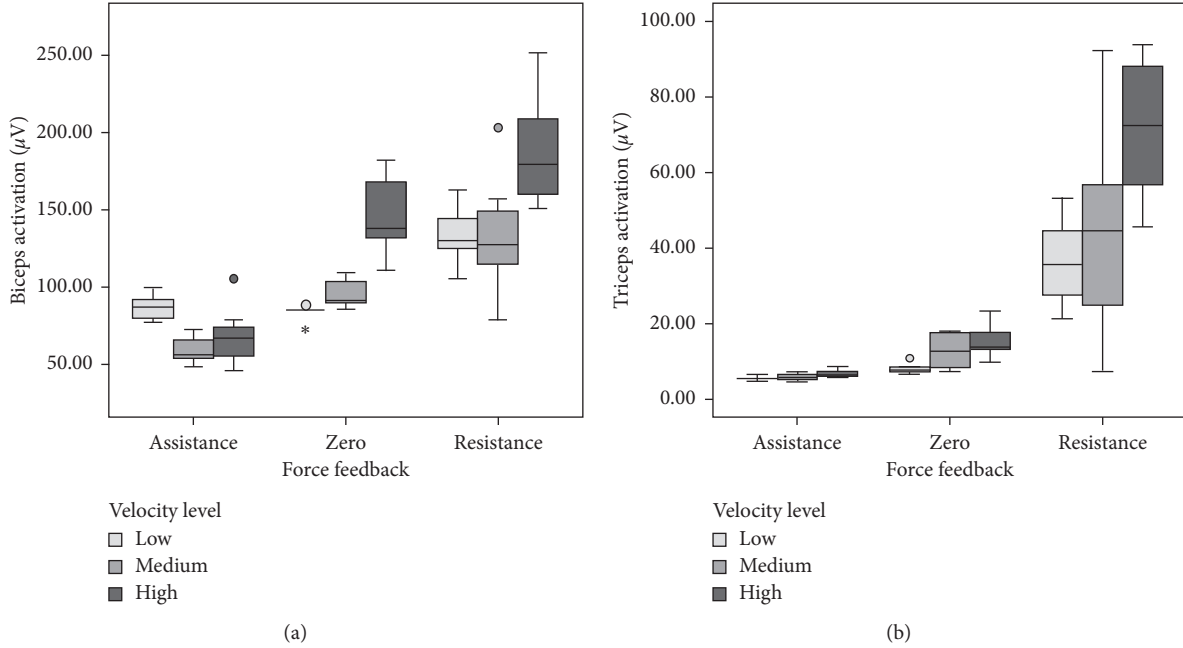


FIGURE 7: Observed amplitudes of the postprocessed muscular activation signals of the isolated flexion/extension elbow's movements for the 3 force × 3 velocity conditions. Main effect factors and significant interactions for force and velocity on both BB (a) and TBL (b) muscles.

TABLE 4: Observed patients' performance during the game tests.

Patient	Working FE RoM (deg)	Performed FE RoM (deg)	FE velocity (deg/s)	FE load (kg)	FE game score (0–100)	Working PS RoM (deg)	Performed PS RoM (deg)	PS velocity (deg/s)	PS game score (0–100)
P1	73 ± 13	101 ± 6	79.22 ± 22.1	0.27 ± 0.14	88.15 ± 15.5	104 ± 13	78 ± 13	46.80 ± 20.90	77.05 ± 0.24
P2	99 ± 15	91 ± 6	86.14 ± 28.44	0.19 ± 0.16	93.40 ± 7.2	123 ± 12	98 ± 13	87.11 ± 44.17	96.50 ± 0.05
P3	81 ± 22	83 ± 16	66.91 ± 13.57	0.29 ± 0.19	64.30 ± 5.3	113 ± 11	83 ± 12	89.14 ± 53.13	87.12 ± 0.07
P4	99 ± 16	101 ± 6	86.14 ± 28.44	0.19 ± 0.16	93.40 ± 7.2	129 ± 11	111 ± 9	85.56 ± 51.01	94.49 ± 0.09
P5	97 ± 14	91 ± 3	112 ± 45.18	0.44 ± 0.11	81.73 ± 11.3	121 ± 23	99 ± 20	53.79 ± 21.88	93.71 ± 0.067
P6	100 ± 4	84 ± 8	88.32 ± 50.92	0.29 ± 0.14	85.29 ± 15.2	112 ± 14	85 ± 2	78.71 ± 27.90	87.63 ± 0.10
P7	95.17 ± 9.38	87.43 ± 18.5	67.10 ± 14.27	0.175 ± 0.04	88.94 ± 15.8	—	—	—	—
P8						123 ± 6	98 ± 5	54 ± 22	93.71 ± 0.067
P9						123 ± 11	94 ± 11	79 ± 28	87.63 ± 0.1
P10						136 ± 8	112 ± 13	44 ± 22	97.19 ± 4.33

high as possible while keeping safe movements' conditions, which resulted in the observed performance in Table 4.

We carried out a correlation analysis between the observed kinetic information of patients during the training and the outcomes of current clinical assessment (JAMAR, VAS, and DASH scores) to elucidate any possible relationship between the patient's clinical condition and the difficulty game conditions.

First, the patient strength given the JAMAR score was found to be negatively correlated ( $r = -0.615$ ) with the mean executed RoM during the game (*performed FE RoM*; Table 4). The contrary was less correlated with the mean

working load (*FE load*,  $r = 0.126$ ) and velocity of movements (*FE velocity*,  $r = -0.172$ ). These correlations can be explained by the fact that even though the achievable range of motion could infer muscular weakness, muscular weakness is not ultimately expressed in the dynamic components of movements (loads and velocity) since for safety requirements, the working loads were calibrated for assuring moderate levels of motion. A moderate negative correlation ( $r = -0.369$ ) between the pain sensation (VAS score) and the performed RoM during FE training (*Performed FE RoM*) indicates that the patients who reported higher pain sensation were more cautious of performing painful

TABLE 5: Results from PCA over observed kinesiology outcomes explaining the first and second components, around 65% and 30% of the variance and defining the *performance* equation as a linear combination of kinesiology information.

Outcome	PC <sub>1</sub>	PC <sub>2</sub>	Performance equation
<i>Flexion/Extension</i>			
RoM <sub>performed</sub>	0.285	0.4424	
Velocity <sub>performed</sub>	0.618	0.5929	Performance <sub>FE</sub> = 0.6238PC <sub>1</sub> + 0.2957PC <sub>2</sub>
Force <sub>performed</sub>	0.7323	0.6729	
<i>Pronation/supination</i>			
RoM <sub>performed</sub>	0.4899	-0.8718	
Velocity <sub>performed</sub>	0.8718	0.4899	Performance <sub>PS</sub> = 0.6844PC <sub>1</sub> + 0.3156PC <sub>2</sub>

TABLE 6: Regression models for predicting kinesiology information of the achieved range of motion, the velocity of movements, and exerted opposing forces, as a function of difficulty input parameters.

Movement	Regression predictive model	No significant effect for the model ( $p > 0.05$ )
FE	RoM* performed = $b_0 + b_1 * \text{RoM}_{\text{work}}$	$t_{\text{task}} * \text{RoM}_{\text{work}}$
FE	Velocity* performed = $b_0 + b_1 * t_{\text{task}} + b_2 * \text{RoM}_{\text{work}}$	—
FE	Force* performed = $b_0 + b_1 * \text{Force}_{\text{work}} + b_2 * t_{\text{task}} * \text{RoM}_{\text{work}}$	$t_{\text{task}}$
PS	RoM* performed = $b_0 + b_1 * \text{RoM}_{\text{work}}$	—
PS	Velocity* performed = $b_0 + b_1 * \text{sequence} + b_2 * \text{balls}_{\text{speed}} + b_3 * \text{sequence} * \text{balls}_{\text{speed}} + b_4 * \text{RoM}_{\text{work}} * \text{balls}_{\text{frequency}}$	$\text{balls}_{\text{frequency}}$ $\text{sequence} * \text{balls}_{\text{number}}$

movements, and thus, they performed smaller RoM. The small correlations found between VAS scores with both working loads (*FE load*) and velocity of movements (*FE velocity*) confirm that the rehabilitation sessions were carried out at moderate dynamic levels.

Regarding the relationship of the self-perception of the ability to perform daily-life activities through the DASH score, we found a positive correlation with the *performed FE RoM* ( $r = 0.417$ ) and a negative correlation with *FE load* ( $r = -0.468$ ). Both correlations highlight that the kinesiological performance of patients was lower in those patients showing higher current disabilities than in patients with less daily-life difficulties, as occurred with patients P3, P5, and P7 who suffered from injuries affecting elbow FE. It is important to notice that patient P1 expressed a high pain sensation in the VAS test but did not show difficulties in *performed FE RoM* because of the primary suffering that was in PS instead of FE movements.

Regarding the PS movements, negative correlations were found between *performed PS RoM* with the DASH score ( $-0.439$ ) and with the JAMAR score ( $r = -0.372$ ). An explanation to the observed correlations is the fact that the higher the level of impairment, the more the difficulty to perform the rehabilitation exercise involving PS movements.

In general, the working RoM<sub>work</sub> was set to be slightly higher than the patient's one (measured during the system calibration). Consequently, the speed of the objects on the screen was set for resulting in mild slow motions (FE and PS velocities) within the performed RoM. For FE, the adaptive loads assigned from zero up to 0.5 kg were well tolerated by the patients. A necessary clarification at this point is that working load for patients remained under the same range applied to healthy volunteers, as can be observed in the force feedback profiles in Figure 6 (with values up to 5 N, equivalent to 0.5 kg loads).

During all the tests, we did not observe any unexpected event that may cause risk to the patients. Moreover, all patients remained calm during the sessions and did not perceive or express any threat due to the system.

Then, with the aim of modelling the kinematic performance score, a PCA was implemented over the training data sets of six patients for FE and seven patients for PS to perform dimension reduction of the data and obtain a metric of *performance* as a linear combination of the normalised values of the observed RoM<sub>performed</sub>, Velocity<sub>performed</sub>, and Force<sub>performed</sub>. Table 5 shows the coefficient values of the two principal components: for FE, the first and second components explain 62.38% and 29.57% of the variance, respectively, while for PS, the first and second components explain 68.44% and 31.56% of the variance, resulting in the *performance* equations in Table 5.

Then, for FE movements, the series of MANOVAs over outcomes revealed significant main factor effects of RoM<sub>work</sub> ( $p < 0.0001$ ) and a significant interaction of  $t_{\text{task}} * \text{RoM}_{\text{work}}$  ( $p < 0.007$ ) for the observed RoM<sub>performed</sub>. For the observed Velocity<sub>performed</sub>, main factors were found for  $t_{\text{task}}$  and RoM<sub>work</sub> ( $p < 0.0001$ ) with no significant interaction. For the observed Force<sub>performed</sub>, main factors were found for  $t_{\text{task}}$  ( $p = 0.05$ ), Force<sub>work</sub> ( $p < 0.0001$ ), and a significant interaction of  $t_{\text{task}} * \text{Force}_{\text{work}}$  ( $p < 0.0001$ ). On the contrary, for PS movements, main factor effects of RoM<sub>work</sub> ( $p < 0.0001$ ) for RoM<sub>performed</sub> were revealed; for Velocity<sub>performed</sub>, main factor effects of sequence ( $p < 0.0001$ ), balls<sub>frequency</sub> ( $p < 0.0001$ ), and balls<sub>speed</sub> ( $p < 0.024$ ) and a significant interaction between sequence \* balls<sub>number</sub> ( $p < 0.01$ ), sequence \* balls<sub>speed</sub> ( $p < 0.032$ ), and RoM<sub>work</sub> \* balls<sub>frequency</sub> ( $p = 0.05$ ) were revealed.

Consequently, the predictive regression models given the equations in Table 6 were obtained, as a function of the difficult input parameters estimated over the corresponding training data. The regression models presented a significant

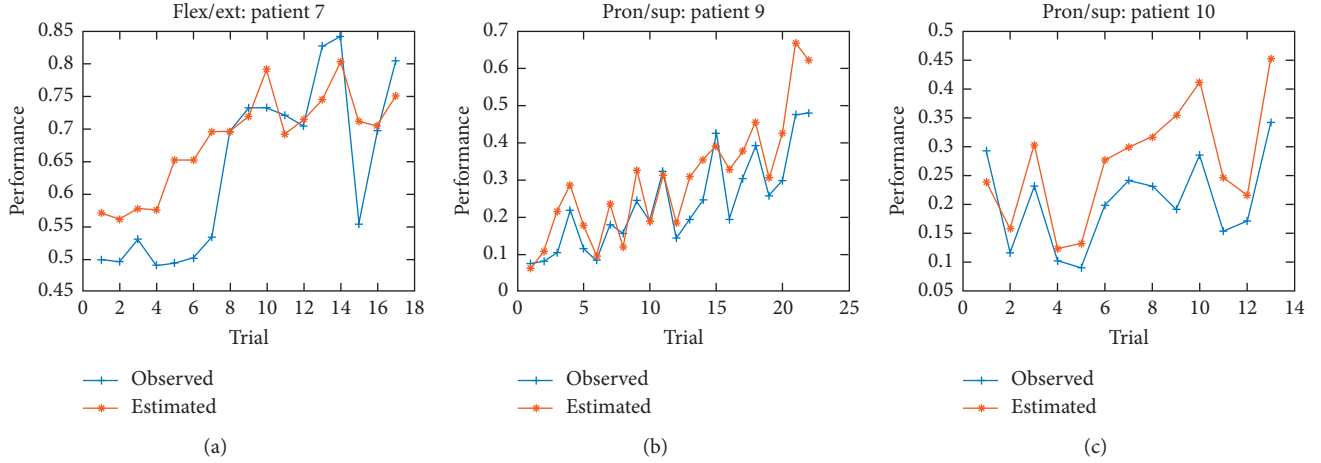


FIGURE 8: Comparison of the performance (from 0 to 1) between the predicted and observed score for the group of three testing patients: (a) patient 7 for FE, and (b) patient 9 and (c) patient 10 for PS movements.

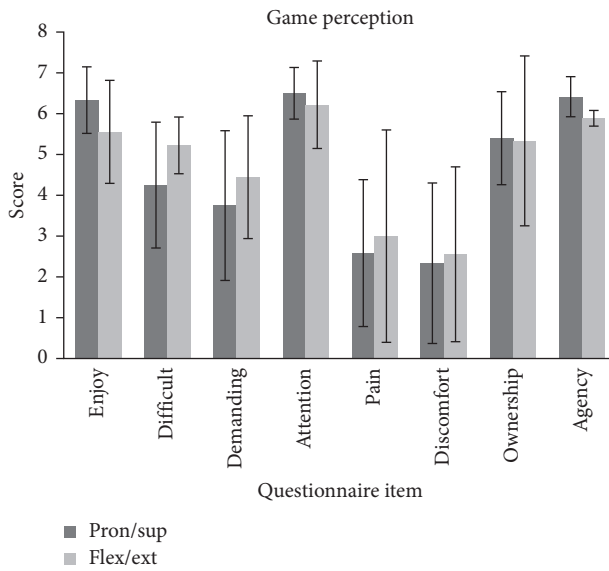


FIGURE 9: Observed values of the self-reported scores of the ad hoc questionnaire for assessing the perception and opinion of the system by the patients. Items *enjoy*, *difficult*, *fatigue*, *attention*, *pain*, and *annoyance* evaluated the confidence and acceptance of the system, while *ownership* and *agency* assessed the embodiment experience during the sessions.

correlation of  $r=0.837$  (the Pearson coefficient) comparing the predicted and observed performance over one patient data for FE and  $r=0.917$  over two patients data for PS. This correlation indicates a good agreement between the estimated performance during the setting up of the difficult training parameters and the observed performance during the training under such parameters, as shown in Figure 8.

Figure 9 shows the observed scores of the self-rated questionnaire for assessing the opinion and experience of the patients about the system. We adopted the criteria of considering a median score  $\geq 5$ , as the indication that the diverse aspects were experienced highly. Patients found the games enjoyable (median of  $6.50 \pm 0.82$  in *enjoy* for PS and

$5.50 \pm 1.26$  for FE). They experienced neutral difficulty ( $4.50 \pm 0.82$  for PS and  $5 \pm 0.69$  for FE in *difficult*) and neutral *fatigue* ( $4.00 \pm 1.97$  for PS and  $4.50 \pm 1.50$  for FE), and the sessions were enough demanding for keeping their *attention* quite high ( $6.75 \pm 0.75$  in *attention* for PS and  $6.50 \pm 1.07$  for FE). Regarding the perceived side effects, most patients expressed feeling some mild *pain* ( $2.00 \pm 2.02$  for PS and  $2.50 \pm 2.60$  for FE) and low *annoyance* ( $1.50 \pm 2.16$  for PS and  $2.50 \pm 2.14$  for FE). High embodiment sensation of the system reflected in the high scores for the *ownership* ( $5.00 \pm 1.29$  for PS and  $5.00 \pm 2.08$  for FE) and *agency* ( $6.25 \pm 0.50$  for PS and  $6 \pm 0.19$  for FE) sensations over the virtual avatar. Finally, at the end of the session, besides the questionnaire, they verbally express their high interest in participating in a more extended clinical study with the system.

## 5. Discussion

The present work has three important aspects: (i) the development for the first time of a robotic-VR-mediated application specific for the orthopaedic rehabilitation of the forearm, (ii) the development of a predictive model of patient performance for aiding the individualisation of the training exercises regarding observed kinesiology information, and (iii) an evaluation of the system by two healthy subjects and a group of patients to study its acceptance and the feasibility of carrying out clinical studies.

The system was specially developed for covering the clinical needs of orthopaedic rehabilitation of injured upper limbs affecting the forearm mobility, similarly as the manual method. Diversely from current neurorehabilitation robotic systems, in this approach, three essential aspects were considered of particular interest in orthopaedics: the recovery of functional range of motion [9, 51], muscular strength, and pain reduction [5, 49]. The system integrates some elements already reported separately for neurorehabilitation, such as resistive [26] and assistive force fields and jerk trajectories [25], but combined and adapted in a new methodology that satisfies the particular needs of isometric passive, active, or active-assistive motion training of single joints. An important

characteristic is that it allows the therapist to assign different training loads, imposing incremental motion tasks starting from small training arcs and mild force loads up to a painless normal range of motion and moderate force loads.

The restoration of functional ranges of motion is constrained by the system to be progressively incremented with small steps, during all the assisted treatment process, in particular for the flexion/extension arc from the current ranges up to a minimum functional range of motion of 100° [51] and for pronation/supination up to a functional range of 50° [9, 51]. In this way, the system guarantees the gradual and careful tuning up of the task motion requirements to the patients. Slight increments in working loads are also possible through small increases in the intensity of the force feedback, but at any moment up to moderate tolerated levels observed during the calibration phase at the beginning of each session. This characteristic is crucial to avoid harmful movements that may result in severe side effects such as destabilisation, inflammation, and oedema or time delay in the rehabilitation process, with the consequent risk of developing joint stiffness and contracture.

In the field of neurorehabilitation, a current trend is the development of adaptive methods for the individualisation training with the aim of the optimisation of neuroplasticity and motor relearning [28, 56, 57]. In the scope of orthopaedic rehabilitation, this would play an essential role in stimulating the patient to perform progressively more challenging movements to promote the motivation and adherence to the treatment and is more important as a crucial tool in modulating the incremental kinesiologic requirements of patients through time. To this aim, the system includes a predictive model of kinesiologic performance which scores the patient evolution as a function of the online range of motion, force feedback intensity, and velocity of movements. This module enables the possibility to manually personalise the difficulty level of the therapy during the game in a systematic quantitative manner. This information is also useful for managing and reporting online and historical data of the patient evolution during the treatment by the therapist.

Regarding the evaluation of the system, the observed increments in amplitude in the sEMG signals of the volunteers showed that the system allows assigning significant different levels of working loads, due to the combination of required strength and velocity. The analysis over the mean amplitude and mean frequency of the sEMG signals confirmed that the different loads effectively demanded different levels of motor unit activations at the arm muscles, but for safety always keeping the activations below muscular fatigue [54, 55].

The observed mean force feedback intensity remained similar for both healthy participants and patients (below the equivalent load of 0.5 kg). Moreover, since the resulting training profiles of the two healthy volunteers corresponded to profiles conceived for patients, we argue that the working load may be modulated safely by the therapist, according to the observed progress of the patient during the treatment. At this point, we also reviewed the relationship of the observed kinesiology metrics and the current clinical outcomes (VAS, JAMAR, and DASH), and due to the observed correlations between metrics and the clinical scores, we may conclude

that the motion tasks were programmed efficiently from mild to moderate demanding.

In fact, the results of the experimental sessions indicate that it is possible to modulate the expected patient performance during the sessions, as a function of kinesiology metrics computed in real time, through the combination of difficulty game parameters. The metrics consider the achieved range of motion, the velocity of movements, and the tolerated opposing forces for the flexion/extension movements, while the range of motion and the velocity of movements for pronation/supination. Moreover, the implemented prediction model of performance shows a good agreement between the estimated scores before and during the training, indicating that it is possible to objectively assign therapeutic levels systematically, which we argue may play an essential role for the individualisation of the therapy and the optimal evolution through the treatment.

The questionnaire for assessing the system revealed that all patients enjoyed playing the games and that the assigned difficulty levels were well balanced and demanded their high attention, which for motor improvement through cognitive activities is crucial. The questionnaires also confirmed that patients felt a mild perception of pain, which is line with the reported scores with the VAS test. Interestingly, patients experienced a high embodiment sensation of the virtual representation of their limb in the scenarios; patients were able to see their forearm, but still perceived the sensation of ownership of the virtual representation of their injured limbs [58]. This fact could be valuable for the incorporation of new proprioceptive exercises and as a biofeedback method that helps the patients to be aware of their current physical limitations, such as abnormal movement synergies, compensatory movements, and limited mobility, among other aspects difficult to perceive at first sight during daily activities. Moreover, this issue could be valuable to design new games more related to daily-life situations, promoting the (re)embodiment of the injured limb in their body schema, especially during the early mobilisation stage.

Patients perceived slightly more difficult the game for FE than for PS movements because they performed free movements for PS with the forearm static, while for FE variable force-resistant movements for placing the hand at different positions in space.

The experimental sessions were designed in the same conditions that would be applied during robotic-assisted physiotherapy sessions. During the tests, we incremented the difficulty levels from the observed motion capacity of the patients after the calibration phase. The increments include force resistance levels and working range of motion risings, decrements in the task's time, increasing number of targets, and different sequences of position targets. No matter the difficulty levels, we did not observe any unexpected event that may cause risk to the patients. Moreover, all patients remained calm during the sessions and did not perceive or express any threat generated by the system, even when experiencing more challenging conditions.

Since the experimental conditions were designed to be applied similarly to sessions during the assisted therapy and we did not observe risk situations during the tests, we are

confident that the system was well accepted. Moreover, we conclude that the system is safe enough to clinically validate it in an interventional study, as a next research step shortly.

However, regarding the estimated ranges of motion of patients with the system at the beginning of the session, we observed an underestimation concerning the standard clinical outcome. A factor that may affect the precision of the inverse kinematic algorithm is that, for computing the joint angles of the upper limb from the wrist position in space, a fixed posture of the shoulder is assumed, so avoiding slight trunk adjustment postures by patients bias the estimation. Additionally, the algorithm also depends on input parameters such as the dimensions of the arm and forearm, so manual errors in such measures may also influence the inaccuracy. Consequently, the range evaluation must be considered as an indicative measure of kinesiologic performance during the training, but not as a valid clinical value. Therefore, it would be desirable to incorporate other technologies such as wearable sensors [59, 60] for the precise assessment of other kinetic aspects such as compensatory movements.

Another limitation is that the current state of the system does not enable the possibility of force feedback during the pronation/supination treatment like other systems conceived for orthopaedic rehabilitation [35–37], which may reduce the chances of shortening the recovery period because of the impossibility to assign variable resistant exercises. By fortune, even if the effects of pronation/supination recovery cannot be neglected for strength recovery, it accounts in less extent than elbow strengthening training [33], so our system can be still a significant tool for aiding the rehabilitation process of the forearm. Since the robot design followed an end-effector based approach, instead of an orthotic one [14], the system is unable to impose strict joint constraints mechanically. So is not feasible for the very first period of the physiotherapy after immobilisation; in this case, not before seven days after the withdrawal of the splint immobiliser. Therefore, even if the system enables the possibility of providing small assistive forces to the patient, we figure out from the experiments that this feature has no practical clinical use. On the contrary, it would be more helpful to provide small-to-moderate resistive forces after the first week of manual mobilisation.

A third limitation is that, for the moment, the kinesiology performance calibration corresponded to pilot tests with patients performing mild exercising, as observed with high games scores (hits versus failures), which would lead to biases in the estimated performance probably below optimal intensities levels. Moreover, since the hits/failure rates in the game may involve cognitive abilities and not necessarily kinesiology performance, it is not still clear if there is a direct correlation between game and kinesiology scores that would lead in mechanisms for balancing the physical and cognitive requirements to patients. So, to optimise both their performance and cognitively demanding tasks (involving attention, perception, the complexity of the game, and motivation, among other), more research in nonlinear predictive modelling is required.

Finally, due to the limited number of patients, the statistical results would be interpreted as preliminary evidence of the feasibility of the proposed methodology, but more

comparative studies are needed with more patients and healthy subjects for confirming the entire validity of the proposal.

## 6. Conclusions

Rehabilitation robotics offers the possibility of new methods of physiotherapy in orthopaedics with patients with musculoskeletal injuries, such bone fractures. As a study case, here we presented a new approach to assisted orthopaedic rehabilitation method of the forearm, involving the elbow and wrist joints. Our proposal combines an end-effector robotic system and a virtual-reality mediated software application with the capability of delivering passive, active, and assisted exercising training of flexion/extension and pronation/supination of injured elbow affecting the forearm. The proposed methodology exploits some existing methods reported separately for neurorehabilitation but integrated within a new framework conceived explicitly for the orthopaedics clinical goal of recovery of functional range of motion, strength, pain reduction, and stiffness prevention.

We studied the possibilities of personalising the exercise's intensity and modify it manually according to the kinesiologic performance of the patient, within safe and moderate controlled online increments during the games, in a more systematic way than traditional manual physiotherapy. The results of our experiments in healthy participants and patients showed that the proposed strategy is suitable. Besides its limitations, the present work contributed to promoting the development of new assisted methods in orthopaedics and further research in this area. We conclude that the proposed approach may have the potential of enhancing the current manual methods, incrementing the hours of therapy per patients and the number of patients simultaneously and reducing the treatment discharge periods.

Future work involves the validation of the system during interventional clinical studies combining manual and assisted sessions some days per week during the whole duration of treatments. Additionally, the developing of other scenarios and the extension of the current system to other musculoskeletal deficits of the upper limb involving other movements would be valuable and may promote the development of new physiotherapy patient-specific methods in the scope of orthopaedic rehabilitation.

## Conflicts of Interest

The authors declare that they have no conflicts of interest.

## Acknowledgments

M. A. Padilla-Castañeda thanks CONACYT Mexico and DGAPA-UNAM (PAPIIT-TA100218) for the financial support received. The authors sincerely acknowledge Samuele Olivieri, Gloria Mazzinghi, and Alessandra Gronchi from USL5/Pisa, Italy, for their helpful criticism and discussion regarding this research and the content of our manuscript.

## References

- [1] Centers for Disease Control and Prevention, *National Ambulatory Medical Care Survey: 2013 State and National Summary Tables*, Centers for Disease Control and Prevention, Atlanta, GA, USA, 2013.
- [2] H. H. Handoll, R. Madhok, and T. E. Howe, "A systematic review of rehabilitation for distal radial fractures in adults," *British Journal of Hand Therapy*, vol. 8, no. 1, pp. 16–23, 2003.
- [3] M. Nylenna, K. B. Frønsdal, H. D. Kvernmo et al., *Treatment of Distal Radial Fractures in Adults*, Norwegian Knowledge Centre for the Health Services, Oslo, Norway, 2013.
- [4] G. D. Krischak, A. Krasteva, F. Schneider, D. Gulkin, F. Gebhard, and M. Kramer, "Physiotherapy after volar plating of wrist fractures is effective using a home exercise program," *Archives of Physical Medicine and Rehabilitation*, vol. 90, no. 4, pp. 537–544, 2009.
- [5] M. K. Dekkers and T. L. Nielsen, "Occupational performance, pain, and global quality of life in women with upper extremity fractures," *Scandinavian Journal of Occupational Therapy*, vol. 18, no. 3, pp. 198–209, 2011.
- [6] S. A. Davila and K. Johnston-Jones, "Managing the stiff elbow: operative, nonoperative, and postoperative techniques," *Journal of Hand Therapy*, vol. 19, no. 2, pp. 268–281, 2006.
- [7] C. C. Norkin and D. J. White, *Measurement of Joint Motion: A Guide to Goniometry*, F. A. Davis Company, Philadelphia, PA, USA, 3rd edition, 2003.
- [8] P. Harding, T. Rasekaba, L. Smirneos, and A. E. Holland, "Early mobilisation for elbow fractures in adults," *Cochrane Database of Systematic Reviews*, no. 6, article CD008130, 2011.
- [9] K. Parmelee-Peters and S. W. Eathorne, "The wrist: common injuries and management," *Primary Care: Clinics in Office Practice*, vol. 32, no. 1, pp. 35–70, 2005.
- [10] K. Valdes, "A retrospective pilot study comparing the number of therapy visits required to regain functional wrist and forearm range of motion following volar plating of a distal radius fracture," *Journal of Hand Therapy*, vol. 22, no. 4, pp. 312–318, 2009.
- [11] A. Frisoli, F. Salsedo, M. Bergamasco, B. Rossi, and M. C. Carboncini, "A force-feedback exoskeleton for upper-limb rehabilitation in virtual reality," *Applied Bionics and Biomechanics*, vol. 6, no. 2, pp. 115–126, 2009.
- [12] M. Mihelj, T. Nef, and R. Riener, "ARMin II-7 DoF rehabilitation robot: mechanics and kinematics," in *Proceedings of the 2007 IEEE International Conference on Robotics and Automation*, pp. 4120–4125, Roma, Italy, April 2007.
- [13] T. Nef, M. Guidali, and R. Riener, "ARMin III—arm therapy exoskeleton with an ergonomic shoulder actuation," *Applied Bionics and Biomechanics*, vol. 6, no. 2, pp. 127–142, 2009.
- [14] N. Jarrasse, G. Morel, J. Paik, and V. Pasqui, "Design and acceptability assessment of a new reversible orthosis," in *Proceedings of the 2008 IEEE/RSJ International Conference on Intelligent Robots and Systems*, pp. 1933–1939, Nice, France, September 2008.
- [15] R. C. V. Loureiro and W. S. Harwin, "Reach & grasp therapy: design and control of a 9-DOF robotic neuro-rehabilitation system," in *Proceedings of the 2007 IEEE 10th International Conference on Rehabilitation Robotics*, pp. 757–763, Noordwijkerhout, Netherlands, June 2007.
- [16] L. F. Lucca, "Virtual reality and motor rehabilitation of the upper limb after stroke: a generation of progress?," *Journal of Rehabilitation Medicine*, vol. 41, no. 12, pp. 1003–1100, 2009.
- [17] M. S. Cameirao, S. B. i. Badia, E. Duarte, A. Frisoli, and P. F. M. J. Verschuren, "The combined impact of virtual reality neurorehabilitation and its interfaces on upper extremity functional recovery in patients with chronic stroke," *Stroke*, vol. 43, no. 10, pp. 2720–2728, 2012.
- [18] D. K. A. Singh, N. A. Mohd Nordin, N. A. A. Aziz, B. K. Lim, and L. C. Soh, "Effects of substituting a portion of standard physiotherapy time with virtual reality games among community-dwelling stroke survivors," *BMC Neurology*, vol. 13, no. 1, pp. 1–7, 2013.
- [19] J.-H. Shin, M.-Y. Kim, J.-Y. Lee et al., "Effects of virtual reality-based rehabilitation on distal upper extremity function and health-related quality of life: a single-blinded, randomized controlled trial," *Journal of NeuroEngineering and Rehabilitation*, vol. 13, no. 1, pp. 1–10, 2016.
- [20] G. B. Prange, M. J. Jannink, C. G. Groothuis-Oudshoorn, H. J. Hermens, and M. J. IJzerman, "Systematic review of the effect of robot-aided therapy on recovery of the hemiparetic arm after stroke," *Journal of Rehabilitation Research and Development*, vol. 43, no. 2, p. 171, 2006.
- [21] P. Staubli, T. Nef, V. Klamroth-Marganska, and R. Riener, "Effects of intensive arm training with the rehabilitation robot ARMin II in chronic stroke patients: four single-cases," *Journal of NeuroEngineering and Rehabilitation*, vol. 6, no. 1, p. 46, 2009.
- [22] A. C. Lo, P. D. Guarino, L. G. Richards et al., "Robot-assisted therapy for long-term upper-limb impairment after stroke," *New England Journal of Medicine*, vol. 362, no. 19, pp. 1772–1783, 2010.
- [23] A. Frisoli, C. Procopio, C. Chisari et al., "Positive effects of robotic exoskeleton training of upper limb reaching movements after stroke," *Journal of NeuroEngineering and Rehabilitation*, vol. 9, no. 1, p. 36, 2012.
- [24] T. Nef, M. Mihelj, and R. Riener, "ARMin: a robot for patient-cooperative arm therapy," *Medical & Biological Engineering & Computing*, vol. 45, no. 9, pp. 887–900, 2007.
- [25] M. Guidali, A. Duschau-Wicke, S. Broggi, V. Klamroth-Marganska, T. Nef, and R. Riener, "A robotic system to train activities of daily living in a virtual environment," *Medical & Biological Engineering & Computing*, vol. 49, no. 10, pp. 1213–1223, 2011.
- [26] L. Zollo, L. Rossini, M. Bravi, G. Magrone, S. Sterzi, and E. Guglielmelli, "Quantitative evaluation of upper-limb motor control in robot-aided rehabilitation," *Medical & Biological Engineering & Computing*, vol. 49, no. 10, pp. 1131–1144, 2011.
- [27] P. Maciejasz, J. Eschweiler, K. Gerlach-Hahn, A. Jansen-Troy, and S. Leonhardt, "A survey on robotic devices for upper limb rehabilitation," *Journal of NeuroEngineering and Rehabilitation*, vol. 11, no. 1, p. 3, 2014.
- [28] R. Chemuturi, F. Amirabdollahian, and K. Dautenhahn, "Adaptive training algorithm for robot-assisted upper-arm rehabilitation, applicable to individualised and therapeutic human-robot interaction," *Journal of NeuroEngineering and Rehabilitation*, vol. 10, no. 1, p. 102, 2013.
- [29] F. J. Badesa, R. Morales, N. Garcia-Aracil, J. M. Sabater, A. Casals, and L. Zollo, "Auto-adaptive robot-aided therapy using machine learning techniques," *Computer Methods and Programs in Biomedicine*, vol. 116, no. 2, pp. 123–130, 2013.
- [30] S. R. Saunders, "Physical therapy management of hand fractures," *Physical Therapy*, vol. 69, no. 12, pp. 1065–1076, 1989.
- [31] S. Hoppenfeld and V. L. Murthy, *Treatment and Rehabilitation of Fractures*, Lippincott Williams & Wilkins, Philadelphia, PA, USA, 2000.
- [32] C. E. Nash, S. M. Mickan, C. B. Del Mar, and P. P. Glasziou, "Resting injured limbs delays recovery: a systematic review," *Journal of Family Practice*, vol. 53, no. 9, pp. 706–712, 2004.

- [33] P. S. Issack and K. A. Egol, "Posttraumatic contracture of the elbow: current management issues," *Bulletin/Hospital for Joint Diseases*, vol. 63, no. 3-4, pp. 129–136, 2006.
- [34] P. D. Kim, M. W. Gafe, and M. P. Rosenwasser, "Elbow stiffness: etiology, treatment, and results," *Journal of the American Society for Surgery of the Hand*, vol. 5, no. 4, pp. 209–216, 2005.
- [35] J. Allington, S. J. Spencer, J. Klein, M. Buell, D. J. Reinkensmeyer, and J. Bobrow, "Supinator Extender (SUE): a pneumatically actuated robot for forearm/wrist rehabilitation after stroke," in *Proceedings of the Annual International Conference of the IEEE Engineering in Medicine and Biology Society*, pp. 1579–1582, Honolulu, HI, USA, July 2011.
- [36] M. H. Rahman, M. Saad, J. P. Kenné, and P. S. Archambault, "Exoskeleton robot for rehabilitation of elbow and forearm movements," in *Proceedings of the 2010 18th Mediterranean Conference on Control Automation (MED)*, pp. 1567–1572, Marrakech, Morocco, June 2010.
- [37] A. U. Pehlivan, F. Sergi, A. Erwin, N. Yozbatiran, G. E. Francisco, and M. K. O'Malley, "Design and validation of the RiceWrist-S exoskeleton for robotic rehabilitation after incomplete spinal cord injury," *Robotica*, vol. 32, no. 8, pp. 1415–1431, 2014.
- [38] D. Buongiorno, E. Sotgiu, D. Leonardis, S. Marcheschi, M. Solazzi, and A. Frisoli, "WRES: a novel 3 DoF WRist ExoSkeleton with tendon-driven differential transmission for neuro-rehabilitation and teleoperation," *IEEE Robotics and Automation Letters*, vol. 3, no. 3, pp. 2152–2159, 2018.
- [39] I. Vanderniepen, R. Van Ham, M. Van Damme, and D. Lefever, "Design of a powered elbow orthosis for orthopaedic rehabilitation using compliant actuation," in *Proceedings of the 2008 2nd IEEE RAS & EMBS International Conference on Biomedical Robotics and Biomechatronics*, pp. 801–806, Scottsdale, AZ, USA, 2008.
- [40] C. Sicuri, G. Porcellini, and G. Merolla, "Robotics in shoulder rehabilitation," *Muscles, Ligaments and Tendons Journal*, vol. 4, no. 2, pp. 207–213, 2014.
- [41] C. Nerz, L. Schwickert, C. Becker, S. Studier-Fischer, J. A. Müßig, and P. Augat, "Effectiveness of robot-assisted training added to conventional rehabilitation in patients with humeral fracture early after surgical treatment: protocol of a randomised, controlled, multicentre trial," *Trials*, vol. 18, no. 1, p. 589, 2017.
- [42] L. Schwickert, J. Klenk, A. Stähler, C. Becker, and U. Lindemann, "Robotic-assisted rehabilitation of proximal humerus fractures in virtual environments: a pilot study," *Zeitschrift für Gerontologie und Geriatrie*, vol. 44, no. 6, pp. 387–392, 2011.
- [43] M. Bergamasco, C. A. Avizzano, A. Frisoli, E. Ruffaldi, and S. Marcheschi, "Design and validation of a complete haptic system for manipulative tasks," *Advanced Robotics*, vol. 20, no. 3, pp. 367–389, 2006.
- [44] M. A. Padilla-Castañeda, "A virtual reality system for robotic-assisted orthopedic rehabilitation of forearm and elbow fractures," in *Proceedings of the 2013 IEEE/RSJ International Conference on Intelligent Robots and Systems (IROS)*, pp. 1506–1511, Tokyo, Japan, November 2013.
- [45] M. A. Padilla-Castañeda, A. Frisoli, S. Pabon, and M. Bergamasco, "The modulation of ownership and agency in the virtual hand illusion under visuotactile and visuomotor sensory feedback," *Presence: Teleoperators and Virtual Environments*, vol. 23, no. 2, pp. 209–225, 2014.
- [46] M. A. Padilla-Castañeda, E. Sotgiu, A. Frisoli, and M. Bergamasco, "A robotic & virtual reality orthopedic rehabilitation system for the forearm," *Studies in Health Technology and Informatics*, vol. 181, pp. 324–328, 2012.
- [47] D. Tolani, A. Goswami, and N. I. Badler, "Real-time inverse kinematics techniques for anthropomorphic limbs," *Graphical Models*, vol. 62, no. 5, pp. 353–388, 2000.
- [48] R. W. Bohannon, A. Peolsson, N. Massy-Westropp, J. Desrosiers, and J. Bear-Lehman, "Reference values for adult grip strength measured with a Jamar dynamometer: a descriptive meta-analysis," *Physiotherapy*, vol. 92, no. 1, pp. 11–15, 2006.
- [49] A. M. Carlsson, "Assessment of chronic pain. I. Aspects of the reliability and validity of the visual analogue scale," *Pain*, vol. 16, no. 1, pp. 87–101, 1983.
- [50] R. Padua, L. Padua, E. Ceccarelli et al., "Italian version of the disability of the arm, shoulder and hand (dash) questionnaire: cross-cultural adaptation and validation," *Journal of Hand Surgery*, vol. 28, no. 2, pp. 179–186, 2003.
- [51] B. F. Morrey, L. J. Askew, and E. Y. Chao, "A biomechanical study of normal functional elbow motion," *Journal of Bone and Joint Surgery*, vol. 63, no. 6, pp. 872–877, 1981.
- [52] H. J. Hermens, Commission des Communautés européennes, and Biomedical and Health Research Programme, SENIAM : European Recommendations for Surface Electromyography: Results of the SENIAM Project, [Pays-Bas]: Roessingh Research and Development, Enschede, Netherlands, 1999.
- [53] M. V. Sanchez-Vives, B. Spanlang, A. Frisoli, M. Bergamasco, and M. Slater, "Virtual hand illusion induced by visuomotor correlations," *PLoS One*, vol. 5, no. 4, Article ID e10381, 2010.
- [54] M. Gonzalez-Izal, A. Malanda, E. Gorostiaga, and M. Izquierdo, "Electromyographic models to assess muscle fatigue," *Journal of Electromyography and Kinesiology*, vol. 22, no. 4, pp. 501–512, 2012.
- [55] I. Kuorinka, "Restitution of EMG spectrum after muscular fatigue," *European Journal of Applied Physiology and Occupational Physiology*, vol. 57, no. 3, pp. 311–315, 1988.
- [56] M. S. Cameirão, S. B. i. Badia, E. D. Oller, and P. F. Verschuren, "Neurorehabilitation using the virtual reality based Rehabilitation Gaming System: methodology, design, psychometrics, usability and validation," *Journal of NeuroEngineering and Rehabilitation*, vol. 7, no. 1, p. 48, 2010.
- [57] D. J. Reinkensmeyer, E. Burdet, M. Casadio et al., "Computational neurorehabilitation: modeling plasticity and learning to predict recovery," *Journal of NeuroEngineering and Rehabilitation*, vol. 13, no. 1, p. 42, 2016.
- [58] L. D. Walsh, G. L. Moseley, J. L. Taylor, and S. C. Gandevia, "Proprioceptive signals contribute to the sense of body ownership," *Journal of Physiology*, vol. 589, no. 12, pp. 3009–3021, 2011.
- [59] J. K. Lee, E. J. Park, and S. N. Robinovitch, "Estimation of attitude and external acceleration using inertial sensor measurement during various dynamic conditions," *IEEE Transactions on Instrumentation and Measurement*, vol. 61, no. 8, pp. 2262–2273, 2012.
- [60] M. El-Gohary and J. McNames, "Human joint angle estimation with inertial sensors and validation with a robot arm," *IEEE Transactions on Biomedical Engineering*, vol. 62, no. 7, pp. 1759–1767, 2015.

## Research Article

# Experimental Characterization of NURSE, a Device for Arm Motion Guidance

Betsy Dayana Marcela Chaparro-Rico ,<sup>1,2</sup> Daniele Cafolla ,<sup>2</sup> Marco Ceccarelli ,<sup>2</sup> and Eduardo Castillo-Castaneda ,<sup>1</sup>

<sup>1</sup>*Instituto Politécnico Nacional-CICATA Querétaro, Cerro Blanco 141, Colinas del Cimatario, 76090 Santiago de Querétaro, QRO, Mexico*

<sup>2</sup>*Laboratory of Robotics and Mechatronics (LARM), University of Cassino and Southern Lazio, Via Di Biasio 43, 03043 Cassino, Italy*

Correspondence should be addressed to Betsy Dayana Marcela Chaparro-Rico; [betsychaparro@hotmail.com](mailto:betsychaparro@hotmail.com)

Received 24 February 2018; Accepted 20 May 2018; Published 3 July 2018

Academic Editor: Antonio Fernández-Caballero

Copyright © 2018 Betsy Dayana Marcela Chaparro-Rico et al. This is an open access article distributed under the Creative Commons Attribution License, which permits unrestricted use, distribution, and reproduction in any medium, provided the original work is properly cited.

This paper presents an experimental characterization of NURSE, a device for arm motion guidance. The laboratory setup and testing modes are presented to explain the experimental procedure. Two exercises for the upper limb exercise are used to test the NURSE behaviour, and successful results are presented. Trajectories and linear accelerations are tested when the device performs the two exercises without and with load. In addition, torque and power consumption are considered to check the NURSE behaviour.

## 1. Introduction

Every year, 15 million people worldwide suffer a stroke; more than 70 percent must deal with mobility impairment and cognitive disabilities [1]. Additionally, the arm mobility can be affected by neurological, muscle, and joint diseases [2]. Lymphatic and vascular disorders can also reduce arm mobility [3]. On the contrary, the arm mobility can be also affected by traumatic and overuse injuries of the shoulder, elbow, and wrist [3, 4]. In such a case, exercises are necessary to recover a suitable range of motion by strengthening, flexing, and extending the muscles and the joints [5]. However, the number of trained human therapists who can provide this support is limited, while the demand is growing, particularly in elderly people [6, 7]. The required exercises for an assistive therapy should be designed by a specialist according to the medical diagnosis, and it can be vary from a specialist to another [3, 8, 9]. However, all exercises start from the basic movements of the human arm seen in [3, 4, 8, 10, 11]. During a traditional exercise, the specialist assists the limb motion. However, it is difficult for the

therapist to keep the same quality of motions during long-therapy sessions. In addition, the motion cannot be controlled, and a feedback of the patient evolution is difficult to obtain. While there remain a number of tasks that only human therapists can perform, many rehabilitation exercises are mainly highly repetitive. This is where robotic systems are useful since they can reproduce the same task countless times, with precision and accuracy without fatigue or loss of attention [12]. It has been proved that use of robotic systems benefits the rehabilitation process [13, 14]. In addition, the use of robotic systems reduces the recovery time by 30% [13]. Several devices have been developed for arm motion assistance. However, there are several issues to solve in the existing robotic devices such as they are costly and they have bulky structures very difficult to adjust to the patient arm.

The existing devices for arm motion assistance can be classified into three groups: nonactuator devices, exoskeletons, and end-effector devices. The nonactuator devices are frequently used by rehabilitation centers since they have significant lower costs, are easier to use, and are inherently safe. An example is the handboard to trace the number 8

[15], and the mechanism is composed of a roller skate for the arm support, a table with a guide with an 8 shape, and pieces of different weights to apply resistance to the motion during the therapy. However, the mechanism offers only one exercise, and the arm motion is not controlled. Another example is the skateboard [16, 17]. The skateboard is a known mechanism composed of a board with wheels that allow movements on a horizontal plane. The patient should perform the movements by himself/herself. Since the skateboard is a cheap mechanism, it is widely used. However, by using the skateboard, the therapy motion cannot be controlled. However, the nonactuator devices do not have movement correction. Within the exoskeletons group, ArmeoPower can be found [18]. ArmeoPower has six degrees of freedom to perform 3D motions and a graphical interface for virtual interaction. However, ArmeoPower is difficult to wear, costly, and has a bulky frame. Another exoskeleton is MEDARM [19], which can assist the arm motion on a horizontal plane; it is actuated by cables and has 3 degrees of freedom. The MEDARM exoskeleton is adjustable for users of different sizes. However, MEDARM needs a bulky frame structure, is difficult to transport and construct, and has been proposed only to assist the right arm, and it is difficult to align the exoskeleton joints with the human arm joints. Another exoskeleton named "CAREX" is proposed in [20]. The exoskeleton is actuated by seven cables and has five degrees of freedom. However, CAREX needs a very huge structure to support the seven motors that move the cables. In addition, the cables can be dangerous for the subject since they move close to his/her head. Other exoskeletons with similar disadvantages to ArmeoPower, MEDARM, and CAREX can be seen in [21–23]: in [21], an exoskeleton is proposed to assist just the shoulder motion, but it is difficult to wear; in [22], an exoskeleton is proposed to assist the elbow and wrist joints, but it has a bulky frame structure and it is not comfortable to use since the frame must be placed in the middle of the patient's legs so that the arm gets the proper position; in [23], an exoskeleton named "ARMin III" is proposed, but like ArmeoPower, it is difficult to wear and has a bulky frame. As seen in [18–23], the main issues in the exoskeletons are that the exostulations have joint axes fully determined as well as physiological movements, but robot axes have to be aligned with anatomical axes and are very difficult to transport, construct, and wear. In addition, the exoskeletons are very difficult to adapt to different anthropometric sizes. An example of an end-effector device can be seen in [16]. The device is based on a planar parallel mechanism 3RRR. The device can assist the arm motion on a horizontal, vertical, or inclined plane by performing several trajectories within its workspace. However, the device has large links and presents stiffness problems. In [24], an end-effector device is proposed to assist the arm motion. The forearm of the user is supported by an end-effector device, and the device can assist the shoulder/elbow flexion and extension without other trajectories. The disadvantage of this end-effector device is that it covers a small workspace and offers few types of

exercises. In [25], a portable end-effector device is proposed for arm exercises on an inclined plane. The device is composed of two actuators that are actuated by cables and a hand grip device. The device trajectories are limited by four guides that constrain the end-effector movement along straight lines, and the device cannot perform other types of exercises. In [26], MIT-MANUS is presented, a commercial and known device for arm therapy that has been developed in the early 1990s. MIT-MANUS is principally composed of a five-bar mechanism and a modular end-effector. The robotic arm helps in the shoulder and elbow motion on a horizontal plane, and the modular end-effector allows the movements of the wrist joint. Currently, MIT-MANUS has a clinical version that is named "InMotion ARM™" as pointed out in [27]. However, the device has a reduced workspace in terms of the range of possible motions. Furthermore, the device is not portable and it requires to be operated by highly trained personnel. Another end-effector device named "REAplan" is presented in [28]. The device is based on the Cartesian mechanism with a handle that is moved on a horizontal plane to assist the arm motion. However, REAplan has a bulky and heavy structure so that is difficult to transport. In addition, it has a reduced workspace in relation to the required link sizes. However, the end-effector devices present advantages with respect to the exoskeletons such as they present a simple structure and control and they are easy to adjust to the patient.

As seen in the above examples, the main issues to consider about the existing devices for arm motion are that the devices with a large workspace are very difficult to transport, construct, and wear as seen in [18–23]; the existing portable devices cover a small workspace [16, 24–28] and offer few types of exercises [24, 25]; and the widely used basic mechanisms do not have motion control during the therapy or they perform a single trajectory as seen in [15, 17].

In order to solve the above issues, NURSE (cassiNo-qUeretaro uppeR-limb aSsistive dEvice) was developed as an alternative solution for arm motion assistance with advantages over the existing devices. NURSE is an end-effector device composed of a mechanism, a controller, and a user interface. NURSE is based on a mechanism of 2 degrees of freedom whose workspace is amplified by using a pantograph. NURSE can assist the arm motion during a rehabilitation therapy and the arm motion of elderly people during an exercise. The main advantages of NURSE are presented in this paper together with the experimental characterization.

## 2. Exercises for Arm Motion Guidance

In order to assist the arm motion during a therapy, two exercises for upper limb rehabilitation and exercise have been designed by the authors as reported in [29] (Figure 1). The considered exercises can be used in patients recovering from injuries and neurological, muscular, and joint diseases. Moreover, they can also be used for the arm exercise by elderly people. Figure 1(a) shows exercise no. 1 that has been designed to treat the shoulder. The exercise consists of

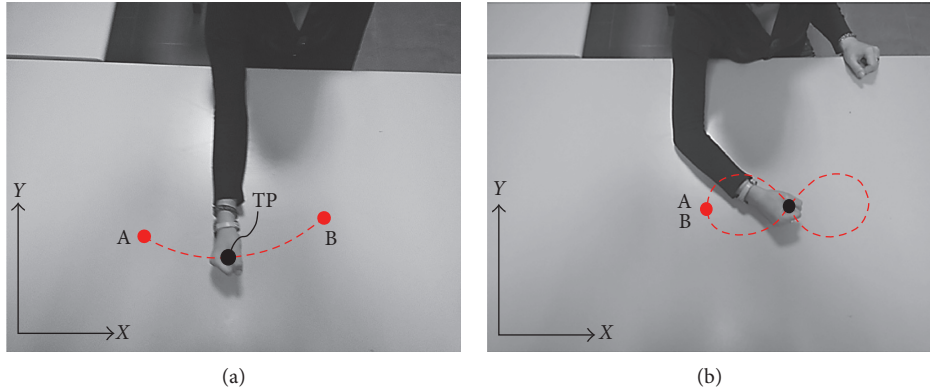


FIGURE 1: The two considered exercises for upper limb rehabilitation and exercise: (a) exercise no. 1 to treat the shoulder joint; (b) exercise no. 2 to treat both shoulder and elbow joints.

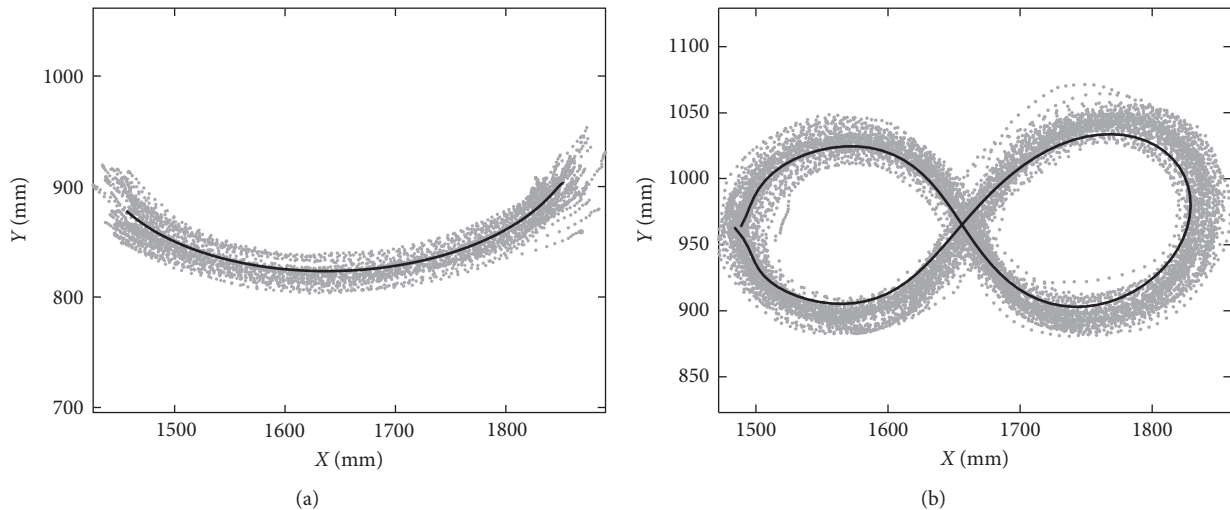


FIGURE 2: Reference trajectories generated by regression analysis (in black) and the trajectories acquired from the 12 subjects: (a) trajectories for exercise no. 1 to treat the shoulder joint; (b) trajectories for exercise no. 2 to treat both the shoulder and elbow joints.

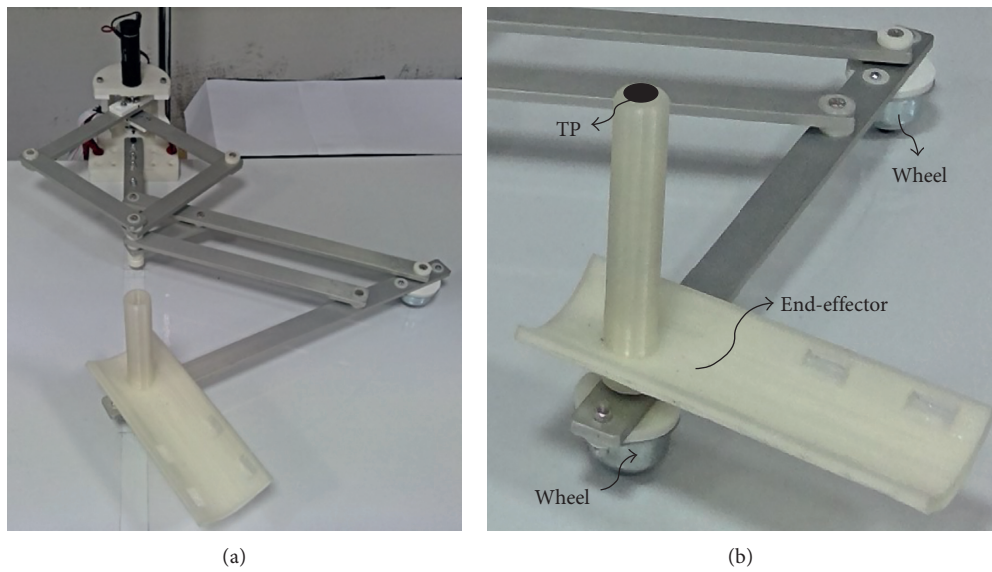


FIGURE 3: NURSE: (a) a prototype; (b) the tracing point (TP) on the end-effector and wheels.

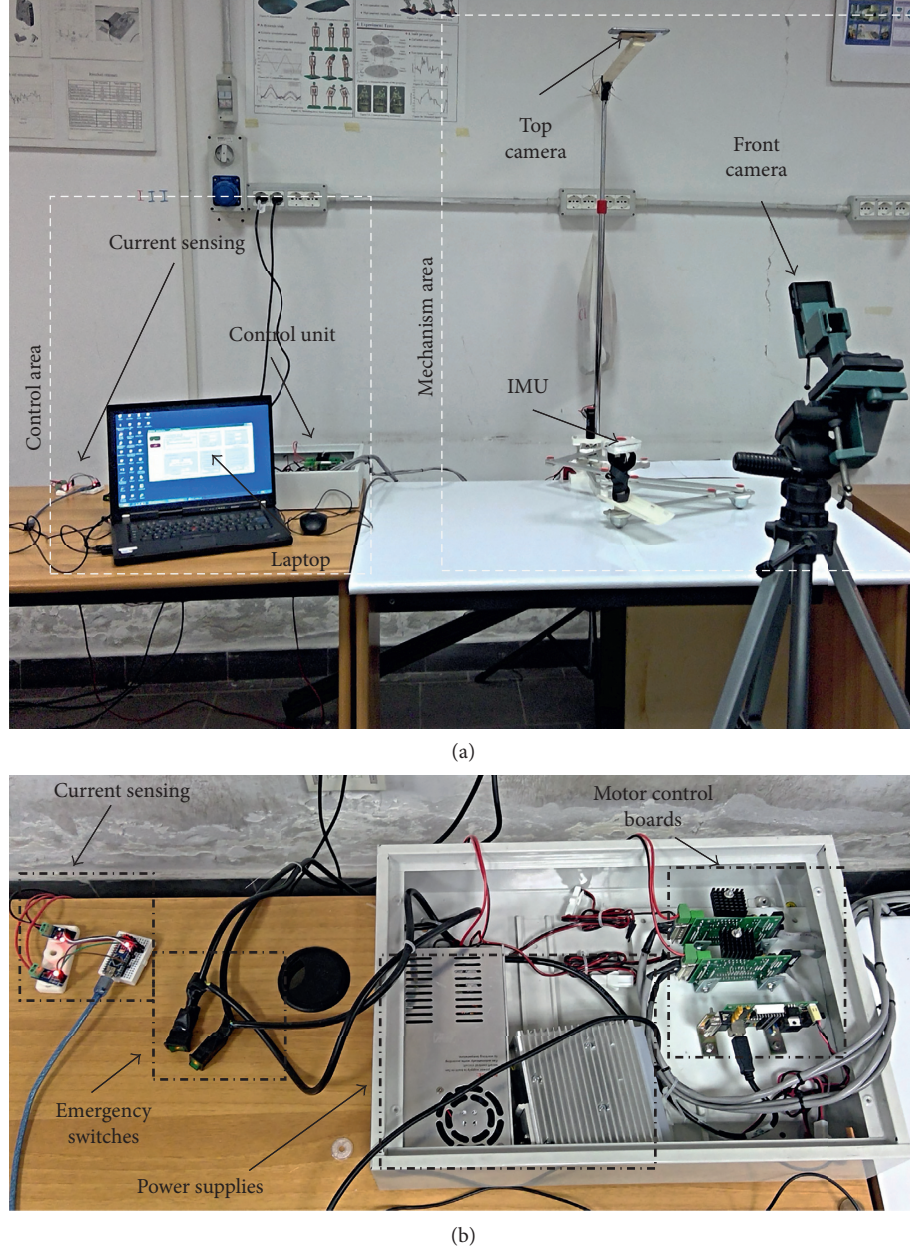


FIGURE 4: Experiment layout: (a) overview of the lab setup; (b) control area details.

performing a horizontal shoulder flexion by tracing the trajectory in red dotted lines with a tracing point (TP) from the point A to the point B (Figure 1(a)). Figure 1(b) shows exercise no. 2 that has been designed to treat both the shoulder and elbow joints. The exercise consists of tracing the number 8 with the TP. Exercise no. 2 starts and ends in the same point. Since the path to trace the number 8 is complex, it is also used as a reference trajectory to evaluate the behaviour of robots that perform human tasks [30].

The procedure for the motion design of the considered exercises is explained in [29]. The reached coordinates of the TP with respect to an XY reference frame were used for the design motion. Since in an assistive therapy, the patient's

hand is guided by a specialist to perform a desired exercise, it is assumed that a device for motion assistance should perform the path of the same exercise. A Kinect vision system [31] was used to carry out the data collection of the arm motion from 12 subjects that performed the above exercises. The subjects performed each exercise during 12 repetitions. From the collected trajectories, a reference trajectory was generated for each exercise by using regression analysis as reported in [29]. Figure 2 shows the trajectories generated for each exercise and the trajectories acquired by the Kinect vision system. It is important to notice that other arm exercises have also been designed in [29].

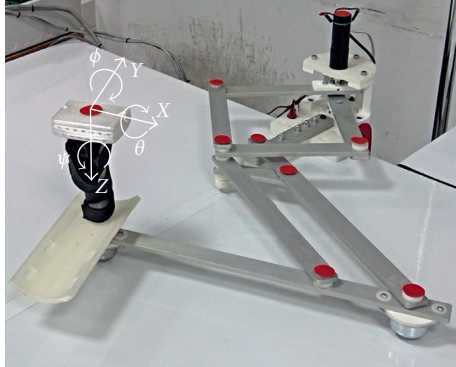


FIGURE 5: Markers for image processing.

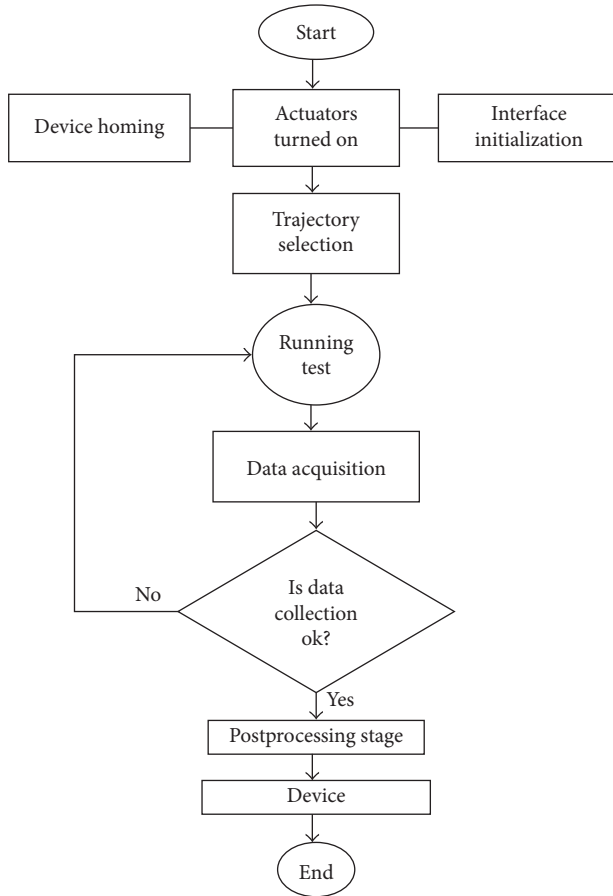
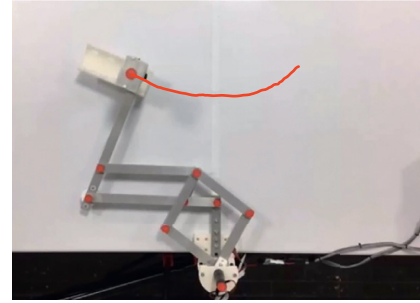


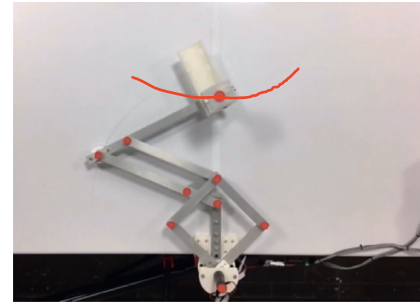
FIGURE 6: Experiment flow chart.

TABLE 1: Experiment to test NURSE.

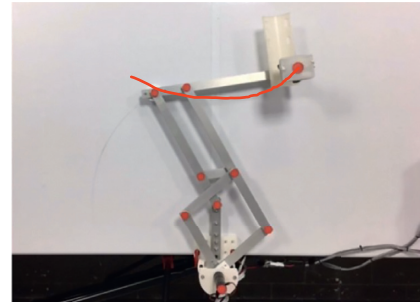
Test no.	Description	Inputs	Outputs
1	Perform exercise no. 1	$X, Y$	$X_m, Y_m, a_x, a_y, p, \tau_1$ , and $\tau_2$
2	Perform exercise no. 2		



(a)



(b)



(c)

FIGURE 7: Some snapshots of test no. 1 without load during repetition no. 1 together with the trajectory obtained by image processing (in red): (a) the first sample position; (b) the second sample position; (c) the third sample position.

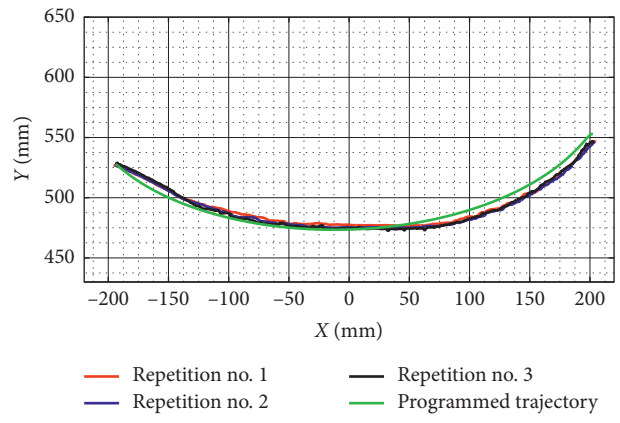


FIGURE 8: Comparison between the programmed trajectory and the TP trajectories from three repetitions during test no. 1 without load.

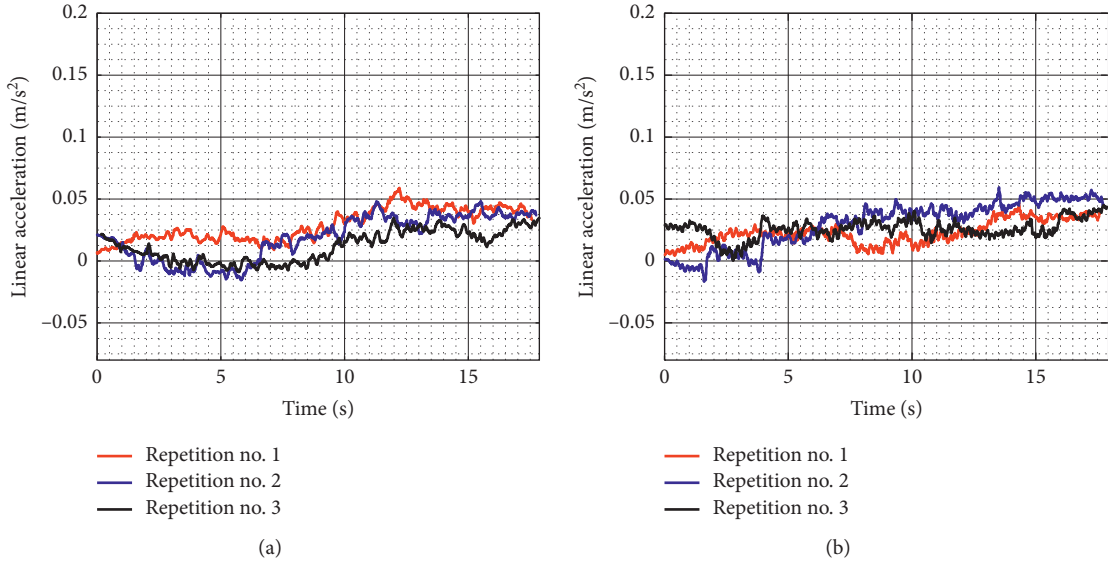


FIGURE 9: Acquired linear acceleration during test no. 1 without load for the three repetitions seen in Figure 8: (a) X linear acceleration; (b) Y linear acceleration.

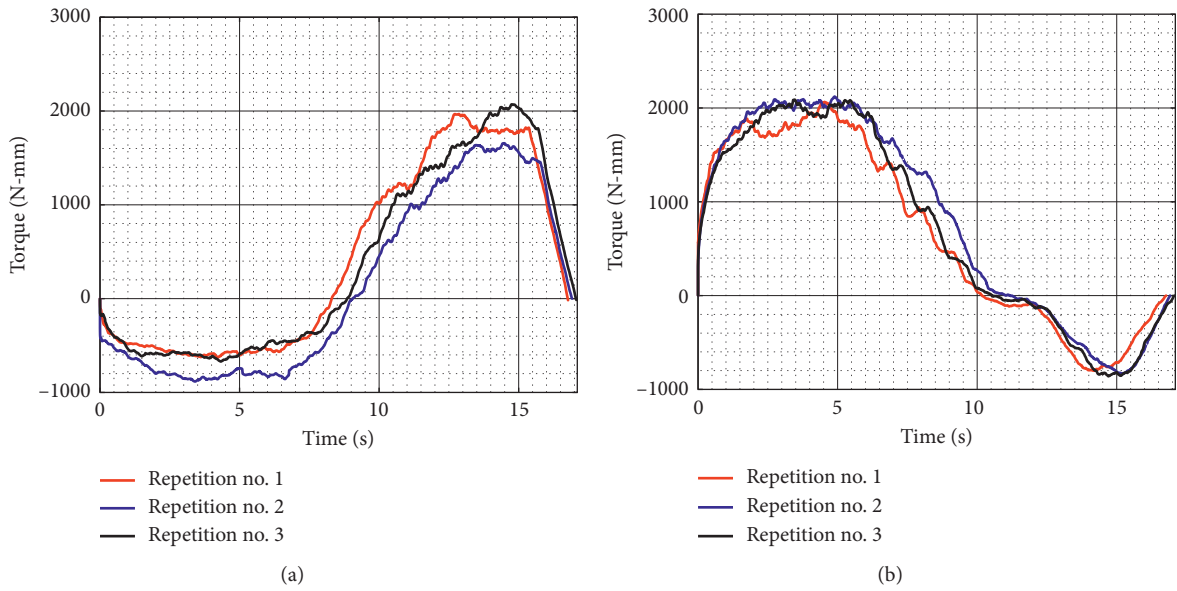


FIGURE 10: Computed torques during test no. 1 without load for the three repetitions seen in Figure 8: (a) Motor 1; (b) Motor 2.

### **3. Laboratory Setup and Testing Modes**

NURSE has been conceived and designed to solve all the issues that have been mentioned in Introduction, giving the possibility to perform exercises useful for physical therapy or rehabilitation, for treatments of injuries or diseases, for prevention of injuries or diseases, or for physical exercising [32] (Figure 3(a)).

The proposed device is composed of a linkage structure that is driven in planar movements by two actuators. Two wheels are used to support the NURSE structure (Figure 3(b)). The used wheels have omnidirectional balls of stainless steel, and they can support a load of 25 kg each. In addition,

an end-effector has been designed for a comfortable grasping of the user. Figure 3(b) shows the tracing point TP on the NURSE end-effector. The linkage structure is composed of aluminum bars that have a thickness of 6 mm and a width of 25 mm. The mechanism structure weighs 2.6 kg, and it fits into a box of  $35 \times 45 \times 30$  cm. More details of the mechanical design of NURSE are explained in [32, 33]. The mechanism can guide both right and left human arms on a plane within a large workspace to follow whatever desired trajectory [32, 33]. The planar linkage structure is characterized by light links for compact design, low-power consumption, and easy portability. The movements that can be performed by NURSE involve the shoulder and elbow of a human arm in

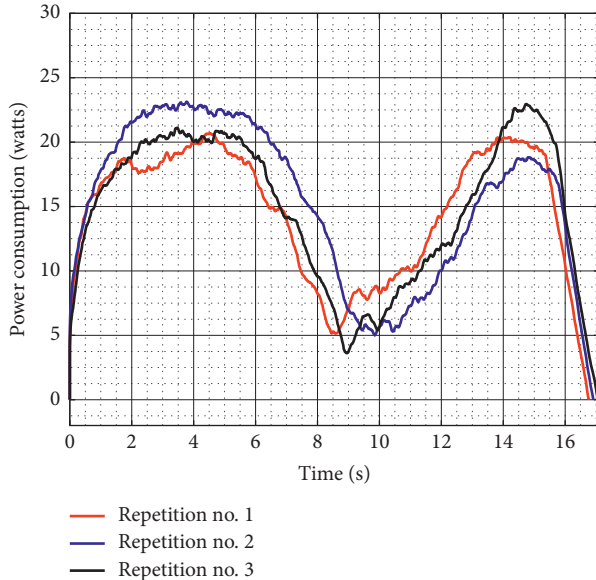
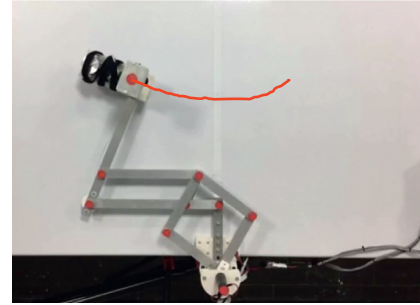
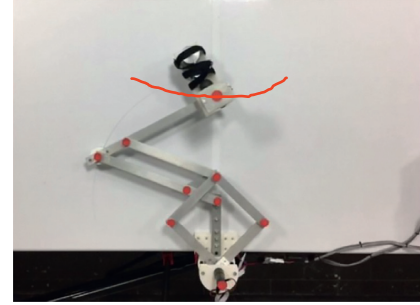


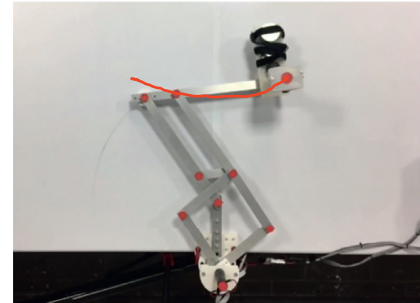
FIGURE 11: Computed power consumption of test no. 1 without load for the three repetitions seen in Figure 8.



(a)



(b)



(c)

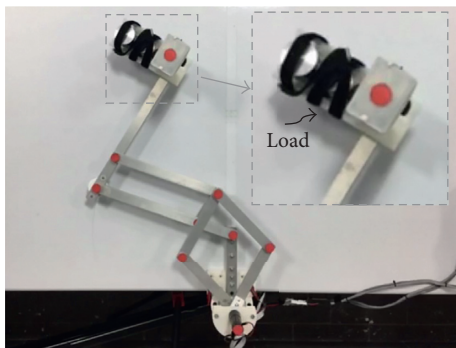


FIGURE 12: A zoomed view of a NURSE end-effector with a load of 520 g.

an independent way or in a coordinated motion. Since NURSE can perform several trajectories of different sizes, it can be used by people of any age, anthropomorphic sizes, and anthropometric sizes, including children and elderly people as pointed out in [32, 33].

To test the performances and the behaviour of NURSE, some experiments have been carried out at LARM laboratory in Cassino. A specific layout has been designed to allow a satisfactory acquisition of the needed data (Figure 4). In Figure 4(a), it is possible to notice that the area can be divided in two subareas, namely, the mechanism area and the control area.

The mechanism area includes the NURSE together with two cameras. One camera has been installed on the top of NURSE being planar to its workspace, while the other camera has been installed in front of NURSE. Furthermore, an IMU (inertial measurement unit) sensor has been placed on the TP.

The control area consists of a laptop in which an interface sends the positions for the NURSE motors according to a selected arm exercise, the control unit, and the current-sensing modules as in Figure 4(b). Each actuator is connected to a control

FIGURE 13: Some snapshots of test no. 1 with a load of 520 g during repetition no. 1 together with the trajectory obtained by image processing (in red): (a) the first sample position; (b) the second sample position; (c) the third sample position.

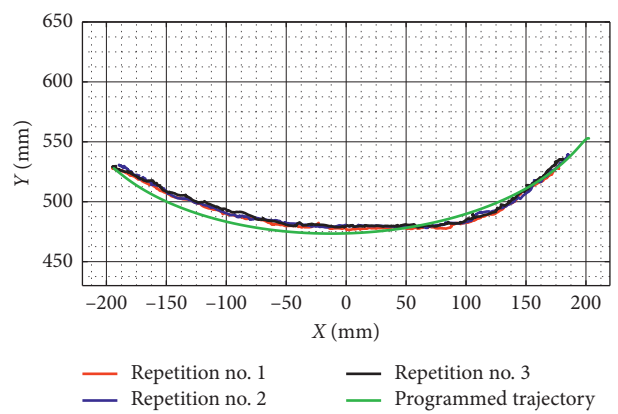


FIGURE 14: Comparison between the programmed trajectory and the TP trajectories from three repetitions during test no. 1 with a load of 520 g.

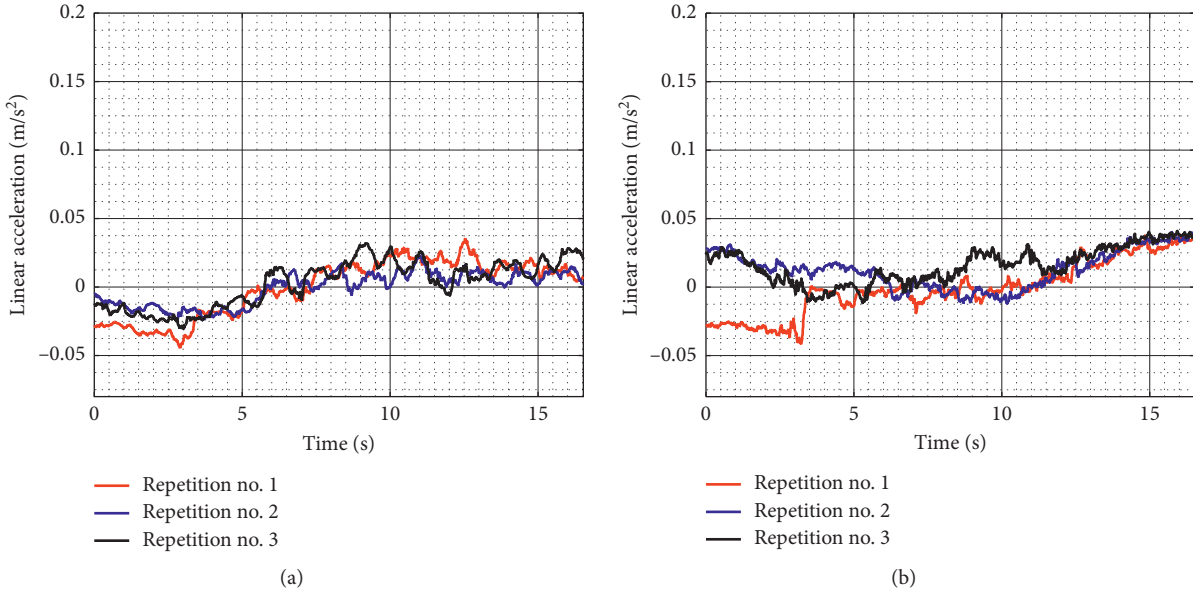


FIGURE 15: Acquired linear acceleration during test no. 1 with a load of 520 g for the three repetitions seen in Figure 14: (a) X linear acceleration; (b) Y linear acceleration.

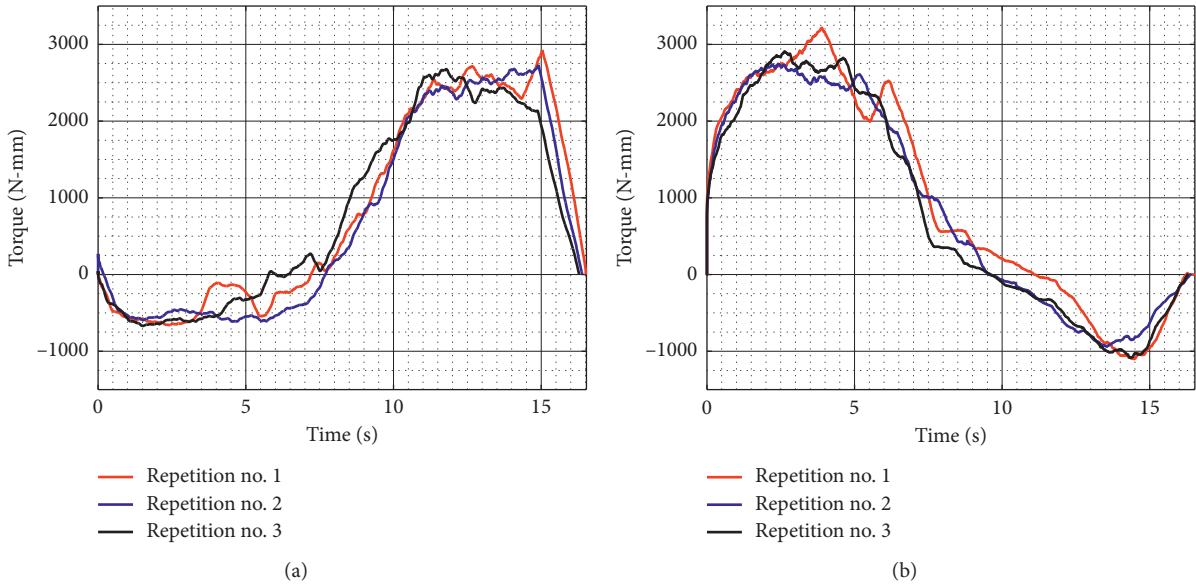


FIGURE 16: Computed torques during test no. 1 with a load of 520 g for the three repetitions seen in Figure 14: (a) Motor 1; (b) Motor 2.

board that will generate the trajectories to reproduce the selected exercise from the interface. The current-sensing module is composed of two current sensors, and each sensor is connected to each motor. Finally, one emergency switch turns off the motor amplifier, while the second turns off the entire system.

The top camera has been used to track the movement of the TP to validate if the programmed trajectory is satisfactorily reproduced by NURSE; to do so, some markers (red color circles) have been placed on the structure for the motion tracking by image processing (Figure 5). The front camera allows for an overview of the working area.

The placed IMU sensor on the TP can be used to measure the angular displacement in terms of roll ( $\theta$ ), pitch ( $\Phi$ ), and yaw ( $\psi$ ) and to acquire the linear acceleration along X, Y, and Z-axes as shown in Figure 5.

The two current sensors based on the Hall effect are used to compute the power consumption and check the behaviour of each actuator.

The experiments are carried out following the flow chart shown in Figure 6. Before running a test, the device is set manually in the home position, the actuator is turned on, and the interface is initialized. After that, the exercise to be performed is selected, the exercise trajectory is sent to the motor

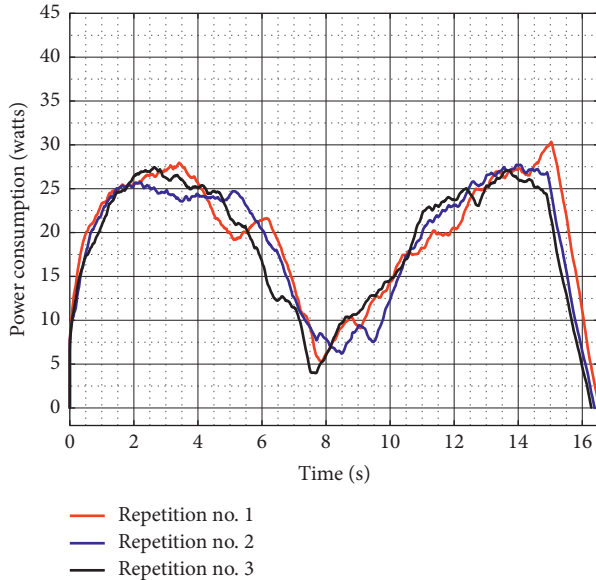


FIGURE 17: Computed power consumption during test no. 1 with a load of 520 g for the three repetitions seen in Figure 14.

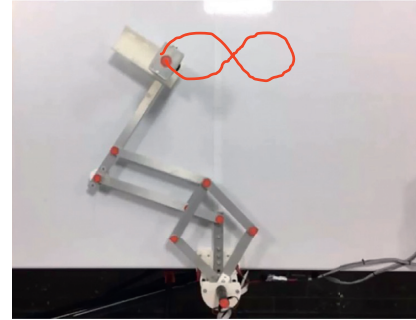
control board, and the test runs reproducing the desired task. While the experiment is running, the data are acquired from the cameras and the sensors. When the exercise ends, the data are collected and checked to evaluate if there is any data discrepancy due to sensors or video acquisition failure. In such a case, the test is repeated; otherwise, the postprocessing stage starts and the device characterization is carried out to evaluate the performance of NURSE.

Table 1 shows parameters of the tests that have been carried out in order to characterize the NURSE behaviour. The references trajectories of exercise nos. 1 and 2 in Figure 2 are used to carry out the tests. In test no. 1, NURSE performs exercise no. 1 during three repetitions. In test no. 2, NURSE performs exercise no. 2 during three repetitions. Both tests are carried out without load and with a load of 520 g by using a velocity of 396 °/s. The used load of 520 g is equivalent to 30% of the average weight of the forearm together with the hand, and it has been considered enough for lab experiments. In both tests, the positions of the TP are programmed in the control ( $X$ ,  $Y$ ) as inputs.

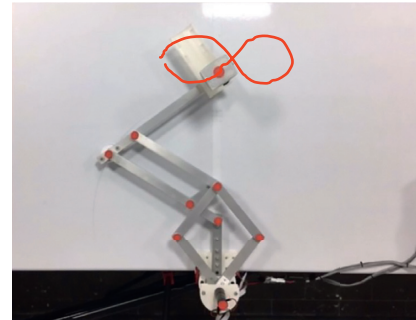
After the acquisition, the positions of the TP ( $X_m$ ,  $Y_m$ ) are obtained by image processing. The positions of the TP are used to validate if the device is able to perform the programmed trajectory. The linear accelerations of the TP ( $a_x$ ,  $a_y$ ) are acquired by the IMU sensor, and they can be used to evaluate the smoothness of the motion as an important aspect for user safety. Using the acquired motor's current, it is possible to compute the torque of each motor ( $\tau_1$ ,  $\tau_2$ ) and the power consumption ( $p$ ) of NURSE to evaluate if the actuators struggle while replicating the task.

#### 4. Test Results

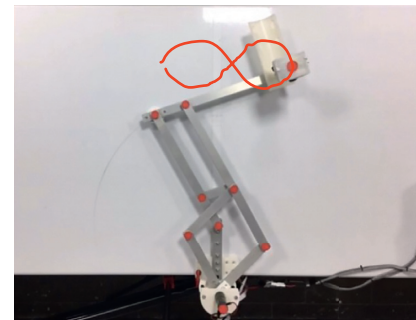
Test no. 1 has been carried without load during three repetitions. Figure 7 shows three snapshots of the video while the test is carried out during repetition no. 1. In addition, Figure 7



(a)



(b)



(c)

FIGURE 18: Some snapshots of test no. 2 without load during repetition no. 1 together with the trajectory obtained by image processing (in red): (a) the first sample position; (b) the second sample position; (c) the third sample position.

shows the trajectory obtained from the marker on the TP. Figure 8 shows the trajectory programmed in the device and the trajectories obtained from the marker on the TP during repetition nos. 1, 2, and 3. As shown in Figure 8, the trajectories obtained from the marker on the TP are close to the programmed one with a maximum deviation of 10 mm. This deviation is related with the accuracy of the home position since it is set manually. However, the repeatability deviation between the trajectories performed by NURSE has a maximum value of 3 mm for test no. 1 without load.

Figure 9 shows the linear accelerations acquired from the TP during test no. 1 when the device is unloaded for the three repetitions as seen in Figure 8. The linear accelerations in  $X$  have a maximum value of  $0.058 \text{ m/s}^2$  and a minimum value of  $-0.015 \text{ m/s}^2$ , and linear accelerations in  $Y$  have a maximum value of  $0.059 \text{ m/s}^2$  and a minimum value of  $-0.015 \text{ m/s}^2$ . The linear acceleration values in  $X$  and  $Y$  are

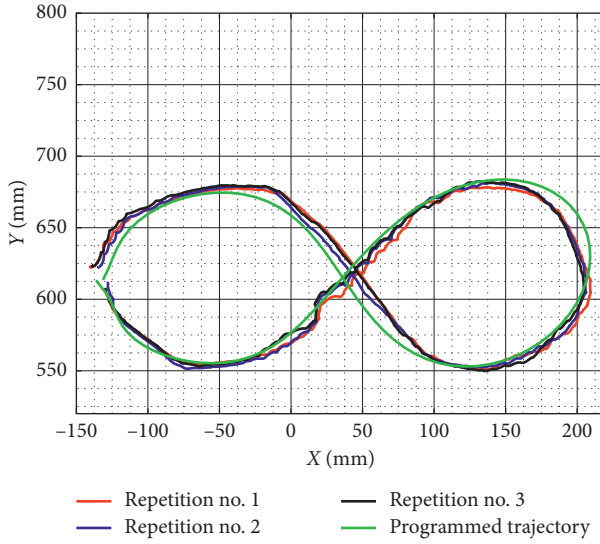


FIGURE 19: Comparison between the programmed trajectory and the TP trajectories from three repetitions during test no. 2 without load.

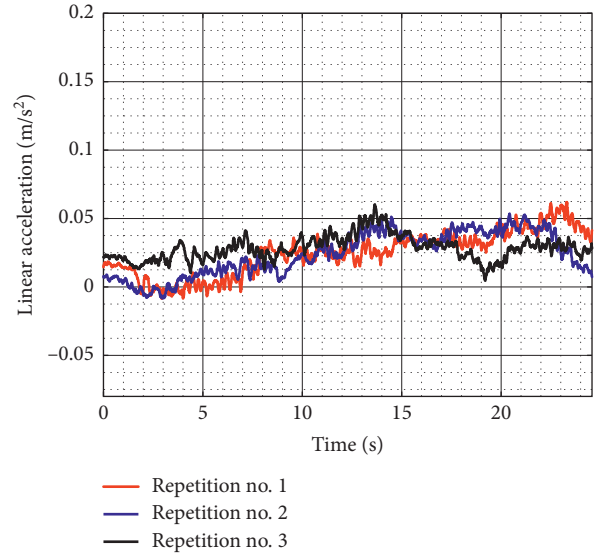
negligible, and it shows that the movement of the TP is smooth. The spikes in the linear acceleration are due to the backlash of the wheels.

Figure 10 shows the acquired motor torques during test no. 1 when the device is unloaded for the three repetitions as seen in Figure 8. Motor 1 reaches a maximum magnitude of 2,071 N-mm, and Motor 2 reaches a maximum magnitude of 2,119 N-mm. The torque values confirm that commercial servomotors can be used for NURSE motion. In addition, the torques curves show a symmetrical behaviour between Motor 1 and Motor 2.

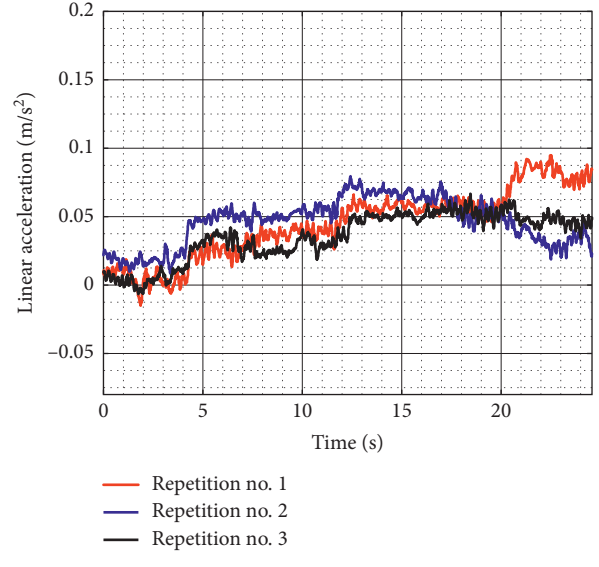
Figure 11 shows the power consumption of NURSE without load during test no. 1. The power consumption reaches a maximum value of 23.130 W. The power consumption values confirm that NURSE works with low-power consumption when it is unloaded.

Similarly, test no. 1 has been carried out with a load of 520 g during three repetitions. Figure 12 shows a zoomed view of a NURSE end-effector with the load of 520 g. Some snapshots of the test with the acquired trajectory from the TP during repetition no. 1 are shown in Figure 13. Figure 14 shows the trajectories acquired from the TP during the three repetitions and the programmed one. When NURSE is loaded in test no. 1, the deviation between the trajectories acquired from the TP and the programmed one has a maximum value of 13 mm. The deviation when NURSE is loaded is 3 mm greater than the deviation when NURSE is unloaded. However, this difference is negligible, and it can also be related with the accuracy of the home position as mentioned above. It is important to notice that the repeatability deviation between the trajectories performed by NURSE has a maximum value of 4.5 mm for test no. 1 with load.

The linear accelerations acquired from the TP during test no. 1 with a load of 520 g are shown in Figure 15. The linear accelerations in X have a maximum value of  $0.036 \text{ m/s}^2$  and a minimum value of  $-0.045 \text{ m/s}^2$ , and linear accelerations in Y



(a)



(b)

FIGURE 20: Acquired linear acceleration during test no. 2 without load for the three repetitions seen in Figure 19: (a) X linear acceleration; (b) Y linear acceleration.

have a maximum value of  $0.041 \text{ m/s}^2$  and a minimum value of  $-0.039 \text{ m/s}^2$ . Therefore, the linear acceleration values in X and Y are also negligible when the device is loaded. Thus, NURSE can reproduce the exercise of test no. 1 when it is loaded as smoothly as when it is unloaded.

When the device is loaded during test no. 1, the torque of the Motor 1 reaches a maximum magnitude of 2,926 N-mm and Motor 2 has a maximum magnitude of 3,217 N-mm (Figure 16). As seen in Figure 16, the torque increases around 1,098 N-mm when the device is loaded with respect to the torque when it is unloaded as seen in Figure 10. However, the torque values confirm that NURSE can also be moved by commercial motors in the loaded condition.

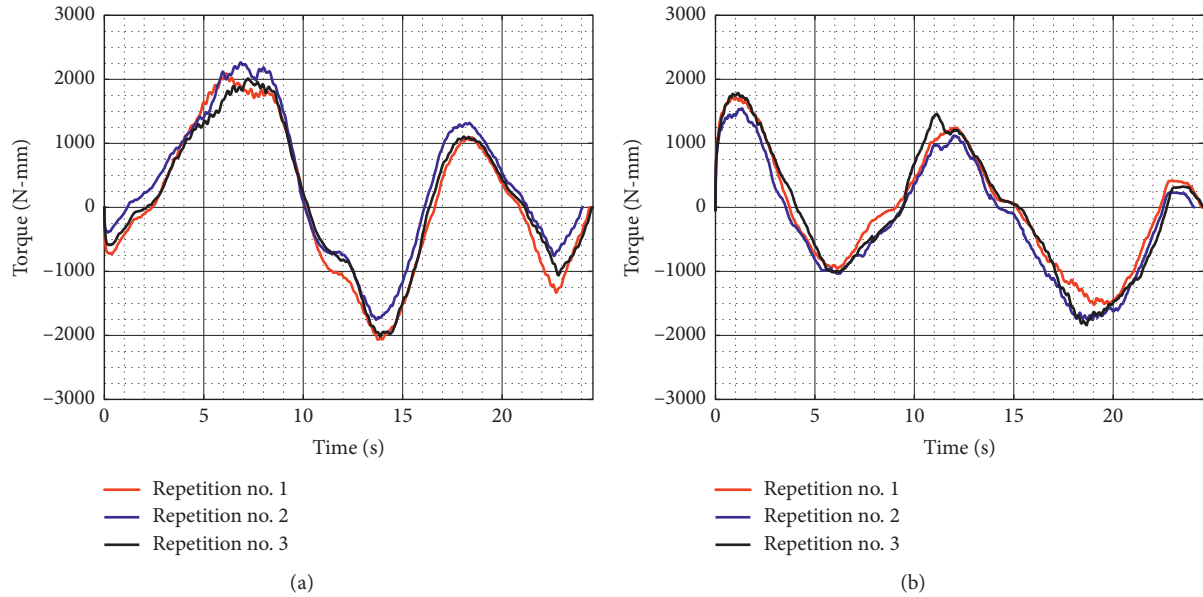


FIGURE 21: Computed torques during test no. 2 without load for the three repetitions seen in Figure 19: (a) Motor 1; (b) Motor 2.

The power consumption when NURSE is loaded has a maximum value of 30.35 W for test no. 1 (Figure 17). Thus, it increased 7.220 W with respect to the power consumption when NURSE is unloaded. Therefore, the NURSE low-power consumption characteristic remains.

Test no. 2 has been carried out without load during three repetitions. In Figure 18 are shown some snapshots of NURSE when it is performing repetition no. 1 together with the trajectory acquired from the TP. Figure 19 shows the trajectories acquired from the TP during repetition nos. 1, 2, and 3 and the programmed one. As seen in Figure 19, the trajectories performed by the NURSE to trace the number 8 are close to the programmed one with a maximum deviation of 16 mm. The deviation in test no. 2 is greater than the deviation in test no. 1 since the 8 shape has more changes in direction and is being more complex to perform than the trajectory for horizontal shoulder flexion. On the contrary, the backlash of NURSE wheels can affect the motion more when it has several changes of direction than when it maintains a same direction. However, the repeatability deviation between the trajectories performed by NURSE has a maximum value of 8.22 mm for test no. 2 without load. Despite the fact that the wheels backlash can affect the trajectory shape during test no. 2, the linear accelerations acquired from the TP show that the motion remains smooth as seen in Figure 20, where the linear accelerations in X have a maximum value of  $0.062 \text{ m/s}^2$  and a minimum value of  $-0.008 \text{ m/s}^2$  and linear accelerations in Y have a maximum value of  $0.095 \text{ m/s}^2$  and a minimum value of  $-0.015 \text{ m/s}^2$ . As seen in Figure 20, the linear acceleration values during test no. 2 have remained in the same range than the linear accelerations during test no. 1.

Figure 21 shows the torque required by Motor 1 and Motor 2 during test no. 2 without load. Motor 1 reaches a maximum torque of 2,264 N-mm, and Motor 2 reaches a maximum torque of 1,840 N-mm. As seen in Figure 21, the

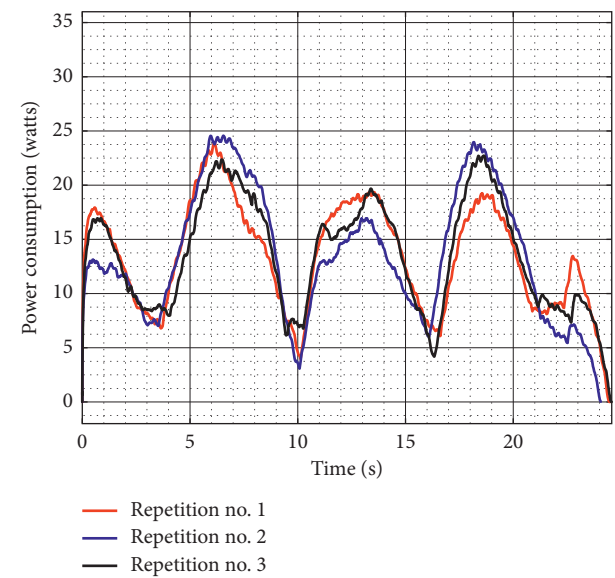


FIGURE 22: Computed power consumption during test no. 2 without load for the three repetitions seen in Figure 19.

torques reached by the motors without load during test no. 2 remain in the same range than the torques in test no. 1 without load. Therefore, it shows that when NURSE is unloaded, it requires a similar force to perform the trajectory for horizontal shoulder flexion than it requires to perform the number 8. The latter is confirmed also by the power consumption that presents a maximum value of 24.510 W (Figure 22). The power consumption during test no. 2 without load increases only 1.380 W with respect to the value in test no. 1 without load. Therefore, NURSE maintains low-power consumption while tracing the number 8.

Similarly, test no. 2 has been carried out during three repetitions by using a load of 520 g. Figure 23 shows some

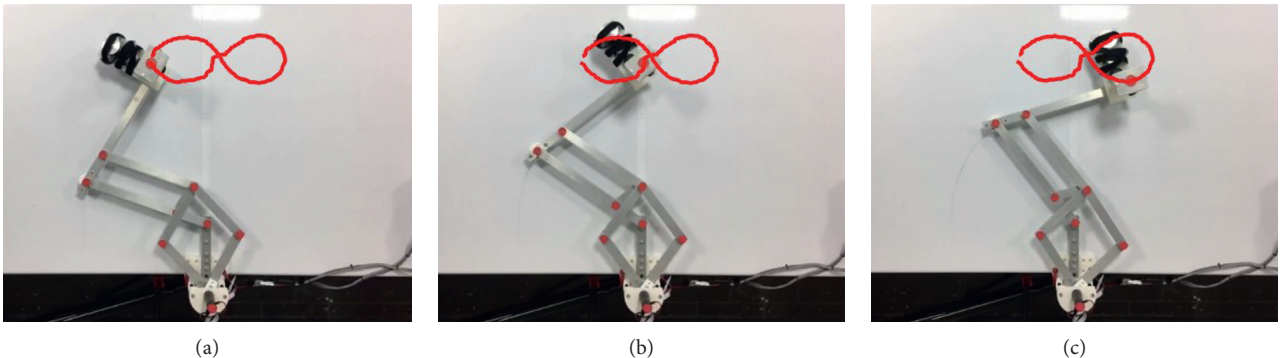


FIGURE 23: Some snapshots of test no. 2 with a load of 520 g during repetition no. 1 together with the trajectory obtained by image processing (in red): (a) the first sample position; (b) the second sample position; (c) the third sample position.

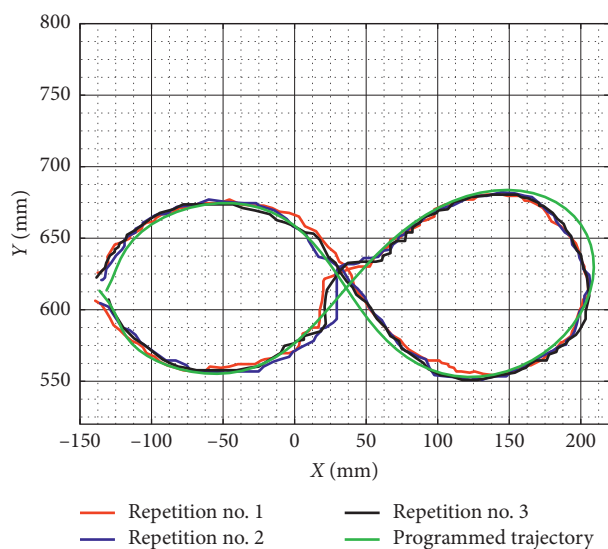


FIGURE 24: Comparison between the programmed trajectory and the TP trajectories from three repetitions during test no. 2 with a load of 520 g.

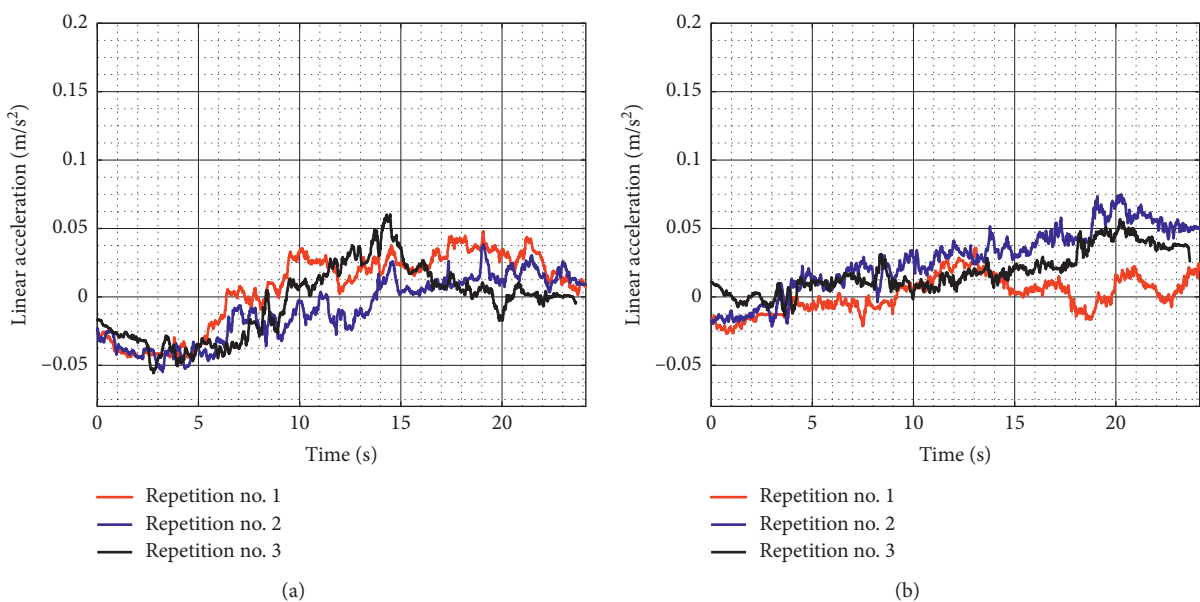


FIGURE 25: Acquired linear acceleration during test no. 2 with a load of 520 g for the three repetitions seen in Figure 24: (a) X linear acceleration; (b) Y linear acceleration.

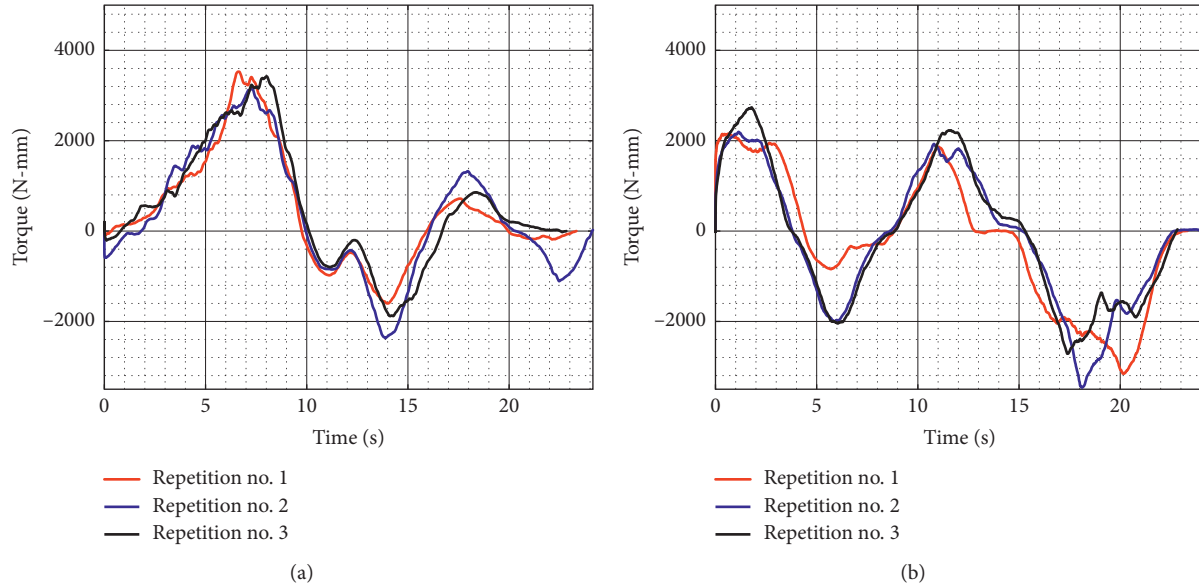


FIGURE 26: Computed torques during test no. 2 with a load of 520 g for the three repetitions seen in Figure 24: (a) Motor 1; (b) Motor 2.

snapshots of NURSE when it is performing repetition no. 1. As seen in Figure 24, the trajectories acquired from the TP during repetition nos. 1, 2, and 3 are close to the programmed one with a maximum deviation of 21 mm. However, the repeatability deviation between the trajectories performed by NURSE has a maximum value of 11.94 mm for test no. 2 with load. Although the wheels backlash introduces deviation in the motion to perform the trajectories, the linear accelerations acquired from the TP show that NURSE motion continues to be smooth with the linear accelerations in  $X$  having a maximum value of  $0.062 \text{ m/s}^2$  and a minimum value of  $-0.056 \text{ m/s}^2$  and linear accelerations in  $Y$  having a maximum value of  $0.075 \text{ m/s}^2$  and a minimum value of  $-0.026 \text{ m/s}^2$  (Figure 25). As seen in Figures 9, 15, 20, and 25, the linear accelerations acquired from the TP are maintained around the same range. Therefore, it can be said that NURSE can reproduce the trajectories with a smooth motion during test nos. 1 and 2 with and without load.

The torque of Motor 1 reached a maximum magnitude of 3,527 N-mm, and the torque of Motor 2 reached a maximum magnitude of 3,464 N-mm, Figure 26. In test no. 2, the torque increases 310 N-mm with respect to the torque when the device is loaded in test no. 1 (Figure 16). It can be said that NURSE needs more force when performing the exercise of test no. 2 than when performing the exercise of test no. 1 both in loaded conditions. However, the torque values are in a range that always can be reached by commercial servomotors. The power consumption has a maximum value of 37.080 W as seen in Figure 27. Therefore, the power consumption increased 6.730 W with respect to the obtained values during test no. 1 with a load as seen in Figure 17. However, NURSE continues to have low-power consumption also to trace the number 8 in loaded conditions.

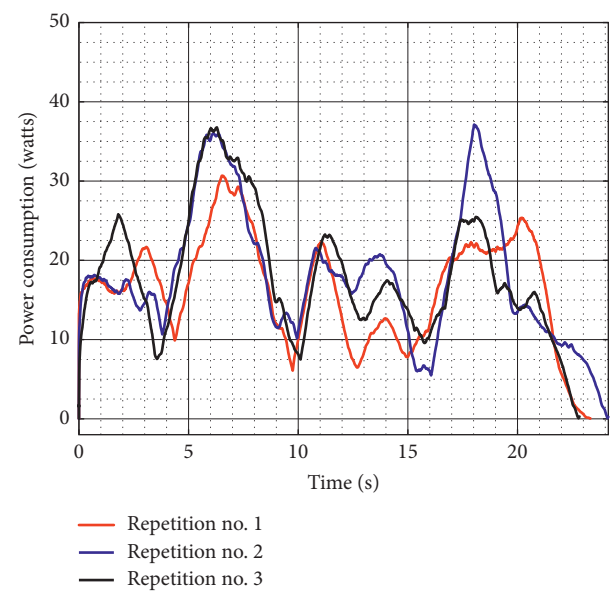


FIGURE 27: Computed power consumption during test no. 2 with a load of 520 g for the three repetitions seen in Figure 24.

## 5. Conclusions

NURSE, a device for arm motion assistance, is presented with an experimental characterization. NURSE can assist the motion of both right and left human arms during a rehabilitation therapy or during the arm exercise for elderly people. The NURSE behaviour has been characterized by performing tests of several exercises for upper limb rehabilitation or training, whereas in this paper, two significant ones have been discussed. The tests have successfully been carried out without and with load by looking at trajectory tracking, linear acceleration, torque, and power

consumption. The examined trajectories during the tests show that NURSE is able to perform a trajectory near to the programmed one with a minimum deviation of 16 mm when it is unloaded and a maximum deviation of 21 mm in the loaded condition. The trajectories performed by NURSE during reported test no. 1 have a satisfactory maximum repeatability deviation of 3 mm when it is unloaded and 4.5 mm when it is loaded. The trajectories performed by NURSE during reported test no. 2 have a satisfactory maximum repeatability deviation of 8.22 mm between them when it is unloaded and 11.94 mm when it is loaded. The linear accelerations during test nos. 1 and 2 have been successfully measured within a satisfactory range of minimum  $-0.008 \text{ m/s}^2$  and maximum  $0.095 \text{ m/s}^2$  with a smooth NURSE motion. The NURSE motors operated with a maximum torque of 3,527 N-mm occurring during test no. 2 with load as a feasible result for commercial servomotors. NURSE worked with low-power consumption without and with a load. The maximum power consumption has been 37.080 W and it has been reached during test no. 2 with load. The experimental results show that NURSE is capable of reproducing successfully different exercises with a smooth motion and a proper low-power consumption.

## Conflicts of Interest

The authors declare that they have no conflicts of interest.

## Acknowledgments

Betsy Dayana Marcela Chaparro-Rico thankfully acknowledges CONACYT for the financial support for her Ph.D. studies at Instituto Politécnico Nacional in Mexico with a program for a double Ph.D. degree at the University of Cassino and Southern Lazio.

## References

- [1] National Stroke Association, *Mobility after Stroke*, National Stroke Association, Centennial, CO, USA, 2018, [https://www.stroke.org/sites/default/files/resources/NSA\\_Mobility\\_brochure.pdf](https://www.stroke.org/sites/default/files/resources/NSA_Mobility_brochure.pdf).
- [2] I. P. Corona-Acosta, "Development of a mechatronic device for rehabilitation of the upper extremity (shoulder-elbow-wrist)," Master thesis, Instituto Politécnico Nacional-CICATA UNIDAD QUERÉTARO, Santiago de Querétaro, QRO, Mexico, 2015, in Spanish.
- [3] T. M. Skirven, A. L. Osterman, J. Fedorczyk, and P. C. Amadio, *Rehabilitation of the Hand and Upper Extremity*, Vol. 2, Elsevier Health Sciences, Toronto, ON, Canada, 6th edition, 2011.
- [4] S. J. Hall, *Basic Biomechanics*, McGraw-Hill, New York, NY, USA, 6th edition, 2012.
- [5] J. Rippe, S. McCarthy, and W. M. Abbott, *The Joint Health Prescription: 8 Weeks to Stronger, Healthier, Younger Joints*, Ballantine Books, New York, NY, USA, 2002.
- [6] P. Maciejasz, J. Eschweiler, K. Gerlach-Hahn, A. Jansen-Troy, and S. Leonhardt, "A survey on robotic devices for upper limb rehabilitation," *Journal of NeuroEngineering and Rehabilitation*, vol. 11, no. 3, pp. 1–29, 2014.
- [7] World Health Organization (WHO), *The Global Burden of Disease: 2004 Update*, WHO, Geneva, Switzerland, 2008, [http://www.who.int/healthinfo/global\\_burden\\_disease/2004\\_report\\_update/en/](http://www.who.int/healthinfo/global_burden_disease/2004_report_update/en/).
- [8] D. Knudson, *Fundamentals of Biomechanics*, Springer, Chico, CA, USA, 2nd edition, 2007.
- [9] W. E. Prentice, *Rehabilitation Techniques in Sports Medicine*, McGraw-Hill Education, Boston, MA, USA, 4th edition, 2003.
- [10] I. Kapandji, *The Physiology of the Joints*, Vol. 3, Churchill Livingstone, New York, NY, USA, 2008.
- [11] L. Ombregt, *A System of Orthopaedic Medicine*, Churchill Livingstone Elsevier, Edinburgh, Scotland, 3rd edition, 2013.
- [12] R. Riener, T. Nef, and G. Colombo, "Robot-aided neuro-rehabilitation of the upper extremities," *Medical and Biological Engineering and Computing*, vol. 43, no. 1, pp. 2–10, 2005.
- [13] C. G. Burgar, P. S. Lum, P. C. Shor, and H. F. Machiel Van der Loos, "Development of robots for rehabilitation therapy: the Palo Alto VA/Stanford experience," *Journal of Rehabilitation Research and Development*, vol. 37, no. 6, pp. 663–673, 2000.
- [14] P. S. Lum, C. G. Burgar, P. C. Shor, M. Majmundar, and M. Van der Loos, "Robot-assisted movement training compared with conventional therapy techniques for the rehabilitation of upper-limb motor function after stroke," *Archives of Physical Medicine and Rehabilitation*, vol. 83, no. 7, pp. 952–959, 2002.
- [15] S. L. Mediatic, *Figure 8 System*, Ref. NC99110, 2016, <http://www.mediatic.com/productos.aspx?tipo=1&pag=77&idprod=632>, in Spanish.
- [16] I. P. Corona-Acosta and E. Castillo-Castaneda, "Dimensional synthesis of a planar parallel manipulator applied to upper limb rehabilitation," in *Multibody Mechatronic Systems, Mechanisms and Machine Science*, H. M. E. Ceccarelli, Ed., vol. 25, pp. 443–452, Springer, Cham, Switzerland, 2015.
- [17] AliMed, *Ergo Arm Skate*, Ref. 8591, 2018, <https://www.alimed.com/ergo-arm-skate.html>.
- [18] Hocoma, *ArmeoPower*, 2017, <https://www.hocoma.com/solutions/armeo-power/>.
- [19] S. J. Ball, I. E. Brown, and S. H. Scott, "A planar 3DOF robotic exoskeleton for rehabilitation and assessment," in *Proceedings of the 29th Annual Conference of the IEEE EMBS*, pp. 4024–4027, Cité Internationale, Lyon, France, August 2007.
- [20] Y. Mao and S. Kumar-Agrawal, "Design of a cable-driven arm exoskeleton (CAREX) for neural rehabilitation," *IEEE Transactions on Robotics*, vol. 28, no. 4, pp. 922–931, 2012.
- [21] C. T. O'Neill, N. S. Phipps, L. Cappello, S. Paganoni, and C. J. Walsh, "A soft wearable robot for the shoulder: design, characterization, and preliminary testing," in *Proceedings of the 2017 International Conference on Rehabilitation Robotics (ICORR)*, pp. 1672–1678, QEII Centre, London, UK, July 2017.
- [22] H. Bian, Z. Chen, H. Wang, and T. Zhao, "Mechanical design of EFW Exo II: a hybrid exoskeleton for elbow-forearm-wrist rehabilitation," in *Proceedings of the 2017 International Conference on Rehabilitation Robotics (ICORR)*, QEII Centre, London, UK, July 2017.
- [23] T. Nef, M. Guidali, and R. Riener, "ARMin III—arm therapy exoskeleton with an ergonomic shoulder actuation," *Applied Bionics and Biomechanics*, vol. 6, no. 2, pp. 127–142, 2009.
- [24] J. Annisa, S. Mohamaddan, M. S. Jamaluddin et al., "Development of upper limb rehabilitation robot prototype for home setting," in *Proceedings of the 5th Brunei International Conference on Engineering and Technology (BICET 2014)*, pp. 1–6, Bandar Seri Begawan, Brunei, November 2014.
- [25] D. Campolo, F. Widjaja, and J. Klein Hubert, "An apparatus for upper body movement," US Patent Application No. US20150302777A1, USPTO, Alexandria, VA, USA, 2015.

- [26] H. I. Krebs, N. Hogan, M. L. Aisen, and B. T. Volpe, "Robot-aided neurorehabilitation," *IEEE Transactions on Rehabilitation Engineering*, vol. 6, no. 1, pp. 75–87, 1998.
- [27] Bionik Laboratories, *Inmotion Arm*, Bionik Laboratories, Toronto, ON, Canada, 2018, <http://bionikusa.com/healthcarereform/upper-extremity-rehabilitation/inmotion2-arm/>.
- [28] P. Leconte and R. Ronsse, "Performance-based robotic assistance during rhythmic arm exercises," *Journal of Neuro-Engineering and Rehabilitation*, vol. 13, no. 1, pp. 1–16, 2016.
- [29] B. D. M. Chaparro-Rico, E. Castillo-Castaneda, M. Ceccarelli, and D. Cafolla, "Design and test of therapy exercise for human arms," in *Proceedings of the 5th International Workshop on Medical and Service Robots (MESROB 2016)*, Graz, Austria, July 2016.
- [30] S. Chatzis, D. Korkinof, and Y. Demiris, "A quantum-statistical approach toward robot learning by demonstration," *IEEE Transactions on Robotics*, vol. 28, no. 6, pp. 1371–1381, 2012.
- [31] Microsoft, *User's Manual Microsoft: Kinect SDK*, 2015, <https://msdn.microsoft.com>.
- [32] B. D. M. Chaparro-Rico, D. Cafolla, M. Ceccarelli, and E. Castillo-Castañeda, "Device for arm motion assistance," Italian Application Patent No. IT102016000107499, October 2016.
- [33] B. Chaparro-Rico, D. Cafolla, M. Ceccarelli, and E. Castillo-Castaneda, "Design and simulation of an assisting mechanism for arm exercises," in *Advances in Italian Mechanism Science, Mechanisms and Machine Science*, G. Boschetti and A. Gasparetto, Eds., vol. 47, pp. 115–123, Springer, Cham, Switzerland, 2017.

## Research Article

# Human-Inspired Reflex to Autonomously Prevent Slip of Grasped Objects Rotated with a Prosthetic Hand

Zachary Ray and Erik D. Engeberg 

*Florida Atlantic University, Boca Raton, FL 33431, USA*

Correspondence should be addressed to Erik D. Engeberg; eengeberg@fau.edu

Received 16 February 2018; Accepted 17 April 2018; Published 24 June 2018

Academic Editor: Rafael Morales

Copyright © 2018 Zachary Ray and Erik D. Engeberg. This is an open access article distributed under the Creative Commons Attribution License, which permits unrestricted use, distribution, and reproduction in any medium, provided the original work is properly cited.

Autonomously preventing grasped objects from slipping out of prosthetic hands is an important feature for limb-absent people since they cannot directly feel the grip force applied to grasped objects. Oftentimes, a satisfactory grip force in one situation will be inadequate in different situations, such as when the object is rotated or transported. Over time, people develop a grip reflex to prevent slip of grasped objects when they are rotated with respect to gravity by their natural hands. However, this reflexive trait is absent in commercially available prosthetic hands. This paper explores a human-inspired grasp reflex controller for prosthetic hands to prevent slip of objects when they are rotated. This novel human-inspired grasped object slip prevention controller is evaluated with 6 different objects in benchtop tests and by 12 able-bodied subjects during human experiments replicating realistic tasks of daily life. An analysis of variance showed highly significant improvement in the number of successfully completed cycles for both the benchtop and human tests when the slip prevention reflex was active. An object sorting task, which was designed to serve as a cognitive distraction for the human subjects while controlling the prosthetic hand, had a significant impact on many of the performance metrics. However, assistance from the novel slip prevention reflex mitigated the effects of the distraction, offering an effective method for reducing both object slip and the required cognitive load from the prosthetic hand user.

## 1. Introduction

Approximately 541,000 people in the USA are living with an upper limb loss [1]; however, only 30%–50% of amputees use an electromyogram- (EMG-) controlled prosthetic hand or arm [2]. This high rejection rate is often because commercially available prostheses do not effectively solve problems for many limb-absent people, not because they are unavailable to them [3]. There is still a significant difference between prosthetic and human hands. This is due in no small part to the fact that the skin on the human hand has numerous sensory receptors which provide feedback to the central nervous system. These include the fast responding Pacinian and Meissner's corpuscles and the slow responding Ruffini corpuscle and Merkel cells. Each has unique sensory functions including the detection of vibration frequency, object texture, and finger pose, as well as grasp stability and force to name a few [4]. They provide highly efficient neural feedback allowing for a 0.06–0.08 second response to the

onset of the object slip [5]. Replicating the functionality and autonomous control of a human hand with modern-day prostheses is a challenging task.

Most powered prosthetic hands, such as the Motion Control Hand (MCH), currently used have a single degree of freedom (DOF) to enable a three fingered pinch grasp. However, there have been great advances recently toward more dexterous prostheses, such as the Vincent hand (Vincent Systems), the Bebionic hand (RSL Steeper), and the i-limb (Touch Bionics) [6].

Powered prosthetic hands are often controlled using a set of EMG preamplifiers placed on antagonistic muscles [7]. EMG signals are typically band-pass filtered, rectified, and amplified to obtain a functional motor control signal where the muscle contraction controls the force or speed of the hand [8, 9]. Although EMG control is a well-established technique used for the actuation of prostheses, improvements must be made in order to lessen the need for the user's visual attention and the cognitive control burden [9, 10].

Many myoelectric prosthetic hands have a powered wrist joint for pronation and supination [11]. While controlling the wrist joint, clinical practice does not allow the user to simultaneously control the grip force of grasped objects. A majority of clinical upper limb prostheses in use today are operated open loop [12], which can lead to frustrating situations where objects are inadvertently dropped as the user cannot directly feel if there is a sufficient grip force to prevent slip as the object is being rotated by the wrist. Even if the operator could visually determine if the grip force was insufficient [13], it would be difficult to react quickly enough to halt slip after the grasped object begins to slide due to EMG filter time constants that are prevalent in clinically available prosthesis control schemes [2].

Grasped object slip prevention is important for prosthetic hands because the user has no direct sense of the applied grip force, making it common to inadvertently drop objects [14, 15]. There are two main approaches to autonomously prevent grasped objects from being accidentally dropped: reactive and proactive. In reactive slip prevention, specialized tactile sensors [16, 17] can be used to detect when a grasped object slips and the grip force can be autonomously increased to prevent the object from being dropped [18, 19]. With proactive slip prevention, as incorporated within the SensorHand Speed [20], risky situations can be identified that are likely to induce slip and the grip force is autonomously increased prior to the onset of slip. These scenarios include unfavorable grip force to load force ratios [20, 21] or increased velocity [22] and acceleration [23] of the wrist, and both of which are likely to destabilize the grasp safety margin and cause objects to be dropped.

Commonly used objects, such as tools, beverages, and personal items, require grip force compensation to prevent slip when rotated with respect to gravity [24]. For example, when an object is grasped with a human hand and pronated such that the grip axis is aligned with gravity, the object is likely to slip as the shift in the object's center of mass location creates a different torque at the fingertips. However, this trait is absent in prosthetic hands and could be problematic when limb-absent operators rotate grasped objects with a powered wrist or their residual limb.

Because limb-absent people have mentioned that autonomous slip prevention is a desirable trait for prosthetic hands (Table 2 in [14]), the focus of this paper is on the development of a novel proactive slip prevention controller. The human-inspired trait of autonomously increasing the grip force as grasped objects are rotated with respect to gravity [25] will be implemented within a hybrid force-position sliding mode controller [26]. Results from benchtop experiments using the human-inspired slip prevention controller reliant upon hand orientation feedback (HOF) with respect to gravity while grasping six different objects with the MCH are presented [27]. New additions to this paper over that previously presented [27] include data from 12 able-bodied subjects who used the Motion Control Hand with and without HOF during an object sorting task.

## 2. Prosthetic and Robotic Systems

**2.1. The Motion Control Hand.** The Motion Control Hand (Motion Control, Inc. Salt Lake City, USA) has a single DOF. It is instrumented with an A1321 Hall effect sensor (Allegro Micro Systems Inc., Worcester, USA) used to measure the distance between the thumb and forefingers which are connected via a motor-driven four-bar linkage. Strain gauges on the thumb measure normal force ( $F_N$ ) of the grasp. The hand is also equipped with a gyro (IDG-300, InvenSense, Inc., Santa Clara, CA, USA), which is used to measure the orientation of the wrist with respect to gravity.

State space equations [28] to describe the single DOF MCH are given by

$$\dot{x}_1 = x_2, \quad (1)$$

$$\dot{x}_2 = -\frac{B}{J}x_2 - \frac{K}{J}(x_{1C} - x_1) + \frac{n}{J}E - \frac{D}{J}, \quad (2)$$

where  $x_1$  is the distance between the fingertips,  $x_{1C}$  is the position when the MCH makes contact with a given object, and  $x_2$  is the velocity.  $E$  is the voltage input, and  $J$  is the inertia of the system.  $K$  and  $B$  are the combined stiffness and damping of the grasped object-hand system, respectively;  $n$  is a constant derived from the gear ratio, armature resistance, and torque constant of the motor.  $D$  is the cumulative unknown and potentially nonlinear disturbances affecting the system.

**2.2. Yaskawa SIA10F Robotic Arm.** Motoman's SIA10F is a seven DOF robotic arm to which the Motion Control Hand is attached. Only the distal joint of the arm was necessary for this study to simulate human pronation and supination of the wrist as described in [25]. The SIA10F robotic arm utilizes the FS100 controller and DX100 Teach Pendant.

## 3. Sliding Mode Controller

Sliding mode control (SMC) has been implemented for prosthetic hands in the past using a hybrid force-position control law [29], which is particularly useful for prosthetic hands because it facilitates an ability to control both the force and the position of the hand through a single input. When grasping an object, the desired force from the operator is  $F_D$ , which is realized using an outer force control loop to form a force error signal. This force error signal yields the desired position of the hand:

$$x_D = G_F(F_D - F_N). \quad (3)$$

This force error, shown as the difference between  $F_D$  and the measured normal force of the hand  $F_N$ , is scaled by the gain,  $G_F$ . To enable sliding mode control, a position error is next formed as

$$e = x_D - x_1, \quad (4)$$

with which a sliding manifold is formed as

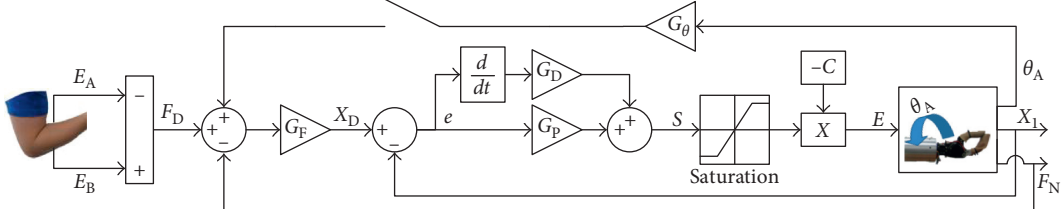


FIGURE 1: Diagram of the sliding mode controller. When the upper loop is closed, hand orientation feedback modulates the grip force.

$$S = G_P e + G_D \dot{e}, \quad (5)$$

where  $G_P$  is the proportional gain and  $G_D$  is the derivative gain. This enables control over the applied grip force as well as the position of the hand even if an object is not grasped.

The sliding mode controller (Figure 1) has been demonstrated to be robustly stable using the following control law:

$$E = -C \text{ sat}(S). \quad (6)$$

The constant,  $C$ , is based on an upper bound estimate on the torques acting on the motor of the hand and  $\text{sat}$  represents the saturation function to partially linearize the controller and prevent undesirable chatter or oscillations. Refer [26] for more details about this controller and [30] for discussion about the stability of sliding mode control for a broad class of systems.

#### 4. Human-Inspired Reflexive Slip Prevention Controller

Based on prior research, it is clear that the human grip force is coupled to wrist motions to maintain grasp stability [31]. A human-inspired prosthetic hand control strategy will be developed in this paper to mimic this trait. Prosthetic hand orientation feedback will be used to impart the anthropomorphic trait of modulating the grasp force based on pronation and supination motions of the wrist with respect to gravity, which had been studied in people [25]. This is a proactive slip prevention technique that is used to increase the grasp force when the grip axis is rotated through the field of gravity so that grasped objects are not inadvertently dropped. The specific control mechanism to enable this biomimetic trait is to feed back the measured wrist angle into the outer force feedback loop so that the desired position becomes

$$x_D = G_F (F_D - F_N + G_\theta \theta_A). \quad (7)$$

The orientation of the hand with respect to gravity is denoted by  $\theta_A$  in rad, and  $G_\theta$  is a proportional gain. With the inclusion of this positive feedback term, the applied grip force is increased relative to the rotation of the wrist relative to gravity, to mimic the human trait of proactive slip prevention during wrist rotation [25]. This sliding mode controller with HOF is shown in Figure 1 when the upper switch is closed.

Note that this HOF controller is robustly stable since the error term is still minimized by the sliding mode controller (6); the wrist angle feedback can be thought of as an

autonomous modifier of the hand operator's desired force signal. This is useful to reduce the cognitive burden required to operate prosthetic hands as will be subsequently shown.

#### 5. Experimental Methods

The sliding mode controller is implemented using Simulink (MathWorks, Natick, USA) and the real-time windows target kernel. Data were recorded at a rate of 1 kHz.

For each experiment, the hand is initially set to grasp a given object, with the grip axis in the plane of gravity (Figure 2(a)). Once grasped, the hand pronates  $\pi/2$  rad in 0.5 seconds (Figure 2(b)). The hand remains oriented with the grip axis perpendicular to gravity for 2 seconds (Figure 2(c)). It then supinates back to the start position with the grip axis in line with gravity in 0.5 seconds (Figure 2(d)). The hand remains in this position with the grip axis in line with gravity (Figure 2(e)) for 2 seconds, at which time the entire cycle (Figures 2(a)–2(e)) is repeated by the Yaskawa arm according to a predetermined program.

**5.1. Benchtop Tests.** Six relatively common items numbered one through six in Figure 3 were used in this study. The figure shows the grasp location of the thumb for each grasped item represented by the superimposed white thumbprint. The copper tube (Object 1, 262 g) was grasped at one end to induce a noticeable gravitational torque when the grip axis was rotated out of the plane of gravity. The grasp location for the paintbrush (Object 2, 57 g) was its wooden handle. The sealed aluminum soda can (Object 3, 386 g) was grasped around its middle. The compliant scrap metal (Object 4, 164 g) was used to show how the control system reacted to a deformable object. The scrap metal had a stiffness of 2.4 N/mm over the range of deformations imparted in this study. The compliant foam football (Object 5, 25 g) had a stiffness of 0.47 N/mm. The aluminum block (Object 6, 461 g) was also tested prior to use by the human subjects.

Each of the six objects was subjected to two different benchtop tests. The first test involved observing how the MCH performed the pronation/supination task without the influence of HOF. Each object was grasped with the minimum grip force and then subjected to the predefined rotations (Figures 2(a)–2(e)). The second test was identical to the first but with the HOF included (7) by closing the top feedback loop shown in Figure 1. Each test was repeated for ten trials, and each trial consisted of ten possible pronation/supination cycles. The cycle count stopped if the object was dropped.

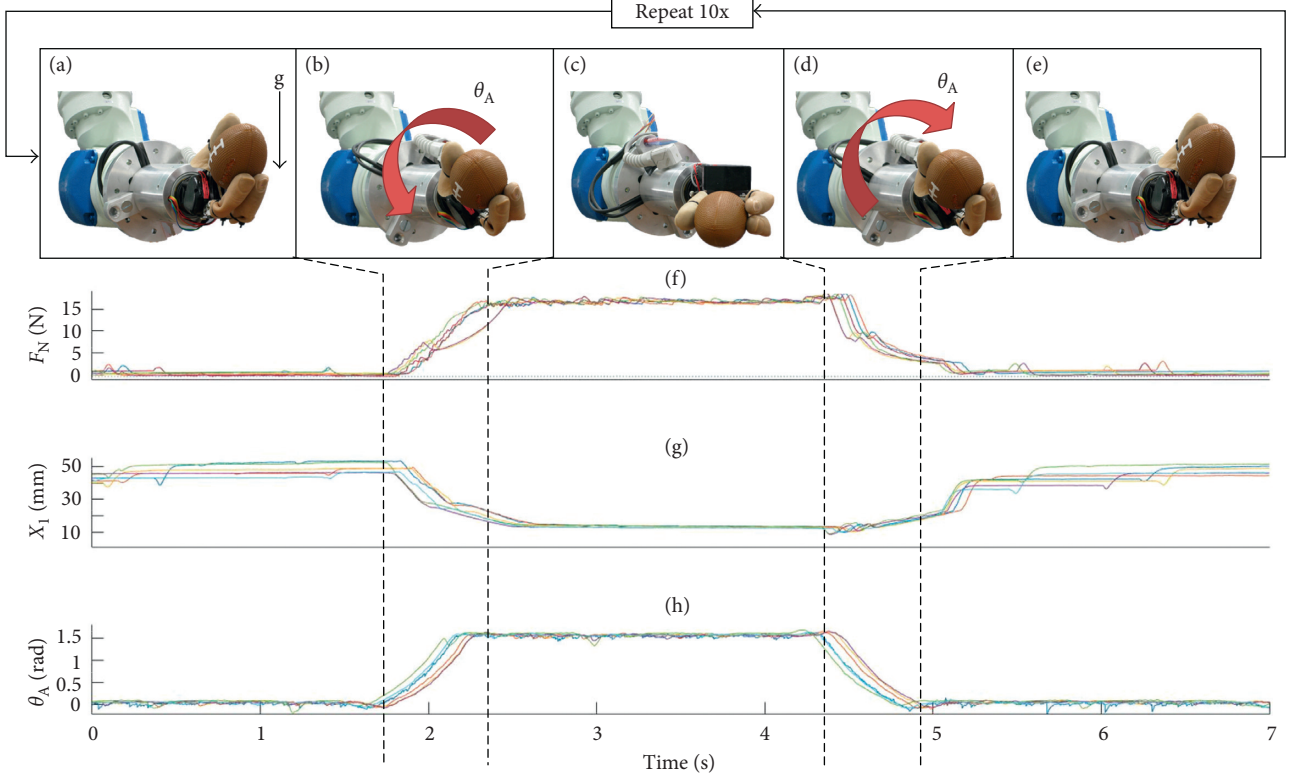


FIGURE 2: (a-e) Pronation-supination motion sequence aligned with (f) normal force, (g) fingertip distance, and (h) wrist angle.

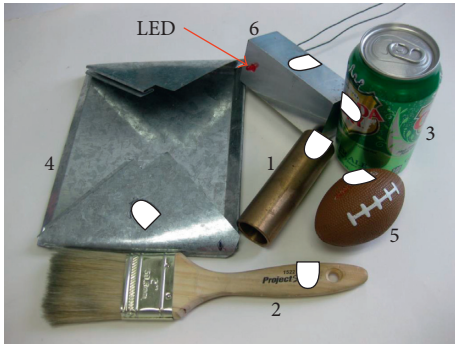


FIGURE 3: The grasped and rotated items includes (1) copper tube (262 g), (2) paintbrush (57 g), (3) full soda can (386 g), (4) compliant sheet metal (164 g), (5) stress football (25 g), and (6) aluminum block (461 g) equipped with a LED to indicate if the object was squeezed too tightly during the human trials. The superimposed white thumbprint shows how the item was grasped.

The effect of each object and the use of the human-inspired HOF on the number of successful cycles completed were analyzed using a two-factor ANOVA test.

**5.2. Human Trials.** Twelve able-bodied subjects (four females and eight males) participated in this experiment. All subjects gave voluntary written and informed consent in accordance with the approved IRB protocol.

Each subject was allowed approximately 15 minutes to familiarize him or herself with EMG control while the

experimenter calibrated the EMG hardware (MyoLab II, Motion Control, Inc. Salt Lake City, USA) for each individual. The subject sat comfortably in an office chair facing the prosthetic hand with the EMG preamplifiers strapped to the forearm of his or her nondominant hand. One preamplifier was placed atop the extensor digitorum communis muscle, and the other preamplifier was placed over the flexor carpi radialis [32].

The dominant hand was kept free for a sorting task performed in the second half of this experiment. This sorting task served as an additional cognitive load that is similar to sorting tasks performed daily; it consisted of separating a mix of four types of nuts and bolts (50 pieces total) into unique containers. Figure 4 shows a diagram of the testing environment including the data flow for the EMG to the DAQ (green) and signals sent to and from the robot (dashed blue). All subjects were timed as they completed the sorting task three times prior to EMG experimentation. This baseline test provided information on the individual's sorting rate while unhindered by the additional task of EMG control.

All subjects participated in four different sets of experiments with the MCH grasping the instrumented aluminum block (Figure 3, Object 6). Each of the four tests was repeated for three trials, and each trial consisted of ten possible pronation/supination cycles. The total number of completed cycles depended on the subject's success rate. The first two tests performed by all subjects were either EMG control without HOF or EMG control with HOF. The third and fourth tests were the same as the first two; however, the subjects in these cases were also asked to simultaneously

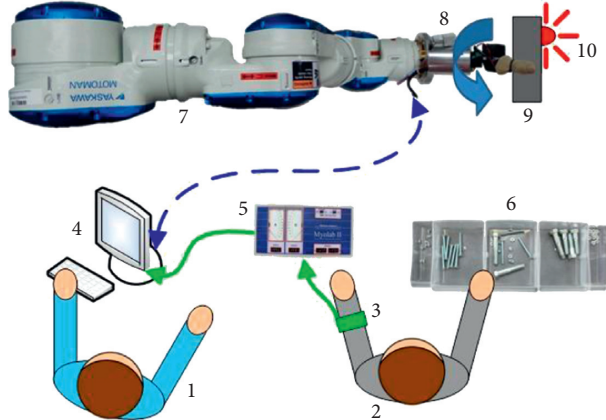


FIGURE 4: Test environment: (1) test operator; (2) test subject; (3) EMG preamplifiers strapped to the subject's forearm; (4) computer running Simulink; (5) MyoLab II for EMG signal processing; (6) sorting task; (7) Yaskawa seven DOF robot arm; (8) Motion Control Hand; (9) aluminum block, Object 6 in Figure 3; (10) LED indicator showing a failure if the object was squeezed too tightly.

TABLE 1: Testing order for the 12 subjects who were separated into four groups. The first two EMG tests were done without the sorting task, and the third and fourth EMG tests were done with the sorting task.

Group	Without sorting		With sorting	
	Test 1	Test 2	Test 3	Test 4
1	HOF	No HOF	HOF	No HOF
2	HOF	No HOF	No HOF	HOF
3	No HOF	HOF	HOF	No HOF
4	No HOF	HOF	No HOF	HOF

perform the previously mentioned nuts and bolts sorting task. The twelve subjects were separated into one of the four different groups (three subjects per group) and performed each experimental condition in different orders to counterbalance the impact of learning with the different control configurations and tasks (Table 1).

Two failure conditions were possible for each test: a break condition and a drop condition. The instrumented aluminum block (Figure 3, Object 6) used in this study was equipped with an LED which lit up if the break condition force threshold was surpassed. The strain gauges in the MCH's thumb were used to determine the normal force applied to the object. The normal force for the break condition threshold was set to offer a moderate challenge while rotating the object. The number of breaks per trial was recorded in Simulink, but the testing continued regardless of break failures. If the object was dropped, the drop failure condition was tallied and the failed trial was terminated. The outline of the MCH's thumb was traced onto the block, and it was also considered a "drop" failure if the object slipped out of the traced area. During the third and fourth tests involving the sorting task, the number of nuts and bolts correctly sorted was also recorded for each trial from which the average rate of sorting was calculated.

After completing the experiments, each person was also asked to subjectively rate the difficulty of each of the four

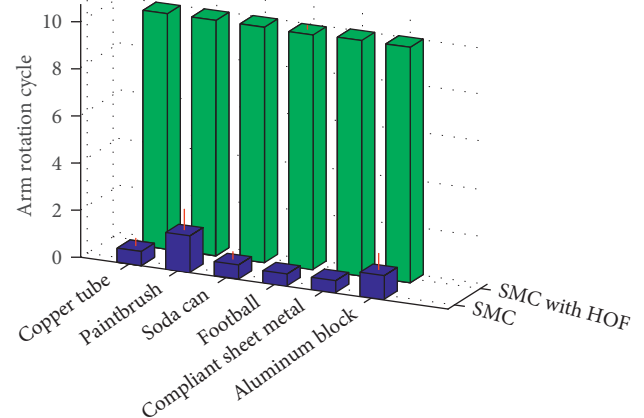


FIGURE 5: The number of successful cycles completed using the SMC without HOF is shown in blue, while the number of successful cycles completed using the SMC with HOF is shown in green for each object tested. Red lines indicate the standard deviations.

experimental combinations with and without being required to sort objects with or without HOF. A scale of 1 to 10 was used with 1 being difficult and 10 being easy.

The statistical significance of individual subject performance, HOF, and the sorting task on the collected data for number of successful cycles, drops, and breaks was analyzed using a three-factor ANOVA test. Also, the effect of variance caused by subject performance and HOF on the sorting count and sorting rate was analyzed using a two-factor ANOVA test. These analyses were performed to ascertain whether HOF with or without the cognitive load from the sorting task significantly impacted the performance metrics and whether or not there was interaction among any of the factors. Statistical significance of the subjective ratings was analyzed using a nonparametric Wilcoxon rank sum test for equal medians.

## 6. Results

**6.1. Benchtop Tests.** The data plots of Figure 2 illustrate the grip force,  $F_N$ , the distance between the MCH's fingers,  $x_1$ , and the angle of the wrist,  $\theta_A$ . The normal force (Figure 2(f)) applied to the grasped object increased to compensate for the wrist rotation with HOF. The tip-to-tip distance between the finger and thumb of the MCH (Figure 2(g)) decreased as the compliant object deformed, but it remained nearly constant when grasping rigid objects. The wrist pronated and supinated through the  $\pi/2$  radians (Figure 2(h)) in 0.5 seconds.

Objects grasped by the MCH without HOF were most frequently dropped on the first or second cycle. The objects grasped with HOF remained in the hand for all cycles with the exception of one football rotation cycle (Figure 5). The variance in the number of successful cycles completed was significantly impacted by the unique object and HOF ( $p < 0.01$ ), but not their interaction ( $p > 0.05$ ). The overall average number of successful cycles completed for each object was  $0.79 \pm 0.37$  for SMC and  $9.99 \pm 0.03$  for SMC with HOF.

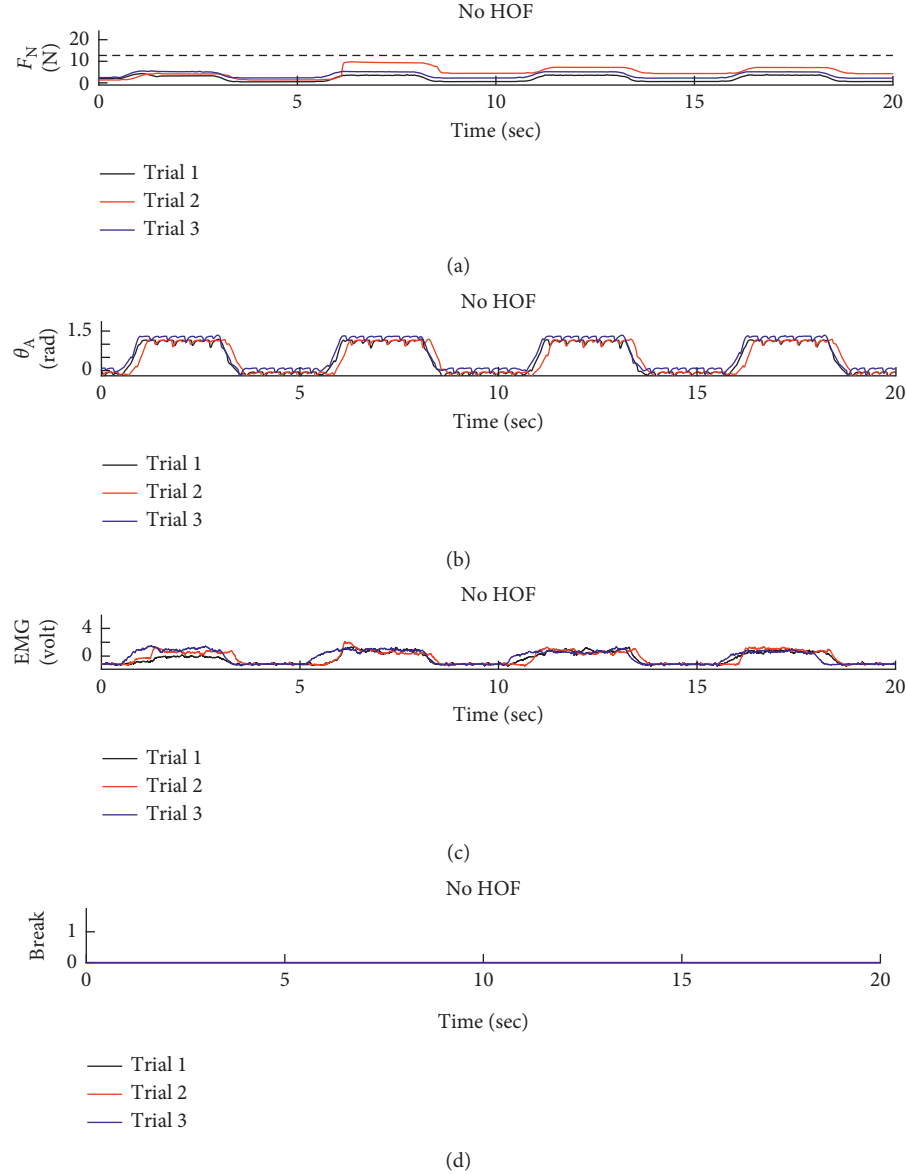


FIGURE 6: Test data for Group 2, Subject 1. This dataset shows the subject using EMG to control the hand. This subject was able to maintain a steady grip while focused on the task at hand.

**6.2. Human Subject Results.** Sample data for two different tests are presented for a subject with a relatively high level of skill with EMG control of the prosthetic hand in Figures 6 and 7. The first two subplots in each figure show the normal force and wrist angle similar to the benchtop tests. The dashed line in the normal force subplots shows the break failure threshold. Notice that this threshold is not crossed in Figure 6(a) like it is in Figure 7(a). The additional cognitive load represented by the sorting task is apparent in the EMG signals of Figures 6(c) and 7(c) as the subject is unable to focus entirely on a single task. An example of a break failure is recorded as shown in Figure 7(d). The EMG input signals for each trial are included in these figures. These signals show a nearly proportional relationship between the EMG signal and the normal force the hand applies to the object.

The number of successfully completed cycles shown in Figure 8 shows the efficacy of the artificial slip prevention reflex afforded by HOF. Each test had a maximum of three possible drop failures, and the total number of drops is shown in Figure 9. In these figures, S1, S2, and S3 are the first, second, and third human subjects in each of the four groups. The overall average and standard deviation for the number of successfully completed cycles and number of drops is shown in Table 2. The sorting task had a significant impact on the number of drops and total number of successful cycles, but the HOF significantly improved this metric (Table 3).

The maximum possible number of break failures for each test was 30 (three trials with ten pronation/supination cycles each) if the object was not dropped. Figure 10 shows the total number of break failures by each subject

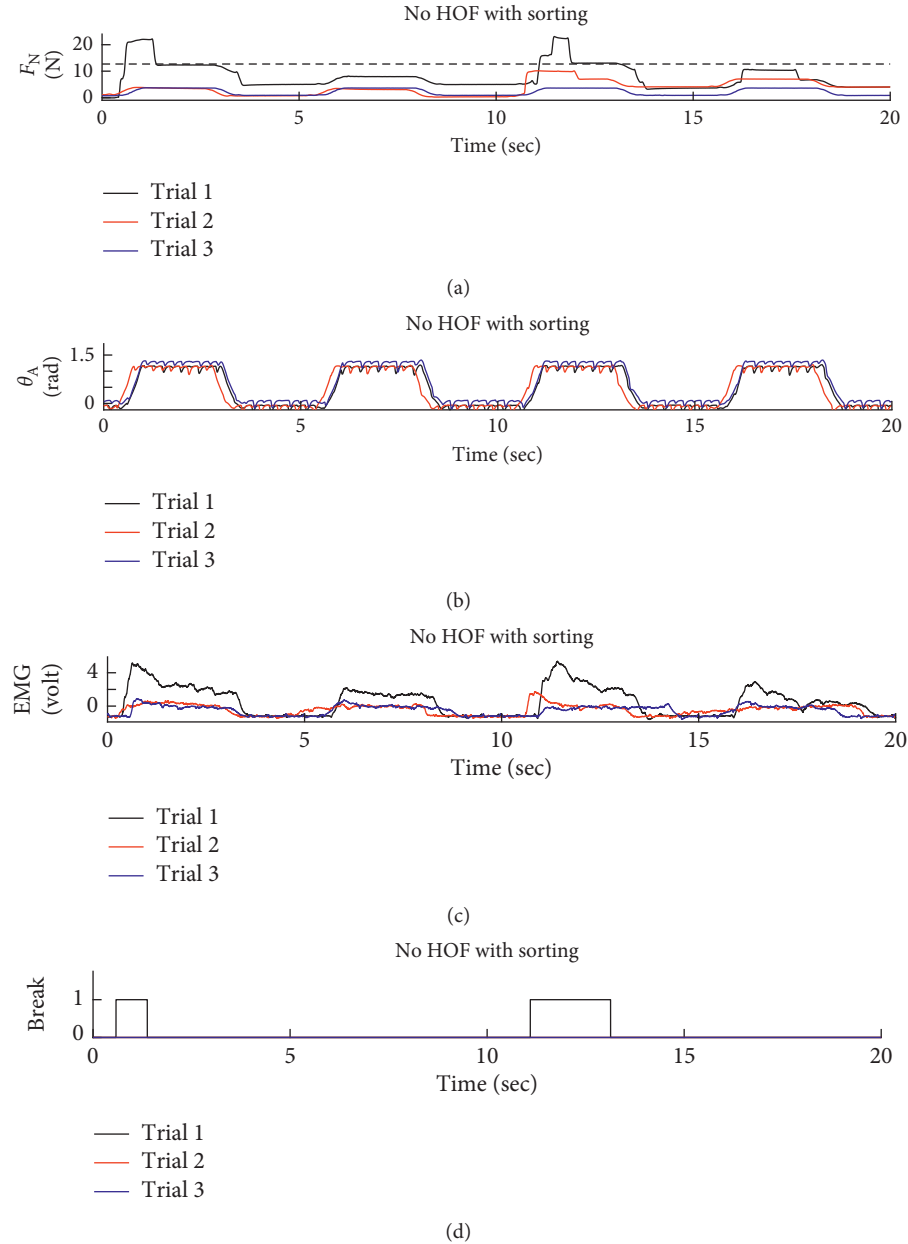


FIGURE 7: Test data for Group 2, Subject 1. This dataset shows the subject using EMG to control the hand without the assistance of HOF while simultaneously sorting parts. This subject was unable to maintain the same level of focus resulting in the grasp force exceeding the dashed line which represents the break threshold.

for every test. The overall average and standard deviation for number of break failures is shown in Table 2. The total break count was not significantly impacted by the sorting task, but it was significantly improved with the use of HOF (Table 3).

The number of parts sorted and the completion time for the sorting task were recorded and compared to the baseline case when the subjects sorted the nuts and bolts prior to controlling the hand. The average sorting rate was calculated from three iterations of the sorting task for each subject to serve as a baseline comparison to the sorting rate obtained while controlling the hand with and without HOF. The total number of parts sorted was summed for each of the three trials performed with and without HOF (Figure 11).

The average sorting rate was then determined based on the number of parts sorted and the duration of the successful cycles for each trial. The overall average and standard deviation for these is shown in Table 2. It is clear that more parts were sorted with HOF and the sorting rate was fairly consistent. An ANOVA test reveals that the total number of parts sorted was significantly more with HOF (Table 3) because the objects were not dropped meaning that the subject had the maximum possible amount of sorting time. The influence of the subject was insignificant (Table 3). The sorting rate was different in the sense that HOF was not a significant factor, and the subject was a significant factor (Table 3). This can be attributed to the fact that each

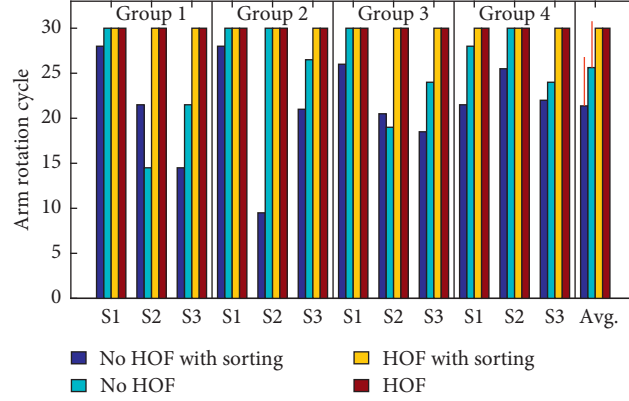


FIGURE 8: Total number of successful cycles out of 30 (10 for each of the 3 trials) attempted trials. S1, S2, and S3 are the first, second, and third subjects in each of the four groups.

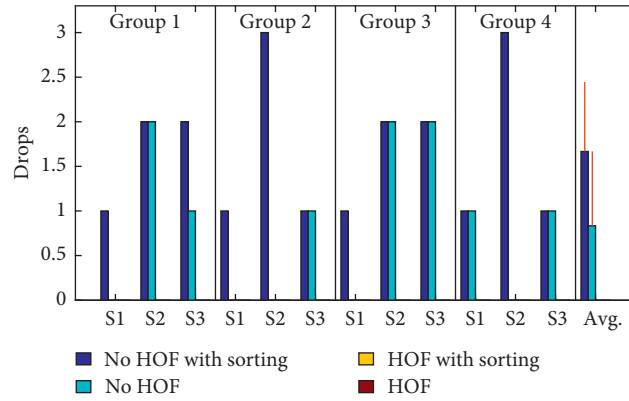


FIGURE 9: Total number of drop failures for each test out of 3.

TABLE 2: The overall average  $\pm$  standard deviation of each performance metric for each of the four tests.

Performance metric	Without HOF with sorting	Without HOF without sorting	With HOF with sorting	With HOF without sorting
Successful cycles	$21.4 \pm 5.43$	$25.6 \pm 5.15$	$30.0 \pm 0.00$	$30.0 \pm 0.00$
Drop count	$1.67 \pm 0.778$	$0.833 \pm 0.835$	$0.000 \pm 0.000$	$0.000 \pm 0.000$
Break count	$4.33 \pm 2.77$	$2.92 \pm 2.54$	$0.167 \pm 0.577$	$0.000 \pm 0.000$
Sort count	$91.4 \pm 27.1$	—	$129 \pm 15.2$	—
Sort rate	$0.819 \pm 0.187$	—	$0.870 \pm 0.115$	—
Subjective ranking	$4.17 \pm 1.59$	$6.33 \pm 1.50$	$8.50 \pm 1.00$	$9.92 \pm 0.289$

TABLE 3: *p* values from the three-factor ANOVA showing the level of effect that the subject's performance, the HOF, and the sorting task had on the collected data shown in the columns. It is clear that HOF had a highly significant impact on all data except the sorting rate, which was primarily affected by the individual subject's performance. The sorting task had a significant impact on all data except the break count.

Variable	Successful cycles	Drop count	Break count	Break rate	Sort count	Sort rate
Subject	0.194	0.440	0.255	0.254	0.095	0.012
HOF	0.000	0.000	0.000	0.000	0.000	0.221
Sorting	0.043	0.025	0.131	0.029	—	—
Subject HOF	0.194	0.440	0.296	0.350	0.943	0.397
Subject sorting	0.500	0.500	0.368	0.347	—	—
HOF sorting	0.043	0.025	0.224	0.045	—	—
Subject HOF sorting	0.989	1.000	0.984	0.862	—	—

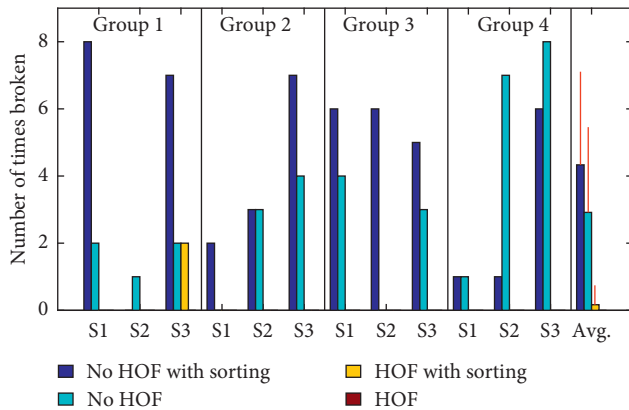


FIGURE 10: Total number of break failures for the 12 individual subject's successful number of cycles out of 30.

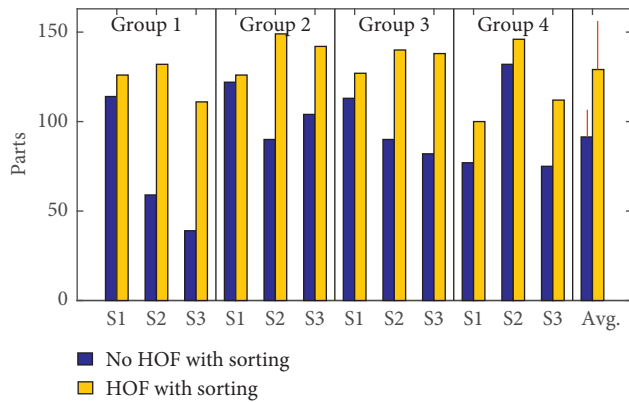


FIGURE 11: Total number of parts sorted out of 150 (50 for each of the 3 trials).

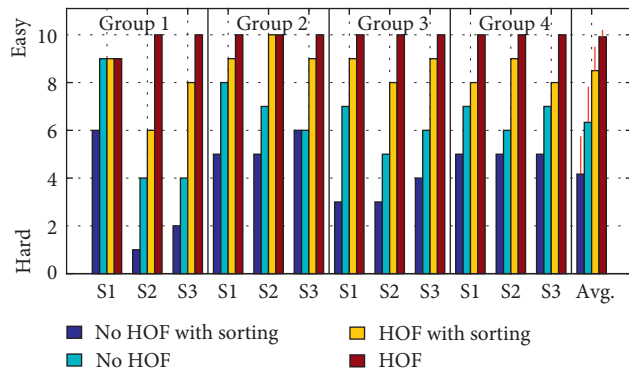


FIGURE 12: Subjective difficulty rating for each test scaling from 1 (hard) to ten (easy).

subject sorted at an individual pace of which the HOF was independent.

Subjects provided a qualitative rating of the difficulty for each test ranging from one (very difficult) to ten (very easy) shown in Figure 12. As expected, the sorting task increased the difficulty, but the tests performed without HOF were rated much more difficult than those with HOF. Overall averages and standard deviations for the subjective ranking

are shown in (Figure 12). The order of the subjective ranking of the tests from easiest to hardest was statistically proven to be HOF without sorting, HOF with sorting, no HOF without sorting, and finally no HOF with sorting (Figure 12).

The order in which subjects attempted each test was structured to counterbalance the effect of a learning curve for the overall group of 12 subject's EMG operation of the MCH (Table 1). An ANOVA study showed the subject's influence on the data collected due to learning curve to be insignificant (Table 3).

## 7. Discussion

The increased use of sensor feedback will likely be more common in future prosthetic hand designs to allow more functional human-inspired closed loop control [33]. In this paper, both benchtop and human-controlled prosthetic hand experiments have demonstrated the utility of a novel grasped object slip prevention reflex enabled by HOF with respect to gravity for the MCH. Extension of the HOF slip prevention technique to multi-DOF hands such as the i-limb would be simple provided the forward kinematics equations were used to calculate the orientation of the grip axis. Another solution to circumvent the need for forward kinematics (which would require joint angle sensors) is to embed a small accelerometer into the distal link of the prosthetic finger to assess the grip axis orientation with respect to gravity. This would be useful for different grasp types such as power grip, precision grip, lateral pinch, and key grip [34]. It may also be useful to incorporate this control system into more complex hand synergies, similar to the one discussed in [7].

Even with advanced surgical procedures such as targeted muscle reinnervation [35], there will likely be less biocontrol signals available than controllable DOFs in the next generation of dexterous prosthetic hands such as the DEKA arm [35] and Modular Prosthetic Limb [36], both of which have powered wrists. Thus, there will be a continued need in the future for human-inspired low-level control algorithms [37, 38] such as the slip prevention reflex enabled by HOF to alleviate the operator's cognitive burden and reduce training time to gain proficiency.

## 8. Conclusion

The human-inspired grasped object slip prevention reflex enabled by hand orientation feedback dramatically improved the prosthetic hand's ability to maintain a precision grip on objects that were subjected to wrist pronation and supination. Benchtop tests showed the utility of the technique with six different objects with a wide range of mechanical characteristics. Human tests showed far fewer drop and break failures for each object and person with HOF. A realistic sorting task performed during testing showed the usefulness of HOF for all 12 human subjects, which was further corroborated in their qualitative controller evaluations. The object was broken and dropped much less frequently with the use of HOF while still sorting at approximately the same speed. Additionally, it would be easy

to scale the technique to powered prosthetic elbows and shoulders. This human-inspired slip prevention reflex provides an inexpensive and practical way to anthropomorphically prevent grasped object slip while rotating objects, which would be very useful for prosthetic hands.

## Conflicts of Interest

The authors declare that they have no conflicts of interest.

## Acknowledgments

This research was supported in part by the National Science Foundation (Award nos. 1317952 and 1536136) and the National Institutes of Health (Award no. 1R01EB025819).

## References

- [1] K. Ziegler-Graham, E. MacKenzie, P. Ephraim, T. Travison, and R. Brookmeyer, "Estimating the prevalence of limb loss in the US: 2005–2050," *Archives of Physical Medicine and Rehabilitation*, vol. 89, no. 3, pp. 422–429, 2008.
- [2] A. Fougner, O. Stavdahl, P. Kyberd, Y. Losier, and P. Parker, "Control of upper limb prostheses: terminology and proportional myoelectric control-a review," *IEEE Transactions on Neural Systems and Rehabilitation Engineering*, vol. 20, no. 5, pp. 663–677, 2012.
- [3] E. Biddiss, D. Beaton, and T. Chau, "Consumer design priorities for upper limb prosthetics," *Disability and Rehabilitation: Assistive Technology*, vol. 2, no. 6, pp. 346–357, 2007.
- [4] R. S. Dahiya, G. Metta, M. Valle, and G. Sandini, "Tactile sensing—from humans to humanoids," *IEEE Transactions on Robotics*, vol. 26, no. 1, pp. 1–20, 2010.
- [5] R. S. Johansson and G. Westling, "Roles of glabrous skin receptors and sensorimotor memory in automatic control of precision grip when lifting rougher or more slippery objects," *Experimental Brain Research*, vol. 56, no. 3, pp. 550–564, 1984.
- [6] J. Belter, J. Segil, A. Dollar, and R. Weir, "Mechanical design and performance specifications of anthropomorphic prosthetic hands: a review," *Journal of Rehabilitation Research and Development*, vol. 50, no. 5, pp. 599–618, 2013.
- [7] B. Kent, N. Karnati, and E. Engeberg, "Electromyogram synergy control of a dexterous artificial hand to unscrew and screw objects," *Journal of NeuroEngineering and Rehabilitation*, vol. 11, no. 1, p. 41, 2014.
- [8] C. J. De Luca, "The use of surface electromyography in biomechanics," *Journal of Applied Biomechanics*, vol. 13, no. 2, pp. 135–163, 1997.
- [9] M. Oskoei and H. Hu, "Myoelectric control systems-a survey," *Biomedical Signal Processing and Control*, vol. 2, no. 4, pp. 275–294, 2007.
- [10] F. Cordella, A. Ciancio, R. Sacchetti et al., "Literature review on needs of upper limb prosthesis users," *Frontiers in Neuroscience*, vol. 10, 2016.
- [11] N. Bajaj, A. Spiers, and A. Dollar, "State of the art in prosthetic wrists: commercial and research devices," in *Proceedings of the International Conference on Rehabilitation Robotics*, Singapore, August 2015.
- [12] I. Saunders and S. Vijayakumar, "The role of feed-forward and feedback processes for closed-loop prosthesis control," *Journal of NeuroEngineering and Rehabilitation*, vol. 8, no. 1, p. 60, 2011.
- [13] E. Engeberg and S. Meek, "Enhanced visual feedback for slip prevention with a prosthetic hand," *Prosthetics and Orthotics International*, vol. 36, no. 4, pp. 423–429, 2012.
- [14] E. Biddiss and T. Chau, "Upper limb prosthesis use and abandonment: a survey of the last 25 years," *Prosthetics and Orthotics International*, vol. 31, no. 3, pp. 236–257, 2007.
- [15] P. Kyberd, C. Wartenberg, L. Sandsjo et al., "Survey of upper-extremity prosthesis users in Sweden and the United Kingdom," *Journal of Prosthetics and Orthotics*, vol. 19, no. 2, pp. 55–62, 2007.
- [16] J. Fishel and G. Loeb, "Bayesian exploration for intelligent identification of textures," *Frontiers in Neurorobotics*, vol. 6, pp. 1–20, 2012.
- [17] M. Vatani, E. Engeberg, and J. Choi, "Force and slip detection with direct-write compliant tactile sensors using multi-walled carbon nanotubes/polymer composites," *Sensors and Actuators A: Physical*, vol. 195, pp. 90–97, 2013.
- [18] E. Engeberg and S. Meek, "Adaptive sliding mode control for prosthetic hands to simultaneously prevent slip and minimize deformation of grasped objects," *IEEE/ASME Transactions on Mechatronics*, vol. 18, no. 1, pp. 376–385, 2013.
- [19] Y. Yamada, H. Morita, and Y. Umetani, "Slip phase isolating: impulsive signal generating vibrotactile sensor and its application to real-time object regrip control," *Robotica*, vol. 18, no. 1, pp. 43–49, 2000.
- [20] G. Puchhammer, "The tactile slip sensor: integration of a miniaturized sensory device on an myoelectric hand," *Orthopadie*, vol. 1, pp. 7–12, 2000.
- [21] N. Wettels, A. Parnandi, J. Moon, G. Loeb, and G. Sukhatme, "Grip control using biomimetic tactile sensing systems," *IEEE/ASME Transactions on Mechatronics*, vol. 14, no. 6, pp. 718–723, 2009.
- [22] B. Kent and E. Engeberg, "Robotic hand acceleration feedback to synergistically prevent grasped object slip," *IEEE Transactions on Robotics*, vol. 33, no. 2, pp. 492–499, 2017.
- [23] E. Engeberg, M. Frankel, and S. Meek, "Biomimetic grip force compensation based on acceleration of a prosthetic wrist under sliding mode control," in *Proceedings of the IEEE Robotics and Biomimetics Conference*, Pasadena, CA, USA, February 2008.
- [24] R. Balasubramanian, L. Xu, P. Brook, J. Smith, and Y. Matsuoka, "Physical human interactive guidance: identifying grasping principles from human-planned grasps," *IEEE Transactions on Robotics*, vol. 28, no. 4, pp. 899–910, 2012.
- [25] R. Johansson, J. Backlin, and M. Burstedt, "Control of grasp stability during pronation and supination movements," *Experimental Brain Research*, vol. 128, no. 1-2, pp. 20–30, 1999.
- [26] E. D. Engeberg, S. G. Meek, and M. A. Minor, "Hybrid force-velocity sliding mode control of a prosthetic hand," *IEEE Transactions on Biomedical Engineering*, vol. 55, no. 5, pp. 1572–1581, 2008.
- [27] Z. Ray and E. D. Engeberg, "Hand orientation feedback for grasped object slip prevention with a prosthetic hand," in *Proceedings of the Conference on Recent Advances in Robotics*, Florida, USA, May 2016.
- [28] N. Nise, *Control Systems Engineering*, John Wiley and Sons, Singapore, 3rd edition, 2002.
- [29] E. Engeberg, "A physiological basis for control of a prosthetic hand," *Biomedical Signal Processing and Control*, vol. 8, no. 1, pp. 6–15, 2013.
- [30] J. Slotine and W. Li, *Applied Nonlinear Control*, Prentice Hall, Upper Saddle River, NJ, USA, 2002.

- [31] M. Werremeyer and K. Cole, "Wrist action affects precision grip force," *Journal of Neurophysiology*, vol. 78, no. 1, pp. 271–280, 1997.
- [32] F. Netter, *Atlas of Human Anatomy*, Novartis, Basel, Switzerland, 2nd edition, 1998.
- [33] B. Matulevich, G. E. Loeb, and J. A. Fishel, "Utility of contact detection reflexes in prosthetic hand control," in *Proceedings of the IEEE/RSJ International Conference on Intelligent Robots and Systems (IROS)*, pp. 4741–4746, Tokyo, Japan, November 2013.
- [34] C. Connolly, "Prosthetic hands from touch bionics," *Industrial Robot*, vol. 35, pp. 290–293, 2008.
- [35] T. Kuiken, G. Li, B. Lock et al., "Targeted muscle reinnervation for real-time myoelectric control of multifunction artificial arms," *Journal of the American Medical Association*, vol. 301, no. 6, pp. 619–628, 2009.
- [36] M. S. Johannes, J. D. Bigelow, J. M. Burck, S. D. Harshbarger, M. V. Kozlowski, and T. Van Doren, "An overview of the developmental process for the modular prosthetic limb," *Johns Hopkins APL Technical Digest*, vol. 30, no. 3, pp. 207–216, 2011.
- [37] B. A. Kent and E. D. Engeberg, "Human-inspired feedback synergies for environmental interaction with a dexterous robotic hand," *Bioinspiration and Biomimetics*, vol. 9, no. 4, p. 046008, 2014.
- [38] B. Kent, J. Lavery, and E. Engeberg, "Anthropomorphic control of a dexterous artificial hand via task dependent temporally synchronized synergies," *Journal of Bionic Engineering*, vol. 11, no. 2, pp. 236–248, 2014.

## Research Article

# Evaluating the Effects of Kinesthetic Biofeedback Delivered Using Reaction Wheels on Standing Balance

Muhammad Raheel Afzal<sup>1</sup>, Amre Eizad<sup>1</sup>, Carlos Ernesto Palo Peña<sup>1</sup>,  
and Jungwon Yoon<sup>1</sup>

<sup>1</sup>School of Integrated Technology, Gwangju Institute of Science and Technology, Gwangju 61005, Republic of Korea  
<sup>2</sup>School of Mechanical and Aerospace Engineering, Gyeongsang National University, Jinju 52828, Republic of Korea

Correspondence should be addressed to Jungwon Yoon; jyoon@gist.ac.kr

Received 15 February 2018; Revised 20 April 2018; Accepted 8 May 2018; Published 11 June 2018

Academic Editor: Rafael Morales

Copyright © 2018 Muhammad Raheel Afzal et al. This is an open access article distributed under the Creative Commons Attribution License, which permits unrestricted use, distribution, and reproduction in any medium, provided the original work is properly cited.

Aging, injury, or ailments can contribute to impaired balance control and increase the risk of falling. Provision of light touch augments the sense of balance and can thus reduce the amount of body sway. In this study, a wearable reaction wheel-based system is used to deliver light touch-based balance biofeedback on the subject's back. The system can sense torso tilt and, using reaction wheels, generates light touch. A group of 7 healthy young individuals performed balance tasks under 12 trial combinations based on two conditions each of standing stance and surface types and three of biofeedback device status. Torso tilt data, collected from a waist-mounted smartphone during all the trials, were analyzed to determine the efficacy of the system. Provision of biofeedback by the device significantly reduced RMS of mediolateral (ML) trunk tilt ( $p < 0.05$ ) and ML trunk acceleration ( $p < 0.05$ ). Repeated measures ANOVA revealed significant interaction between stance and surface on reduction in RMS of ML trunk tilt, AP trunk tilt, ML trunk acceleration, and AP trunk acceleration. The device shows promise for further applications such as virtual reality interaction and gait rehabilitation.

## 1. Introduction

Standing with a stable posture is a capability that most of us take for granted and so considered to be a simple task. The reality, on the contrary, is totally opposite to this assumption. The achievement of the stable standing posture is possible through a synergetic collaboration of various faculties of the human body. The mechanism for maintaining postural stability can be divided into three parts: sensing, processing, and actuation. The sense of balance is achieved by the utilization of the vestibular system, visual input from the eyes, and proprioceptive input from the lower extremities [1]. The communication and processing of all the sensor data are carried out by the central nervous system (CNS), which generates the actuation signals according to those data, which are also communicated by the CNS. The actuation signals are implemented by the musculoskeletal system [2]. A weakness, injury, or disorder of any of these

systems involved may hamper the execution of the balance maintaining task, leading to postural instability [3]. The faculties involved may be weak due to congenital disorders or degraded due to aging, disease, or injury, thus causing postural instability. Reduced postural control, apart from causing lack of confidence and reduced independence, may also be the cause of falling, thereby causing injury [4]. Therefore, remedial measures need to be taken to improve postural control.

The remedial measures include the implementation of various rehabilitation strategies [5]. Rehabilitation strategies include exercises or tasks that enhance posture control and are tailored according to the particular patient and modified according to their progress [6]. The task performance is sometimes accompanied by the use of various assistive devices such as orthotics, systems that induce a particular pattern of movement and biofeedback systems [7]. It is in the realm of these devices that modern engineering technology is now being extensively applied [8–10]. The inclusion of

automated systems in the rehabilitation process can reduce therapist involvement, allowing them to provide service to a greater number of patients. Compact and cost efficient systems may even allow the user to use them and perform rehabilitation tasks in the comfort of their own home, increasing the chance of the patients adhering to the prescribed exercises till the desired level of rehabilitation has been achieved [11].

One group of rehabilitation devices that is being explored for automated rehabilitation is the biofeedback generation devices [12]. These devices provide feedback to the user according to their performance. This feedback is in a form that can be perceived by the user using one or more of their senses. The different modes of feedback commonly exploited for balance rehabilitation are visual [13–16], audio [17–19], and haptic [20–22]. The haptic feedback is further divided into tactile and kinesthetic feedback. These modes may also be used in conjunction with each other to form a multimodal system. Such multimodal systems, with one system previously developed by us [23], have also shown positive outcomes with regards to balance rehabilitation [24]. The visual cue systems require display devices which make the overall system cumbersome and inappropriate for use as a wearable device. The audio-based system is more compact, but it utilizes the sense of hearing which is already being utilized by the user for listening to the therapist's commands and other environmental sounds. Thus, the haptic-based systems are most suited for unobtrusive delivery of biofeedback.

In the field of kinesthetic haptic biofeedback, one point of great interest is the concept of "light touch." Light touch refers to a fingertip contact with a rigid surface that involves forces which are not strong enough to give mechanical support to the person but are strong enough to be perceived by the somatosensory system. This very low force stimulus when processed by the CNS acts to augment the proprioceptive input coming to the brain and can thus make up for the weakened balance sensing capability. Light touch is known to improve postural control [25–27]. We have previously developed a system that utilized light-touch biofeedback delivered to the hand by a Phantom Omni® device for balance training [28]. We have also devised a multimodal biofeedback generation system for balance training by combining light-touch biofeedback from the Phantom Omni device with a visual biofeedback provision system [23, 29]. Experiments with both these systems produced promising results, but the biggest limitation in both cases was that the systems were not portable. A further variation of light touch is interpersonal light touch. This refers to very low force generating contact of parts of the body with another person or a static or moving object. Interpersonal light touch is not just limited to fingertip contact but also encompasses touch at other parts of the body. It has been seen that interpersonal light touch also acts to reduce body sway [30]. Johannsen et al. have shown that, under some test conditions, interpersonal light touch to the shoulder yields better results than fingertip contact during performance of balancing tasks [31]. Krishnamoorthy et al. have shown that light-touch interface of a fixed device with

the neck and head has a more profound effect in improving the postural stability than that with the finger [32]. Therefore, further exploration of interpersonal light touch, administered to a part of the body other than the finger, such as the subject's back, as a balance rehabilitation tool is warranted. Furthermore, to the best of authors' knowledge, a wearable system for inducing light touch on a subject's back without the involvement of another person has not yet been evaluated. A wearable system, by virtue of its wearability, is usually easier to use and less cumbersome than fixed or portable systems. Therefore, exploration of the possibility to apply currently available technology to devise a wearable, controlled light touch-inducing system is also warranted. Such a wearable system may benefit rehabilitation of subjects with balance impairment. A wearable haptic biofeedback system may also be used at home by individuals who find it difficult to go to a clinic for therapy sessions.

The system presented in this paper utilizes the concept of interpersonal light touch by inducing forces on the user's back to give them feedback of their body sway. It is a wearable system where instead of using a stationary object or another person to generate the reaction forces, we have utilized reaction wheels (RWs). The torso tilt is sensed using an on-board inertial measurement unit (IMU), and the data are processed by an on-board microcontroller which then actuates four RWs to generate the torque required to induce the light touch. In this paper, we have evaluated the effect of these cues as a balance biofeedback on young healthy subjects performing various standing tasks.

## 2. Materials and Methods

**2.1. System Description.** We have devised a rather simple, easy-to-use system that consists of a wearable RW-based biofeedback generation device and a PC-based system for device configuration and viewing and logging of sensor data [33]. Although the biofeedback device is designed to function as a stand-alone device without being connected to the PC, during experimental trials, it is connected to the PC for monitoring purposes. A smartphone-based torso tilt sensing module is also used during experimental trials; it is not part of the biofeedback system and is only used to gather experimental data. The biofeedback device and smartphone both communicate with the PC over a Wi-Fi link to allow completely wireless operation. The feedback device has an on-board IMU which it uses to sense any changes in its orientation. The values read for the IMU are communicated to the microcontroller where they are processed to determine torso tilt in the mediolateral (ML) plane. Based on this calculated tilt angle, the microcontroller generates control signals for the RW motors. The data are also communicated to the PC where it is stored for if further processing is desired. The body sway values measured by the smartphone are also communicated to the PC where they are stored for any further analysis. The block diagram of the complete experimental setup with indication of data flow is shown in Figure 1(a).

The feedback device generates intuitive balance cues in the form of light touch generated due to the induction of torque from the RW. The device is composed of four RWs

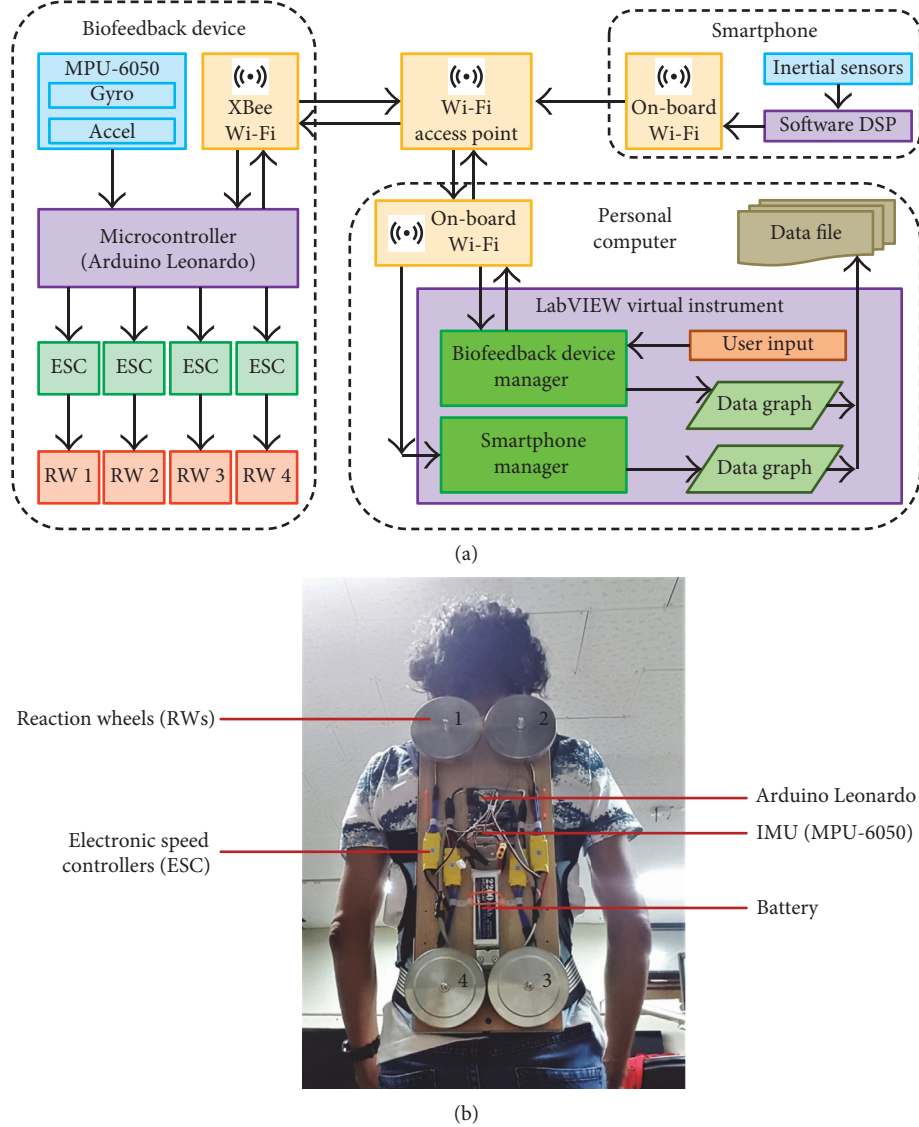


FIGURE 1: System Design. (a) Block diagram of the experimental setup with indication of data flows. The smartphone is not part of the biofeedback system and is used for data collection purposes only. The biofeedback device can function on its own, and the PC is only required for an initial configuration of the device and for data monitoring and logging. (b) Developed hardware of the biofeedback device as worn by a participant during testing.

attached to an easy-to-wear harness. The wheel motors are connected to electronic speed controllers (HW25\30A ESC) which allow the on-board Arduino microcontroller (Arduino Leonardo by DFRobot) to control the motors. The microcontroller takes sensory input from the IMU (MPU-6050 by Invensense). A lithium polymer battery is used as the power source for this module, and communication is handled using an XBee Wi-Fi transceiver. The biofeedback device prototype as worn by a participant with labeled parts is shown in Figure 1(b).

The RWs are usually used in spacecraft for attitude control, but their compact design makes them ideal for use in applications where low magnitude torque is required. Every RW used in our system consists of a brushless DC motor (A2212/13T, 1000 KV) attached to a high-inertia flywheel. When this flywheel is accelerated or decelerated,

a reaction torque is induced on the motor [34]. A simple representation of this phenomenon is shown in Figure 2(a).

The reaction torque induced on the motor is, by virtue of the motor's connection with the mounting harness, converted into a linear force that is perceived by the user as light touch. The device is worn by the user like a backpack with two shoulder straps and one strap at the waist. The torque generated by the RW manifests itself as forces acting on the contact areas of these straps with the user's body. These forces, instead of being felt at individual points, provide a total sensation of lightly trying to tilt the user's body to the right-hand or left-hand side.

Our feedback device consists of 4 RWs arranged in an “X”-shaped configuration. The RW pairs located at the ends of each diagonal work in tandem to generate torque in one direction, so the “X”-shaped configuration allows for the

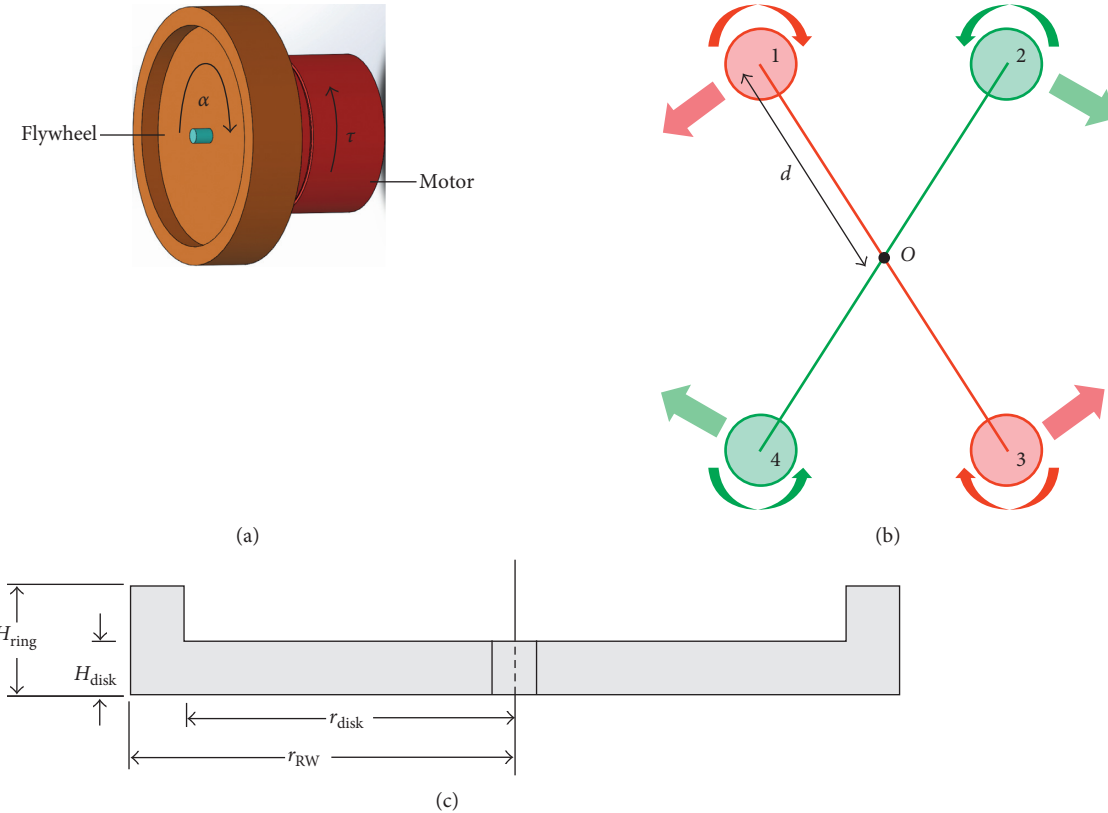


FIGURE 2: (a) Torque production in a reaction wheel assembly due to angular acceleration. (b) Layout of the RW in the biofeedback device with dimensional labels. (c) Cross section of the biofeedback device flywheel with dimensional labels.

generation of torques in two directions. The arrangement of RW with accompanying dimensional tags is shown in Figure 2(b). The touch forces generated by these torques correspond to mediolateral (ML) trunk tilt in both the right and left directions [33]. When the user's torso tilt towards their right-hand side exceeds the set threshold, leftward-directed cue is generated, and vice versa. The cue itself consists of a singular impulse application of force every time the torso tilt exceeds the set threshold. The amount of torque experienced by the motor is dependent on the amount of acceleration taking place and the moment of inertia of the RW (Figure 3(a)). Moment of inertia of a rotating body is the measure of its mass and its distance from the axis of rotation. The moment of inertia for the wheel used in this research is calculated using (1). The variables used in this equation are defined in Figure 2(c). Since the device is designed to be wearable, its size is limited, and thus, the size of the components used is also restricted. Therefore, the selected wheel diameter is 10 cm:

$$I_{RW} = \rho \frac{\pi}{2} [H_{ring}(r_{RW}^4 - r_{disk}^4) + H_{disk}r_{disk}^4]. \quad (1)$$

Using (1), the moment of inertia of each of the RW used in this research is  $I_{RW} = 1.625 \times 10^{-4} \text{ kgm}^2$ .

The separation distance between the centers of the wheels is  $d = 19.5 \text{ cm}$ . The total mass moment of inertia of the RW array about its center was found using the parallel axis theorem, which yielded the following equation:

$$I_{tot} = 4(I_{RW} + m_W d^2), \quad (2)$$

where  $d$  is the distance of the wheel center from the center of rotation of the device and  $m_W$  is the mass of the wheel found using the following equation:

$$m_W = \rho \pi [r_{RW}^2 h_{ring} - r_{disk}^2 (h_{ring} - h_{disk})]. \quad (3)$$

The mass of each RW was found to be  $m_W = 0.130 \text{ kg}$ . Therefore, from (2), the total mass moment of inertia of the complete RW array is  $I_{tot} = 0.0204 \text{ kgm}^2$ . The RWs were empirically tested in couples to validate the design. The maximum force generated by each RW couple was 1.24 N and can thus be considered as light touch. The device has a total weight of 4.20 kg inclusive of all its components. Figure 3(b) shows the net force being generated by the system in relation to the torso tilt.

**2.2. Experimental Setup.** The PC-based module of the system runs the LabVIEW environment in which an application is developed to receive data from the biofeedback device and the smartphone tilt sensor for display and logging and allows the operator to configure the biofeedback device. The program utilizes bidirectional UDP communication over Wi-Fi to communicate with the devices. It can receive sensor data from the feedback device and can be used to switch the RW motors on and off and to control their speed. Communication with the smartphone is unidirectional; the PC only receives

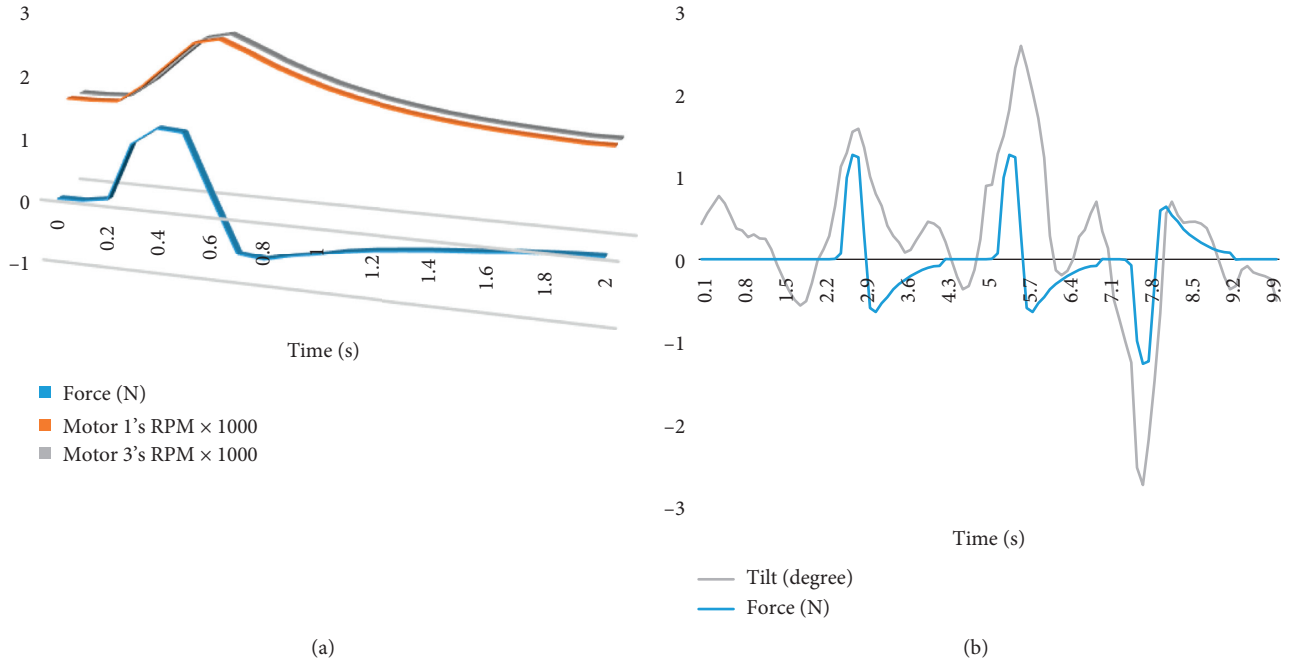


FIGURE 3: (a) Representative plot of motor 1 and motor 3 RPM and the consequently generated force. (b) The force generated by the system in relation to the torso tilt.

body sway data from the module. The smartphone used in this research is a Pantech Vega IM-A850L that has a quad-core 1.5 GHz CPU with 2 GB of RAM and runs the Android® operating system. We have previously utilized the smartphone as a reliable body sway assessment tool during both stance and gait conditions [23, 28, 29, 35–37]. The smartphone runs an application that measures the trunk tilt in terms of the ML and anteroposterior (AP) angles and sends these data via UDP over Wi-Fi to the PC.

Seven healthy young participants took part in the experimental study and performed prescribed balance tasks to check the effectiveness of biofeedback provided by our system. The details of these participants are given in Table 1. None of the subjects had any history of sensorimotor disorders. This study was conducted according to the Declaration of Helsinki and had ethical approval from the Institutional Review Board at the Gwangju Institute of Science and Technology. All subjects gave written informed consent prior to data collection.

The subjects were asked to wear the feedback device and the smartphone in order to conduct the experimental tests. The feedback device is provided with straps so that it can be worn like a backpack, and the smartphone is attached to the waist with the help of an elastic belt. For the purpose of conducting the experiments presented here, the cue generation threshold for trunk tilt was set at  $\pm 1^\circ$  about the vertical. With all the hardware in place and configuration completed, the subjects were asked to maintain their balance while standing with two distinct stance postures on two distinct surfaces for 30 seconds each. The data obtained during first and last 5 seconds of each trial were not utilized during analysis. The prescribed stance postures were tandem-Romberg and single-leg. In tandem-Romberg stance, one foot is placed in front of the other with heel of the anterior foot touching the toe of the

TABLE 1: Details of the young healthy subjects who participated in the study.

Participants	Age (year)	Height (cm)	Weight (kg)	Gender
7	$27 \pm 3$	$161 \pm 9$	$70 \pm 6.5$	Male = 6 Female = 1

posterior foot, and the nondominant leg is in the posterior position. In single-leg stance, the subject stands on the non-dominant leg with the contralateral limb held in approximately  $20^\circ$  of hip flexion,  $45^\circ$  of knee flexion, and neutral position in the frontal plane. Subject's kicking preference is used to determine leg dominance. The surfaces used in these tests were solid ground and a platform made of foam. The platform was used to simulate soft ground conditions. It had the dimensions of  $600 \times 600 \times 150$  mm and was made using high resilience foam that had a density of  $48 \text{ kg/m}^3$  and tensile strength of 83 kPa. The subjects were explained appropriate utilization of kinesthetic biofeedback for balance control prior to start of the experimental trials. The biofeedback device worn by the subjects delivered light-touch balance cues. The subjects, utilizing these cues, tried to achieve the objective of balancing themselves in the prescribed stance on the designated surface. The stance conditions and surface conditions would enable us to identify the efficacy of the proposed system when operated under different conditions. We anticipated that the system will have greater efficacy when the user is performing balance tasks in relatively more unstable conditions.

Each participant performed balancing tasks under a total of twelve trial combinations composed of three conditions of the biofeedback device, two ground conditions, and two distinct standing postures ( $3 \times 2 \times 2 = 12$ ). The three biofeedback device conditions were as follows: not wearing the

TABLE 2: A summary representation of all the testing conditions used in the experimental trials along with their related abbreviation tags.

Stance condition	Surface condition					
	Ground (G)			Foam (F)		
Tandem-Romberg (T)	NTG	OTG	BTG	NTF	OTF	BTF
Single-leg (S)	NSG	OSG	BSG	NSF	OSF	BSF

device, wearing the device but it is not providing any biofeedback, and wearing the device while it is providing biofeedback. The participants stood on normal ground for stable support and on a foam platform that simulated unstable ground conditions. The two standing postures assumed by the participants were the tandem-Romberg stance and the one-leg stance.

Balancing trials under the mentioned 12 different sets of conditions were carried out with all the conditions being applied to all the participants in a random order. The abbreviations associated with the testing conditions are tabulated in Table 2. “N” refers to trials done without wearing the biofeedback device. “O” refers to trials done while wearing the device but it is not switched on. “B” refers to trials done while wearing the device and it is switched on and providing biofeedback.

**2.3. Data Collection and Analysis.** Body sway is a meaningful indicator that can be used to recognize the balance of a human being during upright standing posture [38]. The smartphone attached to the subjects’ waist measured trunk tilt angles during trials and communicated them wirelessly to the PC. The ML and AP, trunk tilt, and acceleration data were recorded on the PC. In postexperimental analysis, RMS values of ML trunk tilt, AP trunk tilt, ML trunk acceleration, and AP trunk acceleration were calculated. Afterwards, we carried out statistical analysis of the recorded data to make detailed observations about balance performance [39]. Using dependent *t*-test, we compared the body sway under N and O conditions with statistical significance defined as  $p < 0.05$ . A 3-way repeated measures ANOVA was conducted (factors: feedback (O, B), stance (T, S), and surface (G, F)) for analysis of the trunk tilt and acceleration parameters. In addition, we calculated reduction in RMS values of ML trunk tilt (RMS-ML-tilt-R), AP trunk tilt (RMS-AP-tilt-R), ML trunk acceleration (RMS-ML-acceleration-R), and AP trunk acceleration (RMS-AP-acceleration-R) by calculating absolute difference between O and B conditions. A 2-way repeated measures ANOVA was conducted to investigate the effects of stance (factor) and surface (factor) on reduction of RMS values of ML trunk tilt, AP trunk tilt, ML trunk acceleration, and AP trunk acceleration. Post hoc multiple comparison tests were conducted using the Bonferroni correction method.

### 3. Results and Discussion

Mean  $\pm$  standard deviation (SD) for all subjects’ RMS of ML trunk tilt, RMS of AP trunk tilt, RMS of ML trunk

acceleration, and RMS of AP trunk acceleration are shown in Table 3. Results of the *t*-tests showed that there was no statistically significant difference between N (without wearing the biofeedback device) and O (wearing the device, but it is not switched on) for the dependent variables (ML trunk tilt, AP trunk tilt, ML trunk acceleration, and AP trunk acceleration) in all trial conditions (Table 4). This shows that wearing the device did not significantly affect the users’ balance.

Table 5 shows the statistics of the 3-way repeated measures ANOVA with factors: feedback, stance, and surface. Results of the 3-way repeated measures ANOVA revealed that all main effects and interactions were significant for RMS of ML trunk tilt. Post hoc analysis revealed significant difference of RMS of ML trunk tilt at all levels of each factor and between factors. However, RMS of AP trunk tilt exhibited significant main effects and interactions of the stance and surface factors. The post hoc analysis revealed significant difference of RMS of AP trunk tilt at all levels of surface and stance factors and between these factors. RMS of ML trunk acceleration exhibited significant main effects of feedback, stance, and surface and interaction of the stance and surface. Post hoc analysis revealed significant difference of RMS of ML trunk acceleration at all levels of each factor and between factors. RMS of AP trunk acceleration exhibited significant main effects and interaction of the stance and surface factors. The post hoc analysis revealed a significant difference of RMS of AP trunk acceleration at all levels of surface and stance factors and between these factors.

Results of the 2-way repeated measures ANOVA revealed that both main effects and the interaction were insignificant for RMS-ML-acceleration-R, RMS-AP-tilt-R, and RMS-AP-acceleration-R. However, main effects of stance ( $p$  value = 0.012), surface ( $p$  value = 0.003), and stance  $\times$  surface interaction ( $p$  value = 0.005) were statistically significant for RMS-ML-tilt-R. Due to significant interaction, post hoc analysis was conducted to evaluate simple main effects for RMS-ML-tilt-R (Figure 4). Statistically significant difference was found in reduction of RMS values of ML trunk tilt between tandem-Romberg and single-leg stance on ground ( $p$  value = 0.020) and on foam ( $p$  value = 0.039) surfaces. Statistically significant difference was also found in reduction of RMS values of ML trunk tilt between ground and foam conditions in tandem-Romberg stance ( $p$  = 0.002). However, no statistically significant difference in reduction of RMS values of ML trunk tilt was found between ground and foam conditions in single-leg stance. From this result, we can observe that reduction in RMS of ML trunk tilt was more on the foam surface relative to the ground as expected. However, when comparing stance conditions, the reduction in RMS of ML trunk tilt was more in tandem-Romberg stance in comparison to the single-leg stance. This outcome can be attributed to the deficiency of AP directional cues/assistance from the system.

In this paper, the effect of provision of kinesthetic biofeedback on the subject’s back for balance is presented. When the means and standard deviations (SD) of the data collected during experimental trials are observed, it shows that provision of biofeedback delivered by our system

TABLE 3: RMS values of the measured parameters.

Parameter	Stance	Surface					
		Ground (G)			Foam (F)		
		N	O	B	N	O	B
ML trunk tilt (degree)	Tandem-Romberg (T)	0.5192 ± 0.0381	0.4961 ± 0.0223	0.4234 ± 0.0102	1.3747 ± 0.0668	1.3724 ± 0.1051	1.1019 ± 0.0564
	Single-leg (S)	1.1251 ± 0.0450	1.1287 ± 0.0257	1.0582 ± 0.0124	2.1152 ± 0.0391	2.0980 ± 0.0256	2.0058 ± 0.0411
AP trunk tilt (degree)	Tandem-Romberg (T)	1.0172 ± 0.0374	1.0219 ± 0.0470	1.0328 ± 0.2759	1.9030 ± 0.0552	1.9048 ± 0.0574	1.8932 ± 0.0501
	Single-leg (S)	1.6114 ± 0.0287	1.6205 ± 0.0238	1.6274 ± 0.0275	2.4284 ± 0.0368	2.4318 ± 0.0446	2.4104 ± 0.0249
ML trunk acceleration ( $\text{m/s}^2$ )	Tandem-Romberg (T)	0.0635 ± 0.0025	0.0629 ± 0.0029	0.0514 ± 0.0018	0.1062 ± 0.0026	0.1054 ± 0.0037	0.0926 ± 0.0043
	Single-leg (S)	0.0956 ± 0.0016	0.0946 ± 0.0034	0.0858 ± 0.0031	0.1459 ± 0.0032	0.1451 ± 0.0036	0.1348 ± 0.0049
AP trunk acceleration ( $\text{m/s}^2$ )	Tandem-Romberg (T)	0.0614 ± 0.0196	0.0619 ± 0.0012	0.0620 ± 0.0011	0.1082 ± 0.0029	0.1075 ± 0.0038	0.1079 ± 0.0034
	Single-leg (S)	0.1063 ± 0.0027	0.1070 ± 0.0038	0.1066 ± 0.0031	0.1621 ± 0.0023	0.1613 ± 0.0028	0.1618 ± 0.0019

reduced body sway in the participants. This may be attributed to the somatosensory augmentation provided by the haptic biofeedback. Somatosensory augmentation is known to improve standing stability [40]. In order to evaluate the effects of the biofeedback device, RMS of ML and AP trunk tilt, and RMS of ML and AP trunk acceleration are observed. The device currently provides balance cues in the ML direction upon trunk sway in the ML direction. Therefore, the results obtained in the ML direction are the focus of this research. RMS of ML trunk tilt has been shown to be a reliable marker of postural control in multiple prior studies [41–43]. Likewise, RMS of ML trunk acceleration has been shown to be a reliable measure of judging balance during standing trials [44–46]. During the study, the participants exhibited no significant differences in RMS of ML trunk tilt and RMS of ML trunk acceleration, between not wearing the device (N) and wearing the device with no feedback conditions (O). This shows that the wearing of the device did not affect the postural stability of the participants. On the contrary, while comparing RMS of ML trunk tilt under no feedback (O) and biofeedback (B) conditions, statistically significant differences were found in all stance and surface conditions. Similar results for RMS of ML trunk acceleration were observed. Hence, kinesthetic biofeedback generated by our system had a significant effect on the postural stability of the subjects. This is in line with our hypothesis that application of light-touch cues to a subject's back works to reduce their body sway. 2-way repeated measures ANOVA revealed significant interaction between stance and surface on reduction in RMS of ML trunk tilt between no device and biofeedback conditions. This indicates that the amount of postural stability improvement varies in relation to the stance and the surface conditions. In contrast, there was no significant interaction between stance and surface on reduction in RMS of ML trunk acceleration, RMS of AP trunk tilt, and RMS of AP trunk acceleration between no device and biofeedback conditions.

The system generates a force magnitude of 1.24 N which can be considered as light touch-based biofeedback and is sufficient for standing balance tasks as evidenced in previous

TABLE 4: Comparison of N and O trial conditions with *t*-test (*p* value).

Parameter	Stance condition	Surface condition	
		Ground (G)	Foam (F)
ML trunk tilt	Tandem-Romberg (T)	0.084	0.950
	Single-leg (S)	0.779	0.103
AP trunk tilt	Tandem-Romberg (T)	0.825	0.847
	Single-leg (S)	0.299	0.817
ML trunk acceleration	Tandem-Romberg (T)	0.310	0.390
	Single-leg (S)	0.351	0.547
AP trunk acceleration	Tandem-Romberg (T)	0.541	0.278
	Single-leg (S)	0.498	0.180

related works [26, 27]. It might be necessary to increase the force magnitude in order to apply this biofeedback method during locomotor tasks as previous related works dealing with light-touch feedback during walking have utilized up to 4 N force [47, 48]. A number of recent studies have reported on the promising effects of vibrotactile biofeedback on standing balance [49, 50]. Thus, it is a point of interest to study this system for provision of kinesthetic biofeedback in comparison with a vibrotactile balance biofeedback system to determine the differences in their performance. A study to compare the neurophysiological effects that these systems may have on a particular set of users is also envisioned.

A limitation of this study is the small number of participants, but several other published works related to effect of biofeedback devices have also reported trials with small sample size [51, 52]. Through the testing carried out during this research, we not only were able to judge the effects of the device on performance of prescribed balance tasks but also were able to uncover some shortcomings of the current device prototype. The participants were able to wear the device with ease, but they were not comfortable with its weight. They were in general view that wearing the device for extended period of time will become uncomfortable due to its weight. Reduction in weight of the system is thus a point of consideration for our future work. This may be possible through variations in material selection so that the system

TABLE 5: ANOVA statistics of the dependent variables.

Effect	Parameter			
	ML trunk tilt	AP trunk tilt	ML trunk acceleration	AP trunk acceleration
Feedback	$F(1, 6) = 86.645, p < 0.001$	$F(1, 6) = 0.497, p = 0.507$	$F(1, 6) = 104.653, p < 0.001$	$F(1, 6) = 0.165, p = 0.699$
Stance	$F(1, 6) = 2368.311, p < 0.001$	$F(1, 6) = 2120.584, p < 0.001$	$F(1, 6) = 1500.545, p < 0.001$	$F(1, 6) = 2900.932, p < 0.001$
Surface	$F(1, 6) = 5434.270, p < 0.001$	$F(1, 6) = 2305.391, p < 0.001$	$F(1, 6) = 4238.458, p < 0.001$	$F(1, 6) = 2899.990, p < 0.001$
Feedback × stance	$F(1, 6) = 10.457, p = 0.018$	$F(1, 6) = 0.181, p = 0.686$	$F(1, 6) = 2.500, p = 0.165$	$F(1, 6) = 0.062, p = 0.811$
Feedback × surface	$F(1, 6) = 23.599, p = 0.003$	$F(1, 6) = 2.351, p = 0.176$	$F(1, 6) = 0.600, p = 0.468$	$F(1, 6) = 0.628, p = 0.458$
Stance × surface	$F(1, 6) = 42.320, p = 0.001$	$F(1, 6) = 13.773, p = 0.010$	$F(1, 6) = 7.235, p = 0.036$	$F(1, 6) = 26.467, p = 0.002$
Feedback × surface × stance	$F(1, 6) = 18.800, p = 0.005$	$F(1, 6) = 0.129, 0.732$	$F(1, 6) = 0.001, p = 0.981$	$F(1, 6) = 0.043, p = 0.842$

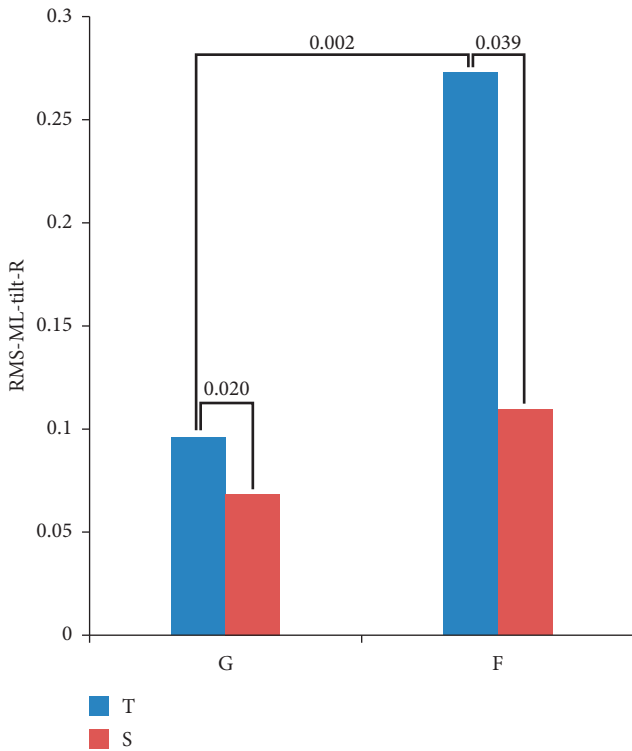


FIGURE 4: Result of post hoc simple main effects analysis following the 2-way repeated measures ANOVA. Reduction in RMS of ML trunk tilt is compared for the different stance and surface. The bars represent the mean reduction in RMS of ML trunk tilt.

may become suitable for application in extended rehabilitation schemes. One such scheme is the use of haptic biofeedback devices in conjunction with virtual reality to enhance poststroke balance and mobility [53]. As the system provides balance cues in the ML direction only, to enhance its capabilities, there is a need to make it a two-dimensional cue delivery system that can provide cues in both the ML and AP directions. In order to do this, the appropriate layout of reaction wheels needs to be determined and hardware needs to be developed that can generate the desired forces without being too heavy. The

current study didn't identify the effects of added weight of the system on the balance recovery of the users during large sway. In future work, we will also observe the postural control of the users in detail under condition of postural perturbations.

#### 4. Conclusions

A wearable biofeedback device which generates light-touch biofeedback in correspondence to torso movement in the ML directions is evaluated in this research. The tests were conducted with participants without any balance impairments, and imbalance was induced by the use of imbalance inducing standing stances and an unstable standing surface. The level of balance achieved by the participants was judged based on their body sway in ML and AP. The outcomes observed during initial trials with healthy young subjects point towards an important addition to the balance training procedures. We observed that our method of delivering kinesthetic biofeedback can be applied to balance rehabilitation through the use of specifically designed balance tasks. Being wearable, the system has high potential for use at home or in outpatient clinics for balance training exercises. Experimental trials conducted with young healthy subjects supported the feasibility of the system as a balance training aid. In future prototype, the system should be designed to minimize the current limitations. We plan to use this system to perform long-term balance training of individuals with upright balance issues. Furthermore, exploiting the wearable nature of the system, we also plan to explore the benefits of utilizing this device as a balance assistance aid during gait.

#### Data Availability

Data supporting the conclusions of this research are included within the article.

#### Conflicts of Interest

The authors declare that there are no conflicts of interest regarding the publication of this paper.

## Acknowledgments

This research work was supported by the National Research Foundation of Korea (NRF) (2017R1A2B4011704), Dual Use Technology Program of Civil and Military, and Global University Project (GUP) 2018 Grant by GIST.

## References

- [1] L. M. Nashner, "Analysis of stance posture in humans," in *Motor Coordination*, pp. 527–565, Springer, New York, NY, USA, 1981.
- [2] B. S. Hassan, S. Mockett, and M. Doherty, "Static postural sway, proprioception, and maximal voluntary quadriceps contraction in patients with knee osteoarthritis and normal control subjects," *Annals of the Rheumatic Diseases*, vol. 60, no. 6, pp. 612–618, 2001.
- [3] C. M. Sackley, "Falls, sway, and symmetry of weight-bearing after stroke," *International Disability Studies*, vol. 13, no. 1, pp. 1–4, 1991.
- [4] S. J. Herdman, M. C. Schubert, and R. J. Tusa, "Strategies for balance rehabilitation," *Annals of the New York Academy of Sciences*, vol. 942, no. 1, pp. 394–412, 2001.
- [5] M. B. Badke, T. A. Shea, J. A. Miedaner, and C. R. Grove, "Outcomes after rehabilitation for adults with balance dysfunction," *Archives of Physical Medicine and Rehabilitation*, vol. 85, no. 2, pp. 227–233, 2004.
- [6] B. A. Alsalaheen, S. L. Whitney, A. Mucha, L. O. Morris, J. M. Furman, and P. J. Spar托, "Exercise prescription patterns in patients treated with vestibular rehabilitation after concussion," *Physiotherapy Research International*, vol. 18, no. 2, pp. 100–108, 2013.
- [7] S. Hesse, "Rehabilitation of gait after stroke: evaluation, principles of therapy, novel treatment approaches, and assistive devices," *Topics in Geriatric Rehabilitation*, vol. 19, no. 2, pp. 109–126, 2003.
- [8] N. U. Ahamed, K. Sundaraj, R. B. Ahmad, and S. M. Rahman, "Biosensors assisted automated rehabilitation systems: a systematic review," *International Journal of the Physical Sciences*, vol. 7, pp. 5–17, 2012.
- [9] S. Patel, H. Park, P. Bonato, L. Chan, and M. Rodgers, "A review of wearable sensors and systems with application in rehabilitation," *Journal of Neuroengineering and Rehabilitation*, vol. 9, no. 1, p. 21, 2012.
- [10] N. U. Ahamed, K. Sundaraj, R. B. Ahmad, S. Nadarajah, P. T. Shi, and S. M. Rahman, "Recent survey of automated rehabilitation systems using EMG biosensors," *Journal of Physical Therapy Science*, vol. 23, no. 6, pp. 945–948, 2011.
- [11] R. Forkan, B. Pumper, N. Smyth, H. Wirkkala, M. A. Ciol, and A. Shumway-Cook, "Exercise adherence following physical therapy intervention in older adults with impaired balance," *Physical Therapy*, vol. 86, no. 3, pp. 401–410, 2006.
- [12] H. Huang, S. L. Wolf, and J. He, "Recent developments in biofeedback for neuromotor rehabilitation," *Journal of Neuroengineering and Rehabilitation*, vol. 3, no. 1, p. 11, 2006.
- [13] J. F. Bayouk, J. P. Boucher, and A. Leroux, "Balance training following stroke: effects of task-oriented exercises with and without altered sensory input," *International Journal of Rehabilitation Research*, vol. 29, no. 1, pp. 51–59, 2006.
- [14] B. Lange, S. Flynn, R. Proffitt, C. Y. Chang, and A. "Skip" Rizzo, "Development of an interactive game-based rehabilitation tool for dynamic balance training," *Topics in Stroke Rehabilitation*, vol. 17, no. 5, pp. 345–352, 2010.
- [15] A. Srivastava, A. B. Taly, A. Gupta, S. Kumar, and T. Murali, "Post-stroke balance training: role of force platform with visual feedback technique," *Journal of the Neurological Sciences*, vol. 287, no. 1, pp. 89–93, 2009.
- [16] W. Young, S. Ferguson, S. Brault, and C. Craig, "Assessing and training standing balance in older adults: a novel approach using the 'Nintendo Wii' Balance Board," *Gait and Posture*, vol. 33, no. 2, pp. 303–305, 2011.
- [17] C. Franco, A. Fleury, P. Y. Gumery, B. Diot, J. Demongeot, and N. Vuillerme, "iBalance-ABF: a smartphone-based audio-biofeedback balance system," *IEEE Transactions Biomedical Engineering*, vol. 60, no. 1, pp. 211–215, 2013.
- [18] M. Dozza, F. B. Horak, and L. Chiari, "Auditory biofeedback substitutes for loss of sensory information in maintaining stance," *Experimental Brain Research*, vol. 178, no. 1, pp. 37–48, 2007.
- [19] L. Chiari, M. Dozza, A. Cappello, F. B. Horak, V. Macellari, and D. Giansanti, "Audio-biofeedback for balance improvement: an accelerometry-based system," *IEEE Transactions on Biomedical Engineering*, vol. 52, no. 12, pp. 2108–2111, 2005.
- [20] M. R. Afzal, Y. Jan, S. Hassan, and J. Yoon, "Analysis of active haptic feedback effects on standing stability," in *Intelligent Robotics and Applications*, J. Lee, M. C. Lee, H. Liu, and J. H. Ryu, Eds., pp. 154–164, Springer, Berlin, Heidelberg, Germany, 2013.
- [21] K. H. Sienko, V. V. Vichare, M. D. Balkwill, and C. Wall III, "Assessment of vibrotactile feedback on postural stability during pseudorandom multidirectional platform motion," *IEEE Transactions on Biomedical Engineering*, vol. 57, no. 4, pp. 944–952, 2010.
- [22] B. C. Lee, J. Kim, S. Chen, and K. H. Sienko, "Cell phone based balance trainer," *Journal of Neuroengineering and Rehabilitation*, vol. 9, no. 1, p. 10, 2012.
- [23] M. R. Afzal, M. K. Oh, H. Y. Choi, and J. Yoon, "A novel balance training system using multimodal biofeedback," *Biomedical Engineering Online*, vol. 15, no. 1, p. 42, 2016.
- [24] K. E. Bechly, W. J. Carender, J. D. Myles, and K. H. Sienko, "Determining the preferred modality for real-time biofeedback during balance training," *Gait and Posture*, vol. 37, no. 3, pp. 391–396, 2013.
- [25] M. Kouzaki and K. Masani, "Reduced postural sway during quiet standing by light touch is due to finger tactile feedback but not mechanical support," *Experimental Brain Research*, vol. 188, no. 1, pp. 153–158, 2008.
- [26] J. J. Jeka and J. R. Lackner, "Fingertip contact influences human postural control," *Experimental Brain Research*, vol. 79, no. 2, pp. 495–502, 1994.
- [27] J. J. Jeka, "Light touch contact as a balance aid," *Physical Therapy*, vol. 77, no. 5, pp. 476–487, 1997.
- [28] M. R. Afzal, H. Y. Byun, M. K. Oh, and J. Yoon, "Effects of kinesthetic haptic feedback on standing stability of young healthy subjects and stroke patients," *Journal of Neuroengineering and Rehabilitation*, vol. 12, no. 1, p. 27, 2015.
- [29] M. R. Afzal, M. K. Oh, and J. Yoon, "Development of a multimodal biofeedback system for balance training," in *Proceedings of the IEEE International Conference on Advanced Intelligent Mechatronics (AIM)*, pp. 658–663, Busan, Republic of Korea, July 2015.
- [30] L. Johannsen, A. Guzman-Garcia, and A. M. Wing, "Interpersonal light touch assists balance in the elderly," *Journal of Motor Behavior*, vol. 41, no. 5, pp. 397–399, 2009.
- [31] L. Johannsen, A. M. Wing, and V. Hatzitaki, "Contrasting effects of finger and shoulder interpersonal light touch on standing balance," *Journal of Neurophysiology*, vol. 107, no. 1, pp. 216–225, 2012.

- [32] V. Krishnamoorthy, H. Sliper, and M. L. Latash, "Effects of different types of light touch on postural sway," *Experimental Brain Research*, vol. 147, no. 1, pp. 71–79, 2002.
- [33] M. R. Afzal, C. E. Palo Peña, and J. Yoon, "Development of a wearable device based on reaction wheels to deliver kinesthetic cues for balance training," in *Proceedings of the International Conference on Control, Automation and Systems (ICCAS)*, pp. 1926–1929, Jeju, Republic of Korea, October 2017.
- [34] M. J. Sidi, *Spacecraft Dynamics and Control: A Practical Engineering Approach*, Cambridge University Press, Cambridge, UK, 1997.
- [35] M. R. Afzal, M. K. Oh, C. H. Lee, Y. S. Park, and J. Yoon, "A portable gait asymmetry rehabilitation system for individuals with stroke using a vibrotactile feedback," *BioMed Research International*, vol. 2015, Article ID 375638, 16 pages, 2015.
- [36] M. R. Afzal, S. Pyo, M. K. Oh, Y. S. Park, B. C. Lee, and J. Yoon, "Haptic based gait rehabilitation system for stroke patients," in *Proceedings of the IEEE/RSJ International Conference on Intelligent Robots and Systems (IROS)*, pp. 3198–3203, Deajeon, Republic of Korea, October 2016.
- [37] M. R. Afzal, S. Pyo, M. K. Oh, Y. S. Park, and J. Yoon, "Identifying the effects of using integrated haptic feedback for gait rehabilitation of stroke patients," in *Proceedings of the IEEE International Conference on Rehabilitation Robotics (ICORR)*, pp. 1055–1060, London, UK, July 2017.
- [38] R. W. Baloh, S. Corona, K. M. Jacobson, J. A. Enrietto, and T. Bell, "A prospective study of posturography in normal older people," *Journal of the American Geriatrics Society*, vol. 46, no. 4, pp. 438–443, 1998.
- [39] M. R. Afzal, S. Pyo, M. K. Oh, Y. S. Park, and J. Yoon, "Evaluating the effects of delivering integrated kinesthetic and tactile cues to individuals with unilateral hemiparetic stroke during overground walking," *Journal of Neuroengineering and Rehabilitation*, vol. 15, no. 1, p. 33, 2018.
- [40] P. B. Shull and D. D. Damian, "Haptic wearables as sensory replacement, sensory augmentation and trainer—a review," *Journal of Neuroengineering and Rehabilitation*, vol. 12, no. 1, p. 59, 2015.
- [41] K. H. Sienko, M. D. Balkwill, L. I. Oddsson, and C. Wall, "The effect of vibrotactile feedback on postural sway during locomotor activities," *Journal of Neuroengineering and Rehabilitation*, vol. 10, no. 1, p. 93, 2013.
- [42] C. Wall III, "Application of vibrotactile feedback of body motion to improve rehabilitation in individuals with imbalance," *Journal of Neurologic Physical Therapy*, vol. 34, no. 2, p. 98, 2010.
- [43] F. B. Horak, M. Dozza, R. Peterka, L. Chiari, and C. Wall III, "Vibrotactile biofeedback improves tandem gait in patients with unilateral vestibular loss," *Annals of the New York Academy of Sciences*, vol. 1164, no. 1, pp. 279–281, 2009.
- [44] R. Moe-Nilssen, "Test-retest reliability of trunk accelerometry during standing and walking," *Archives of Physical Medicine and Rehabilitation*, vol. 79, no. 11, pp. 1377–1385, 1998.
- [45] S. L. Whitney, J. L. Roche, G. F. Marchetti et al., "A comparison of accelerometry and center of pressure measures during computerized dynamic posturography: a measure of balance," *Gait and Posture*, vol. 33, no. 4, pp. 594–599, 2011.
- [46] M. Mancini, F. B. Horak, C. Zampieri, P. Carlson-Kuhta, J. G. Nutt, and L. Chiari, "Trunk accelerometry reveals postural instability in untreated Parkinson's disease," *Parkinsonism and Related Disorders*, vol. 17, no. 7, pp. 557–562, 2011.
- [47] R. Boonsinsukh, L. Panichareon, and P. Phansuwan-Pujito, "Light touch cue through a cane improves pelvic stability during walking in stroke," *Archives of Physical Medicine and Rehabilitation*, vol. 90, no. 6, pp. 919–926, 2009.
- [48] R. Boonsinsukh, L. Panichareon, V. Saengsirisuwan, and P. Phansuwan-Pujito, "Clinical identification for the use of light touch cues with a cane in gait rehabilitation poststroke," *Topics in Stroke Rehabilitation*, vol. 18, no. 1, pp. 633–642, 2011.
- [49] B. C. Lee, A. Fung, and T. A. Thrasher, "The effects of coding schemes on vibrotactile biofeedback for dynamic balance training in Parkinson's disease and healthy elderly individuals," *IEEE Transactions on Neural Systems and Rehabilitation Engineering*, vol. 26, no. 1, pp. 153–160, 2018.
- [50] T. Bao, W. J. Carender, C. Kinnaird et al., "Effects of long-term balance training with vibrotactile sensory augmentation among community-dwelling healthy older adults: a randomized preliminary study," *Journal of Neuroengineering and Rehabilitation*, vol. 15, no. 1, p. 5, 2018.
- [51] C. Z. Ma, Y. P. Zheng, and W. C. Lee, "Changes in gait and plantar foot loading upon using vibrotactile wearable biofeedback system in patients with stroke," *Topics in Stroke Rehabilitation*, vol. 25, no. 1, pp. 20–27, 2018.
- [52] A. U. Alahakone and S. A. Senanayake, "A real-time system with assistive feedback for postural control in rehabilitation," *IEEE/ASME Transactions on Mechatronics*, vol. 15, no. 2, pp. 226–233, 2010.
- [53] J. Fung and C. F. Perez, "Sensorimotor enhancement with a mixed reality system for balance and mobility rehabilitation," in *Proceedings of the 2011 Annual International Conference of the IEEE Engineering in Medicine and Biology Society, EMBC*, pp. 6753–6757, Boston, MA, USA, August–September 2011.

## Review Article

# Assessing Effectiveness and Costs in Robot-Mediated Lower Limbs Rehabilitation: A Meta-Analysis and State of the Art

Giorgio Carpino<sup>1</sup>, Alessandra Pezzola,<sup>1</sup> Michele Urbano,<sup>2</sup> and Eugenio Guglielmelli<sup>1</sup>

<sup>1</sup>Laboratory of Biomedical Robotics and Biomicrosystems, Università Campus Bio-Medico di Roma, 00128 Rome, Italy

<sup>2</sup>Polyclinic General Direction, Università Campus Bio-Medico di Roma, 00128 Rome, Italy

Correspondence should be addressed to Giorgio Carpino; g.carpino@unicampus.it

Received 12 February 2018; Revised 6 April 2018; Accepted 22 April 2018; Published 4 June 2018

Academic Editor: Carlo Ferraresi

Copyright © 2018 Giorgio Carpino et al. This is an open access article distributed under the Creative Commons Attribution License, which permits unrestricted use, distribution, and reproduction in any medium, provided the original work is properly cited.

Robots were introduced in rehabilitation in the 90s to meet different needs, that is, reducing the physical effort of therapists. This work consists of a meta-analysis of robot-mediated lower limbs rehabilitation for stroke-affected patients; it aims at evaluating the effectiveness of the robotic approach through the use of wearable robots or operational machines with respect to the conventional approach (i.e., manual rehabilitation therapy). The primary assessed outcome is the patient's ability to recover walking independence, whereas the secondary outcome is the average walking speed. The therapy acceptability and the treatment costs are also assessed. The assessment shows that the robot-mediated therapy is more effective than the conventional one in reaching the primary outcome. As for the secondary outcome, there is no significant difference between the robotic (wearable robots or operational machines) and the conventional approach. Rehabilitation using wearable robots has a greater acceptability than the conventional one. This does not apply to operational machines. The cost of robotic treatment with wearable robots ranges from double to triple the cost of the conventional approach. On the contrary, rehabilitation using operational machines costs the same as the conventional treatment. Robotic rehabilitation based on operational machines is the most cost-effective approach.

## 1. Introduction

The introduction of robots in rehabilitation therapy dates back to the 1990s [1]. Since then, the rehabilitation therapy has been led by the following factors: (i) modern medicine is based on objective assessments and quantitative benchmarking of the impact of different therapeutic approaches; (ii) conventional rehabilitation therapy (i.e., manual rehabilitation therapy) is an intense, time-consuming activity, which requires high physical effort for health workers; (iii) recent studies on neuroplasticity related to functional recovery in patients with brain injuries have highlighted that patients benefit from activity-dependent rehabilitation therapies. These factors usually require the execution of repetitive exercises, aimed at a well-defined goal. The patient has to have an active role during the rehabilitation session in order to stimulate the whole system of sensorimotor coordination, including the stages of imagination and planning

of the motor task. Therefore, there are unmet or not completely met needs in the conventional approach to the motor rehabilitation such as availability of measurable outcomes, repeatability of the rehabilitation tasks, and active patient engagement.

Robotic solutions for assisted therapy meet all these needs [2, 3]. Rehabilitation robotics is a new technological branch related to the application of robot technology in medical fields. Nowadays, rehabilitation robots are a key enabling technologies to help people who suffer limb movement disorder to restore the normal physiological muscular activity with the possibility of gain-measurable outcomes. Robot-mediated rehabilitation aims at developing new solutions for assisted therapy, thus allowing an objective functional assessment of patients. Due to the advantages of their accuracy and reliability, rehabilitation robots can provide an effective way to improve the outcome of stroke or postsurgical rehabilitation. Robotic technology offers

(i) accuracy, precision, and simple tools for the modelling of the human behaviour; (ii) repeatable and continuous movements of the human districts to rehabilitate; and (iii) active engagement of the patients during the rehabilitation tasks, that is, through virtual reality-based exercises.

Robotic devices for rehabilitation fall into two broad categories (i.e., the ones considered in this paper) based on the relationship between the movements of the human body and those of the machine [4]:

(i) Operational machines: The physical interface between the robot and human body is in a defined part of the body, usually the effectors. For these machines, the trajectories of the robot end-effector and the human end-effector in the operational space are physically coupled. In the joint space, instead, the trajectories of the robot joints and the human joints can be significantly different, so that, kinematic schemes can also be selected based on only the specific requirements of the target application scenario.

(ii) Wearable robots: In these machines, a large portion of the human body (typically the whole affected limb) is in continuous physical contact with the robot. In most cases, a biomimetic exoskeleton kinematic structure is selected. Therefore, not only the trajectories of the robot end-effector and the human end-effector are the same in the operational space but also the trajectories of the robot joints approximate those of the human joints in the joint space. These systems require advanced biomechatronic design approaches in order to mimic human-like joints motion, while minimizing invasiveness for the patient in terms of weight, dimensions, and so on. To overcome these challenging problems, nonbiomimetic wearable robots are also currently under investigation in a few pilot research projects recently launched in Europe and the U.S. [5, 6].

Wearable robots for walking rehabilitation can be divided in turn into nonportable and portable systems, depending on whether they are fixed to a specific environment or not. Portable systems are autonomous while nonportable systems require a source of energy. Rehabilitation wearable robots can also be classified as robots for rehabilitation on treadmill and robots for overground walking rehabilitation [7, 8].

Lokomat (Hocoma AG, Volketswil, Switzerland), trade name for the DGO (Driven Gait Orthosis), is one of the most widely used wearable robots. It is a nonportable robot for treadmill rehabilitation, with an anthropomorphic non-redundant structure. It assists and guides the hip and knee movements in the sagittal plane, while the ankle joint is not actuated [9]. LOPES (lower-extremity powered exoskeleton) is another example of nonportable robot. It assists flexion/extension and abduction/adduction of the hip and flexion/extension of the knee [10]. ALEX (active leg exoskeleton) is a wearable robot for treadmill rehabilitation with two actuated degrees of freedom, which allow movement in the sagittal plane of the hip and knee joints [11]. AutoAmbulator and Walkbot are nonportable robotic systems with a mechanical structure very similar to Lokomat [12, 13].

ReWalk (ReWalk Robotics, Marlborough, US) is a mobile exoskeleton that allows overground rehabilitation. The battery and the controllers are inside the backpack that the patient wears on his shoulders. It is primarily used for SCI patients, and it must be used in conjunction with crutches [14].

Gait Trainer GT I (Reha-Stim, Berlin, Germany) is one of the most widespread operational machines for walking rehabilitation, and it consists of two footplates connected with the patient's feet mimicking the walking cycle [15]. Gait Master 4 is another operational machine based on the movement of two footplates moved by a connecting rod-crank system. The footplates allow the movement of the human effector back and forth (to simulate the walk) or up and down (up/down the stairs) [16].

In this paper, the authors provide a cost-effectiveness assessment to compare, in terms of efficiency, conventional rehabilitation therapies to wearable robot-/operational machine-mediated rehabilitation for the treatment of stroke-affected patients. The present work aims at assessing the effectiveness of the two therapeutic approaches and evaluating the costs for both types of procedure.

## 2. Materials and Methods

**2.1. Assessment of Effectiveness.** The authors have carried out a review of the articles at the state of the art, which compares the effectiveness of robot-mediated and conventional rehabilitation in stroke-affected patients. The analysis is based on average recovery of patients treated with the two approaches. The study includes all the articles in the Cochrane review [17] and more recent studies [13, 18–21]. The studies included in this review focus on patients who suffered a first stroke, who are over 18 years old (with an average age ranging between 48 and 71 years old), who have sufficient cognitive and communication skills that allow a correct understanding of the rehabilitation session, and who do not suffer cardiac, psychological, and orthopaedic contraindications. The authors have included studies on patients in acute and subacute phases (time elapsed since the ictal event not exceeding three months), on chronic patients, and on patients with different levels of disability. The patient groups range from patients who are able to walk independently even before the beginning of the rehabilitation therapy to patients who are completely dependent to walk.

All clinical trials are based on the random division of patients into two groups: group A and group B.

- (i) Group A: patients in this group underwent a rehabilitation programme consisting of several sessions of robot-mediated therapy and some additional manual therapy session.
- (ii) Group B: patients in this group underwent conventional therapy only.

Depending on the particular study, machines used for the robot-mediated rehabilitation of patients in the group A are wearable robots (Lokomat in most of the articles, but also AutoAmbulator, Anklebot, and Walkbot in one study each) or operational machines (Gait Trainer I in all cases except

one where Gate Master 4 is used). In both cases, training with a BWS (Body Weight Support) is carried out; a 30–40% of body weight support during the first rehabilitation session is applied. The body weight support is progressively reduced as the patient recovered his/her locomotor ability.

At the end of the rehabilitation process, the primary outcome is the ability of the patients to recover walking independence. The secondary outcome is the average walking speed. The acceptability of the therapy is assessed taking into account the number of dropouts, that is to say, the number of patients who do not complete the entire rehabilitation process.

The authors have applied the same statistical methods as those used in the Cochrane review [17], although not explicitly described here, but suggested by the homonymous statistical group in the “Cochrane Handbook for Systematic Reviews of Interventions” [22]. The odds ratio (OR) is calculated for each article. It measures the number of patients who recovered walking independence at the end of the robotic treatment compared to the conventional one, as well as to quantify the number of dropouts. The OR is calculated as follows:

$$OR_i = \frac{a_i \cdot d_i}{b_i \cdot c_i}, \quad (1)$$

where  $a_i$  is the number of patients in group A who recovered independence in walk at the end of the planned rehabilitation process,  $b_i$  is the number of patients in group A who did not recover independence in walk,  $c_i$  is the number of patients in group B who recovered independence in walk, and  $d_i$  is the number of patients in group B who did not recover independence in walk. Similarly,  $a_i$ ,  $b_i$ ,  $c_i$ , and  $d_i$  can be used to measure the number of patients who completed or not the entire rehabilitation process.

The Mantel-Haenszel (MH) random-effects method is used for meta-analysis and to calculate the Overall OR, which takes into account the results of each article:

$$OR_{MH} = \frac{\sum w_i^{MH} \cdot OR_i}{\sum w_i^{MH}}, \quad (2)$$

with  $w_i^{MH} = b_i \cdot c_i / n_i$ , where  $n_i = a_i + b_i + c_i + d_i$ . If no participant or if every participant in the study achieved the ability to walk independently, the OR of the  $i$ th article is considered “not estimable,” and it is, thus, not included in the meta-analysis. When this situation just occurs only in one of the two groups (A or B), a modified formula is used.  $OR_i$  is calculated by adding a factor equal to 0.5 to each element in (1).

The confidence interval (CI) is calculated taking into account the overall standard error  $SE(\ln OR_{MH})$ , according to the following formula:

$$95\% CI = \left[ e^{\ln OR_{MH} - 1.96 \cdot SE(\ln OR_{MH})}, e^{\ln OR_{MH} + 1.96 \cdot SE(\ln OR_{MH})} \right], \quad (3)$$

with  $SE(\ln OR_{MH}) = \sqrt{(1/2)((E/R^2) + (F + G/R \cdot S) + (H/S^2))}$ , where  $R = \sum a_i \cdot d_i / n_i$ ,  $S = \sum b_i \cdot c_i / n_i$ ,  $E = \sum (a_i + d_i) \cdot a_i \cdot d_i / n_i^2$ ,  $F = \sum (a_i + d_i) \cdot b_i \cdot c_i / n_i^2$ ,  $G = \sum (b_i + c_i) \cdot a_i \cdot d_i / n_i^2$ , and  $H = \sum (b_i + c_i) \cdot b_i \cdot c_i / n_i^2$ .

If 95% CI includes value 1 (no effect), the result described by the corresponding OR does not demonstrate a clear effectiveness, and it is not considered significant.

The mean difference (MD) is used to calculate the secondary outcome:

$$(MD \vec{v})_i = \vec{v}_i^{RT} - \vec{v}_i^{CT} \text{ (m/s)}, \quad (4)$$

where  $\vec{v}_i^{RT}$  is the average speed that patients reached at the end of the robotic therapy, and  $\vec{v}_i^{CT}$  is the average speed that patients reached at the end of the conventional therapy.

The inverse variance (IV) random-effects method is used to calculate the Overall MD:

$$(MD \vec{v})_{IV} = \frac{\sum w_i \cdot (MD \vec{v})_i}{\sum w_i} \text{ (m/s)}, \quad (5)$$

with  $w_i = 1/SE(MD \vec{v})_i^2$ , where  $SE(MD \vec{v})_i^2$  is the variance of the  $i$ th article.

The CI is calculated taking into account the overall standard error  $SE(MD \vec{v})_{IV}$ , according to the following formula:

$$95\% 2CI = [(MD \vec{v})_{IV} - 1.96 \cdot SE(MD \vec{v})_{IV}; (MD \vec{v})_{IV} + 1.96 \cdot SE(MD \vec{v})_{IV}], \quad (6)$$

with  $SE(MD \vec{v})_{IV} = 1/\sqrt{\sum w_i}$ . If 95% CI includes the value 0 (no effect), the result described by the corresponding MD does not demonstrate a clear effectiveness, and it is not considered significant.

Establishing the abovementioned statistical methods, the authors verified to be able to exactly reproduce the same results reported in the Cochrane review [17] (with a difference of maximum 0.02). Therefore, they carried out the calculations again, considering also the 5 more recent studies [13, 18–21], that perfectly fit in terms of inclusion criteria for the patients and the type of trials with the papers included in the Cochrane review.

**2.2. Costs Analysis.** Although in most of the studies patients were hospitalised for rehabilitation therapy, the authors take into account only the costs of the rehabilitation therapy, whereas hospitalisation costs are not considered, as they are effectively the same in the robotic and conventional approaches. Costs of medications, meals, and electricity are identical because the duration of the rehabilitation process, in all studies included in this review, is the same for patients of group A and B. The same applies to health cost reimbursements from the Lazio Region, which are the same in Italy for the conventional- and robot-mediated therapies [23]:

- (i)  $C_h^{\text{therapist}}$  (€/h), hourly cost of a single physiotherapist
- (ii)  $n^{\text{therapists}}$ , average number of therapists per session per patient
- (iii)  $t^{\text{session}}$  (min), average session duration
- (iv)  $n^{\text{sessions}}$ , average number of sessions for the entire rehabilitation process for patients mentioned in the articles.

The hourly cost of conventional therapy ( $C_h^{\text{Conventional}}$ ), cost per session ( $C_{\text{session}}^{\text{Conventional}}$ ), and cost of the entire rehabilitation process ( $C_{\text{total}}^{\text{Conventional}}$ ) are calculated. The cost estimate of the robot-mediated treatment takes into account the abovementioned parameters and also the cost to purchase the robot ( $C_{\text{Robot-purchase}}$  (€)), the number of years to amortise the robot ( $y^{\text{amortization}}$  (years)), and the annual routine maintenance cost ( $C_{\text{maintenance}}$  (€/year)).

The hours of potential use of the robot in a health facility are estimated to calculate the hourly cost of the robot (and the cost per session). Physiotherapists' working shifts are taken into account to get an idea of how many hours per day the robot can be used for rehabilitation sessions. Two possible working shifts were identified in collaboration with the Polyclinic General Direction of Campus Bio-medico (Rome, Italy), amounting to a total of 36 weekly working hours. The cost of the robotic therapy is, therefore, calculated for both shifts:

- (i) "1st case": robot used 7.12 hours per day, 5 days a week. This is the total amount of weekly working hours of a single therapist.
- (ii) "2nd case": robot used 12 hours per day, 6 days a week. This is the total amount of weekly working hours of two therapists, one working in the morning and the other in the afternoon.

This allows to calculate the hourly cost ( $C_h^{\text{Robot}}$ ), the cost per session ( $C_{\text{session}}^{\text{Robot}}$ ), and the cost of the entire rehabilitation process ( $C_{\text{total}}^{\text{Robot}}$ ) for the robotic therapy.

The cost estimate for the entire training process of the two groups (A and B) takes into account, for both approaches (robotic and conventional), the additional cost of conventional therapy in the clinical trials as extra training for patients in both groups:

$$C_{\text{total}}^{\text{patient}} = C_{\text{total}}^{\text{(Robot or Conventional)}} + C_{\text{additional}} \quad (7)$$

This means that (7) is calculated taking into account the cost of the specific rehabilitation process ( $C_{\text{total}}^{\text{Robot}}$  for group A and  $C_{\text{total}}^{\text{Conventional}}$  for group B), plus the additional cost of conventional therapy extra sessions.

**2.3. Cost-Effectiveness Analysis.** The ICER (incremental cost-effectiveness ratio) is calculated to compare the efficiency of the two approaches (conventional versus robotic) and to determine which one is most cost-effective:

$$\text{ICER} = \frac{C_A - C_B}{E_A - E_B}, \quad (8)$$

where  $C_A$  and  $C_B$  are the cost of the entire rehabilitation process for robot-mediated therapy and conventional therapy, respectively, whereas  $E_A$  and  $E_B$  measure the effectiveness of each therapy in terms of primary outcome, that is to say, the Overall OR for walking independence, or in terms of secondary outcome, the Overall MD of walking speed.

When calculating the ICER, it is important to distinguish whether the difference in effectiveness is expressed in terms

of OR or MD. When the difference in effectiveness ( $E_A - E_B$ ) is expressed in terms of Overall OR,  $C_A$  and  $C_B$  are calculated by multiplying the cost of the entire rehabilitation process per patient ( $C_{\text{total}}^{\text{patient}}$ ) per the average number of treated patients. When the difference in effectiveness ( $E_A - E_B$ ) is expressed in terms of Overall MD,  $C_A$  and  $C_B$  costs are equal to  $C_{\text{total}}^{\text{patient}}$ . In both cases, robot-mediated therapy is more effective than the conventional therapy when the ICER value is low. A low value at the ICER ratio numerator indicates a small difference in cost between the two approaches, whereas a high value at the denominator marks a high OR or MD, which means that the robotic therapy is much more effective than the conventional therapy. The more the OR is  $>1$  or MD is  $>0$ , the more the robot-mediated therapy is effective compared to the conventional one. Therefore, the ICER is the difference in terms of cost for the two approaches, weighted by the difference of effectiveness.

### 3. Results and Discussion

**3.1. Effectiveness.** A number of 26 trials are included with a total of 1064 patients, all of them affected by a stroke for the first time. 60% of the patients are men and 40% are women, 70% are affected by ischemic stroke and 30% by haemorrhagic stroke, and 50% have a left hemiparesis and 50% a right hemiparesis. The total number of sessions and their duration and frequency are the same in group A and group B.

The authors have selected the appropriate number of articles to assess the primary and secondary outcomes, as well as the therapy acceptability in three different cases:

- (1) Robot-mediated therapy for group A based on the use of both wearable robots and operational machines.
- (2) Robot-mediated therapy for group A based on the use of wearable robots,
- (3) Robot-mediated therapy for group A based on the use of operational machines.

In all the three cases, the robot-mediated therapy is more effective than the conventional one to recover the patient walking independence (Overall OR  $> 1$ ) with statistically significant results ( $p$  value  $< 0.05$  and 95% CI not including value 1), as shown in Figure 1. The OR is equal to 2.38 in the first case ( $p$  value  $< 0.0001$ , 95% CI between 1.68 and 3.39), 2.28 in the second case ( $p$  value = 0.0038, CI between 1.31 and 4.00), and 2.45 in the third case ( $p$  value = 0.0001, 95% CI between 1.56 and 3.85).

As for the average walking speed achieved at the end of the rehabilitation process, the robotic therapy is slightly more effective than the conventional one (Overall MD is 0.04 m/s,  $p$  value = 0.0026, 95% CI between 0.01 and 0.06). Operational machines, in particular, are more effective than wearable robots, as shown in Figure 2. Operational machines MD is 0.14 m/s ( $p$  value  $< 0.0001$ , 95% CI between 0.09 and 0.19). Wearable robots have a null MD, which means that wearable robots are as effective as conventional therapy.

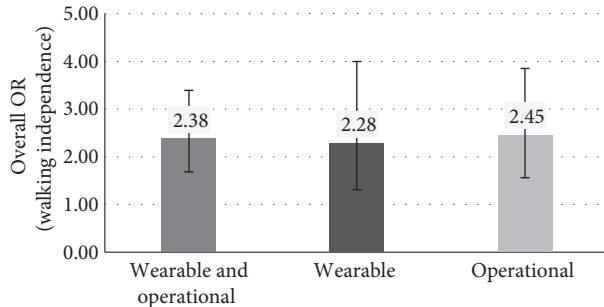


FIGURE 1: Overall OR (and 95% CI) for independence in walk in the three different cases based on the type of robot used for the rehabilitation of patients in group A.

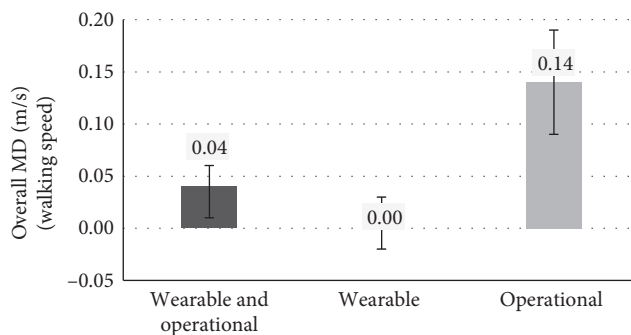


FIGURE 2: Overall MD (and 95% CI) for walking speed in the three different cases based on the type of robot used for the rehabilitation of patients in group A.

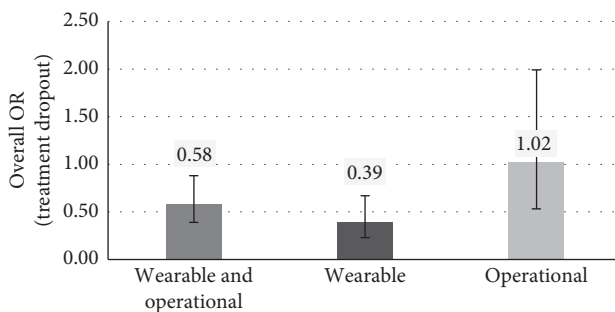


FIGURE 3: Overall OR (and 95% CI) for dropouts in the three different cases based on the type of robot used for the rehabilitation of patients in group A.

However, this result is not statistically significant ( $p$  value = 0.89, 95% CI between -0.02 and 0.03).

Regarding the acceptability, the robotic therapy is more effective than the conventional one with OR equal to 0.58 ( $p$  value = 0.01, 95% CI between 0.39 and 0.88), as shown in Figure 3. OR < 1 indicates fewer dropouts. However, the results show differences based on the type of robot used for the rehabilitation of patients in group A. The therapy based on the use of wearable robots is much more acceptable than the conventional one (OR = 0.39,  $p$  value = 0.0007, 95% CI between 0.23 and 0.67). The therapy based on the use of operational machines has the same acceptability as the

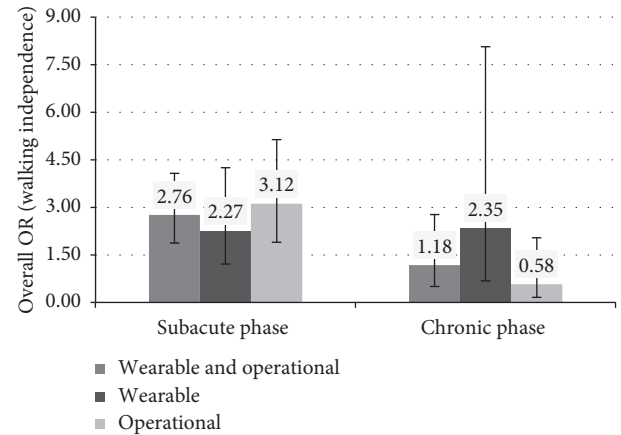


FIGURE 4: Overall OR (and 95% CI) for walking independence based on the type of robot and the condition of patients (chronic versus subacute phase).

conventional one (OR = 1.02). However, this result is not statistically significant ( $p$  value = 0.95, 95% CI between 0.53 and 1.99).

The authors distinguish between the results for the primary and secondary outcomes depending on patient conditions, that is to say, patients in the subacute or chronic phase.

The use of different types of robots to recover the independence in walk produces different results, as shown in Figure 4. The therapy based on the use of wearable robots is more effective than the conventional one for patients both in the chronic (OR = 2.35,  $p$  value = 0.17, 95% CI between 0.68 and 8.07) and subacute phases (OR = 2.27,  $p$  value = 0.01, 95% CI between 1.21 and 4.25). The therapy based on the use of operational machines is extremely more effective than the conventional one for patients in the subacute phase (OR = 3.12,  $p$  < 0.0001, 95% CI between 1.90 and 5.14), but it is less effective than the conventional therapy for chronic patients. However, this result is not statistically significant (OR = 0.58,  $p$  value = 0.40, 95% CI between 0.16 and 2.04).

With regards to walking speed, results show no big difference between patients in the subacute or chronic phases, as shown in Figure 5. The therapy based on the use of operational is more effective than the conventional one for both patients in the subacute and chronic phases. For patients in the chronic phase, MD is equal to 0.14 m/s ( $p$  value = 0.01, 95% CI between 0.03 and 0.26). Similar results are obtained for patients in the subacute phase: MD is equal to 0.14 m/s ( $p$  value < 0.0001, 95% CI between 0.09 and 0.19). The therapy based on the use of wearable robots is as effective as the conventional one for patients in the subacute phase (MD = 0 m/s), but the result is not statistically significant ( $p$  value = 0.77, 95% CI between -0.02 and 0.03) and less effective than the conventional one for chronic patients (MD = -0.02 m/s), but the result is still not statistically significant ( $p$  value = 0.68, 95% CI between -0.10 and 0.06).

**3.2. Costs.** Similar to the effectiveness analysis, three types of comparisons between training costs for the two groups (A

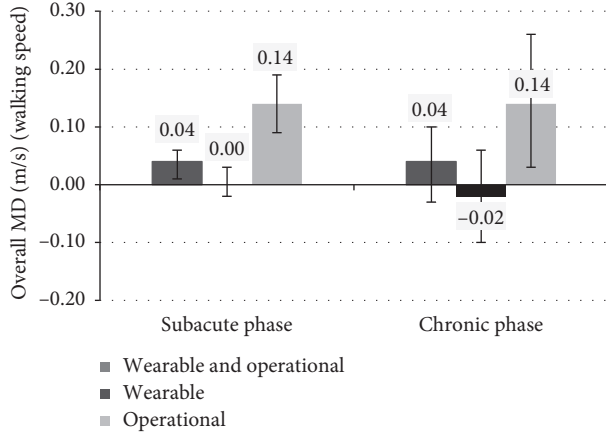


FIGURE 5: Overall MD (and 95% CI) for walking speed based on the type of robot and the condition of patients (chronic versus subacute phase).

and B) are carried out. The first comparison is based on all the articles included in the review, irrespective of the type of robot used for the therapy (operational machine or wearable robot). The other two comparisons focus on two subcases: one based only on studies on wearable robots and the other only on studies on operational machines.

The results are based on a 20 €/h cost per therapist (as per 2014 Collective Bargaining Agreement in Italy) and 5 years to amortise the robot, as per “high-tech medical equipment” tax rate [24]. The annual robot maintenance cost is calculated as 10% of the robot value. For wearable robots, the reference value is set to the Lokomat cost, that is, € 330,000.00. For operational machines, the reference value is set to the Gait Trainer GT I, that is, € 30,000.00. For the robotic therapy in general—regardless of the type of robot—the robot purchase cost is, thus, set equal to € 225,000.00, which is the average between the costs of Lokomat and Gait Trainer GT I weighted by the number of reference articles.

Table 1 shows the parameters used to calculate costs and the relative results, when comparing the conventional therapy to the robot-mediated one, in both the cases described in section “Cost Analysis.” As it could be imagined, the robot-mediated therapy is more expensive and, therefore, less economically sustainable than the conventional one. The cost estimate shows very different results for the therapy based on the use of wearable robot and the one based on operational machines.

Table 2 summarises the hourly cost and total cost (for the full rehabilitation of a patient) for conventional therapy, wearable robots therapy, and operational machines therapy. The therapy with wearable robots costs about three times more than the conventional one considering 12.7 hours of possible use of the robot for 5 days a week (“1st case”). The cost decreases and is about two times more than the cost of the conventional therapy when it is based on 12 hours of possible use of the robot for 6 days a week (“2nd case”). The cost of the therapy with operational machines, on the contrary, is the same as the cost of the conventional therapy

TABLE 1: Costs analysis of robotic therapy versus conventional therapy: parameters and cost estimate results.

	Robotic		Conventional
	1st case	2nd case	
<i>Parameters</i>			
$C_h^{\text{therapist}}$ (€/h)	20.00	20.00	20.00
$n_{\text{therapists}}$	1	1	1.19
$t_{\text{session}}$ (min)	52.72	52.72	52.72
$n_{\text{sessions}}$	17.91	17.91	17.91
$C_{\text{Robot purchase}}$ (€)	225,000.00	225,000.00	—
$y_{\text{amortization}}$ (years)	5	5	—
$C_{\text{maintenance}}$ (€/year)	22,500.00	22,500.00	—
Daily robot use (hours per day)	7.12	12	—
Weekly robot use (days per week)	5	6	—
<i>Results</i>			
$C_{\text{therapy}}$ (€/h)	56.46	38.03	23.80
$C_{\text{session}}$ (€/session)	52.44	35.32	22.10
$C_{\text{total}}^{\text{patient}}$ (€)	1,023.36	716.76	480.10

TABLE 2: Hourly cost and total cost: comparison between conventional, wearable robots, and operational machines therapies.

	Conventional	Wearable robot		Operational robot	
		1st case	2nd case	1st case	2nd case
$C_h^{\text{therapy}}$ (€/h)	23.80	73.48	46.44	24.86	22.40
$C_{\text{total}}^{\text{patient}}$ (€)	480.10	1,353.71	866.21	491.00	458.56

in the “1st case” and even lower than the cost of the conventional therapy in the “2nd case.”

**3.3. Cost-Effectiveness (ICER).** ICER estimates are carried out for the three cases described in section “Effectiveness.” For each case, two different values of ICER are calculated—the first is based on the cost estimate of the robotic therapy in the “1st case” and the second in the “2nd case.”

Figure 6 shows ICER values regarding patients recovering walking independence. For the robot-mediated therapy in general, without considering the type of robot, ICER is € 4,565.21 in the “1st case” and is lower in the “2nd case,” € 1,988.74. Taking into account, instead the type of robot, results are very different. The wearable robots therapy has a higher ICER: € 7,889.21 in the “1st case” and € 3,612.89 in the “2nd case.” The ICER for operational machines therapy is much lower and amounts to € 71.27 in the “1st case.” Increasing the number of hours of possible use of the robot (“2nd case”), the ICER has a negative value (€ -193.47). This means that the operational machines therapy is not only 2.45 times more effective than the conventional one in the case of patients recovering independence in walk (as shown by the Overall OR), but also

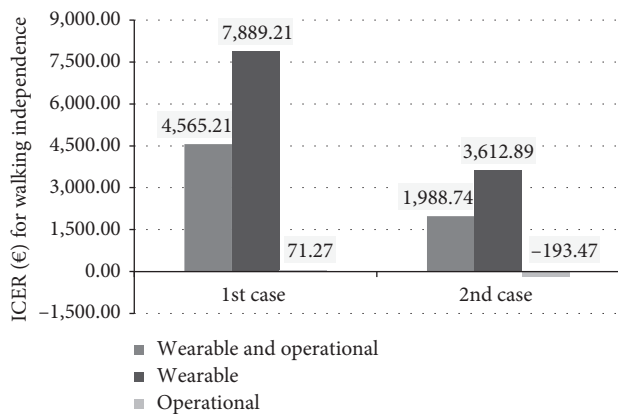


FIGURE 6: ICER values related to the independence in walk in the different cases based on the type of robot used and on the hours of potential use of the robot.

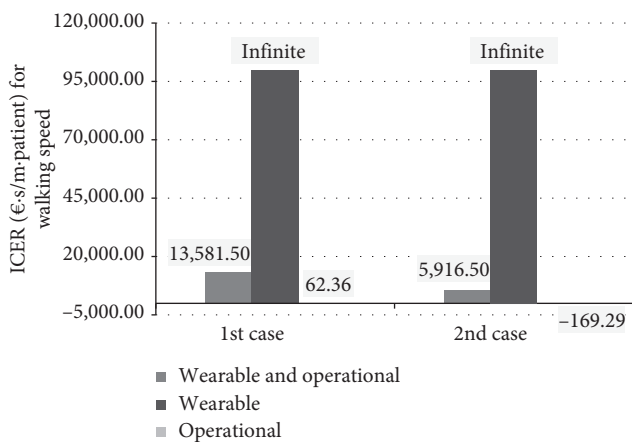


FIGURE 7: ICER values related to the independence in walking in the different cases based on the type of robot used and on the hours of potential use of the robot. Divergent ICER, for graphic purposes, set equal to € 100,000.00.

the therapy is even more economically sustainable, as it allows to save € 193.47.

Figure 7 shows ICER values of patients recovering average walking speed. The ICER of the operational machines therapy is 62.36 (€/patient)/(m/s) in the “1st case”. This means that the robotic therapy costs approximately € 60 more than the conventional one per patient per meter per second of recovered walking speed. In the “2nd case,” the ICER is negative (-169.29 €/patient/m/s).

Results are very different for wearable robots: the ICER for them is divergent being present a zero at denominator in (8) (Overall MD = 0 m/s both in the “1st case” and in the “2nd case”).

#### 4. Conclusions

Robot-mediated therapy has proven to be more effective than conventional therapy in the treatment of stroke-affected patients. Overall OR results show that the robotic therapy enables a larger number of patients to recover independence in walk, compared to the conventional therapy.

This applies to all analysed cases, being the therapy based on the use of wearable robots or operational machines and being the patients in a chronic or subacute phase. This is particularly interesting since the time that patients in group A spent for robotic therapy is less than the time that patients in group B spent for conventional therapy. In the analysed studies, the duration of the rehabilitation session and the total number of sessions are the same for both groups. However, for patients in group A, about half of the session time is not spent training with the robot but rather setting-up the machine. In conventional therapy for patients in group B, the session is entirely dedicated to the rehabilitation procedure. The therapy based on the use of operational machines is the most effective treatment, with the highest Overall OR. This may be due to limitations of wearable robots. For instance, in the case of exoskeletons when the coupled joint-links are not perfectly aligned with the human joints, undesired high forces are produced [25]. This makes the robot a danger to the patient, as well as an obstacle to his/her movement. This does not happen with operational machines. Operational machines are more effective for patients in the subacute phase, whereas wearable robots are more effective for patients in the chronic phase. These results, however, are not statistically significant and require further study in the future. In terms of secondary outcome, robot-mediated therapy has the same effectiveness as conventional therapy. To sum up, robotic therapy is particularly effective in the treatment of critical patients, who are unable to walk independently before starting the rehabilitation process. For critical patients, the most important goal is to recover the walking autonomy, which is more easily achieved through robotic therapy. For patients who are already able to walk autonomously, the main goal is to recover walking speed; thus, the robotic therapy is not particularly convenient for them. Further studies are needed to assess the effectiveness of robot-mediated therapy with wearable robots to achieve the secondary outcome. Current results on this aspect are still not statistically significant.

As for therapy acceptability, patients who underwent robotic therapy with wearable robots have the lowest number of dropouts. This result is rather unexpected, as the authors thought that robot-mediated therapy would not be well accepted. A possible explanation may lie in the fact that the therapist is always present during the sessions, supervising the patient, prompting his/her active participation, and making him/her feel safe. In addition to this, the robot reduces the physical effort required to the patient and relieves his/her fatigue, especially when he/she is in difficulty. Another element to take into consideration is that the wearable robot allows patients to walk as of the very first session. This could have a positive impact on the patient's psychological response, by increasing his/her self-confidence and motivation to keep on training.

As for the economic point of view, robotic therapy based on the use of wearable robots has proven to be very expensive. Costs decrease as the hours of possible use of the robot increase. The gap between the cost of robotic and conventional therapies is considerable. Robotic therapy based on the use of operational machines is the most

economically sustainable method due to the low purchasing cost. It must be said, however, that the cost of robot-mediated and conventional therapies is estimated based on the assumption that training time is the same for both therapies. The fact that the duration of the rehabilitation therapy is the same for patients in both groups A and B is based on what is reported in the articles included in this study. This, in addition to the lack of information on posttraining patients quality of life, means that the authors can evaluate only some of the direct medical costs of the therapy. It is not possible to make a comparison between the two rehabilitation approaches in terms of nonmedical direct costs (i.e., social services, home care, transportation, etc.) nor indirect costs (i.e., working days lost by the patient due to treatment and health care, working days lost in terms of lower productivity of working patients, etc.). Also, the fact that patients of both groups (A and B) underwent a programme with a similar structure does not allow to analyse other possible cost differences related, for instance, to days of hospitalisation for patients locomotion recovery. The authors, thus, highly recommend organizing clinical trials differently. Rather than having all patients undergoing a rehabilitation therapy, which has the same duration, it might be useful to set “targets” (sufficient values of effectiveness) and assess patients’ recovery time against such “targets.” This would allow for a more realistic assessment of the cost of robot-mediated and conventional therapies, which takes into account rest days for patients to achieve “targets” and the other aspects mentioned above. Future clinical trials should also consider different methods for a proper assessment of nonmedical direct and indirect costs.

Taking into account both economic aspect and effectiveness, the cost difference between robotic therapy and conventional therapy is reduced. ICER results for the primary outcome show that the therapy based on wearable robots is more effective than the conventional one but also more expensive. This trend is even more evident if we consider ICER results for the secondary outcome. In this case, the ICER is divergent. This means that an infinite amount of resources would have to be spent to increase the patient’s walking speed. In other words, robot-mediated therapy based on the use of wearable robots has a cost for benefit equal to 0. It is “infinitely” less efficient than conventional therapy. On the contrary, rehabilitation therapy based on operational machines is the most cost-effective one, as ICER values are very low and in some cases, even negative.

In conclusion, the study shows that robotic therapy based on the use of operational machines is the most efficient strategy. It is much more effective than the conventional one, with statistically significant results, both in terms of patients’ recovery of walking ability and walking speed. It is also much more economically sustainable than robotic therapy based on the use of wearable robots, as its cost is similar, if not lower, than the cost of conventional therapy. However, the therapy which has the highest patients’ acceptability is the one based on the use of wearable robots.

The investigated topic, and in general the assessment studies on medical devices, is relatively new with respect to the studies on drugs, the scientific evidence is sparse, and the

attempts to collect information are challenging but the need of the assessment for medical device is crucial for supporting the decision-making process [26].

## Conflicts of Interest

The authors declare that there are no conflicts of interest regarding the publication of this paper.

## References

- [1] W. S. Harwin, J. L. Patton, and V. Reggie Edgerton, “Challenges and opportunities for robot-mediated neuro-rehabilitation,” *Proceedings of the IEEE*, vol. 94, no. 9, pp. 1717–1726, 2006.
- [2] D. P. Ferris, G. S. Sawicki, and A. Domingo, “Powered lower limb orthoses for gait rehabilitation,” *Topics in Spinal Cord Injury Rehabilitation*, vol. 11, no. 2, pp. 34–49, 2005.
- [3] M. Fairley, *I, Robot: Robotic Technology Adds a New Dimension to Orthotics*, Western Media LLC, Northglenn, CO, USA, 2009.
- [4] E. Guglielmelli, M. J. Johnson, and T. Shibata, “Guest editorial, special issue on rehabilitation robotics,” *IEEE Transactions on Robotics*, vol. 25, no. 3, pp. 477–480, 2009.
- [5] D. Accoto, F. Sergi, N. L. Tagliamonte, G. Carpino, A. Sudano, and E. Guglielmelli, “Robomorphism: a nonanthropomorphic wearable robot,” *IEEE Robotics and Automation Magazine*, vol. 21, no. 4, pp. 45–55, 2014.
- [6] N. L. Tagliamonte, F. Sergi, G. Carpino, D. Accoto, and E. Guglielmelli, “Human-robot interaction tests on a novel robot for gait assistance,” in *Proceedings of the IEEE International Conference on Rehabilitation Robotics ICORR*, pp. 1–6, Seattle, WA, USA, June 2013.
- [7] S. Sargsyan, V. Arakelian, and S. Briot, “Robotic rehabilitation devices of human extremities: design concepts and functional particularities,” in *Proceedings of the 11th Biennial Conference on Engineering Systems Design and Analysis ESDA*, pp. 1–10, Nantes, France, July 2012.
- [8] S. Hussain, S. Q. Xie, and G. Liu, “Robot assisted treadmill training: mechanisms and training strategies,” *Medical Engineering and Physics*, vol. 33, no. 5, pp. 527–533, 2011.
- [9] G. Colombo, “The lokomat: a driven ambulatory orthosis,” *Medicine Orthopaedics Technology*, vol. 6, pp. 178–181, 2000.
- [10] J. Veneman, R. Kruidhof, E. Hekman, R. Ekkelenkamp, E. V. Asseldonk, and H. van der Kooij, “Design and evaluation of the LOPES exoskeleton robot for interactive gait rehabilitation,” *IEEE Transaction on Neural Systems and Rehabilitation Engineering*, vol. 15, no. 3, pp. 379–386, 2007.
- [11] S. Banala, S. H. Kim, S. Agrawal, and J. Scholz, “Robot assisted gait training with active leg exoskeleton (ALEX),” *IEEE Transaction on Neural Systems and Rehabilitation Engineering*, vol. 17, no. 1, pp. 2–8, 2009.
- [12] J. A. Galvez and D. J. Reinkensmeyer, “Robotics for gait training after spinal cord injury,” *Topics in Spinal Cord Injury Rehabilitation*, vol. 11, no. 2, pp. 18–33, 2005.
- [13] S. Y. Kim, L. Yang, I. J. Park et al., “Effects of Innovative WALKBOT robotic-assisted locomotor training on balance and gait recovery in hemiparetic stroke: a prospective, randomized, experimenter blinded case control study with a four-week follow-up,” *IEEE Transactions on Neural Systems and Rehabilitation Engineering*, vol. 23, no. 4, pp. 1–7, 2015.
- [14] A. Esquenazi, M. Talaty, A. Packel, and M. Saulino, “The ReWalk powered exoskeleton to restore ambulatory function to individuals with thoracic-level motor-complete spinal cord

- injury," *American Journal of Physical Medicine and Rehabilitation*, vol. 91, no. 11, pp. 911–921, 2012.
- [15] S. Hesse and D. Uhlenbrock, "A mechanized gait trainer for restoration of gait," *Journal of Rehabilitation Research and Development*, vol. 37, no. 6, pp. 701–708, 2000.
  - [16] N. Tanaka, H. Saitou, T. Takao et al., "Effects of gait rehabilitation with a footpad-type locomotion interface in patients with chronic post-stroke hemiparesis: a pilot study," *Clinical Rehabilitation*, vol. 26, no. 8, pp. 686–695, 2012.
  - [17] J. Mehrholz, B. Elsner, C. Werner, J. Kugler, and M. Pohl, "Electromechanical-assisted training for walking after stroke (review)," *Cochrane Database of Systematic Reviews*, no. 7, pp. 1–100, 2013.
  - [18] M. P. M. van Nunen, K. H. L. Gerrits, M. Konijnenbelt, T. W. J. Janssen, and A. de Haan, "Recovery of walking ability using a robotic device in subacute stroke patients: a randomized controlled study," *Disability and Rehabilitation: Assistive Technology*, vol. 10, no. 2, pp. 141–148, 2014.
  - [19] L. W. Forrester, A. Roy, A. Krywonis, G. Kehs, H. I. Krebs, and R. F. Macko, "Modular ankle robotics training in early subacute stroke: a randomized controlled pilot study," *Neurorehabilitation and Neural Repair*, vol. 28, no. 7, pp. 678–687, 2014.
  - [20] C. P. Kelley, J. Childress, C. Boake, and E. A. Noser, "Over-ground and robotic-assisted locomotor training in adults with chronic stroke: a blinded randomized clinical trial," *Disability and Rehabilitation: Assistive Technology*, vol. 8, no. 2, pp. 161–168, 2013.
  - [21] R. S. Calabro, S. Reitano, A. Leo, R. De Luca, C. Melegari, and P. Bramanti, "Can robot-assisted movement training (Lokomat) improve functional recovery and psychological well-being in chronic stroke? Promising findings from a case study," *Functional Neurology*, vol. 29, no. 2, pp. 139–141, 2014.
  - [22] J. J. Deeks, J. P. T. Higgins, and D. G. Altman, "Analysing data and undertaking meta-analyses," in *Cochrane Handbook for Systematic Reviews of Interventions*, Wiley, Hoboken, NJ, USA, 2008.
  - [23] Official Bulletin of Lazio Region, n° 56, Subject: Approval of the regional tariff for the compensation of hospital care services D. M. 18.10.2012.
  - [24] Italian Ministerial Decree of the 31st of December 1988 and modified with the Italian Ministerial Decree of the 28th of March 1996, established by the Italian Ministry of Finance.
  - [25] M. Cenciarini and A. M. Dollar, "Biomechanical considerations in the design of lower limb exoskeletons," in *Proceedings of the IEEE International Conference on Rehabilitation Robotics ICORR*, pp. 297–302, Zurich, Switzerland, July 2011.
  - [26] World Health Organization, "Needs assessment for medical devices," in *WHO medical device technical series*, WHO, Geneva, Switzerland, 2011.

## Research Article

# Dynamic Modeling and Interactive Performance of PARM: A Parallel Upper-Limb Rehabilitation Robot Using Impedance Control for Patients after Stroke

Hui Guang ,<sup>1</sup> Linhong Ji ,<sup>1</sup> Yingying Shi,<sup>2</sup> and Berno J. E. Misgeld<sup>3</sup>

<sup>1</sup>Department of Mechanical Engineering, Tsinghua University, Beijing, China

<sup>2</sup>Department of Mechanical Engineering, Beihang University, Beijing, China

<sup>3</sup>Helmholtz-Institute for Biomedical Engineering, RWTH Aachen University, Aachen, Germany

Correspondence should be addressed to Linhong Ji; [jilh@tsinghua.edu.cn](mailto:jilh@tsinghua.edu.cn)

Received 1 June 2017; Revised 15 September 2017; Accepted 13 February 2018; Published 5 April 2018

Academic Editor: Carlo Ferraresi

Copyright © 2018 Hui Guang et al. This is an open access article distributed under the Creative Commons Attribution License, which permits unrestricted use, distribution, and reproduction in any medium, provided the original work is properly cited.

The robot-assisted therapy has been demonstrated to be effective in the improvements of limb function and even activities of daily living for patients after stroke. This paper presents an interactive upper-limb rehabilitation robot with a parallel mechanism and an isometric screen embedded in the platform to display trajectories. In the dynamic modeling for impedance control, the effects of friction and inertia are reduced by introducing the principle of virtual work and derivative of Jacobian matrix. To achieve the assist-as-needed impedance control for arbitrary trajectories, the strategy based on orthogonal deviations is proposed. Simulations and experiments were performed to validate the dynamic modeling and impedance control. Besides, to investigate the influence of the impedance in practice, a subject participated in experiments and performed two types of movements with the robot, that is, rectilinear and circular movements, under four conditions, that is, with/without resistance or impedance, respectively. The results showed that the impedance and resistance affected both mean absolute error and standard deviation of movements and also demonstrated the significant differences between movements with/without impedance and resistance ( $p < 0.001$ ). Furthermore, the error patterns were discussed, which suggested that the impedance environment was capable of alleviating movement deviations by compensating the synergetic inadequacy between the shoulder and elbow joints.

## 1. Introduction

Stroke is caused by cerebrovascular accident and is one of the leading diseases of disability, motor disorder, and deterioration of activities of daily living (ADL). The incidences in the European Union and the United States are approximately one million and 0.8 million per year, respectively [1, 2], and thirty percent of patients suffer recurrent attacks, which results in increasing demand for rehabilitation services.

For patients after stroke, the task-repetitive training has been demonstrated to be effective in improving their upper and lower extremity functions and ADL [3]. To meet the requirement for repetitive training, various upper-limb rehabilitation robots have been developed over the past twenty years, which are generally classified into two categories [4]: end-effector robots, such as DIAGNOBOT [5], CARR [6],

MIT-MANUS [7], MIME [8], GENTLE/s [9], and exoskeleton robots, such as CADEN-7 [10], RUPERT [11], BONES [12], and ARMin [13]. Since the robotic rehabilitation exhibits the advantages in terms of high-dosage, high-intensity, and task-specific training [14], randomized controlled trials comparing the robot-assisted and conventional therapy have yielded significant effects of robots on the improvements of limb function [15, 16] and even ADL [17].

Although many robots for the upper-limb rehabilitation have been developed, mechanical design, control, and training methods remain an area of interest. As pointed out by Belda-Lois et al. [18], robot-assisted rehabilitation could be enhanced by means of precisely controllable assistance or resistance, enhanced training motivation through interactive feedback, and quantifiable and objective measures of subject performance. Besides, cost should also be considered [19].

Generally, the exoskeleton robots take individual joint motions into account to minimize abnormal postures and joint motions. Nevertheless, due to the complexity of the human upper-limb anatomy, the instantaneous centers of rotation of the upper-limb joints are changed with movement [20], which causes the inconvenience of joint axis alignments and raises interactive force between human and robots [21], thereby obstructing the development and application of the exoskeleton robots. In contrast to exoskeleton robots, end-effector robots are simple and cost-effective and can adapt to patients with diverse somatotypes [4]. Despite the disadvantage of end-effector robots in joint training, extensive research has also demonstrated their effectiveness and superiority for improving upper-limb function and ADL in comparison with conventional therapies [14].

Compared to serial mechanisms, parallel mechanisms exhibit inherent advantages of low inertia, high stiffness, and satisfactory payload capability [22, 23]. More importantly, as the end-effector is controlled in parallel, the errors of the joint control are not accumulated and amplified by serial counterparts, and thus the manipulator is less affected by joint clearance and has higher precision in aspects of position, stiffness, and interactive force control [12]. Therefore, parallel manipulators have been recently applied to rehabilitation robots, including shoulder [12, 24], wrist [25], hip [26], and upper-limb rehabilitation devices [27].

Another issue is that understanding sensorimotor physiology is more imperative prior to developing a rehabilitation robot. For instance, one aspect is how individual joints, as well as segments, are coordinated to achieve the task. In physiology, limb movements are perceived in an egocentric reference frame, in which targets are defined with respect to the trunk or head. In contrast, an allocentric reference frame represents the coordinate system external to the body [28]. However, for current training robots, target and actual trajectories are presented in a standing monitor, which is a virtual environment based on the allocentric reference frame for patients. Thus, patients are required to transform the targets and movements in the virtual environment to the egocentric reference frame to accomplish the task, causing difficulties in perception and sensorimotor control. Besides, it might weaken the effect of proprioceptive training since the actual positions do not directly correspond to virtual positions.

Based on the issues discussed above, a novel end-effector-based upper-limb rehabilitation robot, which is named PARM, is developed with a parallel mechanism and patient-frame-based interactive feedback to enhance training performance. Distinct from other rehabilitation robots, a monitor was embedded in the platform to show target and actual trajectories, providing isometric direct visual feedback for patients. The trajectories displayed on the platform screen were the same as the actual trajectories in movement space, particularly in the aspects of scale, position, and direction. Therefore, patients could perceive targets and movements in the egocentric reference frame, which should improve the motor recovery and proprioceptive training. As the precise control of position, stiffness, and force contributes to training effects [18], the impacts of friction and acceleration

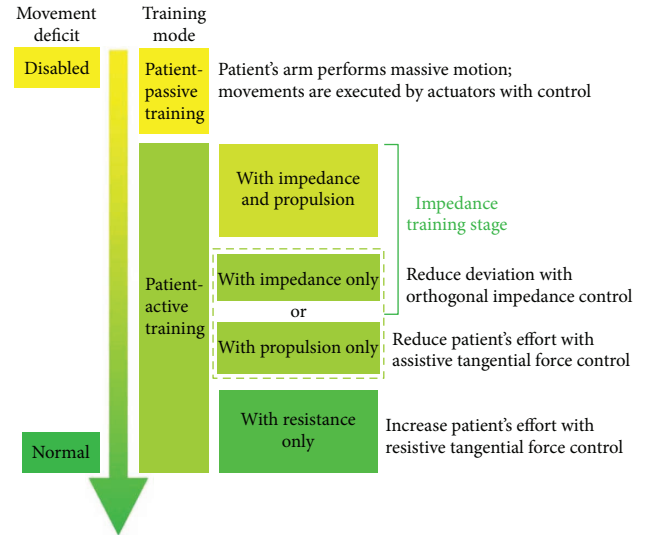


FIGURE 1: Training modes of PARM for stroke patients.

were incorporated to improve the control precision. Consistent with the robots such as MIT-MANUS [7], an assist-as-needed strategy was also introduced in PARM to improve interaction between patients and robots. In the assist-as-needed control, patients determine the manipulator in terms of position, velocity, and acceleration; thus, the reference positions are variable with the movement and associated with real-time deviations.

To summarize, the novelty of our work is the strategy based on the orthogonal deviation for assist-as-needed impedance control, which aims to obtain the equilibrium positions and calculate impedance force, and the hardware which adopts parallel mechanism and isometric visual feedback. Simulated and experimental results validated the dynamic modeling and impedance control. Since the mechanism of the impedance control contributing to the motor coordination is still less clear, the functional interaction between impedance control and movements was also discussed.

## 2. Apparatus and Specification

The rehabilitation robot PARM aims to improve the motor performance of stroke patients by enhancing movement interaction between the patients and the robot. This interactive robot incorporates multiple training modes for patients with diverse disability and recovery stages, which are summarized as patient-passive training and patient-active training (Figure 1). Arbitrary reference trajectories are predefined by therapists prior to training. In the patient-passive training, the movements are entirely actuated by the robot with position control, in which the robot is a mechanical admittance whereas the patient's arm is regarded as an impedance. Contrastively, in the patient-active training, movements are initiated and actuated by patients with partially assistance or resistance. For instance, in the training with impedance and propulsion, the impedance force towards the target trajectory aims to rectify deviations, while

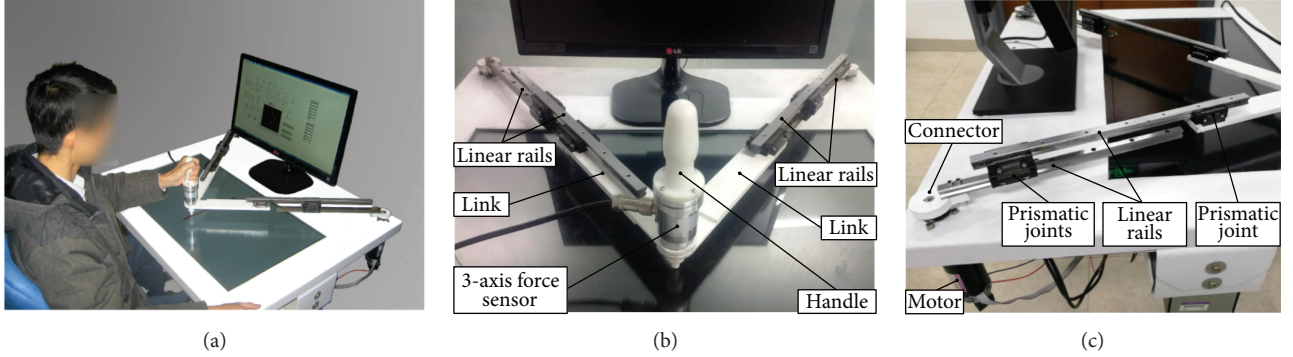


FIGURE 2: Mechanical construction of PARM. (a) Robot overview. (b) Robot parallel mechanism. (c) Motor and joint connections.

the propulsive force towards the movement direction could reduce the active force of the patient, which decreases the task difficulty. Conversely, the resistance force against the movement direction increases the movement effort.

To increase the benefit of robot-aided therapy, control schemes should be customized for individuals and adopted to patients' deficits in upper-limb motor function, based on their poststroke stages and clinical assessments. For subacute patients, since they are generally unable to perform voluntary arm-reaching tasks due to dystonia, training is mainly executed in patient-passive modality. For chronic patients (more than 6 months poststroke), robot-aided therapies are generally performed in patient-active modalities to enhance patient engagement. Specifically, when patients could perform inaccurate arm-reaching tasks, impedance control is applied for this training stage to rectify deviations and improve their abilities in motor control. Besides, for patients with low strength, propulsion in movement direction is included to reduce the movement effort. However, for the patients having coordinated motor control, impedance control is removed. Instead, resistance in movement direction might be involved to match their motor function and improve training outcomes.

PARM mainly consisted of a lifting platform, two monitors, a five-bar parallel mechanism with two motors and actuators, and a three-axis force sensor (Figure 2). A horizontal monitor was embedded in the platform to display the reference trajectory and actual trajectories, providing direct visual feedback for patients, while a standing monitor was used to display the configuration of training parameters and quantitative assessments. Additionally, the inclination and height of the platform could be adjusted to make the trajectories conveniently observed for patients.

The five-bar parallel mechanism RPRPR (revolute-prismatic-revolute-prismatic-revolute) is shown in Figures 2(b) and 2(c). Linear rails were adopted to increase movement range of end-effector and improve kinematic precision, and linear bearing blocks constituted the prismatic joints to reduce friction. Each side consisted of three prismatic joints and two linear rails, and thereby the minimal length of each side was the length of a rail, while the maximal length was the sum of two rails and a link. During movement, the length of two sides was accordingly adjusted to the two revolute joints controlled by the motors.

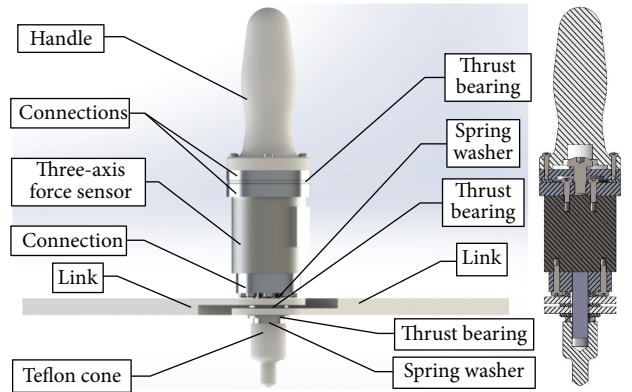


FIGURE 3: End-effector components.

The parallel mechanism was actuated by two Maxon RE50 DC motors with shaft keys, and connectors concatenated the linear rails and motors by screws and shaft keys, respectively. The motors were fixed on the platform and in serial with angle encoders, and the nominal voltage, maximum torque, and torque constant of the motor were 36 V, 418 mNm, and 60.4 mNm/A, respectively. The Maxon gearboxes EP52C, whose gear ratios were 43 : 1, modulated the motor outputs. The motors were actuated by Maxon EPOS2 70/10, and control programs were coded in LabVIEW (NI, USA).

In the patient-active training, an assisted-as-needed strategy was introduced by employing impedance control. To improve the control precision of manipulator impedance, a three-dimensional force sensor was mounted on the end-effector, which could additionally record the interactive force between patients and the robot for quantitative assessments. The sensor signals were collected by Arduino board (Mega 2560) and subsequently transmitted to PC through USB serial communication. The end-effector components are shown in Figure 3. Since the angle between the upper-limb and the links changed with movements when patients hold the handle, the handle had one independently rotational degree of freedom (DoF) with respect to the links, and the revolute friction was reduced by thrust bearings. The cone below the end-effector was used to indicate movement positions, and Teflon was adopted to reduce the friction with screen. In addition, the revolute joint of two links was constituted by an axis, and friction was also reduced by thrust bearings.

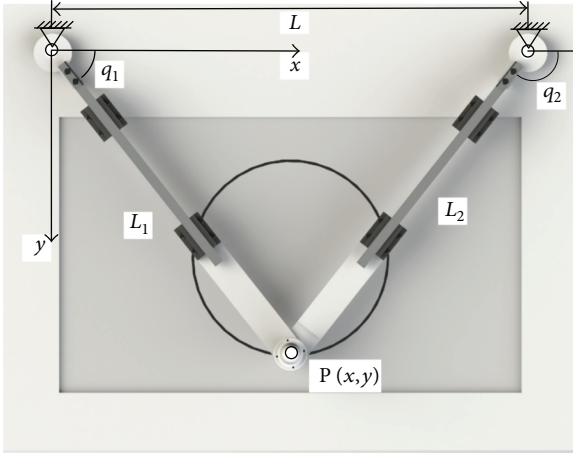


FIGURE 4: Kinematic diagram of PARM.

### 3. Kinematic and Dynamic Modeling

**3.1. Kinematics of PARM.** PARM has two DoF actuated by two servo motors, and the kinematic diagram is shown in Figure 4. The end-effector position  $P(x, y)$  was determined by the joints  $Q(q_1, q_2)$ , which is given by

$$\begin{aligned} x &= \frac{L \tan q_2}{\tan q_2 - \tan q_1}, \\ y &= \frac{L \tan q_1 \tan q_2}{\tan q_2 - \tan q_1}, \end{aligned} \quad (1)$$

where  $L$  means the distance between two joints.

Patient-passive control is based on the inverse kinematics of the robot arm. For continuous predefined trajectories  $g(x, y, t)$ , controlled joints  $Q$  is calculated as

$$\begin{aligned} q_1 &= \tan^{-1} \frac{y}{x}, \\ q_2 &= \pi - \arctan \frac{y}{L-x}. \end{aligned} \quad (2)$$

The calculated joint angles are implemented with position control of servo motors.

Deriving (1), Jacobian matrix  $J_p$  denotes the relationship between the end-effector and joint velocity, which is given by

$$\begin{bmatrix} \dot{x} \\ \dot{y} \end{bmatrix} = J_p \begin{bmatrix} \dot{q}_1 \\ \dot{q}_2 \end{bmatrix}. \quad (3)$$

Besides, link lengths  $L_1$  and  $L_2$  were adjusted automatically to the joint angles  $q_1$  and  $q_2$  as

$$\begin{aligned} L_1 &= \frac{L \sin q_2}{\sin q_2 - \sin q_1}, \\ L_2 &= \frac{L \sin q_1}{\sin q_2 - \sin q_1}. \end{aligned} \quad (4)$$

Similarly, the relation between the elongation velocity of the two links  $\dot{L}(\dot{L}_1, \dot{L}_2)$  and the joint angular velocity  $\dot{Q}(\dot{q}_1, \dot{q}_2)$  is expressed by Jacobian matrix  $J_L$  as

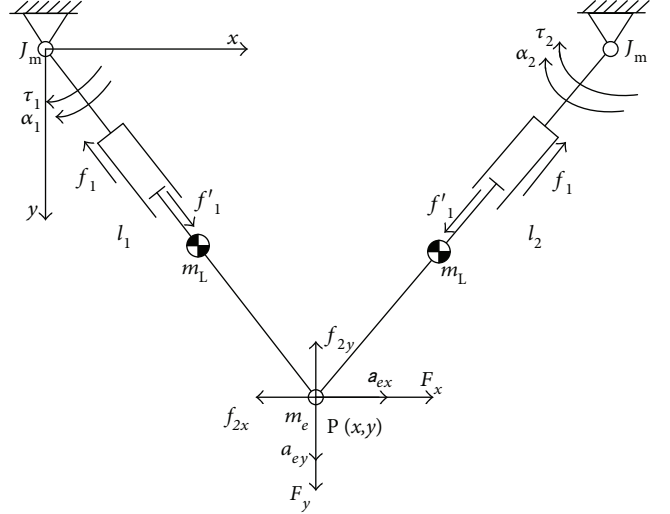


FIGURE 5: Robotic dynamics of the mechanism. In this diagram,  $\tau_1$  and  $\tau_2$  denote the motor torques;  $f_1$  and  $f'_1$  are the friction in the prismatic joint;  $f_{2x}$  and  $f_{2y}$  denote the friction between the end-effector and platform;  $F_x$  and  $F_y$  denote the interactive force between patients and the robot;  $m_L$ ,  $m_e$ , and  $J_m$  denote the inertia of the link, end-effector, and the moment of inertia of the motor shaft, respectively;  $\alpha$  and  $a$  represent the acceleration of the joints and end-effector, respectively.

$$\begin{bmatrix} \dot{L}_1 \\ \dot{L}_2 \end{bmatrix} = J_L \begin{bmatrix} \dot{q}_1 \\ \dot{q}_2 \end{bmatrix}. \quad (5)$$

**3.2. Dynamic Modeling of PARM.** For dexterous and accurate control of a manipulator, inertia and friction should be considered. In this study, it is hypothesized that three components constituted the motor torques. Namely, the first component counteracted friction; another component compensated the inertia of the end-effector, links, and motor-gear system; the last component generated the manipulator impedance and achieved the flexibility. The dynamic diagrams of the mechanism and motor-gear system are shown in Figures 5 and 6, respectively, where the arrows indicate the positive references.

**3.2.1. Friction Component.** In this study, the principle of virtual work was utilized to deduce the equilibrium relations. Specifically,  $\Delta Q(\delta q_1, \delta q_2)$  and  $\Delta P(\delta x, \delta y)$  were virtual displacement of the motor joints and end-effector, respectively, and  $\Delta L(\delta L_1, \delta L_2)$  was the corresponding virtual change of link length. In the patient-active training, the end-effector was mechanical impedance, and conversely, the human arm was regarded as mechanical admittance [29]. Thus, the equation can be written as

$$F \Delta P^T + \tau_f^T \Delta Q^T = f_1 \text{sign}(\Delta L) \Delta L^T - F_2 \Delta P^T, \quad (6)$$

where  $\tau_f$  denotes the joint torques counteracting friction and external force;  $F(F_x, F_y)$  is the external force acting on the end-effector;  $f_1$  represents the friction in the prismatic joint;  $F_2(f_{2x}, f_{2y})$  means the friction between the end-effector and

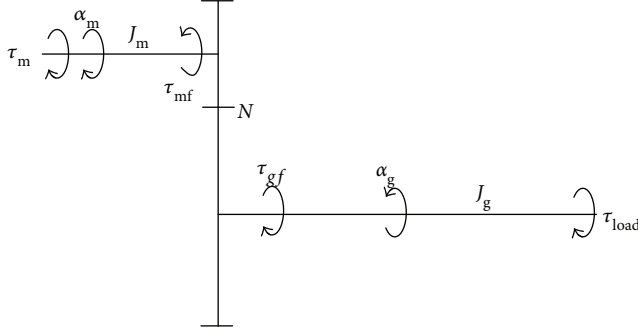


FIGURE 6: Dynamics of the motor-gear system.  $J_m$  and  $J_g$  denote the moments of inertia of the motor and gear shafts, respectively;  $\tau_{mf}$ ,  $\tau_{gf}$  and  $\alpha_m$ ,  $\alpha_g$  are the friction torques and angular accelerations of the two shafts, respectively;  $\tau_m$  and  $\tau_{load}$  represent the motor and load torques, respectively;  $N$  is the gear ratio.

platform, and  $f_2 = \|F_s\|$ . Based on (3) and (5), (6) can be deduced as

$$\begin{aligned} F \mathbf{J}_p \Delta Q^T + \tau_f^T \Delta Q^T &= f_1 \text{sign}(\mathbf{J}_L \Delta Q^T)^T \mathbf{J}_L \Delta Q^T \\ &+ f_2 \frac{(\mathbf{J}_p \Delta Q^T)^T}{\|\mathbf{J}_p \Delta Q^T\|} \mathbf{J}_p \Delta Q^T. \end{aligned} \quad (7)$$

To calculate the component of the joint torques which only counteracted the friction, the external force should be excluded. Eliminating the term  $\Delta Q^T$ , (7) can be written as

$$\tau_f = f_1 \mathbf{J}_L^T \mathbf{S}_1 + f_2 \mathbf{J}_p^T \mathbf{S}_2, \quad (8)$$

where the joint-parameter matrixes  $\mathbf{S}_1 = \text{sign}(\mathbf{J}_L \dot{Q}^T)$  and  $\mathbf{S}_2 = \mathbf{J}_p \dot{Q}^T / \|\mathbf{J}_p \dot{Q}^T\|$ .

According to the motor-gear system shown in Figure 6, motor torque  $\tau_1$  counteracting the friction is derived as

$$\tau_1 = \frac{1}{N} (\tau_f + \text{diag}(\text{sign } \dot{Q}) \tau_{gf}) + \text{diag}(\text{sign } \dot{Q}) \tau_{mf}, \quad (9)$$

where  $\tau_{mf}$  and  $\tau_{gf}$  denote the friction torques of motor and gear shafts, respectively, and  $N$  is the gear ratio.

**3.2.2. Inertia Component.** The joint torque  $\tau_a$  was assumed to compensate the inertia force generated by joint angular acceleration  $\ddot{Q}(\ddot{q}_1, \ddot{q}_2)$  and end-effector acceleration  $\ddot{P}(\ddot{x}, \ddot{y})$ , which can be calculated as

$$\tau_a = \text{diag}(J_L, J_R) \ddot{Q}^T + m_e \mathbf{J}_p^T \ddot{P}^T, \quad (10)$$

where  $m_e$  denotes the mass of the end-effector, and  $J_L$  and  $J_R$  are the moments of inertia of left and right links, respectively.

The end-effector acceleration could be obtained by the derivative of (3), which is given by

$$\ddot{P}^T = \dot{\mathbf{J}}_p \dot{Q}^T + \mathbf{J}_p \ddot{Q}^T. \quad (11)$$

In summary, the motor torque  $\tau_2$  counteracting the inertia force could be calculated as

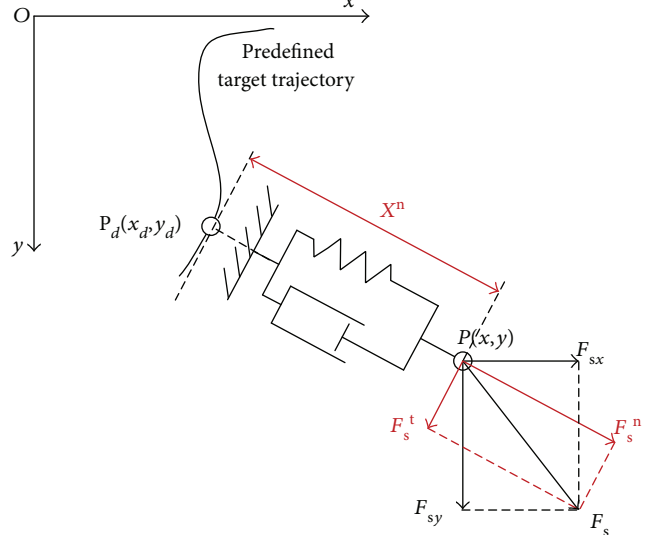


FIGURE 7: Diagram of the strategy based on the orthogonal deviation.

$$\tau_2 = \frac{1}{N} \tau_a + \left( J_m + \frac{1}{N^2} J_g \right) \ddot{Q}^T, \quad (12)$$

where  $J_m$  and  $J_g$  are the moments of inertia of the motor and gear shafts, respectively.

#### 4. Impedance Control for Assist-as-Needed Training

In impedance control, the end-effector behaves as a damped spring-mass system, which is represented in a single DoF system as

$$F_{\text{ext}} = M \ddot{x} + C \dot{x} + K(x - x_d), \quad (13)$$

where  $F_{\text{ext}}$  denotes the external force; parameters  $M$ ,  $C$ , and  $K$  are the dynamic parameters of the end-effector corresponding to mass, damping, and spring, respectively;  $x_d$  represents the desired equilibrium position, while  $x$  denotes the actual end-effector position.

In robot-aided training, the predefined target trajectory  $g(x, y)$  meant the movement that patients were expected to track, which was, however, supposed to be different with the actual trajectory due to movement error. Actual trajectories were obtained by joint sensors and forward kinematics. Assume  $P_d(x_d, y_d)$  denoted the desired position on the predefined target trajectory, when  $P(x, y)$  was the actual end-effector position. Since the reference position  $P_d$  determined the direction and magnitude of the impedance force, it was significant to search the appropriate reference position. In assist-as-needed training, patients determined the manipulator in terms of position, velocity, and acceleration; thus, the reference positions were variable with movements and associated with the real-time deviations. In this study, the strategy based on the orthogonal deviation was proposed to define the desired equilibrium positions for arbitrary predefined trajectories. As illustrated in Figure 7, the curve represents the

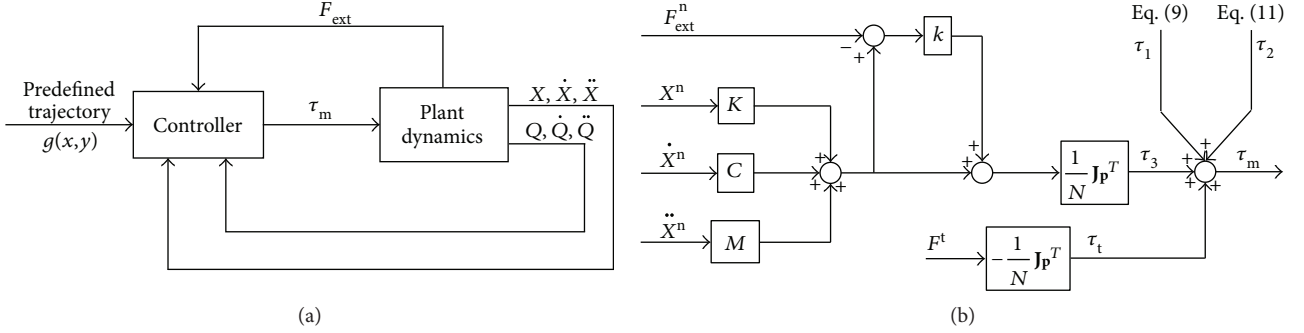


FIGURE 8: Control schemes of impedance and propulsion/resistance control. (a) Overview. (b) Controller diagram.  $X^n, \dot{X}^n, \ddot{X}^n$ , and  $F_{\text{ext}}^n$  are calculated by the strategy based on orthogonal deviation (Figure 7), and  $F^t$  denotes propulsion/resistance force.

predefined target trajectory, and force  $F_{sx}$  and  $F_{sy}$  are the interactive force detected by the three-axis force sensor in  $x$  and  $y$  directions, respectively. In this strategy, the direction of the actual position relative to the reference point was orthogonal to the tangent of the predefined trajectory at the equilibrium position, which indicated that the reference position  $P_d$  was the point on the predefined trajectory closest to the current position  $P$ . Therefore, the tangent component of the external force with respect to the equilibrium point provided the propulsive force  $F_s^t$  along the trajectory, while the normal component force  $F_s^n$  was supposed to be the impedance force ( $F_{\text{ext}}$ ) shown in (13), and  $X^n$  denotes the deviation input to the impedance control.

The dynamic modeling was used to calculate the motor torques to generate the required impedance according to deviations and impedance parameters. However, even though the dynamic modeling incorporated friction and inertia, control errors inevitably occurred in experiments; thus, the force sensor was utilized to obtain actual interactive force as feedback to reduce the errors. Since the acceleration and friction components have been discussed in Section 3, let  $\tau_3$  be the motor torque-generating manipulator impedance, which is given by

$$\tau_3 = \frac{1}{N} \mathbf{J}_p^T [M(1+k)\ddot{X}^n + C(1+k)\dot{X}^n + K(1+k)X^n - kF_s^n], \quad (14)$$

where  $k$  denotes the error feedback coefficient.

As the tangent force illustrated in Figure 7, for propulsion/resistance control, motor torque  $\tau_t$  is implemented as

$$\tau_t = -\frac{1}{N} \mathbf{J}_p^T F^t, \quad (15)$$

where  $F^t$  denotes corresponding assistive/resistive tangent force along the predefined trajectory.

Summarizing (9), (12), (14), and (15), as the control scheme shown in Figure 8, the motor torque for impedance control is calculated as

$$\tau_m = \tau_1 + \tau_2 + \tau_3 + \tau_t. \quad (16)$$

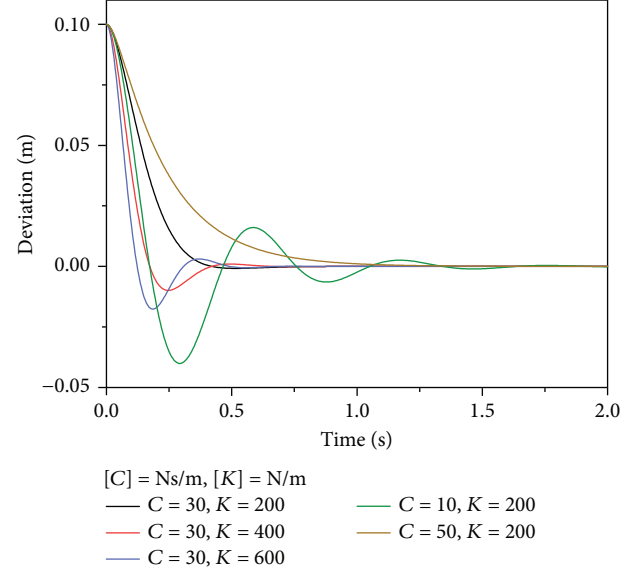


FIGURE 9: Manipulator responses with different impedance parameters.

## 5. Simulations and Experiments

**5.1. Impedance Parameter Determination.** Impedance parameters  $M$ ,  $C$ , and  $K$ , which determined the dynamic behavior of the manipulator, were optimized by simulations. Specifically, it was supposed that the end-effector was released from the initial coordinates  $P_0(0.5,0.4)$  m, while the equilibrium position was  $P_d(0.4,0.4)$  m.  $M$  was set to 0.8 kg, which was the approximately actual mass of the end-effector, whereas the damping and stiffness coefficients  $C$  and  $K$  ranged from 10 to 50 Ns/m and 200 to 600 N/m, respectively. The dynamic responses of the manipulator in the absence of external interaction are shown in Figure 9. The result showed that the oscillation deteriorated with larger  $K$  and smaller  $C$  and the response time and overshoot were the least when  $K = 200$  N/m and  $C = 30$  Ns/m. Therefore,  $K$  and  $C$  were set to 200 N/m and 30 Ns/m for experiments, respectively.

**5.2. Comparison between Experimental and Desired Responses.** To validate the dynamic modeling and impedance control, an experiment of the deviation-regression response,

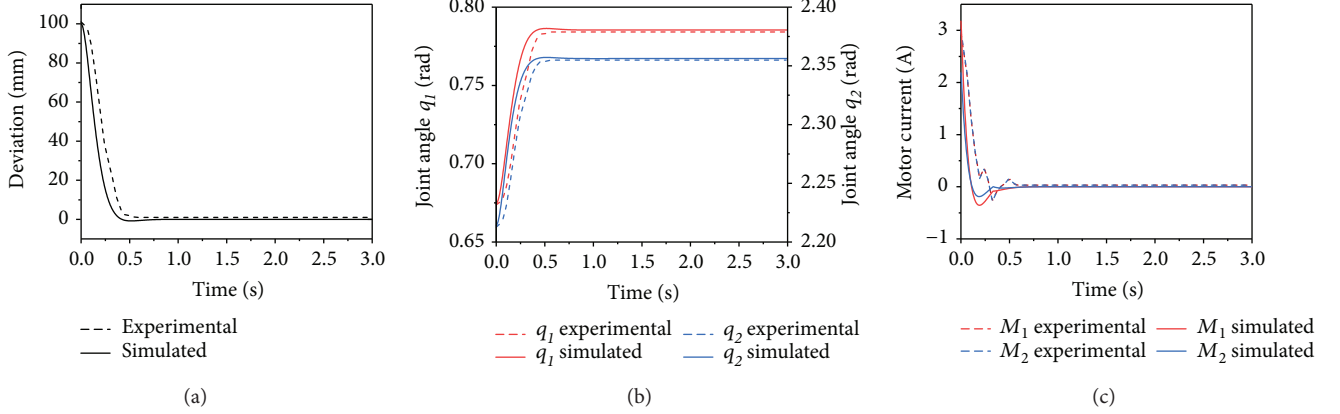


FIGURE 10: Experimental and desired results during the response from the deviated position to the equilibrium position with impedance control. (a) End-effector response. (b) Joint response. (c) Motor current response.

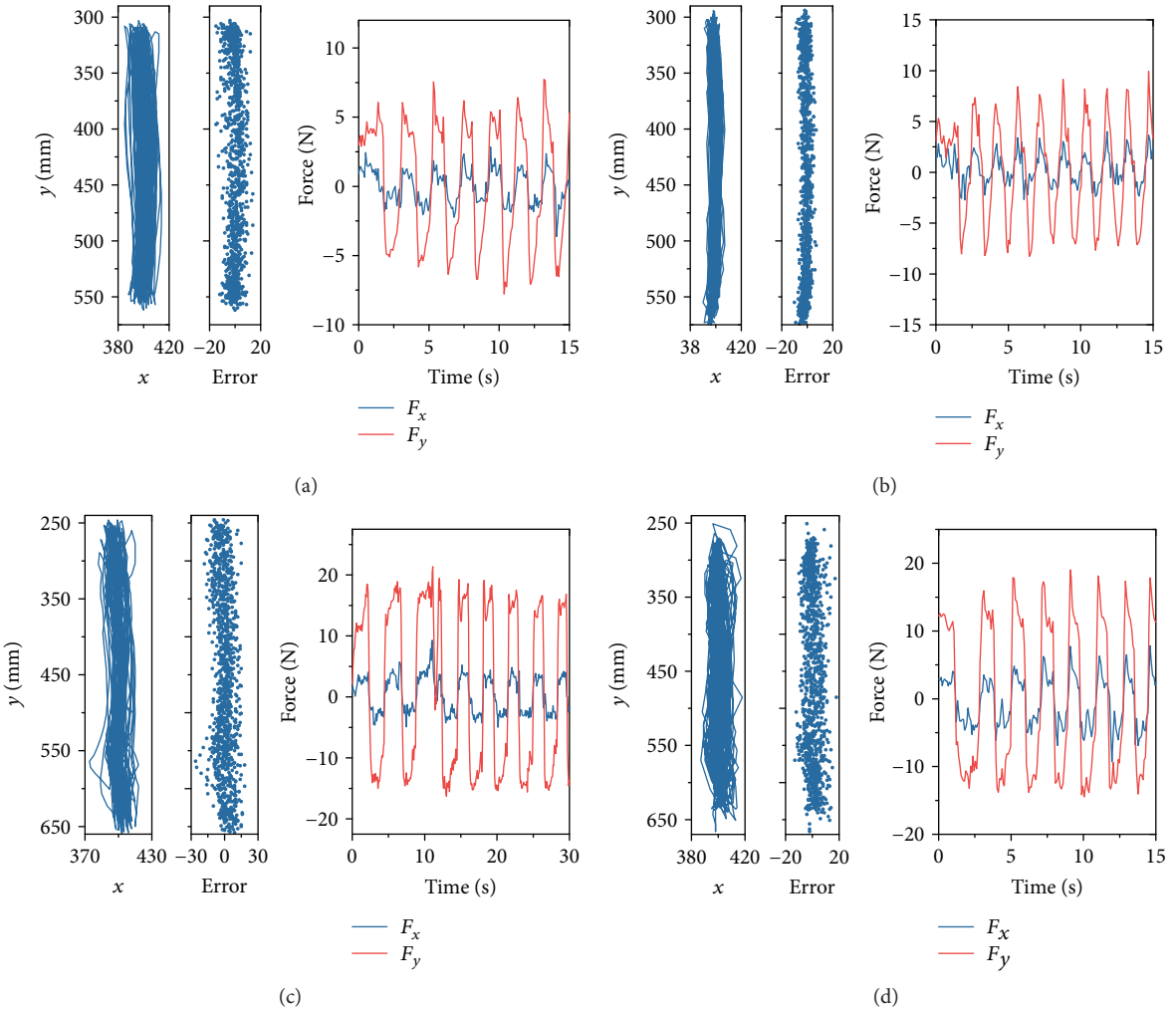


FIGURE 11: Trajectories, errors, and interactive force of the rectilinear movements (a) without impedance or resistance, (b) with impedance only, (c) with resistance only, and (d) with impedance and resistance simultaneously.  $x$  and error are measured by mm.

which was the same as the simulation introduced in Section 5.1, was conducted. The comparisons between the experimental and desired results indicated by simulations are shown in Figure 10. As shown in Figures 10(a) and 10(b),

the experimental responses of the end-effector and joints are approximately the same as the desired response, and the steady-state errors are approximately zero, indicating the accuracy and validity of the dynamic modeling and

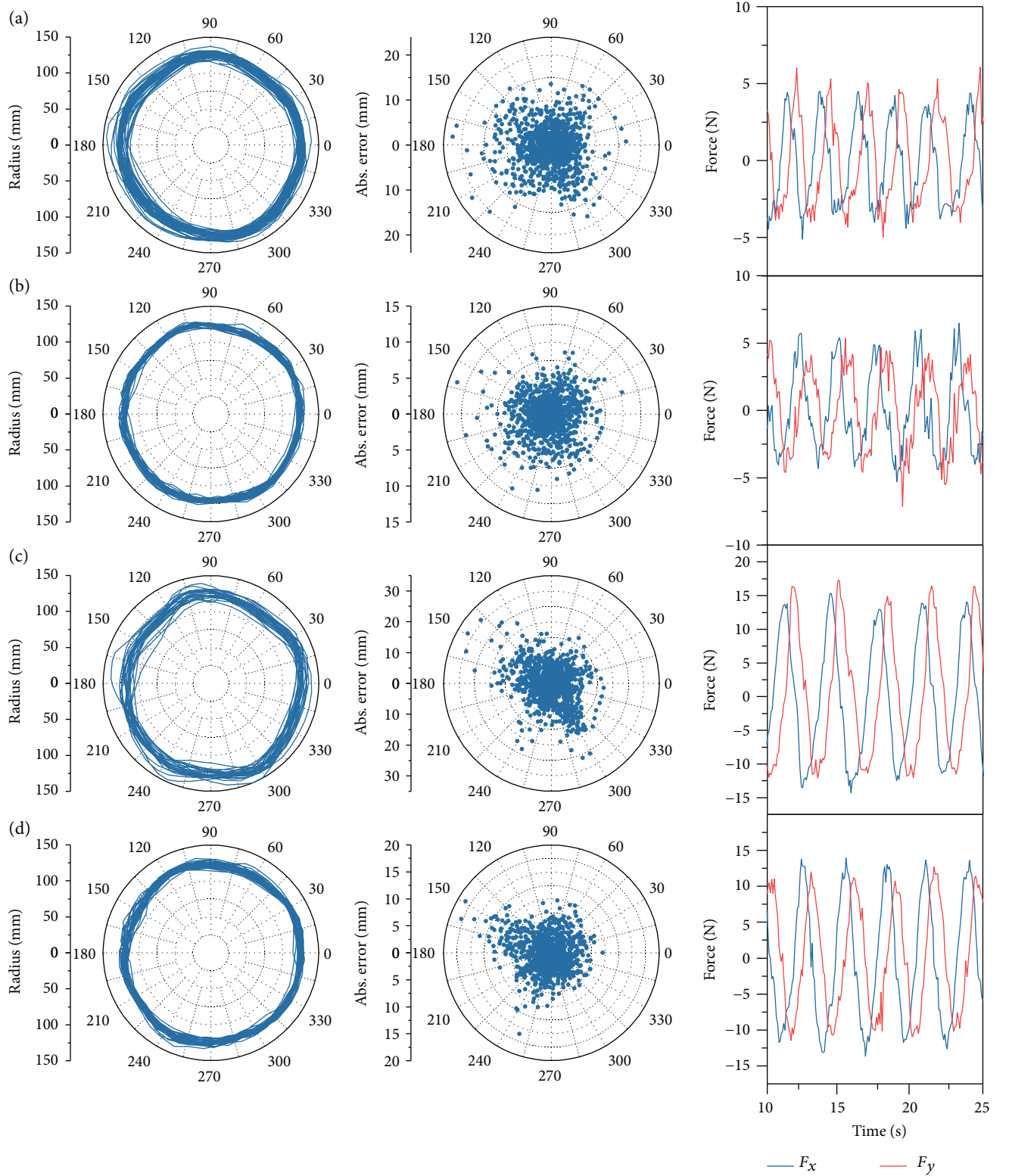


FIGURE 12: Trajectories, errors, and interactive force of the circular movements (a) without impedance or resistance, (b) with impedance only, (c) with resistance only, and (d) with impedance and resistance simultaneously.

impedance control. Figure 10(c) shows the simulated and experimental motor currents, where  $M_1$  and  $M_2$  denote the motor currents of motors 1 and 2, which actuate the  $q_1$  and

$q_2$ , respectively. Consistent with Figures 10(a) and 10(b), the current responses also demonstrate the consistency between the actual dynamic performance and the modeling.

**5.3. Movement Experiments.** In order to discuss how impedance interacted with participants and the error pattern during movements, movement experiments were performed. A healthy male subject, who was 23 years old and left-handed, participated the experiments. The subject performed the movements of two representative types, that is, rectilinear repetitions and clockwise circular repetitions. Furthermore, each moment was performed under four conditions, that is, without impedance or resistance, with impedance only, with resistance only, and with impedance and resistance simultaneously. The resistance force was set to 8 N, which was implemented with (15), and the reference line in rectilinear repetition was set as  $x_d = 400$  mm, while the radius of circular movements was 125 mm with respect to the center at  $P_c(400, 425)$  mm. Since the movement speed could affect the accuracy, the repetition frequencies of rectilinear and circular movements were set to 0.5 Hz and 0.35 Hz, respectively. Each experiment lasted 100 seconds, and the interval time between two experiments was 1 hour to eliminate experimental interactions. The experimental protocol was approved by the Ethics Committee of Tsinghua University, Beijing, China.

The trajectories, errors, and interactive force of rectilinear and circular movements are represented in Figures 11 and 12, respectively. The repetitions in rectilinear movements were indicated by the alternation of  $F_y$  (Figure 11), while the force alternations in  $x$  and  $y$  directions both suggested the repetitions of circular movements (Figure 12). In circular movements, the signals of  $F_x$  and  $F_y$  were both sinusoidal with time, and the phase of  $F_y$  lagged behind that of  $F_x$  by  $\pi/2$ . The maximal  $F_y$  in rectilinear movements and the maximal  $F_x$  and  $F_y$  in circular moments with resistance were larger than those without resistance by 8 N in average, which also validated the force control. Additionally, the results indicated that fewer errors were observed in the presence of impedance, whereas the performance deteriorated in the presence of resistance.

To assess the movement accuracy, the mean absolute error (MAE) and standard deviation (SD) were employed to evaluate the deviation of the movements. The brackets indicated the nonsignificant differences ( $p > 0.05$ ), while the significances at  $p < 0.001$  were observed between other groups (Figure 13). The results showed that the rectilinear movement with impedance only had minimal MAE and SD. Specifically, the impedance could significantly decrease the MAEs, whereas the MAEs were significantly increased in the presence of resistance, for both rectilinear and circular movements. Significant differences were also noted between the two groups under the same condition. In addition, the results suggested that the SDs were larger in the absence of impedance and in the presence of resistance, demonstrating that the impedance and resistance mediated the movements by affecting the MAE and SD simultaneously.

Since the impedance control could reduce the deviations significantly, it was essential to discuss the functional mechanism of the impedance for motor control, which incorporated two sides: theoretical and practical aspects. Theoretically, according to the impedance control proposed

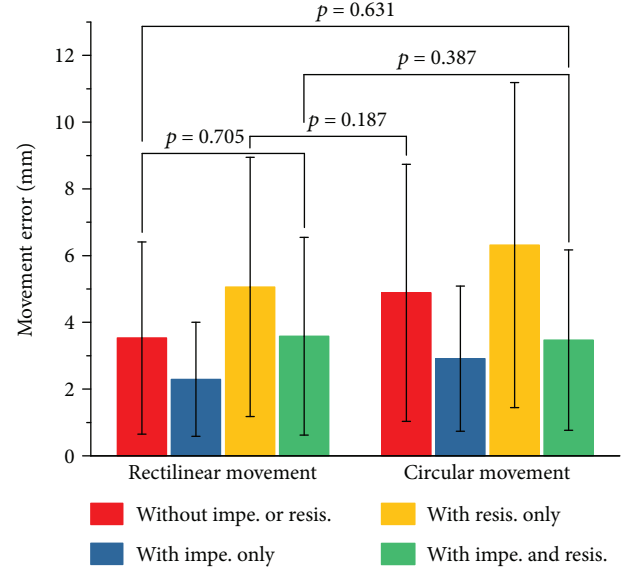


FIGURE 13: Statistics of absolute errors, where the brackets indicate nonsignificant differences ( $p > 0.05$ ), and the significances at  $p < 0.001$  are observed between other groups.

by Hogan [29], the main function of the impedance is to determine the interactive force given a deviation, in which case the manipulator is an impedance whereas the environment is an admittance. The generated impedance force is opposite to the deviation from the desired trajectory, which pulls the patient arm towards the desired trajectory as a “virtual damped spring” and alleviates movement deviations as compensative assistance. On the other hand, to interpret the functional mechanism of the impedance in practice, it is imperative to elucidate how the impedance interacts with participants, which is directly reflected by the error patterns in these movements. The kinematic analysis is shown in Figure 14, which indicates the statistic error patterns with respect to the positions. For rectilinear repetitions in  $y$  direction, the mean errors with respect to  $y$  positions presented the “arched deviations” within 300 to 550 mm, which reached the maximum at 425 mm (Figure 14(a)). The “arched effect” probably attributed to the inadequate synergy between the shoulder and elbow joints. Particularly, the contribution of the elbow joint motion was more than that of the shoulder joint; thus, the movements tended to present arc trajectories with respect to the elbow joint. As presented in Figure 14(a), the “arched effect” could be alleviated by impedance control. In circular repetitions, the maximal deviation occurred at polar angles of approximately 140 and 300 degrees (Figure 14(b)), which were close to the occasions when the elbow angles reached the maximum and minimum, respectively. Motor performance tended to decrease when close to the joint boundary, and the inadequacy of the elbow angles was supposed to be compensated by shoulder abduction and adduction, which might lead to movement errors but could be alleviated by impedance control. In summary, impedance environment was capable of alleviating movement deviations by compensating the synergistic inadequacy between shoulder and elbow joints, particularly when the

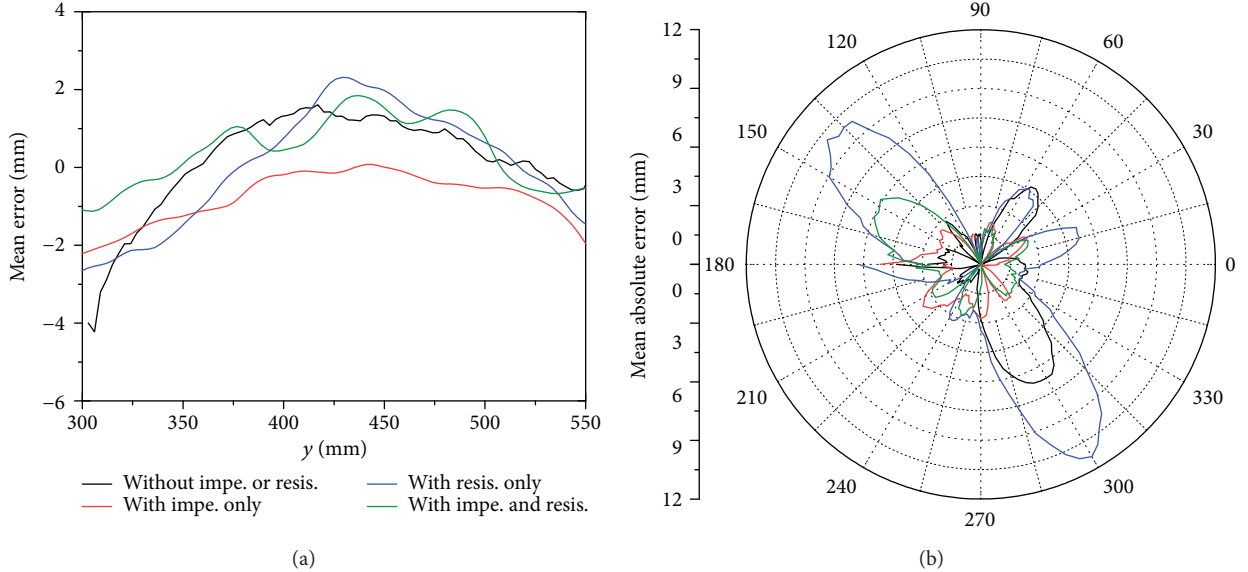


FIGURE 14: Statistic error patterns of the rectilinear and circular movements. (a) Mean errors with respect to  $y$ -position of rectilinear movements. (b) Mean absolute errors with respect to the polar angles of circular movements.

movements were close to the joint boundary. Although the efficiency of impedance control regarding dynamic modeling and movement performance was demonstrated by experiments, nevertheless, the physical interaction between robot and human and the contribution to rehabilitation process still required further experiments performed on stroke patients.

## 6. Conclusions

This paper presented the design, dynamics, impedance control, and experiments of PARM: a parallel rehabilitation robot using impedance control to enhance interactive training. The parallel mechanism was introduced to reduce the inertia and improve the stiffness, capability, and precision. The motion perception and interaction could be improved by embedding an isometric screen. Apart from the mechanical design, the principle of virtual work and derivative of Jacobian matrix were incorporated to eliminate the frictional and inertial influence. Besides, the strategy based on orthogonal deviation was proposed to achieve the impedance control in assist-as-needed training. Comparisons between desired and experimental responses validated the dynamic modeling and impedance control. To investigate the influence of impedance for movements, movement experiments were also performed. The results showed that the errors of circular movements were mostly larger than those of rectilinear movements and demonstrated the significant differences between movements with/without impedance and resistance ( $p < 0.001$ ), where the lowest and highest MAEs were noted in the presence of impedance and resistance, respectively. Furthermore, the “arched effect” was observed in rectilinear repetitions, and the deviation tended to occur when the motion was close to the joint boundary, but the impedance environment was capable of alleviating movement deviations by compensating the synergistic inadequacy between

the shoulder and elbow joints. For the prospect of robot-assisted therapy, PARM could provide a reference for human-robot interaction in aspects of mechanical design, dynamic modeling, and assist-as-needed control.

## Conflicts of Interest

The authors declare that they have no competing financial interest.

## Acknowledgments

This research is supported by the National Natural Science Foundation of China (no. U1613207).

## References

- [1] A. G. Thrift, T. Thayabaranathan, G. Howard et al., “Global stroke statistics,” *International Journal of Stroke*, vol. 12, no. 1, pp. 13–32, 2017.
- [2] D. Mozaffarian, E. J. Benjamin, A. S. Go et al., “Executive summary: heart disease and stroke statistics-2016 update: a report from the American Heart Association,” *Circulation*, vol. 133, no. 4, pp. 447–454, 2016.
- [3] L. H. Thomas, B. French, J. Coupe et al., “Repetitive task training for improving functional ability after stroke,” *Stroke*, vol. 48, no. 4, pp. e102–e103, 2017.
- [4] H. S. Lo and S. Q. Xie, “Exoskeleton robots for upper-limb rehabilitation: state of the art and future prospects,” *Medical Engineering & Physics*, vol. 34, no. 3, pp. 261–268, 2012.
- [5] M. E. Aktan and E. Akdoğan, “Design and control of a diagnosis and treatment aimed robotic platform for wrist and forearm rehabilitation: DIAGNOBOT,” *Advances in Mechanical Engineering*, vol. 10, no. 1, pp. 1–10, 2018.
- [6] M. Zhang, S. Q. Xie, X. Li et al., “Adaptive patient-cooperative control of a compliant ankle rehabilitation robot (CARR) with

- enhanced training safety,” *IEEE Transactions on Industrial Electronics*, vol. 65, no. 2, pp. 1398–1407, 2018.
- [7] H. I. Krebs, M. Ferraro, S. P. Buerger et al., “Rehabilitation robotics: pilot trial of a spatial extension for MIT-Manus,” *Journal of Neuroengineering and Rehabilitation*, vol. 1, no. 1, p. 5, 2004.
  - [8] P. S. Lum, C. G. Burgar, M. V. der Loos, P. C. Shor, M. Majmundar, and R. Yap, “MIME robotic device for upper-limb neurorehabilitation in subacute stroke subjects: a follow-up study,” *Journal of Rehabilitation Research and Development*, vol. 43, no. 5, pp. 631–642, 2006.
  - [9] R. Loureiro, F. Amirabdollahian, M. Topping, B. Driessens, and W. Harwin, “Upper limb robot mediated stroke therapy—GENTLE/s approach,” *Autonomous Robots*, vol. 15, no. 1, pp. 35–51, 2003.
  - [10] J. C. Perry, J. Rosen, and S. Burns, “Upper-limb powered exoskeleton design,” *IEEE/ASME Transactions on Mechatronics*, vol. 12, no. 4, pp. 408–417, 2007.
  - [11] S. Balasubramanian, R. Wei, M. Perez et al., “RUPERT: an exoskeleton robot for assisting rehabilitation of arm functions,” in *2008 Virtual Rehabilitation*, pp. 163–167, Vancouver, BC, Canada, August 2008.
  - [12] J. Hunt, H. Lee, and P. Artermiadis, “A novel shoulder exoskeleton robot using parallel actuation and a passive slip interface,” *Journal of Mechanisms and Robotics*, vol. 9, no. 1, article 011002, 2017.
  - [13] T. Nef, M. Guidali, and R. Riener, “ARMin III-arm therapy exoskeleton with an ergonomic shoulder actuation,” *Applied Bionics and Biomechanics*, vol. 6, no. 2, 142 pages, 2009.
  - [14] W. H. Chang and Y. H. Kim, “Robot-assisted therapy in stroke rehabilitation,” *Journal of Stroke*, vol. 15, no. 3, pp. 174–181, 2013.
  - [15] M. H. Milot, S. J. Spencer, V. Chan et al., “A crossover pilot study evaluating the functional outcomes of two different types of robotic movement training in chronic stroke survivors using the arm exoskeleton bones,” *Journal of Neuroengineering and Rehabilitation*, vol. 10, no. 1, p. 112, 2013.
  - [16] R. Bertani, C. Melegari, M. C. De Cola, A. Bramanti, P. Bramanti, and R. S. Calabro, “Effects of robot-assisted upper limb rehabilitation in stroke patients: a systematic review with meta-analysis,” *Neurological Sciences*, vol. 38, no. 9, pp. 1561–1569, 2017.
  - [17] J. Mehrholz, A. Hädrich, T. Platz, J. Kugler, and M. Pohl, “Electromechanical and robot-assisted arm training for improving generic activities of daily living, arm function, and arm muscle strength after stroke,” *Cochrane Database of Systematic Reviews*, no. 6, article CD006876, 2012.
  - [18] J. M. Belda-Lois, S. Mena-del Horno, I. Bermejo-Bosch et al., “Rehabilitation of gait after stroke: a review towards a top-down approach,” *Journal of Neuroengineering and Rehabilitation*, vol. 8, no. 1, p. 66, 2011.
  - [19] Z. Qian and Z. Bi, “Recent development of rehabilitation robots,” *Advances in Mechanical Engineering*, vol. 7, no. 2, Article ID 563062, pp. 1–11, 2014.
  - [20] R. A. R. C. Gopura, D. S. V. Bandara, K. Kiguchi, and G. K. I. Mann, “Developments in hardware systems of active upper-limb exoskeleton robots: a review,” *Robotics and Autonomous Systems*, vol. 75, pp. 203–220, 2016.
  - [21] Y. Akiyama, Y. Yamada, and S. Okamoto, “Interaction forces beneath cuffs of physical assistant robots and their motion-based estimation,” *Advanced Robotics*, vol. 29, no. 20, pp. 1315–1329, 2015.
  - [22] M. Luces, J. K. Mills, and B. Benhabib, “A review of redundant parallel kinematic mechanisms,” *Journal of Intelligent & Robotic Systems*, vol. 86, no. 2, pp. 175–198, 2017.
  - [23] X. J. Liu and J. Wang, “A new methodology for optimal kinematic design of parallel mechanisms,” *Mechanism and Machine Theory*, vol. 42, no. 9, pp. 1210–1224, 2007.
  - [24] J. Klein, S. Spencer, J. Allington, J. E. Bobrow, and D. J. Reinckensmeyer, “Optimization of a parallel shoulder mechanism to achieve a high-force, low-mass, robotic-arm exoskeleton,” *IEEE Transactions on Robotics*, vol. 26, no. 4, pp. 710–715, 2010.
  - [25] A. Gupta, M. K. O’Malley, V. Patoglu, and C. Burgar, “Design, control and performance of RiceWrist: a force feedback wrist exoskeleton for rehabilitation and training,” *The International Journal of Robotics Research*, vol. 27, no. 2, pp. 233–251, 2008.
  - [26] J. Li, S. Li, L. Zhang, C. Tao, and R. Ji, “Position solution and kinematic interference analysis of a novel parallel hip-assistive mechanism,” *Mechanism and Machine Theory*, vol. 120, pp. 265–287, 2018.
  - [27] H. Taheri, S. A. Goodwin, J. A. Tigue, J. C. Perry, and E. T. Wolbrecht, “Design and optimization of partner: a parallel actuated robotic trainer for neurorehabilitation,” in *2016 38th Annual International Conference of the IEEE Engineering in Medicine and Biology Society (EMBC)*, pp. 2128–2132, Orlando, FL, USA, August 2016.
  - [28] D. Colombo, S. Serino, C. Tuena et al., “Egocentric and allocentric spatial reference frames in aging: a systematic review,” *Neuroscience & Biobehavioral Reviews*, vol. 80, pp. 605–621, 2017.
  - [29] N. Hogan, “Impedance control: an approach to manipulation: part I—theory,” *Journal of Dynamic Systems, Measurement, and Control*, vol. 107, no. 1, p. 1, 1985.

## Research Article

# Motor Imagery-Based Brain-Computer Interface Coupled to a Robotic Hand Orthosis Aimed for Neurorehabilitation of Stroke Patients

Jessica Cantillo-Negrete<sup>1</sup>, Ruben I. Carino-Escobar,<sup>1</sup> Paul Carrillo-Mora<sup>1</sup>,<sup>2</sup>  
David Elias-Vinas,<sup>3</sup> and Josefina Gutierrez-Martinez<sup>1</sup>

<sup>1</sup>Instituto Nacional de Rehabilitación, Division of Medical Engineering Research, 14389 Mexico City, Mexico

<sup>2</sup>Instituto Nacional de Rehabilitación, Division of Neurosciences, 14389 Mexico City, Mexico

<sup>3</sup>Centro de Investigación y de Estudios Avanzados del IPN, Section of Bioelectronics, 07360 Mexico City, Mexico

Correspondence should be addressed to Jessica Cantillo-Negrete; jessica.cantillo.negrete@gmail.com

Received 17 December 2017; Accepted 13 February 2018; Published 3 April 2018

Academic Editor: Carlo Ferraresi

Copyright © 2018 Jessica Cantillo-Negrete et al. This is an open access article distributed under the Creative Commons Attribution License, which permits unrestricted use, distribution, and reproduction in any medium, provided the original work is properly cited.

Motor imagery-based brain-computer interfaces (BCI) have shown potential for the rehabilitation of stroke patients; however, low performance has restricted their application in clinical environments. Therefore, this work presents the implementation of a BCI system, coupled to a robotic hand orthosis and driven by hand motor imagery of healthy subjects and the paralysed hand of stroke patients. A novel processing stage was designed using a bank of temporal filters, the common spatial pattern algorithm for feature extraction and particle swarm optimisation for feature selection. Offline tests were performed for testing the proposed processing stage, and results were compared with those computed with common spatial patterns. Afterwards, online tests with healthy subjects were performed in which the orthosis was activated by the system. Stroke patients' average performance was  $74.1 \pm 11\%$ . For 4 out of 6 patients, the proposed method showed a statistically significant higher performance than the common spatial pattern method. Healthy subjects' average offline and online performances were of  $76.2 \pm 7.6\%$  and  $70 \pm 6.7$ , respectively. For 3 out of 8 healthy subjects, the proposed method showed a statistically significant higher performance than the common spatial pattern method. System's performance showed that it has a potential to be used for hand rehabilitation of stroke patients.

## 1. Introduction

Stroke is the first cause of disability worldwide [1]. Loss of motor function, known as hemiparesis, is one of the most disabling consequences of stroke, which usually affects both upper and lower limbs from one side of the body. If stroke patients engage in therapy in the first 6 months after the initial symptoms appear, they have a 70% chance of regaining motor function in their affected hand [2, 3].

Assistive technologies such as robotic devices could increase the number of patients that receive therapy within this time. In addition, robotic devices have produced stroke rehabilitation outcomes at least as effective as those achieved with traditional therapies [4]. Brain-computer

interfaces (BCI) are another type of assistive technology; these systems provide an artificial communication channel between the brain and an external device such as a robotic orthosis [5, 6]. BCIs based on motor imagery (MI) of affected limbs have shown great potential as a tool for brain plasticity enhancement [7, 8].

MI is a mental rehearsal of movements of a limb, for example, the hand or foot, without muscle activation [9–11]. MI elicits distinctive patterns in the electrical activity of the sensory-motor cortex, mainly in the frequency bands known as mu (8–13 Hz) and beta (14–30 Hz) [9, 12]. An MI-based BCI system is comprised of four stages; the first one is an electrical signal acquisition module such as electroencephalography (EEG). EEG is a noninvasive

technique, has a good time resolution, and is easy to accept by patients. Preprocessing is the second stage of a BCI system; in this stage, signal artefacts such as eye movements, power line noise, and muscle activity are filtered from EEG recordings [13, 14]. The third stage is encompassed by feature extraction methods which preserve only significant information of the BCI user's intentions. Finally, the fourth stage is the classification phase, in which the extracted features are interpreted as the BCI user's intentions; linear discriminant analysis (LDA) is the most used classification technique reported in BCI publications [15, 16]. One of the most effective feature extraction methods is the common spatial pattern (CSP) algorithm, which computes a set of spatial filters that optimally differentiate two classes of MI. To achieve good classification accuracies using the CSP algorithm, the temporal filtering of the EEG signal must be performed on a specific frequency band. Usually, this band is selected in the mu and beta frequency range. Two other parameters that need to be set up are the time interval from which the features are going to be extracted and the subset of spatial filters involved in the feature extraction process [17].

The performance of CSP can be enhanced by selecting subject-specific parameters. Therefore, modifications to the original CSP method have been proposed to include this aspect. One of such modifications is known as filter bank common spatial patterns (FBCSP); this method performs an automatic frequency band selection for temporal filtering of the EEG [18]. FBCSP algorithm employs a filter bank that decomposes the EEG into different frequency bands. Each frequency band is spatially filtered using the CSP algorithm; afterwards, the extracted features for each band are selected with either the Mutual Information-based Best Individual Feature (MIBIF) or the Mutual Information-based Rough Set Reduction (MIRSR) algorithms. Classification is performed only with the selected features [18, 19]. Although, FBCSP performance was higher than CSP, statistically significant differences were not observed between both methods. A bank of filters and CSP are useful for MI; however; in order to increase classification performance other feature selection algorithms could be implemented. Feature selection is an optimisation problem; therefore, artificial intelligence techniques, such as particle swarm optimisation (PSO), could be applied for finding a solution for it.

PSO was originally proposed by Shi and Eberhart [20] and inspired by the social behaviour of bird flocks while searching for food. PSO performs a search in the space of the problem, with the aid of a population (called swarm) of individuals (called particles). Each particle executes a search based on its current position and velocity in the search space. In each iteration (called generations), the position and velocity of the particles are updated according to their best previous position (local search) and the best position of the swarm (global search). In terms of EEG properties, PSO can be applied to select which combination of extracted EEG features provides higher classification accuracies if used as inputs for a classifier. In each iteration (generation), several combinations of selected EEG features (particles) comprise possible inputs for a classifier. After all combinations have

been used to train the classifier, and afterwards test it, classification accuracies for each combination (or other optimisation metrics) can be used to compare the fitness of each combination of EEG features. With this fitness information obtained for each combination, a new set of EEG feature combinations can be generated (a new generation of particles), which could contain a solution with higher classification accuracy than the ones tested in previous generations. This process is repeated until a stop criterion (like a number of generations or achieving a fitness value) is met. To the authors' knowledge, few reported studies describe the use of PSO as a feature selection algorithm for BCI systems. For example, Wei and Wei propose a frequency band selection using PSO and CSP algorithms; selection is based on the best classification accuracies achieved by the BCI. They evaluated their method using MI information from publicly available dataset IVa from BCI competition III. Classification performances were higher using the frequency bands selected by PSO than the ones computed with a broader frequency band [21]. Atyabi et al. proposed a PSO-based method to reduce the number of electrodes and the number of features used for MI classification. The authors evaluated their method with datasets IVa and IIIa from BCI Competition III [22]. Xu et al. evaluated a PSO-based algorithm for CSP frequency band and time selection using a database comprised of finger MI of 18 healthy subjects. They observed better offline performances with PSO than with a statistical approach for frequency and time band selection [23]. These works show that PSO can increase classification performance of MI while also decreasing the number of employed features; therefore, PSO could be a good feature selection method for BCI.

Recent studies have reported better motor rehabilitation outcomes using MI-based BCIs coupled to robotic assistive devices than the ones achieved with only robotic assistive devices [24, 25]. Some of the advantages of these combined systems are that they are noninvasive, are fully automated, and could increase brain plasticity. Some studies have evaluated the performances of these BCI systems with healthy subjects [6], as well as some proofs of concept [26, 27] and a randomised controlled trial [28] that have demonstrated positive rehabilitation outcomes for stroke patients. Even though BCI systems coupled to robotic assistive devices have shown promising outcomes for stroke rehabilitation, to date, none of such systems are used in clinical practice.

Reasons for this include the fact that most BCI systems are still under development in research centres and universities, are usually assessed offline, and have quite different performances in online tests. In addition, new processing stages designed for stroke rehabilitation BCI systems are not tested with EEG information of these patients. Therefore, tests must be performed to evaluate if an MI-based BCI is capable of classification of user's intentions and activation of external devices in online implementations, with a processing stage previously tested with stroke patients' data.

In this work, an MI-based BCI is implemented and tested; the system is aimed to be driven by hand MI. A novel signal processing stage comprised of a bank of filters, CSP for feature extraction, PSO for feature selection, and LDA for

TABLE 1: Patients' clinical and demographic data.

Patient	Gender	Age	Hemiparesis	Evolution	Injury location
1	Male	50	Right	7 months	Posterior limb of left the internal capsule
2	Female	57	Right	36 months	Left pulvinar nucleus of the thalamus extending to the left internal capsule and ipsilateral lateral ventricle
3	Male	58	Left	2 months	Right basal ganglia with involvement of the posterior limb of ipsilateral internal capsule
4	Female	79	Left	1 month	Posterior limb of the right internal capsule
5	Male	46	Left	3 months	Lenticular nucleus, internal capsule, and right corona radiata
6	Male	45	Left	3 months	Right side of the brainstem

classification was designed. The proposed algorithm was evaluated offline with a sample of stroke patients' and healthy subjects' data and afterwards online tests were performed with the healthy subjects as users of the system. For online tests, MI was used to activate a robotic hand orthosis to evaluate the feasibility of the complete BCI system aimed for neurological rehabilitation of stroke patients.

## 2. Materials and Methods

**2.1. Participants.** The sample for this study comprised 8 healthy subjects (mean =  $23.9 \pm 1.3$  years) and 6 patients diagnosed with stroke (mean =  $55.8 \pm 12$  years). Both healthy subjects and stroke patients were required to have a normal performance in the subscales of digit detection and visual detection of the neuropsychological test NEUROPSI (this test has been validated for Spanish-speaking population) [29]. In addition, all subjects were naïve to BCI, with normal or corrected to normal vision, without any history of other neurological/psychiatric diseases and right-handed (at least 90% according to the Mexican adaptation of the Edinburgh handedness inventory [30]). In order to be considered for inclusion in the study, patients had to have a first stroke event of subcortical localisation, confirmed by a neurologist by means of neuroimaging studies (magnetic resonance or computed tomography) and total or partial paresis of one of their hands. Subcortical stroke patients were selected since their brain damage does not involve the brain cortex and, therefore, they were less likely to present significant cognition impairments. Before the EEG recordings were performed, the participants signed an informed consent approved by the Ethics and Research Committee of the National Institute of Rehabilitation in Mexico. Clinical and demographic data of the patients are shown in Table 1.

**2.2. EEG Acquisition.** A g.USBamp biosignal amplifier from g.tec was used for EEG acquisition. EEG was acquired with 24 bits of resolution and sampling rate of 256 Hz. Active EEG electrodes were used for acquisition, with 11 electrodes placed over the scalp of the participants, in positions C3, C4, Cz, T3, T4, F3, F4, Fz, P3, P4, and Pz of the international 10–20 system. Ground placement was set in the AFz position, and the reference electrode was placed in the right earlobe. To verify that no real movements were elicited during MI, electromyography

(EMG) was recorded from the *flexor digitorum superficialis* and *flexor digitorum profundus* muscles of both forearms. For the offline tests, each healthy subject participated in two sessions and performed in consecutive days with 120 trials recorded in total. To avoid exhaustion, stroke patients participated in four recording sessions which were performed in consecutive days, with 120 trials recorded in total. For the online tests, healthy subjects performed in consecutive days two additional sessions, with another 120 trials recorded in total. Subjects were instructed to sit in a comfortable armchair, with a computer monitor placed at 1.5 m in front of them. They were directed, by visual cues shown in the monitor, to perform either rest with their open eyes or MI from their paralysed hand (dominant hand in case of healthy subjects). EEG acquisition was performed using a similar strategy as the one followed by the Graz paradigm [31]. Figure 1 shows that the rest interval of the trials lasted 3 s and the MI interval lasted 5 s.

**2.3. Offline Implementation and Validation of the Processing Stage.** For offline implementation, a window of one-second length was extracted from 1.5 s to 2.5 s to obtain the rest information for each trial (REST). Another window of one-second length was extracted from the 3.5 to 4.5 s time interval of each trial, to obtain the MI information of the trials, as observed in Figure 1. These time windows were selected based on previous studies which show that differentiation between MI and REST classes is higher in these time intervals [32]. The FBCSP algorithm encompassed the processing stage of the BCI system, and PSO was used for feature selection (named FBCSP + PSO). A block diagram of the algorithm's implementation is shown in Figure 2.

The following is a detailed description of the algorithm's implementation:

- (a) Temporal filtering: EEG data were filtered to obtain 6 frequency subbands, each 4 Hz broad and with 1 Hz of overlapping in order to avoid loss of information. Encompassing both alpha and beta frequency bands were as follows: 8–12 Hz, 12–16 Hz, 16–20 Hz, 20–24 Hz, 24–28 Hz, and 28–32 Hz. A 60 Hz band-stop filter was also applied to the EEG signals. All filters were FIR filters of the 30th order, selected for their linear phase features.

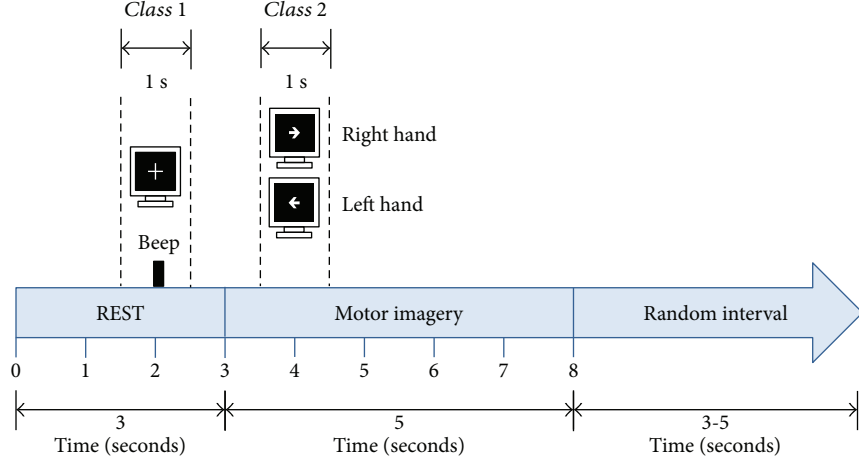


FIGURE 1: Illustration of the experimental paradigm. Dotted lines show the time windows extracted from EEG signals.

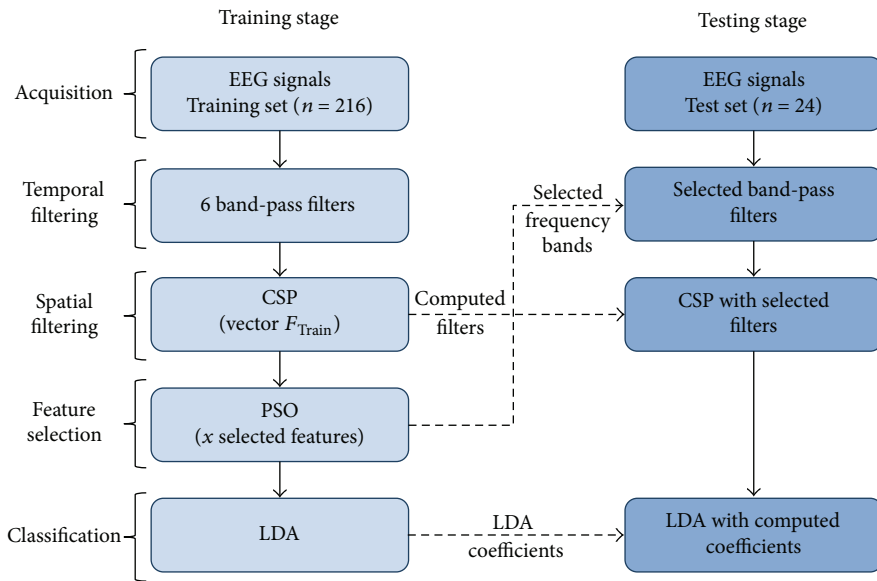


FIGURE 2: Block diagram of FBCSP + PSO implementation.

(b) Spatial filter: For the EEG data filtered in each subband, spatial filters were computed with the CSP algorithm. CSP performs a linear transformation on the EEG data, to obtain features whose variances are optimal for classification of two classes of MI, in a specific frequency band. Details of the CSP implementation can be found in the works of Blankertz et al. [17] and Ramoser et al. [33]. In this work, spatial filters were computed using the MATLAB command  $\mathbf{W} = \text{eig}(\mathbf{S}_1, \mathbf{S}_1 + \mathbf{S}_2)$  as suggested in the abovementioned works.  $\mathbf{W}$  is the matrix containing the spatial filters, and  $\mathbf{S}_1$  and  $\mathbf{S}_2$  are the covariance matrices of MI and REST computed from the EEG data of each filtered frequency subband. In the implementation of the original CSP, only the first and last  $m$  columns of the  $\mathbf{W}$  matrix ( $m$  is generally 2) are used to generate the feature vector used for classification. With the goal of having a greater chance of

finding the optimal subband for each patient, in this work, all possible features were extracted with CSP. The feature vector generated in this work for each trial  $i$  is comprised as follows:

$$\mathbf{f}_i = [f_{1,i}; f_{2,i}; f_{3,i}; f_{4,i}; f_{5,i}; f_{6,i}]. \quad (1)$$

Therefore, CSP features computed for the training set comprised for  $nt$  trials are

$$\mathbf{F}_{\text{Train}} = [f_1; f_2; f_3; f_4; \dots; f_{nt}], \quad \mathbf{F}_{\text{Train}} \in \mathbb{R}^{nt \times 66}. \quad (2)$$

And the true class vector of the training set is

$$\mathbf{y}_{\text{Train}} = [y_1; y_2; y_3; y_4; \dots; y_{nt}]. \quad (3)$$

- (c) Feature selection: PSO was used for selecting a subset of features from  $F_{\text{Train}}$ , in order to decrease both the classification error and the number of selected features. Equation (4) describes PSO implementation.

$$\begin{aligned} v_i^{n+1} &= w \cdot v_i^n + c_1 \cdot r_1 \cdot (\text{PBest}_i^n - x_i^n) \\ &\quad + c_2 \cdot r_2 \cdot (\text{GBest}_g^n - x_i^n), \\ x_i^{n+1} &= x_i^n + v_i^{n+1}, \end{aligned} \quad (4)$$

where  $x_i^n$  and  $v_i^n$  are the position and velocity of the  $i$ th particle of the  $n$ th generation. In this work, 50 particles and 50 generations were used.  $w$  is the inertial weight of PSO which linearly descends from 0 to 1 as generations of PSO are computed.  $c_1$  and  $c_2$  are positive constants set to 1.  $r_1$  and  $r_2$  have random values between 0 and 1, which coupled to  $c_1$  and  $c_2$  set the local and global search properties of PSO.  $\text{PBest}_i^n$  is the best position reached by the  $i$ th particle in the  $n$ th generation.  $\text{GBest}_g^n$  is the best position ( $g$ ) reached by the entire swarm in the  $n$ th generation. The maximum position value that a particle could reach was 1 and the minimum was 0. Maximum speed of each particle was set to 1 and minimum speed to 0. In this work, the search space of PSO was  $1 \times D$ , where  $D$  equals 66 and was comprised of the 66 features that can be selected. Each computed solution with PSO is a subset of the selected features. Solution values are in the range from 0 to 1. If the value of an element of the solution was higher or equal to 0.5, then the corresponding feature was selected. The original CSP algorithm states that selected features must be paired, so in this work, complementary features of the selected ones were also included, in case they were not originally selected by PSO. Selected features from the training set were used for designing an LDA classifier. PSO fitness value was computed using

$$\text{value} = (\text{err} \times 2) + \left( \frac{\text{nselec}}{66} \right), \quad (5)$$

where err is the computed classification error from the training set. nselec is the number of selected features. Variables err and nselec/66 have values ranging from 0 to 1. Both parameters err and nselec are summed so that PSO is able to perform a reduction of both classification error and the number of features used for classification. The err value was multiplied by 2 so that the optimization priority of PSO is the reduction of the classification error over the selection of a lower number of features. The stop criteria used for PSO was either achieving 0% of classification error or 50 generations.

- (d) Classification: With the final selected features ( $x$ ) and the training set, an LDA classifier was designed, which was later evaluated with the testing set. Features selected with PSO in the training stage were

the same as the ones used for the testing stage of the classifiers. LDA performance was measured by computing the percentage of classification accuracy (%CA). In this offline stage, the necessary parameters for the online stage were computed. These parameters were the spatial filters for each frequency subband and the LDA coefficients.

A stratified cross-validation of  $10 \times 10$ -fold was used to avoid bias in the computation of %CA. Classifiers were tested using totally different datasets than the ones used for training. For each fold and repetition, the FBCSP + PSO algorithm was calculated. The 100 values of %CA obtained from this procedure were used to compute the average %CA for each participant.

The performance of the FBCSP + PSO was compared with that of the original CSP (on filtered data between 8 to 32 Hz) using the same training and test subsets. A preliminary version of the proposed algorithm was presented by Cantillo-Negrete et al. [34].

**2.4. Robotic Hand Orthosis.** Since rehabilitation of stroke patients with robotic assistive devices has advantages, a right-hand robotic orthosis was developed in previous works to couple it with the BCI [35, 36]. This orthosis comprised a 3D printed frame of polylactic acid (PLA). The orthosis linear actuators can provide passive flexion and extension movements to the fingers. A closed-loop system was used to sense the moment in which each finger reaches its maximum extension or flexion. The orthosis has a wireless Bluetooth communication with the processing stage of the BCI. The Bluetooth protocol was programmed in both MATLAB® and in a microcontroller attached to the electronic control circuit of the orthosis. The orthosis has four different actuators; however, for this study, all actuators were set to perform flexion and then extension of the hand fingers.

**2.5. Online Implementation of the Designed BCI System.** A graphical user interface (GUI) was programmed using MATLAB, comprised of user's/patient's data, a processing stage, a screen for visual cues presentation, and wireless Bluetooth configuration. Communication was established with the g.USBamp amplifier by means of an adaptor API (available from g.tec). The online processing stage was optimised to process windows of one-second length of the EEG signal. Healthy subjects' spatial filters and LDA coefficients computed for each selected frequency subband in the offline stage were programmed in the online BCI system. The BCI paradigm used for the online implementation was the same as the one used for the offline one, with the addition of the feedback provided by the robotic orthosis. For the online implementation, 6 windows of one-second length each were analysed. The first 3 windows comprised REST and the next 3 windows for MI. As soon as each window had elapsed, data recorded from them were processed in the GUI using the proposed FBCSP + PSO method and the LDA classifier. Afterwards, a classification output was generated which indicated if the time window was classified as REST or as right hand MI. Therefore, for each trial, the system performed 6

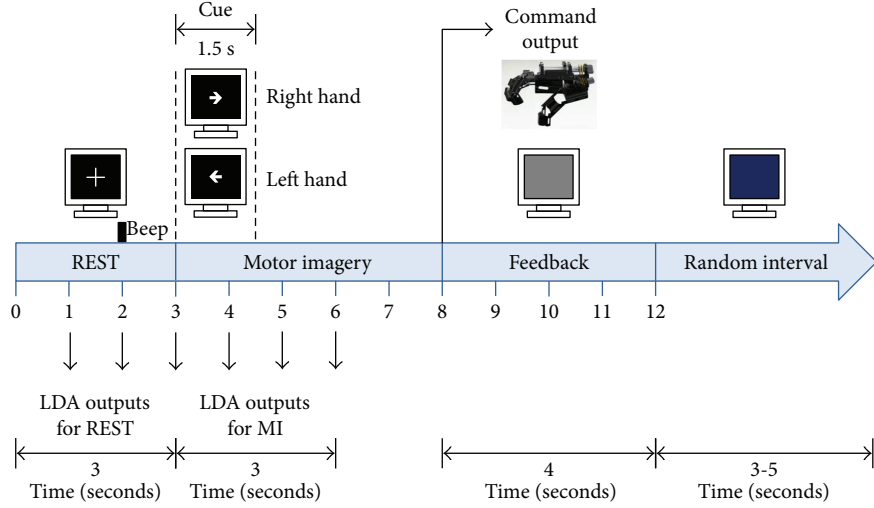


FIGURE 3: Timeline of the online BCI system, depicting a single trial.

classification outputs. A total of 20 trials were recorded for each run, and 3 runs were performed for each session. A total of 2 sessions were performed in consecutive days recording 720 LDA outputs for the REST class and 720 for the MI class. Online %CA was computed per healthy subject by comparing the expected output with the real one.

The robotic hand orthosis was activated by a Bluetooth command sent from the computer, immediately after the MI time interval, only if 2 out of 3 motor imagery time windows were correctly detected by the processing stage. Within the orthosis activation time, the monitor displayed a grey background. The percentage of trials in which the orthosis was activated, regarded as percentage of correct trials (%CT), was computed for all the 120 trials per healthy subject. Activation of the orthosis was comprised of the opening and closing of the healthy subjects' fingers. After each run (20 trials), performance feedback was shown in the computer monitor by using faces with different degrees of smiling expressions. For example, if %CT was in the 100–90 interval, the most smiling face was shown to the subject, and if %CT was below 60%, the most serious face was shown. A depiction of the online processing stage is shown in Figure 3.

Averaged online processing time was computed for all the performed trials. This was the average time required by the preprocessing, FBCSP + PSO, and LDA stages to generate a classification output. A PC with a Core i5 processor of 2.53 GHz and 8 GB of RAM was used for running the GUI with the BCI processing stage. S1 Video shows the complete BCI system in an online test.

**2.6. Statistical Analysis.** In order to assess the reliability of the BCI system, the practical level of chance was computed as explained by Müller-Putz et al. [37]. This practical level of chance is defined as the upper confidence interval of a random classifier's accuracy. Practical level of chance was calculated with a binomial distribution using a significance level of 0.5, with 120 trials encompassing the data of each class.

Equations (5) and (6) show the computation of the practical level of chance.

$$\tilde{p} = \frac{k+2}{n+4}, \quad (6)$$

$$\text{Practical level of chance} = \tilde{p} + \sqrt{\frac{\tilde{p}(1-\tilde{p})}{n+4}} \left(1 - \frac{\alpha}{2}\right), \quad (7)$$

where  $\tilde{p}$  is the probability of correct classification,  $k$  is the expected number of correctly classified trials,  $n$  is the number of trials,  $z_{1-\alpha/2}$  is the  $1 - \alpha/2$  quantile of the standard distribution, and  $\alpha$  is the level of significance. The computed %CAs were compared with the practical level of chance to assess if BCI performance was significantly higher than chance [37].

A Lilliefors-corrected Kolmogorov-Smirnov test ( $\alpha = 0.05$ ) was used to test if stroke patients' and healthy subjects' %CAs for offline tests (obtained from  $10 \times 10$ -fold cross-validation) followed a Gaussian distribution. The tests showed that the offline %CAs computed with FBCSP + PSO, and CSP for both groups did not have a Gaussian distribution. Therefore, nonparametric Mann-Whitney  $U$  tests ( $\alpha = 0.05$ ) were used for comparing the offline %CAs computed with FBCSP + PSO and CSP. A Lilliefors-corrected Kolmogorov-Smirnov test ( $\alpha = 0.05$ ) showed that healthy subjects' offline and online averaged %CAs had a Gaussian distribution. Therefore, a paired  $t$ -test ( $\alpha = 0.05$ ) was used for comparing offline with online %CAs. Pearson's correlation and linear regression analyses were performed for measuring relationships between online %CA and %CT.

### 3. Results

**3.1. Offline Analysis.** Figure 4 shows the offline %CA computed with stroke patients' data with FBCSP + PSO and CSP. Results of the statistical analysis are also shown. The calculated practical level of chance for all experiments was 56.2%. It can be observed that for all patients %CAs were

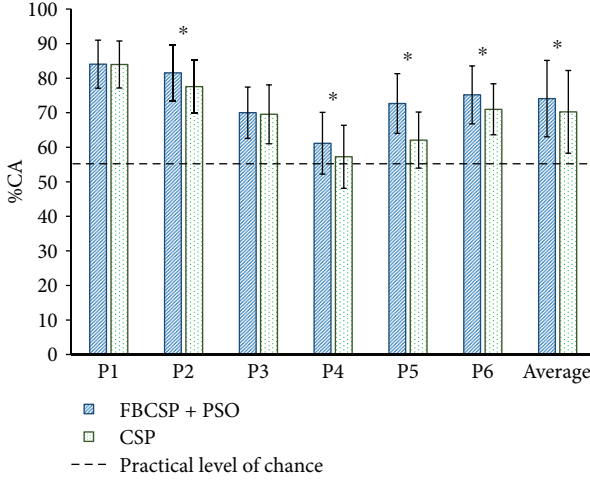


FIGURE 4: Offline classification accuracy percentages (%CAs) computed with data from 6 patients. The dotted line shows the practical level of chance (56.2%). The asterisk (\*) indicates that the %CA of FBCSP + PSO was statistically significantly higher ( $p < 0.05$ ) than CSP.

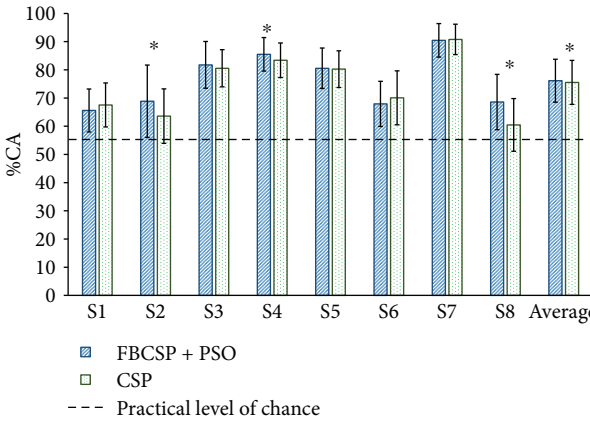


FIGURE 5: Offline classification accuracy percentages (%CAs) computed with data from 8 healthy subjects. The dotted line shows the practical level of chance (56.2%). The asterisk (\*) indicates that the %CA of FBCSP + PSO was statistically significantly higher ( $p < 0.05$ ) than CSP.

above the practical level of chance ( $p < 0.05$ ) for both methods. For 4 out of 6 patient's data, %CA for the FBCSP + PSO algorithm was statistically significantly higher ( $p < 0.05$ ) than the %CA for the CSP algorithm. For 2 patients, there were no statistically significant differences ( $p < 0.05$ ) between the %CA for both methods. The averaged %CA for all stroke patients computed with FBCSP + PSO ( $74.1 \pm 11\%$ ) was statistically significantly higher ( $p < 0.05$ ) than the %CA obtained with CSP ( $70.2 \pm 12\%$ ).

Figure 5 shows the offline performance for healthy subjects' using the FBCSP + PSO and CSP algorithms. The %CA for all subjects were above the practical level of chance ( $p < 0.05$ ) with both algorithms. For 3 out of 8 healthy subjects, FBCSP + PSO was statistically significantly higher ( $p < 0.05$ ) than CSP. For the other subjects, no

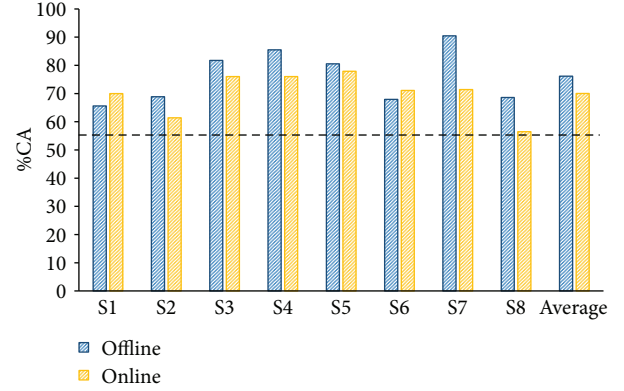


FIGURE 6: Online and offline classification accuracy percentages (%CAs) computed with data from 8 healthy subjects. The dotted line shows the practical level of chance (56.2%).

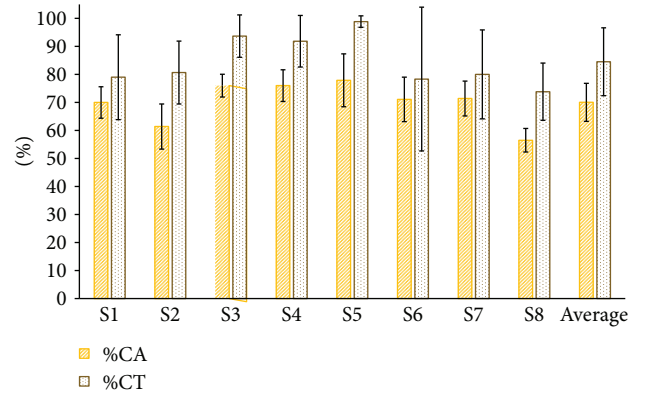


FIGURE 7: Online classification accuracy percentages (%CA) and correct trial percentages (%CT) from 8 healthy subjects.

statistically significant differences ( $p < 0.05$ ) were found between the %CA for both methods. Averaged %CA for the FBCSP + PSO method ( $76.2 \pm 7.6\%$ ) was statistically significantly higher ( $p < 0.05$ ) than the one obtained with CSP ( $75.5 \pm 7.8\%$ ).

**3.2. Online Analysis.** Figure 6 shows healthy subjects' online performances. For all subjects, online %CA was above the practical level of chance ( $p < 0.05$ ). Averaged offline %CA ( $76.2 \pm 7.6\%$ ) was higher compared to online tests ( $70 \pm 6.7\%$ ); however, there was no statistically significant difference ( $p > 0.05$ ) between them.

Figure 7 shows subjects' online %CA ( $70 \pm 6.7\%$ ) and %CT ( $84.5 \pm 12.1\%$ ). Using Pearson's analysis, a 0.8 correlation between %CA and %CT was found. In addition, a linear regression analysis showed an  $r^2$  value of 0.64. Averaged online processing time was of  $0.04 \pm 0.01$  s.

## 4. Discussion

The proposed BCI system was tested with stroke patients' and healthy subjects' data. Offline performances computed with FBCSP + PSO and CSP were above the practical level

of chance for all stroke patients and healthy subjects. However, for 4 out of 6 patients, FBCSP + PSO showed a statistically significant higher performance of their paralysed hand compared to CSP. In addition, 3 out of 8 healthy subjects' offline tests using FBCSP + PSO also showed statistically significant higher performances than CSP. Furthermore, for none of the stroke patients and healthy subjects, FBCSP + PSO performance was significantly lower than CSP. Ang et al. also performed an evaluation of their FBCSP using MIRSR for MI classification. Their algorithm was tested with a public database comprised of 9 healthy subjects and compared with the performance of CSP. However, FBCSP trained with MIRSR performances were not statistically significantly higher than CSP (with a 7 to 35 Hz frequency band) [19], unlike FBCSP + PSO in which the performance was statistically significantly higher than CSP. Therefore, FBCSP + PSO could be a better option for an MI BCI processing stage than CSP since it showed significantly higher performances for both stroke patients and healthy subjects.

The heuristic nature of PSO implies that its performance will not be limited by statistical features of the search space, since the method does not need to compute inverse matrices or other computations which often present restrictions, especially for high dimensional search spaces. Offline performances of the BCI system show that PSO implementation for feature selection of FBCSP allows this method to have better performances than CSP. This performance is achieved by using a multiobjective optimisation for the PSO algorithm by setting a higher importance to the LDA's classification than to the number of selected features in the fitness function.

The system's average processing time ( $0.04 \pm 0.01$  s) was lower than the time window used for EEG acquisition (1 s), which makes possible the online implementation of the system.

Stroke patients' offline performances ( $74.1 \pm 11\%$ ) were similar to the ones reported by Ang et al. with a sample of 46 stroke patients, which achieved an average offline performance of 74% using 27 EEG channels and an FBCSP with MIBIF algorithm. However, in the present work, only 11 EEG channels were recorded. In addition, stroke patients' offline performances were higher than online performances reported using other state-of-the-art BCI designs. For example, Morone et al. performed an acquisition of 61 EEG channels from 8 stroke patients. The goal of the study was to assess if the recruited patients could perform an online grasping of a virtual hand. They reported an average %CA of  $57 \pm 24\%$  [26]. Performances computed with the proposed BCI were also higher than the ones reported by Zhang et al. They recruited 8 stroke patients for the evaluation of a BCI coupled to a functional electrical stimulator. They processed 19 EEG channels with a modified CSP algorithm for feature extraction and support vector machines for classification. The average performance of their BCI system was 66% [38].

Healthy subjects' average online performance ( $70 \pm 6.7\%$ ) was higher than the one reported in a study with a similar feedback, using a hand exoskeleton by Witkowski et al. [39]. In the study, a %CA of 67.4% was reported ( $63.59 \pm 10.8$  of sensitivity and  $71.3 \pm 11.02$  of specificity), using 5

EEG channels, in a sample of 12 healthy subjects. In another study with a hand exoskeleton feedback reported by Tang et al., healthy subjects' online performance was  $84.29 \pm 2.11\%$ . However, only 4 subjects with good MI ability were recruited and 24 EEG electrodes were used [40]. Healthy subjects' online performances using the proposed BCI system were not significantly lower than the offline ones. Therefore, the proposed FBCSP + PSO processing stage should be able to handle the increased signal artefacts present in an online acquisition.

Offline and online tests allow us to suggest that stroke patients' online performance with the proposed BCI is likely to be around 70% or at least higher than the practical level of chance.

Online %CT was positively correlated with the %CA of the system, which implies that the feedback shown to users reflected their ability to voluntary elicit hand MI. This is important since showing a correct feedback to patients motivates them to keep a successful MI strategy or to seek different approaches if feedbacks indicate low performances.

This study showed that the proposed FBCSP + PSO processing stage and robotic orthosis feedback are suitable for a BCI aimed for neurorehabilitation. However, tests involving patients using the system are still required to evaluate its neuroplasticity-enhancement capabilities. The participants of these future tests should include patients with cortical stroke located in the dominant and nondominant hemisphere. The observed performance differences show that FBCSP + PSO could be a better option than CSP for feature extraction in an MI-based BCI. However, online acquisition data from a higher sample of patients participating in a randomized controlled trial are still necessary to completely describe the potential of the proposed BCI system as a neurorehabilitation tool for stroke patients. Another study limitation is that 2 sessions were performed per participant, and a higher number could provide information on performance variations across time. Therefore, the next step in the system's assessment should be to define a therapy schedule, which should include the lessons learned from this study which are to use FBCSP + PSO as processing stage, %CT for patient's feedback, 3 runs of 20 trials each per day, and a somatosensory feedback using a robotic hand orthosis.

## 5. Conclusions

This work presents a BCI system evaluation using a processing stage comprised of FBCSP + PSO combined with LDA and feedback provided by a robotic orthosis. PSO as a feature selection algorithm for FBCSP allows reducing the problem's dimensionality and achieving better classification performances, compared to those obtained if only the original CSP is used.

The present study shows that with the proposed BCI design patients are likely to be able to control a hand robotic orthosis using motor imagery of their paralysed hand. Therefore, the next developing stage of the system will be to perform a randomised controlled study involving direct EEG acquisition from patients. The BCI system designed in this study combines the advantages of a robotic device and motor

imagery, which have separately produced good results for stroke patients' rehabilitation. Therefore, if the proposed BCI system design is introduced into the clinical practice it would provide medical facilities with a tool that could aid stroke patient's functional recovery.

## Conflicts of Interest

The authors declare that there are no conflicts of interest regarding the publication of this article.

## Acknowledgments

The authors would like to thank Consejo Nacional de Ciencia y Tecnología for the support under Grant SALUD-2015-2-262061. The authors would like to thank Marlene Galicia-Alvarado for her helpful comments and Jose Antonio Barraza-Madrigal for helping in the design of the graphical user interface used in this work. Special thanks are given to the patients and healthy subjects for their participation in this study.

## Supplementary Materials

S1 Video shows a user of the proposed BCI system while performing right motor imagery. The robotic hand orthosis, computer screen with visual cues, and the graphical user interface can also be observed. In each trial, if the classifier stage of the BCI detected subject's motor imagery, passive hand finger flexion and extension was provided by the orthosis. After all trials of one session had been presented to the user, its BCI performance was shown on the computer screen. (*Supplementary Materials*)

## References

- [1] E. J. Benjamin, M. J. Blaha, S. E. Chiuve et al., "Heart disease and stroke statistics—2017 update: a report from the American Heart Association," *Circulation*, vol. 135, no. 10, pp. e146–e603, 2017.
- [2] A. Houwink, R. H. Nijland, A. C. Geurts, and G. Kwakkel, "Functional recovery of the paretic upper limb after stroke: who regains hand capacity?," *Archives of Physical Medicine and Rehabilitation*, vol. 94, no. 5, pp. 839–844, 2013.
- [3] R. H. M. Nijland, E. E. H. van Wegen, B. C. Harmeling-van der Wel, G. Kwakkel, and on behalf of the EPOS Investigators, "Presence of finger extension and shoulder abduction within 72 hours after stroke predicts functional recovery: early prediction of functional outcome after stroke: the EPOS cohort study," *Stroke*, vol. 41, no. 4, pp. 745–750, 2010.
- [4] S. E. Farmer, V. Durairaj, I. Swain, and A. D. Pandyan, "Assistive technologies: can they contribute to rehabilitation of the upper limb after stroke?," *Archives of Physical Medicine and Rehabilitation*, vol. 95, no. 5, pp. 968–985, 2014.
- [5] G. Pfurtscheller, C. Guger, G. Muller, G. Krausz, and C. Neuper, "Brain oscillations control hand orthosis in a tetraplegic," *Neuroscience Letters*, vol. 292, no. 3, pp. 211–214, 2000.
- [6] C. E. King, K. R. Dave, P. T. Wang et al., "Performance assessment of a brain-computer interface driven hand orthosis," *Annals of Biomedical Engineering*, vol. 42, no. 10, pp. 2095–2105, 2014.
- [7] M. Mihara, N. Hattori, M. Hatakenaka et al., "Near-infrared spectroscopy-mediated neurofeedback enhances efficacy of motor imagery-based training in poststroke victims: a pilot study," *Stroke*, vol. 44, no. 4, pp. 1091–1098, 2013.
- [8] N. Mrachacz-Kersting, N. Jiang, A. J. T. Stevenson et al., "Efficient neuroplasticity induction in chronic stroke patients by an associative brain-computer interface," *Journal of Neurophysiology*, vol. 115, no. 3, pp. 1410–1421, 2016.
- [9] G. Pfurtscheller and F. H. Lopes da Silva, "Event-related EEG/MEG synchronization and desynchronization: basic principles," *Clinical Neurophysiology*, vol. 110, no. 11, pp. 1842–1857, 1999.
- [10] S. Kraeutner, A. Gionfriddo, T. Bardouille, and S. Boe, "Motor imagery-based brain activity parallels that of motor execution: evidence from magnetic source imaging of cortical oscillations," *Brain Research*, vol. 1588, pp. 81–91, 2014.
- [11] G. Pfurtscheller, C. Brunner, A. Schlogl, and F. H. Lopes da Silva, "Mu rhythm (de)synchronization and EEG single-trial classification of different motor imagery tasks," *NeuroImage*, vol. 31, no. 1, pp. 153–159, 2006.
- [12] C. Andrew and G. Pfurtscheller, "On the existence of different alpha band rhythms in the hand area of man," *Neuroscience Letters*, vol. 222, no. 2, pp. 103–106, 1997.
- [13] O. Bertrand, F. Perrin, and J. Pernier, "A theoretical justification of the average reference in topographic evoked potential studies," *Electroencephalography and Clinical Neurophysiology/Evoked Potentials Section*, vol. 62, no. 6, pp. 462–464, 1985.
- [14] W. Y. Hsu, "Independent component analysis and multiresolution asymmetry ratio for brain-computer interface," *Clinical EEG and Neuroscience*, vol. 44, no. 2, pp. 105–111, 2013.
- [15] J. Muller-Gerking, G. Pfurtscheller, and H. Flyvbjerg, "Designing optimal spatial filters for single trial EEG classification in a movement task," *Clinical Neurophysiology*, vol. 110, no. 5, pp. 787–798, 1999.
- [16] J. Ye and T. Xiong, "Computational and theoretical analysis of null space and orthogonal linear discriminant analysis," *Journal of Machine Learning Research*, vol. 7, pp. 1183–1204, 2006.
- [17] B. Blankertz, R. Tomioka, S. Lemm, M. Kawanabe, and K. R. Muller, "Optimizing spatial filters for robust EEG single-trial analysis," *IEEE Signal Processing Magazine*, vol. 25, no. 1, pp. 41–56, 2008.
- [18] K. K. Ang, Z. Y. Chin, H. Zhang, and C. Guan, "Filter Bank common spatial pattern (FBCSP) in brain-computer Interface," in *2008 IEEE International Joint Conference on Neural Networks (IEEE World Congress on Computational Intelligence)*, pp. 2390–2397, Hong Kong, China, June 2008.
- [19] K. K. Ang, Z. Y. Chin, C. Wang, C. Guan, and H. Zhang, "Filter bank common spatial pattern algorithm on BCI competition IV datasets 2a and 2b," *Frontiers in Neuroscience*, vol. 6, 2012.
- [20] Y. Shi and R. C. Eberhart, "A modified particle swarm optimizer," in *1998 IEEE International Conference on Evolutionary Computation Proceedings. IEEE World Congress on Computational Intelligence (Cat. No.98TH8360)*, pp. 69–73, Anchorage, AK, USA, May 1998.
- [21] Q. Wei and Z. Wei, "Binary particle swarm optimization for frequency band selection in motor imagery based brain-computer interfaces," *Bio-medical Materials and Engineering*, vol. 26, no. s1, pp. S1523–S1532, 2015.

- [22] A. Atyabi, M. H. Luerssen, and D. M. W. Powers, "PSO-based dimension reduction of EEG recordings: implications for subject transfer in BCI," *Neurocomputing*, vol. 119, pp. 319–331, 2013.
- [23] P. Xu, T. Liu, R. Zhang, Y. Zhang, and D. Yao, "Using particle swarm to select frequency band and time interval for feature extraction of EEG based BCI," *Biomedical Signal Processing and Control*, vol. 10, pp. 289–295, 2014.
- [24] B. Várkuti, C. Guan, Y. Pan et al., "Resting state changes in functional connectivity correlate with movement recovery for BCI and robot-assisted upper-extremity training after stroke," *Neurorehabilitation and Neural Repair*, vol. 27, no. 1, pp. 53–62, 2012.
- [25] S. R. Soekadar, N. Birbaumer, M. W. Slutsky, and L. G. Cohen, "Brain machine interfaces in neurorehabilitation of stroke," *Neurobiology of Disease*, vol. 83, pp. 172–179, 2015.
- [26] G. Morone, I. Pisotta, F. Pichiorri et al., "Proof of principle of a brain-computer interface approach to support poststroke arm rehabilitation in hospitalized patients: design, acceptability, and usability," *Archives of Physical Medicine and Rehabilitation*, vol. 96, no. 3, pp. S71–S78, 2015.
- [27] D. Broetz, C. Braun, C. Weber, S. R. Soekadar, A. Caria, and N. Birbaumer, "Combination of brain-computer interface training and goal-directed physical therapy in chronic stroke: a case report," *Neurorehabilitation and Neural Repair*, vol. 24, no. 7, pp. 674–679, 2010.
- [28] A. Ramos-Murguialday, D. Broetz, M. Rea et al., "Brain-machine interface in chronic stroke rehabilitation: a controlled study," *Annals of Neurology*, vol. 74, no. 1, pp. 100–108, 2013.
- [29] F. Ostrosky-Solis, E. Gómez-Pérez, A. Ardila et al., *Batería Neuropsicológica NEUROPSI Atención y Memoria, 6 a 85 años de edad*, Bookstore, Mexico, 2003.
- [30] R. Cuencas, B. V. Seggern, R. Toledo, and E. Harrell, "El inventario de Edimburgo: evaluación de la lateralidad cerebral en una población Mexicana," *Salud Mental*, vol. 13, no. 2, pp. 11–17, 1990.
- [31] G. Pfurtscheller and C. Neuper, "Motor imagery and direct brain-computer communication," *Proceedings of the IEEE*, vol. 89, no. 7, pp. 1123–1134, 2001.
- [32] J. Cantillo-Negrete, J. Gutiérrez-Martínez, T. B. Flores-Rodríguez, R. I. Cariño-Escobar, and D. Elías-Viñas, "Characterization of electrical brain activity related to hand motor imagery in healthy subjects," *Revista De Investigacion Clinica*, vol. 66, Supplement 1, pp. 111–121, 2014.
- [33] H. Ramoser, J. Müller-Gerking, and G. Pfurtscheller, "Optimal spatial filtering of single trial EEG during imagined hand movement," *IEEE Transactions on Rehabilitation Engineering*, vol. 8, no. 4, pp. 441–446, 2000.
- [34] J. Cantillo-Negrete, R. I. Carino-Escobar, and J. Gutierrez-Martinez, "Increasing stroke patients motor imagery classification by selecting features with particle swarm optimisation," in *Proceedings of the 7th Graz Brain-Computer Interface Conference 2017*, pp. 52–57, Graz, Austria, September 2017.
- [35] M. Martinez-Valdes, J. L. Cruz-Vargas, J. Gutierrez-Martinez et al., "Mechanical structure prototype and control unit for an active orthosis for a human had," in *2014 Pan American Health Care Exchanges (PAHCE)*, pp. 1–4, Brasilia, Brazil, April 2014.
- [36] J. Cantillo-Negrete, R. I. Carino-Escobar, D. Elias-Vinas, and J. Gutierrez-Martinez, "Control signal for a mechatronic hand orthosis aimed for neurorehabilitation," in *2015 Pan American Health Care Exchanges (PAHCE)*, pp. 1–4, Vina del Mar, Chile, March 2015.
- [37] J. R. Müller-Putz, R. Scherer, C. Brunner, R. Leeb, and G. Pfurtscheller, "Better than random? A closer look on BCI results," *International Journal of Bioelectromagnetism*, vol. 10, pp. 52–55, 2008.
- [38] H. Zhang, H. Liang, Y. Liu, H. Wang, and L. Zhang, "An iterative method for classifying stroke subjects' motor imagery EEG data in the BCI-FES rehabilitation training system," in *Foundations and Practical Applications of Cognitive Systems and Information Processing*, S. Fuchun, H. Dewen, and L. Huaping, Eds., pp. 363–373, Springer Berlin Heidelberg, Berlin, 2014.
- [39] M. Witkowski, M. Cortese, M. Cempini, J. Mellinger, N. Vitiello, and S. R. Soekadar, "Enhancing brain-machine interface (BMI) control of a hand exoskeleton using electrooculography (EOG)," *Journal of Neuroengineering and Rehabilitation*, vol. 11, no. 1, p. 165, 2014.
- [40] Z. Tang, S. Sun, S. Zhang, Y. Chen, C. Li, and S. Chen, "A brain-machine interface based on ERD/ERS for an upper-limb exoskeleton control," *Sensors*, vol. 16, no. 12, 2016.

## Research Article

# A Lower Limb Rehabilitation Robot in Sitting Position with a Review of Training Activities

Trinnachoke Eiammanussakul  and Viboon Sangveraphunsiri 

*Department of Mechanical Engineering, Faculty of Engineering, Chulalongkorn University, Bangkok, Thailand*

Correspondence should be addressed to Viboon Sangveraphunsiri; viboon.s@chula.ac.th

Received 17 November 2017; Revised 3 February 2018; Accepted 20 February 2018; Published 1 April 2018

Academic Editor: Rafael Morales

Copyright © 2018 Trinnachoke Eiammanussakul and Viboon Sangveraphunsiri. This is an open access article distributed under the Creative Commons Attribution License, which permits unrestricted use, distribution, and reproduction in any medium, provided the original work is properly cited.

Robots for stroke rehabilitation at the lower limbs in sitting/lying position have been developed extensively. Some of them have been applied in clinics and shown the potential of the recovery of poststroke patients who suffer from hemiparesis. These robots were developed to provide training at different joints of lower limbs with various activities and modalities. This article reviews the training activities that were realized by rehabilitation robots in literature, in order to offer insights for developing a novel robot suitable for stroke rehabilitation. The control system of the lower limb rehabilitation robot in sitting position that was introduced in the previous work is discussed in detail to demonstrate the behavior of the robot while training a subject. The nonlinear impedance control law, based on active assistive control strategy, is able to define the response of the robot with more specifications while the passivity property and the robustness of the system is verified. A preliminary experiment is conducted on a healthy subject to show that the robot is able to perform active assistive exercises with various training activities and assist the subject to complete the training with desired level of assistance.

## 1. Introduction

Robots for rehabilitation have gained more attentions in many research due to some benefits over conventional therapy by physiotherapists. For example, robots for locomotion training on a treadmill primarily aim to replace physical demand of the therapist labor because the task is ergonomically unfavorable and tiring [1]. Without physical burden, numbers of repetition and duration of the training session can be increased [2–4]. While the performance of a therapist could vary from day to day [1] and intervention techniques by expert and unexperienced therapists are different [5, 6], a robot follows the certain control algorithm and provides systematic intervention to the patient. Moreover, robots are able to obtain and record data such as position, velocity, interaction force, or biosignal with various kinds of sensors. This quantitative data can be used for further offline analysis, which leads to objective evaluation of the patient's recovery [3, 4], or even used for adapting robot's behavior corresponding the patient's current condition. Rehabilitation robots are also able to perform different types of exercises and varieties

of movement [2, 7, 8]. Moreover, the robot can be implemented with games [9] or virtual reality system [10] in order to promote active participation of the patient. Robots for stroke rehabilitation have shown their effectiveness in many clinical trials worldwide.

The lower limb rehabilitation robots can be categorized into 2 types according to exercise posture [11]. The first type is a robot for training in sitting/lying position which benefits the patient who still suffers from muscle weakness and cannot stand or walk safely [5, 12]. By excluding concern of balance, the patient may be more independent and able to focus on the training [13]. This kind of robot allows the patient to strengthen muscle, develop endurance, and increase joint mobility and movement coordination [4]. Another type of the robot is for training while standing/walking. The gait training robot in literature was developed to train either over ground or on a treadmill with a body weight support mechanism. However, the gait training robot is only suitable for the patient that has adequate endurance and ability to stand [14].

Training modalities used in robots for stroke rehabilitation are often divided into four groups, namely, passive,

active assistive, active, and active resistive exercises [15]. Exercises may be prescribed to a stroke patient corresponding to the stage of recovery [3] and the muscle tone [2, 16], which can be graded according to the muscle contraction observability, ability to move a limb against gravity and external resistance [17]. In the preliminary stage, the patient with very low muscle strength should conduct passive training, for example, moving the patient's limb along a predefined trajectory by another person or an exercise device known as continuous passive machine (CPM). Passive exercise could improve movement ability, maintain range of motion, and reduce muscle atrophy. In the intermediate stage, the patient with some degree of muscle strength should perform active assistive, active, or active resistive exercise. Active assistive exercise allows the patient to move the limb by himself with assistance provided by another person when needed. Active exercise allows the patient to move by his own effort without external assistance and resistance. In active resistive mode, the robot provides force opposing the movement of the patient. This exercise aims to strengthen muscle of the patient who is already able to move his limb over the full range of motion. Different motion and amount of resistive force can be applied to achieve a variety of strengthening training such as isometric, isotonic, and isokinetic exercise. There are many types of force that could be applied to the patient as resistance. Resistive exercise in conventional rehabilitation can be done against weight, elastic bands, in the pool, or by an exercise machine [14]. In the advanced rehabilitation stage, the objective of the exercise is to regain function related to activities in daily living such as balancing and gait training.

Apart from training modalities, training activities also have to be selected appropriately to an individual. Because the lower limb rehabilitation robots in sitting/lying position get rid of the stability concern, the robots are able to perform a variety of training activities. It is interesting to study how these training activities are selected and what are benefits of each training activity for a stroke patient. This knowledge would be useful in developing robots suitable for stroke rehabilitation.

This article focuses on the lower limb rehabilitation robots for training in sitting/lying position. In Section 2, the training activities performed by this type of robot are reviewed. Description of the robot is shown in Section 3. The control system and the impedance control law proposed in our previous work [18] for active assistive exercises are discussed in Section 4. Experiments conducted to study the performance of the system are also presented in this section. The experiment by a healthy subject in Section 5 demonstrates the robot behavior while performing training activities with many levels of assistance. Finally, the conclusion of the research article is made on Section 6.

## 2. Review of Training Activities of Robots for Stroke Rehabilitation

Training activities performed by lower limb stroke rehabilitation robots in sitting/lying position are summarized in Table 1. Types and actuated degrees of freedom of the robots

are also reported since they are corresponding to the training activities. Foot robotic orthoses and footplate-based end-effector robots are able to actuate only at ankle joint and foot section. End-effector robots (nonfootplate-based type) are usually able to perform movements involving hip, knee, and ankle joints in the sagittal plane. On the other hand, exoskeletons whose structure and joint axes aligned with those of human body are able to perform the movement of a single joint or multiple joints.

Robots in lower limb rehabilitation after stroke are developed with different concepts of the training. Some robots are able to perform a certain training activity and modality. Anklebot [19] is able to train ankle joint with active assistive training modality while the lower limb paediatric therapy device by Chrif et al. [20] was designed for leg press exercise performing with active resistive training modality. Besides, some robots can perform many training activities but with a certain training modality. For example, the horizontal lower limb rehabilitation training robot by Guo et al. [5] is able to train lower limbs in six actions according to the traditional Chinese medicine technique with passive training modality, whereas ViGRR [21] can perform gait trajectory following and leg press exercise with active resistive training modalities. Moreover, some robots are able to perform only one training activity but with various kinds of training modality. MOTOMed [22] can perform cycling exercise with passive, active assistive, and active resistive training modalities while Vi-RABT [12] can train ankle joint with active assistive and active training modalities. The other robots are able to perform many training activities and modalities. The ankle rehabilitation robot by Yoon et al. [7] is able to train ankle joint or perform gait trajectory following at the ankle joint with passive, active assistive, and active resistive training modalities. Physiotherabot [2] is able to perform many training activities at hip and knee joints with passive, active assistive, and active resistive training modalities. Lower limb rehabilitation robot in our previous research [18] can be used for therapeutic exercises at hip, knee, and ankle joints. Because the robot structure is exoskeleton, it can perform both single- and multiple-joint training. The desired trajectory of the robot can be easily customized. Therefore, range, pattern, and speed of the movement can be arbitrarily adjusted to suit with the patient condition. It is also able to perform passive, active assistive, and active resistive training modalities. The robot is designed for versatile training for a stroke patient in sitting position.

According to Table 2, training activities can be categorized as single-joint training and multiple-joint training. The single-joint training involves the movement of a specific joint (hip, knee, or ankle joint) in one or several degrees of freedom. It can be performed by foot robotic orthoses, footplate-based end-effector robots, and exoskeletons. On the other hand, the multiple-joint training consists of the simultaneous movement of several joints for performing exercises such as leg press, cycling, and gait trajectory following. Some robots are able to perform a customized movement by using recorded data (e.g., position, velocity, and interaction force) obtained during the robot teaching session by a physiotherapist. The multiple-

TABLE 1: Training activities of stroke rehabilitation robot in sitting/lying position.

Robot	Robot type	Actuated DOFs	Training activities	Training modalities
Anklebot	Foot robotic orthosis	Ankle dorsiflexion/plantar flexion, inversion/eversion	Training at ankle joint	Active assistive
Vi-RABT	Footplate-based end-effector robot	Ankle dorsiflexion/plantar flexion, inversion/eversion	Training at ankle joint	Active assistive, active
Ankle rehabilitation robot by Yoon et al.	Footplate-based end-effector robot	Ankle dorsiflexion/plantar flexion, inversion/eversion, metatarsophalangeal flexion/extension	Training at ankle joint, gait trajectory following	Passive, active assistive, active resistive
Lower limb paediatric therapy device by Chrif et al.	End-effector robot	Movement in sagittal plane	Leg press	Active resistive
Horizontal lower limb rehabilitation training robot by Guo et al.	End-effector robot	Movement in sagittal plane, ankle internal/external rotation	Training at single/multiple joints	Passive
ViGRR	End-effector robot	Movement in sagittal plane	Gait trajectory following, leg press	Active resistive
MOTOMed	End-effector robot	Movement in sagittal plane	Cycling	Passive, active assistive, active resistive
Physiotherabot	Exoskeleton	Hip flexion/extension, abduction/adduction, knee flexion/extension	Training at single/multiple joints, customized movement	Passive, active assistive, active resistive
Lower limb rehabilitation robot in our previous research	Exoskeleton	Hip flexion/extension, knee flexion/extension, ankle flexion/extension	Training at single/multiple joints, customized movement	Passive, active assistive, active resistive

TABLE 2: Training modalities implemented in each training activity.

Training activity	Passive	Active assistive	Active	Active resistive
Single-joint training (at hip, knee, or ankle joint)	x	x	x	x
Multiple-joint training				
Leg press				x
Cycling	x	x		x
Gait trajectory following				x
Customized movement		x		

joint training can be conducted by end-effector robots and exoskeletons.

Single-joint training is usually selected for range of motion exercise which can be performed with passive, active assistive, or active training modalities. In addition, single-joint training is also chosen when improvement of functional ability of a specific joint is required. For example, the ankle joint is targeted for the training by some rehabilitation robots because stroke patients are usually unable to activate dorsiflexor muscle to lift the foot up. This problem leads to walking impairments of the patients such as toe dragging in the swing phase and foot slapping in the heel strike phase. Besides, the patients might have excessive inversion which causes lateral instability in the stance phase of the gait [19]. Anklebot and Vi-RABT apply active assistive training modality to provide assistance to a patient while using the

robots to move a cursor in computer games. The benefits of the training are supported by results of clinical trials on chronic stroke patients with Anklebot. It was shown that the patients had better motor control (increased targeting accuracy and faster and smoother movements) and walking ability (increased walking velocity, durations of paretic single support, and nonparetic step length which could be a result from greater push-off of the paretic foot) [23–25].

There are varieties of exercise that involve training of multiple joints such as leg press, cycling, gait trajectory following and customized movement. The developers of the robots selected one or several kinds of these exercises to achieve different aspects of the stroke recovery.

Leg press exercise is extensively used in sport and neuromuscular rehabilitation. It aims to strengthen muscles across multiple joints of the lower limbs in sitting/lying

position [26]. This exercise is able to activate leg muscles in a similar level compared to bodyweight exercises such as chair rise and hip thrust [27]. Moreover, it is found that chronic stroke patients not only gain strength on both affected and nonaffected legs but also have improvement in balance, walking ability, and functional performance [28, 29].

Cycling is an alternative exercise to walking for stroke patients who have difficulty in maintaining balance and independent gait [30]. It provides continuous repetitions of movement which promotes coordination of muscle synergies. Its kinematic pattern is also similar to walking as it requires flexion and extension of hip, knee, and ankle joints as well as activation of antagonist muscles in alternating and coordinated manner. In addition, because the range of motion in cycling is greater than that in walking, cycling could help maintaining functional range of motion as a preparation for gait training in the future [31]. It was found that the stationary cycling training is able to enhance dynamic balance, muscle strength, and walking ability of chronic stroke patients [30]. MOTOMed, which was specifically designed for cycling exercise, had been used in clinical trials on stroke patients. It was found that stroke patients who performed resistive exercise with the device had improvement in walking distance in 2 and 6 minutes walking test, increase in comfortable speed, and lower time spent on "Up & Go" test [22].

Walking is a functional task of lower limbs and the goal of rehabilitation. However, the task consists of complex movement that requires force generation for body weight support, coordination, and weight shifting [31]. Gait training of a stroke patient who still suffers from muscle weakness demands great physical effort from both the patient and several physiotherapists. Therefore, duration and numbers of repetition in a gait training session in an upright position might not be enough to gain effective rehabilitation outcome [1]. Some robots are able to perform gait training for stroke patients in sitting/lying position. These robots recorded gait trajectories from healthy subjects to create a reference data for training stroke patients. The ankle rehabilitation robot by Yoon et al. performs isokinetic exercise by following ankle and foot (metatarsophalangeal joint) reference trajectory. On the other hand, ViGRR implements resistive exercise against virtual damping and inertia to interact with the patient during the gait trajectory following task.

Because physical characteristics may differ among stroke patients and from day to day, the training should be customized individually at the beginning of each training session. Physiotherabot was developed to train a stroke patient with any movement pattern taught by a physiotherapist. Once the movement is recognized, the robot will train a stroke patient with that movement as if the training is performed by a physiotherapist.

### 3. Lower Limb Rehabilitation Robot

The lower limb rehabilitation robot in this project is developed for movement training in sitting position. It aims to be used by patients who have severe hemiparesis condition. These patients are not comfortable to use typical treadmill-training devices at the beginning of training activities. The

sitting position robot is more preferable especially at the beginning state of training. The lower limb rehabilitation robot in this study as shown in Figure 1 consists of a powered exoskeleton, a counterbalance mechanism, a control unit, and a monitor screen (not shown in the figure).

The exoskeleton is able to move in the sagittal plane at hip, knee, and ankle joints. The hip joint allows 45° flexion and 0° extension. The knee joint is able to move in the range of 110° flexion and 0° extension. The ankle joint permits 20° dorsiflexion and 45° plantar flexion. These ranges of motion are ensured by mechanical stoppers placed at the end of the joint movement range.

Figure 2 illustrates components of the cable transmission mechanism of a robot joint (the knee joint is shown, e.g.). The mechanism is actuated by a brushless servomotor (SANYO DENKI). Sizes of the motors are 400 W for hip and knee joints and 200 W for the ankle joint. Specifications of the motors are provided in Table 3. The pulley A, which is mounted at the end of the motor shaft, drives the pulley B via cable. The second stage of the cable transmission is done by the shaft connected to the pulley B. Another end of this shaft works as a small pulley for driving the pulley C via cable. With the shaft connected between the pulley C and the shank segment, the shank segment rotates about the knee joint axis with respect to the pulley C.

The torque requirements (maximum torque) of hip and knee joints are considered when lower limbs stretch out in sitting position while the torque requirement for the ankle joint is considered at neutral sitting position. According to anthropomorphic data [32], for a human with 100 kg weight and 180 cm height, torque requirements for hip, knee, and ankle joints are 67.331, 18.598, 1.945 N·m, respectively. For the robot joint design, transmission ratios of hip, knee, and ankle joints are chosen so that continuous torque provided by the robot joints is sufficient for the torque requirements. Specifications of the robot joints are shown in Table 4.

To achieve backdrivability of the robot joints, the inertia of the corresponding robot segment must be lower than the reflected motor inertia (the product of the square of the transmission ratio and the inertia of the motor) [33]. The ranges of inertia of thigh, shank, and foot segments according to their minimum and maximum lengths are given in Table 5. It can be noticed that the reflected motor inertias of hip, knee, and ankle joints are always lower than the moments of inertia of thigh, shank, and foot segments about their proximal joint axes, respectively. Therefore, it can be concluded that the robot joints are backdrivable.

The counterbalance mechanism is designed to reduce effects of the gravitational load due to robot's weight. The mechanism consists of vertical guide rods, linear bearings, a 12 kg mass, and a cable which wraps around a series of idlers to link the thigh segment of the exoskeleton and the 12 kg mass together. The guide rods and idlers are mounted on the control unit. The weight of the 12 kg mass generates counterbalance moment about the hip joint whose magnitude corresponds to the hip joint angle in order to counteract the moment due to robot's weight. With this counterbalance mechanism, the torque requirement of the hip joint transmission mechanism is reduced up to 20.7 N·m.

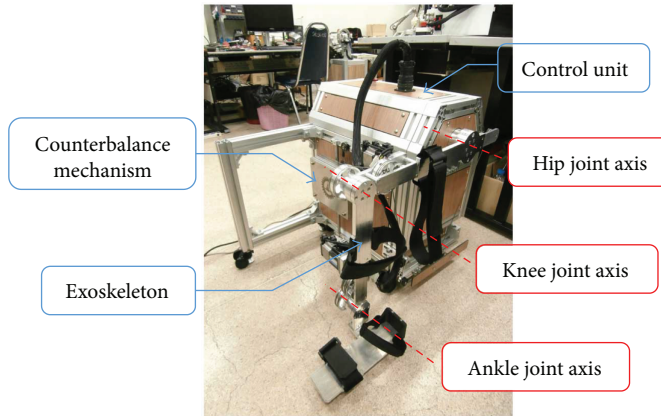


FIGURE 1: Lower limb rehabilitation robot in sitting position consisted of an exoskeleton (with hip, knee, and ankle joints), the counterbalance mechanism, and the control unit.

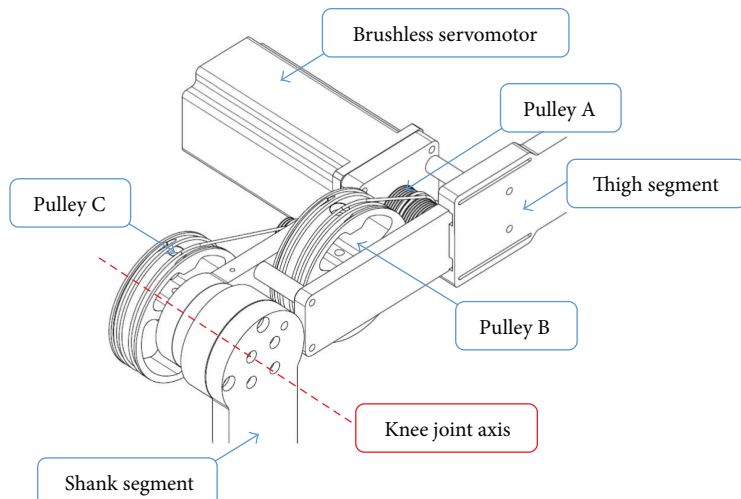


FIGURE 2: Cable transmission mechanism of the knee joint.

TABLE 3: Specifications of brushless servomotors.

Power (W)	Peak stall torque (N·m)	Rated torque (N·m)	Rated speed (rpm)	Inertia ( $\times 10^{-4} \text{ kg} \cdot \text{m}^2$ )
400	4.8	1.27	3000	0.412
200	2.2	0.637	3000	0.219

TABLE 4: Specifications of the robot joints.

Joint	Transmission ratio	Continuous torque (N·m)	Reflected motor inertia ( $\text{kg} \cdot \text{m}^2$ )
Hip	57.76:1	73.36	0.137
Knee	15:1	19.05	$9.27 \times 10^{-3}$
Ankle	15:1	9.56	$4.93 \times 10^{-3}$

Both the exoskeleton and the counterbalance mechanism are installed on the control unit as a single platform. The control unit also contains a DC power supply, a

TABLE 5: Dimensions and inertia properties of the robot segments.

Segment	Length (mm)	Moment of inertia about the proximal joint axis ( $\text{kg} \cdot \text{m}^2$ )
Thigh	365–465	0.141–0.258
Shank	365–465	0.140–0.259
Foot	75–95	0.006–0.007

computer unit, a data acquisition card, motor amplifiers, an emergency stop button, and other electronic devices.

#### 4. Control System

The lower limb rehabilitation robot is developed to train a subject with various training activities and modalities. Control algorithm for each training modality had been introduced in the previous work [18]. In this study, the control algorithm for active assistive exercise is described in more detail.

**4.1. Control Strategy.** In active assistive exercise, a patient moves his limb in desired movements. The assistance on the patient's limb exerted by a physiotherapist will be given as much as necessary to achieve the task and only when needed.

Modern rehabilitation robots have realized this intervention technique, which is usually called the “assist-as-needed” control strategy, into their controllers. One of the most popular controllers is an impedance controller. This controller simulates the interaction between human and a robot with a function between force and kinematic variables (position, speed, and acceleration). The robot will interact to the environment (which is human, in this case) as if it is connected to virtual mechanical components such as springs, dampers, and masses. Since the characteristics of the human-robot interaction is controlled rather than position, the impedance controller allows some degree of position error and does not enforce the movement of the robot to follow the exact reference trajectory. This allows both spatial and temporal variability of the movement which does not only improve motor coordination and walking ability [34] but also promote active participation of the patient [3, 35]. Both variability and active participation are important factors for motor recovery as they provoke neuroplasticity and motor learning [35–37].

**4.2. Control Architecture.** The control algorithm for each joint of the robot as shown in Figure 3 consists of 3 cascaded loops which are outer, middle, and inner loops. The outer control loop is implemented with the impedance controller whose control law ( $P$ ) is shown in (1). It establishes the relationship between joint angle error ( $e_\theta$ ) and the magnitude of desired torque ( $\tau_d$ ). In literature, many impedance control laws for rehabilitation robots were nonlinear such as Gaussian [12], polynomial [35, 38], or exponential [39] function. With a nonlinear impedance control law, low desired torque is generated for small position error but the magnitude of the desired torque increases with higher rate compared to the change of position error. This controller characteristic encourages a patient to move voluntarily if the position error is within acceptable tolerance. However, these control laws usually consist of one control gain. This could limit how the magnitude of desired torque changes with respect to position error. Therefore, the impedance control law developed for the robot in this research has two control gains  $K_1$  and  $K_2$ , so the relationship between joint angle error and desired torque can be defined with more specifications. The proce-

dure to select proper control gains will be presented in the next section of the article. Moreover, the impedance control law also considers the magnitude of desired force due to joint velocity error as represented by the last term in (1). The control gain  $K_d$  determines the magnitude of the damping force which could reduce oscillation of the human-robot interaction. It is noticed that the impedance controller in (1) is similar to a PD controller.

$$\tau_d = K_1 (\exp(K_2 |\theta_{j,d} - \theta_j|) - 1) \operatorname{sgn}(\theta_{j,d} - \theta_j) + K_d d/dt(\theta_{j,d} - \theta_j). \quad (1)$$

The saturation function is applied after the impedance control law to limit the maximum assistance force to be generated by the robot. The required gravitational torque ( $\tau_g$ ) is also added to the desired torque to cancel the load at the robot joint due to robot's weight. For the hip joint, the required gravitational torque is reduced by the moment generated by the counterbalance mechanism. The resultant control signal is used as the torque reference for the middle control loop. A PI controller with control gains  $K_o$  and  $I_o$  is used to ensure perfect torque tracking.

The output of the torque controller in the middle control loop is used as the reference signal for the inner control loop. Another PI controller with control gains  $K_i$  and  $I_i$  is implemented to generate control signal to the motor driver in order to actuate a robot joint with inertia of  $J$ . The encoder mounted on the motor shaft measures the motor position. It can be used to estimate the position of the robot joint ( $\theta_j$ ) by dividing the motor position by the total transmission ratio ( $N$ ) of the robot joint. The velocity of the robot joint ( $\dot{\theta}_j$ ) is differentiated from the estimated joint position.

Motor current ( $i$ ) measured by the motor driver is detected due to the elastic force from the transmission mechanism. The magnitude of the elastic force is the product of the mechanism stiffness  $K$  and position difference between angle of the robot joint and angle at the load side that might be disturbed by an environment ( $\theta_{dis}$ ). The joint torque is obtained from the motor current multiplied by the torque constant ( $K_t$ ) of the motor and the total transmission ratio of the joint.

By viewing the impedance controller as a PD controller,  $P$  becomes  $K_d s + K_p$ . The open loop transfer function of the system is derived as

$$\frac{\tau}{e_\theta} = \frac{NKK_t(K_d s + K_p)(K_i s + I_i)(K_o s + I_o)}{Js^4 + K_i s^3 + (I_i + NKK_t + NKK_t K_i K_o)s^2 + NKK_t(K_i I_o + K_o I_i)s + NKK_t I_i I_o}. \quad (2)$$

From (2), the system is strictly stable since the coefficient of the denominator is positive. Moreover, it can be noticed that the relative degree of the system is 1. Therefore, the

phase shift of the system in response to sinusoidal inputs is always less than 90 degrees such that the Nyquist plot of (2) lies entirely in the right half complex plane. With these

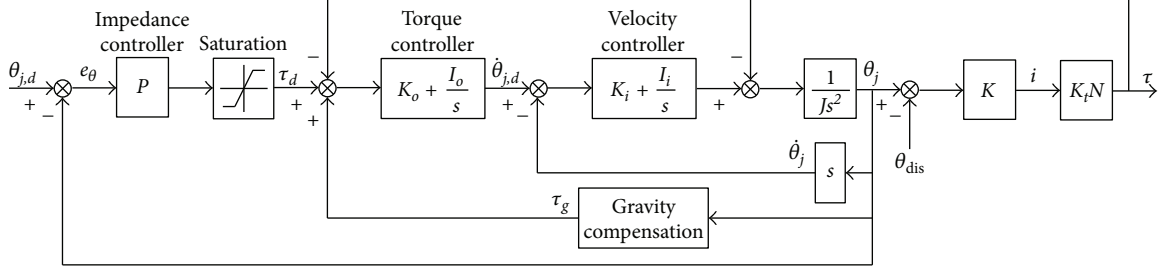


FIGURE 3: Block diagram of control algorithm for active assistive exercise.

characteristics, it can be concluded that the system is strictly stable or passive [40]. This property implies that the system cannot output more energy than that was input into the system. In other words, stability of the interaction between the robot and an environment is guaranteed.

**4.3. Control Gain Selection Procedure.** The magnitude of the desired torque due to joint angle error ( $\tau_{d,e_\theta}$ ) is defined by the first term in the impedance control law (1)

$$\tau_{d,e_\theta} = K_1(\exp(K_2 e_\theta) - 1), \quad (3)$$

where  $e_\theta = |\theta_{j,d} - \theta_j|$  is the magnitude of error between desired and actual joint position. It is noted that the function  $\text{sgn}(e_\theta)$  shown in (1) is for determining the direction of the desired torque, so it is omitted in (3).

Differentiating (3) with respect to position error, the rate of change of desired torque is obtained

$$\frac{d\tau_{d,e_\theta}}{de_\theta} = K_1 K_2 \exp(K_2 e_\theta). \quad (4)$$

The initial rate of change of desired torque (by setting  $e_\theta = 0$ ) is

$$\left. \frac{d\tau_{d,e_\theta}}{de_\theta} \right|_{e_\theta=0} = K_1 K_2, \quad (5)$$

so

$$K_2 = \frac{1}{K_1} \left( \left. \frac{d\tau_{d,e_\theta}}{de_\theta} \right|_{e_\theta=0} \right). \quad (6)$$

Substituting (4) into (3) yields

$$\tau_{d,e_\theta} = K_1 \left[ \exp \left( \frac{e_\theta}{K_1} \left( \left. \frac{d\tau_{d,e_\theta}}{de_\theta} \right|_{e_\theta=0} \right) \right) - 1 \right]. \quad (7)$$

By specifying the maximum desired torque generated by the controller ( $\tau_{d,e_\theta}^{\max}$ ) and the maximum allowable position error ( $e_\theta^{\max}$ ), it is found that

$$\tau_{d,e_\theta}^{\max} = K_1 \left[ \exp \left( \frac{e_\theta^{\max}}{K_1} \left( \left. \frac{d\tau_{d,e_\theta}}{de_\theta} \right|_{e_\theta=0} \right) \right) - 1 \right]. \quad (8)$$

If the initial rate of change of desired torque is known, the

control gain  $K_1$  can be obtained by solving (5) numerically. Next, the control gain  $K_2$  can be calculated from (4).

**4.4. Effects of the Impedance Controller Gains on the Robot Response.** To study the effect of the nonlinear relationship between joint angle error and desired torque in (1). The ankle joint of the robot is tested with three sets of control gains as shown in Table 6. The control gains  $K_1$  and  $K_2$  are chosen so that the controller generates the maximum ankle torque (10 N·m) at joint angle errors of 0.03, 0.05, and 0.07 rad with different initial rate of change of desired torque ( $K_1 K_2$ ) as seen in Figure 4. The control gain  $K_d$  is the same for the controllers A, B, and C.

The objective of this experiment is to investigate the response due to the disturbance torque at robot's ankle joint which is implemented with controllers A, B, and C. During this experiment, no human subject is included and the disturbance torque is generated in robot's program by adding it before the torque control loop. The desired joint angle is always fixed at zero while the magnitude of the disturbance torque changes over time. Its magnitude increases from zero to the maximum value in 1 second. The maximum disturbance torque is hold for another second. Then, the magnitude decreases from the maximum value to zero in 1 second and is kept at zero until the end of each tests. The maximum magnitude of the disturbance torque is chosen as 1, 4, 7, and 10 N·m. This experiment simulates the circumstance when a human subject performs a movement training with the robot. At first, the subject gradually moves out of the desired path, stays at some position errors, and finally gets back to the desired path. The disturbance torque on robot's controller is caused from the position deviation from the desired path.

Figure 5 shows the ankle position of the robot during the experiment with the controllers A, B, and C. Generally, it could be seen that the controller A always produces the highest angle error (deviation from the desired angle which is zero in this experiment) while the controller C generates the smallest angle error. The higher the magnitude of the disturbance torque, the higher the controllers produce angle error. During the first second, the controller A produces angle error which increases with varying rate as the magnitude of the disturbance torque is rising. On the contrary, the controller C creates angle error almost proportional to the magnitude of the disturbance torque. This difference originates from the relationship between angle error and torque generated by the controllers. As seen from Figure 4, the slope of the

TABLE 6: Impedance control gains of the ankle joint.

Controller	Initial rate of change of desired torque	Angle error at the maximum torque (rad)	$K_1$	$K_2$	$K_d$
A	30	0.07	0.81	37.01	2.0
B	100	0.05	3.98	25.13	2.0
C	300	0.03	43.42	6.91	2.0

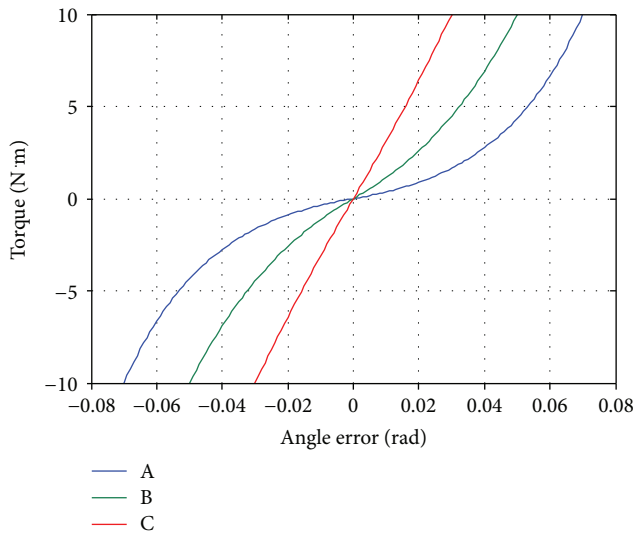


FIGURE 4: Relationship between angle error and torque generated by controllers A, B, and C of the ankle joint.

relationship of the controller A is very different at low and high angle error while the slope of the relationship of the controller C is almost constant. Therefore, with the same amount of change in the magnitude of the disturbance torque, the angle error produced by the controller A changes much faster than that by the controller C. The varying rate of angle change can also be found in the experiment with the controller B too, but the change is not as obvious as the controller A. While the magnitude of the disturbance torque is at the maximum value, the ankle angle in each case is constant. It can be noticed from Figure 5(d) that the angle error almost reached the certain error used in the controller design (0.07, 0.05, and 0.03 rad for the controllers A, B, and C). When the magnitude of the disturbance force is decreasing from its maximum value, the trends of the angle change by each controllers are also the same as in the first second of the experiment. After the magnitude of the disturbance torque reaches zero, it could be seen that the ankle position does not converge to zero. The remaining angle error is highest in the experiment with the controller A and lowest in the experiment with controller C. It is found that torque generated by these controllers is only around  $-0.3\text{ N}\cdot\text{m}$  (not shown in Figure 5). Since friction in the robot mechanism is minimized by the robot design and the manufacturing of the robot parts, it is believed that the remaining angle errors are mainly due to the imperfect gravity compensation.

It can be concluded from this experiment that both control gains  $K_1$  and  $K_2$  determine how the robot responds to external torque. In order to obtain desired interaction between a human and the robot, these control gains should be selected appropriately. They can be calculated by using specified initial rate of change of the desired torque and maximum allowable angle error and torque. As demonstrated by the experimental results, the initial rate of change of desired torque defines the robot response at low angle error while the maximum angle error and torque determine the limit of the robot response. Therefore, if high angle error is allowed during the movement training, low initial rate of change of desired torque and high maximum angle error should be chosen. For more strict movements, high initial rate of change of desired torque and low maximum angle error should be selected. The maximum torque can be set according to the maximum capacity of the robot actuator or the amount of assistance required by an individual patient for a movement training. In the rest of the article, the impedance control gains of hip, knee, and ankle joints are selected with the same criterions used in this section. However, the maximum torque of hip and knee joints is 50 and 20  $\text{N}\cdot\text{m}$ , respectively. The controllers A, B, and C are named as low, medium, and high assistance controllers, respectively. Table 7 summarizes the impedance control gains of the robot joints in each mode.

**4.5. Robot Response due to External Impact Force.** In Section 4.2, it was shown that the robot controller is passive. This property ensures the stability of the interaction between the robot and an environment. In this experiment, the robot is tested under impact force to verify the system's robustness in the sense of withstanding external impacts. During the experiment, there is no human subject worn the exoskeleton. The impact force is applied at the foot segment of the exoskeleton while it is fixed at a certain position (at hip, knee, and ankle angle of 0.703, 0.097, and 0.0 rad, resp.). The intensity of the impact force is high enough to reach the torque limit of at least one of the robot joints within a short period of time (torque limits for hip, knee, and ankle joints are 50, 20, and 10  $\text{N}\cdot\text{m}$ , resp.). The impedance control gains used in this experiment are referred to Table 7.

As seen in Figure 6, during the impact, hip, knee, and ankle angles deviate from the desired fixed position. Some robot joints generate torque at their maximum limit during the impact. Even though, the robot joint torque reaches the maximum limit as illustrated by flat peaks of torque signals, the robot joints finally get back to the desired position after few oscillations. This experiment has shown that the system is robust to external large impact force. Moreover, it confirms the stability of the system when interacting to an environment.

## 5. Experiment by a Healthy Subject with Various Training Activities

**5.1. Method.** To train a human subject with the robot as shown in Figure 7, the subject has to sit on a chair with an adjustable inclination backseat next to the control unit. Next,

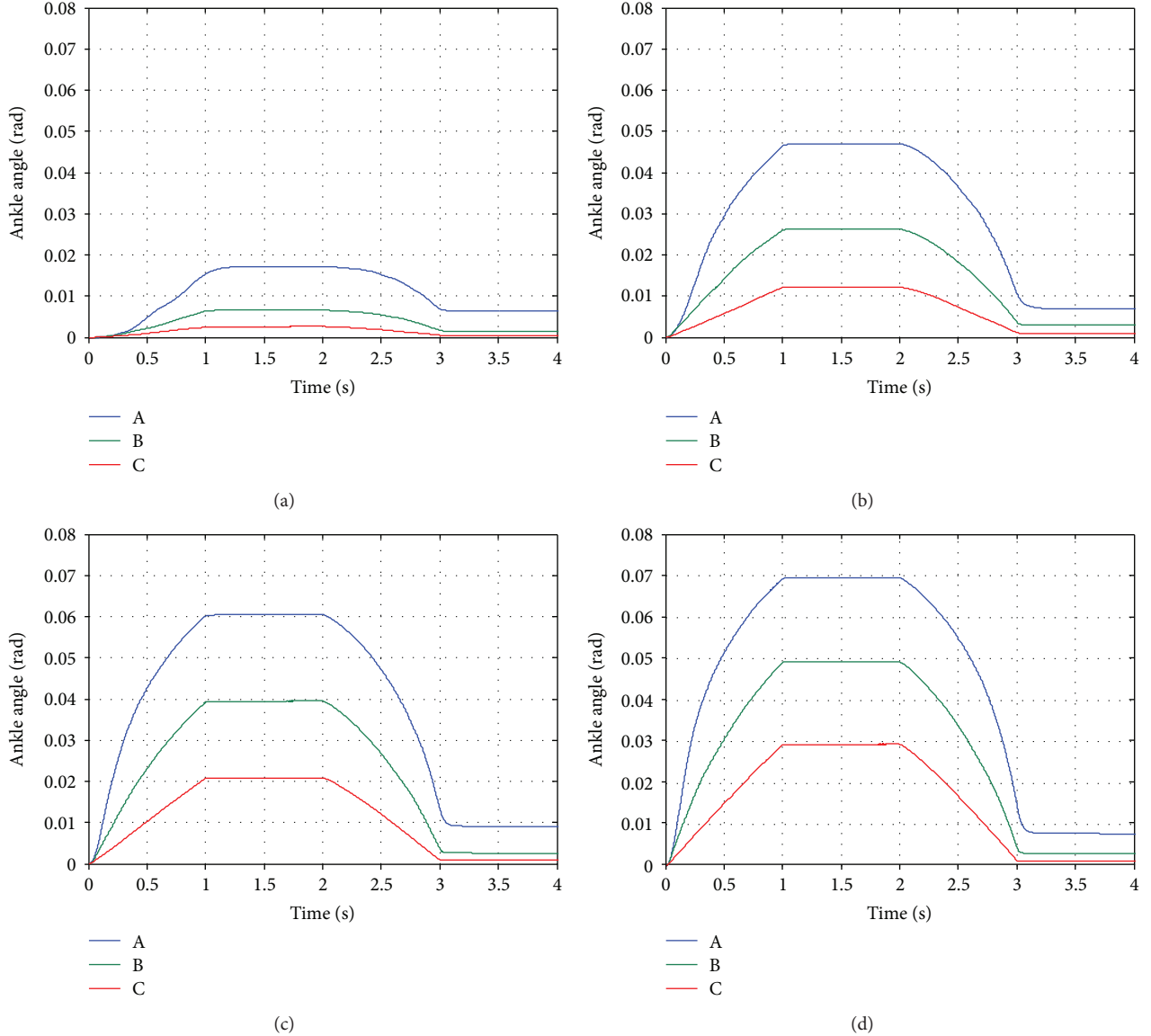


FIGURE 5: Response of robot's ankle joint implemented with the controllers A, B, and C as a result from the disturbance torque with maximum magnitude of (a) 1.0 N·m, (b) 4.0 N·m, (c) 7.0 N·m, and (d) 10.0 N·m.

TABLE 7: Impedance control gains for hip, knee, and ankle joints in low, medium, and high assistance mode.

Joint	Low assistance mode			Medium assistance mode			High assistance mode		
	$K_1$	$K_2$	$K_d$	$K_1$	$K_2$	$K_d$	$K_1$	$K_2$	$K_d$
Hip	0.44	67.62	5.0	1.38	72.30	5.0	3.20	93.67	5.0
Knee	0.59	50.71	4.0	2.14	46.73	4.0	6.29	47.65	4.0
Ankle	0.81	37.01	2.0	3.98	25.13	2.0	43.42	6.91	2.0

lengths of the exoskeleton segments are adjusted so that the robot fits on the subject's leg where the axes of hip, knee, and ankle joints of the subject are aligned with robot joint axes. Then, Velcro straps are used to fasten the subject's leg and the exoskeleton together at thigh, shank, and foot segments.

Before the training session, the reference path must be defined by teaching the robot. By manually moving the exoskeleton (and the subject's leg) to the starting point of the desired movement, the robot operator can use the user interface shown on the monitor screen to record the current joint position of the robot. The next points of the desired movement are also obtained while moving the exoskeleton and recording a sequence of the desired position. When the teaching is done, the reference path for the training is generated by connecting a series of the selected points with straight lines. The desired joint angles are linearly interpolated between a selected point and the consecutive point. The repetition of the path can be selected as moving back and forth or as a cycle (the last point connected to the first point). The desired path can be generated to perform various

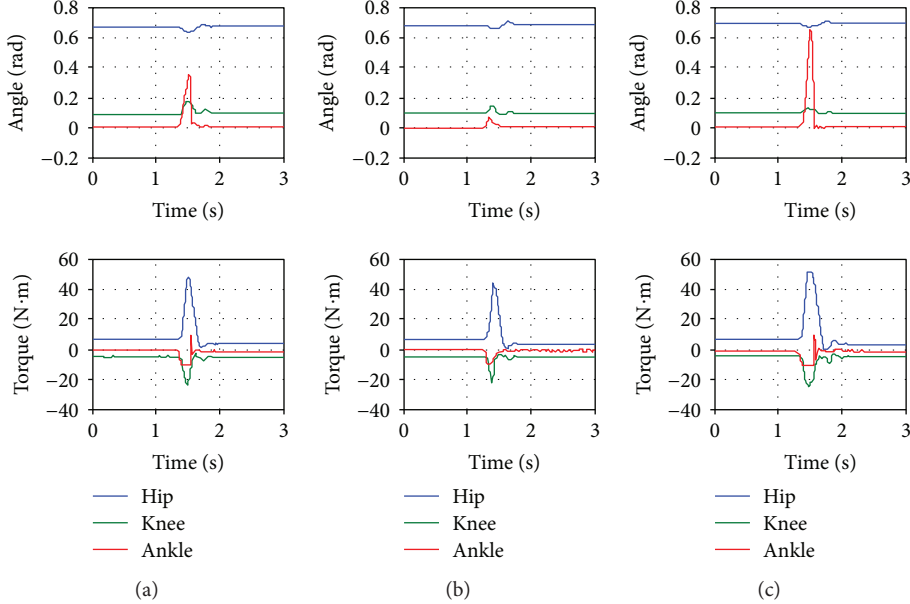


FIGURE 6: Response of the robot due to external impact force with control gains for (a) low assistance mode, (b) medium assistance mode, and (c) high assistance mode.



FIGURE 7: Training a subject with the robot.

training activities both single-joint and multiple-joint training. Figure 8 presents the reference path of seated marching exercise (for hip flexion exercise), the single-joint training at knee and ankle joint, and cycling exercise both in joint space and Cartesian space. The virtual leg of the subject is illustrated as triangles for thigh (pink), shank (blue), and foot (yellow) segments. It is displayed on the monitor screen as a visual feedback to the subject while tracking the reference trajectory.

Once the reference trajectory is generated, the operator must select the trajectory speed and assistance level. When the training starts, the reference position moves from the first point to the last point along the reference path and repeats the movement. Actual joint angle and torque are recorded at the frequency of 100 Hz and shown on the monitor screen. The training session continues until the “stop” button on the user interface is pressed.

In this study, a preliminary experiment was conducted on a volunteered healthy subject (male, age 28 years, weight 65 kg, height 168 cm, and without history of

neurological disorder). The training activities include seated marching exercise, training at knee and ankle joints, and cycling training whose reference paths are shown in Figure 8. The subject is informed to keep tracking the reference trajectory, which is shown on a monitor screen along with the current position of the robot, as much as possible. Speed of the trajectories in Cartesian space is set as a constant throughout the training. However, for the single-joint training, when reaching the first and the last point of the reference path, the movement is paused for one second. Each training consists of 8 cycles of movement. Control gains  $K_1$ ,  $K_2$ , and  $K_d$  used in this experiment are referred to Table 7.

**5.2. Statistical Data Analysis.** The data of the movement is separated into data from each cycle. Time spent on a cycle is normalized so that 0% represents the start of the cycle and 100% is the end of the cycle. Average angle ( $\bar{\theta}_{i\%}$ ) and assistance torque ( $\bar{T}_{i\%}$ ) at  $i\%$  of a movement cycle are calculated from

$$\bar{\theta}_{i\%} = \frac{\sum_{j=1}^n \theta_{i\%}^j}{n}, \quad (9)$$

$$\bar{T}_{i\%} = \frac{\sum_{j=1}^n T_{i\%}^j}{n},$$

where  $n$  is the number of movement cycles which is equal to 8 for this experiment, and  $\theta_{i\%}^j$  and  $T_{i\%}^j$  are angle and torque at  $i\%$  of the  $j^{\text{th}}$  cycle. The average data profile is obtained by connecting average angle from 0% to 100%.

The root mean square value is chosen as the representative of the average data in a movement cycle. The root mean square error ( $e_{\theta_{\text{ref}} - \bar{\theta}_{\text{rms}}}$ ) between the reference

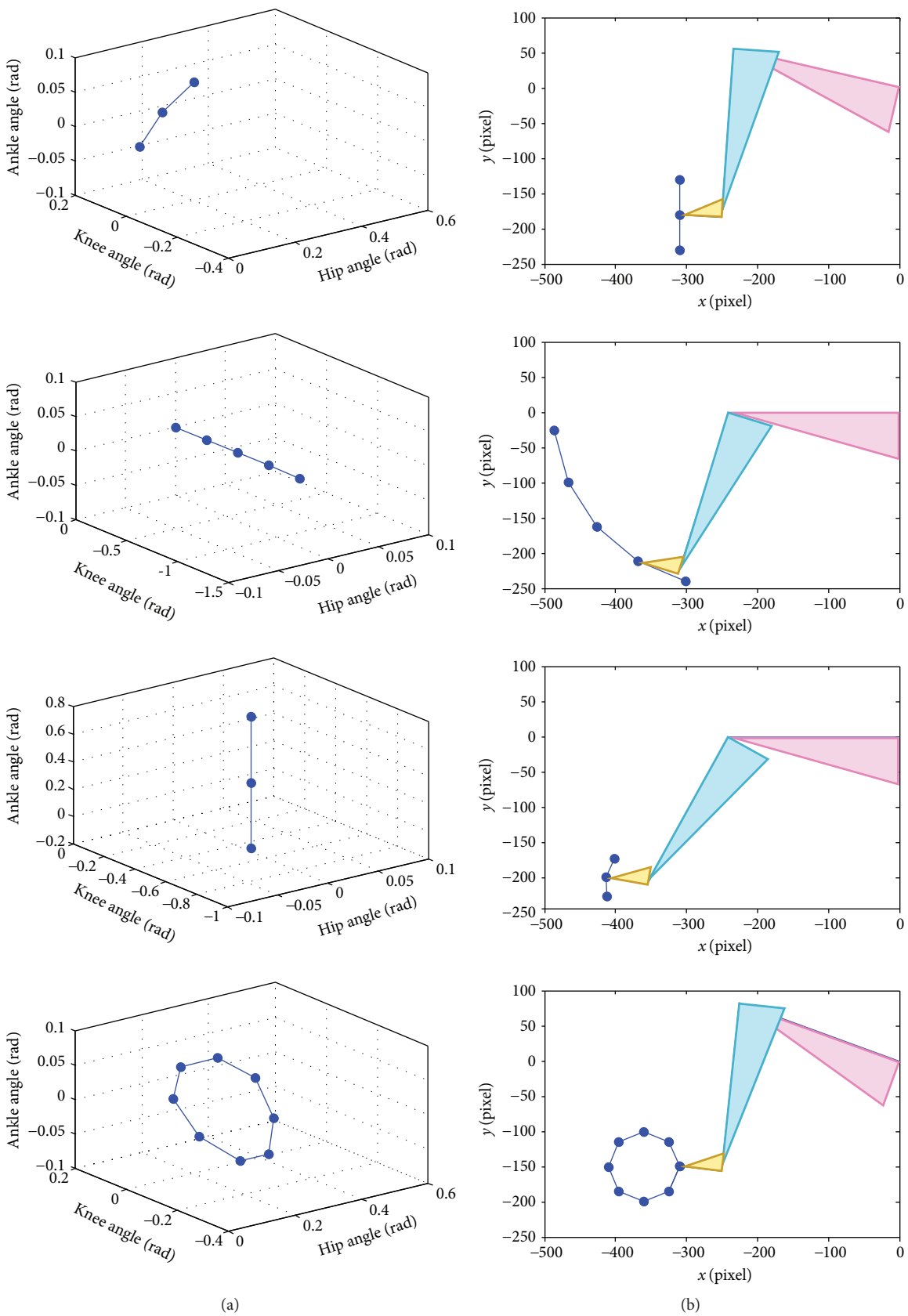


FIGURE 8: Reference paths for seated marching exercise, the single-joint training at knee and ankle joint, and cycling exercise in (a) joint space and (b) Cartesian space.

trajectory ( $\theta_{\text{ref}}$ ) and the average trajectory ( $\bar{\theta}$ ) is computed as follows:

$$e_{\theta_{\text{ref}}, \bar{\theta}, \text{rms}} = \sqrt{\frac{\sum_{k=1}^N (\theta_{\text{ref},i\%} - \bar{\theta}_{i\%})^2}{N}}, \quad (10)$$

where  $N$  is the number of data in one cycle of movement (index  $k = 1$  and  $k = N$  refers to data at 0% and 100%). Note that the reference trajectory is the same in every movement cycle, so  $\theta_{\text{ref},i\%}$  is not averaged.

To determine the deviation between the trajectory of each movement cycle and the average trajectory, another error that compares the angle of the  $j^{\text{th}}$  cycle to the average angle at  $i\%$  ( $e_{\theta-\bar{\theta},i\%}^j$ ) is described by

$$e_{\theta-\bar{\theta},i\%}^j = \theta_{i\%}^j - \bar{\theta}_{i\%}^j. \quad (11)$$

The root mean square error of the  $j^{\text{th}}$  cycle ( $e_{\theta-\bar{\theta}, \text{rms}}^j$ ) is

$$e_{\theta-\bar{\theta}, \text{rms}}^j = \sqrt{\frac{\sum_{k=1}^N (e_{\theta-\bar{\theta},i\%}^j)^2}{N}}. \quad (12)$$

The standard deviation of the root mean square error ( $SD_{e_{\theta-\bar{\theta}, \text{rms}}^j}$ ) is calculated to identify the variation of data from 8 movement cycles:

$$SD_{e_{\theta-\bar{\theta}, \text{rms}}} = \sqrt{\frac{\sum_{j=1}^n (e_{\theta-\bar{\theta}, \text{rms}}^j - \bar{e}_{\theta-\bar{\theta}, \text{rms}})^2}{n}}, \quad (13)$$

where

$$\bar{e}_{\theta-\bar{\theta}, \text{rms}} = \frac{\sum_{j=1}^n e_{\theta-\bar{\theta}, \text{rms}}^j}{n}. \quad (14)$$

The root mean square average torque ( $\bar{T}_{\text{rms}}$ ) is derived as follows:

$$\bar{T}_{\text{rms}} = \sqrt{\frac{\sum_{k=1}^N (\bar{T}_{i\%})^2}{N}}, \quad (15)$$

where  $\bar{T}_{i\%}$  is the torque averaged from 8 movement cycles at  $i\%$ . The root mean square average torque is a good representation showing the amount of assistance torque provided to a subject because the value of positive and negative sign is not canceled out. The direction of the assistance torque can be observed from the average torque profile.

### 5.3. Results

**5.3.1. Seated Marching Exercise.** In Figure 9, the average hip trajectory and torque obtained from 8 movement cycles and 3 different assistance levels are shown with respect to movement cycle percentage (0% and 100% represent the start and the end of each movement cycle). The movement starts by performing hip flexion (increasing hip angle) and pauses for one second (constant maximum hip angle) and then performing hip extension (decreasing hip angle) and

pauses for another one second (constant minimum hip angle to complete the cycle). One cycle of the movement takes 9.45 seconds.

According to Table 8, the training with low assistance has the highest angle error. In Figure 9, the average trajectory of low assistance training has the largest deviation from the reference trajectory while the average trajectory of medium and high assistance training is closer to the reference trajectory, respectively. The variation of the actual trajectory in 8 movement cycles as compared to the average trajectory can be identified by the standard deviation. It is noticed from Table 8 that the highest variation is found in the training with low assistance. Moreover, the average assistance torque during the training with low assistance also has the lowest magnitude. It can also be seen in Figure 9(b) that the torque profiles in low, medium, and high assistance training are similar when compared at each percentage of the movement cycle.

**5.3.2. Training at Knee Joint.** Figure 10 shows the average knee angle and torque during the training at knee joint. The movement starts by performing knee extension (decreasing knee angle) and pauses for one second (constant minimum knee angle) and then performing knee flexion (increasing knee angle) and ends after another one-second pause (constant maximum knee angle). Hip and ankle joints do not move, so their reference angles are fixed at zero. One cycle of the movement takes 24.43 seconds.

As shown in Table 9, the low assistance training has the highest error between the average and the reference trajectory. The standard deviation which shows variation of the actual trajectory in 8 movement cycles compared to the average trajectory is highest in the low assistance training. Besides, the lowest magnitude of average assistance torque is found in the low assistance training. As seen from Figure 10(b), the shapes of torque profiles are similar in low, medium, and high assistance training.

**5.3.3. Training at Ankle Joint.** The average ankle angle and torque during the training are shown in Figure 11. The movement starts from performing ankle plantar flexion (increasing ankle angle) and pauses for one second and then performing ankle dorsiflexion (decreasing ankle angle) and pauses for another one second. During the training, the knee angle is fixed at a negative constant angle to avoid the foot slapping on the floor. One cycle of the movement takes 6.13 seconds.

According to Table 10, the highest error between the average and the reference trajectory is found in the low assistance training. Large variation of the actual trajectory in 8 movement cycles compared to the average trajectory also occurs in the low assistance training. Moreover, the robot provides the lowest average assistance torque to the subject in low assistance training. It could be noticed that the variations of the movement in the medium and high assistance are similar. The torque profiles in low, medium, and high assistance as shown in Figure 11(b) are also resemblant.

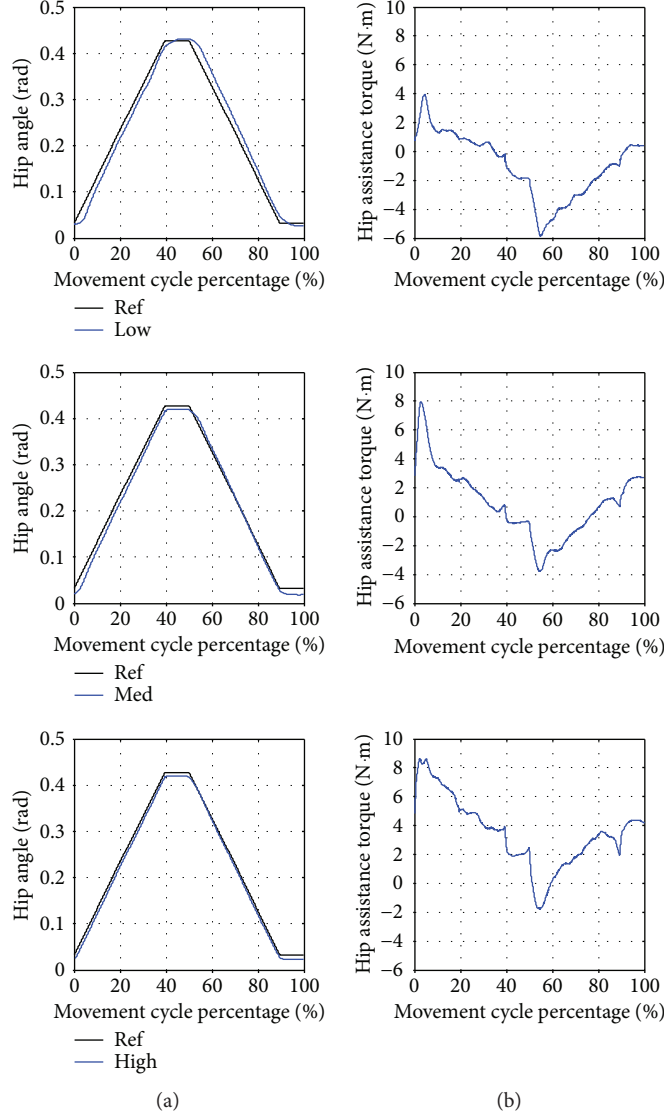


FIGURE 9: Seated marching exercise with low (Low), medium (Med), and high (High) assistance. (a) Average hip angle compared to the reference trajectory (Ref.). (b) Average hip assistance torque.

TABLE 8: Statistical data of the hip joint from the seated marching exercise.

Level of assistance	$e_{\theta_{ref}-\bar{\theta}_{rms}}$ (rad)	$SD_{e_{\theta_{ref}-\bar{\theta}_{rms}}}$ ( $\times 10^{-4}$ rad)	$\bar{T}_{rms}$ (N·m)
Low	0.0198	28.31	2.40
Medium	0.0123	11.04	2.57
High	0.0090	6.55	4.25

**5.3.4. Cycling Exercise.** In Figure 12, the average angle and assistance torque of hip, knee, and ankle joints are compared when training with low, medium, and high assistance level. As noticed from Figure 13(b), the starting point of the movement is located at  $(x, y) = (-310 \text{ pixel}, -150 \text{ pixel})$  and the direction of the movement is counterclockwise around the center of the circle located at  $(x, y) = (-360 \text{ pixel}, -150 \text{ pixel})$ .

The cycling reference trajectory includes the movement of hip and knee joints while the ankle angle is fixed at zero. The reference trajectory is created from straight lines connecting reference points to the consecutive points. The movement is continuous, so there is no pause in a movement cycle. One cycle of movement takes 11.45 seconds.

As noticed from Table 11, the highest error between the average and reference trajectory almost occurs in the training with low assistance. High variation of the movement is also likely to be found in the low assistance training compared to the medium and high assistance training. Furthermore, the average assistance torque applied by the robot is usually low in the low assistance training while the medium and high assistance training tend to generate higher magnitude of assistance torque. It can be seen from Figure 12(b) that the shapes of torque profiles for low, medium, and high assistance are similar. Figure 13 compares the average trajectory to the reference trajectory when the subject trained with

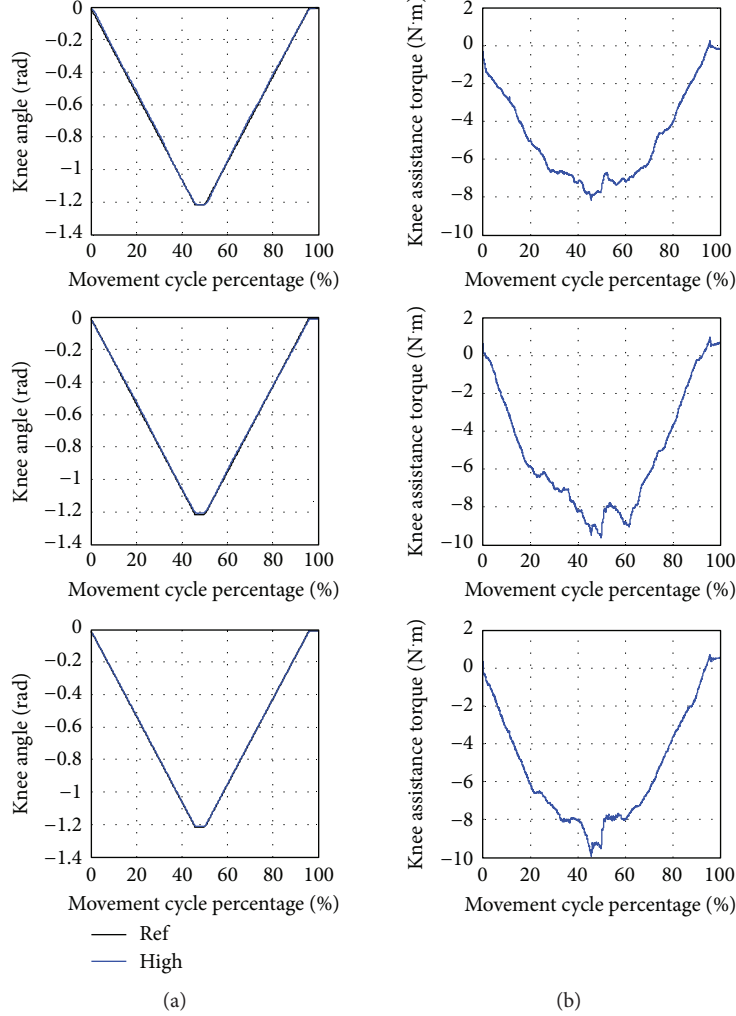


FIGURE 10: Training at knee joint with low (Low), medium (Med), and high (High) assistance. (a) Average knee angle compared to the reference trajectory (Ref). (b) Average knee assistance torque.

TABLE 9: Statistical data from the training at knee joint.

Level of assistance	$e_{\theta_{ref}-\bar{\theta}_{rms}}$ (rad)	$SD_{e_{\theta_{ref}-\bar{\theta}_{rms}}}$ ( $\times 10^{-4}$ rad)	$\bar{T}_{rms}$ (N·m)
Low	0.0107	23.26	5.35
Medium	0.0077	16.97	5.97
High	0.0033	9.00	6.05

low, medium, and high assistance. The average trajectories as seen in joint space and Cartesian space are closed to the reference trajectory with some degree of angle error.

**5.3.5. Discussion.** The experiment has shown that the robot is able to train the subject with many activities and levels of assistance. The subject can track the reference trajectories with some angle errors. The magnitude of the error is usually high in low assistance training followed by medium and high assistance training.

The variation of the movement can be determined from the standard deviation which derived from the comparison between the actual trajectories in 8 movement cycles and the average trajectory. It was found that the low assistance training is likely to have the highest movement variation for hip, knee, and ankle joints in any training activities. In other words, the subject has more freedom to move on his own in the low assistance, even though the patterns of the movement in each cycles are not consistent.

The average magnitude of assistance torque is usually lowest in the low assistance training. Shapes of the torque profiles for low, medium, and high assistance are similar when comparing at each movement cycle percentage. It could be seen that there are abrupt changes of the torque profile in the seated marching exercise and the single-joint training at knee and ankle joints at the transitions before and after the movement pauses. These might result from the speed of the trajectory which is set as a constant and absence of smooth changes at these transitions. Assistance torque changes rapidly in order to create acceleration/deceleration for stopping or initiating the movement. These abrupt

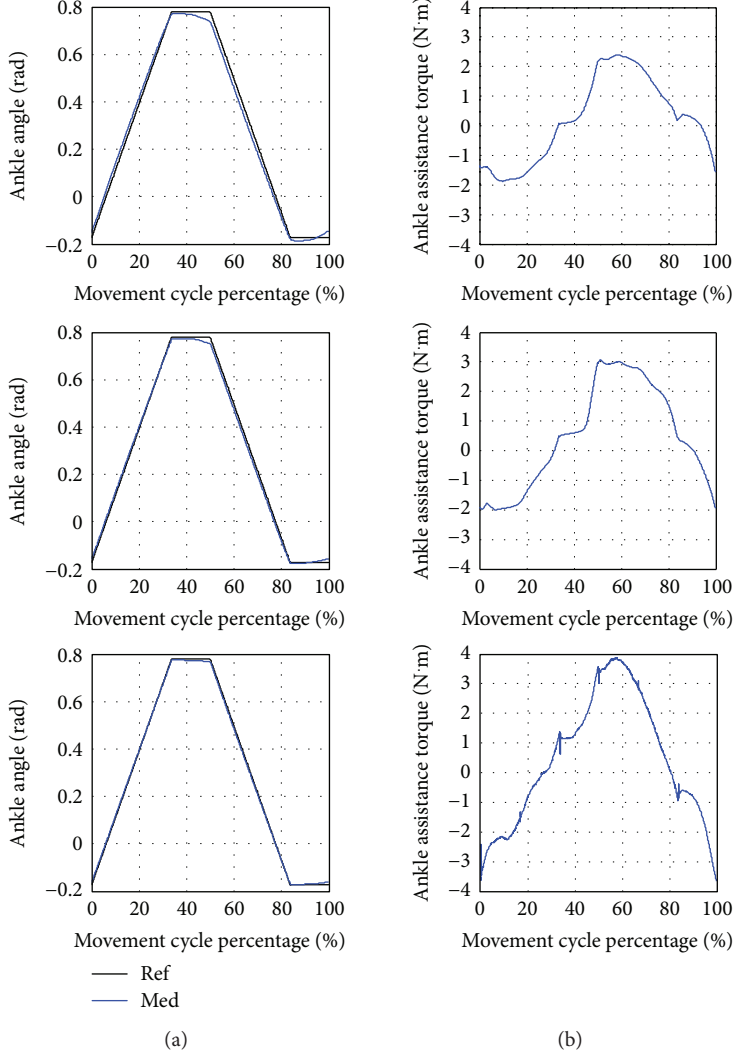


FIGURE 11: Training at ankle joint with low (Low), medium (Med), and high (High) assistance. (a) Average ankle angle compared to the reference trajectory (Ref). (b) Average ankle assistance torque.

TABLE 10: Statistical data from the training at ankle joint.

Level of assistance	$e_{\theta_{ref} - \bar{\theta}, rms}$ (rad)	$SD e_{\theta_{ref} - \bar{\theta}, rms} (\times 10^{-4})$ rad)	$\bar{T}_{rms}$ (N·m)
Low	0.0253	19.56	1.4
Medium	0.0141	4.42	1.81
High	0.0071	5.00	2.15

changes are also found in the cycling exercise when changing the reference point. Although the speed remains constant, the direction of the movement changes at the reference points. Thus, assistance torque changes suddenly in order to create acceleration for changing the direction of the movement at these transitions.

## 6. Conclusion

Lower limb rehabilitation robots in sitting position have been researched extensively. Rehabilitation robots were developed

into many types and targeted at different degrees of freedom for the physical therapy. Training activities performed by these robots differ according to robot's configuration and the selection of training modalities. These activities can be categorized as single-joint and multiple-joint training. The single-joint training focuses on the movement of an individual joint such as hip, knee, or ankle joint. On the other hand, the multiple-joint training associates the movement of many joints in the same time so that a variety of exercises such as leg press, cycling, gait trajectory following, or customized movement could be performed. Some robots were developed to perform a specific training activity while the others are able to perform several training activities.

A lower limb rehabilitation robot in sitting position for stroke patients was developed in the previous research. It has three degrees of freedom at hip, knee, and ankle joints which allow movements of lower limbs in sagittal plane. This robot is able to perform many training activities and modalities. The control system for active assistive exercise is described in detail. The impedance control law implemented

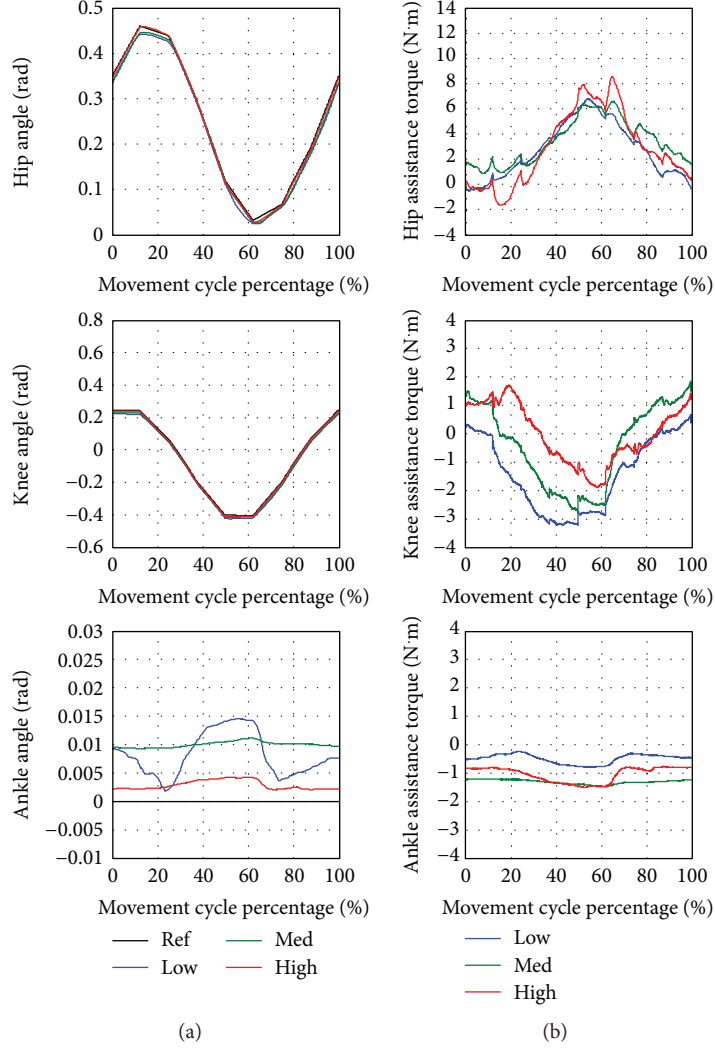


FIGURE 12: Cycling exercise with low (Low), medium (Med), and high (High) assistance. (a) Average hip, knee, and ankle angle compared to the reference trajectory (Ref). (b) Average hip, knee, and ankle assistance torque.

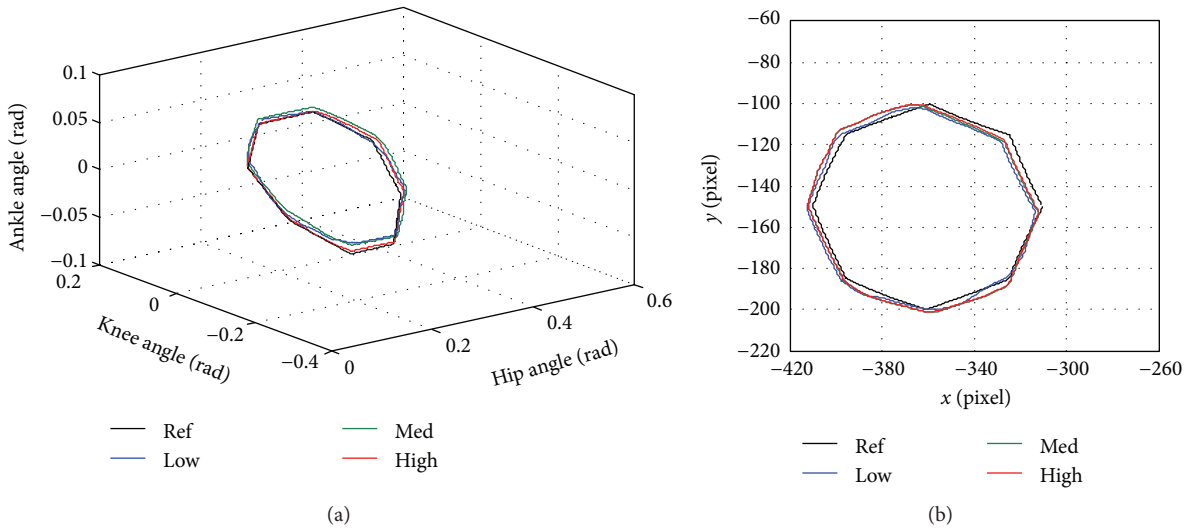


FIGURE 13: Cycling trajectory compared to the reference trajectory (Ref) with low (Low), medium (Med), and high (High) assistance in (a) joint space and (b) Cartesian space.

TABLE 11: Statistical data from the cycling training.

Statistical data	Low assistance			Medium assistance			High assistance		
	$e_{\theta_{ref}-\bar{\theta},rms}$ (rad)	$SD_{e_{\theta-\bar{\theta},rms}}$ ( $\times 10^{-4}$ rad)	$\bar{T}_{rms}$ (N·m)	$e_{\theta_{ref}-\bar{\theta},rms}$ (rad)	$SD_{e_{\theta-\bar{\theta},rms}}$ ( $\times 10^{-4}$ rad)	$\bar{T}_{rms}$ (N·m)	$e_{\theta_{ref}-\bar{\theta},rms}$ (rad)	$SD_{e_{\theta-\bar{\theta},rms}}$ ( $\times 10^{-4}$ rad)	$\bar{T}_{rms}$ (N·m)
Hip	0.0125	25.31	3.50	0.0104	8.76	3.82	0.0041	9.14	4.11
Knee	0.0199	29.76	1.91	0.0150	6.91	1.50	0.0073	2.82	1.02
Ankle	0.0090	13.09	0.52	0.0100	1.29	1.31	0.0030	2.82	1.08

by the developed rehabilitation robot uses two constants to define the relationship between angle error and desired torque to be generated by a robot joint. With the damping term in the impedance control law, the passivity property of the system is verified. These control gains are chosen based on the initial rate of change of desired torque, maximum allowable angle error and torque. Different sets of control gains result in different robot response due to disturbance torque. The robot is also tested under impact force to prove its robustness. The experiment conducted on a healthy subject has shown that the robot is able to perform many training activities such as seated marching exercise, single-joint training at knee and ankle joints, and cycling exercise with active assistive training modality and with many levels of assistance. It is found that low assistance training usually produces the highest error between the average trajectory and the reference trajectory. This implies that the subject is not restricted to move exactly along the reference trajectory. The standard deviation is derived by comparing the movement in each cycle to the average trajectory so that the variation of the movement could be investigated. The greatest movement variation is likely to be found in low assistance training than in medium and high assistance training. High angle deviation and movement variation in low assistance training imply that the subject could move the limbs with more freedom. The assistance torque is provided by the robot to ensure the completion of the movement. It is also found that the low assistance training usually generates the lowest magnitude of the assistance torque. Abrupt changes in assistance torque, which can be noticed in each training activity, result from the rapid change in speed and direction of the reference trajectory.

In future research, the movement of the robot at the transitions should be improved by smoothing the change in speed and direction at the transitions. Clinical trials should be conducted on stroke patients to verify the effectiveness of the robot and control system for stroke rehabilitation task.

## Conflicts of Interest

The authors declare that there is no conflict of interest regarding the publication of this paper.

## Acknowledgments

This research work is a part of the project supported by the National Research University Project, Office of Higher Education Commission, Project nos. WCU-013-HR-57 and CU-59-005-IC and also supported by the Research Pyramid

and Chula Research Scholar project, the Second Century Research Policy of Chulalongkorn University, 2016–2018, and the 100th Anniversary Chulalongkorn University Fund for Doctoral Scholarship.

## References

- [1] G. Colombo, M. Joerg, R. Schreier, and V. Dietz, "Treadmill training of paraplegic patients using a robotic orthosis," *Journal of Rehabilitation Research and Development*, vol. 37, no. 6, pp. 693–700, 2000.
- [2] E. Akdogan and M. A. Adli, "The design and control of a therapeutic exercise robot for lower limb rehabilitation: Physiotherabot," *Mechatronics*, vol. 21, no. 3, pp. 509–522, 2011.
- [3] W. Meng, Q. Liu, Z. Zhou, Q. Ai, B. Sheng, and S. Xie, "Recent development of mechanisms and control strategies for robot-assisted lower limb rehabilitation," *Mechatronics*, vol. 31, pp. 132–145, 2015.
- [4] I. Díaz, J. J. Gil, and E. Sánchez, "Lower-limb robotic rehabilitation: literature review and challenges," *Journal of Robotics*, vol. 2011, 11 pages, 2011.
- [5] B. Guo, J. Han, X. Li, T. Fang, and A. You, "Research and design of a new horizontal lower limb rehabilitation training robot," *International Journal of Advanced Robotic Systems*, vol. 13, no. 1, pp. 10–10, 2016.
- [6] J. A. Galvez, A. Budovitch, S. J. Harkema, and D. J. Reinkensmeyer, "Trainer variability during step training after spinal cord injury: implications for robotic gait-training device design," *The Journal of Rehabilitation Research and Development*, vol. 48, no. 2, pp. 147–160, 2011.
- [7] J. Yoon, J. Ryu, and K.-B. Lim, "Reconfigurable ankle rehabilitation robot for various exercises," *Journal of Robotic Systems*, vol. 22, no. S1, pp. S15–S33, 2006.
- [8] F. Zhang, Z. G. Hou, L. Cheng et al., "iLeg—a lower limb rehabilitation robot: a proof of concept," *IEEE Transactions on Human-Machine Systems*, vol. 46, no. 5, pp. 761–768, 2016.
- [9] T. B. Pasqual, G. A. P. Caurin, and A. A. G. Siqueira, "Serious game development for ankle rehabilitation aiming at user experience," in *2016 6th IEEE International Conference on Bio-medical Robotics and Biomechatronics (BioRob)*, Singapore, June 2016.
- [10] A. Mirelman, B. L. Patritti, P. Bonato, and J. E. Deutsch, "Effects of virtual reality training on gait biomechanics of individuals post-stroke," *Gait & Posture*, vol. 31, no. 4, pp. 433–437, 2010.
- [11] W. Wang, Z. G. Hou, L. Tong, F. Zhang, Y. Chen, and M. Tan, "A novel leg orthosis for lower limb rehabilitation robots of the sitting/lying type," *Mechanism and Machine Theory*, vol. 74, pp. 337–353, 2014.
- [12] A. B. Farjadian, M. Nabian, C. Mavroidis, and M. K. Holden, "Implementation of a task-dependent anisotropic impedance

- controller into a 2-DOF platform-based ankle rehabilitation robot," in *2015 IEEE International Conference on Robotics and Automation (ICRA)*, Seattle, WA, USA, May 2015.
- [13] D. A. Brown, S. Nagpal, and S. Chi, "Limb-loaded cycling program for locomotor intervention following stroke," *Physical Therapy*, vol. 85, no. 2, pp. 159–168, 2005.
  - [14] J. C. Grotta, G. W. Albers, J. P. Broderick et al., *Stroke: Pathophysiology, Diagnosis, and Management*, Elsevier, China, 6th edition, 2016.
  - [15] A. Basteris, S. M. Nijenhuis, A. H. A. Stienen, J. H. Buurke, G. B. Prange, and F. Amirabdollahian, "Training modalities in robot-mediated upper limb rehabilitation in stroke: a framework for classification based on a systematic review," *Journal of Neuroengineering and Rehabilitation*, vol. 11, no. 1, pp. 111–115, 2014.
  - [16] H. I. Krebs, J. J. Palazzolo, L. Dipietro et al., "Rehabilitation robotics: performance-based progressive robot-assisted therapy," *Autonomous Robots*, vol. 15, no. 1, pp. 7–20, 2003.
  - [17] H. M. Clarkson, *Musculoskeletal Assessment: Joint Motion and Muscle Testing*, Wolters Kluwer/Lippincott Williams & Wilkins Health, China, 3rd edition, 2013.
  - [18] T. Eiammanussakul and V. Sangveraphunsiri, "Lower limb rehabilitation robot in sitting position for various therapeutic exercises," in *2017 in Proceedings of the 9th International Conference on Bioinformatics and Biomedical Technology - ICBBT '17*, pp. 112–116, Lisbon, Portugal, May 2017.
  - [19] A. Roy, H. I. Krebs, D. J. Williams et al., "Robot-aided neurorehabilitation: a novel robot for ankle rehabilitation," *IEEE Transactions on Robotics*, vol. 25, no. 3, pp. 569–582, 2009.
  - [20] F. Chrif, T. Nef, M. Lungarella, R. Dravid, and K. J. Hunt, "Control design for a lower-limb paediatric therapy device using linear motor technology," *Biomedical Signal Processing and Control*, vol. 38, pp. 119–127, 2017.
  - [21] K. J. Chisholm, K. Klumper, A. Mullins, and M. Ahmadi, "A task oriented haptic gait rehabilitation robot," *Mechatronics*, vol. 24, no. 8, pp. 1083–1091, 2014.
  - [22] A. Kamps and K. Schüle, "Cyclic movement training of the lower limb in stroke rehabilitation," *Neurologie & Rehabilitation*, vol. 11, no. 5, pp. S1–S12, 2005.
  - [23] R. N. Goodman, J. C. Rietschel, A. Roy et al., "Increased reward in ankle robotics training enhances motor control and cortical efficiency in stroke," *Journal of Rehabilitation Research and Development*, vol. 51, no. 2, pp. 213–228, 2014.
  - [24] L. W. Forrester, A. Roy, H. I. Krebs, and R. F. Macko, "Ankle training with a robotic device improves hemiparetic gait after a stroke," *Neurorehabilitation and Neural Repair*, vol. 25, no. 4, pp. 369–377, 2011.
  - [25] A. Roy, L. W. Forrester, and R. F. Macko, "Short-term ankle motor performance with ankle robotics training in chronic hemiparetic stroke," *The Journal of Rehabilitation Research and Development*, vol. 48, no. 4, pp. 417–429, 2011.
  - [26] E. Badics, A. Wittmann, M. Rupp, B. Stabauer, and U. A. Zifko, "Systematic muscle building exercises in the rehabilitation of stroke patients," *NeuroRehabilitation*, vol. 17, no. 3, pp. 211–214, 2002.
  - [27] J. Vinstrup, J. Calatayud, M. D. Jakobsen et al., "Electromyographic comparison of conventional machine strength training versus bodyweight exercises in patients with chronic stroke," *Topics in Stroke Rehabilitation*, vol. 24, no. 4, pp. 242–249, 2016.
  - [28] S. M. Son, M. K. Park, and N. K. Lee, "Influence of resistance exercise training to strengthen muscles across multiple joints of the lower limbs on dynamic balance functions of stroke patients," *Journal of Physical Therapy Science*, vol. 26, no. 8, pp. 1267–1269, 2014.
  - [29] R. Fernandez-Gonzalo, C. Nissemark, B. Åslund, P. A. Tesch, and P. Sojka, "Chronic stroke patients show early and robust improvements in muscle and functional performance in response to eccentric-overload flywheel resistance training: a pilot study," *Journal of Neuroengineering and Rehabilitation*, vol. 11, no. 1, pp. 150–110, 2014.
  - [30] S. J. Kim, H. Y. Cho, Y. L. Kim, and S. M. Lee, "Effects of stationary cycling exercise on the balance and gait abilities of chronic stroke patients," *Journal of Physical Therapy Science*, vol. 27, no. 11, pp. 3529–3531, 2015.
  - [31] D. Barbosa, C. P. Santos, and M. Martins, "The application of cycling and cycling combined with feedback in the rehabilitation of stroke patients: a review," *Journal of Stroke and Cerebrovascular Diseases*, vol. 24, no. 2, pp. 253–273, 2015.
  - [32] D. A. Winter, *Biomechanics and Motor Control of Human Movement*, John Wiley & Sons Inc, USA, 4th edition, 2009.
  - [33] A. Sutapun and V. Sangveraphunsiri, "A 4-DOF upper limb exoskeleton for stroke rehabilitation: kinematics mechanics and control," *International Journal of Mechanical Engineering and Robotics Research*, vol. 4, no. 3, pp. 269–272, 2015.
  - [34] M. D. Lewek, T. H. Cruz, J. L. Moore, H. R. Roth, Y. Y. Dhaher, and T. G. Hornby, "Allowing intralimb kinematic variability during locomotor training poststroke improves kinematic consistency: a subgroup analysis from a randomized clinical trial," *Physical Therapy*, vol. 89, no. 8, pp. 829–839, 2009.
  - [35] A. Duschau-Wicke, J. von Zitzewitz, A. Caprez, L. Lünenburger, and R. Riener, "Path control: a method for patient-cooperative robot-aided gait rehabilitation," *IEEE Transactions on Neural Systems and Rehabilitation Engineering*, vol. 18, no. 1, pp. 38–48, 2010.
  - [36] A. Pennycott, D. Wyss, H. Vallery, V. Klamroth-Marganska, and R. Riener, "Towards more effective robotic gait training for stroke rehabilitation: a review," *Journal of Neuroengineering and Rehabilitation*, vol. 9, no. 1, p. 65, 2012.
  - [37] B. M. Fleerkotte, B. Koopman, J. H. Buurke, E. H. F. van Asseldonk, H. van der Kooij, and J. S. Rietman, "The effect of impedance-controlled robotic gait training on walking ability and quality in individuals with chronic incomplete spinal cord injury: an explorative study," *Journal of Neuroengineering and Rehabilitation*, vol. 11, no. 1, p. 26, 2014.
  - [38] S. K. Banala, S. K. Agrawal, and J. P. Scholz, "Active leg exoskeleton (ALEX) for gait rehabilitation of motor-impaired patients," in *2007 IEEE International Conference on Rehabilitation Robotics*, pp. 401–407, Noordwijk, Netherlands, June 2007.
  - [39] X. Jin, X. Cui, and S. K. Agrawal, "Design of a cable-driven active leg exoskeleton (C-ALEX) and gait training experiments with human subjects," in *2015 IEEE International Conference on Robotics and Automation (ICRA)*, pp. 5578–5583, Seattle, WA, USA, May 2015.
  - [40] J. J. E. Slotine and W. Li, *Applied Nonlinear Control*, Prentice-Hall Inc., USA, 1st edition, 1991.

## Review Article

# A Review of Robotics in Neurorehabilitation: Towards an Automated Process for Upper Limb

E. D. Oña<sup>1</sup>, R. Cano-de la Cuerda<sup>1</sup>, P. Sánchez-Herrera,<sup>2</sup> C. Balaguer,<sup>1</sup> and A. Jardón<sup>1</sup>

<sup>1</sup>*Robotics Lab, Department of Systems Engineering and Automation, University Carlos III of Madrid, Avda. de la Universidad 30, 28911 Leganés, Madrid, Spain*

<sup>2</sup>*Department of Physical Therapy, Occupational Therapy, Physical Medicine and Rehabilitation, University King Juan Carlos, Avda. de Atenas s/n, 28922 Alcorcón, Madrid, Spain*

Correspondence should be addressed to E. D. Oña; eona@ing.uc3m.es

Received 17 November 2017; Revised 26 January 2018; Accepted 8 February 2018; Published 1 April 2018

Academic Editor: Carlo Ferraresi

Copyright © 2018 E. D. Oña et al. This is an open access article distributed under the Creative Commons Attribution License, which permits unrestricted use, distribution, and reproduction in any medium, provided the original work is properly cited.

Robot-mediated neurorehabilitation is a growing field that seeks to incorporate advances in robotics combined with neuroscience and rehabilitation to define new methods for treating problems related with neurological diseases. In this paper, a systematic literature review is conducted to identify the contribution of robotics for upper limb neurorehabilitation, highlighting its relation with the rehabilitation cycle, and to clarify the prospective research directions in the development of more autonomous rehabilitation processes. With this aim, first, a study and definition of a general rehabilitation process are made, and then, it is particularized for the case of neurorehabilitation, identifying the components involved in the cycle and their degree of interaction between them. Next, this generic process is compared with the current literature in robotics focused on upper limb treatment, analyzing which components of this rehabilitation cycle are being investigated. Finally, the challenges and opportunities to obtain more autonomous rehabilitation processes are discussed. In addition, based on this study, a series of technical requirements that should be taken into account when designing and implementing autonomous robotic systems for rehabilitation is presented and discussed.

## 1. Introduction

According to the findings obtained in the context of a Global Initiative on Neurology and Public Health carried out by the World Health Organization (WHO), many of the neurological disorders are chronic and progressive, constitute a global public health problem [1], and affect especially the elderly people. In addition, a higher life expectancy makes the population of people over 60 increasingly higher [2]. The main patient groups served by the rehabilitation service in the United Kingdom are for neurological pathologies, as a survey reported [3]. 70% of respondents provided neurological rehabilitation services for people with stroke, multiple sclerosis, traumatic brain injury, degenerative neurological diseases, and other neuromuscular conditions. Other services that were represented were those that provided rehabilitation to people with severe single-incident brain injury (10%), spinal

injury (9%), amputees (5%), musculoskeletal disability (4%), learning disabilities (1%), and pain (1%). In Spain, a similar situation is detected where musculoskeletal and articular disability (50%), neurological diseases (15%), traumatic injuries (29%), and others (6%) were treated in the rehabilitation services [4].

This situation, together with the need for rehabilitation and assistance for people with disabilities, means that robotic care and rehabilitation may play an important role in the years ahead.

Nowadays, research on the use of robotic systems in different fields related to healthcare is widespread [5–7]. In the field of rehabilitation, scientific literature shows various classifications of such systems according to their level of interaction [8], the extremities that are treated [9–12], the modularity of the rehabilitation robots [13, 14], control strategies [15, 16], and the effectiveness of treatment

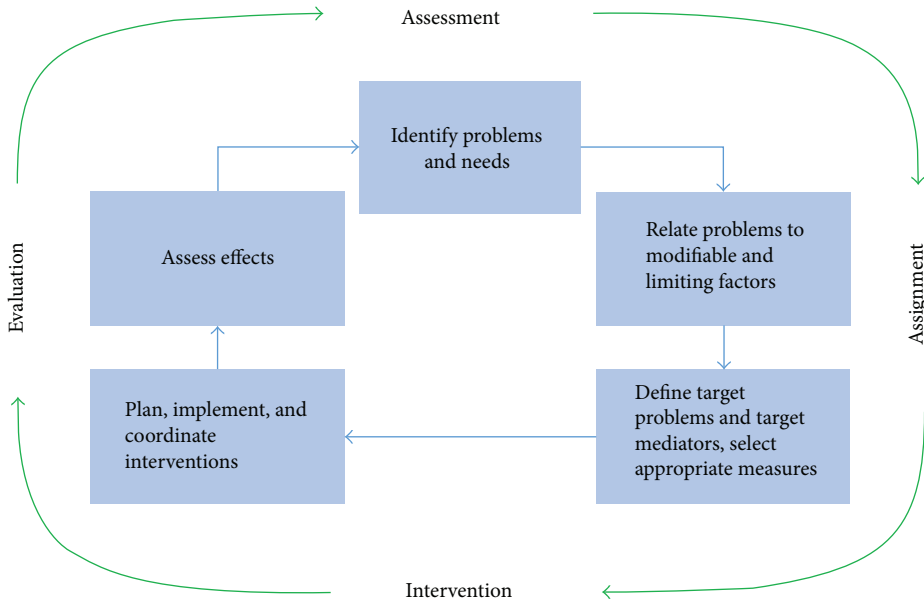


FIGURE 1: The rehabilitation cycle [21].

[17–20]. However, no analysis has been done of the rehabilitation process as such, and the contribution of robotics in the different stages of the rehabilitation cycle or process has not been studied.

In this paper, a systematic literature review is conducted to identify the contribution of robotics for upper limb neurorehabilitation highlighting its relation with the rehabilitation cycle and to clarify the prospective research directions in the development of an autonomous rehabilitation process.

## 2. The Rehabilitation Process

The World Report on Disability by the WHO and World Bank [21] provides a definition of rehabilitation: “a set of measures that assist individuals who experience, or are likely to experience, disability to achieve and maintain optimal functioning in interaction with their environments.”

Despite this, the term rehabilitation covers a wide field of applications, being a subject to different connotations in a world characterized by a profound cultural diversity. Meyer et al. [22] provided a conceptual description of rehabilitation: “it is the health strategy which is based on the WHO’s integrative model of functioning, disability, and health, with the goal to enable persons with health conditions experiencing or likely to experience disability to achieve and to maintain optimal functioning in interaction with the environment.”

The health strategies can be different, but they can share a series of steps to improve the patient’s health status throughout the rehabilitation process. This process involves the identification of a person’s problems and needs, relating the problems to relevant factors of the person and the environment, defining rehabilitation goals, planning and implementing the measures, and assessing the effects [21]. This approach is named the rehabilitation cycle (see Figure 1), which is taken from the World Report on Disability [21],

and it was previously stated by Stucki and Sangha [23] and modified by Steiner et al. [24].

In a simplified way, the rehabilitation cycle includes four steps: assessment, assignment, intervention, and evaluation. The process takes place on two levels: the first corresponds to the guidance provided along the continuum of care and the second refers to the provision of a specific service [25].

From the point of view of the care guide, the assessment consists of the identification of the problems and needs of the person, the analysis of rehabilitation potential and prognosis, the definition of the long-term service, and the goals of the intervention program. Assignment refers to the inclusion of the person in a program of intervention in the most appropriate service for the treatment of their needs. For the guidance perspective, no specifications appear in the intervention. Evaluation refers to the service and the achievement of the intervention goal.

From the perspective of providing a specific service, the assessment includes the identification of the problems, the review and potential modification of the service or goals of the intervention program, the definition of the first goals of the rehabilitation cycle, and the objectives of the intervention. The assignment step refers to the allocation of professionals and health interventions necessary to achieve the intervention objectives. The intervention consists in the specification of the techniques, measures, and the definition of target values that must be achieved within a predetermined period of time. Finally, the evaluation determines the achievements of the objectives with respect to the specific indicators, the goals of the rehabilitation cycle, and, ultimately, the goals of the intervention program. It also includes the decision regarding the need for another intervention cycle based on a new assessment.

**2.1. The Rehabilitation Team.** Rehabilitation requires the services of multiple healthcare providers who possess unique

skills, training, and expertise that are employed for the full restoration of the patients' function and their optimal reintegration into all aspects of life [26]. Rehabilitation professionals have recently favoured the concept of "patient-centred therapy." This is not meant to trivialize the patient's needs but rather to emphasize the patient as the director and arbiter of the interventions according to the patient's own desires [27].

The integration of the different medical means can be done through three working models [26, 28]: (a) *multidisciplinary team model*—in which team members interact and communicate among themselves, knowing the work of all the components and offering an evaluation and parallel but independent work; (b) *interdisciplinary team model*—where the team members share a formal space in which information is exposed (designed to facilitate the flow of lateral communication) and decisions are made around one or several common objectives (in this way, the treatments performed by the different professionals are not independent); and (c) *transdisciplinary team model*—which not only promotes communication among group members but also acquires knowledge from other related disciplines and incorporates them into the practice [29].

Because the interdisciplinary model is designed to facilitate lateral communication, it is theoretically better suited for rehabilitation teams [28].

**2.2. Rehabilitation Measures and Outcomes.** Rehabilitation measures are a set of recovery actions that target body functions and structures, activities and participation, environmental factors, and personal factors.

Rehabilitation outcomes are the benefits and changes in the functioning of an individual over time that are attributable to a single measure or set of measures [30]. These outcomes can be evaluated by the three main dimensions of the International Classification of Functioning, Disability and Health (ICF) [31]: body functions and structures, activities, and participation.

### 3. Neurological Rehabilitation

A particular case of rehabilitation is aimed at treating the problems caused by disorders affecting the nervous and neuromuscular system, known as neurorehabilitation. These types of disorders can produce mental or physical disabilities or both and are chronic and/or progressive.

Neurological rehabilitation can be defined as a process that aims to optimize a person's participation in society and sense of well-being. This definition highlights several important features: rehabilitation is not a particular type of intervention; the focus is on the patient as a person; the goals relate to social functioning, as well as health or well-being; and it is not a process restricted to patients who may recover, partially or completely, but applies to all patients left with long-term problems [32]. This will act on the deficiency, the limitation of activity, and the restriction of participation, constituting a holistic therapeutic approach [33].

The complexity of the problems caused by a neurological damage highlights even more the need for a team to work on its treatment, the interdisciplinary model being the

most used [34]. The composition of the interdisciplinary team in neurorehabilitation is not completely defined, but there is a consensus on the basic members who should constitute the team. According to the Union of European Medical Specialists (UEMS), the interdisciplinary team must include the following medical professionals: physical therapist, rehabilitation nurses, rehabilitation physicians, occupational therapists, speech-language pathologist, psychologists, social workers, orthopaedics, and nutritionists [35].

The rehabilitation cycle shown in Figure 1 applies to the case of neurological rehabilitation with some nuances that are discussed below.

**3.1. Assessment.** The rehabilitation process starts with collecting data from the patient and others to establish: the problems; the causes of, and factors influencing, each problem; and the wishes and expectations of all interested parties. It is also important to consider the prognosis based on the diagnosis, natural history, distribution, and severity and type of the impairment, as well as other personal, social, and environmental factors [36].

To this end, a series of objective scales have been developed to assess the level of independence of patients. The three main domains of the ICF can be used with this aim as a clinical tool [37, 38]:

- (i) Impairments: the typical body functions that need to be assessed in the neurological patient are those related to the functions of the joints, muscles, movements, and sensation and cognitive functions. Thus, some constructs of relevance are muscle, ranges of movement, attention, memory, and balance. There are scales classically encompassed at this level such as Beck Depression Inventory, Behavioral Inattention Test, Canadian Neurological Scale, Clock Drawing Test, Frenchay Aphasia Screening Test, Fugl-Meyer Assessment of Motor Recovery after Stroke, General Health Questionnaire-28, Geriatric Depression Scale, Hospital Anxiety and Depression Scale, Mini-Mental State Examination, Modified Ashworth Scale, Montreal Cognitive Assessment, Motor-Free Visual Perception Test, National Institutes of Health Stroke Scale, and Orpington Prognostic Scale.
- (ii) Activity: when examining a patient's activities, the therapist will examine whether they can do not only the tasks but also the quality with which the task is performed. According to Lennon's study [39], one of the most used scales for measuring the independence in stroke rehabilitation was the Barthel Index, followed by the Rivermead Motor Assessment and Functional Independence Measuring. More than a quarter of therapists (28%) were using outcome tools that they had devised themselves, which had not been tested for reliability or validity. Other examples of scales at this level are the following: Action Research Arm Test, Berg Balance Scale, Box and Blocks Test, Chedoke-McMaster Stroke Assessment

Scale, Clinical Outcome Variables, Functional Ambulation Categories, National Rehabilitation Reporting System, Frenchay Activities Index, Modified Rankin Handicap Scale, Motor Assessment Scale, Nine-Hole Peg Test, Rivermead Mobility Index, Timed “Up and Go” Test, and Wolf Motor Function Test.

- (iii) Participation: this is a more complex concept than impairments and activities, but it is fundamental to understand the patients and their life and help with planning treatment. Physiotherapy assessment of participation therefore focuses on those activities or roles in which patients take part in, patients are hindered in, and patients wish to work on and which could be improved and will inevitably deteriorate. Common scales used are the following: Canadian Occupational Performance Measure, EuroQol Quality of Life Scale, London Handicap Scale, Medical Outcomes Study Short Form 36, Nottingham Health Profile, Reintegration to Normal Living Index, Stroke-Adapted Sickness Impact Profile, Stroke Impact Scale, and Stroke Specific Quality of Life Scale.

**3.2. Planning of Treatment.** According to the pathology, the rehabilitation team designs a specific plan based on the diagnosis (problems identification) and disability of the patient. It is necessary to identify clear objectives related to the functional problems. Rehabilitation objectives normally follow the SMART rule because they must be specific, measurable, achievable, relevant, and time-limited [32].

There are three key areas that the rehabilitation process is broken down: (1) approaches that reduce disability; (2) approaches designed to acquire new skills and strategies, which will maximize activity; and (3) approaches that help to alter the environment, both physical and social, so that a given disability carries with it minimal consequent handicap. The planning of a neurological rehabilitation program should consider the previous three approaches, in addition to the SMART rule.

**3.3. Intervention: Specific Methods.** Specific rehabilitation interventions include those related to physical medicine, occupational therapy, speech and language therapy, dysphagia management, neurophysiological interventions, psychological assessment and interventions, nutritional therapy, and other interventions [25]. A wide range of specific techniques is used in the practice of rehabilitation [40]. These techniques used to treat different patients vary considerably across different geographical locations.

At present, the evidence suggests that to be effective, rehabilitation requires the practice of activities in the most relevant possible environments, rather than undertaking analytical exercises aimed at changing impairments [41]. This is sometimes referred to as task-specific training. However, other approaches are known such as facilitation techniques (such as Bobath concept, Brunnstrom technique, Kabat method, or Rood method), modern techniques (such as treadmill training with body weight support, constraint-

induced movement therapy, or functional electrical stimulation), or compensation techniques.

**3.4. Evaluation.** In this phase, the physical condition of the patient is reevaluated in order to determine the effectiveness of the treatment, based on the SMART objectives [32] initially raised. The considerations for discharge in the case of the neurological patient are very varied, since the clinician must determine whether the improvement achieved is sufficient from the medical point of view of the patient (patient-centred practice).

Previous quantitative investigations and case studies have shown that the use of patient-centred goal planning with adults undergoing neurological rehabilitation can improve self-perceived and observed goal performance and satisfaction [42]. A patient-centred approach involves goals that are set by the patient on the basis of his or her own definition of the problems. This approach enables greater self-determination and control and enhances the person's potential for active participation.

In addition, one must take into account the underlying pathological process, the chronic nature of certain pathologies, the need for supervision and/or the continuity in the absence of an expressive face-to-face rehabilitation treatment, or the degenerative and progressive character of some neurological pathologies, such as Parkinson's disease, multiple sclerosis, or Alzheimer's disease.

## 4. Robotics in Healthcare: Neurorehabilitation of Upper Limb

In this section, this review will highlight the particular aspects of the rehabilitation cycle applied to upper limb neurorehabilitation performed with the assistance of any kind of robotic system.

### 4.1. Material and Method

**4.1.1. Search Methods.** The authors undertook a literature search in October 2017 about robot-assisted upper limb rehabilitation in neurological diseases, using keywords such as robot, neurological, rehabilitation, upper, limb, extremity, arm, hand, neurorehabilitation, intervention, assisted therapy, treatment design, and various combinations. The databases were Brain, Science Direct, PubMed/Medline, and IEEE. Only papers written in English were considered, and the search was extended to the whole database. Studies were included when (1) systems for upper limb training (uni- and bilateral) were used; (2) systems are based on end-effector and exoskeleton devices (commercially available or not); (3) the clinical intervention was conducted; and (4) the effects of the robot-assisted therapy were investigated.

**4.2. Robotics in Neurorehabilitation of Upper Limb.** According to the Strategic Research Agenda for Robotics in Europe (SPARC) [43], healthcare is seen as a combination of three subdomains: (1) clinical robotics—systems that support care (diagnosis) and cure (surgery) processes; (2) rehabilitation—covering postoperative or postinjury care where direct physical interaction with a robot system will

either enhance recovery or act as a replacement for lost function; and (3) assistive robotics—covering other aspects of robotics within the healthcare process where the primary function of the robotic system is to provide assistive help either to carers or directly to patients either in hospital or in a specialist care facility.

Thus, devices to train (robot-aided therapies), support (exoskeletons), or replace (prostheses) impaired activities or impaired body functions and structures are covered in rehabilitation robotics. In this way, robots are presented as a useful tool in the recovery process in neurological treatment. Such systems participate actively and help the therapist to perform a better rehabilitation process. However, it is not clear in what way and to what extent robotic systems provide this help during the rehabilitation cycle. To improve the quality of help provided, it must be identified how and when the aid is administered.

The summary presented in Table 1 collects the information obtained from the study of several robot-aided neurorehabilitation systems for the upper extremities. The systems selected have been used in clinical trials with patients suffering motor function problems derived from different neurological disorders. A comprehensive reading has been made to identify how robotic assistance has been used, how it has contributed and in which phases of the rehabilitation process. Thus, the present review identifies what the robotic system contributes to the rehabilitation cycle in a quantitative way (measurements), the way it does it (automatic or not), and the phase in which it participates (assessment, assignment, or intervention). Notice that the same robotic systems could cover several phases of the rehabilitation cycle. The more phases are covered, the more automated will be the rehabilitation process.

Rehabilitation, like many aspects of human behaviour, can be thought of as a purposive problem-solving activity [44]. The following review draws upon the problem-solving process from a patient-centred perspective in neurorehabilitation.

**4.2.1. Assessment Approaches.** As previously indicated, the starting and ending component of the rehabilitation cycle is the functional assessment. It is important to take into account that most of the assessments performed by robotic systems are not functional assessments (carried out in baseline and follow-up stages of treatment), and its provided outcomes are indicators of a patient's performance. Currently, functional assessment is still carried out by traditional tests and scales provided by therapists. The main features of the robot-aided systems reviewed related to the assessment phase of the rehabilitation cycle are described as follows:

(1) *Assessment Mode.* Assessment of the patient's performance can be carried out in two modes: automatic or non-automatic. The automatic mode corresponds with the online data analysis, that is, during the development or at the end of the session. On the contrary, the nonautomatic mode corresponds with the offline data analysis (after of the end of the session).

(2) *Assessment Method.* Robotic rehabilitation systems present evaluation methods that are based on the biomechanical data they are able to acquire. Based on such data, a rapid report that could be performed in an online or offline mode is provided to the therapist. 74% of the reviewed systems have not specified assessment methods, but propose an evaluation method based on the offline analysis of the biomechanical data acquired during therapy. In these studies, a later analysis of the stored information is done, applying algorithms to obtain information on the patient's performance. However, besides having an automatic record of information, only 26% of the systems perform online processing of these parameters by using specific software (e.g., INMOTION, IPAM, AMADEO, ARMEO, and T-WREX).

(3) *Provided Outcome.* Robot-assisted systems have the advantage of providing a reliable and objective quantitative rapid assessment, based on the comparison of the metrics acquired during therapy. However, this assessment is at the level of impairment but does not provide information on how such impairment influences the activities of the patient's daily life. The most automated are commercially available systems like INMOTION ROBOTS, ARMEO-SPRING, AMADEO, REOGO, and DIEGO. They have an online processing that generates a report at the end of the therapy session. However, the reliability of these automatic assessments, although they are based on objective measures, has not been validated with respect to determining, on their own, whether the rehabilitation has been adequate or not. Also, robot-mediated measurements have even smaller dissemination. For this reason, most of the systems reviewed carry out additional clinical evaluation, using functionality scales that are of standardized use at the clinical level, such as those mentioned in Section 3.1, which are still the "gold standard" for measuring outcomes. The interpretation of these scales allows the therapist to determine in an objective way the health condition of the patient and the effectiveness of the treatment.

(4) *Functional Assessment.* Given the importance of making a correct evaluation, it is necessary to highlight the need to use standardized tools and procedures. The classification of the ICF is very useful for this functional assessment. The use of these standard functional scales as the main output of the rehabilitation systems would provide a better and more collaborative way to determine the effectiveness of the therapy based on the metrics obtained by the rehabilitation systems themselves. Currently, this issue is addressed by INMOTION software (INMOTION EVAL) that, based on multiple regression models, calculates Fugl-Meyer Assessment (FMA), Motor Status Score (MSS), Motor Power (MP), and Modified Ashworth Scale (MAS) from the robot-based metrics. These measurements of motor control are highly correlated with the traditional scales [45].

**4.2.2. Clinical Decision Support.** As previously mentioned, it is important to emphasize that the complexity of a neurorehabilitation treatment usually requires the participation of a work team. Therefore, it is important that the patient's

TABLE 1: Review of robot-aided system for upper limb neurorehabilitation.

System	Automatic assessment	Assessment method	Provided outcome	Assessment			Assignment			Task-specific training	Method	Interaction	Measurements
				Functional assessment	Therapy planning support	Method	Rehabilitation target	Reach (payload simulation)					
<i>End-effector-type system</i>													
ACT-3D [61]	No	Offline data analysis	Difference between sessions	FMA	No	N/A	Shoulder; elbow	Yes	Reach (payload simulation)	VR; haptic; auditory	Kinematic data; force		
ARM GUIDE [62, 63]	No	Offline data analysis	Difference between sessions	CM; RLAFT	No	N/A	Shoulder; elbow	Yes	Passive; active assisted; active resistance	VR; haptic	Kinematic data; force; straightness; smoothness		
BRACCIO DI FERRO [64, 65]	No	Offline data analysis	Difference between sessions	FMA; MAS	No	N/A	Shoulder; elbow	Yes	Active assisted; active resistance; gravity compensation	VR; haptic	Kinematic data; force; smoothness; accuracy		
GENTLE/S [66, 67]	No	Offline data analysis	Visual comparison of data trends (slopes)	FMA; MoAS; MAS; NSA; SCT	Yes	Haptic Master software allows the therapist to define the exercise path	Shoulder; elbow	Yes	Passive; assisted; active; trajectory correction	VR; haptic	Kinematic data; force		
INMOTION EVAL			Robot calculates 13 evidence-based measures of motor control that are highly correlated with traditional scales	FIM; FMA; MP; NIHSS	Yes	Selection of the therapeutic exercise games; progress measurement of determined medical necessity; assesses treatment based upon measurable gains	Shoulder; elbow	Yes	Passive; active assisted; active resistance; gravity compensation	VR; haptic	Kinematic and kinetic data (position, direction, distance, area, time, force, smoothness, accuracy); performance measures		
INMOTION ARM [59, 68]	Yes												
IPAM [69, 70]	Yes	IPAM software	Virtual environment feedback	FMA	Yes	Automatically generated exercises based on a clinical assessment of the patient (automated tasks)	Shoulder; elbow	Yes	Passive; active resistance; active; reach	VR; haptic	Kinematic data; force		

TABLE 1: Continued.

System	Automatic assessment	Assessment method	Assessment		Assignment		Rehabilitation target	Task-specific training	Intervention	
			Provided outcome	Functional assessment	Therapy planning support	Method			Method	Interaction
MEMOS [71, 72]	Yes	Online data analysis	Score proportional to the voluntary motor activity developed during the task	FMA; MSS; MRC; MP	No	N/A	ARM: not a specific joint	Yes	Passive; active resistance; active	Kinematic data; force
MINE [73]	No	Offline data analysis	Difference between sessions	FMA; MSS; BI; FIM; MP; MAS	No	N/A	Shoulder; elbow	Yes	Passive; active assisted; active resistance; bilateral	Kinematic data; force [bimanual]
NEREBOT [74, 75]	Yes	Online data analysis	Feedback based on patient's effort	FMA; MRC; FIM; MAS; FAT; BBT	No	Therapist defines the exercise by choosing via points and adjusts robot parameters according to the type of exercise		No	Passive; active assisted; active	VR; auditory
REHAROB [76, 77]	Yes	Online data analysis	Feedback based on patient's effort	FMA; FIM; MAS; RMA; BI; BMR	Yes	Therapist can choose exercises from any therapeutic school (Bobath, Kabat, etc.)		No	Passive	N/A
AMADEO TYROMOTION [78–80]	Yes	Tyros software	Difference between sessions	FMA; MRC; MI; MAS; FIM; COPM	Yes	Tyros software creates a therapy report and therapy progress		Yes	Passive; active assisted; active	VR
BIMANUTRACK [81, 82]	No	Offline data analysis	Difference between sessions	FMA; WMFT; RMA; MAS	Programming of individually adjusted natural gait trajectories; real-time simulation of the programmed foot trajectory		Forearm; wrist	No	Active; passive [bilateral]	N/A
HWARD [83, 84]	No	Offline data analysis	Difference between sessions	ARAT; BBT; FMA; NIHSS; GDS; NSA; 9-HPT; SIS; MAS	No	N/A	Wrist; hand	Yes	Passive; active assisted; active resistance	VR

TABLE 1: Continued.

System	Automatic assessment	Assessment method	Assessment provided outcome	Functional assessment	Therapy planning support	Assignment Method	Rehabilitation target	Task-specific training	Intervention Method	Interaction	Measurements
REOGO [85, 86]	Yes	Advanced management software	Evolution of measurements	FMA; MFT	Yes	engaging exercises and games for various rehabilitation objectives	Shoulder; elbow; wrist; hand	Passive; active; guided; free	VR; haptic	Kinematic data; accuracy; smoothness; force; muscle tone	
DIEGO [78, 87]	Yes	Tyros software	Evolution of measurement	N/A	Yes	Selection of therapy games	ARM; not a specific joint; shoulder	Yes	VR; haptic	Kinematic data; motoric function; force proprioception	
<i>Exoskeleton/Orthosis system</i>											
L-EXOSPERCRO [88]	No	Offline data analysis	Difference between sessions	FMA; MAS; BAS	Yes	Selection of different trajectories in the same virtual environment	Shoulder; elbow	Yes	Active assisted; gravity compensation [uni- and bilateral]	VR	Kinematic data; force; accuracy
MYOPRO [89–91]	No	EMG signals	Difference between sessions	MAS; BBT; FMA; MAL-AOU; MAL-HW	No	N/A	Elbow	Yes	Active assisted	Haptic	Kinematic data; force
WREX [92]	No	Offline data analysis	Difference between sessions	N/A	No	N/A	Shoulder; elbow	Yes	Active assisted; gravity compensation	N/A	Kinematic data; force
ARMEOSPRING (T-WREX) [93–95]	Yes	Java Therapy 2.0 software	Difference between sessions	FMA; RFT; BBT; BBTD	Yes	Selection of therapy games	Shoulder; elbow; forearm	Yes	Passive; gravity compensation	VR; haptic	Kinematic data; force
MENTOR PRO (hand) [96–98]	No	Offline data analysis	Monitoring of patient's progress in DLA	N/A	No	N/A	Wrist; hand; fingers	No	Active (only extension)	VR	Kinematic data
HEXORR [99]	No	Offline data analysis	Difference between sessions	ARAT; FMA; MAS	No	N/A	Metacarpus [interfalangica]	Yes	Passive; active assisted; active; gravity compensation	Haptic	Kinematic data; force grasping patterns

TABLE 1: Continued.

System	Automatic assessment method	Assessment		Assignment		Intervention	
		Provided outcome	Functional assessment	Therapy planning support	Method	Rehabilitation target	Task-specific training
RUTGERS MAPTER II [100, 101]	Yes	Online data analysis	Performance meter	JTHF; FMA	No	N/A	Hand
SUPINATOR-EXTENDER [102]	No	Offline data analysis	Difference between sessions	N/A	No	N/A	Forearm; wrist
T-WREX [95, 103]	Yes	Java Therapy software	Monitoring of a patient's progress by skilled rehabilitation therapist	FMA; RFT; BBT	No	N/A	Shoulder; elbow; forearm; wrist; hand
WOTAS [104]	No	Offline data analysis	Difference between sessions	FTMTRS	No	N/A	Elbow; forearm; wrist
ARMEOPOWER (ARM-IN III) [93, 105, 106]	Yes	GIANTS game engine	Difference between sessions	FMA	Yes	Choose from several VR therapy tasks	Passive; gravity compensation
ARM-IN [107, 108]	Yes	Online data analysis	Difference between sessions	N/A	Yes	Allows different therapy modes, robot interface for patient (PRI) and therapist (TRI) HMI module for interaction between the user and the Gentle robot; database for storing patient information	Shoulder; elbow; forearm; wrist
GENTLE/G [109]	Yes	Online data analysis	Performance meter	N/A	Yes	Passive; active assisted; active resistance; gravity compensation	Passive; assisted; active; trajectory correction
						VR; haptic	Kinematic data (position, direction, distance); force

TABLE 1: Continued.

System	Assessment			Assignment			Intervention			
	Automatic assessment	Assessment method	Provided outcome	Functional assessment	Therapy planning support	Method	Rehabilitation target	Task-specific training	Method	Interaction
Rupert [110, 111]	No	Offline data analysis	Difference between sessions	WMFT; FMA	No	N/A	Shoulder; elbow; forearm; wrist	Passive; active assisted; active	VR; haptic	[motor activity; stroke impact scale; stroke recovery scale]

9-HPT: 9 Hole Peg Test; ARAT: Action Research Arm Test; BAS: Bimanual Activity Scale; BBT: Box and Blocks Test; BBTID: BBT (without picking up blocks); BI: Barthel Index; BMR: British Medical Research; CM: Chedoke-McMaster; COPM: Canadian Occupational Performance Measure; FAT: Frenchay Arm Test; FIM: Functional Independence Measure; FMA: Fugl-Meyer Assessment; FTMTRS: Fahn-Tolosa-Marin Tremor Rating Scale; GDS: Geriatric Depression Scale; JTHF: Jebsen Test of Hand Function; MAL-AOU: Activity Log-Amount of Use; MAL-HW: Motor Activity Log-How Well; MAS: Modified Ashworth Scale; MFT: Manual Functional Test; MI: Motricity Index; MoAS: Motor Assessment Scale; MP: Motor Power; MRC: Medical Research Council; MSS: Motor Status Score.

progress information is available to the entire work team, according to the interdisciplinary model. The management of information is one of the more time-consuming tasks that facilitate the decision-making of the therapist. Currently, there are several electronic medical record (EMR) software for the management of the patient's data [46], including based on artificial intelligence [47]. Thus, one of the important aids incorporated in robot-assisted systems is the administration and storage of data automatically, which allows the generation of updated monitoring reports.

The results of the review show that 45% of the systems (the commercial ones) also provide some kind of help in the elaboration of the therapy. The most common assistance is through offering a set of exercises, games (REOGO, DIEGO, and ARMEO), or therapy protocols (INMOTION system) that can be configured or combined by the therapist. One of the systems (REHAROB) also allows the option of selecting exercises that are based on the intervention methods most used in physical rehabilitation, such as the Bobath or Kabat method. On the other hand, in-depth analysis of the data recorded robot-aided therapy, as well as allowing rapid functional assessment, serves as a tool for decision support to determine the patient's discharge. The INMOTION system allows discharge plots to be generated based on the performance of 5 tests that register kinematics and kinetics data. To the authors' knowledge, there are no commercial systems able to automatically generate a complete rehabilitation strategy from the initial functional assessment data and thus the therapist still has to properly identify the patient's problems by means of a reliable diagnosis and the right choice of clinical measures to evaluate the effectiveness of the treatment.

**4.2.3. Rehabilitation Approaches and Outcomes.** Typically, rehabilitation occurs for a specific period of time but can involve single or multiple interventions delivered by an individual or a team of rehabilitation workers and can be needed from the acute or initial phase immediately following recognition of a health condition through postacute and maintenance phases. Rehabilitation reduces the impact of a broad range of health conditions. Further, neurorehabilitation is often still based on therapists' expertise, with competition among different schools of thought, generating substantial uncertainty about what exactly a neurorehabilitation robot should do [48].

Robot-aided systems allow the training of an impaired limb in multiple sessions and in a systematic way, without loss of efficiency. With respect to the target region of treatment, the number of joints that the same system is capable of treating has been identified. No devices covering the movement of all joints of the upper limb have been found, that is, the shoulder, elbow, wrist, and hand (including fingers joints). The ARMEOSPRING, INMOTION, and ARMEOPOWER systems manage to cover the shoulder and elbow joints and also to train the flexoextension of the wrist and the manual grip, excepting finger joints.

The effectiveness of treatments based on task-specific training in robot-assisted interventions is demonstrated. So it is understandable that 86% of the review systems consider this approach. It is observed that the systems have more than

one operating mode (passive, active, active-assisted, or active resistance). This represents a great advantage when considering treatment measures in a flexible way and better adapted to the type of injury. Some systems describe the mechanisms of action of the robots, which can offer assistance to the movement or gravity compensation through cable-based transmissions or pneumatic actuator systems. The pneumatic actuator systems offer the advantage of producing large forces with low weight added to the device, while cable transmission systems have greater shock absorption, smoothness in movement, and greater versatility in their passage through the joints.

Finally, all the robotics rehabilitation systems reviewed are able to acquire and automatically store biomechanical metrics during the therapy. Depending on each robotic system, it can measure the workspace, joint movement ranges, and force exerted, as well as the quality in terms of the precision and smoothness of the trajectories. Other measures derived from the previous ones for a certain interval of time are the speed of execution and completion of the tasks, as well as the reaction times. The acquisition and storage of these parameters are immediate due to the inherent sensorization of the robotic systems (encoders, force sensors, current sensors, etc.). These are objective records due to the robotic intrinsic sensory systems.

## 5. Towards Autonomous Rehabilitation Processes?

The development of autonomous systems is an active line in robotics in general, and with increasing presence in healthcare applications, it is already generating beneficial results as it has done in industry [49]. That is the case of surgical robots in minimally invasive procedures for executing autonomously simple surgical tasks, based on the accuracy of robot movements, image processing algorithms, and cognitive systems. There are many other examples than surgical robotics of translational research applied to healthcare.

The common understanding in the robotic community is that the goal of robotic rehabilitation devices should be to assist therapists in performing the types of activities and exercises they believe give their patients the best chance of a functional recovery. But several barriers have been identified, for the particular case of rehabilitation robotics. The first identified barrier is the lack of effective communication in the planning stage of designing robotics aids, between engineers and therapists. Second, many of the devices are incredibly complicated, from both an engineering and a usability point of view. In fact, "simple-to-use" devices are more likely to be adopted by the clinical community than those that have long set-up times or require multiple therapists and/or aids to use [50]. Another well-known barrier relates to the cost and availability, its relation to the effectiveness of the treatment, and how long the robotic treatment must be applied. Many works discuss these issues. Recent examples are those by Acosta et al., who show that while video games can provide a motivational interface, they are the most effective if designed to target specific impairments [51]. Burgar et al. highlight the importance of providing higher therapy

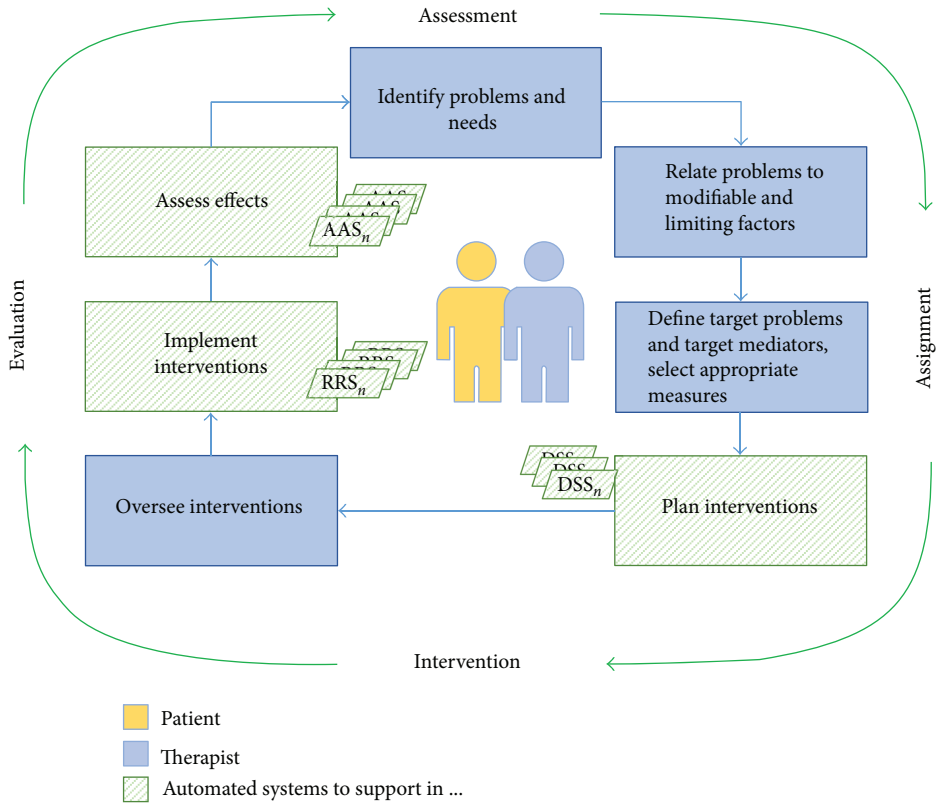


FIGURE 2: The automated rehabilitation cycle.

intensities (hours of therapy per day) in an acute stroke study using the MIME robot [52]. Telemedicine and telerehabilitation are promising topics for building remote monitoring and easy to use rehabilitation systems that could allow the work of therapist with patients at home. Serious games and low-cost sensory devices are arising as very promising tools for breaking this barrier. The last barrier, but not the least from the authors' point of view, is the lack of automation, which greatly increases the total cost of the treatments. There is a huge potential to automate the treatment process.

To apply this automation approach to the rehabilitation process, it is first necessary to identify how the process is developed and identify which are the most susceptible elements to be automated, as well as the requirements and limitations to achieve this purpose.

Based on the review presented in this article, we have identified three main areas within the rehabilitation cycle where robotics is contributing to automation: planning treatment protocols, implementing interventions, and evaluating the treatment's effectiveness. This rehabilitation cycle, shown in the previous Figure 1, is being transformed into a more automated cycle as shown in Figure 2. This transformation adds more detail but does not alter the rehabilitation cycle, thus maintaining the philosophy centred on the user. In this figure, the main actors (patient and therapist) are supported by several automated tools, as it will be explained below.

**5.1. The Automated Rehabilitation Cycle.** This paper proposes a framework for the development of the rehabilitation

cycle that clearly identifies which parts of the process are more likely to be automated, as well as the actors and elements involved. The autonomous rehabilitation cycle would be composed in this way by five elements that are directly correlated with the blocks of the original cycle. According to this approach, three main actors have been identified: user, clinician (understood as the team), and automated systems. Although several automated systems could be available, as denoted in Figure 2, to simplify, we assume that the one used is the best fitted to each case. The appropriate collaboration between the therapy work team and the automated systems is essential to obtain an effective patient-centred rehabilitation process.

The interaction between these three participants during the course of an automated neurological rehabilitation process will be described in Figure 3. First, an initial evaluation (interview and exploration-based) is carried out by the clinician to identify the patient's problems and needs and select the most appropriate treatment measures. Also, the appropriate scales for functional assessment are chosen to quantify the level of functionality impairment caused by the neurological injury. Here, where the first automated system is, the automatic assessment system (AAS) performs the functionality assessment using the same clinically accepted scales. The results obtained with the AAS are automatically updated in the patient's clinical history. In addition, these results serve as input parameters to the second automatic system, the decision support system (DSS). The DSS aims at designing the most optimal treatment protocol for the patient, generating

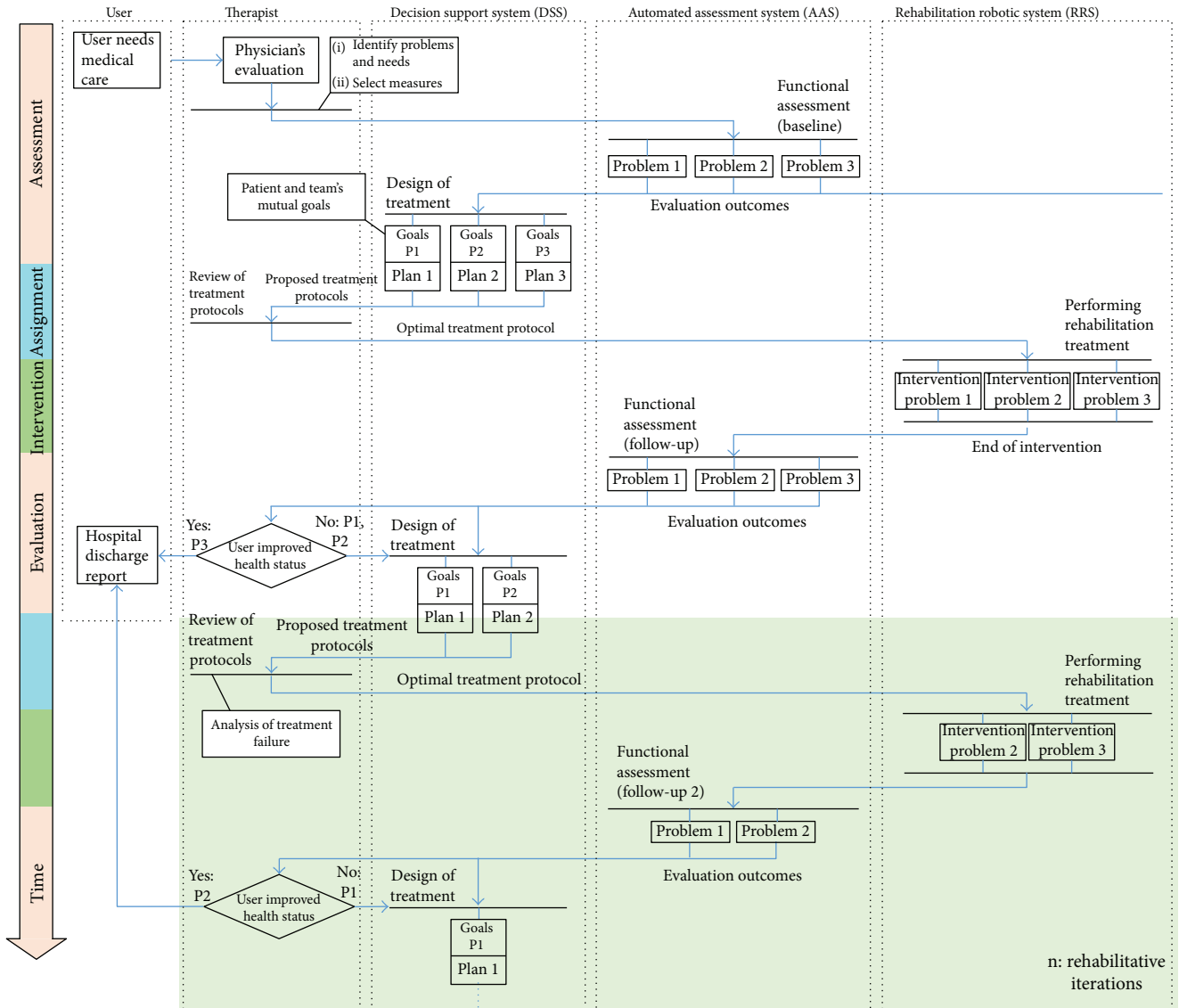


FIGURE 3: Activity diagram for the automation of the rehabilitation process. In the example shown, three functionality problems were identified in the assessment phase: problem 3 is solved after the first intervention, but problems 1 and 2 remain. Then, the rehab cycle is repeated for  $n$  iterations.

the specific intervention plans. This figure is based on the lacks identified in the literature review previously presented.

The therapist discusses with the patient to review and adjust the objectives, deciding which treatment plans proposed by the DSS will be adopted. Then, the selected robotic rehabilitation systems (RRS) perform the intervention. After the intervention with the RRS, an assessment of functionality similar to the initial one is carried out again, in order to quantify the effectiveness of the therapeutic measures. For this, the AAS is used again. Finally, if all the problems identified are considered resolved or accepted by both the clinician and the patient, the rehab cycle is concluded. Otherwise, the necessary iterations will be made to try to solve the remaining problems.

It can be deduced that the proposed automated systems operate separately and independently but that they are intrinsically connected and depend on each other for efficient operation, in coordination with the clinician and the patient.

The methods to extract metrics and share them and their degree of acceptance by both users and health professionals should be rationalized and assessed, as a prerogative to achieve the automation. To design assistance rehabilitation systems, although the focus is on the subject to be treated, it is important to systematize the understanding of the requirements demanded by therapists in order to enable an easier integration of technology in their daily activities [53].

By providing low-cost and easy to access tools for implementing this automated rehabilitation cycle, the viability of extending the rehabilitation cycle can be increased, not only as a temporary activity but also as a lifelong rehabilitation, as needed, for example, for affordable robotic therapy in maintaining function in degenerative disorders.

Thus, in the opinion of the authors, the requirements that the components of a rehabilitation cycle must meet to be more autonomous are described below.

**5.1.1. Automated Assessment Systems (AAS).** As revealed by the analysis of assessment methods in neurorehabilitation, the use of traditional motor and functional scales is the main approach to determine the effectiveness of the rehabilitation process. For this reason, the development of methods based on traditional assessment scales that are widely used and known by specialists in rehabilitation is one of the lines of research that have been highlighted to achieve a more autonomous rehabilitation cycle.

There are already oriented studies in this line of work, taking into account two premises: the method and metrics. Regarding the method, tests that are administered without direct contact of the professional are more suitable to be automated. Concerning metrics, it is essential to assess which ones give relevant information and are less invasive for the subject to be evaluated [54].

It can be seen that the FMA is one of the most used scales employed for the motor assessment in the clinical trials that this review included. So it appears reasonable that the potential for the automation of these kinds of assessment methods is being studied. The application of RGB-D sensors, inertial measurement sensors, and other sensors has allowed the scoring of a part of the FMA to be automated [55]. However, one of the biggest problems with the evaluation using traditional tests is the time they take the therapist to administer. Other works address automatic administration of assessment procedures, such as the case of BBT [56]. Even so, a large number of scales and the variety of methods (sensor-based, tracking systems, computer-based, etc.) make the topic of automating the assessment a very promising line of research.

In this respect, the literature also presents several projects that are focused on the automation of the traditional and still “gold standard” scales. As traditional scales are widely used in clinical trials in rehabilitation, as seen in this article, and because the administration of the evaluation is time-consuming, it appears reasonable that the automation of these kinds of assessment methods is being studied. There is an important difference in emphasis between clinical assessment and measurement. Traditional scales comprise several items. However, measurement concerns the quantification of an attribute and some studies [57] demonstrate that multi-item measures need only a few carefully chosen items to generate reliable and valid estimates.

Following the model of the rehabilitation process, most of the systems reviewed (based on end-effector or exoskeletons) are clearly located within the intervention stages of the rehabilitation cycle. However, a percentage of them (46% end-effector and 43% exoskeletons) addresses the assessment stage, based on the metrics that are obtained from the use of systems in therapy. This assessment serves as a method of “rapid assessment” to support the therapist and inform the patient of the effectiveness of the rehabilitation process, but there are few works that report comparative studies or clinical trials to validate nonclinical metrics.

**5.1.2. Decision Support System (DSS).** Decision support systems based on artificial intelligence (AI-powered DSS) are one of the most active fields in recent years, and it is expected that they will soon contribute to the decision-making

process. In healthcare, a variety of software for EMR management is already available (see Section 4.2.2) to help the therapist in decision-making. However, the diagnosis of diseases still presents serious limitations. We can find numerous smartphone apps that allow an online diagnosis, yet the reliability of the diagnosis is not yet consistent with that of a doctor [58]. Besides, researchers in the artificial intelligence community have started to design robot-assisted rehabilitation devices that implement artificial intelligence methods to improve upon the active assistance techniques found in Section 4.2.3.

Clinical decisions are an important component of the rehabilitation cycle, since they involve the determination of the objectives and design of the rehabilitation treatment. As can be seen in this review, the support provided by automated systems for this kind of task is by providing more reliable and objective information about the motor performance of the user during the intervention, as well as allowing the execution of different types of intervention procedures that can be configured by the clinician.

Regarding the assignment stage of the rehabilitation cycle, there are two steps that could be automated by using artificial intelligence techniques: the planning of intervention treatments and the assignment of the appropriate RRS for intervention.

Related to the planning of intervention treatments, the generation of these protocols is based on different factors that depend on the type of lesion and on how it affects the development of the patient’s daily living activities. Many of the intervention measures are systematized in order to deal with a particular effect (concrete measures for specific problems), but there is no reason to believe that a “one-size-fits-all” optimal treatment exists. Instead, therapy should be tailored (intensity, number of repetitions, and duration of the intervention) to each patient’s needs and abilities [59]. In addition, the protocol planning should consider the available tools (RRS) to execute such protocol in order to assign the appropriate RRS to the type of lesion (e.g., a hand injury cannot be trained by a device designed for elbow training).

Thus, we have identified some requirements that must be met to develop intelligent systems for treatment planning: (1) coherence between technological and traditional outcome measures, for the purpose of a therapeutic intervention based on technology and the problem-solving approach; (2) differentiating these measures according to the level of the effect (mild, moderate, and severe); (3), based on models, to identify the parameters that define an adequate physical condition according to the demographics of the patient and healthy profiles; (4) to be able to estimate the physical condition of the user to compare it with the welfare reference model; and (5) to generate a protocol that can be executed by the available intervention systems.

These requirements imply that the integration of an AI-powered DSS in the automated cycle requires as input parameters the results of the evaluation systems (AAS) and, based on them, generates an optimized treatment protocol that can be executed by the systems of automatic intervention (RRS). This is why special attention is needed to the

development of strategies that allow the integration and collaborative execution of these automated systems.

**5.1.3. Robotic Rehabilitation Systems (RRS).** The developments in medical robotics systems and RRS are fields that have awakened most interest for research in robotics. Due to the direct participation in the intervention phase, the different methods used in rehabilitation (task-oriented, constraint-induced, etc.), and the understanding of what constitutes the most, appropriate therapy has the potential to become an intensively active topic of research [59].

Two main issues have been highlighted: the ability of the RRS to acquire multiple information on patient performance during the development and the fact that from these data an assessment of patient functionality is obtained, even in the same type of score as the traditional scales.

However, the type and amount of information that is obtained depend a lot on the type of robotic system (end-effector or exoskeleton) and the intrinsic sensory system. Also, the parameters derived from the measurements, as indicators of quality (accuracy, smoothness, etc.), can be very heterogeneous. Therefore, a critical issue is to unify the metrics acquired by the RRS, so that they provide as much information as possible for a rapid assessment by the therapist and not just raw data. Thus, among this type of metrics we have the following: range of movement, speed, precision, efficiency, percentage of work of the patient and percentage of work of the robot, and degree of attention in the task. All the works reviewed coincide in capturing the kinematic data; however, they do not address high-level indicators such as the percentages of robot and patient work (excepting NeRe-Bot that gives it as a percentage) nor the degree of attention.

Another important issue is to promote the adherence of the user to therapy. It is necessary to provide an adequate feedback that motivates the patient. Using virtual reality systems is the most widely used solution for this purpose. However, it is important not only the way in which the feedback is given but also the information provided to the user. In this sense, therapists agree that a visual feedback that tells the user if he has improved his score during the execution of the therapy would be beneficial. Other high-level indicators such as the percentages of robot and patient work, control signal, or kinematic data could be helpful to the user only if they help to show the relevance of the patient's progress.

RRS-type systems are already integrated into the rehabilitation cycle, due to their imminent nature in the intervention; however, addressing the aforementioned questions would allow the rest of the automated components indicated in this paper (AAS and DSS) to take advantage of the objective information that is acquired with the RRS.

## 6. Conclusions

A new automated rehabilitation framework has been proposed based on a literature review of robotic rehabilitation systems (RRS) for the upper limb treatment, highlighting its relation with the rehabilitation cycle. This framework has been presented regarding the implementation of more autonomous rehabilitation procedures. Three automated

elements were described to make up the proposed framework: automated assessment systems (AAS), decision support systems (DSS), and robotic rehabilitation systems (RRS).

The development of AAS should be based on the traditional assessment methods, since the traditional scales are still the "gold standard" for measuring outcomes and determine the effectiveness of treatment. In addition, the outcome provided by the AAS is obtained in an objective way, generating additional information about the user's performance.

Those systems must be complemented with a novel DSS to help in clinical decision-making and treatment planning. The management of the patient's data (EMR) is currently addressed by using specific software based on high-level algorithms and also on artificial intelligence (AI). Optimized treatment protocols customized to the patient's condition are expected to be automatically generated by these DSS. For this purpose, AI is a promising tool. Dealing with multiple objectives in decision-theoretic planning and reinforcement learning algorithms [60] could contribute to allow the optimal protocols to be generated. Thus, the treatment protocols could require only approval or adjustment by the clinician.

To conclude, the implementation of the proposed framework should consider some issues that are summarized as follows:

- (i) The development of strategies for allowing the integration and collaborative execution of these automated systems is needed. It must be considered a proper data management in order to allow the AAS and DSS to use the objective information that is acquired with the RRS. In this way, a communication channel similar to the interdisciplinary team model will be enabled for the automated elements.
- (ii) In the case of the AAS development, the automatic administration of the assessment must be considered and not only the automation of the outcome. Knowledge of the user is as important as system functionality, since without the user's cooperation and acceptance, the system's functionality may be ineffective.
- (iii) The complexity of neurological disorders and its effect normally presents additional diseases concurrent with the primary disorder (comorbidity) that could limit the patient recovery.
- (iv) The feasibility of using AI to generate optimal treatment protocols is still unclear, but considering that AI is a mature science at present, the potential to contribute to the implementation of the proposed DSS is encouraging.
- (v) Clinical protocols are validated through randomized control trials (RCT) where a large number of patients undergo the same treatment. In this regard, the most homogeneous samples must be recruited for RCTs that is challenging because of the inherent nature of neurological disorders.

Robots are currently viewed as advanced therapy tools under a therapist's guidance. However, the implementation of the above-mentioned systems could lead to more autonomous and intelligent processes in neurorehabilitation.

## Conflicts of Interest

The authors declare that they have no conflicts of interest.

## Acknowledgments

The research leading to these results has received funding from the ROBOHEALTH-A project (DPI2013-47944-C4-1-R) funded by the Spanish Ministry of Economy and Competitiveness and from the RoboCity2030-III-CM project (S2013/MIT-2748) funded by Programas de Actividades I+D en la Comunidad de Madrid and cofunded by the Structural Funds of the EU.

## References

- [1] A. Janca, J. A. Aarli, L. Prilipko, T. Dua, S. Saxena, and B. Saraceno, "WHO/WFN survey of neurological services: a worldwide perspective," *Journal of the Neurological Sciences*, vol. 247, no. 1, pp. 29–34, 2006.
- [2] United Nations, *World Population Ageing 2017 Report*, 2017, October, 2017 <http://www.un.org/en/development/desa/population/publications/index.shtml>.
- [3] R. C. Holliday, M. Antoun, and E. D. Playford, "A survey of goal-setting methods used in rehabilitation," *Neurorehabilitation and Neural Repair*, vol. 19, no. 3, pp. 227–231, 2005, 16093413.
- [4] J. Climent Barbera and J. Sanchez-Paya, "Indicadores de salud y medicina de rehabilitacion: estimadores de incapacidad en la poblacion," *Rehabilitacion*, vol. 30, pp. 277–286, 1996.
- [5] K. S. G. Chua and C. W. K. Kuah, "Innovating with rehabilitation technology in the real world: promises, potentials, and perspectives," *American Journal of Physical Medicine & Rehabilitation*, vol. 96, no. 10, pp. S150–S156, 2017.
- [6] H. M. Van der Loos, D. J. Reinkensmeyer, and E. Guglielmelli, "Rehabilitation and health care robotics," in *Springer Handbook of Robotics*, B. Siciliano and O. Khatib, Eds., pp. 1685–1728, Springer International Publishing, Cham, 2016.
- [7] P. Gomes, "Surgical robotics: reviewing the past, analysing the present, imagining the future," *Robotics and Computer-Integrated Manufacturing*, vol. 27, no. 2, pp. 261–266, 2011, Translational Research – Where Engineering Meets Medicine.
- [8] H. Huang, S. L. Wolf, and J. He, "Recent developments in biofeedback for neuromotor rehabilitation," *Journal of Neuroengineering and Rehabilitation*, vol. 3, no. 1, p. 11, 2006.
- [9] P. Poli, G. Morone, G. Rosati, and S. Masiero, "Robotic technologies and rehabilitation: new tools for stroke patients' therapy," *BioMed Research International*, vol. 2013, 8 pages, 2013.
- [10] A. A. Timmermans, H. A. Seelen, R. D. Willmann, and H. Kingma, "Technology-assisted training of arm-hand skills in stroke: concepts on reacquisition of motor control and therapist guidelines for rehabilitation technology design," *Journal of Neuroengineering and Rehabilitation*, vol. 6, no. 1, p. 1, 2009.
- [11] I. Diaz, J. J. Gil, and E. Sanchez, "Lower-limb robotic rehabilitation: literature review and challenges," *Journal of Robotics*, vol. 2011, Article ID 759764, 11 pages, 2011.
- [12] X. Lv and Z. Wu, "Review of robot-assisted gait rehabilitation after stroke," *Journal of Rehabilitation Robotics*, vol. 2013, pp. 3–8, 2013.
- [13] Z. Qian and Z. Bi, "Recent development of rehabilitation robots," *Advances in Mechanical Engineering*, vol. 7, no. 2, Article ID 563062, 2014.
- [14] L. Rodriguez-Prunotto, R. Cano-de la Cuerda, A. Cuesta-Gomez, I. M. Alguacil-Diego, and F. Molina-Rueda, "Terapia robótica para la rehabilitación del miembro superior en patología neurológica," *Rehabilitación*, vol. 48, no. 2, pp. 104–128, 2014.
- [15] L. Marchal-Crespo and D. J. Reinkensmeyer, "Review of control strategies for robotic movement training after neurologic injury," *Journal of Neuroengineering and Rehabilitation*, vol. 6, no. 1, p. 20, 2009.
- [16] T. Yan, M. Cempini, C. M. Oddo, and N. Vitiello, "Review of assistive strategies in powered lower-limb orthoses and exoskeletons," *Robotics and Autonomous Systems*, vol. 64, pp. 120–136, 2015.
- [17] A. C. Lo, P. D. Guarino, L. G. Richards et al., "Robot-assisted therapy for long-term upper-limb impairment after stroke," *New England Journal of Medicine*, vol. 362, no. 19, pp. 1772–1783, 2010.
- [18] G. Kwakkel, B. J. Kollen, and H. I. Krebs, "Effects of robot-assisted therapy on upper limb recovery after stroke: a systematic review," *Neurorehabilitation and Neural Repair*, vol. 22, no. 2, pp. 111–121, 2008.
- [19] N. Norouzi-Gheidari, P. S. Archambault, and J. Fung, "Effects of robot-assisted therapy on stroke rehabilitation in upper limbs: systematic review and meta-analysis of the literature," *Journal of Rehabilitation Research and Development*, vol. 49, no. 4, pp. 479–496, 2012.
- [20] J. M. Veerbeek, A. C. Langbroek-Amersfoort, E. E. H. van Wegen, C. G. M. Meskers, and G. Kwakkel, "Effects of robot-assisted therapy for the upper limb after stroke: a systematic review and metaanalysis," *Neurorehabilitation and Neural Repair*, vol. 31, no. 2, pp. 107–121, 2017.
- [21] World Health Organization, *World Report on Disability*, 2011, October 2017, <http://www.who.int/en/>.
- [22] T. Meyer, C. Gutenbrunner, J. Bickenbach, A. Cieza, J. Melvin, and G. Stucki, "Towards a conceptual description of rehabilitation as a health strategy," *Journal of Rehabilitation Medicine*, vol. 43, no. 769, pp. 765–769, 2011.
- [23] G. Stucki and O. Sangha, "Principles of rehabilitation," *Rheumatology*, vol. 1, pp. 517–530, 1998.
- [24] W. A. Steiner, L. Ryser, E. Huber, D. Uebelhart, A. Aeschlimann, and G. Stucki, "Use of the icf model as a clinical problem-solving tool in physical therapy and rehabilitation medicine," *Physical Therapy*, vol. 82, no. 111, pp. 1098–1107, 2002.
- [25] World Health Organization, *Neurological Disorders: Public Health Challenges*, 2006, October 2017, [http://www.who.int/mental\\_health/neurology/neurodiso/en/](http://www.who.int/mental_health/neurology/neurodiso/en/).
- [26] J. King, T. Nelson, K. Blankenship, T. Turturro, and A. Beck, *Rehabilitation Team Function and Prescriptions, Referrals, and Order Writing, Rehabilitation Medicine: Principles and*

- Practice*, J. A. Delisa, Ed., Lippincott Williams & Wilkins, Philadelphia, PA, USA, 4th edition, 2005.
- [27] M. McColl, N. Gerein, and F. Valentine, "Meeting the challenges of disability: models for enabling function and well-being," in *Occupational Therapy: Enabling Function and Well-Being*, pp. 509–528, Slack, Thorofare, NJ, USA, 1997.
- [28] M. Ramiro-Gonzalez and C. Gonzalez Alted, "El equipo de trabajo en neurorrehabilitacion," in *Neurorehabilitacion*, R. Cano-de la Cuerda and S. Collado Vazquez, Eds., pp. 61–72, Medica Panamericana, Madrid, Spain, 2012.
- [29] C. Reilly, "Transdisciplinary approach: an atypical strategy for improving outcomes in rehabilitative and long-term acute care settings," *Rehabilitation Nursing*, vol. 26, no. 6, pp. 216–244, 2001.
- [30] E. Finch, *Physical Rehabilitation Outcome Measures: A Guide to Enhanced Clinical Decision Making*, Canadian Physiotherapy Association, Hamilton, ON, Canada, 2nd edition, 2002.
- [31] World Health Organization, *International Classification of Functioning, Disability and Health (ICF)*, 2001, October 2017, <http://www.who.int/classifications/icf/en/>.
- [32] M. P. Barnes, "Principles of neurological rehabilitation," *Journal of Neurology, Neurosurgery & Psychiatry*, vol. 74, no. 90004, pp. 3iv–3iv7, 2003.
- [33] A. J. Thompson, "Neurological rehabilitation: from mechanisms to management," *Journal of Neurology, Neurosurgery & Psychiatry*, vol. 69, no. 6, pp. 718–722, 2000.
- [34] E. L. Miller, L. Murray, L. Richards et al., "Comprehensive overview of nursing and interdisciplinary rehabilitation care of the stroke patient: a scientific statement from the American Heart Association," *Stroke*, vol. 41, no. 10, pp. 2402–2448, 2010.
- [35] V. Neumann, C. Gutenbrunner, V. Fialka-Moser et al., "Interdisciplinary team working in physical and rehabilitation medicine," *Journal of Rehabilitation Medicine*, vol. 42, no. 1, pp. 4–8, 2010.
- [36] D. Katz, V. Mills, and J. Cassidy, "Neurological rehabilitation: a guide to diagnosis, prognosis and treatment planning," in *The Neurological Rehabilitation Model in Clinical Practice* pp. 1–27, Blackwell Science, Oxford, UK.
- [37] P. Kersten, "Principles of physiotherapy assessment and outcome measures," *Physical Management in Neurological Rehabilitation*, vol. 2, pp. 29–46, 2004.
- [38] K. Salter, N. Campbell, M. Richardson et al., "Outcome measures in stroke rehabilitation," in *Evidence-Based Review of Stroke Rehabilitation*, Heart and Stroke Foundation, Canadian Partnership for Stroke Recovery, Ontario, Canada, 2014.
- [39] S. Lennon, "Physiotherapy practice in stroke rehabilitation: a survey," *Disability and Rehabilitation*, vol. 25, no. 9, pp. 455–461, 2003, 12745940.
- [40] V. Pomeroy, S. M. Aglioti, V. W. Mark et al., "Neurological principles and rehabilitation of action disorders: rehabilitation interventions," *Neurorehabilitation and Neural Repair*, vol. 25, Supplement 5, pp. 33S–43S, 2011.
- [41] M. Donaghy, "Principles of neurological rehabilitation," in *Brain's Diseases of the Nervous System*, M. Donaghy, Ed., pp. 165–179, Oxford University Press, Oxford, UK, 12 edition, 2011.
- [42] E. Doig, J. Fleming, P. L. Cornwell, and P. Kuipers, "Qualitative exploration of a client-centered, goal-directed approach to community-based occupational therapy for adults with traumatic brain injury," *American Journal of Occupational Therapy*, vol. 63, no. 5, pp. 559–568, 2009.
- [43] The Partnership for Robotics in Europe SPARC, *Robotics 2020 Multi Annual Roadmap*, Call 2 ICT24 (2015) – Horizon 2020, Brussels, Belgium, 2015.
- [44] A. Davis, S. Davis, N. Moss et al., "First steps towards an interdisciplinary approach to rehabilitation," *Clinical Rehabilitation*, vol. 6, no. 3, pp. 237–244, 1992.
- [45] C. Bosecker, L. Dipietro, B. Volpe, and H. I. Krebs, "Kinematic robot-based evaluation scales and clinical counterparts to measure upper limb motor performance in patients with chronic stroke," *Neurorehabilitation and Neural Repair*, vol. 24, no. 1, pp. 62–69, 2010, 19684304.
- [46] "Capterra," 1999, January 2018, <https://www.capterra.com/electronic-medical-records-software/>.
- [47] "The medical futurist," 2018, January 2018, <http://medicalfuturist.com/top-artificial-intelligence-companies-in-healthcare/>.
- [48] M. Iosa, G. Morone, A. Cherubini, and S. Paolucci, "The three laws of neurorobotics: a review on what neurorehabilitation robots should do for patients and clinicians," *Journal of Medical and Biological Engineering*, vol. 36, no. 1, pp. 1–11, 2016.
- [49] R. Muradore, P. Fiorini, G. Akgun et al., "Development of a cognitive robotic system for simple surgical tasks," *International Journal of Advanced Robotic Systems*, vol. 12, no. 4, p. 37, 2015.
- [50] J. Hidler and P. S. Lum, "The road ahead for rehabilitation robotics," *The Journal of Rehabilitation Research and Development*, vol. 48, no. 4, pp. vii–vix, 2011.
- [51] A. M. Acosta, H. A. Dewald, and J. P. Dewald, "Pilot study to test effectiveness of video game on reaching performance in stroke," *The Journal of Rehabilitation Research and Development*, vol. 48, no. 4, pp. 431–444, 2011.
- [52] C. G. Burgar, S. L. Garber, H. M. Van der Loos, O. PhD, M. S. Deborah Kenney, and P. Shor, "Robot-assisted upper-limb therapy in acute rehabilitation setting following stroke: department of veterans affairs multisite clinical trial," *The Journal of Rehabilitation Research and Development*, vol. 48, no. 4, pp. 445–458, 2011.
- [53] M. Saborowski and I. Kollak, "How do you care for technology?" – care professionals' experiences with assistive technology in care of the elderly," *Technological Forecasting and Social Change*, vol. 93, pp. 133–140, 2015, Science, Technology and the "Grand Challenge" of Ageing.
- [54] W. J. Coster, "Making the best match: selecting outcome measures for clinical trials and outcome studies," *American Journal of Occupational Therapy*, vol. 67, no. 2, pp. 162–170, 2013.
- [55] P. Otten, J. Kim, and S. H. Son, "A framework to automate assessment of upper-limb motor function impairment: a feasibility study," *Sensors*, vol. 15, no. 12, pp. 20097–20114, 2015.
- [56] E. D. Oña, A. Jardón, and C. Balaguer, "The automated box and blocks test an autonomous assessment method of gross manual dexterity in stroke rehabilitation," in *Towards Autonomous Robotic Systems*, Lecture Notes in Computer Science, Y. Gao, S. Fallah, Y. Jin, and C. Lekakou, Eds., pp. 101–114, Springer, Cham, 2017.
- [57] J. Hobart, D. Lamping, J. Freeman et al., "Evidence-based measurement which disability scale for neurologic rehabilitation?," *Neurology*, vol. 57, no. 4, pp. 639–644, 2001.

- [58] H. L. Semigran, D. M. Levine, S. Nundy, and A. Mehrotra, "Comparison of physician and computer diagnostic accuracy," *JAMA Internal Medicine*, vol. 176, no. 12, pp. 1860-1861, 2016.
- [59] H. I. Krebs, J. J. Palazzolo, L. Dipietro et al., "Rehabilitation robotics: performance-based progressive robot-assisted therapy," *Autonomous Robots*, vol. 15, no. 1, pp. 7-20, 2003.
- [60] D. M. Roijers and S. Whiteson, "Multi-objective decision making," *Synthesis Lectures on Artificial Intelligence and Machine Learning*, vol. 11, no. 1, pp. 1-129, 2017.
- [61] M. D. Ellis, T. M. Sukal-Moulton, and J. Dewald, "Impairment-based 3-D robotic intervention improves upper extremity work area in chronic stroke: targeting abnormal joint torque coupling with progressive shoulder abduction loading," *IEEE Transactions on Robotics*, vol. 25, no. 3, pp. 549-555, 2009.
- [62] L. E. Kahn, M. L. Zygman, W. Z. Rymer, and D. J. Reinkensmeyer, "Robotassisted reaching exercise promotes arm movement recovery in chronic hemiparetic stroke: a randomized controlled pilot study," *Journal of Neuroengineering and Rehabilitation*, vol. 3, no. 1, p. 12, 2006.
- [63] D. J. Reinkensmeyer, L. E. Kahn, M. Averbuch, A. McKenna-Cole, B. D. Schmit, and W. Z. Rymer, "Understanding and treating arm movement impairment after chronic brain injury: progress with the arm guide," *Journal of Rehabilitation Research and Development*, vol. 37, p. 653, 2000.
- [64] M. Casadio, V. Sanguineti, P. G. Morasso, and V. Arrichiello, "Braccio di ferro: a new haptic workstation for neuromotor rehabilitation," *Technology and Health Care*, vol. 14, no. 3, pp. 123-142, 2006.
- [65] E. Vergaro, M. Casadio, V. Squeri, P. Giannoni, P. Morasso, and V. Sanguineti, "Self-adaptive robot training of stroke survivors for continuous tracking movements," *Journal of Neuroengineering and Rehabilitation*, vol. 7, no. 1, p. 13, 2010.
- [66] R. Loureiro, F. Amirabdollahian, M. Topping, B. Driessens, and W. Harwin, "Upper limb robot mediated stroke therapy—gentle/s approach," *Autonomous Robots*, vol. 15, no. 1, pp. 35-51, 2003.
- [67] S. Coote, B. Murphy, W. Harwin, and E. Stokes, "The effect of the gentle/s robot-mediated therapy system on arm function after stroke," *Clinical Rehabilitation*, vol. 22, no. 5, pp. 395-405, 2008.
- [68] *Bionik Laboratories Corp*, 2010, October 2017, <https://www.bioniklabs.com/>.
- [69] A. E. Jackson, P. R. Culmer, M. C. Levesley, S. G. Makower, J. A. Cozens, and B. B. Bhakta, "Effector force requirements to enable robotic systems to provide assisted exercise in people with upper limb impairment after stroke," in *2011 IEEE International Conference on Rehabilitation Robotics*, pp. 1-6, Zurich, Switzerland, 2011.
- [70] A. Jackson, P. Culmer, S. Makower et al., "Initial patient testing of ipam a robotic system for stroke rehabilitation," in *2007 IEEE 10th International Conference on Rehabilitation Robotics*, pp. 250-256, Noordwijk, Netherlands, 2007.
- [71] S. Micera, P. N. Sergi, F. Zaccone et al., "A low-cost biomechatronic system for the restoration and assessment of upper limb motor function in hemiparetic subjects," in *2006 The First IEEE/RAS-EMBS International Conference on Biomedical Robotics and Biomechatronics*, pp. 25-30, BioRob, Pisa, Italy, 2006.
- [72] R. Colombo, F. Pisano, S. Micera et al., "Robotic techniques for upper limb evaluation and rehabilitation of stroke patients," *IEEE Transactions on Neural Systems and Rehabilitation Engineering*, vol. 13, no. 3, pp. 311-324, 2005.
- [73] P. S. Lum, C. G. Burgar, M. Van der Loos, P. C. Shor, M. Majmundar, and R. Yap, "Mime robotic device for upper-limb neurorehabilitation in subacute stroke subjects: a follow-up study," *The Journal of Rehabilitation Research and Development*, vol. 43, no. 5, pp. 631-642, 2006.
- [74] S. Masiero, M. Armani, and G. Rosati, "Upper-limb robot-assisted therapy in rehabilitation of acute stroke patients: focused review and results of new randomized controlled trial," *Journal of Rehabilitation Research and Development*, vol. 48, no. 4, pp. 355-366, 2011.
- [75] S. Masiero, M. Armani, G. Ferlini, G. Rosati, and A. Rossi, "Randomized trial of a robotic assistive device for the upper extremity during early inpatient stroke rehabilitation," *Neurorehabilitation and Neural Repair*, vol. 28, no. 4, pp. 377-386, 2014, 24316679.
- [76] A. Toth, G. Fazekas, G. Arz, M. Jurak, and M. Horvath, "Passive robotic movement therapy of the spastic hemiparetic arm with reharob: report of the first clinical test and the follow-up system improvement," in *2005 9th International Conference on Rehabilitation Robotics*, pp. 127-130, ICORR, Chicago, IL, USA, 2005.
- [77] G. Fazekas, M. Horvath, T. Troznai, and A. Toth, "Robot-mediated upper limb physiotherapy for patients with spastic hemiparesis: a preliminary study," *Journal of Rehabilitation Medicine*, vol. 39, no. 7, pp. 580-582, 2007.
- [78] "Tyromotion gmbh," 2007, October 2017, <http://tyromotion.com/>.
- [79] P. Sale, V. Lombardi, and M. Franceschini, "Hand robotics rehabilitation: feasibility and preliminary results of a robotic treatment in patients with hemiparesis," *Stroke Research and Treatment*, vol. 2012, 5 pages, 2012.
- [80] C. H. Hwang, J. W. Seong, and D.-S. Son, "Individual finger synchronized robot-assisted hand rehabilitation in subacute to chronic stroke: a prospective randomized clinical trial of efficacy," *Clinical Rehabilitation*, vol. 26, no. 8, pp. 696-704, 2012.
- [81] S. Hesse, G. Schulte-Tigges, M. Konrad, A. Bardeleben, and C. Werner, "Robot-assisted arm trainer for the passive and active practice of bilateral forearm and wrist movements in hemiparetic subjects," *Archives of Physical Medicine and Rehabilitation*, vol. 84, no. 6, pp. 915-920, 2003.
- [82] H. Schmidt, S. Hesse, C. Werner, and A. Bardeleben, "Upper and lower extremity robotic devices to promote motor recovery after stroke -recent developments," in *2004 26th Annual International Conference of the IEEE Engineering in Medicine and Biology Society*, vol. 2, pp. 4825-4828, San Francisco, CA, USA, 2004.
- [83] C. D. Takahashi, L. Der-Yeghaian, V. H. Le, and S. C. Cramer, "A robotic device for hand motor therapy after stroke," in *2005 9th International Conference on Rehabilitation Robotics*, pp. 17-20, ICORR, Chicago, IL, USA, 2005.
- [84] C. D. Takahashi, L. Der-Yeghaian, V. Le, R. R. Motiwala, and S. C. Cramer, "Robot-based hand motor therapy after stroke," *Brain*, vol. 131, no. 2, pp. 425-437, 2008.
- [85] "Motorika medical ltd," 2004, October 2017, <http://motorika.com/>.

- [86] I. Treger, S. Faran, and H. Ring, "Robot-assisted therapy for neuromuscular training of sub-acute stroke patients. A feasibility study," *European Journal of Physical and Rehabilitation Medicine*, vol. 44, no. 4, pp. 431–435, 2008.
- [87] P. Meyer-Rachner, A. Passon, C. Klauer, and T. Schauer, "Compensating the effects of fes-induced muscle fatigue by rehabilitation robotics during arm weight support," *Current Directions in Biomedical Engineering*, vol. 3, pp. 31–34, 2017.
- [88] A. Montagner, A. Frisoli, L. Borelli et al., "A pilot clinical study on robotic assisted rehabilitation in vr with an arm exoskeleton device," in *2007 Virtual Rehabilitation*, pp. 57–64, Venice, Italy, 2007.
- [89] "Myomo, inc," 2017, October 2017, <http://myomo.com/>.
- [90] S. J. Page, V. Hill, and S. White, "Portable upper extremity robotics is as efficacious as upper extremity rehabilitative therapy: a randomized controlled pilot trial," *Clinical Rehabilitation*, vol. 27, no. 6, pp. 494–503, 2013.
- [91] G. J. Kim, L. Rivera, and J. Stein, "Combined clinic-home approach for upper limb robotic therapy after stroke: a pilot study," *Archives of Physical Medicine and Rehabilitation*, vol. 96, no. 12, pp. 2243–2248, 2015.
- [92] T. Rahman, W. Sample, S. Jayakumar et al., "Passive exoskeletons for assisting limb movement," *Journal of Rehabilitation Research and Development*, vol. 43, no. 5, pp. 583–590, 2006.
- [93] "Hocoma," 1996, October 2017, <https://www.hocoma.com/>.
- [94] D. Gijbels, I. Lamers, L. Kerkhofs, G. Alders, E. Knippenberg, and P. Feys, "The armeo spring as training tool to improve upper limb functionality in multiple sclerosis: a pilot study," *Journal of Neuroengineering and Rehabilitation*, vol. 8, no. 1, p. 5, 2011.
- [95] R. J. Sanchez, J. Liu, S. Rao et al., "Automating arm movement training following severe stroke: functional exercises with quantitative feedback in a gravity-reduced environment," *IEEE Transactions on Neural Systems and Rehabilitation Engineering*, vol. 14, no. 3, pp. 378–389, 2006.
- [96] "Motus nova," 2016, October 2017, <http://motusnova.com/>.
- [97] N. G. Kutner, R. Zhang, A. J. Butler, S. L. Wolf, and J. L. Alberts, "Quality-of-life change associated with robotic-assisted therapy to improve hand motor function in patients with subacute stroke: a randomized clinical trial," *Physical Therapy*, vol. 90, no. 4, pp. 493–504, 2010.
- [98] E. J. Koeneman, R. S. Schultz, S. L. Wolf, D. E. Herring, and J. B. Koeneman, "A pneumatic muscle hand therapy device," in *2004 The 26th Annual International Conference of the IEEE Engineering in Medicine and Biology Society*, vol. 1, pp. 2711–2713, San Francisco, CA, USA, 2004.
- [99] C. N. Schabowsky, S. B. Godfrey, R. J. Holley, and P. S. Lum, "Development and pilot testing of hexorr: hand exoskeleton rehabilitation robot," *Journal of Neuroengineering and Rehabilitation*, vol. 7, no. 1, p. 36, 2010.
- [100] M. Bouzit, G. Burdea, G. Popescu, and R. Boian, "The rutgers master ii-new design force-feedback glove," *IEEE/ASME Transactions on Mechatronics*, vol. 7, no. 2, pp. 256–263, 2002.
- [101] A. Merians, D. Jack, R. Boian et al., "Virtual reality-augmented rehabilitation for patients following stroke," *Physical Therapy*, vol. 82, pp. 898–915, 2002.
- [102] J. Allington, S. J. Spencer, J. Klein, M. Buell, D. J. Reinkensmeyer, and J. Bobrow, "Supinator extender (sue): a pneumatically actuated robot for forearm/wrist rehabilitation after stroke," in *2011 Annual International Conference of the IEEE Engineering in Medicine and Biology Society*, pp. 1579–1582, Boston, MA, USA, 2011.
- [103] R. Sanchez, D. Reinkensmeyer, P. Shah et al., "Monitoring functional arm movement for home-based therapy after stroke," in *2004 The 26th Annual International Conference of the IEEE Engineering in Medicine and Biology Society*, vol. 2, pp. 4787–4790, San Francisco, CA, USA, 2004.
- [104] E. Rocon, J. M. Belda-Lois, A. F. Ruiz, M. Manto, J. C. Moreno, and J. L. Pons, "Design and validation of a rehabilitation robotic exoskeleton for tremor assessment and suppression," *IEEE Transactions on Neural Systems and Rehabilitation Engineering*, vol. 15, no. 3, pp. 367–378, 2007.
- [105] T. Nef and R. Riener, "Shoulder actuation mechanisms for arm rehabilitation exoskeletons," in *2008 2nd IEEE RAS EMBS International Conference on Biomedical Robotics and Biomechatronics*, pp. 862–868, Scottsdale, AZ, USA, 2008.
- [106] M. Guidali, A. Duschau-Wicke, S. Broggi, V. Klamroth-Marganska, T. Nef, and R. Riener, "A robotic system to train activities of daily living in a virtual environment," *Medical & Biological Engineering & Computing*, vol. 49, no. 10, pp. 1213–1223, 2011.
- [107] T. Nef, M. Mihelj, G. Colombo, and R. Riener, "Armin - robot for rehabilitation of the upper extremities," in *Proceedings 2006 IEEE International Conference on Robotics and Automation*, pp. 3152–3157, Orlando, FL, USA, 2006.
- [108] T. Nef, M. Mihelj, and R. Riener, "Armin: a robot for patient-cooperative arm therapy," *Medical & Biological Engineering & Computing*, vol. 45, no. 9, pp. 887–900, 2007.
- [109] R. C. V. Loureiro and W. S. Harwin, "Reach & grasp therapy: Design and control of a 9-dof robotic neuro-rehabilitation system," in *2007 IEEE 10th International Conference on Rehabilitation Robotics*, pp. 757–763, Noordwijk, Netherlands, 2007.
- [110] J. Huang, X. Tu, and J. He, "Design and evaluation of the rupert wearable upper extremity exoskeleton robot for clinical and in-home therapies," *IEEE Transactions on Systems, Man, and Cybernetics: Systems*, vol. 46, no. 7, pp. 926–935, 2016.
- [111] S. Balasubramanian, R. Wei, M. Perez et al., "Rupert: an exoskeleton robot for assisting rehabilitation of arm functions," in *2008 Virtual Rehabilitation*, pp. 163–167, Vancouver, Canada, 2008.

## Research Article

# Rehabilitation of Upper Limb in Children with Acquired Brain Injury: A Preliminary Comparative Study

Elena Beretta,<sup>1</sup> Ambra Cesareo,<sup>2</sup> Emilia Biffi ,<sup>1</sup> Carolyn Schafer,<sup>3</sup> Sara Galbiati,<sup>1</sup> and Sandra Strazzer<sup>1</sup>

<sup>1</sup>Scientific Institute IRCCS Eugenio Medea, Bosisio Parini, Lecco, Italy

<sup>2</sup>Dipartimento di Elettronica, Informazione e Bioingegneria, Politecnico di Milano, Milan, Italy

<sup>3</sup>School of Biomedical Engineering, Science and Health Systems, Drexel University, Philadelphia, PA, USA

Correspondence should be addressed to Emilia Biffi; emilia.biffi@bp.lnf.it

Received 14 November 2017; Accepted 29 January 2018; Published 14 March 2018

Academic Editor: Antonio Fernández-Caballero

Copyright © 2018 Elena Beretta et al. This is an open access article distributed under the Creative Commons Attribution License, which permits unrestricted use, distribution, and reproduction in any medium, provided the original work is properly cited.

Acquired brain injuries (ABIs) can lead to a wide range of impairments, including weakness or paralysis on one side of the body known as hemiplegia. In hemiplegic patients, the rehabilitation of the upper limb skills is crucial, because the recovery has an immediate impact on patient quality of life. For this reason, several treatments were developed to flank physical therapy (PT) and improve functional recovery of the upper limbs. Among them, Constraint-Induced Movement Therapy (CIMT) and robot-aided therapy have shown interesting potentialities in the rehabilitation of the hemiplegic upper limb. Nevertheless, there is a lack of quantitative evaluations of effectiveness in a standard clinical setting, especially in children, as well as a lack of direct comparative studies between these therapeutic techniques. In this study, a group of 18 children and adolescents with hemiplegia was enrolled and underwent intensive rehabilitation treatment including PT and CIMT or Armeo®Spring therapy. The effects of the treatments were assessed using clinical functional scales and upper limb kinematic analysis during horizontal and vertical motor tasks. Results showed CIMT to be the most effective in terms of improved functional scales, while PT seemed to be the most significant in terms of kinematic variations. Specifically, PT resulted to have positive influence on distal movements while CIMT conveyed more changes in the proximal kinematics. Armeo treatment delivered improvements mainly in the vertical motor task, showing trends of progresses of the movement efficiency and reduction of compensatory movements of the shoulder with respect to other treatments. Therefore, every treatment gave advantages in a specific and different upper limb district. Therefore, results of this preliminary study may be of help to define the best rehabilitation treatment for each patient, depending on the goal, and may thus support clinical decision.

## 1. Introduction

Acquired brain injuries are nonprogressive, nonhereditary brain injuries acquired sometime after birth and are the leading cause of long-term disability and death in children and young adults. Resulting from trauma, hypoxia, stroke, infection, or a variety of other sources, ABIs can lead to a wide variety of impairments, including deficiencies in cognitive, behavioral, metabolic, motor, perceptual motor, and/or sensory brain functions. In particular, a number of ABIs lead to significant hemiplegia [1], a weakness or paralysis on one side of the body, with relevant effects on the upper limb functionality [2].

In cases of hemiplegia, the aim of rehabilitation of the upper limbs is to prevent the disuse of the impaired side of the body. Many studies in literature have shown that therapy involving sensorimotor exercises to simulate meaningful tasks used in daily life increases the functional recovery of the affected upper limb [3, 4]. Realistic contexts of functional activities, such as reaching or pointing towards an everyday object, help patients acquire control strategies to compensate for muscle weakness and inaccuracies [5].

In order to rehabilitate the upper limbs, there are a variety of treatments available. Physical therapy (hereafter PT) is standard practice worldwide, but there are other types. Therapy aided by a robotic exoskeleton is noted for its

capability of supporting repetitive and high-intensity training tasks as well as its ability to reliably track patients' motor progress by quantitatively measuring patients' movement kinematics and forces, rather than relying on subjective impressions [6]. When combined with interactive programs such as virtual reality, robot-aided therapy can assign functional meaning to the therapy, creating a motivating environment [6–9]. Studies involving robotic therapy have shown improvements in upper limb coordination and fluency of movement in the hands and fingers of children with cerebral palsy [10, 11].

Constraint-Induced Movement Therapy (CIMT) involves constraining the nonimpaired upper extremity in order to encourage use of the impaired side. CIMT therapy often involves intensive repetitive tasks directed by a therapist in order to practice motor movements [12]. CIMT is a rehabilitative methodology widely used nowadays, even on infants below one year of age (named baby-CIMT); it is considered feasible and without adverse effects [13]. Studies involving CIMT had shown improvements in the reaction time and movement-path length and improved smoothness in actions of the impaired limb in adults, with the overall goal to increase functional use and support cortical reorganization [12, 14–19].

There are numerous standardized clinical functional scales used for the assessment and evaluation of upper limb impairment and activity limitation. The majority of these utilize an ordinal-level scoring system, with scores assigned to the patient by the observing physician or therapist. Another way to assess upper limb activity is through kinematic data from 3D motion capture. Kinematic data is more objective and quantifiable, and there are a myriad of metrics available for calculation, both temporal, such as time and velocity, and spatial, such as joint angles and trunk displacement. However, the protocol for the measurement of kinematics is less standardized and can be difficult to compare, especially when dealing with child subjects [14].

Although previous studies have shown promising results of CIMT and robot-aided therapy in children [9, 12, 20], there is a lack of quantitative evaluations of effectiveness in a standard clinical setting as well as a lack of direct comparative studies between these therapeutic techniques.

The purpose of the present study is to quantify and compare the effects of constraint, robot-aided, and physical therapies in the rehabilitation of upper limbs of children and adolescents after ABI measured by both functional scales and kinematic data. Preliminary results have been presented in [21].

## 2. Materials and Methods

A group of children/adolescents with hemiplegia was enrolled in the study.

**2.1. Subjects.** In order to be included in this study, participants had to be 4–18 years old, had to have a clinical form of hemiplegia and a severe acquired brain injury, and had to have the ability to understand and follow test instructions. Patients were excluded from the study if they had severe

muscle spasticity and/or contracture, a diagnosis of severe learning disabilities or behavioral problems, visual or hearing difficulties that would impact on function and participation, previously undergone restraint therapy, or injections of antispasticity drugs (e.g., Botox or Dysport) into the upper limb musculature in the 6 months leading up to the beginning of the trial.

Taking these criteria into consideration, eighteen children/adolescents (hereafter, participants) (9 M and 9 F, mean age:  $12.28 \pm 5.13$  years) were recruited: ten had right-sided and eight had left-sided impairments. The mean age at injury was  $10.95 (\pm 4.88)$  years. Eight participants had a traumatic brain injury, seven participants had a stroke, two participants had a brain injury due to encephalitis, and one participant had a brain injury due to other causes. They took part in the clinical protocol  $1.25 (\pm 1.02)$  years after the injury.

All parents were informed about the study and signed a consent statement. The study was approved by the Ethics Committee of the Scientific Institute IRCCS Eugenio Medea, located in Bosisio Parini, Italy, in accordance with the declaration of Helsinki.

**2.2. Rehabilitative Protocol.** The rehabilitation program included two consecutive four-week periods of treatment, attended in a random order: one period of physical therapy (PT) and one period of a rehabilitative treatment, randomly chosen between Constraint-Induced Movement Therapy (CIMT) and training with Armeo®Spring.

PT treatment was administered in five 45-minute sessions per week for each of the four weeks. PT emphasized fine and gross motor skills and multimodal exploration, with the overall goal of successfully performing independent daily living skills such as self-care and eating. It was based on motor control and motor-learning theories, task-oriented and customized on the single patient's functional status. Fine motor skills included monomanual and bimanual grasping and use of individual fingers, while gross motor skills focused on reactive balance responses and postural support. There were four types of task goals: perceptual motor activities; activities of reaching, grasping, holding, and manipulating; activities for posture and balance; and self-care and daily living activities.

During Constraint-Induced Movement Therapy (CIMT), a restraining thermoplastic splint was worn on the unaffected hand, preventing subjects from flexing their fingers or grasping objects. Even though the thumb was locked in a fixed position against the index finger, children could use the hand for support or to break a fall. The splint was worn for at least 3 consecutive hours a day, every day of the week for 4 weeks. While the splint was worn, children/adolescents underwent an intensive rehabilitation program to simulate play sessions and a daily living activity. Unimanual activities performed included memory cards, puzzles, playing bowls and cards, using a spoon or fork, and/or dusting a surface.

Armeo®Spring is an exoskeleton with five degrees of freedom that uses springs (rather than robotic actuators) to guarantee passive arm weight support and guidance (Figure 1). By adapting to each patient's individual morphology and residual ability, the Armeo exoskeleton enables



FIGURE 1: The exoskeleton Armeo®Spring.

users to achieve a large range of motion in a 3D workspace. Subjects using Armeo were given 45-minute treatment sessions 5 times a week for 4 weeks. In each session, subjects used dedicated system software to simulate intense and meaningful tasks targeting different upper arm joints and regions. Physical therapists oversaw each session; adjusted the exercises, weight compensation, and maximal active workspace according to each subject's progress; and performed setup and maintenance on the Armeo system. As patients improved, physical therapists would increase the difficulty level and number of repetitions of the games, as well as introduce more difficult games into the training system.

**2.3. Evaluation.** Experimental subjects participated in two types of therapy and were evaluated with functional scales and with upper limb kinematic analysis at pre-treatment (T0), post-first treatment (T1), and post-second treatment (T2).

**2.3.1. Functional Scales.** Clinical data in terms of age at trauma, etiology, and severity were collected at T0 while the Quality of Upper Extremities Skills Test (QUEST), the Melbourne Assessment of Unilateral Upper Limb Function, and the Gross Motor Function Measure (GMFM) were assessed in the clinical examination at T0, T1, and T2.

The Quality of Upper Extremities Skills Test (QUEST) is an internationally validated scale designed to measure treatment outcome in children with upper extremity movement disorders. It explores four domains: dissociated movement, grasp, weight bearing, and protective extension. The dissociated movement domain includes items that counter typical patterns of spastic synergy, representing each joint of the upper limb. Grasp items are based on normal hand grasps as described in developmental literature, arranged in a hierarchical and developmental framework. Weight bearing and protective extension are based on normal developmental sequence and are scored hierarchically based on the degree of abnormality as represented by joint positions. The domain score is a summed-item score converted into a standardized percentage, and the total score is the average of domain scores, with higher scores representing a better quality of movement [22].

The Melbourne Assessment of Unilateral Upper Limb Function, abbreviated to the Melbourne Assessment [23], is a criterion-referenced test developed for use with patients with neurological impairment. The Melbourne Assessment scores the quality of unilateral upper-limb motor function based on items involving reach, grasp, release, and manipulation. In comparison to the Melbourne Assessment, items on the QUEST have been designed also to provide information about postural responses [23, 24].

The GMFM measures the child's overall functional abilities and consists of 88 items, divided into the following sections: (1) lying and rolling, (2) sitting, (3) crawling and kneeling, (4) standing, and (5) walking, running, and jumping. Each section contributes to the total GMFM score [25].

**2.3.2. Kinematics.** The evaluation consisted of two tasks completed by the subjects, namely horizontal-reaching movements and vertical-reaching movements, while an optoelectronic system for motion capture recorded the kinematics of the participants.

**(1) Horizontal Reaching.** During this task, the subject was seated at a table adjusted to a level to support the subject's arms. A stationary marker target was placed on the table along the subject's midline, at a distance equal to 80% of the subject's arm length away from the body. Both hands were to rest on the table, with the hand performing the task to trace the midline path from the body to the marker target and back and the other hand stationary for support (Figure 2(a)). Neither the trunk nor the head were constrained, but the subject was asked to complete the movements as precisely and concisely as possible. The horizontal task was completed three times with each arm by each subject.

**(2) Vertical Reaching.** During the vertical-reaching task (Figure 2(b)), the subject seated comfortably on a chair with a pole with an adjustable support in front of him/her. The pole was adjusted in order to have the edge of the support aligned with the subject's knees. In the starting position, the participant had the tested arm pronated with the finger leaning on the edge of the pole's support. The upper arm was in a neutral adducted position with approximately 90° flexion at the elbow. The participant's other hand was resting on the knee. The subject was asked to move the index finger upward along the pole, following a thin adhesive stripe, as fast as possible but with a maximum precision, reaching the maximum height allowed (but remaining in the seated position) and then returning to the initial position. Neither the trunk nor the head were constrained. The vertical task was completed three times with each arm by each subject.

**(3) Equipment and Kinematic Variables.** The task was recorded using the BTS OEP System (BTS Bioengineering), with 8 cameras with semi-infrared rays that acquire at a frequency of 60 Hz and submultiples. 12 semispherical, retro-reflective markers were placed on specific body landmarks: two markers were placed on the trunk—one above vertebrae C7 and the other on the upper part of sternum. Ten markers

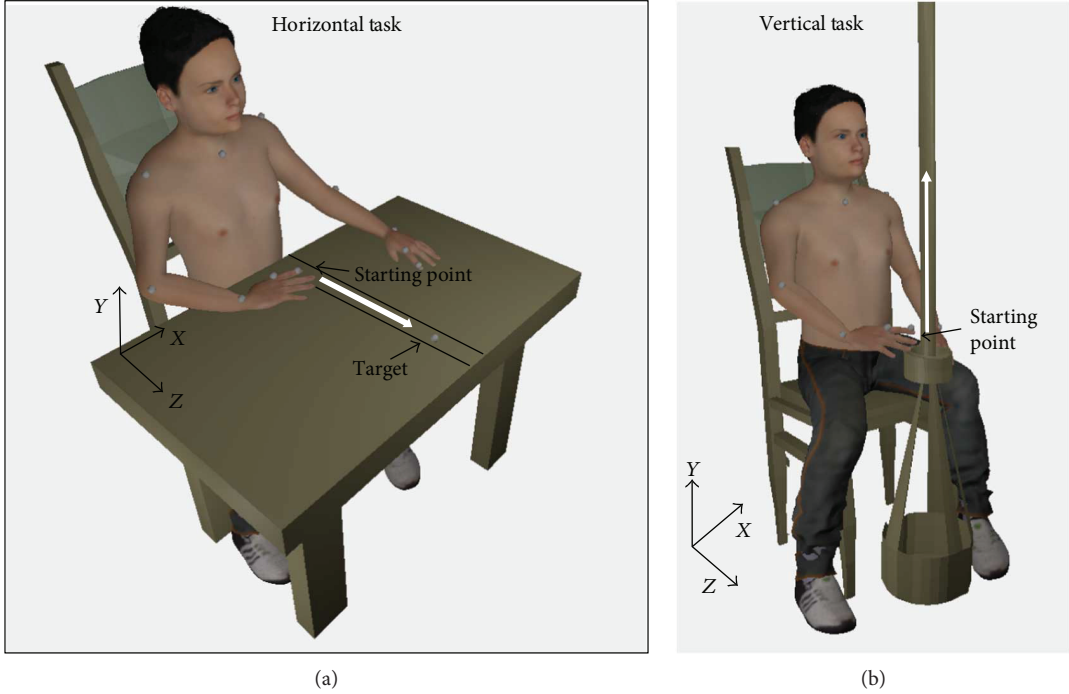


FIGURE 2: 3D sketch of the testing setup, for the horizontal task (left panel) and the vertical task (right panel). Gray dots are the retroreflective markers.

were placed bilaterally on the acromion, elbow, wrist (ulnar styloid processes), second metacarpal head, and fingernail of the index (Figure 2). The system was able to extrapolate the 3D coordinates of each marker in space and reconstruct the trajectory of each for the whole duration of the movement. Data were analyzed using MATLAB: at first, data were filtered by means of a low-pass filter with a cutoff frequency of 10 Hz. Then, for each movement, three phases were identified, as described in [12]: going phase ( $F_{go}$ ), representing the movement towards the target marker starting from the rest position; adjusting phase ( $F_{adj}$ ) that is dedicated to precisely locating the target; and returning phase ( $F_{ret}$ ) representing the movement towards the starting point. For each phase, many parameters were calculated, both for the horizontal- and the vertical-reaching tasks. In particular, kinematic parameters were divided into three categories and are reported in Table 1:

- (i) *End-point (finger) metrics*: parameters belonging to this category were computed using end-point (finger) kinematic data and provide information about speed of execution, accuracy, efficiency, and smoothness of the movement.
- (ii) *Joint kinematics*: angles at the elbow and shoulder were computed as described in previous studies [5, 26]; then, ranges of motion (ROMs) and angular velocity were computed for elbow and shoulder.
- (iii) *Trunk compensation*: information derived mainly from the marker placed on the sternum, describing the compensatory movements of the trunk during the reaching movements.

Data were gathered from patients before and after each of the two sets of treatment. Data were divided into groups based on the treatment (namely PT, CIMT, and Armeo) and analyzed comparing treatment type, independently from the order of occurrence of treatments.

**2.4. Statistical Analysis.** Both clinical scale results and the data extracted from the kinematic trials were analyzed in MATLAB using nonparametric statistics, since the Shapiro–Wilk test highlighted a number of data parameters not normally distributed.

To evaluate differences between groups at pretreatment, the Kruskal–Wallis test followed by the Mann–Whitney test with the Bonferroni correction as post hoc analysis were used. Further, the chi-square test was used to check the uniformity of the samples at the beginning of treatment, with regard to sex, etiology, age, distance from event, GCS, and QI. For each treatment, the Wilcoxon test for paired samples was used to compare pre- and posttreatment results, both for kinematic variables and functional scales. To compare treatments, for each variable, the difference ( $\Delta$ ) between post- and pretreatment values was computed, and the Kruskal–Wallis test was used to compare the three treatments, followed by the Mann–Whitney test with the Bonferroni correction as post hoc. For all statistical comparisons, it has defined a maximum value of accepted possible error equal to 5% ( $p = 0.05$ ).

### 3. Results

All children performed the horizontal task and were evaluated with kinematic analysis, while 2 children did not perform the vertical task. 9 subjects ( $N = 9$  for horizontal

TABLE 1: Kinematic variables computed for the horizontal and vertical task.

		Horizontal task	Vertical task
<i>End-point (finger) metrics</i>			
Hand path ratio ( $P_{go}$ ) HPR <sub>go</sub>	A measure of how directly the hand moves toward the target, computed as the ratio between the length of the real subject's hand (finger) path and the length of the theoretical or desired trajectory. This metric quantifies the movement efficiency.	✓	✓
Displacement along $y$ -axis, Y-FD	The difference between the maximum and the minimum $y$ coordinate during the whole movement, representing the vertical displacement of the finger.		✓
Movement time ( $P_{go}$ ) MT <sub>go</sub>	Time from the onset to the offset of the going phase quantifies the movement speed and upper extremity function within the given task.	✓	
Target error	It is a measure of the movement quality in terms of accuracy, computed as the maximum distance from the index finger to the target during the adjusting phase.	✓	
Mean velocity ( $P_{go}$ ) MV <sub>go</sub>	Mean arm velocity attained during the going phase computed from the speed profile of the finger.	✓	✓
Number of velocity peaks (Tot), #VP <sub>tot</sub>	It is a quality measure of the movement smoothness computed from the speed profile of the finger during the whole movement.	✓	✓
<i>Joint kinematics</i>			
Joint ROMs	Range of motion for the elbow (flex-extension) and the shoulder (abduction-adduction and flex-extension) computed as the difference between the maximum and the minimum angle, considering the whole movement.	✓	✓
Mean angular velocity (MAV)	Mean angular velocity during elbow flex-extension and shoulder abduction-adduction or flex-extension, during the going phase.	✓	✓
<i>Trunk compensation</i>			
Trunk 3D path	3D path length of the marker placed on the sternum	✓	✓
Displacement along $z$ -axis ( $P_{go}$ ), Z-TD <sub>go</sub>	Displacement of the marker placed on the sternum along the $z$ -axis (towards the target) during the going phase. It quantifies trunk flexion.	✓	
Displacement along $x$ -axis ( $P_{go}$ ), X-TD <sub>go</sub>	Displacement of the marker placed on the sternum along the $x$ -axis during the going phase. It quantifies trunk lateral bending.		✓

task,  $N = 9$  for vertical task) underwent the CIMT rehabilitative treatment, and 9 subjects ( $N = 9$  for horizontal task,  $N = 8$  for vertical task) completed successfully the Armeo protocol; as 6 patients left the study before its end, only 12 ( $N = 12$  for horizontal task,  $N = 11$  for the vertical task) subjects were included into the PT group. Specifically, 6 participants out of 9 underwent CIMT as first treatment, 8 patients out of 9 underwent Armeo as first treatment, and 4 patients out of 12 underwent PT as first treatment.

**3.1. Differences among Groups at Pretreatment.** First, a comparison among groups in terms of group features (sex, etiology, age, distance from event, GCS, and QI) and functional evaluations was performed at the beginning of each protocol. No differences were found among groups in terms of group features except for a significant difference (Kruskal-Wallis  $p$  value = 0.02) in etiology, specifically between Armeo (etiological prevalence of "traumatic brain injury") and CIMT (etiological prevalence of "hemorrhagic stroke"; Mann-Whitney with Bonferroni correction  $p$  = 0.02). Furthermore, many significant differences (Kruskal-Wallis  $p$  value < 0.05) were found in pretreatment functional evaluations among different treatments, mainly in the group that performed Armeo. CIMT and Armeo groups differed in terms of the QUEST-A (80.47 (24.61), 54.69 (12.50),  $p$  < 0.01), QUEST-C (100 (10), 76 (16),  $p$  =

0.01), QUEST-tot (70.88 (21.54), 56.63 (7.03),  $p$  = 0.02), Melbourne Assessment (81.00(13.50), 40.00 (37.00),  $p$  = 0.02), and GMFM-C (98.00 (2.75), 73.00 (27.75),  $p$  = 0.03). Moreover, PT and Armeo differed in terms of the QUEST-C (98.00 (12.00), 76.00 (16.00),  $p$  = 0.03) and Melbourne Assessment (72.00 (17.53), 40.00 (37.00),  $p$  = 0.03). In contrast, CIMT and PT groups were comparable at the initial evaluation.

The kinematic data between each group before treatment were also analyzed. For the horizontal task, it was found there was a significant difference in the target error (Figure 3(e)) (Kruskal-Wallis  $p$  value < 0.01), with Mann-Whitney highlighting lower target error before CIMT ( $p$  value < 0.01) and PT ( $p$  value < 0.05) than Armeo.

With regard to the vertical task, a difference in the finger displacement along the  $y$ -axis (Y-FD) emerged (Kruskal-Wallis  $p$  value < 0.01), highlighting higher displacement before CIMT than Armeo (Mann-Whitney  $p$  value < 0.01). In addition, many differences in terms of range of motion emerged, describing a condition characterized by higher functional ranges of motion before CIMT than Armeo, in particular for elbow flex-extension (Kruskal-Wallis  $p$  value = 0.02, Mann-Whitney  $p$  value < 0.01), shoulder abduction-adduction (Kruskal-Wallis  $p$  value < 0.01, Mann-Whitney  $p$  value < 0.01), and shoulder flex-extension (Kruskal-Wallis  $p$  value < 0.01, Mann-Whitney  $p$  value < 0.01).

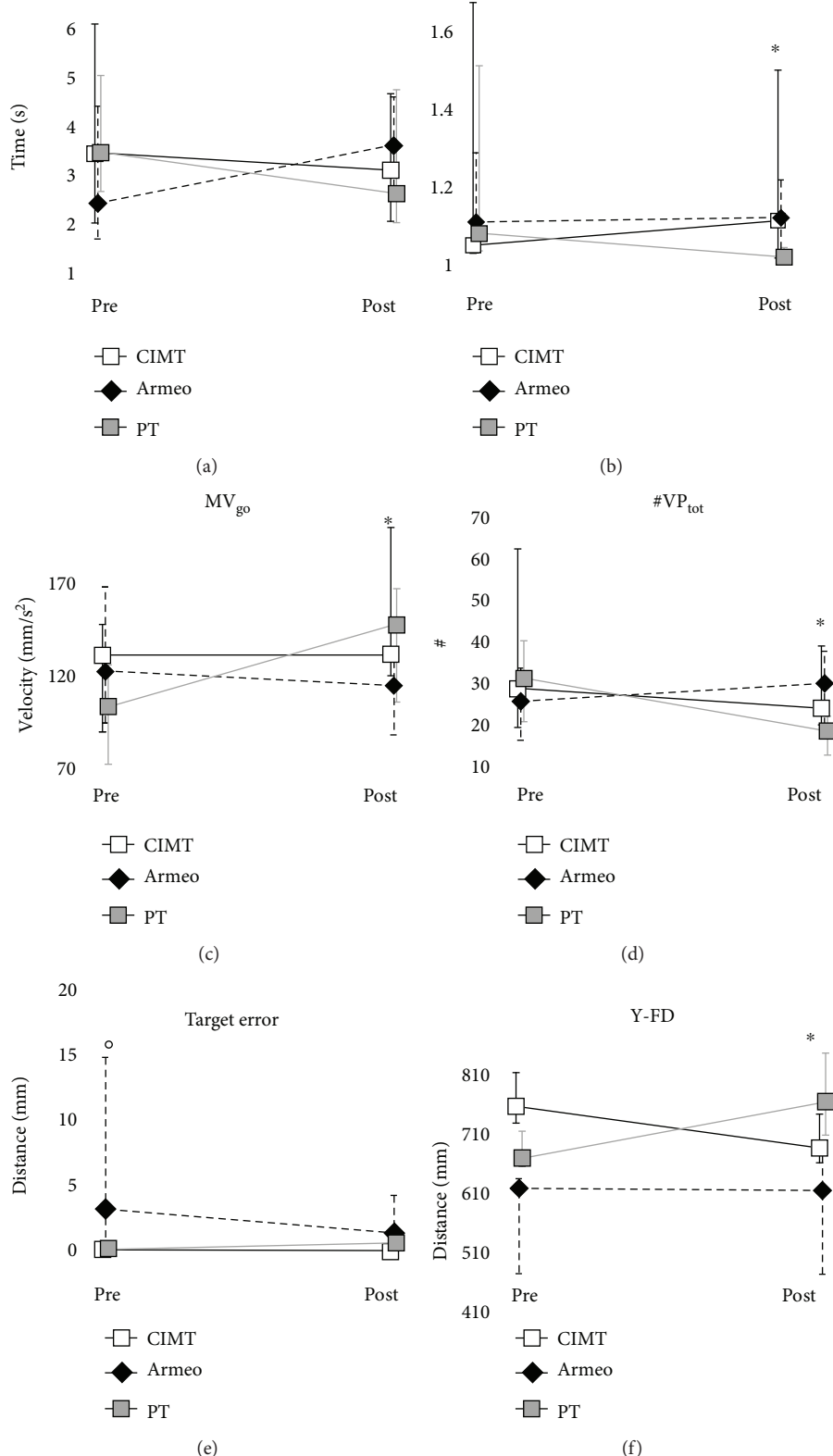


FIGURE 3: Effect of treatments on end-point metrics. For the horizontal task, pre- and posttreatment values of (a) movement time, (b) hand path ratio during the going phase, (c) mean velocity of the finger during the going phase, (d) total number of velocity peaks, and (e) target error are reported for CIMT (black line), Armeo (black dashed line), and PT (grey line). For the vertical task, pre- and posttreatment values of displacement of (f) the finger along y-axis are reported for CIMT (black line), Armeo (black dashed line) and PT (grey line). Data are reported as median (IQR). \* $p < 0.05$  Wilcoxon test, before PT versus after PT; ° $p < 0.05$  Mann–Whitney post hoc test at pretreatment, Armeo versus CIMT, Armeo versus PT.

TABLE 2: Median (IQR) of functional scales before (pre) and after (post) each treatment. The sample size is  $n=8$  for the CIMT,  $n=9$  for the Armeo, and  $n=11$  for the PT groups.  $P$  values refer to Wilcoxon test. Bold values:  $p < 0.05$ .

	Pretreatment	Posttreatment	$p$ value
<b>CIMT (<math>n = 8</math>)</b>			
QUEST-tot	70.88 (21.54)	82.02 (17.10)	<b>0.03</b>
QUEST-A	80.47 (24.61)	86.72 (21.48)	<b>0.04</b>
QUEST-B	77.78 (15.74)	77.78 (17.59)	0.11
QUEST-C	100.00 (10.00)	100.00 (3.00)	0.18
QUEST-D	59.73 (30.56)	59.73 (25.00)	0.18
Melbourne Assessment %	81.00 (13.50)	82.50 (7.25)	<b>0.02</b>
GMFM total	214.00 (20.50)	249.00 (18.00)	0.07
<b>Armeo (<math>n = 9</math>)</b>			
QUEST-tot	56.63 (7.03)	56.63 (9.43)	0.07
QUEST-A	54.69 (12.50)	54.69 (15.63)	0.11
QUEST-B	55.56 (14.81)	55.56 (14.81)	0.32
QUEST-C	76.00 (16.00)	80.00 (16.00)	0.11
QUEST-D	41.67 (8.33)	41.67 (8.33)	0.08
Melbourne Assessment %	40.00 (37.00)	43.00 (26.00)	<b>0.03</b>
GMFM total	204.50 (28.25)	214.00 (21.75)	0.07
<b>PT (<math>n = 11</math>)</b>			
QUEST-tot	70.49 (14.81)	73.36 (18.95)	<b>0.01</b>
QUEST-A	70.31 (17.97)	76.56 (14.85)	<b>0.02</b>
QUEST-B	70.37 (16.67)	77.78 (20.37)	0.89
QUEST-C	98.00 (12.00)	100.00 (12.00)	0.10
QUEST-D	44.40 (13.89)	52.78 (19.45)	<b>0.04</b>
Melbourne Assessment %	72.00 (17.53)	77.00 (18.50)	0.14
GMFM total	240.00 (28.50)	240.50 (26.25)	0.07

**3.2. Changes in Functional Scales Dependent on Treatment.** Table 2 shows values of functional scales before and after each treatment.  $p$  values are the results of the Wilcoxon test for paired data. The table highlights several changes that were conveyed by the CIMT treatment in the QUEST scale (medium effect size,  $d = 0.6$ ) as well as in the Melbourne Assessment (large effect size,  $d = 1.1$ ). Armeo treatment caused improvements in the Melbourne Assessment (large effect size,  $d = 0.9$ ) while the PT protocol in the QUEST scale (large effect size,  $d = 0.9$ ) [27]. No changes in GMFM were detected.

The comparison among the three treatments, considering the variations between post- and pretreatments did not show any significant difference (Kruskal–Wallis test  $p > 0.05$ ).

**3.3. Changes in Kinematics Dependent on Treatment.** For the horizontal task, the improvement of mean angular velocity during shoulder flex-extension was found for CIMT. Several improvements were also found after PT treatment concerning end-point metrics (Figure 3): the significant reductions of  $HPR_{go}$  (Figure 3(b)) and  $\#VP_{tot}$  (Figure 3(d)) as well as

an increase of  $MV_{go}$  (Figure 3(c)) suggest enhanced efficiency and smoothness of distal movement. Moreover, a trend of improvement was observed with regard to the  $MT_{go}$  which decreased after PT ( $p = 0.08$ , decreases in 8 out of 12 children). With regard to Armeo, no significant differences were found between pre- and posttreatments with regard to end-point metrics; in contrast, a significant but small (i.e., 0.52 degrees) reduction of ROM of shoulder flex-extension emerged (reduces in 8 out of 9 children). No significant differences emerged with regard to the compensatory movement of the trunk after CIMT, Armeo, and PT. Pre-/post values of kinematic parameters extracted for the horizontal task for each treatment are shown in Table 3.

With regard to the vertical task, no significant differences emerged for CIMT and Armeo treatments between pre- and postevaluations; on the contrary, some improvements emerged after PT, in particular an increase of  $Y-FD$  (Wilcoxon  $p$  value = 0.02) (Figure 3(f)) and of the mean angular velocity of the elbow flex-extension (Wilcoxon  $p$  value = 0.03). Trends of improvement, even if not significant, were observed: with regard to compensatory movements of the trunk, a reduction of trunk lateral bending emerged after CIMT ( $X-TD_{go}$ :  $p = 0.05$ ); also, a trend of increase of movement efficiency was observed after Armeo ( $HPR_{go}$ :  $p = 0.08$ ,  $HPR_{go}$  increases in 6 children out of 8), and after PT, increase of shoulder abduction-adduction ROM ( $p = 0.05$ , increase in 9 out of 11 children) was observed. Pre-/post values of kinematic parameters extracted for the vertical task for each treatment are shown in Table 4.

The comparison of variations (post-pre) among the three treatments highlighted a significant difference in ROM of the shoulder during flex-extension (Kruskal–Wallis  $p = 0.02$ ) that decreased after Armeo while it increased after CIMT (Mann–Whitney  $p = 0.03$ ) and a significant difference in the mean angular velocity of the shoulder in flex-extension during the going phase (Kruskal–Wallis  $p = 0.01$ ) that increased after CIMT while it decreased after PT (Mann–Whitney  $p = 0.01$ ).

For the vertical task, a difference between groups emerged with regard to the modification of the ROM of shoulder abduction-adduction during the going phase (Kruskal–Wallis  $p = 0.03$ ) that increased after PT while it was reduced after Armeo (Mann–Whitney  $p = 0.05$ ). Also, compensatory movements of the trunk, namely  $X-TD_{go}$  (Kruskal–Wallis  $p = 0.03$ ), were reduced after CIMT while they increased after PT (Mann–Whitney  $p = 0.04$ ).

## 4. Discussion

In children affected by acquired hemiplegia, several treatments were developed to improve functional recovery of the upper limbs.

In hemiplegic patients, the rehabilitation of the upper limb skills is crucial, because the recovery has an immediate impact on patient quality of life. Recent literature documents demonstrate the great effort made by rehabilitation facilities to enhance the recovery of motor function [28]. Two of the most widely used rehabilitation methods used for this aim are CIMT (Constraint-Induced Movement Therapy) and

TABLE 3: Kinematic variables before (pre) and after (post) each treatment for the horizontal task. Data are presented as median (IQR). The sample size is  $n = 9$  for the CIMT,  $n = 9$  for the Armeo, and  $n = 12$  for the PT groups.  $p$  values refer to the Wilcoxon test. Bold values:  $p < 0.05$ .

	Horizontal task parameters	Pretreatment	Posttreatment	$p$ value
CIMT ( $n = 9$ )				
	MT <sub>go</sub> [s]	3.42 (4.08)	3.08 (2.62)	0.25
	HPR <sub>go</sub>	1.05 (0.64)	1.11 (0.48)	0.73
End-point metrics	MV <sub>go</sub> [mm/s]	95.74 (60.63)	111.72 (49.20)	0.50
	#VP <sub>tot</sub>	28.67 (43.00)	24.00 (19.00)	0.16
	Target error	0 (0)	0 (0)	0.88
	ROM shoulder flex-ext [°]	45.82 (5.35)	47.57 (12.46)	0.25
	ROM shoulder abd-add [°]	13.54 (2.49)	19.32 (19.32)	0.10
Joint kinematics	ROM elbow flex-ext [°]	47.55 (21.26)	44.37 (14.17)	0.91
	MAV shoulder flex-ext [°/s]	3.92 (4.52)	7.16 (5.95)	<0.01
	MAV shoulder abd-add [°/s]	12.70 (7.95)	14.19 (7.31)	0.65
	MAV elbow flex-ext [°/s]	13.49 (6.21)	18.12 (9.45)	0.16
Trunk	Trunk 3D path	39.12 (21.06)	34.29 (16.60)	0.91
	Z-TD <sub>go</sub>	90.11 (78.62)	74.94 (42.20)	0.65
Armeo ( $n = 9$ )				
	MT <sub>go</sub> [s]	2.41 (2.73)	3.59 (2.10)	0.50
	HPR <sub>go</sub>	1.11 (0.26)	1.12 (0.18)	0.73
End-point metrics	MV <sub>go</sub> [mm/s]	122.18 (73.32)	114.65 (39.97)	0.43
	#VP <sub>tot</sub>	25.67 (17.33)	30.00 (20.72)	0.91
	Target error	3.14 (14.44)	1.30 (3.91)	0.36
	ROM shoulder flex-ext [°]	45.52 (9.59)	45.00 (15.86)	0.01
	ROM shoulder abd-add [°]	13.61 (7.40)	16.13 (4.72)	0.20
Joint kinematics	ROM elbow flex-ext [°]	31.52 (14.30)	27.27 (16.73)	0.65
	MAV shoulder flex-ext [°/s]	6.68 (6.59)	6.03 (8.17)	0.72
	MAV shoulder abd-add [°/s]	15.42 (9.90)	13.37 (4.77)	0.16
	MAV elbow flex-ext [°/s]	14.44 (9.91)	9.63 (9.44)	0.73
Trunk	Trunk 3D path	352.52 (195.01)	443.60 (189.82)	0.73
	Z-TD <sub>go</sub>	136.16 (44.51)	158.63 (54.40)	1.00
PT ( $n = 12$ )				
	MT <sub>go</sub> [s]	3.44 (2.38)	2.61 (2.73)	0.08
	HPR <sub>go</sub>	1.08 (0.47)	1.02 (0.03)	0.03
End-point metrics	MV <sub>go</sub> [mm/s]	103.36 (53.40)	147.31 (61.05)	0.04
	#VP <sub>tot</sub>	31.17 (19.50)	18.50 (9.25)	0.02
	Target error	0.10 (0.26)	0.67 (0.53)	0.31
	ROM shoulder flex-ext [°]	44.95 (17.62)	43.23 (8.31)	0.97
	ROM shoulder abd-add [°]	17.73 (8.68)	12.82 (14.56)	0.42
Joint kinematics	ROM elbow flex-ext [°]	41.45 (19.07)	39.57 (28.90)	0.57
	MAV shoulder flex-ext [°/s]	5.88 (8.31)	5.42 (3.57)	0.52
	MAV shoulder abd-add [°/s]	11.68 (3.76)	16.72 (14.28)	0.11
	MAV elbow flex-ext [°/s]	12.82 (8.81)	13.85 (7.39)	0.42
Trunk	Trunk 3D path	313.42 (186.79)	300.32 (182.32)	0.18
	Z-TD <sub>go</sub>	90.01 (102.48)	108.07 (91.19)	0.85

robot-aided therapy. The plurality of treatments necessitates a comparison of the effectiveness of each; in addition, the current lack of availability of quantitative methods makes the use of objective measures of functional recovery essential. Next to the functional scales, the clinic has recently

introduced methods of kinematic analysis of the upper limb movement to get more objective and quantifiable measures.

In this study, we evaluated a group of children and adolescents with upper limb movement impairment after ABI that underwent intensive rehabilitation treatment. The

TABLE 4: Kinematics variables before (pre) and after (post) each treatment for the vertical task. Data are presented as median (IQR). The sample size is  $n = 9$  for the CIMT,  $n = 8$  for the Armeo, and  $n = 11$  for the PT groups.  $p$  values refer to Wilcoxon test. Bold values:  $p < 0.05$ .

	Vertical task parameters	Pretreatment	Posttreatment	$p$ value
CIMT ( $n = 9$ )				
End-point metrics	HPR <sub>go</sub>	1.10 (0.89)	1.09 (0.61)	0.09
	Y-FD [mm]	757.14 (84.78)	686.79 (81.75)	0.30
	MV <sub>go</sub> [mm/s]	150.57 (47.00)	209.59 (76.55)	0.65
	#VP <sub>tot</sub>	48.00 (18.67)	42.67 (39.00)	0.34
Joint kinematics	ROM shoulder flex-ext [°]	116.56 (22.72)	106.45 (38.87)	0.15
	ROM shoulder abd-add [°]	126.69 (15.41)	126.20 (35.95)	1.00
	ROM elbow flex-ext [°]	56.61 (11.46)	62.26 (18.99)	0.31
	MAV shoulder flex-ext [°/s]	22.43 (16.58)	25.06 (26.00)	0.84
Trunk	MAV shoulder abd-add [°/s]	18.74 (13.24)	19.66 (8.48)	0.46
	MAV elbow flex-ext [°/s]	15.59 (8.19)	18.50 (6.62)	0.74
	Trunk 3D path	477.38 (103.88)	386.72 (157.66)	0.20
	X-TD <sub>go</sub>	58.35 (25.96)	49.77 (18.30)	0.05
Armeo ( $n = 8$ )				
End-point metrics	HPR <sub>go</sub>	1.43 (0.39)	1.26 (0.14)	0.08
	Y-FD [mm]	618.80 (160.00)	615.27 (217.03)	0.84
	MV <sub>go</sub> [mm/s]	125.76 (107.67)	152.51 (66.25)	1.00
	#VP <sub>tot</sub>	46.46 (26.83)	35.67 (32.83)	0.31
Joint kinematics	ROM shoulder flex-ext [°]	66.93 (34.99)	69.95 (41.34)	0.55
	ROM shoulder abd-add [°]	54.39 (48.41)	56.59 (24.32)	0.31
	ROM elbow flex-ext [°]	38.32 (11.65)	35.09 (10.73)	0.64
	MAV shoulder flex-ext [°/s]	13.96 (16.62)	9.56 (9.38)	0.15
Trunk	MAV shoulder abd-add [°/s]	13.85 (10.24)	14.05 (8.53)	0.46
	MAV elbow flex-ext [°/s]	8.78 (6.28)	10.49 (5.33)	0.74
	Trunk 3D path	351.34 (58.49)	303.72 (130.18)	0.46
	X-TD <sub>go</sub>	46.51 (25.83)	52.57 (11.13)	0.55
PT ( $n = 11$ )				
End-point metrics	HPR <sub>go</sub>	1.15 (0.49)	1.12 (0.48)	0.20
	Y-FD [mm]	669.71 (58.56)	764.82 (138.49)	<b>0.02</b>
	MV <sub>go</sub> [mm/s]	185.59 (106.09)	194.79 (41.96)	0.52
	#VP <sub>tot</sub>	56.00 (42.33)	36.00 (32.42)	0.97
Joint kinematics	ROM shoulder flex-ext [°]	95.13 (36.11)	99.75 (16.26)	0.32
	ROM shoulder abd-add [°]	103.43 (67.88)	121.15 (18.94)	0.05
	ROM elbow flex-ext [°]	57.71 (23.32)	62.54 (15.12)	0.43
	MAV shoulder flex-ext [°/s]	26.50 (20.66)	22.46 (13.69)	0.40
Trunk	MAV shoulder abd-add [°/s]	18.99 (14.07)	18.21 (10.20)	0.58
	MAV elbow flex-ext [°/s]	16.36 (4.14)	18.98 (5.86)	<b>0.03</b>
	Trunk 3D path	347.89 (155.03)	348.67 (180.99)	0.17
	X-TD <sub>go</sub>	49.77 (8.77)	66.22 (24.72)	0.10

rehabilitation program included two consecutive four-week periods of treatment, attended in a random order: one period of physical therapy (PT) and one period of a rehabilitative treatment randomly chosen between Constraint-Induced Movement Therapy (CIMT) and training with the exoskeleton Armeo®Spring. The aim of this study was to compare the effect of different types of treatments on functional abilities in a group of children and adolescents suffering from ABI.

Clinical functional scales and upper limb kinematics data were used as assessment tools.

Only a very low number of studies have previously quantified recovery of upper limbs in children after ABI; our study investigated a very wide perspective in terms of movement (kinematic data), gross motor performance, and hand function. Also, attention was focused on both clinical-functional scales and kinematic data during different types of treatment.

In terms of functional scale, the most significant improvements were obtained after CIMT. In fact, this treatment demonstrated progress in both the QUEST and Melbourne Assessment. The other treatments produced significant changes in a single assessment scale: Armeo modified the Melbourne Assessment score and thus increased the quality of the upper limb movement, while PT produced a significant improvement in the QUEST scale, in particular in postural responses. All these improvements had a large effect size, except for the QUEST scale in the CIMT group.

Therefore, CIMT seems to still be the most effective treatment as evidenced by the literature of the past 20 years [29], significantly improving both the quality of motor limb function (analyzed by the Melbourne Assessment) and postural responses and selective motility (evaluated by the QUEST) [30].

The kinematic analysis of movements during horizontal as well as vertical tasks showed several improvements in terms of efficiency and smoothness of end-effector movements and elbow angular velocity after PT, suggesting its positive influence on distal movements. In contrast, CIMT conveyed more changes at the shoulder and trunk districts that means improvements of proximal kinematics and reduction of compensatory movements. An improvement of the movement efficiency was observed after Armeo treatment: specifically, not only a trend of increase of the hand-path ratio during the vertical reaching but also a significant reduction of the shoulder flex-extension in the horizontal task was observed. Compared with other treatments, Armeo showed an improvement of shoulder abduction-adduction during the vertical task (i.e., a reduction of compensatory movements of the shoulder). These opposing results may be due to the mechanical constraints that the exoskeleton gives during therapy.

More generally, PT seems to be more effective in terms of kinematic variations than CIMT and Armeo: a possible hypothesis is that, since PT was often provided as a second treatment, this depends on a sort of summation effects of the two treatments. Moreover, it has to be noted that the PT sample size is bigger than the other treatments. Compared to a previous work [12], our data after CIMT showed smaller improvements; this may depend on the duration of the treatment, that is, 4 weeks in the current manuscript versus 10 weeks in the work by Cimolin and coworkers. The results of the present study are in line with those by Cope and collaborators [31] where there were improvements of the functional scales but just few trends of improvement with regard to the kinematics after a 2-week rehabilitation with CIMT in children with hemiplegia.

With respect to the treatment with Armeo, the small number of significant improvements can be attributed to the fact that patients who were assigned to this type of treatment were on average more functionally compromised at the beginning of their rehabilitative path, with an important limitation of the upper limb distal level. Specifically, they had worse functional abilities at the hand level and lower functional ranges of motion at joint levels. It is already known, indeed, that patients with a moderate degree of impairment seem to benefit the most [31].

None of the three treatments changed the gross motor skills (no significant changes in GMFM) because the patients recruited for the upper limb treatment, generally, had a framework of global consolidated skills and the rehabilitation was more concerned with the functionality of the upper limb and not with gross motor abilities.

The kinematic data allow us to make objective measurements of the movement characteristics of patients after ABI. Kinematic analysis, known in the literature especially for gait analysis, proves to be able to describe very well the upper limb movements and is a valuable aid in discriminating with greater precision the modifications that each treatment cause.

This study has some limitations. The small number of participants resulted in limited strength with regard to the statistical findings. A larger sample could provide the opportunity to make a deeper investigation of the differences between the treatments. In addition, with a larger group of children, it would be possible to investigate whether the improvements are greater in patients who start the treatment closer to the time of their injury, by comparing the results of the program between children with shorter and longer postinjury times. A bigger sample would also allow to evaluate the effects on functional abilities of different matching of treatments.

Another critical point concerns the group of patients who received robotic treatment with Armeo. They had overall worse limb function when beginning treatment than the other patients and even than other groups performing this treatment [10, 11], and this could have determined the lack of improvement in kinematic data.

Despite these limitations, the present study has interesting clinical implications: from the rehabilitation point of view, this study allowed the development of assessment and treatment protocols that can be used for all patients with ABI that undergo rehabilitation treatments aimed at improving the use of the upper limbs. Further, the results of this study also allow us to give more precise information about the type of treatment to be offered to children suffering from hemiplegia from ABI. In fact, we can choose the treatments after identifying the target that one wants to reach in the single patient, for example, improve the quality of unilateral upper-limb motor function or increase postural responses. Moreover, in some patients, the integration of multiple treatments will be indicated because they are complementary and not only differently effective.

In conclusion, this study investigated the effects of different types of upper-limb rehabilitative treatments on the functional improvement of children and adolescents with ABIs. It was found that CIMT treatment is overall the most effective in terms of quality in motor limb function and postural responses as evidenced by functional scales, while physical therapy and robot exoskeleton-aided therapy convey improvements only in the QUEST and Melbourne Assessment, respectively. Kinematic analysis results suggest that CIMT is able to foster proximal movement improvements, in particular at the shoulder joint. In the contrary, PT showed good results in terms of distal movements, including increase of finger speed and fluidity. Finally, Armeo treatment

conveyed improvements in the shoulder performing the vertical but also a reduction of its functionality in the horizontal one. These data suggest that these treatments are complementary and that it would be important to offer to hemiplegic children a combination of these protocols depending on the main rehabilitative goal. Future works will investigate the ability to prescribe specific treatments in order to maximize patient improvements.

## Conflicts of Interest

The authors declare that they have no conflicts of interest.

## Acknowledgments

The authors would like to thank the physiotherapists that performed the rehabilitation treatments and functional evaluations and all the patients and their families that were involved in this study. The work was supported by the Italian Ministry of Health (Ricerca Corrente 2015–2016).

## References

- [1] S. Gazzellini, S. Strazzer, M. Stortini et al., “Pediatric rehabilitation of severe acquired brain injury: a multicenter survey,” *European Journal of Physical and Rehabilitation Medicine*, vol. 48, no. 3, pp. 423–431, 2012.
- [2] M. A. Wallen, S. Mackay, S. M. Duff, L. C. McCartney, and S. J. O’flaherty, “Upper-limb function in Australian children with traumatic brain injury: a controlled, prospective study,” *Archives of Physical Medicine and Rehabilitation*, vol. 82, no. 5, pp. 642–649, 2001.
- [3] C. Butefisch, H. Hummelsheim, P. Denzler, and K. H. Mauritz, “Repetitive training of isolated movements improves the outcome of motor rehabilitation of the centrally paretic hand,” *Journal of the Neurological Sciences*, vol. 130, no. 1, pp. 59–68, 1995.
- [4] H. T. Hendricks, J. van Limbeek, A. C. Geurts, and M. J. Zwarts, “Motor recovery after stroke: a systematic review of the literature,” *Archives of Physical Medicine and Rehabilitation*, vol. 83, no. 11, pp. 1629–1637, 2002.
- [5] G. Thielman, T. Kaminski, and A. M. Gentile, “Rehabilitation of reaching after stroke: comparing 2 training protocols utilizing trunk restraint,” *Neurorehabilitation and Neural Repair*, vol. 22, no. 6, pp. 697–705, 2008.
- [6] F. Frascarelli, L. Masia, G. Di Rosa et al., “The impact of robotic rehabilitation in children with acquired or congenital movement disorders,” *European Journal of Physical and Rehabilitation Medicine*, vol. 45, no. 1, pp. 135–141, 2009.
- [7] S. Masiero, M. Armani, and G. Rosati, “Upper-limb robot-assisted therapy in rehabilitation of acute stroke patients: focused review and results of new randomized controlled trial,” *Journal of Rehabilitation Research and Development*, vol. 48, no. 4, pp. 355–366, 2011.
- [8] C. Colomer, A. Baldovi, S. Torrome et al., “Efficacy of Armeo®-Spring during the chronic phase of stroke. Study in mild to moderate cases of hemiparesis,” *Neurología*, vol. 28, no. 5, pp. 261–267, 2013.
- [9] V. Doerbeck, A. Nallinger, H. Burger et al., “Integration of Armeo Spring pediatrics in inpatient rehabilitation of children and adolescents with hemiparesis,” *Neuropediatrics*, vol. 43, no. 2, 2012.
- [10] E. Peri, E. Biffi, C. Maghini et al., “Quantitative evaluation of performance during robot-assisted treatment,” *Methods of Information in Medicine*, vol. 55, no. 1, pp. 84–88, 2016.
- [11] A. C. Turconi, E. Biffi, C. Maghini, E. Peri, F. Servodio Iammarone, and C. Gagliardi, “Can new technologies improve upper limb performance in grown-up diplegic children?,” *European Journal of Physical and Rehabilitation Medicine*, vol. 52, no. 5, pp. 672–681, 2016.
- [12] V. Cimolin, E. Beretta, L. Piccinini et al., “Constraint-induced movement therapy for children with hemiplegia after traumatic brain injury: a quantitative study,” *The Journal of Head Trauma Rehabilitation*, vol. 27, no. 3, pp. 177–187, 2012.
- [13] A. C. Eliasson, L. Nordstrand, L. Ek et al., “The effectiveness of baby-CIMT in infants younger than 12 months with clinical signs of unilateral-cerebral palsy; an explorative study with randomized design,” *Research in Developmental Disabilities*, vol. 72, pp. 191–201, 2018.
- [14] M. Alt Murphy and C. K. Häger, “Kinematic analysis of the upper extremity after stroke—how far have we reached and what have we grasped?,” *Physical Therapy Reviews*, vol. 20, no. 3, pp. 137–155, 2015.
- [15] M. R. El-Helou, M. L. Zamzam, M. M. Fathalla et al., “Efficacy of modified constraint-induced movement therapy in acute stroke,” *European Journal of Physical and Rehabilitation Medicine*, vol. 51, no. 4, pp. 371–379, 2015.
- [16] S. L. Wolf, C. J. Winstein, J. P. Miller et al., “Effect of constraint-induced movement therapy on upper extremity function 3 to 9 months after stroke: the EXCITE randomized clinical trial,” *JAMA*, vol. 296, no. 17, pp. 2095–2104, 2006.
- [17] M. Caimmi, S. Carda, C. Giovanzana et al., “Using kinematic analysis to evaluate constraint-induced movement therapy in chronic stroke patients,” *Neurorehabilitation and Neural Repair*, vol. 22, no. 1, pp. 31–39, 2008.
- [18] C. Y. Wu, C. L. Chen, S. F. Tang, K. C. Lin, and Y. Y. Huang, “Kinematic and clinical analyses of upper-extremity movements after constraint-induced movement therapy in patients with stroke: a randomized controlled trial,” *Archives of Physical Medicine and Rehabilitation*, vol. 88, no. 8, pp. 964–970, 2007.
- [19] C. Y. Wu, K. C. Lin, H. C. Chen, I. H. Chen, and W. H. Hong, “Effects of modified constraint-induced movement therapy on movement kinematics and daily function in patients with stroke: a kinematic study of motor control mechanisms,” *Neurorehabilitation and Neural Repair*, vol. 21, no. 5, pp. 460–466, 2007.
- [20] P. Langhorne, F. Coupar, and A. Pollock, “Motor recovery after stroke: a systematic review,” *Lancet Neurology*, vol. 8, no. 8, pp. 741–754, 2009.
- [21] A. Cesareo, E. Beretta, E. Biffi, S. Strazzer, and G. Reni, “A comparative study among constraint, robot-aided and standard therapies in upper limb rehabilitation of children with acquired brain injury,” in *XIV Mediterranean Conference on Medical and Biological Engineering and Computing 2016*, pp. 673–678, Springer, Cham, 2016.
- [22] C. DeMatteo, M. Law, D. Russell, N. Pollock, P. Rosenbaum, and S. Walter, *QUEST: Quality of Upper Extremity Skills Test*, Neurodevelopmental Research Unit, Chedoke Campus, Chedoke-McMasters Hospital, Hamilton, ON, 1992.

- [23] L. M. Johnson, M. J. Randall, D. S. Reddihough, L. E. Oke, T. A. Byrt, and T. M. Bach, "Development of a clinical assessment of quality of movement for unilateral upper-limb function," *Developmental Medicine and Child Neurology*, vol. 36, no. 11, pp. 965–973, 1994.
- [24] M. Randall, J. B. Carlin, P. Chondros, and D. Reddihough, "Reliability of the Melbourne assessment of unilateral upper limb function," *Developmental Medicine and Child Neurology*, vol. 43, no. 11, pp. 761–767, 2001.
- [25] D. J. Russell, P. L. Rosenbaum, D. T. Cadman, C. Gowland, S. Hardy, and S. Jarvis, "The gross motor function measure: a means to evaluate the effects of physical therapy," *Developmental Medicine and Child Neurology*, vol. 31, no. 3, pp. 341–352, 1989.
- [26] M. Alt Murphy, C. Willen, and K. S. Sunnerhagen, "Kinematic variables quantifying upper-extremity performance after stroke during reaching and drinking from a glass," *Neurorehabilitation and Neural Repair*, vol. 25, no. 1, pp. 71–80, 2011.
- [27] S. S. Sawilowsky, "New effect size rules of thumb," *Journal of Modern Applied Statistical Methods*, vol. 8, no. 2, pp. 597–599, 2009.
- [28] G. Kelly, S. Mobbs, J. N. Pritkin et al., "Gross motor function Measure-66 trajectories in children recovering after severe acquired brain injury," *Developmental Medicine and Child Neurology*, vol. 57, no. 3, pp. 241–247, 2015.
- [29] M. A. Rocca, A. C. Turconi, S. Strazzer et al., "MRI predicts efficacy of constraint-induced movement therapy in children with brain injury," *Neurotherapeutics*, vol. 10, no. 3, pp. 511–519, 2013.
- [30] K. Klingels, P. De Cock, K. Desloovere et al., "Comparison of the Melbourne assessment of unilateral upper limb function and the quality of upper extremity skills test in hemiplegic CP," *Developmental Medicine & Child Neurology*, vol. 50, no. 12, pp. 904–909, 2008.
- [31] S. M. Cope, X. C. Liu, M. D. Verber, C. Cayo, S. Rao, and J. C. Tassone, "Upper limb function and brain reorganization after constraint-induced movement therapy in children with hemiplegia," *Developmental Neurorehabilitation*, vol. 13, no. 1, pp. 19–30, 2010.

## Research Article

# Social Robotics in Therapy of Apraxia of Speech

José Carlos Castillo , Diego Álvarez-Fernández , Fernando Alonso-Martín, Sara Marques-Villarroya , and Miguel A. Salichs 

Departamento de Sistemas y Automática, Universidad Carlos III de Madrid, 28911 Madrid, Spain

Correspondence should be addressed to José Carlos Castillo; jocastil@ing.uc3m.es

Received 24 November 2017; Accepted 15 January 2018; Published 11 March 2018

Academic Editor: Carlo Ferraresi

Copyright © 2018 José Carlos Castillo et al. This is an open access article distributed under the Creative Commons Attribution License, which permits unrestricted use, distribution, and reproduction in any medium, provided the original work is properly cited.

Apraxia of speech is a motor speech disorder in which messages from the brain to the mouth are disrupted, resulting in an inability for moving lips or tongue to the right place to pronounce sounds correctly. Current therapies for this condition involve a therapist that in one-on-one sessions conducts the exercises. Our aim is to work in the line of robotic therapies in which a robot is able to perform partially or autonomously a therapy session, endowing a social robot with the ability of assisting therapists in apraxia of speech rehabilitation exercises. Therefore, we integrate computer vision and machine learning techniques to detect the mouth pose of the user and, on top of that, our social robot performs autonomously the different steps of the therapy using multimodal interaction.

## 1. Introduction

Apraxia of speech (AOS) is a neurological disorder in which the messages from the brain to the mouth are disrupted, and the person cannot move his/her lips or tongue to say sounds properly. This condition is caused by a damage in the left hemisphere of the brain generated by strokes, Alzheimer's or brain traumas, among others. The severity of the apraxia depends on the nature of the brain damage. AOS is also known as acquired apraxia of speech, verbal apraxia, and dyspraxia [1].

The focus of intervention is on improving the planning, sequencing, and coordination of muscle movements for speech production. The muscles of speech often need to be “retrained” to produce sounds correctly and sequence sounds into words. Exercises are designed to allow the person to repeat sounds over and over and to practice correct mouth movements for sounds [2]. Currently, there are three different interventions for AOS rehabilitation: (i) intervention based on motor control: these exercises consist of producing phonemes and sequences of phonemes through accurate, controlled, and conscious movements. The aim of these therapies is to

automate such movements to be subsequently performed unwittingly; (ii) intervention based on augmented systems: these methods include several input channels to improve the therapy results. Audio and images are traditionally mixed to help remembering how to pronounce difficult and long words; and (iii) interventions based on melodies: these therapies are adopted in patients that preserve an auditive comprehension of the language. In these cases, the patient has to imitate different melodies proposed that remark the stressed syllables of the words, establishing the rhythm of the melodies [3]. These interventions are frequently planned as intensive, one-on-one speech-language therapy sessions for both children and adults. Thus, the repetitive exercises and personal attention needed to improve AOS are difficult to deliver in group therapy [4].

In recent years, robots are gaining popularity in rehabilitation therapies, mainly in traumatology, where the robot holds the user's weight or helps moving a determined limb. Robots have been proven to be effective in assisting the therapist to provide safe and intensive rehabilitation training for the stroke subjects. Nevertheless, in the general setting of these systems, a therapist is still responsible for the nonphysical interaction and observation of the patient by maintaining

a supervisory role of the training, while the robot carries out the actual physical interaction with the patient. In most applications, rehabilitation robots have been mainly employed in lower and upper limb therapy [5–8].

Rehabilitation using robotics is generally well tolerated by patients and has been found to be an effective adjunct to therapy in individuals suffering from motor impairments, especially due to stroke. Therefore, we believe that robotics can be introduced to other rehabilitation areas such as AOS. To the extent of our knowledge, this proposal is innovative as robotic technologies have not been applied to this field so far. We propose following the first kind of intervention presented in this section in which the user repeats exercises to practice mouth movements; in our case, we take inspiration from mouth poses associated to the five vowels in the Spanish tongue. Here, “a” is pronounced like the “a” in the word “father” (/a/); “e” is pronounced like the “a” in the word “date” (/e/), except that it is shorter and crisper; “i” is pronounced like the “ee” in the word “see” (/i/); “o” is pronounced like the “o” in the word “no” (/o/); and “u” is pronounced like the “e” in the word “new” (/u/). Thus, we propose using some of these sounds because their pronunciation imply different poses of the mouth, associated to a range of muscular movements.

We believe that a social robot could help in AOS therapy offering a new and eye-catching way of assisting in the exercises. The robot adds to the therapy some new resources such as a screen to stimulate the patient, offering a visual reinforcement to the exercises. Additionally, the human-robot interaction (HRI) capabilities of a social robot could enhance the traditional therapy, maximizing the human resources while keeping a personalized treatment. That is, a therapist could take care of more patients having robots develop parts of the treatments.

We propose using machine learning techniques for vowel pose recognition and identification. The input information is collected by an RGB-D device, a *Microsoft Kinect*, and with this information, the system obtains mouth poses which are used in the exercises to guide the users. Interaction is performed through a multimodal system that integrates body expressions, voice interaction, and a graphical user interface (GUI), and all of these modalities are developed to give instructions to the patient as well as encourage him/her during the exercise.

The rest of this manuscript is structured as follows: Section 2 provides the insights of current therapies for AOS, presents new robotic developments for physical therapy and cognitive rehabilitation, and analyses some face detection and classification techniques related to our approach. Next, Section 3 presents the details of our proposal, describing its main phases. Section 4 presents the experiments conducted to validate our work along with the robotic platform, the social robot Mini, and the metrics for evaluating the approach. This section also presents the preliminary results from integrating and testing the AOS exercises in the social robot. Finally, Section 5 analyses the main contributions of our work and draws the main conclusions.

## 2. Related Work

The ability of speech is commonly affected after suffering Alzheimer’s, dementia, or a stroke. Traditional speech therapies focus on mitigating this problem in case of cognitive impairment or rehabilitating in case of cerebrovascular accidents. The recovery time in these cases is around three years [9] in which speech therapy yields positive results in most cases. Apart from this line of therapy, there are others such as music therapy that are usually applied to patients with neurological problems, generally elders. In the case of music, the therapy consists of patients emitting singing and emitting sounds from given melodies in order to improve pitch, variability, and intelligibility of speech [10]. Tomaino and Sacks [11] demonstrated that music therapy helps reorganizing the brain function in patients with brain alterations.

Apart from traditional therapies, technology is being incorporated to health environments. More precisely, robotics is gaining importance, mainly in the fields of physical therapy and cognitive rehabilitation. In these cases, exercises are supervised by therapists who are in charge of selecting the tasks to perform and monitor the procedure [12]. The robot Paro is a good example of the application of robots in cognitive therapy. It imitates a baby harp seal and has been used in therapy with elder people with dementia, increasing the willingness of patients to communicate and a steady increase in physical interaction, not only between patients and the robot but also among patients as well [13, 14]. Another robotic platform used in cognitive therapy is Babyloid, a baby-like robot designed to be taken care of [15]. This robot is intended for recreational therapy in which the robot becomes a pet instead of an animal. These proposals are mainly intended for interaction with elderly people with moderate cognitive impairments.

Other robotic platforms provide a higher degree of interaction in therapies with people with mild cognitive problems. This is the case of Eldertoy [16], a robot developed to achieve both entertaining and gerontological capabilities. This robot offers different interaction channels to communicate with users: gestures, voice, touch-screen, and external actuators. Therapy with this robot is conceived through manipulation and display multimedia content. Therefore, therapy specialists are furnished with a tool able to run games by using the sensors integrated in the platform. The robot Mini is another proposal for therapy with elders in early stages of Alzheimer’s or dementia [17, 18]. Mini is a plush-like desktop robot that offers functionalities related to safety, personal assistance, entertainment, and stimulation. In this work, we aim to extend the capabilities of Mini to conduct speech therapy. More details about the robot design and features can be found in Section 3.

Another research area integrated in our work is computer vision. The literature offers several approaches for face detection and recognition [19, 20]. Applications range from people recognition [21], surveillance [22] to emotion detection and regulation [23, 24]. Although there are several techniques to retrieve facial features, this problem is still challenging since most of the approaches are highly dependent on the face orientation. In this work, we have integrated

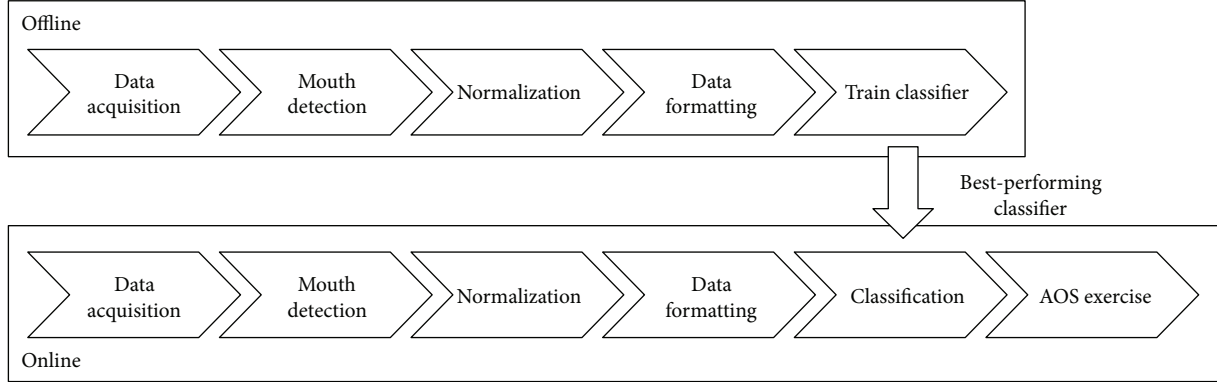


FIGURE 1: Proposed approach pipeline. The upper path corresponds to the offline analysis for assessing the best classifier. The lower path corresponds to the software running in the robot with the speech therapy exercise.

Stasm, an active shape model-based approach coupled to a support vector machine (SVM) classifier that retrieves facial features [20]. Out of these features, the user's mouth is represented with 18 3D points, which will be the input for the machine learning algorithm.

Apart from detecting the mouth, recognizing the mouth pose is crucial to have an algorithm that can be integrated into a speech therapy application. Machine learning has been widely applied in face recognition and recognition of facial expressions [25, 26]. Within the number of techniques, SVM, Adaboost, linear discriminant analysis or, more recently, deep learning [27], among others, try to cope with known problems such as different poses, illumination, ages, and occlusions that nowadays still pose a challenge. In our work, we test several classifiers integrated within Sci-Kit learn [28], an open-source machine learning library written in Python language. It provides feature classification, regression, and clustering algorithms.

### 3. Materials and Methods

This section presents the details of the proposed approach that allows a social robot, equipped with a 3D camera, to conduct an AOS exercise autonomously. Figure 1 shows the main steps of our proposal, which is roughly divided into two operation modes. First, we need to assess the classifier that performs best for our kind of data. In this process, we acquire information from users, preprocess it, and train a set of classifiers to select the best-performing one. This classifier is used next online, thus integrated in the robotic platform where the speech therapy application uses the mouth pose detected to conduct the exercises. Note that the four first steps are the same in both approaches.

**3.1. Mouth Detection from RGB-D Data.** The system described here uses a Microsoft Kinect, which provides RGB images and depth data synchronized both in terms of time and field of view. After information acquisition is performed, the system extracts face features in 2D using the open-source library Stasm [20]. Then, those features are translated into 3D points which are finally classified to recognize the mouth pose (see Figure 2).

The mouth detection process is composed by two main steps. Data acquisition is performed through a middleware specifically designed to work with *RGB-D* devices, *OpenNI* (*OpenNI* website: <http://openni.ru/>). Two information flows are generated from the Kinect device: an *RGB* image stream and a point cloud containing depth information. Next, the system processes the *RGB* data to identify the mouth within a detected face using *Stasm*. This library characterizes a face with 77 points of which 18 belong to the mouth. These points are next matched to the depth information from the camera and formatted to be used in the next phase, mouth pose classification. A more detailed description of the mouth detection system can be found in a previous work [29].

**3.2. Machine Learning Tools for Mouth Pose Classification.** In our approach for mouth pose recognition, we aim to test a series of classification techniques integrated within Scikit-Learn [28]. For the classifier selection, we take as a starting point a previous work [29] in which mouth detection was evaluated using WEKA [30], a well-known data mining tool that allows preprocessing, classification, regression, clustering, association rules, and visualization of data. In this case, we wanted to take the study one step further and integrate the best-performing classifier in our robotic platform (WEKA was not directly integrated within the framework ROS). Thus, we compared the performance of the following classifiers:

- (i) *k-Nearest neighbours (k-NN)* is a nonparametric method used for classification and regression in which the input consists of the *k* closest training examples in a feature space [31]. In our problem, the output is a mouth pose where a sample is classified by a majority vote of its neighbours with the object being assigned to the most common class among its *k*-nearest neighbours.
- (ii) *Support vector machine* is a supervised learning technique for classification and regression that builds a hyperplane or set of hyperplanes in a high- or infinite-dimensional space [32]. An SVM can

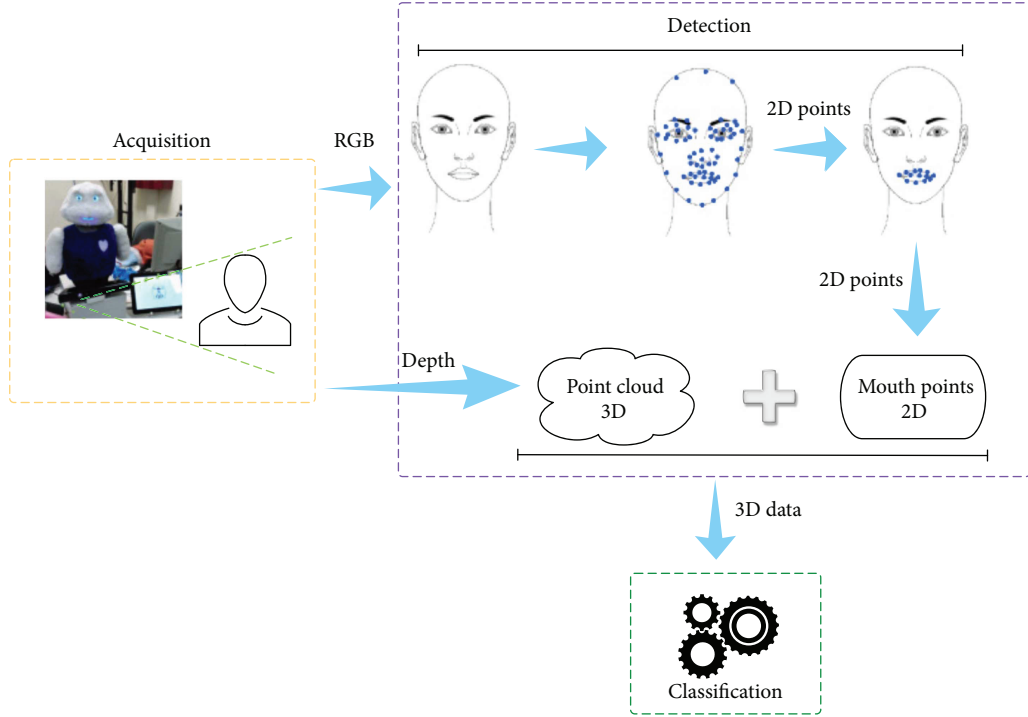


FIGURE 2: Mouth detection pipeline using Stasm.

perform linear and nonlinear classification mapping the inputs into high-dimensional feature spaces.

- (iii) C4.5 is an algorithm that generates a decision tree from a set of training data using the concept of information entropy [33]. At each node of the tree, the algorithm chooses the attribute of the data that most effectively splits the set of samples into subsets enriched in one of the classes. The splitting criterion is the normalized information gain (difference in entropy).
- (iv) *Random forest* is an ensemble learning method for classification and regression that construct multiple decision trees at training time and outputs the class that corresponds to the mode of the possible classes (mouth poses). An advantage of random forest is that this technique mitigates the overfitting problem caused by traditional decision trees [34].

**3.3. Assessing the Best Classifier: Offline Analysis.** Before addressing the logic of the speech therapy exercise, it was necessary establishing which classifier offered better performance with our input data. This operation mode, depicted in the upper path of Figure 1, starts with a data acquisition phase in which the RGB-D device provides colour images and point clouds with the 3D representation of the scene. The next step, mouth detection, works as described in Section 3.1, using Stasm to generate a 3D array of 18 points corresponding to the mouth detected in the input data.

Since the head position in the image varies as the user moves, it is important to normalize the data to establish a

common frame for reference. Thus, the normalization step computes the centroid of the mouth, setting it as the origin of coordinates for the 18 points (see (1), (2), and (3)). Each one of these points is defined by its  $x$ ,  $y$ ,  $z$  components, and therefore, (4), (5), and (6) show that the normalization for each of them is calculated with respect to the centroid.

$$x_{\text{centroid}} = \frac{1}{18} \sum_{i=1}^{18} x_i, \quad (1)$$

$$y_{\text{centroid}} = \frac{1}{18} \sum_{i=1}^{18} y_i, \quad (2)$$

$$z_{\text{centroid}} = \frac{1}{18} \sum_{i=1}^{18} z_i, \quad (3)$$

$$x_{i_{\text{normalized}}} = x_i - x_{\text{centroid}} \quad \forall i \in [1, 18], \quad (4)$$

$$y_{i_{\text{normalized}}} = y_i - y_{\text{centroid}} \quad \forall i \in [1, 18], \quad (5)$$

$$z_{i_{\text{normalized}}} = z_i - z_{\text{centroid}} \quad \forall i \in [1, 18]. \quad (6)$$

These normalized points are formatted in tuples for the classifier. Each tuple composed by 54 values plus the class for each pose was recorded. After the data is formatted, we trained the classifiers previously described in Section 3.2.

**3.4. Online Execution.** The best-performing classifier identified in the previous section is integrated in the online execution mode of our system, described in the lower path of

TABLE 1: Set of utterances to convey messages during the exercise (approximate translation from Spanish).

Situation	Sentence	Details
Congratulating	Very good	General congratulation utterances
	Keep going	
	You are doing great	
	Open a little less your mouth	Corrections in case the user is opening the mouth more than expected
	Open your mouth less	
	Please, close your mouth a bit	
Correcting	Open your mouth a bit more	Corrections in case the user is opening the mouth less than expected
	Open your mouth a bit more	
	Make a bigger mouth	
	You are almost there	Utterance to encourage the user during the exercise
	Keep trying	
	Let us try to say “a” correctly three times	Practicing with “a” pose
Starting exercise	Let us try to say “u” correctly three times	Practicing with “u” pose
	Try to keep your mouth closed for three rounds	Practicing with mouth closed pose
	In 3, 2, 1... Now!	Start signal

Figure 1. The four first steps are common to both offline and online executions as they are intended for data acquisition, detecting the points corresponding to the mouth and normalize them as well as formatting the data for classification. In the online mode, the data formatted is then processed in a classifier which output is used in the AOS exercise to assess the user performance and guide him/her during the session.

When one of the three poses reaches a number of detections, the system selects that pose as the current one and interacts with the user, expressing congratulations in case the pose detected was the one expected, or correcting the user if another pose is detected. A repertoire or corpus of utterances has been created to congratulate and correct the user (see Table 1) as a complement to the images shown in the tablet (see Figure 3). Additionally, the robot expresses gestures with its body to help engaging the user in the exercise. When the user fails to perform the pose, a sad expression is performed while otherwise the robot shows a happy expression (Instead of denning here what they are about, a demo video has been released in which those gestures are clearly demonstrated. The video link is presented at the end of Section 4.4).

In the current version of the system, the process of detecting a mouth pose and congratulating/correcting the

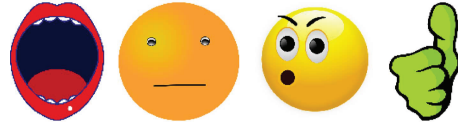


FIGURE 3: Images to give feedback about the mouth pose and the user’s performance. First, image to indicate how to make the “a” pose. Second, image to indicate how the closed-mouth pose should be. Third, image to indicate how to make the “u” pose. Fourth, image to congratulate the user.

user is repeated three times although the system is flexible enough to change and adapt the exercise logic.

## 4. Results and Discussion

**4.1. Robotic Platform: Mini.** The system developed in this work was integrated in Mini, a desktop social robot designed and built at RoboticsLab research group from the Charles III University of Madrid (see Figure 4). Originally, this robot was designed to interact with elder people with mild cognitive impairment [18]. Nevertheless, the capabilities of this platform allows other users and applications such as our current goal.

Mini is equipped with multiple HRI interfaces including automatic speech recognition (ASR) [35], voice activity detection [36], emotion detection [37], a text to speech (TTS) system, a tablet, and an RGB-D device. Moreover, Mini possesses 5 degrees of freedom to allow moving its arms, base, and head. The interaction capabilities complete with touch sensors, two uOled screens for the eyes, RGB LEDs in the cheeks and heart, and a VUmeter as mouth to create the illusion of a talking robot. All of these interfaces are integrated in a natural dialogue management system [38] which enables the robot to carry out natural interactions. Finally, these components are integrated using ROS framework [39].

**4.2. Metrics for Evaluating the Classifiers.** Since our classifiers have to solve a multiclass problem, the metric selected for assessing the best one was the macroaverage F-score. Macroaverage means that the metric is independently computed from each class and then the average is calculated. This metric uses the precision and recall for each class and calculates the mean precision and recall of all classes as shown as follows:

$$\begin{aligned} \text{Precision} &= \frac{\sum_{i=1}^N \text{TP}_i}{\sum_{i=1}^N \text{TP}_i + \text{FP}_i}, \\ \text{Recall} &= \frac{\sum_{i=1}^N \text{TP}_i}{\sum_{i=1}^N \text{TP}_i + \text{FN}_i}, \end{aligned} \quad (7)$$

where  $N$  is the total number of classes,  $\text{TP}_i$  corresponds to the true positives achieved in class  $i$ ,  $\text{FP}_i$  are the false positives for class  $i$ , and  $\text{FN}_i$  are the false negatives in class  $i$ . Then, the

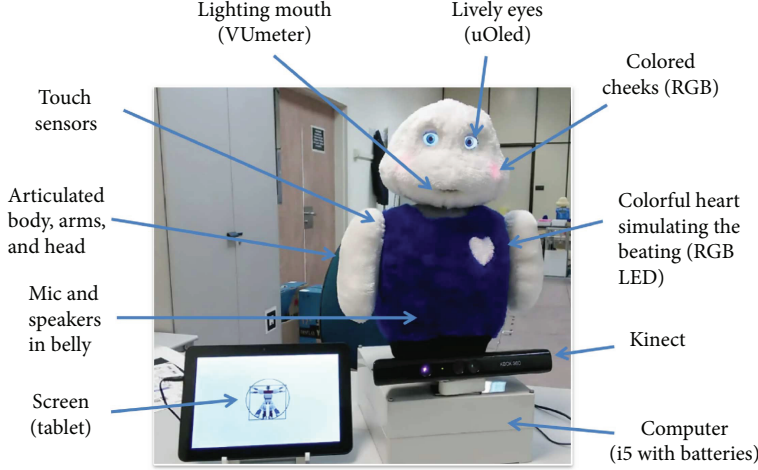


FIGURE 4: Mini, the social robot involved in the experiments [40]. Apart from its plushy shape, the robot is equipped with a series of sensors and actuators for HRI.

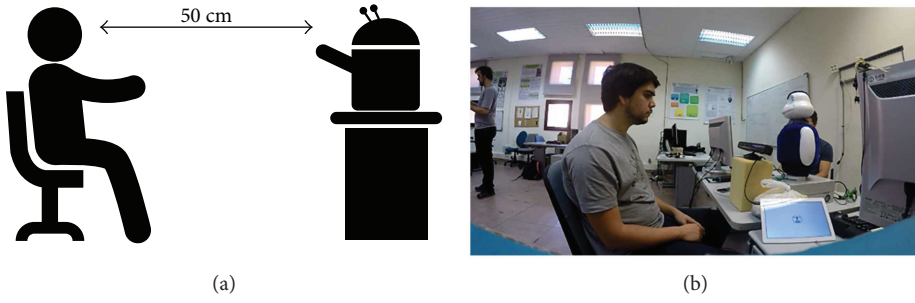


FIGURE 5: Experimental setup. The user was sitting in front of the robot at 0.5 meters, a natural distance for interaction that ensures clear images of the face.

macroaverage  $F$ -score is computed as the harmonic mean of these two values as shown as follows:

$$\text{Macroaverage-}F\text{-score} = \frac{2 \times \overline{\text{precision}} \times \overline{\text{recall}}}{\overline{\text{precision}} + \overline{\text{recall}}}. \quad (8)$$

**4.3. Experiments.** In our experiments, users sit in front of the robot, at 0.5 meters (see Figure 5(a)). A previous study indicated that at a range of 0.5 meters, the detector performance in order to locate the mouth accurately in the face was high, suffering a degradation with the distance that at 2 meters was too poor to achieve reliable detections [29]. Moreover, as shown in Figure 5, right, this distance allows a natural interaction with the robot, for instance with its tablet that is usually placed between the robot and the user. Note that in Figure 5(b), the tablet is on the left side of the robot. In this specific case, the tablet was placed there just for illustrative purposes. Also, the Kinect camera changed the usual location (see Figure 4) to allow a better acquisition of face images.

The following sections detail the experiments conducted to assess the performance of our system and its feasibility for speech therapy. Also, the aim of this set of tests was to select the best classifier for our data. We first tested the performance with the most different poses “a” and “u”, as described in experiment 1. For our second experiment, we added a new “neutral” pose that corresponded to the mouth

closed and carried out experiment 2. 14 users were involved in our experiments, and the method for dividing the datasets was 1-fold cross-validation with 60% of the instances for training and 40% for test.

**4.3.1. Experiment 1: Training 2 Poses.** This experiment is meant to assess the feasibility of the classifiers described in Section 3.2 to distinguish between two mouth poses. Although this set of poses may seem reduced, they are different enough as to implement a range of mouth movements that could be useful in SOA therapy. Moreover, recognizing the mouth is not an easy task, leading to similar representations of different poses as shown in Figure 6. The two first images correspond to the poses associated to “a” and “e,” and the two last ones correspond to “o” and “u.”

In this test, the dataset was composed of 1200 instances for the pose “a” and 1425 for the “u” pose (see Table 2). After the test, two classifiers, C4.5 and SVM, showed promising results, with a macroaverage  $F$ -score of 0.82 and 0.81, respectively, as shown in Table 3. Additionally, Table 4 offers the confusion matrix for the best classifier in this experiment, C4.5, in which we can observe an accuracy that starts to be competitive for our speech therapy application.

**4.3.2. Experiment 2: Training 3 Poses.** In this experiment, a new pose was added to the dataset, mouth closed, to

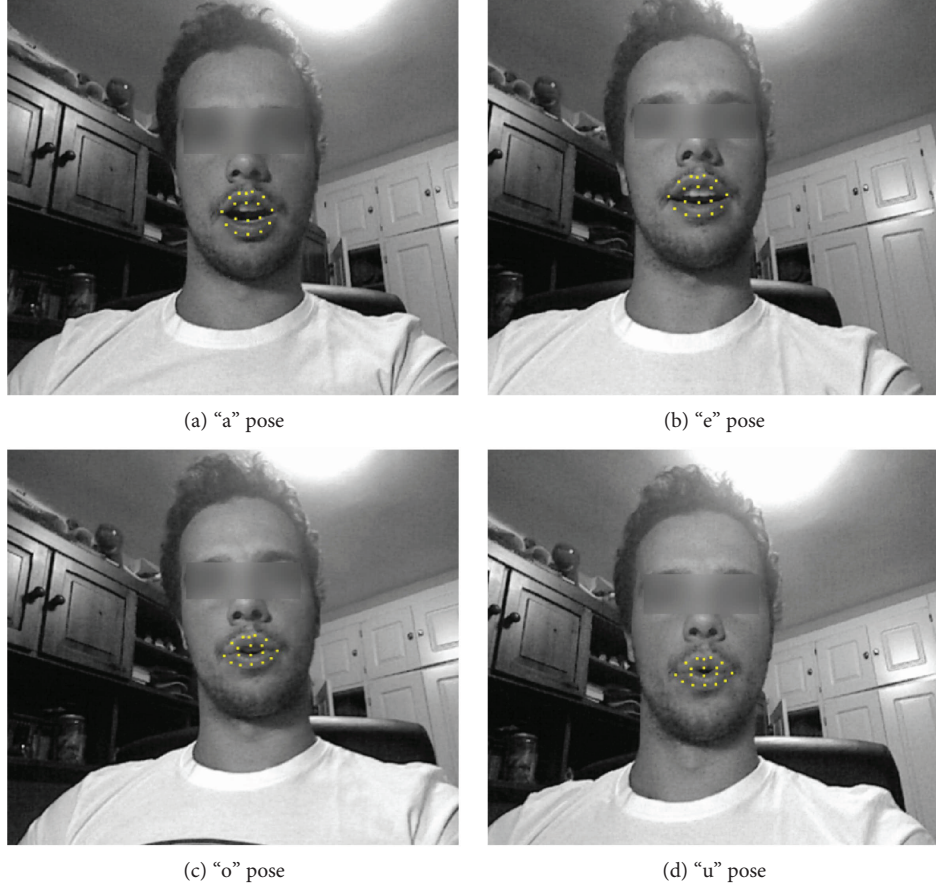


FIGURE 6: Mouth points as detected by Stasm. We can see in this example how there is low variability between some mouth poses.

TABLE 2: Dataset summary for experiments 1 and 2.

Pose	Experiment 1 instances	Experiment 2 instances
“a”	1200	4623
“u”	1425	5250
Mouth closed	N/A	3624
Total	1625	13497

TABLE 3: Results for experiments 1 and 2. Macroaverage  $F$ -score for the four classifiers tested with two mouth poses.

Classifier	Experiment 1: macroaverage $F$ -score	Experiment 2: macroaverage $F$ -score
Random forest	0.57	0.47
C4.5	<b>0.82</b>	<b>0.95</b>
k-NN	0.54	0.93
SVM	0.81	0.63

complement the cases for the AOS exercise. Therefore, a new class, mouth closed, was added to our dataset with 3624 instances. For the previous classes, new instances were added as well, having a total of 4623 instances for the “a” pose and

5250 instances for the “u” pose. Finally, the classifiers were retrained with the new data. The results show that C4.5 is again the best classifier, with k-NN offering competitive performance (see Table 3). Therefore, since C4.5 showed the best behaviour in both experiments, this classifier is the one selected for the online execution.

In this experiment, the results improved with respect to the previous one as shown in the confusion matrix for C4.5 classifier (see Table 5). Here, the recognition rate for the “a” pose reached 95%; in case of the “u” pose, the rate is 93%, and finally for mouth-closed pose, the rate is 99.67%.

**4.4. Integration in the Social Robot.** This section analyses the performance of the detection and classification integrated with the speech therapy application. In this case, users trained the system online in periods ranging between 5 and 10 minutes for the three poses together. Table 6 shows the performance of our pretrained C4.5 classifier when offered new data. We can see how in some cases as in mouth-closed pose that the performance drops to the point that the system is not usable.

At this point, we realised that we needed to perform some training with the new users’ data, but in this case, that training should not be as intensive as in previous experiments. Since the final application is speech therapy, we cannot expect that users will be willing to train the

TABLE 4: Experiment 1: confusion matrix for C4.5 classifier identifying 2 poses.

	Predicted A	Predicted U
Actual A	86%	14%
Actual U	12%	88%

TABLE 5: Experiment 2: confusion matrix for C4.5 classifier identifying 3 poses.

	Predicted A	Predicted U	Predicted mouth closed
Actual A	95%	4%	1%
Actual U	5%	93%	2%
Actual mouth closed	0.03%	0.3%	99.67%

robot for long periods of time. In this case, the users are trained from the system with online detections in periods ranging between 5 and 10 minutes for the three poses together. We believe that this would not cause boredom or fatigue in the users as it only needs to be performed once per new user. With this new data, the performance of the system improves to levels comparable to experiment 1 (see Table 7), and although not reaching the scores achieved in experiment 2 with cross-validation, these levels are high enough to ensure a good detection rate.

In the online execution, we experimentally set the score threshold to consider valid detection to 0.35 and a pose was output after six successful recognitions. In most cases, we noticed that the detection score was close to one, dropping to low values for missdetections. The number of successful recognitions to consider a valid pose directly impacts the execution time of our system since a bigger number would cause a slow response and a smaller number could lead to wrong detections. Therefore, six valid detections were considered as a good tradeoff between time of response and accuracy.

Figure 7 offers an overview of the speech therapy proposal with the different phases where the robot guides the user along the exercise. First, the robot provides a simple explanation about the exercise (see Figure 6) using gestures, voice, and the tablet to convey the messages. Next, the exercise starts and the user should start making the desired pose while the system is detecting and classifying the mouth pose (see Figure 6). Finally, after three successful detections, the robot congratulates the user (see Figure 6). There is also the possibility that the system does not detect the target pose. In this case, the robot corrects the user, explaining how to achieve the desired pose (see Figure 6). Along this exercise, the robot uses voice, gestures, and the tablet to give instructions and feedback to the user. A video has been uploaded with more details about the execution of the system which can be found in <https://youtu.be/XRrIP3BcwCY>.

**4.5. Discussion.** The results and the experimental conditions of the proposed approach are summarized in Table 8. These results show how our proposal provides high accuracy for

TABLE 6: Confusion matrix for the first test with untrained users.

	Predicted A	Predicted U	Predicted mouth closed
Actual A	52%	32%	16%
Actual U	36%	40%	24%
Actual mouth closed	0%	90%	10%

TABLE 7: Confusion matrix for the test retraining the classifier with new user data.

	Predicted A	Predicted U	Predicted mouth closed
Actual A	85%	12%	3%
Actual U	8%	75%	17%
Actual mouth closed	0%	14%	86%

mouth pose classification, up to 0.95 in the cross-validation test. It is worth remarking that the experimental phase in this paper is intended as a proof of concept and that we are currently working on testing it with real users. Additionally, we are aware that mouth poses could change when working with people with motor mouth problems and that this fact could affect the performance of the classifiers. In this regard, our plan is to add real user data and retrain the system when deploying it in real scenarios.

Also, the set of mouth poses recognized may seem too small but for AOS therapy purposes, their differences were considered enough for a first approach. It is our intention involving experts to evaluate the feasibility of our proposal both in terms of poses recognized and the dynamic of the exercise.

## 5. Conclusions

This manuscript introduced an approach for apraxia of speech therapy using a social robot. The system consists of two main phases: an *offline* one in which we train a set of classifiers after detecting and normalizing the mouth information from users and an *online* one that runs in our social robot Mini. This operation runs in real time, integrating the best-performing classifier, and guides the user through an AOS exercise.

The experiments included up to three mouth poses (“a”, “u,” and mouth closed) which we consider are enough for a first approach of therapy for their differences regarding the mouth positions. The classifiers trained on our dataset are composed by information from 14 users in our experiments offline, to assess the best one. In these offline experiments, C4.5 was the best classifier for our data (achieving 0.95 of macroaverage *F*-score), and therefore, it was integrated within the final approach. In the online tests with the whole system integrated in the social robot, we conducted additional experiments with 7 new users, the first one running

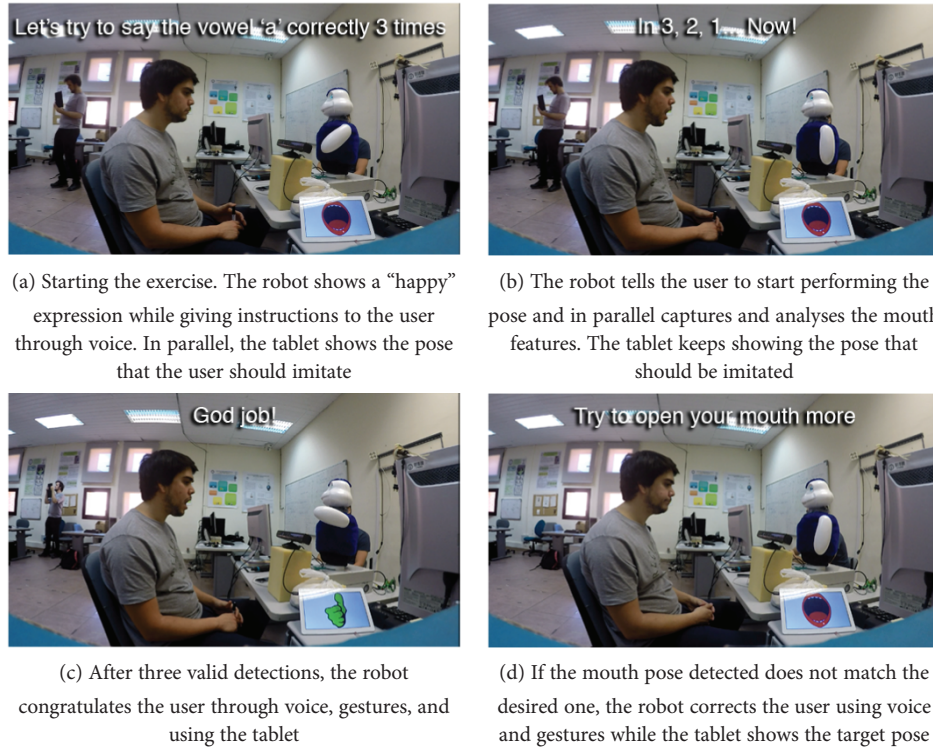


FIGURE 7: Running example of the speech therapy proposal. The robot leads the user through the exercise, encouraging him to keep participating.

TABLE 8: Numbers summarizing the experimental conditions and results of our proposal.

Recognized poses	<b>3 poses</b> (“a,” “u,” mouth closed)
Dataset instances	<b>1625</b> for experiment 1 and <b>13497</b> for experiment 2
Input features per instance	<b>54 features:</b> 18 mouth points * 3 components (x, y, z)
Users involved in the dataset	<b>14 users</b> for the 2 datasets
Classifiers tested	<b>4 classifiers</b>
Metric for comparison	<b>Macroaverage F-score</b>
Best algorithm for classifying poses	<b>C4.5</b> (0.81 and 0.95 of macroaverage F-score in the experiments)
Users involved in the real tests	<b>7 users</b>

the system with untrained data which showed a performance decrease in the mouth poses classification. This motivated the second experiment in which we retrained the classifier adding a small set of samples from the new users. In this case, the performance rose again to competitive values.

We believe that the results achieved in our experiments are promising, and thus, we are intended to proceed with the next stage: testing the AOS exercise with real users and therapists.

To the extent of our knowledge, this proposal is innovative as robotic technologies have not been applied to this field so far.

## Conflicts of Interest

The authors declare that there is no conflict of interest regarding the publication of this paper.

## Acknowledgments

The research leading to these results has received funding from the projects Development of Social Robots to Help Seniors with Cognitive Impairment (ROBSEN), funded by the Spanish Ministry of Economy and Competitiveness, and RoboCity2030-III-CM, funded by Comunidad de Madrid and cofunded by Structural Funds of the EU.

## References

- [1] R. González Victoriano and L. Toledo Rodríguez, “Apraxia del habla: evaluación y tratamiento,” *Revista Neuropsicología, Neuropsiquiatría y Neurociencias*, vol. 15, no. 1, pp. 141–158, 2015.
- [2] American Speech-Language-Hearing Association, *Apraxia of Speech in Adults* November 2017, <https://www.asha.org/public/speech/disorders/ApraxiaAdults/>.

- [3] A. Ygual-Fernández and J. Cervera-Mérida, "Dispraxia verbal: características clínicas y tratamiento logopédico," *Revista de Neurología*, vol. 40, pp. 121–126, 2005.
- [4] National Institute of Deafness and Other Communication Disorders (NIDCD) and U.S. Department of Health & Human Services, *Apraxia of Apeech* October 2017, <https://www.nidcd.nih.gov/health/apraxia-speech> 05.
- [5] J. F. Veneman, R. Kruidhof, E. E. G. Hekman, R. Ekkelenkamp, E. H. F. Van Asseldonk, and H. Van Der Kooij, "Design and evaluation of the lopes exoskeleton robot for interactive gait rehabilitation," *IEEE Transactions on Neural Systems and Rehabilitation Engineering*, vol. 15, no. 3, pp. 379–386, 2007.
- [6] N. Ho, K. Tong, X. Hu et al., "An emg-driven exoskeleton hand robotic training device on chronic stroke subjects: task training system for stroke rehabilitation," in *2011 IEEE International Conference on Rehabilitation Robotics*, pp. 1–5, Zurich, Switzerland, June–July 2011.
- [7] H. S. Lo and S. Q. Xie, "Exoskeleton robots for upper-limb rehabilitation: state of the art and future prospects," *Medical Engineering & Physics*, vol. 34, no. 3, pp. 261–268, 2012.
- [8] D. Copaci, A. Flores, F. Rueda, I. Alguacil, D. Blanco, and L. Moreno, "Wearable elbow exoskeleton actuated with shape memory alloy," in *Converging Clinical and Engineering Research on Neurorehabilitation II*, Biosystems & Biorobotics, pp. 477–481, Springer International Publishing, Cham, 2017.
- [9] O. Juncos and A. Rozas, "Problemas del lenguaje en la tercera edad. Orientaciones y perspectivas de la logopedia," *Revista Galego-Portuguesa De Psi-Coloxía E Educación: revista de estudios e investigación en psicología y educación*, vol. 8, pp. 387–398, 2002.
- [10] N. S. Cohen, "The effect of singing instruction on the speech production of neurologically impaired persons," *Journal of Music Therapy*, vol. 29, no. 2, pp. 87–102, 1992.
- [11] C. M. T. Oliver Sacks, "Music and neurological disorder," *International Journal of Arts Medicine*, vol. 1, no. 1, pp. 10–12, 1992.
- [12] K. Wada, Y. Ikeda, K. Inoue, and R. Uehara, "Development and preliminary evaluation of a caregiver's manual for robot therapy using the therapeutic seal robot PARO," in *19th International Symposium in Robot and Human Interactive Communication*, pp. 533–538, Viareggio, Italy, September 2010.
- [13] K. Takayanagi, T. Kirita, and T. Shibata, "Comparison of verbal and emotional responses of elderly people with mild/moderate dementia and those with severe dementia in responses to seal robot, PARO," *Frontiers in Aging Neuroscience*, vol. 6, p. 257, 2014.
- [14] W. L. Chang, S. Abanovic, and L. Huber, "Use of seal-like robot PARO in sensory group therapy for older adults with dementia," in *2013 8th ACM/IEEE International Conference on Human-Robot Interaction (HRI)*, pp. 101–102, Tokyo, Japan, March 2013.
- [15] Y. Furuta, M. Kanoh, T. Shimizu, M. Shimizu, and T. Nakamura, "Subjective evaluation of use of Babyloid for doll therapy," in *2012 IEEE International Conference on Fuzzy Systems*, pp. 1–4, Brisbane, QLD, Australia, June 2012.
- [16] L. F. Cossío, J. M. L. Salvador, and S. F. Martínez, "Robotics for social welfare," *Journal of Accessibility and Design for All*, vol. 2, no. 1, pp. 94–113, 2012.
- [17] E. Salichs, A. Castro-González, M. Malfaz, and M. Salichs, "Mini: a social assistive robot for people with mild cognitive impairment," in *New Friends 2016. The 2nd International Conference on Social Robots in Therapy and Education*, pp. 29–30, Barcelona/Spain, November 2016.
- [18] M. A. Salichs, I. P. Encinar, E. Salichs, Á. Castro-González, and M. Malfaz, "Study of scenarios and technical requirements of a social assistive robot for Alzheimer's disease patients and their caregivers," *International Journal of Social Robotics*, vol. 8, no. 1, pp. 85–102, 2016.
- [19] S. Zafeiriou, C. Zhang, and Z. Zhang, "A survey on face detection in the wild: past, present and future," *Computer Vision and Image Understanding*, vol. 138, pp. 1–24, 2015.
- [20] S. Milborrow and F. Nicolls, "Active shape models with SIFT descriptors and MARS," in *Proceedings of the 9th International Conference on Computer Vision Theory and Applications*, pp. 380–387, Lisbon, Portugal, 2014.
- [21] W. Zhao, R. Chellappa, P. J. Phillips, and A. Rosenfeld, "Face recognition: a literature survey," *ACM Computing Surveys*, vol. 35, no. 4, pp. 399–458, 2003.
- [22] Z. Kalal, K. Mikolajczyk, and J. Matas, "Face-tld: tracking-learning-detection applied to faces," in *2010 IEEE International Conference on Image Processing*, pp. 3789–3792, Hong Kong, China, September 2010.
- [23] A. Fernández-Caballero, A. Martínez-Rodrigo, J. M. Pastor et al., "Smart environment architecture for emotion detection and regulation," *Journal of Biomedical Informatics*, vol. 64, no. C, pp. 55–73, 2016.
- [24] J. C. Castillo, A. Castro-González, F. Alonso-Martín, A. Fernández-Caballero, and M. A. Salichs, "Emotion detection and regulation from personal assistant robot in smart environment," in *Personal Assistants: Emerging Computational Technologies*, Intelligent Systems Reference Library, pp. 179–195, Springer, Cham, 2018.
- [25] M. S. Bartlett, G. Littlewort, M. Frank, C. Lainscsek, I. Fasel, and J. Movellan, "Recognizing facial expression: machine learning and application to spontaneous behavior," in *2005 IEEE Computer Society Conference on Computer Vision and Pattern Recognition (CVPR'05)*, pp. 568–573, San Diego, CA, USA, June 2005.
- [26] G. Littlewort, M. S. Bartlett, I. Fasel, J. Susskind, and J. Movellan, "Dynamics of facial expression extracted automatically from video," *Image and Vision Computing*, vol. 24, no. 6, pp. 615–625, 2006.
- [27] Y. Sun, Y. Chen, X. Wang, and X. Tang, "Deep learning face representation by joint identification-verification," in *Proceedings of the 27th International Conference on Neural Information Processing Systems*, vol. 2 of NIPS'14, pp. 1988–1996, MIT Press, Cambridge, MA, USA, 2014.
- [28] F. Pedregosa, G. Varoquaux, A. Gramfort et al., "Scikit-learn: machine learning in python," *Journal of Machine Learning Research*, vol. 12, pp. 2825–2830, 2011.
- [29] J. C. Castillo, I. P. Encinar, A. Conti-Morera, Á. C. González, and M. Á. Salichs, "Vowel recognition from RGB-D facial information," in *Ambient Intelligence-Software and Applications-7th International Symposium on Ambient Intelligence (ISAMI 2016)*, Advances in Intelligent Systems and Computing, pp. 225–232, Springer, Cham, 2016.
- [30] M. Hall, E. Frank, G. Holmes, B. Pfahringer, P. Reutemann, and I. H. Witten, "The WEKA data mining software: an update," *ACM SIGKDD Explorations Newsletter*, vol. 11, no. 1, pp. 10–18, 2009.
- [31] N. S. Altman, "An introduction to kernel and nearest-neighbor nonparametric regression," *The American Statistician*, vol. 46, no. 3, pp. 175–185, 1992.

- [32] C. Cortes and V. Vapnik, "Support-vector networks," *Machine Learning*, vol. 20, no. 3, pp. 273–297, 1995.
- [33] J. R. Quinlan, *C4. 5: Programs for Machine Learning*, Morgan Kaufmann Publishers Inc., San Francisco, CA, USA, 1993.
- [34] T. K. Ho, "Random decision forests," in *Proceedings of 3rd International Conference on Document Analysis and Recognition*, pp. 278–282, Montreal, Que., Canada, August 1995.
- [35] F. Alonso-Martín and M. A. Salichs, "Integration of a voice recognition system in a social robot," *Cybernetics and Systems: An International Journal*, vol. 42, no. 4, pp. 215–245, 2011.
- [36] F. Alonso-Martin, A. Castro-González, J. F. Gorostiza, and M. A. Salichs, "Multidomain voice activity detection during human-robot interaction," in *International Conference on Social Robotics*, Lecture Notes in Computer Science, pp. 64–73, Springer, Cham, 2013.
- [37] F. Alonso-Martín, M. Malfaz, J. Sequeira, J. F. Gorostiza, and M. A. Salichs, "A multimodal emotion detection system during human–robot interaction," *Sensors*, vol. 13, no. 12, pp. 15549–15581, 2013.
- [38] F. Alonso-Martín, A. Castro-González, J. F. Gorostiza, and M. A. Salichs, "Augmented robotics dialog system for enhancing human–robot interaction," *Sensors*, vol. 15, no. 12, pp. 15799–15829, 2015.
- [39] M. Quigley, K. Conley, B. Gerkey et al., "ROS: an open-source robot operating system," in *ICRA Workshop on Open Source Software*, vol. 3, p. 5, Kobe, 2009.
- [40] J. C. Castillo, D. Cáceres-Domínguez, F. Alonso-Martín, Á. Castro-González, and M. Á. Salichs, "Dynamic gesture recognition for social robots," in *International Conference on Social Robotics*, Springer, Lecture Notes in Computer Science, pp. 495–505, Springer, Cham, 2017.

## Research Article

# Obtaining Natural Sit-to-Stand Motion with a Biomimetic Controller for Powered Knee Prostheses

**Molei Wu, Md Rejwanul Haque, and Xiangrong Shen**

*Department of Mechanical Engineering, The University of Alabama, 286 Hardaway Hall, P.O. Box 870276, Tuscaloosa, AL 35487-0276, USA*

Correspondence should be addressed to Xiangrong Shen; [xshen@eng.ua.edu](mailto:xshen@eng.ua.edu)

Received 12 June 2017; Revised 8 August 2017; Accepted 9 August 2017; Published 18 September 2017

Academic Editor: Antonio Fernández-Caballero

Copyright © 2017 Molei Wu et al. This is an open access article distributed under the Creative Commons Attribution License, which permits unrestricted use, distribution, and reproduction in any medium, provided the original work is properly cited.

Standing up from a seated position is a common activity in people's daily life. However, for transfemoral (i.e., above-knee) amputees fitted with traditional passive prostheses, the sit-to-stand (STS) transition is highly challenging, due to the inability of the prosthetic joints in generating torque and power output. In this paper, the authors present a new STS control approach for powered lower limb prostheses, which is able to regulate the power delivery of the prosthetic knee joint to obtain natural STS motion similar to that displayed by healthy subjects. Mimicking the dynamic behavior of the knee in the STS, a unified control structure provides the desired control actions by combining an impedance function with a time-based ramp-up function. The former provides the gradual energy release behavior desired in the rising phase, while the latter provides the gradual energy injection behavior desired in the loading phase. This simple and intuitive control structure automates the transition between the two phases, eliminating the need for explicit phase transition and facilitating the implementation in powered prostheses. Human testing results demonstrated that this new control approach is able to generate a natural standing-up motion, which is well coordinated with the user's healthy-side motion in the STS process.

## 1. Introduction

Standing from a seated position is a common yet dynamically challenging task in people's daily life. Due to the vertical ascent of the body's center of gravity, sit-to-stand (STS) transition requires high torque in the knee, far exceeding the joint torque in walking. Various biomechanical studies reported knee peak torques in STS as high as 2.2 Nm/kg (e.g., [1]), while the typical peak torque in natural walking is only 0.615 Nm/kg [2] (both body weight normalized). As a result, STS transition poses a major barrier to the mobility of individuals with lower limb motor impairments, including the transfemoral (TF) amputees (i.e., individuals suffering from above-knee amputations). A related study showed that TF amputees suffer from much higher asymmetry in ground reaction force and knee moments in the sit-to-stand motion, compared with no-amputee healthy individuals [3]. According to the results of this study, the healthy individuals' ground reaction force and knee moment production were

less than 7% asymmetric, while the amputees' asymmetry for ground reaction force was 53~69%, and the asymmetry for knee moments was 110~124%. Note that although a powered TF prosthesis (Power Knee) was used in this study, it generated resistance in the STS and thus produced similar results as the passive devices in the study (C-Leg and Mauch SNS). The inability of existing prostheses in generating enough knee torque and regulating the torque delivery in the STS seriously affects the mobility of the large population of TF amputees in their daily life.

Motivated by this significant performance deficiency of traditional passive TF prostheses, researchers have expended substantial efforts in developing powered devices. The pioneering work in this area was conducted by Flowers and Mann, which uses a hydraulic actuator to actuate the knee joint [4]. However, multiple drawbacks with hydraulics, such as leakage and lack of a compact supply, make it less attractive for prosthetic applications. Currently, most powered transfemoral prostheses are actuated with electric motors

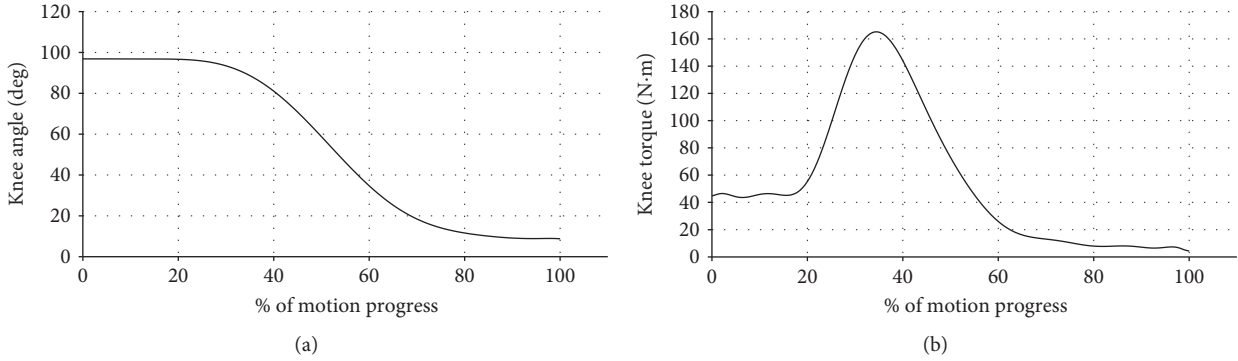


FIGURE 1: Knee position (a) and torque (b) trajectories in the STS motion (plotted for a 75 kg person with the data from [1]).

[5–10], for example, Sup et al. developed a powered knee and ankle prosthesis with both joints powered with a DC motor—ball screw assemblies [8]; Martinez-Villalpando and Herr developed a powered knee prosthesis with two series-elastic actuators positioned in parallel in an agonist-antagonist arrangement [9]; and Hoover et al. developed a myoelectric transfemoral prosthesis, in which the powered knee is controlled with an EMG-based motion controller [10]. Additionally, Ossur, a leading orthopedics company, manufactured the aforementioned Power Knee, the first commercially available powered transfemoral prosthesis. According to the available technical information, the Power Knee is also actuated with an electric motor. In addition to these motor-powered devices, pneumatically actuated prostheses have also been developed by researchers including the authors' group, for example, the prototypes powered with pneumatic cylinders [11] and muscle actuators [12].

The powered prostheses mentioned above are able to actively generate joint torque and power for dynamically challenging tasks such as STS transition. Making full use of such capability, however, requires an effective and reliable controller to regulate the joint power delivery in motion. Currently, a walking controller for powered prostheses has been well established. Typical approaches include echo control, which controls the prosthetic joint to track the recorded sound-side motion with a half-cycle delay [13], and finite-state impedance control, which implements an artificial impedance within each phase of the gait cycle [11]. Electromyography has also been attempted in obtaining the user's motion intent and generating the corresponding motion command [14]. STS control, however, is much less investigated. The Center for Intelligent Mechatronics at Vanderbilt University developed a multimode controller for powered knee and ankle prostheses, in which STS is incorporated as a transitional motion between sitting and standing states [15, 16]. However, no details were provided on the rationale of the controller structure or the determination of the control parameters.

In the research presented in this paper, the authors developed a new control approach to regulate the power and torque delivery in the STS process. As the basis of this approach, an analysis of the biomechanical behavior of the

knee in the STS was conducted, providing the inspiration for the proposed controller structure. Subsequently, curve fitting was conducted to evaluate the validity of the new controller structure, utilizing the existing biomechanical data of the STS motion. This new approach was implemented in a powered knee prosthesis developed in the authors' lab, generating qualitative and quantitative results to evaluate its effectiveness.

## 2. Knee Biomechanical Behavior-Inspired STS Controller

Biomechanics in STS is a heavily investigated topic with a large body of data generated from numerous studies. Ideally, an STS controller should replicate the biomechanical behavior of the knee in this process, providing the prosthesis user a natural control experience. However, exactly replicating the kinetic and kinematic trajectories of the biological knee is unfeasible. Human locomotion is a highly interactive process, in which the human lower limbs interact with the rest of the human body and the environment to obtain coordinated motion. Enforcing the kinetic/kinematic trajectories in the prosthetic knee precludes such interaction, resulting in a poor experience for the prosthesis users. Results of the biomechanical data, on the other hand, provide insight to the dynamic behavior of the knee and thus can be used as the inspiration for the prosthesis controller.

Unlike cyclical motion modes such as walking, STS is a typical transitional motion with clearly defined start (seated position) and end (standing position). The typical joint position and torque trajectories are shown in Figure 1 (data from [1]). The entire process can be divided into two phases with distinct dynamic characteristics, separated by the instant of seat-off (SO):

- (1) Loading phase (from start to SO): with the body weight shifted from the seat to the lower limb, the knee torque increases rapidly to support the body weight and initiate the upward motion. In this phase, the knee position remains almost constant until the final portion of the phase, and the torque increases at a nearly constant rate after the initial dormant period.

- (2) Rising phase (from SO to end): after reaching the maximum value, the knee torque reduces with the joint extension and settles at a steady-state value after the standing position is reached.

Such segmentation of the STS motion can be clearly seen in Figure 1. For a powered knee prosthesis to generate natural motion in this process, the controller should follow the same strategy, generating a knee torque that changes in a way similar to the biological joint torque trajectory. To facilitate the implementation in powered prostheses, the STS controller structure should be adequately simplified while retaining the essence of human biological control. Furthermore, considering the significant intersubject variation among prosthesis users, subject-specific tuning is an indispensable step in fitting a powered prosthesis. Ideally, the number of control parameters should be minimized, and all parameters should have clearly defined physical meanings to make the tuning process intuitive and easy to understand. Based on the multiple requirements above, the authors propose a control structure consisting of a time-based ramp-up function for gradual loading of the knee combined with an impedance function for automatic adjustment of knee torque according to the motion progress:

$$\tau = R(t) \cdot \tau_{\text{imp}}(\theta, \dot{\theta}). \quad (1)$$

In this equation, the impedance function  $\tau_{\text{imp}}$  is defined as

$$\tau_{\text{imp}} = K(\theta - \theta_e) + B\dot{\theta}, \quad (2)$$

where  $\theta$  is the joint position (measured from the knee-straight position),  $\dot{\theta}$  is the joint angular velocity,  $K$  is the stiffness of the virtual spring,  $\theta_e$  is the equilibrium point of the virtual spring, and  $B$  is the damping value of the virtual damper. The ramp-up function  $R(t)$  is defined as

$$R(t) = \begin{cases} \frac{t - t_0}{T} & \text{when } t_0 \leq t \leq t_0 + T \\ 1 & \text{when } t > t_0 + T, \end{cases} \quad (3)$$

where  $t$  is the current time point,  $t_0$  is the starting time point of the ramp-up period, and  $T$  is the length of the ramp-up period.

The impedance function, as the major part of the controller, simulates the dynamics of a mechanical spring combined with a viscous damper. A mechanical spring is energetically conservative, while a viscous damper is dissipative. As such, the simulated spring-damper combination is purely passive, guaranteeing the stability in the control process. The passivity, on the other hand, dictates that all the required artificial mechanical energy (in the form of artificial spring deflection) is to be introduced at the onset of STS motion, such that sufficient power output can be provided while lifting the user in the upward motion. Consequently, the torque output of the spring-damper combination immediately reaches the maximum at the motion onset, as opposed to the gradual increase as shown in the biomechanical data.

The time-based ramp-up function is then introduced to address this problem. As (3) shows, the value of the function

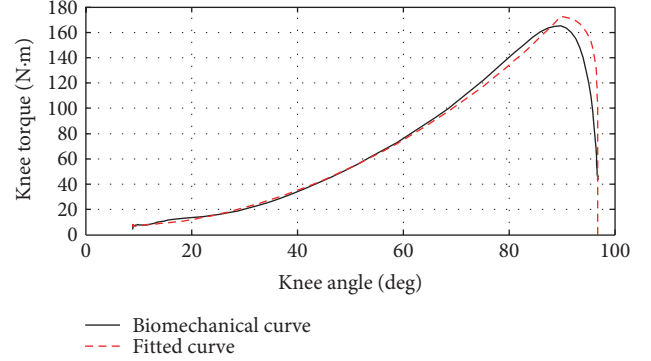


FIGURE 2: Comparison of the fitted knee torque curve versus the knee torque curve in the biomechanical data for the STS motion [1].

increases linearly from 0 to 1 within the ramp-up period and stays at 1 afterwards. As such, it only takes effect in the ramp-up period, providing the gradual energy injection required in the loading phase. It is worth mentioning that the use of the ramp-up function eliminates the need for explicit phase transition from loading to rising as a result of the limited effective period, which significantly simplifies the implementation of controller. Note that other functions may also be used to generate the gradual loading effect in the load phase. For example, a sigmoid function ( $y = 1/(1 + e^{-x})$ ) also monotonically increases from 0 to 1, with the additional advantage of having a continuous derivative. However, such function usually comes with higher computation load than the ramp-up function in the real-time implementation. Furthermore, the ramp-up function has a tunable parameter  $T$  that has a clearly defined physical meaning (the duration of the ramp-up period). As such, it is easier to tune the speed of loading to fit each individual user when the ramp-up function is used.

To validate the controller structure shown by (1), (2), and (3), curve fitting was conducted based on the biomechanical data of knee position/velocity and torque in the STS for a 75 kg subject [1]. Matlab Curve Fitting Toolbox was utilized to obtain the optimal set of values for  $K$ ,  $\theta_e$ ,  $B$ , and  $T$  with the least error from the biomechanical data. Figure 2 shows the comparison of the fitted knee torque curve versus the knee torque trajectory plotted from biomechanical data. The close match between the two curves indicates that the proposed controller structure is able to replicate the dynamic behavior of the biological knee joint in the STS motion with very small error.

Finally, to initiate the control action, the axial load in the prosthesis combined with the knee joint angle serves as the indicator for the user's readiness for the STS motion. When the user prepares for standing up, he/she first bends the knees by a large angle (usually greater than 90°) such that the feet can be directly underneath the body's center of mass. Subsequently, the weight is gradually shifted to the feet, increasing the axial load born by the prosthesis. Based on such biomechanical process, the trigger condition is set as the prosthesis axial load greater than a certain threshold  $F_T$ , and the prosthesis knee angle also greater than a certain threshold  $\theta_T$ . This simple yet effective triggering condition can be easily implemented by using the embedded sensors in the

prosthesis and provides an intuitive and reliable way to initiate the STS motion. If the axial load information is not available, the inclination of the upper body may also serve as a triggering condition, as a user usually leans forward significantly when attempting to stand up. Alternatively, direct human input (e.g., through voice command or a switch) may also be used for this purpose.

### 3. Human Testing Results

To demonstrate the effectiveness of the STS controller, the authors conducted a set of human subject experiments at the Human-Centered BioRobotics (HUB-Robotics) Laboratory at The University of Alabama. The human subject participated in the testing was a 22-year-old male unilateral amputee, 178 cm in height and weighed 57 kg. He was fitted with a powered knee prosthesis prototype developed at HUB-Robotics Lab, namely Alabama Powered Prosthetic Limb-Knee (APPL-K), shown in Figure 3.

The version of the powered knee prosthesis used in this study, APPL-K-E1, was powered by an 8-pole brushless DC motor with 70 W power rating (EC 45 flat, Maxon Motor, Sachseln, Switzerland). For short-term operation, this motor is able to generate a peak torque of 0.2 Nm and a maximum rotation speed of 10,000 rpm. A two-stage transmission of 150:1 gear ratio is used, combining a timing belt drive as the first stage and a harmonic drive gearhead as the second stage. Note that, in the design of the device, reducing the weight and simplifying the system structure was given higher priority than generating higher torque output, and the actuation torque is less than the peak value in the biomechanical data. This issue, however, did not affect the performance of the prosthesis in the STS, as indicated by the experimental results below.

For the implementation of the STS controller, the prosthesis is instrumented with various control components for computing, sensing and regulation of power delivery. The joint position is measured with a rotary magnetic encoder, and the position signal is digitally differentiated to obtain the joint angular velocity information. A custom load cell developed by the Center for Intelligent Mechatronics at Vanderbilt University [17] is mounted between the prosthesis and the standard pyramid connector to measure the axial force in the prosthesis. The power output of the DC motor is regulated with a PWM servo drive (AZBDC20A8, Advanced Motion Controls, Camarillo, CA, USA), which controls the motor current as a function of the PWM duty cycle. The controller is implemented on a microcontroller (Microstick II, Microchip Technology Inc., Chandler, AZ, USA), which communicates with a host desktop computer to record and display experimental results for controller tuning and data analysis.

Due to the limitation of available equipment, the data collected in the testing were all based on the sensors embedded in the prosthesis, primarily the joint angle and torque trajectories. After being fitted with the powered prosthesis, the subject repeated the STS motion to identify the best set of control parameters through his feedback and recorded experimented data. The stiffness of the artificial spring in

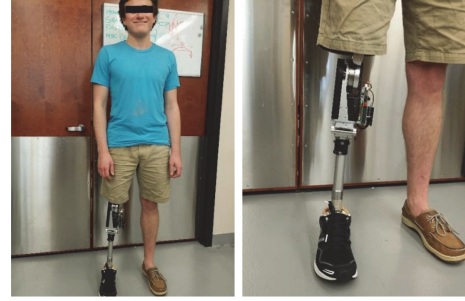


FIGURE 3: The test subject fitted with the powered knee prosthesis.

TABLE 1: The parameters of the STS controller.

$T$ (s)	$K$ (Nm/deg)	$B$ (Nm·s/deg)	$\theta_0$ (deg)
0.47	1.1	0.4	8

the controller  $K$  was increased gradually, providing increasing extensional torque to assist the user to stand up. The final value, with which the user is most comfortable with, generates a peak torque of 25 Nm, much less than that in the biomechanical data. The primary reason, presumably, is that the subject is used to the lack of power supply in his daily-use passive prosthesis, and thus the comfortable level of power supply in his prosthetic joint has been reduced significantly compared with that in a healthy biological joint. This observation, to some extent, validates the original decision of prioritizing low weight over high torque in the prosthesis design.

The damping of the artificial viscous damper was also tuned. With the function of controlling the speed of standing up, the damper reduces the extensional torque or even generates a flexional torque if the extension of the knee becomes too fast. The damping value was also adjusted primarily according to the feedback of the test subject. The finalized controller parameters are shown in Table 1.

The typical trajectories of the experimentally measured prosthetic joint position and torque are shown in Figure 4, and a sequence of snapshots of the STS process is shown in Figure 5. The data window started when the triggering condition was met. As can be seen in Figure 4, the joint position stayed almost as a constant until the rising phase started, and the whole trajectory shows smooth and controlled motion throughout the process. Compared with the biomechanical data shown in Figure 1, the contour of the experimentally measured prosthetic position trajectory is highly similar. For the joint torque trajectory, the dynamics of the loading and rising phases can be clearly identified and distinguished, while the flat peak in the middle of the cycle is a result of the torque saturation (i.e., reaching the maximum torque as dictated by the prosthetic actuator). The overall contour is also similar to that of the biomechanical curve in Figure 1. Matching the observations from these figures, the subject also stated a natural control experience in which the prosthesis motion coordinates with the sound-side leg motion well, and the extensional torque in the prosthesis

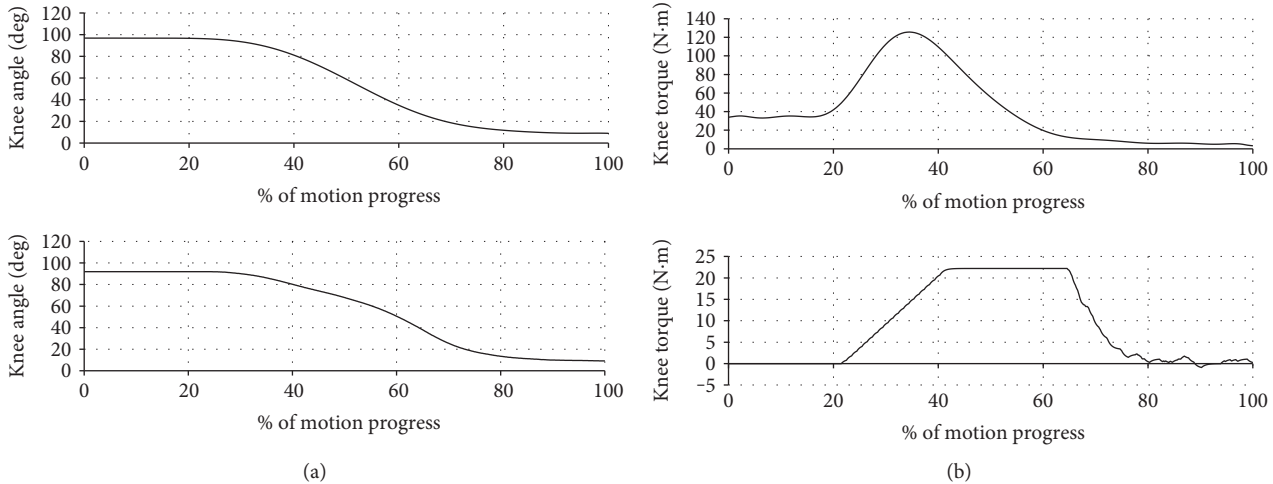


FIGURE 4: Comparison of the typical trajectories of the prosthetic joint versus the biomechanical trajectories in [1]: (a) angle trajectory comparison, with the biomechanical trajectory above the experimental trajectory; (b) torque trajectory comparison, with the biomechanical trajectory (for a 57 kg person) above the experimental trajectory.



FIGURE 5: A sequence of snapshots of the STS motion.

enabled him to stand up with less effort. Such quantitative and qualitative results fully demonstrated the effectiveness of the proposed controller, which provides the prosthesis user a significantly improved experience over the traditional passive prosthesis.

#### 4. Conclusions

In this paper, the authors present a new control approach for powered knee prostheses in the STS motion. The objective was to develop an STS controller that regulates the extensional torque in powered knee prostheses to obtain smooth standing-up motion. As the basis of the controller development, the biomechanical data from prior STS studies were analyzed. The dynamics in the loading and rising phases are vastly different. However, a unique control structure was created, which combines the impedance function with a time-based ramp-up function. The impedance function was introduced to provide the gradual energy release in the rising phase, while the ramp-up function was included to mimic the gradual energy injection behavior in the loading phase. The use of such unified control structure simplifies the controller implementation while maintaining the unique biomechanical characteristics of each motion phase. This new STS controller was implemented on a powered knee prosthesis developed in the authors' lab, and human testing results demonstrated the effectiveness of this approach in

generating smooth standing-up motion according to the user's will.

#### Conflicts of Interest

The authors declare that there is no conflict of interest regarding the publication of this paper.

#### References

- [1] M. Schenkman, R. A. Berger, P. O. Riley, R. W. Mann, and W. A. Hodge, "Whole-body movements during rising to standing from sitting," *Physical Therapy*, vol. 70, no. 10, pp. 638–648, 1990.
- [2] D. A. Winter, *The Biomechanics and Motor Control of Human Gait: Normal, Elderly and Pathological*, University of Waterloo Press, Waterloo, ON, 2nd edition, 1991.
- [3] M. J. Highsmith, J. T. Kahle, S. L. Carey et al., "Kinetic asymmetry in transfemoral amputees while performing sit to stand and stand to sit movements," *Gait & Posture*, vol. 34, no. 1, pp. 86–91, 2011.
- [4] W. C. Flowers and R. W. Mann, "Electrohydraulic knee-torque controller for a prosthesis simulator," *ASME Journal of Biomechanical Engineering*, vol. 99, no. 4, pp. 3–8, 1977.
- [5] D. Popovic and L. Schwirtlich, *Belgrade Active A/K Prostheses*, J. Vries, Ed., *Electrophysiological Kinesiology*, Interm. Congress Ser. No. 804, Excerpta Medica, Amsterdam, The Netherlands, 1988.

- [6] N. Hata and Y. Hori, *Basic Research on Power Limb Using Gait Information of Able-Side Leg*, International Workshop on Advanced Motion Control, 7th edition, 2002.
- [7] K. Fite, J. Mitchell, F. Sup, and M. Goldfarb, "Design and control of an electrically powered knee prosthesis," in *Proceedings of the 2007 IEEE 10th International Conference on Rehabilitation Robotics*, pp. 902–905, Noordwijk, Netherlands, June 2007.
- [8] F. Sup, H. A. Varol, J. Mitchell, T. J. Withrow, and M. Goldfarb, "Preliminary evaluations of a self-contained anthropomorphic transfemoral prosthesis," *IEEE/ASME Transactions on Mechatronics*, vol. 14, no. 6, pp. 667–676, 2009.
- [9] E. C. Martinez-Villalpando and H. Herr, "Agonist-antagonist active knee prosthesis: a preliminary study in level-ground walking," *Journal of Rehabilitation Research & Development*, vol. 46, no. 3, pp. 361–374, 2009.
- [10] C. D. Hoover, G. D. Fulk, and K. B. Fite, "The design and initial experimental validation of an active myoelectric transfemoral prosthesis," *ASME Journal of Medical Devices*, vol. 6, article 011005, 2012.
- [11] F. Sup, A. Bohara, and M. Goldfarb, "Design and control of a powered transfemoral prosthesis," *The International Journal of Robotics Research*, vol. 27, no. 2, pp. 263–273, 2008.
- [12] G. Waycaster, S. K. Wu, and X. Shen, "Design and control of a pneumatic artificial muscle actuated above-knee prosthesis," *Journal of Medical Devices*, vol. 5, no. 3, article 031003, 2011.
- [13] D. L. Grimes, W. C. Flowers, and M. Donath, "Feasibility of an active control scheme for above knee prostheses," *ASME Journal of Biomechanical Engineering*, vol. 99, no. 4, pp. 215–221, 1977.
- [14] S. K. Wu, G. Waycaster, and X. Shen, "Electromyography-based control of active above-knee prostheses," *Control Engineering Practice*, vol. 19, no. 8, pp. 875–882, 2011.
- [15] H. A. Varol, F. Sup, and M. Goldfarb, "Multiclass real-time intent recognition of a powered lower limb prosthesis," *IEEE Transactions on Biomedical Engineering*, vol. 57, no. 3, pp. 542–551, 2010.
- [16] H. A. Varol, F. Sup, and M. Goldfarb, "Powered sit-to-stand and assistive stand-to-sit framework for a powered transfemoral prosthesis," in *2009 IEEE International Conference on Rehabilitation Robotics*, pp. 645–651, Kyoto, Japan, June 2009.
- [17] B. E. Lawson, J. E. Mitchell, D. Truex, A. Shultz, E. Ledoux, and M. Goldfarb, "A robotic leg prosthesis: design, control, and implementation," *IEEE Robotics & Automation Magazine*, vol. 21, no. 4, pp. 70–81, 2014.